



Universitat Autònoma de Barcelona

**ADVERTIMENT.** L'accés als continguts d'aquesta tesi queda condicionat a l'acceptació de les condicions d'ús establertes per la següent llicència Creative Commons:  [http://cat.creativecommons.org/?page\\_id=184](http://cat.creativecommons.org/?page_id=184)

**ADVERTENCIA.** El acceso a los contenidos de esta tesis queda condicionado a la aceptación de las condiciones de uso establecidas por la siguiente licencia Creative Commons:  <http://es.creativecommons.org/blog/licencias/>

**WARNING.** The access to the contents of this doctoral thesis it is limited to the acceptance of the use conditions set by the following Creative Commons license:  <https://creativecommons.org/licenses/?lang=en>

DOCTORAL THESIS

Barcelona 2022

**NANOTARGETED ENDOTHELIAL  
PROGENITOR CELLS-SECRETOME  
THERAPY THROUGH ENDOVASCULAR  
DELIVERY FOR ISCHAEMIC STROKE**

Alba Grayston Morales

---

**PhD programme in Neurosciences**  
Universitat Autònoma de Barcelona (UAB)

**Neurovascular Research Laboratory**  
Vall d'Hebron Research Institute (VHIR)

---

DIRECTOR

Dr. Anna Rosell Novel

TUTOR

Dr. Joan Montaner Vilallonga



This doctoral thesis has been conducted in the Neurovascular research laboratory at the Vall d'Hebron Research Institute (VHIR), and supported by fellowships (FI17/00073 and MV18/00006) and research grants (AC17/00004 and RD16/0019/0021) from the Instituto de Salud Carlos III, and the support of the 2017-SGR-1427 from AGAUR.





## AGRAÏMENTS

---

Amb aquestes pàgines tanco una de les etapes més intenses que he viscut fins ara. L'esforç, la satisfacció i les frustracions que ha comportat tot això potser quedaran entre línies. Però hi ha un grapat de gent que n'ha format part i a qui m'agradaria dedicar unes paraules. Sense vosaltres aquest camí no hauria valgut tant la pena.

Primer de tot, a l'Anna Rosell. Gràcies per obrir-me aquesta porta, per tota la confiança que has dipositat en mi i per brindar-me tantíssimes oportunitats per aprendre al llarg d'aquests anys. Ha estat un plaer créixer amb tu, i celebro tot el que hem aconseguit des d'aquell “nena, estem en ratxa”.

A l'Anna Roig, que ha estat una peça clau. M'ha encantat topar amb aquest projecte que vau engegar plegades i haver-hi pogut aportar el meu nano-gra de sorra. Moltes gràcies per l'ajuda, els consells i els elogis que m'han aixecat els ànims tantes vegades.

A tota la gent amb qui he compartit aquesta etapa al LIN. Em sento molt afortunada d'haver-hi trobat aquest caliu, i m'enduc molts bons records, des de la poiata a la barra. A la generació que ens va fer “el traspàs” i en especial a l'Alba, que ha seguit allà compartint inquietuds i donant-me empenta. A la nova generació, ha estat molt bonic tancar aquest cercle així; Neus, no perdís aquesta llum! A les noies d'amiloide, que han hagut d'escoltar alguna que altra xapa meva dins i fora de les micros; Mar, gràcies pels consells i els ànims per seguir endavant. Al Joan, sempre disposat a repartir optimisme. A tot el 123, teniu un imant per la gent bonica; Alejandro i Joanet, gracias por las charlas, és un plaer seguir coincidint amb vosaltres fora del LIN; Elena, gràcies pels teus ànims aquest últim tram, y a Daisy, por tus abrazos al final del día. Als compis de cafè, a l'Anita i al Chechu, gràcies per alegrar-me els dies, us trobaré a faltar! A la Paula, mi otra (a veces) compañera de cafés, reina de las vitaminas, m'hagués agradat compartir més temps aquí amb tu, molta força i sobretot a gaudir! A la súper línia de Neurorepair; Merch, con todo y después de esta última cuesta que se nos ha hecho tan larga, gracias; Miguel, amb qui he tingut la sort de treballar colze a colze, el mèrit d'aquesta feinada també és teu i estic orgullosa tant del que hem fet plegats com del vincle que hem anat teixint amb el temps. I unes

paraules que es quedaran curtes per a la millor combinació de companyes, confidents i amigues que m'han pogut tocar: Laura, Paula i Júlia, quina sort compartir aquesta experiència amb vosaltres. Ho heu fet tot molt més divertit i amè, dins i fora del lab. Ara sí, el despatx es queda buit, però pleníssim de records que espero que seguim sumant fora d'aquí.

Al Ricardo Guixà, per cedir el seu treball fantàstic per embolicar aquest llibre. Amb qui comparteixo la fascinació reflectida a "Melothesia" per la redundància de patrons fractals a la natura, de la macro- a la nano-escala.

Als Towanda, amb qui vaig començar el trajecte. En la distància o aquí, us sento sempre a prop. Als vallcarqueens, la vostra companyia ha fet que aquesta etapa fos molt més bonica; gràcies per fer-me costat, per escoltar-me, per aconsellar-me, per divertir-me, per donar-me tant escalf. A les persones amb qui vaig compartir un pis molt especial, a la Carlota, la Nunu, l'Helena i les Annes, les que m'han falcat i m'han fet l'escaleta tots aquests anys. A l'Edmon, amb qui he compartit les primeres passes del doctorat, gràcies per seguir aquí i per aquest vincle que hem construït. Als bubbles, amb alguns dels quals vaig rebre la notícia que em fotia en aquest merder ara fa gairebé 5 anys, a l'altra banda del charco. A la colla de Sarrià, sou amor, gràcies pel vostre caliu i el vostre suport, amb la tesi, a la muntanya i a la vida. Al Marc i a la Maria, per tants moments terapèutics. I a les que han estat aquí sempre i a tot arreu, passant per l'institut, la uni, els castells, el circ, els bubbles i més enllà: a l'Andrea, la Helen, la Clot i el Pai. He arribat així i fins aquí gràcies a vosaltres, per molts motius. Gràcies per tantíssim.

A la mama, por tu apoyo incondicional y tu orgullo de madre, por enseñarme a observar y a emocionarme por los pequeños detalles; esta tesis no es nada al lado de todo tu esfuerzo. To dad, who encouraged me to follow this career in the first place, who taught me that "all work and no play makes Alba a dull girl"; thank you for your soothing words and support. A Pablo, por tu complicidad, por estar ahí y preocuparte, por subirme la moral, porque nos lo hemos currado. A Liam y a Clara, por vuestra curiosidad genuina, por ser siempre tan agradecidos y enseñarme lo que

de veritat importa. A la Mire, companya de uni i de pis, amiga, i amb qui tinc la sort de gaudir com a família, gràcies per tota l'energia positiva que em transmetes. A Anna, por tu apoyo y por hacerme sentir siempre que me voy a comer el mundo. A la família que em va obrir els braços a l'inici de tot això: a l'Anna, al Guillem, a la Berta i al Quimet, per ser tan càlids, per tots els detalls que heu tingut amb mi.

Al Ferranji, a qui escullo cada dia. El que em dóna l'empenta i després m'ajuda a frenar. Gràcies per fer-ho tot tan fàcil, per fluir, per entendre'm, per lluitar al meu costat. Per tota la força que m'has donat. Avui ens celebrem, pel que hem aconseguit i per tots els camins que comencen aquí. T'estimo.

Tinc moltíssima sort de comptar amb tota aquesta xarxa de suport. Moltíssimes gràcies a tothom!





# INDEX

<b>THE MAGBBRIS PROJECT .....</b>	<b>1</b>
<b>ABSTRACT.....</b>	<b>5</b>
<b>RESUM.....</b>	<b>7</b>
<b>ABBREVIATIONS.....</b>	<b>9</b>
<b>INTRODUCTION.....</b>	<b>15</b>
<b>1.1. Stroke .....</b>	<b>17</b>
1.1.1. Definition, global burden and risk factors.....	17
1.1.2. Classification and diagnosis .....	18
<b>1.2. Stroke pathophysiology .....</b>	<b>20</b>
1.2.1. Acute phase.....	21
1.2.2. Subacute phase .....	23
1.2.2.1. Neurogenesis .....	24
1.2.2.2. Oligodendrogenesis and white matter remodelling .....	26
1.2.2.3. Angiogenesis .....	26
1.2.2.4. Brain plasticity .....	28
<b>1.3. Current stroke treatments .....</b>	<b>29</b>
1.3.1. Recanalisation therapies .....	29
1.3.2. Rehabilitation therapies .....	30
<b>1.4. Pre-clinical stroke models .....</b>	<b>31</b>
<b>1.5. Experimental therapeutic strategies for stroke.....</b>	<b>34</b>
1.5.1. Cell-based therapies .....	36
1.5.2. Endothelial Progenitor Cells (EPCs).....	38
1.5.2.1. EPCs-derived secretome.....	41
<b>1.6. Brain drug delivery .....</b>	<b>41</b>
1.6.1. The blood-brain barrier.....	41

1.6.2. Strategies for brain drug delivery.....	42
1.6.2.1. Physicochemical modifications of the therapeutic agent.....	43
1.6.2.2. Selective BBB opening.....	44
1.6.2.3. Biological vectors.....	44
1.6.2.4. Nanocarriers.....	45
1.6.2.5. Administration routes.....	47
<b>1.7. Nanomaterial-based treatments for stroke.....</b>	<b>48</b>
<b>1.8. Thesis rationale and hypothesis.....</b>	<b>51</b>
<b>OBJECTIVES.....</b>	<b>53</b>
<b>MATERIALS AND METHODS.....</b>	<b>57</b>
<b>3.1. EPC-secretome, Nanocarriers and Magnet devices.....</b>	<b>59</b>
3.1.1. EPCs isolation.....	59
3.1.2. Secretome collection and concentration.....	59
3.1.3. Nanocarriers synthesis and characterisation.....	60
3.1.4. Secretome encapsulation efficiency and release.....	62
3.1.5. Magnet devices.....	63
3.1.5.1. Validation for magnetic retention.....	64
<b>3.2. Cell culture <i>in vitro</i> studies.....</b>	<b>65</b>
3.2.1. Experimental design and cell types.....	65
3.2.2. Endothelial proliferation assays.....	66
3.2.3. Endothelial tubulogenesis assays.....	67
3.2.4. Endothelial nanocarriers uptake.....	67
<b>3.3. <i>In vivo</i> nanocarriers delivery and cerebral ischaemia.....</b>	<b>68</b>
3.3.1. Experimental design.....	68
3.3.2. MCAO surgery.....	76
3.3.3. Administration route and magnetic retention.....	77

3.3.4. Fluorescent Molecular Imaging (FMI).....	78
3.3.4.1. FMI analysis.....	79
3.3.5. Magnetic Resonance Imaging (MRI).....	80
3.3.5.1. MRI analysis.....	80
3.3.6. Functional tests.....	81
3.3.7. Tissue sampling and processing.....	81
3.3.8. Plasma biochemical analysis .....	84
3.3.9. Prussian blue staining .....	84
3.3.10. Lectin vessel staining .....	84
3.3.11. Infarct volume and intracerebral haemorrhage evaluation .....	85
3.3.12. Brain vessels isolation.....	85
3.3.13. Western blot.....	86
3.3.14. Multiplexed enzyme-linked immunosorbent assays (ELISA).....	88
3.3.15. Singleplex ELISA .....	89
3.3.16. Immunofluorescence .....	89
3.3.17. Fluoro-Jade C staining.....	90
3.3.18. Pilot endovascular delivery study in pigs .....	91
<b>3.4. <i>Ex vivo</i> magnetic retention in a humanised model .....</b>	<b>93</b>
3.4.1. 3D printing.....	93
3.4.2. Micro-catheter-guided infusion and monitoring .....	94
<b>3.5. Statistical analysis.....</b>	<b>94</b>
<b>RESULTS .....</b>	<b>97</b>
<b>4.1. Angiogenic effects of EPCs-secretome on endothelial cells .....</b>	<b>99</b>
<b>4.2. EPCs-secretome encapsulation .....</b>	<b>102</b>
4.2.1. Angiogenic effects after EPCs-secretome encapsulation.....	102
4.2.2. Encapsulation efficiency .....	107

4.2.3. Nanocarriers characterisation for <i>in vivo</i> studies.....	108
<b>4.3. Endovascular administration of magnetised nanocarriers to enhance brain delivery after stroke.....</b>	<b>109</b>
4.3.1. Administration route and magnetic retention .....	109
4.3.2. Safety of hyperacute endovascular administration of magnetised nanocarriers after cerebral ischaemia.....	114
4.3.3. Magnetic field modelling to improve brain nanomaterial retention .....	118
<b>4.4. Endovascular-nanotargeted EPCs-secretome treatment after cerebral ischaemia.....</b>	<b>126</b>
4.4.1. Short-term efficacy after hyperacute endovascular administration of free or nanotargeted EPCs-secretome in ischaemic mice .....	126
4.4.1.1. Short-term functional outcome and brain damage.....	126
4.4.1.2. Effects of free or encapsulated EPCs-secretome on the BBB and the neuro-inflammatory response after cerebral ischaemia.....	130
4.4.2. Long-term efficacy after hyperacute endovascular administration of free or nanotargeted EPCs-secretome in ischaemic mice .....	135
4.4.2.1. Long-term NCs biodistribution .....	135
4.4.2.2. Long-term safety and functional outcome .....	138
4.4.2.3. Effects of free or encapsulated EPCs-secretome on brain angiogenesis.....	142
4.4.2.4. Effects of free or encapsulated EPCs-secretome on neurogenesis and delayed neurodegeneration .....	148
<b>4.5. Translational feasibility of endovascular delivery and magnetic retention for nanomaterial brain retention .....</b>	<b>151</b>
4.5.1. Endovascular nanocarriers delivery in naïve pigs .....	151
4.5.2. 3D vascular model.....	154
<b>DISCUSSION.....</b>	<b>157</b>

5.1. Enhancing brain delivery through endovascular administration and magnetic nanotargeting.....	159
5.2. Neurovascular repair can be achieved through early nanoencapsulated EPCs-secretome intraarterial delivery after stroke reperfusion .....	164
5.3. Paving the way towards the clinical implementation of endovascular treatments, advanced therapies and nanotheranostics .....	172
5.4. Limitations of the study and future perspectives.....	174
CONCLUSIONS .....	177
REFERENCES .....	181
ANNEX I – CURRICULUM VITAE .....	209
ANNEX II – RELATED PUBLICATIONS .....	217
Revascularization and endothelial progenitor cells in stroke .....	219
Effects of aging and comorbidities on endothelial progenitor cells.....	233
PLGA protein nanocarriers with tailor-made fluorescence / .....	247
MRI / PET imaging modalities.....	247
Endovascular administration of magnetised nanocarriers targeting brain delivery after stroke.....	265
Secretome of endothelial progenitor cells from stroke patients promotes endothelial barrier tightness and protects against hypoxia-induced vascular leakage .....	283



# THE MAGBBRIS PROJECT

The present doctoral thesis has been carried out within the framework of a European project titled “**MAGnetic Biomaterials for Brain Repair and Imaging after Stroke (MAGBBRIS)**” (Figure 1).

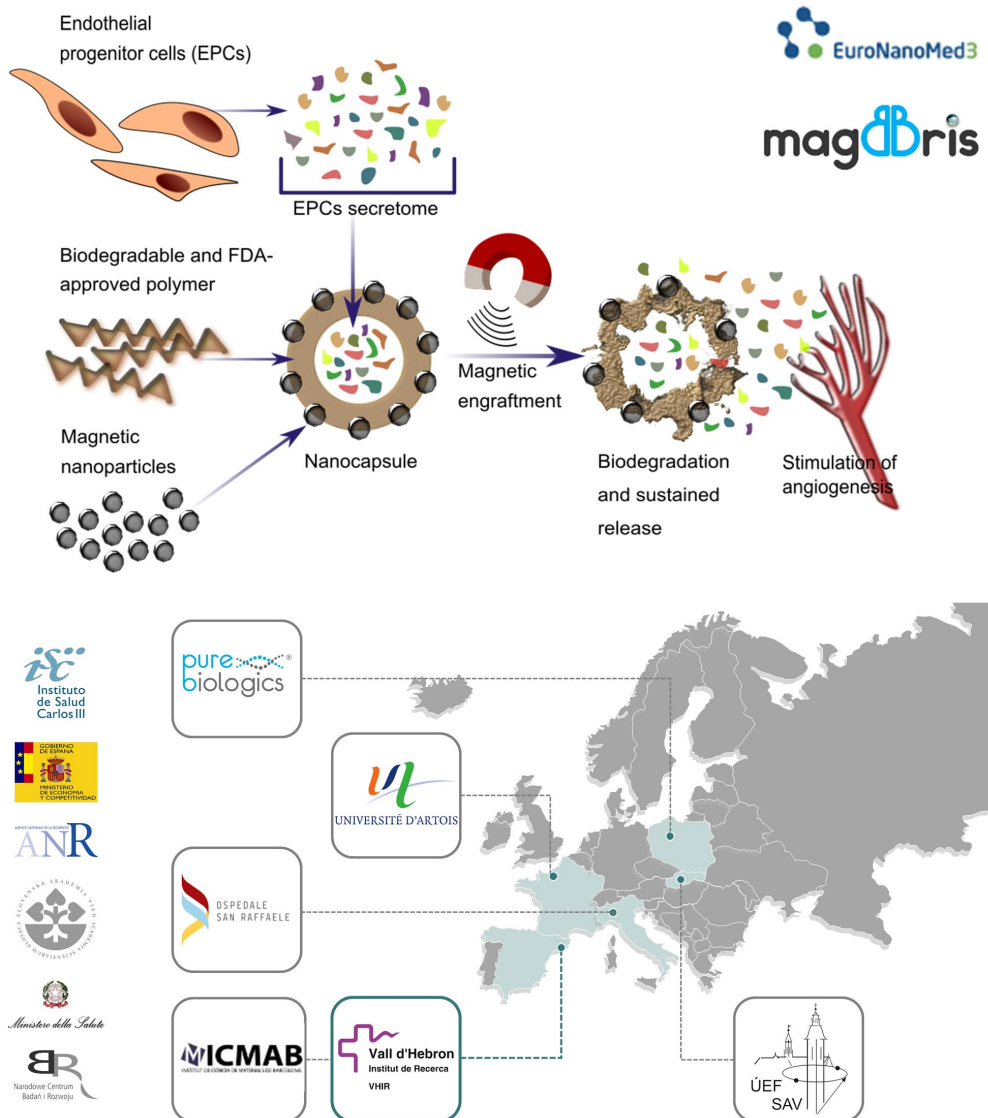


**Figure 1. MAGBBRIS graphical abstract and project consortium.**



The project was founded in the 2017 call within the EuroNanoMed III programme, by 6 different European funding agencies including the Instituto de Salud Carlos III (AC17/00004) at the Neurovascular Research Laboratory, for a duration of 36 months. Our research group was the coordinator of the MAGBBRIS consortium, made up by 6 partners, involving multidisciplinary materials scientists, biomedical and clinical researchers together with industrial partnership (**Table 1**).

**Table 1. MAGBBRIS project consortium.**

<b>Institution (partner number, *coordinator)</b>	<b>Principal Investigator</b>	<b>Funding Organisation, Country</b>
Vall d'Hebron Institut de Recerca (VHIR) (1*)	Anna Rosell	Instituto de Salud Carlos III (ISCIII), Spain
Agencia Estatal Consejo Superior de Investigaciones Científicas (CSIC) (2)	Anna Roig	Ministry of Economy and Competitiveness (MINECO), Spain
University of Artois, Faculty Jean Perrin (3)	Fabien Gosselet	Agence Nationale de la Recherche (ANR), France
Ospedale San Raffaele, Istituto di Ricovero e Cura a Carattere Scientifico (IRCCS) (4)	Maria Picchio	Ministero Della Salute (IMH), Italy
Pure Biologics Ltd (5)	Filip Jelen	Polish National Center for Research and Development (NCBR), Poland
Institute of experimental physics, Slovak Academy of Sciences (SAS) (6)	Peter Kopcansky	Slovak Academy of Sciences (SAS), Slovakia

The aim of the project was to promote tissue repair in the context of ischaemic stroke by taking advantage of nano-biomaterials to deliver therapeutic growth factors secreted by endothelial progenitor cells (EPCs). In order to achieve so, a novel non-invasive local regenerative treatment was proposed to enhance vascular remodelling by the EPCs-secretome encapsulated into polymeric biodegradable and biocompatible nanocapsules (NCs), labelled with magnetic nanoparticles and fluorescent tags allowing their retention and tracking.

Our major roles within the project were to coordinate the consortium and conduct the experiments for EPCs-secretome production, nanocapsules delivery and

magnetic retention validation for *in vitro* (cell cultures) and *in vivo* (pre-clinical stroke model) applications, which are part of the results presented in this doctoral thesis.

The specific work packages defined within the proposal, which relate with the work conducted in this Doctoral Thesis, are described in **Table 2**.

**Table 2. MAGBBRIS work packages.**

	<b>Partners</b>
<b>WP1. Nano-biomaterial synthesis and magnetic targeting</b>	
<b>Milestones:</b> description of EPCs-secretome and well-characterised PLGA-fluorescent/magnetic nanocapsules. Magnet device design based on focused magnets wearable for stroke patients	1, 2, 4, 6
<b>WP2. Functional validation of the therapeutic nanocapsules</b>	
<b>Milestones:</b> <i>in vitro</i> and <i>in vivo</i> safety of the theranostic biomaterial	1, 2, 3, 4
<b>WP3. Secretome/biomaterial production, validation and industrialisation</b>	
<b>Milestones:</b> manufacturing process at industry standards and product validation	All
<b>WP4. Imaging brain responses and magnetic tracking</b>	
<b>Milestones:</b> protocols for MRI and OI of biomaterial delivery and <i>in vivo</i> evaluation of biomaterial efficacy. Proving a successful delivery of magnetic nanocapsules with focused magnets	1, 2, 4, 6
<b>WP5. Coordination, management and dissemination</b>	
<b>Milestones:</b> web page creation, results' dissemination and publications.	All

WP = work package, PLGA = poly(lactic-co-glycolic acid), MRI = magnetic resonance imaging, OI = optical imaging.



## ABSTRACT

---

Stroke remains a leading cause of death and disability worldwide. Hence there is an urgent need to develop therapeutic strategies beyond acute recanalisation. However, this therapeutic development is hampered by a highly complex pathophysiology, added to the challenge of brain drug delivery. In this regard, endothelial progenitor cells (EPCs)-secretome represents a promising cell-free therapy for post-stroke neurovascular repair. Furthermore, mechanical thrombectomy for recanalisation has opened the window to brain drug delivery, which could be further improved by nanomedicine.

This doctoral thesis aimed to enhance brain targeting and neurovascular repair in the context of cerebral ischaemia, through the endovascular delivery and magnetic retention of EPCs-secretome encapsulated in biocompatible and biodegradable polymeric nanocarriers.

The proposed nanocarriers have been functionalised with superparamagnetic iron-oxide nanoparticles (SPIONs) and fluorescent tags for magnetic retention and magnetic resonance/fluorescent molecular imaging (MRI/FMI), respectively. An exhaustive study of their biodistribution by MRI/FMI has shown a great advantage of the intraarterial route combined with magnetic retention through focused magnet devices, to safely enhance brain targeting in a mouse model of cerebral ischaemia. And, importantly, it has been demonstrated that the nanocarriers remain in the target ischaemic brain up to one week, easing the sought-after sustained release of cargo therapeutic factors. Furthermore, the EPCs-secretome has been successfully encapsulated into the polymeric nanocarriers, as seen through both total and specific EPCs-secretome cargo proteins, and the pro-angiogenic therapeutic effects were preserved after the encapsulation-release process, as demonstrated in endothelial cell culture *in vitro* models.

The present study demonstrates the advantage of the therapeutic application of EPCs-secretome through this selective nanotargeted approach against the equivalent

free treatment at similar doses. The results presented herein suggest that hyperacute endovascular delivery of free EPCs-secretome, at the tested dose, might exacerbate the acute post-ischaemic brain damage along with an increased neuro-inflammatory response, while ubiquitously enhancing brain angiogenesis. In contrast, the nanotargeted treatment could selectively enhance brain angiogenesis in the target peri-infarct brain, in the absence of the aforementioned detrimental effects.

As preliminary steps towards the translation of the proposed therapeutic approach to the clinical setting, large animals with gyrencephalic brains and an *ex vivo* humanised vascular model were also used. The present study demonstrates the safety and feasibility of endovascular delivery for brain nanotargeting in pigs, and the efficacy of endovascular delivery and magnetic retention in an *ex vivo* model adapted to the human vascular anatomy and biodynamics.

In summary, this doctoral thesis places the use of polymeric magnetised nanocarriers through endovascular delivery as a promising approach to enhance specific brain targeting of multiple therapeutic agents, such as EPCs-secretome, which could be implemented in the context of mechanical thrombectomies in the clinical scenario.

L'ictus isquèmic segueix sent a dia d'avui una de les principals causes de mortalitat i discapacitat a nivell mundial. Així doncs, és essencial desenvolupar estratègies terapèutiques més enllà de la recanalització aguda. Tanmateix, la cerca de noves teràpies es veu limitada per l'elevada complexitat dels processos fisiopatològics derivats de l'ictus i pel repte que suposa l'arribada d'agents terapèutics al cervell. En aquest sentit, l'ús dels factors secretats per cèl·lules progenitores endotelials (secretoma d'EPCs) representa una estratègia prometedora per promoure la reparació neurovascular la qual estalviaria els riscos associats a les teràpies cel·lulars. Paral·lelament, la trombectomia mecànica per a la recanalització aguda després de l'ictus ha obert una nova possibilitat per administrar fàrmacs directament al cervell, i aquest abordatge podria millorar significativament gràcies a la nanomedicina.

L'objectiu d'aquesta tesi doctoral ha estat augmentar l'arribada de fàrmacs al cervell per promoure la reparació neurovascular després de l'ictus isquèmic mitjançant l'administració intraarterial i el direccionament magnètic del secretoma d'EPCs en nanocàpsules polimèriques biocompatibles i biodegradables.

Les nanocàpsules emprades per a aquest estudi han estat modificades per incorporar nanopartícules de ferro superparamagnètiques (SPIONs) i marcatges fluorescents per al seu direccionament magnètic i monitoratge mitjançant les tècniques d'imatge per ressonància magnètica i per fluorescència molecular, respectivament. L'estudi exhaustiu de la biodistribució d'aquestes nanocàpsules per mitjà de les tècniques esmentades ha demostrat, en un model d'ictus isquèmic en ratolins, que la ruta intraarterial en combinació amb el direccionament magnètic presenta un gran avantatge per augmentar de forma segura l'arribada al cervell.

A més, s'ha observat l'acumulació de nanocàpsules a la regió cerebral infartada fins a una setmana després de l'administració, fet que afavoriria l'alliberament sostingut dels factors terapèutics encapsulats. Per altra banda, aquest treball ha demostrat, a través de l'estudi tant del contingut proteic total com de factors específics, la

possibilitat d'encapsular aquest secretoma i preservar la seva funció pro-angiogènica un cop alliberat, tal com s'ha demostrat en models *in vitro* de cèl·lules endotelials.

El present estudi demostra l'avantatge terapèutic de la implementació d'aquest abordatge nano-dirigit per a l'administració del secretoma d'EPCs, enfront de la teràpia lliure. Els resultats que es mostren aquí suggereixen que l'administració endovascular hiperaguda del secretoma d'EPCs, a la dosi testada, podria exacerbar el dany cerebral post-isquèmic, juntament amb una resposta neuro-inflamatòria incrementada i, per altra banda, promouria la formació de nous vasos sanguinis de manera ubiqua. En canvi, el tractament equivalent nano-dirigit permetria l'angiogènesi selectiva al teixit subjacent a l'infart sense els efectes nocius observats amb el tractament lliure.

Com a pas previ cap a la translació de l'abordatge terapèutic proposat, s'han utilitzat porcs com a models d'animals grans amb cervells girencéfals (propers a l'humà) així com un model *ex vivo* de l'arbre vascular humà. Per una banda, s'ha pogut comprovar la seguretat de l'administració endovascular i la seva eficàcia per al nano-direccionament al cervell en porcs. Finalment, el direccionament de nanocàpsules administrades per via intraarterial i retenció amb camp magnètic també ha estat demostrat per l'ús en humans, en un model que simula l'anatomia i biodinàmica humanes.

En conjunt, els resultats obtinguts en aquesta tesi doctoral posicionen l'ús de nanocàpsules magnètiques per via intraarterial com una estratègia prometedora per augmentar l'arribada de fàrmacs de forma específica al cervell, com per exemple el secretoma d'EPCs. Aquesta estratègia es podria implementar en el context clínic actual, amb l'ús de la trombectomia mecànica.

## ABBREVIATIONS

---

<b>3D</b>	Three-dimensional
<b>ACA</b>	Anterior carotid artery
<b>ACoA</b>	Anterior communicating artery
<b>ALT</b>	Alanine aminotransferase
<b>ARRIVE</b>	Animal research: reporting of <i>in vivo</i> experiments
<b>ASA/AHA</b>	American Stroke Association / American Heart Association
<b>AST</b>	Aspartate aminotransferase
<b>BA</b>	Basilar artery
<b>Balbc</b>	Balbc AnNRj
<b>BBB</b>	Blood-brain barrier
<b>BCA</b>	Bicinchoninic acid
<b>BDNF</b>	Brain-derived neurotrophic factor
<b>bFGF</b>	Basic fibroblast growth factor
<b>BM</b>	Bone marrow
<b>BrdU</b>	5-Bromo-2'-deoxyuridine
<b>BSA</b>	Bovine serum albumin
<b>C57</b>	C57BL/6JRj
<b>Ca<sup>2+</sup></b>	Calcium
<b>CAC</b>	Circulating angiogenic cell
<b>CADASIL</b>	Cerebral autosomal dominant arteriopathy with subcortical infarcts and leukoencephalopathy
<b>CARPA</b>	Complement activation related pseudo-allergy
<b>CBF</b>	Cerebral blood flow
<b>CCA</b>	Common carotid artery
<b>CCK-8</b>	Cell counting kit 8
<b>cCM</b>	Concentrated CM
<b>CD</b>	Cluster of differentiation
<b>cEBM</b>	Concentrated EBM
<b>CK</b>	Creatine kinase
<b>CM</b>	Conditioned medium
<b>CNS</b>	Central nervous system
<b>CT</b>	Computed tomography
<b>CXCL</b>	C-X-C motif chemokine ligand
<b>CXCR</b>	C-X-C motif chemokine receptor



<b>Cy</b>	Cyanine
<b>DAMP</b>	Damage-associated molecular pattern
<b>DCX</b>	Doublecortin
<b>DG</b>	Dentate gyrus
<b>DMEM</b>	Dulbecco's Modified Eagle's Medium
<b>DMSO</b>	Dimethyl sulfoxide
<b>DNA</b>	Deoxyribonucleic acid
<b>DPBS</b>	Dulbecco's PBS
<b>EBM</b>	Endothelial basal medium
<b>EC</b>	Endothelial cell
<b>ECA</b>	External carotid artery
<b>EGM-2</b>	Endothelial cell growth medium 2
<b>ELISA</b>	Enzyme-linked immunosorbent assay
<b>eNOS</b>	Endothelial nitric oxide synthase
<b>EPC</b>	Endothelial progenitor cell
<b>EPO</b>	Erythropoietin
<b>ET-1</b>	Endothelin-1
<b>ETL</b>	Echo train length
<b>F1</b>	Fake 1
<b>F2</b>	Fake 2
<b>FA</b>	Flip angle
<b>FAST</b>	Face, arms, speech, time
<b>FBS</b>	Fetal bovine serum
<b>f-CM</b>	Free CM
<b>FDA</b>	U.S. Food and Drug Administration
<b>FeNdB</b>	Iron-neodymium-boron
<b>FITC</b>	Fluorescein isothiocyanate
<b>FJC</b>	Fluoro-Jade C
<b>FMI</b>	Fluorescent molecular imaging
<b>FOV</b>	Field of view
<b>GCL</b>	Granular cell layer
<b>G-CSF</b>	Granulocyte colony-stimulating factor
<b>GDNF</b>	Glial cell-derived neurotrophic factor
<b>GFAP</b>	Glial fibrillary acidic protein
<b>GM-CSF</b>	Granulocyte-macrophage colony-stimulating factor
<b>HCl</b>	Hydrochloric acid
<b>hEGF</b>	Human endothelial growth factor
<b>hEPC</b>	Human EPC
<b>HGF</b>	Hepatocyte growth factor

<b>HI</b>	Haemorrhage infarction
<b>HR-T2WI</b>	High-resolution T2-weighted image
<b>i.a.</b>	Intraarterial
<b>i.v.</b>	Intravenous
<b>ICA</b>	Internal carotid artery
<b>IFN<math>\gamma</math></b>	Interferon-gamma
<b>IGF-1</b>	Insulin-like growth factor-1
<b>iNOS</b>	Inducible nitric oxide synthase
<b>KC</b>	Keratinocyte-derived chemokine
<b>LACI</b>	Lacunar infarcts
<b>LV</b>	Lateral ventricle
<b>LVO</b>	Large vessel occlusion
<b>M1</b>	Magnet 1
<b>M2</b>	Magnet 2
<b>MCA</b>	Middle cerebral artery
<b>MCAO</b>	Middle cerebral artery occlusion
<b>MCP-1</b>	Monocyte chemoattractant protein 1
<b>MIP-2</b>	Macrophage inflammatory protein 2
<b>miRNA</b>	Micro RNA
<b>MMP</b>	Matrix metalloproteinase
<b>MNC</b>	Mononuclear cell
<b>MRI</b>	Magnetic resonance imaging
<b>mRS</b>	Modified Rankin scale
<b>MT</b>	Mechanical thrombectomy
<b>MTT</b>	3-(4-5-dimethylthiazol-2-yl)-2,5- diphenyl tetrazolium bromide
<b>Na<sup>2+</sup></b>	Sodium
<b>NC</b>	Nanocapsule
<b>NC-CM</b>	cCM-loaded NCs
<b>NC-EBM</b>	cEBM-loaded NCs
<b>NC-W</b>	H <sub>2</sub> O-loaded NCs
<b>NIHSS</b>	National Institute of Health Stroke Scale
<b>NMDA</b>	N-methyl-D-aspartate
<b>NSC</b>	Neural stem cells
<b>OB</b>	Olfactory bulb
<b>OCSP</b>	Oxfordshire Community Stroke Project
<b>OCT</b>	Optimal cutting temperature
<b>OEC</b>	Outgrowth endothelial cell
<b>OPC</b>	Oligodendrocyte precursor cell
<b>PACI</b>	Partial anterior circulation infarcts

<b>PBS</b>	Phosphate buffered saline
<b>PBS-T</b>	PBS-1% Tween20
<b>PCA</b>	Posterior cerebral artery
<b>PCoA</b>	Posterior communicating artery
<b>PDGF</b>	Platelet-derived growth factor
<b>PECAM-1</b>	Platelet endothelial cell adhesion molecule
<b>PH</b>	Parenchymal haematoma
<b>PI3K</b>	Phosphatidylinositol-3kinase
<b>PLGA</b>	Poly(lactic-co-glycolic acid)
<b>PMSF</b>	Phenylmethanesulfonyl fluoride
<b>POCI</b>	Posterior circulation infarcts
<b>PSD95</b>	Postsynaptic density protein 95
<b>PTX-3</b>	Pentraxin 3
<b>RMS</b>	Rostral migratory stream
<b>RNA</b>	Ribonucleic acid
<b>ROI</b>	Region of interest
<b>ROS</b>	Reactive oxygen species
<b>ROSIER</b>	Recognition of stroke in the emergency room
<b>RT</b>	Room temperature
<b>SDF-1</b>	Stromal cell-derived factor 1
<b>SGZ</b>	Subgranular zone
<b>SHH</b>	Sonic Hedgehog
<b>SPION</b>	Superparamagnetic iron oxide nanoparticle
<b>STAIR</b>	Stroke Therapy Academic Industry Roundtable
<b>SVZ</b>	Subventricular zone
<b>T2*WI</b>	T2*-weighted image
<b>T2WI</b>	T2-weighted image
<b>TACI</b>	Total anterior circulation infarcts
<b>TBS-T</b>	Tris-buffered saline-0.1% Tween20
<b>TE</b>	Echo time
<b>TEeff</b>	Effective echo time
<b>TGF-<math>\beta</math></b>	Transforming growth factor- $\beta$
<b>TJ</b>	Tight junction
<b>TNF<math>\alpha</math></b>	Tumour necrosis factor $\alpha$
<b>TNK</b>	Tenecteplase
<b>TOAST</b>	Trial of Org 10172 in Acute Stroke Treatment
<b>tPA</b>	Tissue plasminogen activator
<b>TR</b>	Repetition time
<b>TRE</b>	Total radiant efficiency

<b>TTC</b>	2,3,5-Triphenyltetrazolium chloride
<b>UEA-1</b>	Ulex Europaeus Agglutinin I
<b>uPA</b>	Urokinase-type plasminogen activator
<b>VA</b>	Vertebral artery
<b>VE-Cadherin</b>	Vascular endothelial cadherin
<b>VEGF</b>	Vascular endothelial growth factor
<b>VEGFR2</b>	VEGF receptor 2
<b>vWF</b>	Von willebrand factor
<b>WHO</b>	World Health Organisation
<b>ZO-1</b>	Zonula occludens 1



# INTRODUCTION

---



## 1.1. Stroke

### 1.1.1. Definition, global burden and risk factors

The term ‘stroke’ covers a broad spectrum of cerebrovascular pathological conditions characterised by a disrupted blood flow and consequent infarction or haemorrhage in the central nervous system (CNS), attributable to a vascular obstruction (**ischaemic stroke**) or a non-traumatic focal bleeding (**haemorrhagic stroke**) in the brain parenchyma or ventricular system (intracerebral haemorrhage) or in the subarachnoid space (subarachnoid haemorrhage).<sup>1-3</sup>

Stroke is at present the second leading cause of death and disability worldwide, with over 13 million incident cases and 5.5 million deaths per year.<sup>4</sup> Amongst the European countries members of the World Health Organisation (WHO), stroke is responsible for more than 1 million annual deaths, a 15% of which are premature, before the age of 65 years.<sup>5</sup> Haemorrhagic stroke presents a higher mortality rate, but ischaemic stroke is the most common type, accounting for more than 80% of all strokes.<sup>2,6</sup>

Stroke is a heterogeneous and multifactorial disease with a large variety of additive risk factors and aetiologies, the majority of which are also common for haemorrhagic stroke<sup>6</sup>. The most important **modifiable risk factors** are hypertension, smoking, diet, physical inactivity, hyperlipidaemia, diabetes mellitus, alcohol consumption, and cardiovascular causes. Major **non-modifiable risk factors** include age, sex, race/ethnicity, and genetics, although the latter is increasingly considered as a potentially modifiable risk factor. The sex-related risk depends on age; however, overall women suffer more strokes due to a longer life span. Monogenic disorders accounting for approximately 1-5% of all strokes include conditions such as CADASIL (cerebral autosomal dominant arteriopathy with subcortical infarcts and leukoencephalopathy), sickle cell or Fabry diseases, mitochondrial encephalomyopathy, lactic acidosis, and stroke-like episodes), hereditary cerebral



amyloid angiopathy, or Marfan syndrome. Finally, genetic variants can contribute directly or indirectly to the risk of stroke through other stroke risk factors.<sup>6,7</sup>

This doctoral thesis has been focused on the study of ischaemic stroke, so in the interest of brevity, the term ‘stroke’ will be preferably used from now on.

### 1.1.2. Classification and diagnosis

Beyond the former classification, ischaemic stroke can be subdivided according to the aetiology and vascular distribution (**Table 3**). Stroke **aetiology** is considered to affect prognosis, outcome, and management, and is therefore crucial in acute stroke diagnosis. The Trial of Org 10172 in Acute Stroke Treatment (TOAST) is a system developed to categorise stroke into 5 subtypes based on clinical features and brain, cardiac and extra-cranial arteries imaging, angiography, and laboratory assessments<sup>8,9</sup>. Classification according to the **vascular distribution** is based on the Oxfordshire Community Stroke Project (OCSP) criteria, which divide ischaemic stroke in 4 categories and can be used to predict clinical outcomes<sup>10</sup>.

**Table 3. Ischaemic stroke classification.**

According to the aetiology (TOAST criteria)	
<b>Large-artery atherosclerosis</b>	Large vessel disease (atherosclerosis of cervical/proximal intracranial vessels). 30-43% of cases. >50% stenosis or occlusion of a major brain/cortical artery. Infarcts >15 mm (cortex, cerebellum, brainstem, subcortical regions).
<b>Cardioembolism</b>	Arterial occlusions from cardioembolic sources. 20-31% of cases. Magnetic resonance imaging (MRI): restricted diffusion in multiple and often bilateral vascular territories.
<b>Small-vessel occlusion (lacunar infarcts)</b>	Infarcts of <20 mm, without evidence of other disorders (vascular disease, vasospasm, or cardioembolism). 10-23% of the cases.
<b>Stroke of other determined aetiology</b>	Rare causes: non-atherosclerotic vasculopathies, hypercoagulable states, hematologic disorders, right-to-left vascular shunts, or arterial dissections.
<b>Stroke of undetermined aetiology (cryptogenic)</b>	Multiple causes or no causes found.
Based on the vascular distribution (OCSP classification)	
<b>Lacunar infarcts (LACI)</b>	
<b>Total anterior circulation infarcts (TACI)</b>	
<b>Partial anterior circulation infarcts (PACI)</b>	
<b>Posterior circulation infarcts (POCI)</b>	

Furthermore, according to the presence or absence of acute neurological dysfunction, cerebral infarcts can be classified as **strokes** or **silent cerebral infarcts**, respectively. Awakening with or acute onset of focal neurologic symptoms (limb or facial weakness and/or hemiparesis, limb paraesthesia, dysphasia, headache, and eye movement or visual deficits) is the hallmark of stroke diagnosis.<sup>2</sup> On the other hand, **transient ischaemic attacks (TIAs)** are characterised by an episode of sudden focal neurological dysfunction caused by focal brain ischaemia, but are distinguished from ischaemic stroke by the absence of brain infarction and symptoms duration of less than 24 hours. In this regard, evidence of acute infarction can be determined either from a symptom duration for more than 24 hours or brain imaging.<sup>11</sup>

**Neuroimaging** is crucial to distinguish between ischaemic and haemorrhagic strokes, since the latter is also characterised by acute onset of focal symptoms.<sup>12</sup> Apart from guiding the diagnosis of acute stroke, neuroimaging can also provide information on the aetiology.<sup>9</sup> The current American Stroke Association/American Heart Association (ASA/AHA) guidelines recommend emergency brain evaluation for all patients with suspected acute stroke on first arrival to a hospital before initiating any specific therapy, including non-contrast computed tomography (CT) and MRI.<sup>13</sup> The latter is also crucial to exclude **stroke mimics**, which are conditions that lead to an acute onset of neurological deficits that can be confused with the common symptoms of stroke and therefore represent a significant proportion of hospital stroke admissions.<sup>14</sup>

An important aspect to consider in acute stroke management is time upon neurological symptoms onset, given the medical emergency and as it may determine the treatment eligibility criteria. Several public awareness campaigns have used mnemonics to help identifying key stroke signs to reduce the time from onset to treatment, such as the acronym **FAST** (Face, Arms, Speech, and Time) implemented by the British Department of Health.<sup>15</sup> Efforts have also been put in hastening intervention upon symptoms onset in primary care. The ‘Recognition of stroke in the emergency room’ (**ROSIER**) is a stroke recognition scale designed for its use by

physicians in emergency departments. It is more complete than the FAST tool, including the distinction from stroke mimics.<sup>16</sup>

Finally, the most commonly used scales to assess the motor and neurological deficits are the National Institute of Health Stroke Scale (**NIHSS**) for early stroke severity, and the **modified Rankin Scale (mRS)** which is commonly applied to evaluate stroke functional recovery.<sup>17,18</sup>

### 1.2. Stroke pathophysiology

Upon stroke onset, a complex and time-dependent cascade of events is triggered, which can be broadly divided into the following stages: (i) acute, (ii) subacute, and (iii) chronic (**Figure 2**).

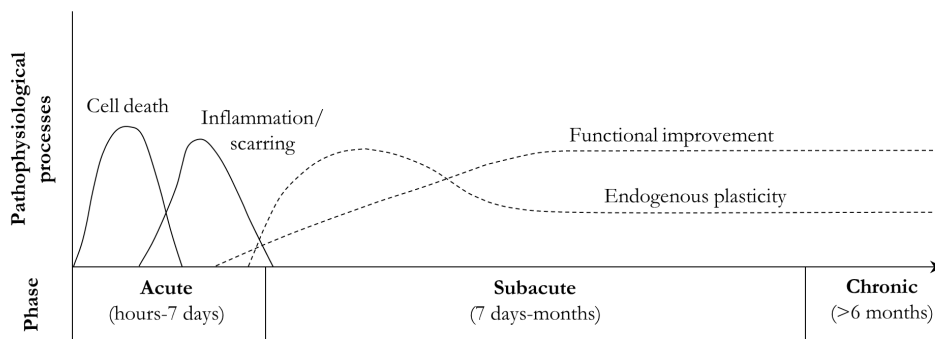


**Figure 2. Chronology of the different pathophysiological phases of stroke.** Figure adapted from Dobkin et al. (2016).<sup>19</sup>

Acute events that may be detrimental for the infarct progression are however essential to promote neurorestorative processes in delayed stages. In this sense, the timely regulation of these pathophysiological mechanisms is crucial for the final outcome. The following sections will focus on the major pathophysiological events occurring within the acute and subacute phases, which lie within the scope of this thesis.

### 1.2.1. Acute phase

Vessel occlusion causes a depletion of oxygen and glucose supply to the brain, inducing an **ischaemic cascade** of events that lead to massive cell death through necrotic, apoptotic and autophagy mechanisms (**Figure 3**). Depending on the extent and duration of hypoperfusion, the tissue that is supplied by the occluded vessel is differentiated in an area of irreversible damage (**infarct core**), a surrounding area of hypoperfused but salvageable tissue (**penumbra**), and hypoperfused tissue but not threatened under normal circumstances (**oligaemia**).<sup>20,21</sup>

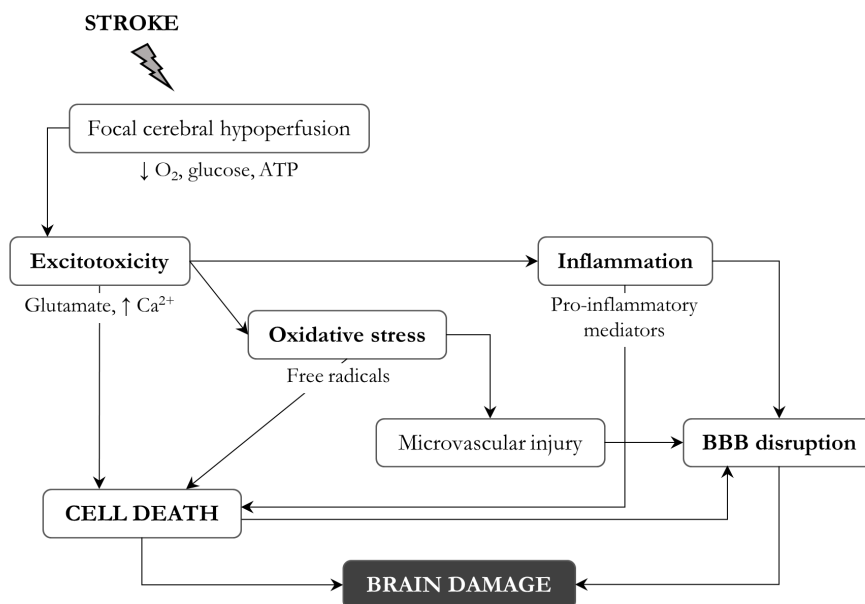


**Figure 3. The ischaemic cascade.** Figure adapted from Lakhan et al. (2009).<sup>22</sup>

The earliest events leading to cell death upon stroke are **oxidative stress** and **excitotoxicity**. The interruption of nutrients' supply to the brain impairs energy-dependent ion transport pumps and re-uptake of excitatory amino acids, namely glutamate, which prompts calcium ( $\text{Ca}^{2+}$ ) influx through the activation of N-methyl-D-aspartate (NMDA) receptors. The resulting intracellular  $\text{Ca}^{2+}$  accumulation triggers the digestion of proteins, lipids and nucleic acids, and disrupts the

mitochondrial function causing more energy depletion, activation of caspase-dependent cell death pathways and production of reactive oxygen species (ROS) that in its turn amplify the ischaemic cascade. Intracellular  $\text{Ca}^{2+}$  accumulation is also accompanied by sodium ( $\text{Na}^{2+}$ ) and chloride influx, causing cytotoxic oedema, while energy depletion is further worsened by neuronal and glial membrane depolarisations, altogether expanding the infarct core.<sup>20,21,23,24</sup>

The production of ROS leads to the release of pro-inflammatory cytokines and chemokines and the expression of leukocyte adhesion molecules in endothelial cells (ECs), mediating the attraction and infiltration of leukocytes into the brain parenchyma. Additionally, complement system activation further contributes to adhesion molecule upregulation, chemotaxis and leukocyte activation. These infiltrating leukocytes facilitate the clearance of debris in the infarcted area, but also release cytotoxic mediators that exacerbate the **inflammatory cascade**, worsening the brain damage. In parallel, dying cells release damage-associated molecular patterns (DAMPs), which induce the activation of microglia and further release of pro-inflammatory cytokines that amplify the inflammatory response.<sup>22,25</sup> Together with inflammation and the microvascular injury caused by oxidative stress, the elevation of matrix metalloproteinases (MMPs), which degrade components of the extracellular matrix, contribute to **blood-brain barrier (BBB) leakage** and thus increased infiltration of immune cells.<sup>26,27</sup>

In contrast to the neuro-inflammatory burst following stroke, the release of pro-inflammatory mediators to the circulation leads to a systemic inflammation that is later counteracted by the so-called **stroke induced immunosuppression**, which increases the risk of systemic infections that worsen the overall functional recovery.<sup>28</sup>

Importantly, in addition to the high complexity of this wave of interrelated events, many of these mechanisms are known to have **controversial functional roles** after stroke, in the sense that a harmful contribution to infarct expansion may be counterbalanced by the participation in delayed repair processes.

For instance, the immune system is known to play a dual role by resolving the post-ischaemic inflammation and contributing to delayed neuroregeneration processes, aside from the aforementioned lesion-amplifying effects. For example, in the late acute phase, the infiltrating pro-inflammatory macrophages (M1 macrophages) shift to anti-inflammatory (M2 macrophages), the latter contributing to the clearance of necrotic debris and releasing trophic factors that facilitate angiogenesis and axonal outgrowth in the subacute and chronic phases.<sup>29,30</sup> Another example for mechanisms acting as a double-edged sword are MMPs, such as MMP-2 or MMP-9, which aside from causing a deleterious disruption of the BBB, are also key mediators in delayed remodelling.<sup>31</sup> Moreover, peri-infarct astrocytes undergo morphological changes and upregulation of the glial fibrillary acidic protein (GFAP), a process known as **reactive astrogliosis**, forming a glial scar that separates the ischaemic core from the surrounding healthy tissue. This mechanism also has a controversial role, as on one hand, reactive astrocytes may limit axonal regeneration through different inhibitory factors, but may also prevent infarct expansion and participate in subacute repair by isolating the injured site from the viable tissue and producing or recycling neurotrophic factors, respectively.<sup>32</sup>

### 1.2.2. Subacute phase

In addition to the abovementioned mechanisms leading to cell death and brain damage, **endogenous repair processes** also take place in response to stroke, most especially during the subacute phase.

This is reflected in some degree of spontaneous recovery in the weeks to months following stroke in human patients, although this **recovery** is often insufficient and largely variable.<sup>33,34</sup> On the other hand, it must be noted that this functional improvement may also arise from compensation mechanisms, which are alternative strategies to overcome a dysfunction and resume daily tasks independently, such as the use of the unaffected limb.<sup>35</sup>

In the recent past decades, relevant scientific breakthroughs such as the discovery of post-natal vasculogenesis<sup>36,37</sup> and neurogenesis<sup>38–40</sup> have brought about great paradigm shifts that contributed to a better understanding of the underlying mechanisms for stroke recovery and leveraged the emergence of therapeutic strategies aiming at the enhancement of endogenous neurorepair processes.

These processes, occurring both in the infarct surrounding and remote areas<sup>41</sup>, are strongly interrelated and include neuronal plasticity, neurogenesis, angiogenesis, oligodendrogenesis and white matter remodelling, amongst others, altogether providing an optimal environment that facilitates brain tissue repair.<sup>42</sup>

### 1.2.2.1. Neurogenesis

Neural stem cells (NSCs) originate from two main neurogenic niches, the **subventricular zone (SVZ)** in the lateral ventricles (LV), and the **subgranular zone (SGZ)** in the dentate gyrus (DG) of the hippocampus. In the healthy brain, NSCs from the SVZ migrate through the rostral migratory stream (RMS) into the olfactory bulbs (OBs), where they mature to interneurons that contribute to olfactory functions, while NSCs originating in the SGZ migrate and differentiate into the granular cell layer (GCL) of the DG, contributing to spatial memory (**Figure 4**).<sup>43,44</sup>

After cerebral ischaemia, NSCs are activated by diverse stimuli that enhance endogenous neurogenesis and alter the migration pattern of neuroblasts towards the injured site to replace the damaged neural cells, including neurons, ependymal cells, astrocytes, and oligodendrocytes.<sup>24</sup> This ectopic migration is mediated through NSCs chemokine receptors that respond to chemokines released in the injured tissue, such as the stromal cell-derived factor 1 (SDF-1)/C-X-C motif chemokine receptor 4 (CXCR4) pathway.<sup>45</sup>

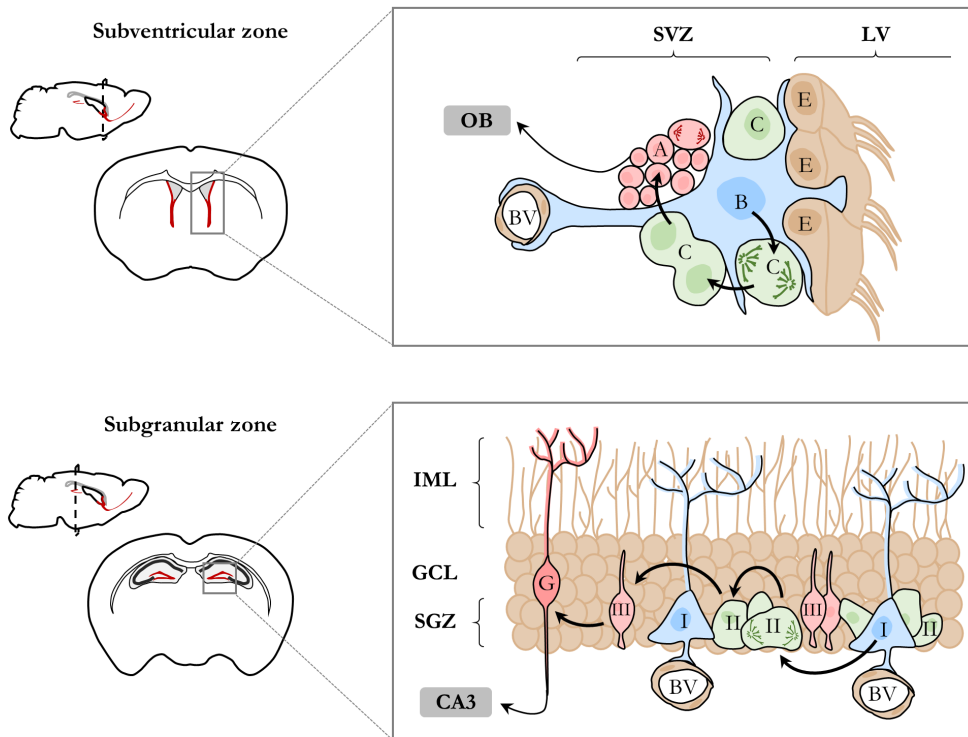


**Figure 4. Neurogenic niches in the adult mouse brain.** In the SVZ, quiescent neural stem cells (type B) become activated and give rise to amplifying cells (Type C). Type C cells generate neuroblasts (Type A), which migrate to the OB along the RMS, where they become mature interneurons. In the SGZ, activated NSCs in the inner molecular layer (IML) (Type I) generate amplifying neural precursor cells (Type II). Type II cells become neuron-committed intermediate progenitors (Type III), and differentiate to granule cells (G) in the GCL, with dendritic arborisation in the IML and axonal projection to CA3. BV = blood vessels; E = ependymal cells. Figure adapted from Fontán-Lozano et al. (2020) and Lim et al. (2016).<sup>46,47</sup>

However, the number and regenerating capacity of these cells is insufficient, and this potential can be further impaired with age or under certain pathological conditions.<sup>24</sup> Depending on the severity and the location of stroke, the ischaemic insult can alter the viability or the cell fate of NSCs. For instance, hypoxia triggers a switch from neurogenesis to astrogliosis through enhanced Notch signalling.<sup>48</sup> Moreover,



although the beneficial neurogenic response seems clearer in the SVZ, hippocampal neurogenesis has been suggested to potentially exert a detrimental role in post-stroke recovery due to maladaptive responses.<sup>49,50</sup>

In this light, a range of mechanisms have been explored in the attempt to protect the NSCs and potentiate neurogenesis, by targeting relevant pathways such as the phosphatidylinositol-3kinase (PI3K), Wnt/ $\beta$ -catenin, Sonic Hedgehog (SHH), and Notch signalling.<sup>24</sup>

### 1.2.2.2. Oligodendrogenesis and white matter remodelling

The neurogenic niche in the SVZ also gives rise to oligodendrocyte precursor cells (OPCs) which, after brain ischaemia involving the white matter, proliferate and migrate to the peri-infarct area in order to become myelinating oligodendrocytes.<sup>51</sup> The formation and maintenance of myelin sheaths by mature oligodendrocytes is essential to isolate neuronal axons, provide metabolic support and facilitate rapid transmission of axon potentials.<sup>52</sup> Other than the obvious beneficial role of oligodendrogenesis for neuroregeneration, neuronal activity also regulates OPCs proliferation and differentiation through excitatory and inhibitory inputs.<sup>32</sup> On the other hand, OPCs seem to be neuroprotective through the release of insulin-like growth factor-1 (IGF-1).<sup>53</sup> A reciprocal crosstalk between both elements is therefore essential for brain repair. Nonetheless, mature oligodendrocytes also impede neural regeneration through neurite outgrowth inhibition mediated by myelin associated inhibitors such as Nogo A.<sup>54</sup> This highlights the importance of molecular and cellular timely modulation during stroke recovery.

### 1.2.2.3. Angiogenesis

New blood vessels can be formed by three mechanisms: (i) vasculogenesis, which occurs during and after embryogenesis by the differentiation of angioblasts and endothelial progenitor cells (EPCs), respectively, (ii) angiogenesis, resulting from the sprouting of new vessels from pre-existing capillaries, and longitudinal extension of

pre-existing vessels (intussusception), and (iii) arteriogenesis, in which vessels become covered by pericytes and vascular smooth muscle cells to form arteries.<sup>55</sup>

Angiogenesis is a key feature for post-stroke recovery and neuronal reorganisation, and has been related to improved survival and functional outcome in both patients and animal models.<sup>56,57</sup> Early after stroke, new blood vessels are formed in the peri-infarct regions. This process involves the coordinated remodelling of the extracellular matrix, extension of ECs behind tip cells and participation of pericytes, under the coordinated effect of growth factors and cytokines. Amongst the main angiogenic factors are the transforming growth factor- $\beta$  (TGF- $\beta$ ), platelet-derived growth factor (PDGF), vascular endothelial growth factor (VEGF) and basic fibroblast growth factor (bFGF). Amongst them, VEGF is the most potent hypoxia-inducible angiogenic factor.<sup>58,59</sup>

Although the formation of new blood vessels seems clearly beneficial for stroke recovery, it is important to consider the risk associated to vascular remodelling in terms of BBB disruption, oedema and haemorrhagic transformation, and the fact that neovascularisation may also lead to immature non-functional vessel formation.<sup>60</sup>

As earlier pointed out, the repair processes taking place in the subacute phase after stroke are strongly interrelated and should be therefore understood as a whole. The **neurovascular unit** is a relatively recent concept in neuroscience that accounts for the relationship between ECs, pericytes, neurons, astrocytes, microglia, and the extracellular matrix. All of these components gather together as an anatomical and functional whole to maintain the BBB integrity, and regulate cerebral homeostasis.<sup>61</sup>

In this regard, there is a close interplay between angiogenesis and the abovementioned processes of neurogenesis and oligodendrogenesis. ECs are known to play a key role in the SVZ and SGZ neurogenic niches through the release of growth factors that maintain their neurogenic potential, while the migration of neuroblasts and OPCs towards to the ischaemic injury occur in chains along vascular tracks.<sup>32,62,63</sup> Moreover, neurogenesis and angiogenesis are casually linked through the

so-called neurovascular niche, and several angiogenic factors such as VEGF have shown neuroprotective and axonal growth boosting effects.<sup>30,57,64</sup>

### 1.2.2.4. Brain plasticity

Brain plasticity and reorganisation are induced during the subacute phase after stroke, in both the peri-infarct and remotely-connected regions. The mechanisms behind brain remodelling include dendritic spine turnover, altered neuronal excitability, and formation of functional neuronal connections. These events are driven by changes in gene expression and cellular responses, which lead to axonal sprouting, synapse formation, changes in synaptic strength and contralateral compensation.<sup>65</sup> The time-course of these events takes places within different overlapping phases, including inflammation and injury resolution, diaschisis by deafferentiation and secondary remote lesions, tissue repair, and compensation processes (**Figure 5**).

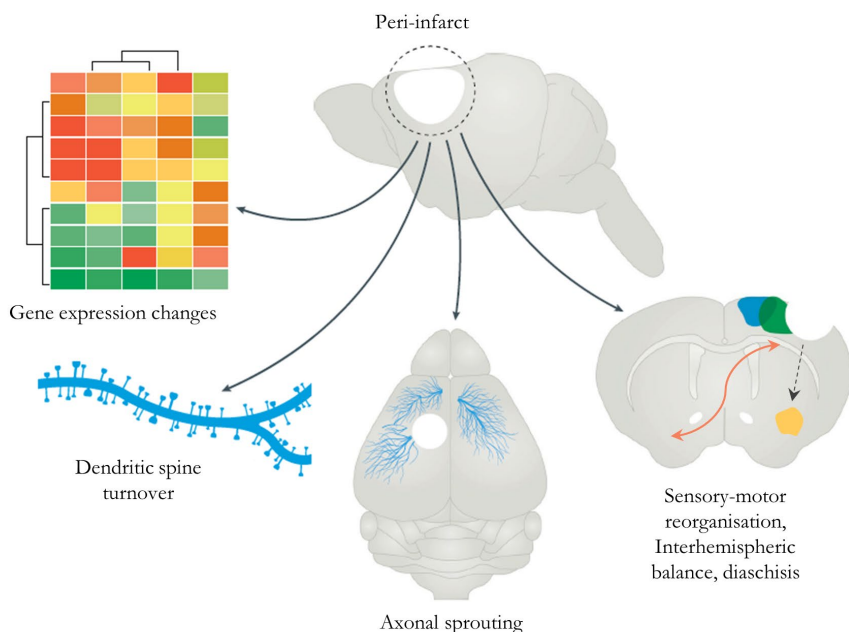


**Figure 5. Endogenous plasticity in subacute stroke.** Figure adapted from Joy et al. 2021.<sup>65</sup>

Such processes are tightly related to functional improvement and successful rehabilitation in stroke patients. Hence, multiple restorative strategies have been focused on the stimulation of post-stroke brain plasticity. However, the window of plasticity is limited and these processes diminish as stroke progresses from the subacute to the chronic phase, when there is little recovery potential. Besides, atypical reorganization and recovery patterns may also occur due to a maladaptive plasticity, which limits recovery after stroke. It is therefore important to tackle these aspects in order to selectively and efficiently boost these mechanisms.<sup>66,67</sup>

### 1.3. Current stroke treatments

#### 1.3.1. Recanalisation therapies

Nowadays, **brain tissue reperfusion** through thrombolysis with tissue plasminogen activator (tPA) and mechanical thrombectomy (MT) for large vessel occlusions (LVO) are the standard of care for acute ischaemic stroke.<sup>13</sup> Furthermore, in the recent years tenecteplase (TNK) has also emerged as an alternative to tPA for LVO strokes, in which tPA is less effective.<sup>68</sup>

Given the narrow time-window (4.5 h upon stroke onset), risk of haemorrhagic transformation and insufficient performance of tPA in LVO strokes, endovascular thrombectomy has been in the spotlight of acute stroke management over the past years.<sup>69</sup> The use of MT started more than 10 years ago<sup>70</sup> as an improved revascularisation strategy against intraarterial (i.a.) plasminogen activators<sup>71,72</sup> and has been refined with the mechanical clot removal. MT is now increasingly used throughout developed countries, with substantially improved devices showing successful recanalisation rates within the first 6 hours after symptoms onset.<sup>73–77</sup> Furthermore, the ASA/AHA guidelines have extended this time window up to 24 h in patients that meet specific eligibility criteria as demonstrated in the DAWN or DEFUSE clinical trials.<sup>13,78,79</sup>

Stroke is a medical emergency where the benefit of these recanalisation therapies is strongly time-dependent. It is estimated that the average infarct progression upon LVO is around the loss of 2 million neurons per minute.<sup>80</sup> Therefore, early diagnosis and treatment initiation are key factors influencing the final outcome. In this regard, **acute stroke care organisation** from pre-hospital care to tertiary stroke centres has greatly improved over the past years with the use of telemedicine, mobile stroke units and the implementation of protocols that optimise the workflow and minimise treatment delay.<sup>81</sup>

### 1.3.2. Rehabilitation therapies

Despite the tremendous advances in acute stroke management, only 25% of all cases are eligible for thrombolysis, while 10-12% are suitable for endovascular treatment.<sup>81</sup> Furthermore, of those patients that are successfully treated, many remain disabled, and the only approved therapy beyond the acute phase is **neurorehabilitation**.<sup>82</sup>

Neurorehabilitative training strategies include task specific or unspecific paradigms such as physical exercise or rehabilitative physiotherapy, the latter being the therapeutic standard. These can be supplemented with upcoming therapeutic strategies such as **brain-computer interfaces** or **artificial intelligence**.<sup>83</sup>

It has been suggested that intensive, high dose or prolonged rehabilitation may enhance the therapeutic benefit.<sup>83,84</sup> However, recovery after stroke is a complex, dynamic, and multifactorial process that is influenced by the interplay amongst genetic, sociodemographic and clinical factors, which highlights the importance of a better understanding and standardisation of post-stroke recovery treatments.<sup>85</sup> In this sense, large-scale and rigorous clinical trials in the field of stroke rehabilitation are scarce and have been introduced only recently and, therefore, there is still a lack of consensus amongst rehabilitative therapies and thorough understanding of the underlying mechanisms for stroke recovery.<sup>82,85</sup>

## 1.4. Pre-clinical stroke models

It is noteworthy that in the particular field of ischaemic stroke, the therapeutic progress in acute recanalisation resulted from clinical trials rather than from animal studies. However, this advance was fuelled by the previous implementation of recanalisation therapies in myocardial infarction and, importantly, despite the enormous advances in acute management, stroke remains a major cause of death and long-term disability worldwide. Plus, this impact is estimated to rise in the near future due to the increasing life-expectancy.<sup>86</sup> Furthermore, we are struggling to address the unmet needs of functional recovery beyond the acute stage, when the only approved therapy is neurorehabilitation, and pharmacological development is hampered by the great complexity of this disease.

Against this backdrop, animal stroke models are intended to mimic the heterogeneous nature of clinical stroke with a high reproducibility and standardisation, adding the possibility of directly analysing the tissue of interest to provide insight into the pathological and therapeutic response mechanisms, and are therefore essential for pre-clinical stroke research.<sup>87</sup> A major drawback of animal stroke models has been the poor translation from pre-clinical studies into successful clinical trials. For this reason, the Stroke Therapy Academic Industry Roundtable Roundtable (STAIR) established in 1999 a series of guidelines for pre-clinical stroke models, which were thereafter updated in order to facilitate the translation of neuroprotective and neurorestorative drugs to human studies.<sup>88</sup> In the same vein, the ARRIVE guidelines (Animal Research: Reporting of *In vivo* Experiments) were developed in 2010 to improve the reporting of animal research, and have also been updated afterwards to improve the reporting of research involving animals.<sup>89</sup>

At present, there are different approaches to model stroke, by experimentally inducing stroke in either healthy young animals or in aged animals presenting relevant comorbidities, as well as using models that exhibit spontaneous stroke development. Ideally, a successful translation from bench to bedside requires animal models that accurately reflect the clinical situation, therefore selecting an appropriate animal

model is crucial. However, clinical stroke is extremely diverse, and for this reason pre-clinical studies should be carried out in different animal models before jumping to the clinical scenario.<sup>90</sup> A large variety of animal species have been used, including mice, rats, rabbits, pigs, cats, dogs, and non-human primates. **Rodents** are currently the most widely used, given the advantages for ethical regulations, low cost, easy monitoring of physiological parameters and reproducible surgical manipulation. Specifically, mice and rats are the most used as these can be genetically modified, which facilitates the study of pathophysiological and drug molecular mechanisms. Anatomically, despite presenting a lysencephalic brain, in contrast to the human gyrencephalic brain, they also present a complete circle of Willis, as well as the anterior and posterior circulation territories, as in humans.<sup>91,92</sup>

Cerebral ischaemia models can be **permanent** or **transitory**, and can also be classified as **global**, when the blood flow is reduced in the whole brain, **focal**, when the blood flow obstruction is restricted to a specific brain region, or **multifocal**, characterised by a patchy cerebral blood flow obstruction. This section will focus on focal models, as this particular group lies within the scope of this thesis (**Table 4**).<sup>93</sup>

For focal cerebral ischaemia models, **middle cerebral artery (MCA) occlusion** is the most common approach, due to its accessibility and because it is one of the most frequently affected arteries in human ischaemic stroke.<sup>87</sup>

Table 4. Most commonly used models of focal ischaemic stroke.

	Procedure	Utility	Strengths	Weaknesses
<b>Transcranial</b>	MCA permanently/ transiently occluded across cranial window. Resembles M2 or peripheral occlusion in humans.	Post-acute neurorepair. Risk factors for stroke recovery. Permanent MCAO for neuroprotection in absence of reperfusion.	Low mortality. Low variability in lesion size.	Requires craniotomy. Sensorimotor deficits mild and largely variable with subtle MCA occlusion site variations.
<b>Intraluminal MCA occlusion</b>	MCA offsprings permanently/transiently occluded by intraluminal silicon-coated nylon monofilament. Proximal LVO resembling M1 occlusion in humans	Neuroprotection. Risk factors for stroke recovery. Post-acute neurorepair. Adjunctive treatments alongside endovascular thrombectomy	Reproducible infarcts and penumbra. Sensorimotor and cognitive deficits. Prompt reperfusion as endovascular treatments.	Mortality. Unsuitable to study thrombolytics. Overestimation of neuroprotective drugs' efficacy due to extent of secondary injury. Prompt reperfusion vs. typical gradual reperfusion in humans.
<b>Cerebral photothrombosis</b>	Systemic delivery of photosensitive dye and transcranial illumination. Occlusion by highly platelet-rich thrombi.	Suitable to study underlying brain plasticity and remodelling mechanisms.	Predefined and circumscribed infarcts. Technically simple. Thrombi similar to those clinically observed.	No penumbra. Intracerebral haemorrhages. Mild sensorimotor deficits, and large spontaneous recovery.
<b>Cerebral (thrombo-) embolism</b>	MCA/branches occluded by synthetic macro- or microspheres, autologous blood clots (resembling M1 occlusion) or stereotactic thrombin injection (usually in M2).	Thrombolytic and neuroprotective drugs. Risk factors for stroke recovery	Clinically relevant stroke model. Penumbra.	Variable infarcts. High mortality (low mortality with thrombin injection). Laborious procedure. Possible clot breakage leading to multifocal ischaemic lesions. Possible off-target occlusions.
<b>Endothelin-1 (ET-1) model</b>	Stereotaxic injection of ET-1 into tissue adjacent to the MCA, resulting in significant, long-lasting vasoconstriction with gradual reperfusion	Studies targeting specific neuroanatomical areas.	Technically simple. Avoids damage to the facial muscles. Penumbra unclear.	High variability in lesion volume

Table adapted from Kumar et al. (2016),<sup>93</sup> Sommer et al. (2017),<sup>94</sup> and Hermann et al. (2019).<sup>91</sup>



### 1.5. Experimental therapeutic strategies for stroke

As earlier mentioned, the benefits of recanalisation treatments are incomplete. In this light, **alternative reperfusion strategies**, such as aptamer systems,<sup>95</sup> sonothrombolysis with magnetic microbubbles<sup>96</sup> and magnetically enhanced thrombolysis with iron nanoparticles,<sup>97</sup> are being studied to increase the safety and efficacy of thrombolysis.

Beyond recanalisation, **neuroprotection** has emerged as a promising strategy to limit infarct damage and/or peri-infarct expansion. A large effort has been put into this field over the past decades, but out of more than 1000 putative neuroprotective therapies, none have been approved in the clinical setting to date.<sup>81</sup> In this regard, the change of perspective from the neuron as a single-target to the neurovascular unit as a whole, together with the emerging strategy to tackle multiple mechanisms and the incorporation of guidelines for rigorous pre-clinical testing, are paving the way for the implementation of such treatments. Amongst the neuroprotective compounds that are being tested in clinical trials are the following: uric acid as an antioxidant (NCT00860366), nerinetide as an inhibitor of protein-protein interactions of the postsynaptic density protein 95 (PSD95) (NCT02930018, NCT04462536), otaplimastat to block the MMPs pathway (NCT01757795, NCT02787278, NCT04479449), cytoprotection through activated protein C and analogues (NCT02222714, NCT00533546), ApTOLL as a toll-like receptor 4 (TLR4) antagonist (NCT04742062, NCT04734548), and selective i.a. hypothermia (NCT05032781, NCT04554797) or Ca<sup>2+</sup> channel blockage with verapamil (NCT02235558, NCT03347786).<sup>98</sup>

Alongside to improving the success of recanalisation and protecting the penumbral tissue, there is a flagrant need to enhance post-stroke recovery. In this regard, different **neurorestorative strategies** are being studied to stimulate and amplify the endogenous restorative mechanisms by means of pharmacological or cell-based

approaches, together with strategies complementary to rehabilitation such as activity and cognitive-based training, robotics and brain-computer interface systems.<sup>34,42</sup>

The combination of pharmacological interventions with rehabilitation has been proposed as a promising restorative strategy, on the basis that treatments enhancing plasticity require physical and behavioural training to strengthen functionally relevant networks. This has been tested with drugs acting on neurotransmitters such as fluoxetine, amphetamine, or dopamine, although clinical trials have been largely negative.<sup>99</sup> Other promising multifaceted strategies with an impact on different regenerative mechanisms include, amongst others, the use of non-coding ribonucleic acids (RNAs)<sup>95</sup> and brain stimulation to modulate the excitability of a target area.<sup>84</sup>

Many studies have focused on the use of specific growth factors, such as brain-derived neurotrophic factor (BDNF), glial cell-derived neurotrophic factor (GDNF), IGF-1, bFGF, erythropoietin (EPO) or granulocyte colony-stimulating factor (G-CSF), involved in intrinsic regenerative processes, or compounds targeting relevant molecular pathways such as the blockage of Nogo A to promote axonal sprouting. However, there is a lack of a clear clinical benefit so far. Although some of the abovementioned factors are known to be both neurotrophic and pro-angiogenic, some experimental therapies promoting a specific regenerative process have turned out to be detrimental for other mechanisms.<sup>100,101</sup> As earlier pointed out, the pathophysiological mechanisms after stroke are orchestrated by the interplay between multiple cell types, thus neurorepair therapies should promote simultaneously neurogenesis, angiogenesis, myelinogenesis and neural plasticity.

Overall, novel therapeutic approaches for a disease of such complexity as stroke should tackle multiple mechanisms in each pathophysiological stage to enhance stroke recovery. Growing knowledge leads to a multimodal strategy combining refined protocols for a rapid acute stroke diagnosis and treatment allocation with selective and timely appropriate neuroprotective and neurorestorative treatments for the foreseeable future.

### 1.5.1. Cell-based therapies

In the past recent decades, cellular therapies have been in the spotlight of stroke research due to their potential multifaceted benefits for neuroprotection, neuroregeneration and immune system modulation.<sup>102,103</sup> Cell-based treatments can be broadly divided into **endogenous** strategies to stimulate existing cells, such as the growth factors mentioned above, or **exogenous** administration of stem or progenitor cells, expecting their differentiation into functional brain cells to replace the damaged tissue. It should be highlighted that the benefits of the latter may result from a combined mechanism, given that exogenous stem/progenitor cells contribute to restorative effects partly through a paracrine effect.<sup>84</sup>

Endogenous strategies present the advantage of avoiding the adverse effects of exogenous therapies such as immune rejection, but the existing stem cell niches are limited in number and may be affected with age and/or comorbidities, as well as by the ischaemic injury, as previously discussed. Moreover, although large cell numbers can be obtained through *ex vivo* expansion, exogenous cell administration has been hampered by difficulties in the engraftment and specific phenotype differentiation.

Additionally, a number of clinical trials have been conducted to assess the safety and efficacy of exogenous stem cell therapies using a variety of cell types from haematopoietic, mesenchymal and neural lineages, different doses, delivery routes and treatment time points after stroke (**Figure 6**). However, the outcomes are inconsistent and the underlying mechanisms remain largely unknown.<sup>104–106</sup> In this regard, induced pluripotent stem cells (iPSCs) therapies, which avoid immune rejection and controversial ethical issues, and represent an advantage against the limited potential of endogenous stem cell niches under certain conditions, have become an appealing cell replacement strategy for stroke. In the past recent years, the refinement of specific cell differentiation protocols, together with cutting-edge tools to corroborate the engraftment and functionality of the transplanted cells, are paving the way towards the clinical application of cell-based therapies for stroke.<sup>107</sup>

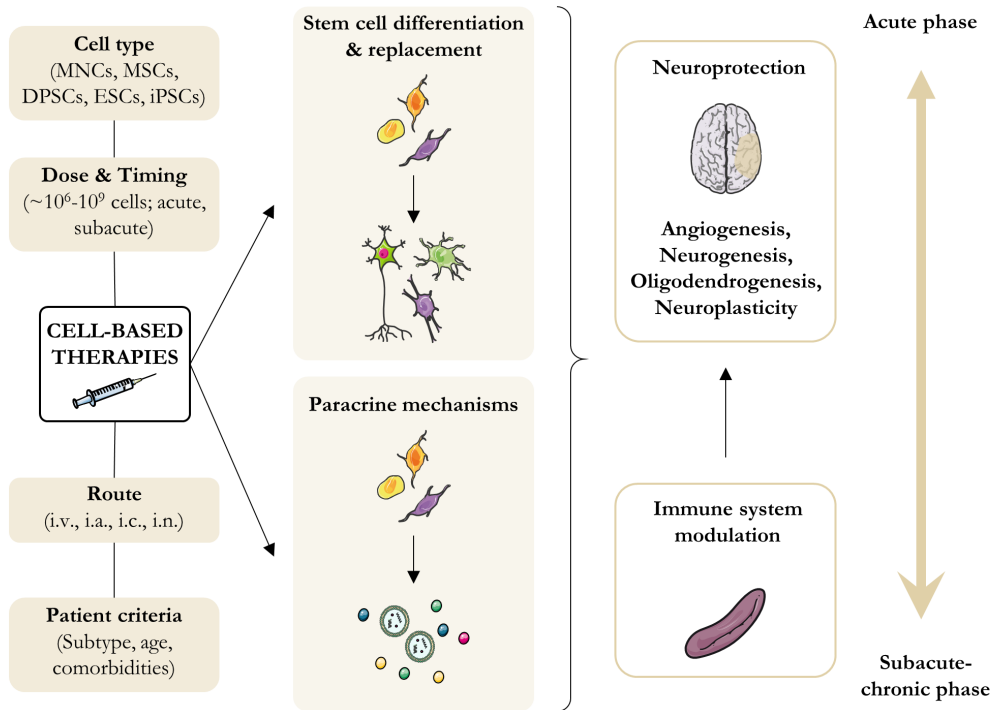


**Figure 6. Cell-based therapies for stroke.** Cellular therapies are a promising therapeutic approach for stroke due to their neuroprotective and neurorestorative effects, and immune system modulation. Despite their potential benefits, there are current unmet challenges such as the choice of the cell type, dose, and transplantation route, or the definition of eligible patients. MNCs: mononuclear cells, MSCs: mesenchymal stem cells, DPSCs: dental pulp stem cells; ESCs: embryonic stem cells; iPSCs: induced pluripotent stem cells; i.v.: intravenous; i.a.: intraarterial; i.c.: intracerebral; i.n.: intranasal.

It should also be highlighted that the beneficial effects of cell therapies are more likely to arise from a paracrine mechanism promoting survival or regeneration of pre-existing brain cells, rather than a direct incorporation to replace the damaged cells.<sup>108</sup> In this light, **cell-based but cell-free therapies** focused on the administration of stem cell-derived secretomes have become an appealing strategy for stroke neurorepair.

Additional hurdles for cellular engraftment and tissue regeneration are liquefactive necrosis in the infarct core and glial scar formation. **Biomaterials**-based therapies may represent a promising tool to address these issues. With this approach, the liquefactive cavity could incorporate biomaterials such as hydrogels or living scaffolds to replace the missing stroma, attract endogenous cells and deliver growth factors or cells. This selective administration would ease regeneration by bridging the lesion with the healthy tissue, and could help overcoming the off-target problems of systemic delivery, a matter that will be discussed in more detail hereinafter.<sup>109</sup>

### 1.5.2. Endothelial Progenitor Cells (EPCs)

Endothelial Progenitor Cells (EPCs) were first identified by Asahara and colleagues in 1997 as cluster of differentiation (CD)-34-positive MNCs with endothelial characteristics. These cells were isolated from adult peripheral blood and showed the capacity to differentiate into ECs and contribute to adult neoangiogenesis.<sup>110</sup> This insight shifted the paradigm that vasculogenesis involving progenitor cells was restricted to embryogenesis. Thereafter, EPCs became a focus of study in the field of regenerative medicine given their role in neovascularisation and vascular repair. Nonetheless, ambiguities around their identity and functions, as well as their limited numbers, have hindered their clinical application.<sup>111</sup>

The most widely accepted **phenotypic definition** of EPCs considers the co-expression of the stem and endothelial cell-surface markers CD34 and VEGF receptor 2 (VEGFR2). However, during the past decades, the term EPCs has been used to describe a wide range of cell types exhibiting phenotypes between the haematopoietic and endothelial lineages.<sup>112</sup> This lack of consistency has been attributed to the low frequencies of these cells in the bloodstream, and the different methods used for their isolation and immunophenotyping.<sup>111,113,114</sup>

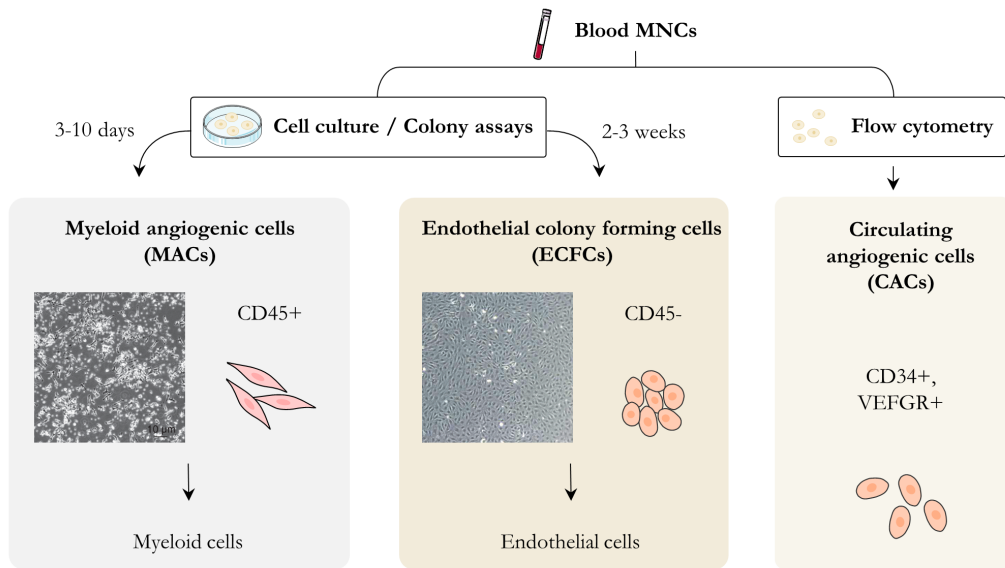


**Figure 7. Methodology used to study EPCs.** Enumeration of EPCs, defined as circulating angiogenic cells (CACs) in blood is performed using flow cytometry. Cell culture/colony assays allow the isolation of well-defined cell populations with vaso-reparative properties such as endothelial colony forming cells (ECFCs) and myeloid angiogenic cells (MACs). Figure adapted from Bhatwadekar et al. (2010) and Medina et al. (2017).<sup>115,116</sup>

In general, two approaches have been used to isolate EPCs from peripheral blood: (i) *in vitro* cell culture and colony assays and (ii) flow cytometry-based assays (Figure 7). Two distinct populations can be obtained using the former protocols depending on the culture time, which were initially named as “early EPCs” and “late EPCs” or “outgrowth endothelial cells (OECs)”, one being haematopoietic, and the other endothelial, respectively.<sup>111</sup> To avoid confusion in defining both cell populations, Medina and colleagues proposed the alternative terms “myeloid angiogenic cells (MACs)” and “endothelial colony forming cells (ECFCs)”, instead of early and late EPCs, respectively.<sup>116</sup>

MACs show pro-angiogenic features through paracrine mechanisms but are unable to form new vessels, and exhibit a phenotype similar to M2 macrophages. Instead,

ECFCs show the ability to form blood vessels both *in vitro* and *in vivo*, and express the markers CD31, CD105, vascular endothelial cadherin (VE-Cadherin)/CD144, CD146, von willebrand factor (vWF), VEGFR2 and ulex europaeus agglutinin 1 (UEA-1), but not CD45 nor monocyte markers, and are fully committed to the endothelial lineage. In the same line, Yoder and colleagues established the definition of EPCs based on the following criteria: (i) circulating cells with clonogenic capacity, (ii) a restricted differentiation towards an endothelial lineage, (iii) showing the ability to form blood vessels both *in vitro* and (iv) *in vivo*, and (v) displaying vessel repair capacities.<sup>112,116</sup>

The characterisation of EPCs has been improved using flow cytometry considering homogeneously highly expressed and stable markers (i.e., CD146, CD144, CD105, CD31), and heterogeneous and unstable markers (i.e., CD34, c-kit, CD133)<sup>117</sup>, yet there is still no consensus for a unique combination of EPC markers.

Regarding the **origin** of EPCs, these have been traditionally thought of as bone marrow (BM)-derived cells that mobilise after an ischaemic event towards the sites of vascular injury. However, other authors have reported to fail in obtaining ECs from the BM culture, which suggests an alternative niche in the vessel wall.<sup>118</sup>

Despite these unresolved questions, there is a growing body of evidence that places EPCs as a promising **therapeutic avenue** for stroke recovery. A number of pre-clinical studies have shown that the administration of EPCs after cerebral ischaemia promotes angiogenesis, vascular repair, neuronal regeneration, neuroprotection, and both short- and long-term functional improvement.<sup>119–125</sup> However, there are only 6 completed or ongoing studies registered at the U.S. National Library of Medicine (ClinicalTrials.gov) testing the therapeutic capacity or diagnostic and prognostic value of EPCs in ischaemic stroke patients (NCT02605707, NCT01468064, NCT02980354, NCT02157896, NCT01289795, NCT03218527).<sup>126</sup> Furthermore, cell-based therapies may lead to adverse effects, such as microemboli or immune rejection<sup>127</sup> and, although several clinical trials have proven the safety of stem cell therapies for stroke, no clear efficacy has been proven to date.<sup>128</sup>

In this light, novel stem cell-based approaches are being investigated for the treatment of stroke, such as the use of cell-derived growth factors, mitochondria, extracellular vesicles, or micro-RNAs (miRNAs).<sup>129–132</sup>

#### 1.5.2.1. EPCs-derived secretome

As earlier stated, the benefits of stem cell therapies are also likely to arise from a paracrine mechanism. In this regard, EPCs are known to release pro-angiogenic factors, such as SDF-1, IGF-1, hepatocyte growth factor (HGF), G-CSF, VEGF, endothelial nitric oxide synthase (eNOS), and inducible nitric oxide synthase (iNOS), and several cytokines, amongst many others.<sup>114</sup>

It is reasonable to think of a potential therapeutic effect of EPC-secretome involving multiple molecular pathways and cell types, considering the large variety of biologically active substances. Most of these factors can promote ECs proliferation and reduce apoptosis, and are also involved in the regulation of endogenous progenitor cells recruitment, vascular growth, and remodelling.<sup>133</sup> Hence, EPC-secretome has been used as a therapeutic strategy in several pre-clinical models such as in hind-limb ischaemia, showing improved hind-limb perfusion and muscle function through neovascularisation and vascular maturation<sup>134</sup>, and in cerebral ischaemia, showing improved functional outcome through vascular remodelling.<sup>135</sup> Aside from its well-known pro-angiogenic capacity, different studies have reported protective and regenerative responses through other mechanisms involving immune regulation or remyelination.<sup>136–140</sup>

## 1.6. Brain drug delivery

### 1.6.1. The blood-brain barrier

Overcoming the challenge of brain drug delivery is an ongoing struggle and this represents an obstacle for CNS diseases drug development.

Brain targeting is hindered mainly by the tight brain capillaries in the BBB. The BBB, which is comprised by microvascular ECs, pericytes and astrocytes, represents the



largest interface for blood-brain exchange. It acts as a physical barrier due to the presence of tight junctions (TJs) between adjacent ECs and the absence of fenestration and pinocytotic activity of these cells, which is essential to isolate brain parenchymal cells from neurotoxic molecules, pathogens and circulating blood cells, thus maintaining brain homeostasis.

Molecules can cross the BBB through a paracellular pathway (between adjacent cells, by passive diffusion) or a transcellular pathway (through the cells, by either passive diffusion, receptor-mediated transport or transcytosis) (**Figure 8**). Only small molecules that are lipid soluble can cross the BBB, while most macromolecules are unable to penetrate the brain endothelium. Nonetheless, even small lipophilic drugs encounter multiple barriers that hamper their delivery in the CNS, such as active efflux mechanisms or degradative enzymes. Furthermore, high lipid solubility may be accompanied by an increased accumulation in off-target tissues.<sup>141</sup>

### 1.6.2. Strategies for brain drug delivery

To meet the challenge of efficient brain drug delivery, many efforts have been put to develop new approaches that improve brain targeting, either by disrupting or circumventing the BBB.

The following sections describe some of the foremost strategies investigated thus far, depicted in **Figure 8**.

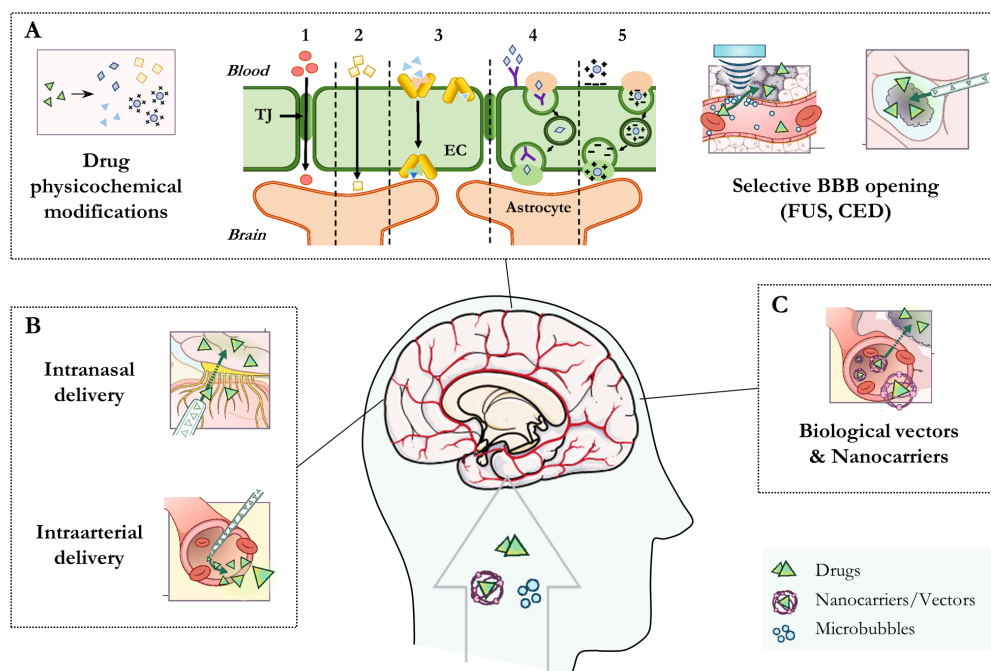


**Figure 8. Different mechanisms for brain drug delivery, including A)** overcoming the BBB through modification of the drugs' physicochemical properties to adapt to the different mechanisms of BBB crossing (1: paracellular pathway, 2: transcellular lipophilic pathway, 3: transport proteins, 4: receptor-mediated transcytosis, or 5: adsorptive transcytosis), or through selective BBB opening, **B)** using selective administration routes, and **C)** directing the drug with carriers (biological vectors or nanocarriers). TJ: tight junction; EC: endothelial cell; BBB: blood-brain barrier; FUS: focused ultrasound; CED: convection enhanced delivery. Figure adapted from Haumann et al. (2022) and Ahlawat et al. (2020)<sup>142,143</sup>

### 1.6.2.1. Physicochemical modifications of the therapeutic agent

Molecular weight, lipophilicity, polar surface area, hydrogen bonding, and charge, are the key physicochemical parameters that determine the ability of passive diffusion of a given compound through the BBB. Thus, a reasonable method to improve brain drug delivery is to select therapeutic compounds based on these parameters. It has also been attempted to add modifications to optimise these features, although

modifying the physicochemical properties of the drugs can secondarily influence off-target biodistribution, and non-specific binding to plasmatic proteins as well as in brain tissue. For this reason, although several studies have proven an enhanced brain drug delivery following this approach, this was not reflected into an increased efficiency.<sup>144</sup>

### 1.6.2.2. Selective BBB opening

A common approach that has been studied to overcome the BBB is the use of **permeability enhancers**, or non-invasive techniques to temporarily open the BBB in order to facilitate drug penetration into the brain. Different BBB opening approaches are being currently studied, including microbubble-mediated focused ultrasound,<sup>145,146</sup> convection enhanced delivery,<sup>147</sup> or the use of nanoagonists<sup>148</sup> and hyperosmolar drugs such as mannitol.<sup>149</sup>

Although promising, especially in the field of brain tumours, some of the aforementioned strategies have raised neuro-inflammatory-related safety concerns that should be carefully considered in the context of the pathophysiology of stroke.<sup>150</sup> In this line and as previously mentioned, the ischaemic cascade following stroke leads to a BBB leakage and potential breakdown. This process, beginning with a hyperacute phase of enhanced permeability (4-6 h after ischaemia), followed by a delayed BBB opening (2-3 days after stroke), could represent a window of opportunity for brain drug delivery. Taking advantage of this biphasic BBB opening, a recent study achieved a selective accumulation of intravenously administered liposomes into the ischaemic mouse brain.<sup>151</sup>

### 1.6.2.3. Biological vectors

Although generally viruses cannot passively cross the BBB, these can transfect a given gene into the targeted cells with a high efficiency. Therefore, **viral vectors** represent a candidate strategy to target the brain. However, they present several limitations such as safety issues mostly related to immunogenicity, high production cost and manufacturing difficulties. Stereotaxic injection and administration into the

cerebrospinal fluid are the most common routes for viral vectors, but these are invasive and have been related to serious adverse effects, while intravenous (i.v.) administration requires high doses and is related to potential off-target delivery.<sup>143</sup> In order to face this challenge, a recent study described the combination of selective BBB opening with microbubble-mediated focused ultrasound and an adenovirus vector gene therapy, as an effective method to enhance brain delivery.<sup>152</sup>

On the other hand, **exosomes** are very attractive drug carriers given their non-immunogenic nature and intrinsic paracrine function across the BBB and within the brain. Exosomes are small extracellular vesicles, secreted by cells as single-membrane lipid bilayer vesicles, which can deliver a variety of biological molecules, such as nucleic acids, proteins, lipids, and carbohydrates.<sup>153,154</sup> Exosomes are particularly attractive for brain drug delivery, since they can be modified to express targeting moieties through surface chemical modification or via genetic engineering of the exosome-producing cells. The former strategy was tested in a study which demonstrated the efficacy of surface-modified exosomes administered intravenously to target the ischaemic brain region in a mouse MCAO model.<sup>155</sup> Furthermore, exosomes seem to have different tissue tropisms depending on their cell type of origin, therefore a promising strategy could be to use an appropriate cell source. In this light, a recent study demonstrated enhanced therapeutic efficacy of NSCs-derived extracellular vesicles compared to mesenchymal stem cells-extracellular vesicles in a mouse thromboembolic stroke model.<sup>156</sup>

#### 1.6.2.4. Nanocarriers

Nanoparticles are organic or inorganic materials that have at least one of their dimensions in the nanometer range, and can be used as drug delivery carriers.<sup>157</sup> They are particularly suitable candidates to improve brain drug delivery due to their size, ability to undergo surface modification, and their potential to load a large variety of molecules, which can be protected from clearance and degradation, and delivered with a selective, controlled and sustained release.<sup>143,158</sup> For these reasons, nanocarriers

have been widely used during the past decades to enhance brain targeting, showing promising results.<sup>144</sup>

There is currently a large variety of nanocarriers that offer multiple properties for tailor-made therapies. Amongst others, **organic nanocarriers** include nanogels, micelles, lipid-based nanocarriers, dendrimers, and polymeric nanoparticles. The latter can be obtained either from synthetic biodegradable polymers, such as poly(lactic-co-glycolic acid) (PLGA), or from natural macromolecular systems, such as chitosan, polysaccharides, or gelatin. **Inorganic nanocarriers** include metal-based nanoparticles such as gold and iron oxide (which possess superparamagnetic properties and are useful as contrast agents), or ceramic materials such as carbon and silica, amongst others (**Figure 9**).<sup>159</sup>

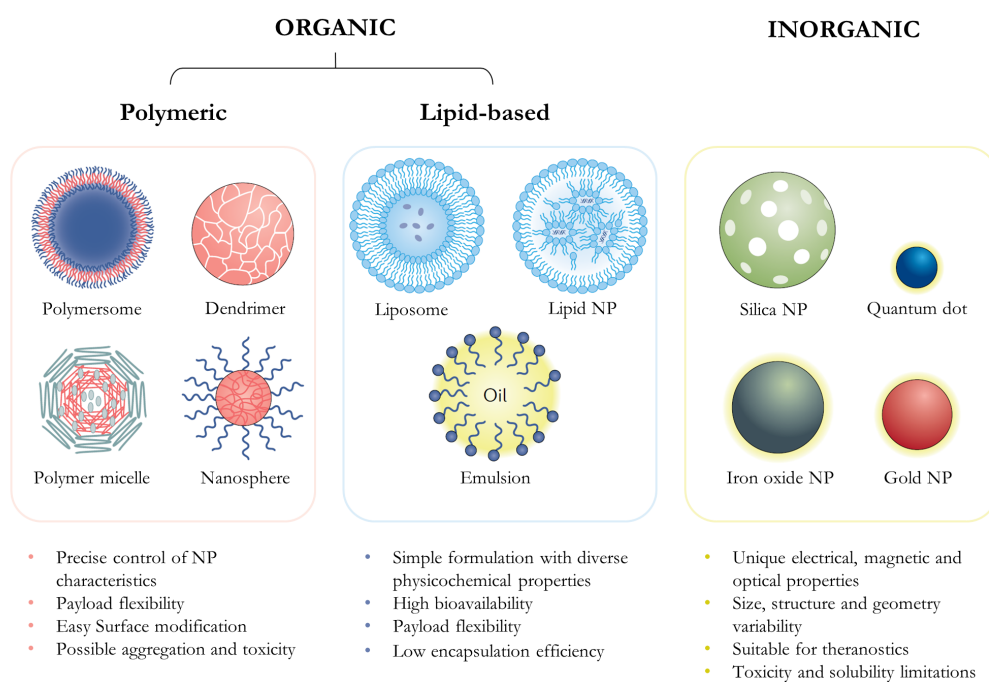


**Figure 9. Types of nanocarriers and advantages/disadvantages of the most commonly used in nanomedicine.** NP: nanoparticles. Figure adapted from Mitchell et al. (2021).<sup>160</sup>

Nanocarriers can cross the BBB in multiple ways, including paracellular and transcellular diffusion, efflux transport, or transcytosis.<sup>161</sup> However, nanomaterials inherently accumulate rapidly after injection in highly perfused reticulo-endothelial system tissues such as the lungs, liver and spleen, limiting their bioavailability in target organs such as the brain.<sup>162</sup> Due to this accumulation in filtering organs, many strategies have been focused on adding affinity moieties to increase tissue specificity, but have been hindered by numerous challenges. Additional limitations associated with the use of these nanoparticles include low transfection efficiency, batch-to-batch variability, poor drug loading capacity, and particle-particle aggregation which difficult their handling.<sup>163</sup> Also, nanocarriers can result in rapid immune-mediated reactions, which have been mechanistically related to the so-called complement activation related pseudo-allergy (CARPA), leading to severe or even fatal consequences. This reaction varies across different species, for example, a study showed an efficient macrophage evasion in murine serum through nanoparticles engineering, which in contrast triggered an extensive complement activation in human serum. Therefore, from a translational perspective, it is of great importance to use appropriate and diverse pre-clinical models in order to predict these responses in humans.<sup>164–166</sup>

Despite the aforementioned challenges, the use of nanocarriers has become an appealing therapeutic and diagnostic tool for multiple diseases including stroke, a matter that will be discussed hereinafter.

#### 1.6.2.5. Administration routes

Local **intraventricular** or **intracerebral** stereotactic injections allow direct parenchymal brain drug delivery, and have been also explored in combination with other techniques such as convection enhanced delivery. However, these are invasive techniques, and therefore alternative strategies are being explored.<sup>167,168</sup>

The **intranasal** route has emerged as promising non-invasive route, which allows a direct delivery of therapeutic agents from the nose to the brain through the olfactory

and trigeminal nerve pathways. It presents the advantage of bypassing the BBB and circumventing the first-pass metabolism, but it is limited by a low tolerable administration volume, low permeability to hydrophilic drugs and low protein brain delivery efficiency.<sup>169</sup> Novel strategies aiming at improving this administration route include its combination with the aforementioned microbubble-mediated focused ultrasound.<sup>170</sup>

The extensive use of mechanical thrombectomy in acute stroke management has also opened a new avenue for **intraarterial** drug delivery to reach the brain vasculature. Taking advantage of this selective route, neuroprotective or neurorestorative treatments could be directly administered in the affected brain regions, partially bypassing filtering organs, thus helping to overcome a significant drawback of systemic drug delivery.<sup>171,172</sup> In this regard, this administration route has already been used in stroke clinical trials to administer autologous stem cells,<sup>173</sup> drugs such as verapamil<sup>174</sup> or to induce cerebral hypothermia by administering cold isotonic saline.<sup>175</sup>

### 1.7. Nanomaterial-based treatments for stroke

To date, only few more than 20 nanomedicines are approved by the U.S. Food and Drug Administration (FDA), including lipid-based, polymeric and inorganic nanomaterials, and none has reached the clinical setting in the field of stroke.<sup>160,176</sup> However, advanced nanosystems are emerging as novel promising tools. Nanoparticles hold a promising theranostic potential for stroke, by increasing the bioavailability and delivery of a given treatment to the ischaemic brain, but also improving stroke diagnosis through molecular brain imaging (**Figure 10**). Moreover, the timing of nanomaterials administration could be adapted to the earlier mentioned stroke biphasic BBB leakage, to further enhance brain drug delivery.<sup>177</sup>

Nanomaterials have been used to improve stroke diagnosis and prognosis by using clinically-relevant **neuroimaging** techniques, such as superparamagnetic iron oxide nanoparticles (SPIONs) as contrast agents for MRI, or gold nanoparticles for CT

imaging. Furthermore, multiple nanomedicine-based strategies have also been used as **therapeutic tools** either to enhance thrombolysis in ischaemic stroke, to limit bleeding in haemorrhagic stroke, or to enhance neuroprotection and neurorepair.<sup>176,178,179</sup>

Amongst the diversity of tools that nanotechnology offers, nanocarriers are particularly interesting due to their capability to add different moieties for a tailored functional mechanism. Aside from the application of SPIONs as contrast agents for MRI, these have also been used to enhance brain targeting through **magnetic retention**,<sup>180,181</sup> as well as to enhance thrombolysis through hyperthermia or magnetically-guided mechanical drilling.<sup>182,183</sup>

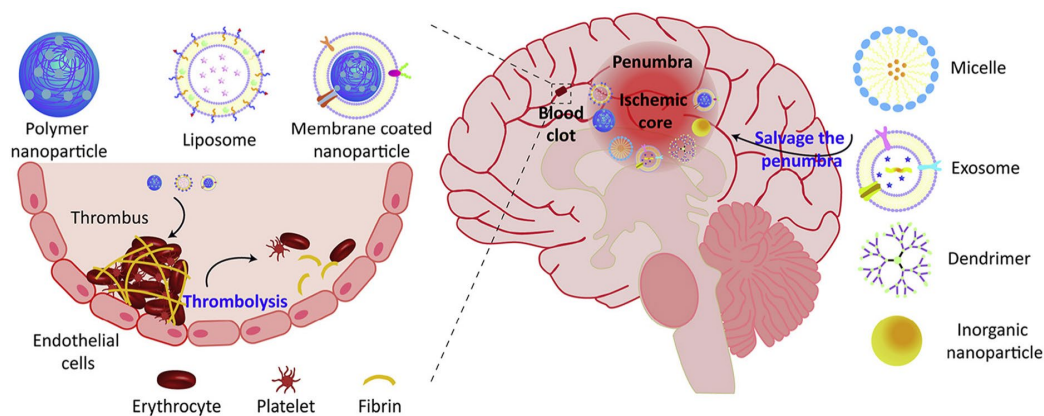


**Figure 10. Nano-drug delivery systems for stroke.** A large variety of nanocarriers are being investigated at different stages after stroke, from acute reperfusion to neuroprotection and tissue repair, including liposomes, dendrimers, nanoparticles, and exosomes, amongst others. Figure adapted from Li et al. (2021).<sup>184</sup>

Together with liposomes, and more recently mesoporous silica nanoparticles, **polymeric nanocarriers** are particularly ideal candidates as delivery vehicles for stroke therapy, due to their biocompatibility, biodegradability and good sustained-release profiles.<sup>185</sup> They present diverse drug loading methods, including encapsulation within the core, entrapping in the polymer matrix, chemically conjugated to the polymer or bound to the surface, and have been extensively used



to deliver oligonucleotides, proteins, and small-molecule drugs to treat stroke. The most common forms of polymeric nanocarriers are **nanocapsules**, consisting of cavities surrounded by a polymeric membrane or shell, and nanospheres, which are solid matrix systems.<sup>160</sup> Polymeric nanocapsules hold a promising potential to improve stroke therapy, as demonstrated by pre-clinical evidence. In this regard, a recent study proved the advantage of PLGA nanocapsules to increase brain delivery and therapeutic efficacy of the cargo drug. This particular study took advantage of the pathophysiological SDF-1/CXCR4 axis after stroke, by using surface coating with membranes derived from NSCs overexpressing CXCR4, which evidences the multiple strategies that nanomedicine can offer to improve stroke therapy.<sup>186</sup>

The present work has been focused on the use of polymeric nanocapsules, therefore the terms ‘nanocapsules’ and ‘nanocarriers’ will be interchangeably used, and the abbreviation ‘NCs’ will be indistinctly referred to both terms from now on.

## 1.8. Thesis rationale and hypothesis

Stroke remains a leading cause of adult disability, thus there is an urgent need to develop therapeutic strategies beyond acute recanalisation. As earlier pointed out, this therapeutic development is hampered by the high-complexity of stroke, added to the challenge of brain drug delivery. In this regard, a multimodal drug delivery approach might be more effective than a single drug delivery method.

To face the aforementioned challenges, and in light of the therapeutic potential of **EPCs-secretome** as a cell-free therapy tackling multiple biological processes, we sought to study its benefits through a guided targeting and controlled release. The aim of the present work is to administer EPCs-secretome in **polymeric nanocarriers**, through **endovascular delivery** and **magnetic retention**, under the hypothesis that the combination of these strategies might be a feasible approach to improve specific **brain targeting and neurovascular repair after stroke**.



# OBJECTIVES

---



The objectives of the present doctoral thesis are the following:

1. To validate the pro-angiogenic effects of stroke patients-derived EPCs-secretome in endothelial cells *in vitro*.
2. To assess the feasibility and efficiency of EPCs-secretome encapsulation into magnetic PLGA nanocapsules for the subsequent release of functional factors.
3. To enhance brain targeting of the proposed nanoformulation in a mouse model of cerebral ischaemia, taking advantage of the endovascular route and improving the magnetic retention in the ischaemic target area, while monitoring the biodistribution and potential toxicity.
4. To study the short-term effects of hyperacute endovascular administration of free or encapsulated EPCs-secretome after cerebral ischaemia.
5. To study the neurovascular repair potential of hyperacute endovascular treatment with free or nanotargeted EPCs-secretome after cerebral ischaemia.
6. To assess the translational feasibility of the endovascular-nanotargeted approach in large animals with gyrencephalic brain and larger vessels/capillaries, and in an *ex vivo* humanised vascular model using a magnet designed for human use.



# MATERIALS AND METHODS

---





### 3.1. EPC-secretome, Nanocarriers and Magnet devices

#### 3.1.1. EPCs isolation

Human EPCs (hEPCs) were isolated from the peripheral blood of a stroke patient (man, 66 years, blood sampling for EPCs-isolation at 24 h post-ischaemic stroke) as previously described<sup>187</sup> and stored in liquid nitrogen until use. The donor did not present any known malignant, infectious, or other neurological diseases than stroke, which were exclusion criteria for the EPCs collection.

Briefly, blood was collected in EDTA tubes by venous puncture, and Ficoll gradient (1.078 g/L) was used to isolate human MNCs. Isolated cells were seeded in fibronectin-coated 12-well plates at a density of  $10^7$  cells/well. Cells were cultured in a 5% CO<sub>2</sub> incubator at 37°C with complete endothelial growth medium (Endothelial Cell Growth Medium-2 (EGM-2) SingleQuots Supplements and Growth Factors; Lonza) containing endothelial cell basal medium (EBM) supplemented with 10% fetal bovine serum (FBS), and the following commercial kit's factors: human endothelial growth factor (hEGF), VEGF, human basic fibroblast growth factor (hFGF-b), recombinant IGF-1 (R3-IGF-1), gentamicin and amphotericin-B (GA-1000), heparin, hydrocortisone and ascorbic acid. After 3 days in culture, non-adherent cells were discarded and the medium was changed every other day. Colonies of OECs appearing 10-20 days after seeding were further expanded. Immunophenotyping of EPCs was confirmed by vWF (Dako), UEA-1 (Sigma-Aldrich), CD34 (Santa Cruz) and VEGFR2 (Santa Cruz). The same outgrowth expanded EPCs were used in all studies.

#### 3.1.2. Secretome collection and concentration

For secretome production, hEPCs ( $10^7$  cells) were resuspended in 25 mL of complete EGM-2-10% FBS and seeded in a T175 flask (175 cm<sup>2</sup>). After 96 h, EPCs were trypsinised and split in three T300 flasks (300 cm<sup>2</sup>). For every T300 flask,  $2 \times 10^7$  cells were seeded in 70 mL of complete EGM-2-10% FBS medium. After 72 h, EPCs

were trypsinised, resuspended ( $2.5 \times 10^8$  cells) in 1 L of EGM-2-10% FBS, and seeded in a CF10 flask (Nunc™ EasyFill™ Cell Factory™ Systems, culture area 6320 cm<sup>2</sup> in 10-layers). After 96 h (100% confluence), the EGM-2-10% FBS medium was discarded and cells were rinsed with phosphate buffered saline (PBS). Next, cells were incubated in 1L of basal Dulbecco's Modified Eagle's Medium (DMEM) for washing, which was discarded after 1 h and replaced with 1 L of EBM. After 24 h, the secretome containing EPCs-released factors, also referred as the EPCs conditioned medium (CM) was collected and filtered/concentrated. In the interest of brevity, the terms secretome and CM will be used interchangeably from now on.

Both CM and fresh protein-free EBM (control) were filtered through a 0.22- $\mu$ m vacuum filter to remove cells and debris. Centricon Plus-70 filters (3 kDa Ultracel-PL membrane, Millipore) were filled with CM/EBM and centrifuged ( $3,500 \times g$ ) at 4°C for 60 min. The concentrated CM (cCM) or EBM (cEBM) were recovered by centrifuging in collection mode at  $1,000 \times g$  for 1 min. Finally, the protein content was determined by Bradford assay and frozen at -80 °C in low-protein binding tubes. All experiments with secretome-loaded NCs have been carried out with the cCM, so the abbreviation NC-CM will be used from now on. Both EBM or cEBM have been used for experimental purposes, however only cEBM was used for encapsulation, so the abbreviation NC-EBM will also be also used in the interest of clarity.

### 3.1.3. Nanocarriers synthesis and characterisation

**The nanocarriers were synthesised and characterised in collaboration with the Group of Nanoparticles and Nanocomposites of Dr. Anna Roig at ICMAB-CSIC within the framework of the MAGBBRIS project.**

PLGA NCs were synthesised by a double emulsion solvent evaporation method and functionalised with SPIONs and/or fluorescent tags (cyanine 5 (Cy5) or cyanine 7.5 (Cy7.5)), and their size and dispersion characteristics were measured by dynamic light scattering, as previously described.<sup>188</sup> Briefly, SPIONs were embedded in the PLGA shell by adding oleic acid-coated SPIONs, with an average diameter of 9 nm, in the

PLGA organic phase during the first emulsification. Modified PLGA-Cy5/7.5 was also added in the organic phase in addition to the commercial PLGA.

For encapsulation, 50  $\mu$ L of either deionised water (MilliQ®, Merck Millipore), cCM or the corresponding cEBM were added during the aforementioned double emulsion solvent evaporation method for a single NCs batch (NC-W, NC-CM or NC-EBM, respectively). Variable protein concentrations are obtained for each secretome batch production so, in order to load a standard secretome concentration for all NC-CM batches, the cCM was lyophilised in a freeze dryer (Lyoquest – Telstar®) for 72 h at -80°C. Then, the lyophilised cCM was reconstituted in MilliQ® deionised water to obtain a final concentration of 15 mg/mL for encapsulation.

The obtained NCs suspension in trehalose aqueous solution was lyophilised and stored at 4°C with desiccant silica gel until each experimental use. The NCs were freshly dispersed at the desired concentration before use, vortexed for 1 min and sonicated in an ultrasound bath for 3 min at 83.3 W/L and 48 kHz.

Details of the different NC batches used in this study are listed in **Table 5**.

**Table 5. Summary of the nanocarriers used for all studies.**

	Z-Average (nm)	Polydispersity index (PDI)
<b>PLGA_SPION_ Cy7.5_H20 (n=10)</b>		
Mean	274.9	0.18
SD	35.6	0.09
<b>PLGA_SPION_ H20 (n=4)</b>		
Mean	266.8	0.15
SD	14.4	0.02
<b>PLGA_SPION_ Cy5_H20 (n=5)</b>		
Mean	248.4	0.17
SD	11.6	0.03
<b>PLGA_SPION_ Cy5_EBM (n=13)</b>		
Mean	295.5	0.23
SD	61.4	0.10
<b>PLGA_SPION_ Cy5_CM (n=16)</b>		
Mean	312.1	0.24
SD	32.0	0.05

### 3.1.4. Secretome encapsulation efficiency and release

Lyophilised NCs encapsulating cCM as well as cEBM as a control were fully dissolved in dimethyl sulfoxide (DMSO) at 100 mg/mL and sonicated during 3 min at 42 kHz to ensure full lysis of the polymer and total release of the protein content. Total protein content was determined directly using the CBQCA protein quantitation kit (Invitrogen™ ref. C6667), which determines the protein concentration based on the production of fluorescent products measurable at an excitation/emission wavelength ( $\lambda_{ex}/\lambda_{em}$ ) of 450 nm/550 nm, respectively, via non-covalent interaction between CBQCA and primary aliphatic amines of proteins. This highly sensitive fluorescence-based method showed compatibility with DMSO, SPIONs, detergents and other substances which interfere with many commonly used protein determination methods. The protein contents in the NC lysates were measured and calculated based on the difference in the fluorescence with the control and a calibration curve drawn with standard albumin solutions. The total protein content was also measured in the secretome used for encapsulation. All determinations were performed in duplicate for each NC batch.

In order to determine specific EPCs-secretome-proteins' content, a configurable multiplexed ELISA was used in cEBM/cCM-loaded NCs, lysed as described above (Human Magnetic Luminex Assay, LXSAHM-06, Luminex code Ml6FbCTe, R&D systems). The following analytes were selected and multiplexed, based on previous proteomics analyses of the EPCs-secretome composition: VEGF, GM-CSF, Angiogenin, and Pentraxin 3 (PTX-3). Angiogenin protein levels were also determined in a single-plex ELISA (Human Angiogenin Quantikine ELISA Kit, DAN00, R&D systems).

The experimental **protein loading** content was expressed as  $\mu\text{g}$  of total protein per mg of NC ( $\mu\text{g}/\text{mg}$ ), or as  $\text{pg}$  of a specific protein per mg of NC ( $\text{pg}/\text{mg}$ ). The **encapsulation efficiency** (EE%) was calculated as follows:

$$\text{EE}\% = \text{Experimental CM loading} / \text{Nominal CM loading} \times 100$$

The biological function of EPCs-CM after collection/concentration, lyophilisation, encapsulation, and **release** was evaluated and compared to the function prior to processing. To do so, NC-CM or NC-EBM were resuspended in EBM (2 mg/mL), and incubated at 37°C on rotation. After 48 h, the solution containing the NCs-cargo release in EBM was collected, centrifuged at 14000 rpm to remove PLGA and SPIONs, and the supernatant was used for *in vitro* cell culture experiments, described hereinafter.

### 3.1.5. Magnet devices

**The magnet devices used for the present study were designed and characterised by the Institute of Experimental Physics at the Slovak Academy of Sciences, in collaboration with Dr. Peter Kopcansky within the framework of the MAGBBRIS project.**

To study the advantages of an external magnetic field for specific brain targeting of the magnetised NCs, two different iron-neodymium-boron (FeNdB) magnets were constructed considering the mouse brain anatomy: permanent Magnet 1 (M1) and focused Magnet 2 (M2), together with non-magnetic pieces serving as controls, differing on the final size: Fake 1 (F1) and Fake 2 (F2).

M1 consists of a circular FeNdB permanent magnet of 5x2 mm covered by a soft iron yoke and a biocompatible polymer support frame (the final size of the device was 8x3 mm). M2 consists of a focused FeNdB magnet with a 2x1 mm matrix of submagnets covered with nickel and a thin biocompatible polyurethane/epoxy film, with a final cylindrical shape of 6x3 mm. F1 and F2 were manufactured as M1 and M2, respectively, except for a brass core instead of FeNdB.

A focused magnetic device prototype was also designed adapted to the human anatomy (M3), as a wearable magnet for patients. M3 was constructed using a patented technology with GIAMAG<sup>®</sup> (GIAnt MAgnet field Gradient) and consists of a curved focused magnet with a matrix of 16 partial magnets covered in gold (40 mm of diameter).

### 3.1.5.1. Validation for magnetic retention

The spatial distribution of the magnetic field and magnetic force of M1 and M2 was characterised with the standard QUICKFIELD software. The modelling was calculated in the plane 3 mm over the surface of the magnet devices. The magnetic field induction and magnetic field gradient of the magnet devices M1 and M2 were measured by 3D Hall probe. The magnetic force was calculated according to the distance from the centre of the magnet at 3 mm in height from the surface.

To test the efficacy of magnetic targeting of the magnet devices, a dust magnetic targeting test was performed. Ferrimagnetic magnetite microparticles (10  $\mu\text{m}$  average diameter) were dispersed in mineral oil and each magnet device was placed at the centre to test the covered distance of magnetic attraction of the magnetic microparticles.

The magnetic targeting efficacy was then validated for the focused magnet (M2) with a simple chicken egg model and MRI by tracking the position of an injected magnetic fluid. The magnetic fluid was prepared with magnetite particles (10 nm average diameter) covered by polyethylene glycol, dissolved in a physiological salt-based solution at a concentration of 0.305 mg/mL. The MRI measurements were performed by using a 7 T BioSpec Bruker system. T2\*-weighted images (T2\*WI) were acquired by Multi Gradient Echo pulse sequence by using the following parameters: repetition time (TR) = 881 ms, starting echo time (TE) = 3 ms, echo-spacing = 3.41 ms (for 10 different TE), flip angle (FA) = 50°, 23 coronal slices of 1 mm slice thickness and 0.5 mm gap, field of view (FOV) = 70 x 58 mm, matrix size = 256 x 256.

The magnetic field and magnetic force for M3 were measured according to the distance from surface and distance from centre of the magnet. The magnetic field and force were measured in the X-Y-Z axis by 3D Hall Probe (connected to a Gaussmeter GM-08). A semiautomatic X-Y scanner (Magscan) adapted with a microcontroller Arduino was used, and the Z axis was manually adjusted.

## 3.2. Cell culture *in vitro* studies

### 3.2.1. Experimental design and cell types

In order to study the potential pro-angiogenic effects of EPCs-secretome, we assessed cell proliferation and tubulogenesis upon treatment in both mouse/human, and endothelial progenitor/mature cells.

Mature immortalised cell lines from the human or mouse cerebral microvasculature (**hCMEC/d3** cells and **bEnd.3** cells, respectively), were used as models of mature brain endothelial cells.<sup>189,190</sup> As models of EPCs, **human OECs** obtained from peripheral blood of a healthy donor (man, 59 years, as described in section 3.1.1, and **mouse OECs** obtained from FVB mouse spleens (Jackson Laboratories, USA), as described elsewhere,<sup>191,192</sup> were also used.

hCMEC/D3 cells were maintained in EGM-2, containing EBM supplemented with 2% FBS, and 1:2 of the commercial kit's factors hEGF, VEGF, hFGF-b, R3-IGF.1, heparin, hydrocortisone and ascorbic acid, and whole GA-1000 aliquot.

bEnd.3 cells were maintained in DMEM-High glucose-pyruvate (Gibco™) supplemented with 10% FBS and penicillin/streptomycin (Gibco™).

Both human and mouse OECs were maintained in EGM-2, containing EBM supplemented with 10% FBS and whole aliquots of the abovementioned bullet kit: hEGF, VEGF, hFGF-b, R3-IGF.1, GA-1000, heparin, hydrocortisone and ascorbic acid.

hCMEC/D3 and bEnd.3 cells were seeded in collagen type I-coated flasks (25 cm<sup>2</sup>), while OECs were seeded in fibronectin-coated flasks (25 cm<sup>2</sup>) and incubated at 37°C and 5% CO<sub>2</sub> in complete medium, which was changed every 2-3 days. For cell passage, all cells were washed with sterile Dulbecco's PBS (DPBS), treated with 1 mL of trypsin and incubated for 5 min at 37°C to disperse the cells. After, cells were centrifuged in the corresponding complete medium at 1500 rpm for 4 min. After



centrifugation, the cell pellet was resuspended with fresh complete medium and seeded correspondingly.

### 3.2.2. Endothelial proliferation assays

Mature ECs or OECs were seeded in collagen I-coated 24-well plates or fibronectin-coated 48-well plates, respectively, in their corresponding complete medium, at the desired density. When reaching a confluence of 80%, complete medium was replaced with the corresponding treatment diluted in non-concentrated basal medium (without growth factors nor FBS): (i) **cEBM**: concentrated EBM, (ii) **CM**: EPC-secretome obtained as described above (section 3.1.2), (iii) **NC-CM**: CM-loaded NC obtained as described above (section 3.1.3), or (iv) **released CM**: NC-CM cargo release, obtained as described above (section 3.1.4). A **control** condition (pure non-concentrated basal medium) was included in all cases.

Cell viability was measured at 24 h/48 h after treatment, using colorimetric assays through tetrazolium salts' metabolisation. The 3-(4-5-dimethylthiazol-2-yl)-2,5-diphenyl tetrazolium bromide (MTT) assay was used for all cases except for the experiments testing NC-EBM or NC-CM release treatment to avoid nanomaterial interference, for which the Cell Counting Kit-8 (CCK-8, Dojindo Molecular Technologies, CK04) was used instead.

Briefly, after 60 min to 120 min incubation with the corresponding dye solution, the absorbance of the resulting formazan crystals diluted in DMSO was determined at 590 nm (MTT), and the absorbance of hydrosoluble formazan was determined in the cell culture supernatant at 450 nm (CCK-8). All conditions when run in duplicates, and cell viability was referred as the percentage compared with the control basal medium condition ( $n \geq 4$ ).

### 3.2.3. Endothelial tubulogenesis assays

An *in vitro* Matrigel® (BD Biosciences, USA) model resembling the extracellular matrix was used to evaluate the role of EPCs-secretome on the angio-vasculogenic functions of mouse or human OECs.

Briefly, OECs were seeded into  $\mu$ -slides ( $\mu$ -Slide Angiogenesis Glass Bottom, IBIDI®) previously coated with cold Matrigel at 37°C for 15 min (to allow polymerisation). After 16-18 h, 2 representative images per well were acquired using an inverted microscope (Eclipse TS100, Nikon) at 4X magnification. Finally, the number of loops (circular vessel-like structures), total tube length (perimeter of complete rings) and covered area were automatically measured using the WimTube software from Wimasis Image Analysis®. A control condition was included in all cases, and all conditions were run in triplicates. The results are expressed as a percentage versus the control condition (n=7).

### 3.2.4. Endothelial nanocarriers uptake

In order to evaluate the potential uptake of NC-CM by mature brain ECs or OECs, a temporal uptake profile was performed in hCMEC/d3 cells or mouse OECs, respectively, as follows.

Briefly, cells were cultured and seeded as previously described, and treated with 50  $\mu$ g/mL of freshly sonicated Cy5-labelled NC during 6, 24 or 48 h. After, cells were stained with the lipophilic DiOC dye (1:200, D275, Invitrogen) for 5 min at 37°C, washed twice in complete EGM-2, then washed twice in DPBS and fixed for 15 min in PFA 4%. Finally, the cells were washed twice in DPBS-Tween, and mounted in Fluoroshield mounting medium with DAPI (F6057, Sigma). Images were acquired at the different conditions using a Zeiss LSM890 confocal microscope at 63X oil magnification.

### 3.3. *In vivo* nanocarriers delivery and cerebral ischaemia

All procedures were approved by the Ethics Committee for Animal Experimentation of the Vall d'Hebron Research Institute and Universitat Autònoma de Barcelona (protocol numbers CEEA 70/18 and 4784) and conducted in compliance with the Spanish legislation and in accordance with the Directives of the European Union. C57BL/6JRj (C57) and Balbc AnNRj (Balbc) adult male mice ( $23.7\pm 1.5$  g and  $23.8\pm 1.2$  g, respectively, 7-9 weeks old), purchased from Janvier laboratories (Saint Berthevin, France), were used for the present study. Mice were housed in groups and kept in a climate-controlled environment on a 12 h light/dark cycle, and both food and water were available *ad libitum*. The total number of animals included for each study and exclusion criteria are listed in the following section and summarised in **Table 6**. All *in vivo* experiments are reported according to the ARRIVE 2.0 guidelines to the best of our possibilities.<sup>89</sup>

#### 3.3.1. Experimental design

##### **Biodistribution study 1: administration route**

To first study the biodistribution of the NC following systemic or endovascular routes and the influence of the first magnet device for brain targeting, randomly assigned naïve Balbc mice were injected either intravenously (n=16) or intraarterially (n=10) with the 1.6 mg *biodistribution dose* of Cy7.5-NC-W (as described in section 3.3.3). Each i.v./i.a. group was further randomly divided into the M1 and the control F1 groups. The fake/magnet devices were implanted for 30 min after the NCs administration and fluorescent molecular imaging (FMI) *in vivo* images were acquired at 30 min, 1 h and 3 h post-injection. After the last acquisition, mice organs were obtained for *ex vivo* FMI, as described in section 3.3.4 (**Figure 11**).

##### **Biodistribution study 2: magnet effect**

To further investigate the influence of the magnetic field on the NCs brain retention, naïve Balbc mice receiving the 1.6 mg *biodistribution dose* of Cy7.5\_NC-W

intraarterially were randomly assigned into the M1 (n=7) and the control F1 (n=8) groups, implanted and administered as mentioned above. A single image acquisition was conducted at 3 h post-injection when the brain was removed and divided into cortical and subcortical regions for the *ex vivo* FMI acquisition (**Figure 11**).

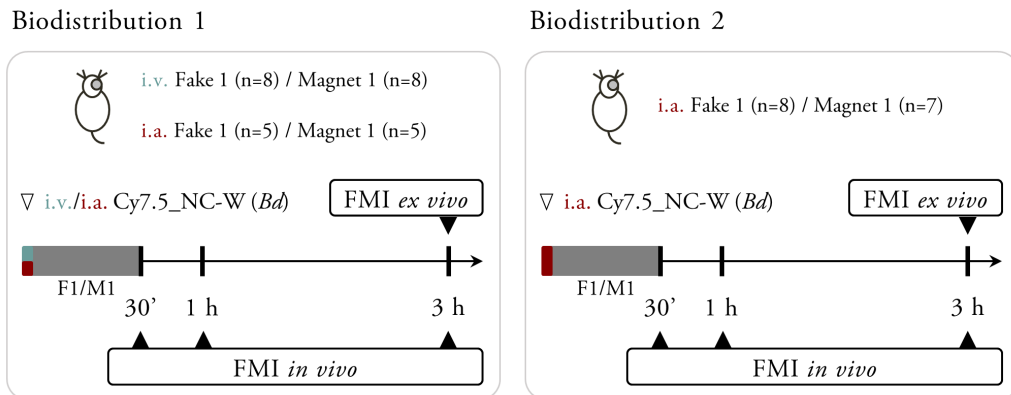
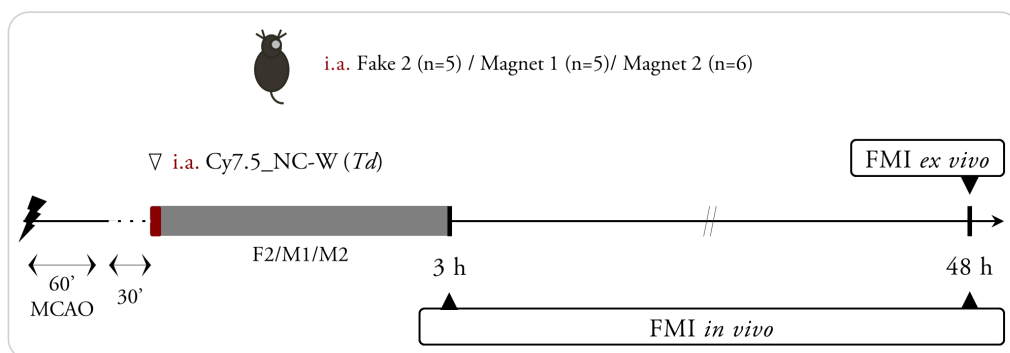


**Figure 11.** Schemes of the experimental design for *Biodistribution studies 1-2*, using healthy Balbc mice receiving 1.6 mg i.a./i.v. Cy7.5-labelled NC-W ( $Bd = Biodistribution\ dose$ ).

### Biodistribution study 3: enhanced magnet effect in cerebral ischaemia

Next, we studied the biodistribution of the NC after hyperacute i.a. administration in the MCAO model, with magnetic retention by two magnet devices with different magnetic fields. A total of 16 C57 mice receiving the 0.8 mg *therapeutic dose* of Cy7.5\_NC-W intraarterially were randomly divided into the two magnet groups (M1 and M2) and a control fake F2 group. The magnet/fake devices were removed after 3 h before the first FMI acquisition time point which was repeated at 48 h post-injection. After the last image acquisition organs were obtained for *ex vivo* FMI (**Figure 12**).

Biodistribution 3



Biodistribution 4

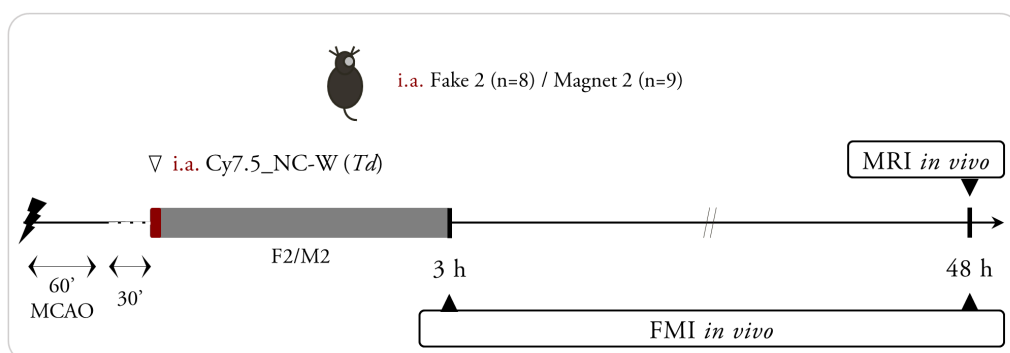


**Figure 12.** Schemes of the experimental design for *Biodistribution studies 3-4*, using ischaemic C57 mice receiving 0.8 mg i.a. Cy7.5-labelled NC-W ( $T_d = \textit{Therapeutic dose}$ ).

**Biodistribution study 4: NCs brain distribution in cerebral ischaemia**

MRI was performed to further characterise the retention and spatial distribution of the NCs in the brain after hyperacute i.a. administration in the MCAO model, with magnetic retention by the M2 device, which showed a better performance in the FMI *Biodistribution study 3*. A total of 17 C57 mice receiving the 0.8 mg *therapeutic dose* of Cy7.5\_NC-W intraarterially, were randomly divided into the M2 and the control F2 groups, implanted and administered as in *Biodistribution study 3*. A single *in vivo* MRI was carried out at 48 h post-injection using a BioSpec 70/30 USR scanner with a 7 T horizontal magnet (Bruker BioSpin, Ettlingen, Germany) equipped with a 72 mm

inner diameter linear volume coil as a transmitter and a mouse brain surface coil as a receiver (**Figure 12**). High-resolution T2-weighted and high-resolution T2\*-weighted images were acquired to visualise the ischaemic lesion and the hypointensities representing the SPION-labelled NCs, respectively (see section 3.3.5).

### Safety study

To assess the safety of hyperacute endovascular NCs administration after cerebral ischaemia, a total of 26 C57 ischaemic mice were randomly assigned into 2 groups: the vehicle group receiving 150  $\mu$ L of saline with a fake magnet (F1) (n=13), and the treatment group receiving the 0.8 mg *therapeutic dose* of NC-W in 150  $\mu$ L of saline with a magnet (M1) (n=13), following the protocols of pre-clinical stroke and endovascular administration, described in sections 3.3.2 and 3.3.3. Both groups were followed for 48 h, when blood was collected from the right ventricle in EDTA tubes for biochemical analysis (see section 3.3.8) and animals were euthanised under deep anaesthesia by cervical dislocation to dissect the brain for 2,3,5-triphenyltetrazolium chloride (TTC) staining and intracerebral haemorrhage evaluation (see section 3.3.11).

A separate group of C57 ischaemic mice (n=8), receiving the 0.8 mg *therapeutic dose* of NC-W intraarterially, were followed for 4 weeks when under deep anaesthesia blood was collected from the right ventricle in EDTA tubes for biochemical analysis. Plasma control samples were also included from naïve C57 mice (n=8) and ischaemic C57 mice without treatment followed at 48 h (n=4) and at 4 weeks (n=8) (**Figure 13**).

Safety

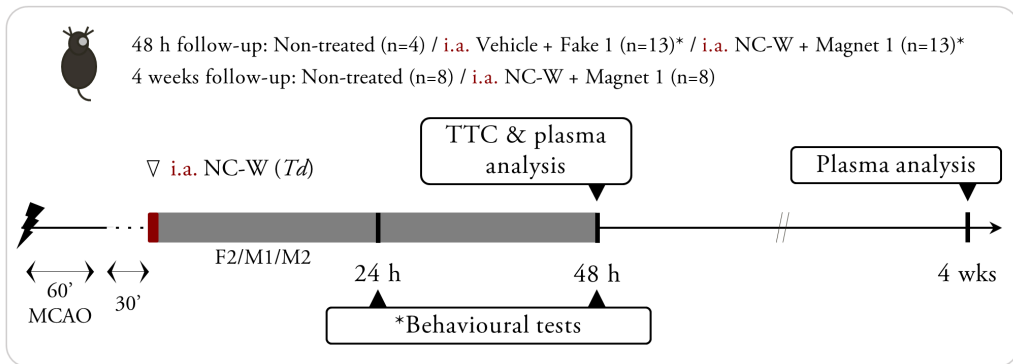


**Figure 13.** Scheme of the experimental design for the *Safety study*, using ischaemic C57 mice receiving 0.8 mg i.a. NC-W (*Td* = *Therapeutic dose*).

**Biodistribution study 5: secretome brain release upon hyperacute i.a. NC-CM administration after cerebral ischaemia**

To study whether the cargo secretome was efficiently delivered to the ischaemic brain upon hyperacute i.a. NC-CM administration after cerebral ischaemia (*Biodistribution dose*), a total of 7 mice were followed for 3 h and euthanised to analyse the secretome proteins in brain homogenates (**Figure 14**).

Biodistribution 5

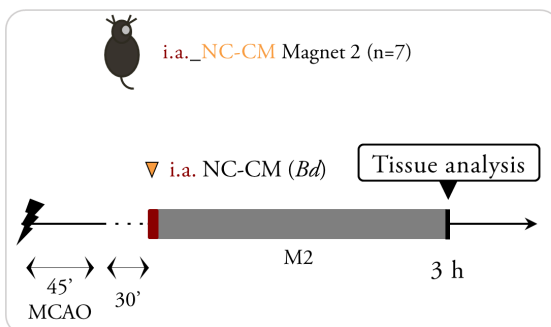


**Figure 14.** Scheme of the experimental design for *Biodistribution study 5*, using ischaemic C57 mice receiving 1.6 mg i.a. NC-CM (*Bd* = *Biodistribution dose*).

### Biodistribution study 6: long-term therapeutic NC biodistribution in cerebral ischaemia

To study the biodistribution along time following the protocol of choice for therapeutic application (i.a. administration of the 0.8 mg *therapeutic dose* of Cy5\_NC-CM, and 3 h magnetic retention with M2), a total of 14 C57 mice were randomly divided into the short-term (48 h post-administration) and long-term (7 days after administration) groups for *in vivo* and *ex vivo* FMI (Figure 15).

#### Biodistribution 6

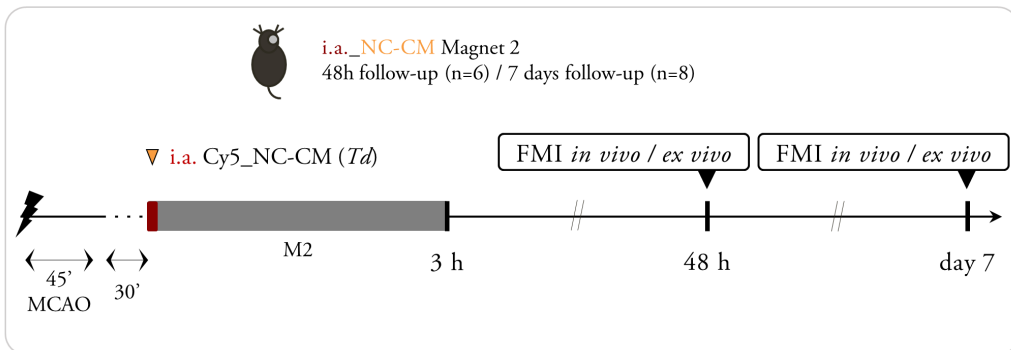


**Figure 15.** Scheme of the experimental design for *Biodistribution study 6*, using ischaemic C57 mice receiving 0.8 mg i.a. Cy5-labelled NC-CM ( $T_d = \textit{Therapeutic dose}$ ).

#### Efficacy study 1

To study the therapeutic efficacy of EPCs-CM encapsulation into magnetic PLGA NCs and hyperacute endovascular administration after cerebral ischaemia, the nanotargeted CM was evaluated together with the non-encapsulated free-secretome (f-CM). To emulate the equivalent *therapeutic dose* of the NC-CM after encapsulation-administration-release, an estimated dose of 7  $\mu\text{g}$  of f-CM was calculated based on the 15 mg/mL concentration of the cCM for encapsulation, and the estimated drug loading in the nanocarriers (section 4.2.2 and Table 8).

To assess the short-term efficacy, a total of 35 C57 ischaemic mice were randomly assigned into 3 groups: the vehicle group receiving 150  $\mu\text{L}$  of saline ( $n=12$ ), a

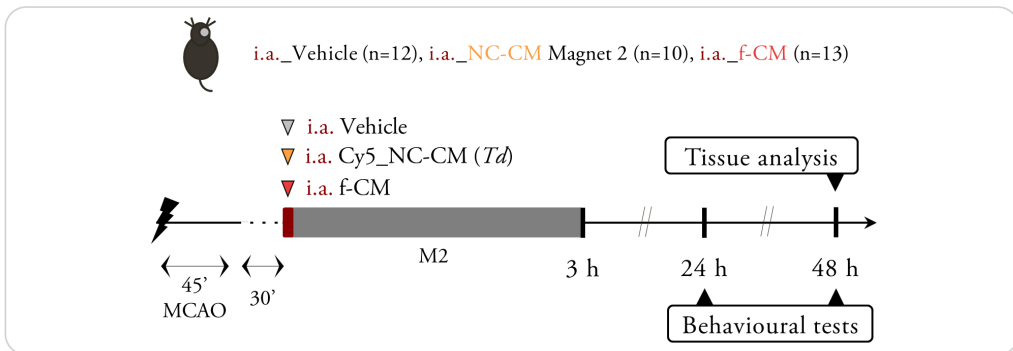


treatment group receiving the 0.8 mg *therapeutic dose* of NC-CM in 150  $\mu$ L of saline with a magnet (M2) (n=10), and a treatment group receiving 7  $\mu$ g of f-CM in 150  $\mu$ L of saline (n=13); **Figure 16**.

### Efficacy study 2

To assess the long-term efficacy, a total of 28 C57 ischaemic mice were randomly assigned into 3 groups: the vehicle group receiving 150  $\mu$ L of saline (n=10), a treatment group receiving the 0.8 mg *therapeutic dose* of NC-CM in 150  $\mu$ L of saline with a magnet (M2) (n=9), and a treatment group receiving 7  $\mu$ g of f-CM in 150  $\mu$ L of saline (n=9); see **Figure 16**. The safety of the therapeutic Cy5\_NC-CM and f-CM was also assessed in animals from *Efficacy studies 1 and 2* through the evaluation of plasma toxicity markers (see section 3.3.8).

#### Efficacy 1



#### Efficacy 2

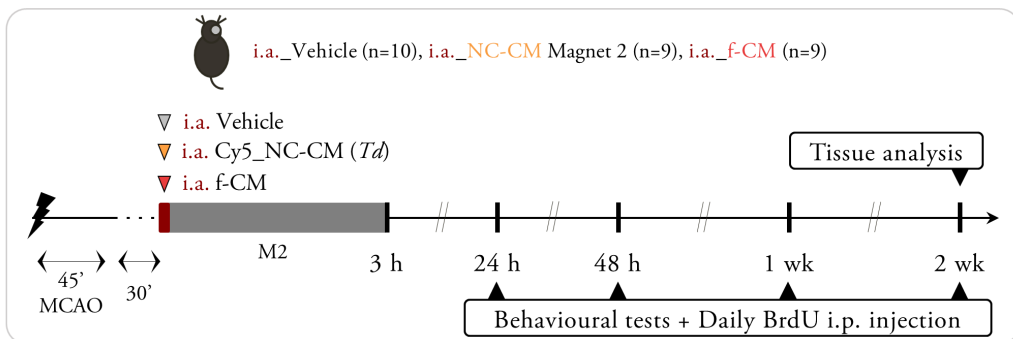


**Figure 16.** Scheme of the experimental design for *Efficacy studies 1 and 2*, using ischaemic C57 mice receiving 0.8 mg of i.a. Cy5-labelled NC-CM (*Td* = *Therapeutic dose*) or 7  $\mu$ g of f-CM.

Table 6. Animals used for the study of nanocarriers delivery in cerebral ischaemia

	Characterisation of the nanotargeted approach				Therapeutic application of the nanoformulation				
	BD-1	BD-2	BD-3	BD-4	Safety	BD-5	BD-6	Efficacy 1	Efficacy 2
<b>Total</b>	50	38	35	17	86	9	22	44	79
<b>Controls</b>	14	15	9	0	8	2	4	0	0
<b>Excluded</b>	8	4	2	0	11	0	0	5	16
<b>Deaths</b>	2	4	8	0	21	0	4	4	35
<b>Included</b>	26	15	16	17	46	7	14	35	28
<b>Strain</b>	Balbc AnNRj	Balbc AnNRj	C57BL/6jRj	C57BL/6jRj	C57BL/6jRj	C57BL/6jRj	C57BL/6jRj	C57BL/6jRj	C57BL/6jRj
<b>MCAO</b>	-	-	60 min	60 min	60 min	45 min	45 min	45 min	45 min
<b>Treatment</b>	Cy7.5-NC ( <i>Bd</i> )	Cy7.5-NC ( <i>Bd</i> )	Cy7.5-NC ( <i>Td</i> )	Cy7.5-NC ( <i>Td</i> )	Vehicle / NC ( <i>Td</i> )	Cy5-NC-CM ( <i>Bd</i> )	Cy5-NC-CM ( <i>Td</i> )	Vehicle / Cy5-NC-CM ( <i>Td</i> ) / F-CM (~ <i>Td</i> )	Vehicle / Cy5-NC-CM ( <i>Td</i> ) / F-CM (~ <i>Td</i> )
<b>Route, Magnet</b>	<i>i.a.</i> / <i>i.v.</i> , M1 (30 min)	<i>i.a.</i> / <i>i.v.</i> , M1 (30 min)	<i>i.a.</i> , M2 (3 h)	<i>i.a.</i> , M2 (3 h)	<i>i.a.</i> , M1 (48 h)	<i>i.a.</i> , M2 (3 h)	<i>i.a.</i> , M2 (3 h)	<i>i.a.</i> , M2 (3 h)	<i>i.a.</i> , M2 (3 h)
<b>Experiments</b>	FMI (30min-3h)	FMI (30min-3h)	FMI (3h-48h)	MRI (48h), Prussian blue (48h)	Functional tests (24h-48h), Infarct & HT (48h), Toxicity (48h-4wk)	ELISA (3h)	FMI (48h-1wk), IF (48h)	Functional tests (24h-48h), Infarct & HT (48h), WB brain vessels (48h), MPX-ELISA total brain (48h), Toxicity (48h)	Functional tests (24h-2wk), IF & FJC (2wk), MPX-ELISA (2wk), Toxicity (2wk)

BD: Biodistribution, *Bd*: Biodistribution dose, *Td*: Therapeutic dose, HT: haemorrhagic transformation, IF: immunofluorescence, MPX: multiplex, FJC: fluoro-jade C

### 3.3.2. MCAO surgery

C57 mice were subjected to 60 min MCAO by introducing an intraluminal filament through the right internal carotid artery (ICA), as described elsewhere.<sup>193</sup> All animals were anaesthetised with isoflurane via facemask (5% for induction, 1.5% for maintenance in air, 79% N<sub>2</sub>:21% O<sub>2</sub>). Body temperature was maintained at 37°C using a self-regulated heating pad connected to a rectal probe. Mice eyes were protected from corneal damage during surgery using an ophthalmic lubricating ointment (Lipolac™; Angelini Farmaceutica, Barcelona, Spain), and analgesia (subcutaneous buprenorphine 0.1 mg/kg; Divasa Farma-Vic S.A., Barcelona, Spain) was given before starting the surgical procedure and daily during the first 5 days after the surgery to minimise their pain and discomfort. Additionally, 0.5 mL of saline were daily administered subcutaneously for post-surgical recovery during the first 5 days. Nutritionally fortified water gel (DietGel Recovery®, ClearH2O®, Portland, ME, USA) was given to mice from *Biodistribution study 4*, *Safety study (long-term)* and *Efficacy study 2* one week prior to surgery for habituation and was available *ad libitum* after surgery to facilitate food intake and favour mid-term survival.

After surgical exposure of the right common carotid artery (CCA) bifurcation into the external carotid artery (ECA) and the ICA, a silicone-coated nylon monofilament (Docol Corporation, Sharon, MA, USA, reference number: 602256PK10Re) was introduced through the ECA and directed towards the ICA to occlude the MCA. Occlusion was monitored by laser doppler flowmetry using a flexible fiberoptic probe (Moor Instruments, Devon, UK) placed on the surface of the distal MCA branch, and confirmed by the decrease of the registered cerebral blood flow (CBF) >80% (100% being considered as the pre-ischaemia CBF value). After occlusion, animals woke up and were re-anaesthetised for reperfusion 60 min later as described above by removing the monofilament. Only animals recovering >80% of CBF after filament removal were finally included.

### 3.3.3. Administration route and magnetic retention

Systemic i.v. administration through the tail vein and i.a. administration through the ICA of the NCs dispersed in saline (either 1.6 or 0.8 mg/animal, corresponding to the *biodistribution* and *therapeutic doses*, respectively) were conducted. The *therapeutic dose* is based on the corresponding iron load for the recommended doses of the FDA-approved iron Endorem® for human use.<sup>194</sup>

The surgical procedure for the i.a. administration was protocolled in the intraluminal MCAO model by cannulating the ECA 30 min after reperfusion under anaesthesia as described above, with a polyimide micro-catheter (0.2-0.22 mm outside diameter, 0.14-0.15 mm inside diameter; MicroLumen, Oldsmar, FL) directed towards the ICA and connected to an infusion pump (PHD 2000 Advance Syringe Pump, Harvard Apparatus, Holliston, Massachusetts, US) at an infusion rate of 75 mL/min, total volume 150 mL (**Figure 17**). Non-ischaemic animals underwent the same surgical procedure as for the intraluminal MCAO model except that the micro-catheter was introduced through the ECA without previously occluding the MCA. Note that the pterygopalatine artery was permanently sutured in all cases to avoid perfusion towards off-target areas. The cortical CBF was registered before, during and after i.a. administration of the NCs as described above and according to the experimental design in each group. On the other hand, for i.v. administrations a volume of 150 mL of the NCs suspension was administered using a 25G needle through the lateral tail vein after vessel dilatation using a heat lamp.

For magnetic retention of the administered NCs, the magnet/fake device was implanted prior to administration, under anaesthesia, on the right (ipsilateral) hemisphere and attached to the skull with superglue. The skin was closed over the device using a surgical glue (Histoacryl®) and was removed after the corresponding magnetic retention time.

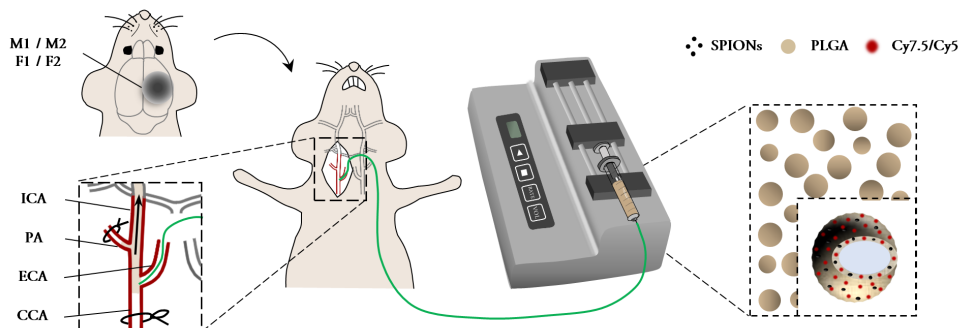


**Figure 17. Endovascular-ICA administration of functionalised NCs.** Scheme of the subcutaneous magnet implantation and the surgical procedure for i.a. NCs administration.

### 3.3.4. Fluorescent Molecular Imaging (FMI)

FMI was performed to characterise the NC batches fluorescence *in vitro* and to track the NCs biodistribution *in vivo* and *ex vivo* in single organs, using a Xenogen IVIS® spectrum imaging system (Perkin Elmer, Waltham, MA) for Cy7.5-labelled NCs, and an IVIS® Lumina LT Series III imaging system (Perkin Elmer, Waltham, MA) for Cy5-labelled NCs. All acquisition settings are detailed in **Table 7**.

For *in vitro* FMI, a series of concentrations ranging from 0.1 mg/mL to 1.5 mg/mL of Cy7.5/Cy5-labelled NC in 100  $\mu$ L of saline were prepared for each batch in a 96-well plate and imaged as detailed above.

The general protocol for the *in vivo* biodistribution studies started with mice being anaesthetised with isoflurane via facemask (5% for induction, 1.5% for maintenance in 95% O<sub>2</sub>) and images being acquired at different time points post-injection according to each experimental design in dorsal and ventral views of the whole body. Between *in vivo* image acquisitions mice recovered from anaesthesia in temperature-controlled recovery cages.

Animals from *Biodistribution studies 1-3* were euthanised by cervical dislocation under anaesthesia after the last *in vivo* acquisition and brain, heart, lungs, liver, spleen, kidneys and bladder were dissected for the *ex vivo* FMI. Animals from *Biodistribution study 6* were euthanised under anaesthesia by exsanguination followed by transcatheter perfusion with cold saline after the last *in vivo* acquisition and brain, lungs, liver, spleen and kidneys were dissected for the *ex vivo* FMI. Animals from the *Pilot study in pigs* (section 3.3.18) were euthanised by i.v. sodium thiopental injection and the brain was removed for the *ex vivo* FMI. All organs were imaged in dorsal and ventral views.

**Table 7. FMI acquisition settings.**

	Excitation wavelength (nm)	Emission wavelength (nm)
<b>Cy7.5-labelled NCs<sup>a</sup></b>		
<i>In vitro</i>	710	820
<i>In vivo</i>	710	820
<i>Ex vivo</i>	745	820
<b>Cy5-labelled NCs<sup>b</sup></b>		
<i>In vitro</i>	640	732
<i>In vivo</i>	640	732
<i>Ex vivo</i>	640	732

<sup>a</sup> Xenogen IVIS® spectrum imaging system

<sup>b</sup> IVIS® Lumina LT Series III imaging system

#### 3.3.4.1. FMI analysis

Background control animals who did not receive fluorescent NCs were also imaged in each *in vivo* and *ex vivo* FMI acquisition for background measures. For quantification, circular regions of interest (ROIs) were manually drawn surrounding the fluorescence signal and total radiant efficiency (TRE; [photons/s]/[ $\mu\text{W}/\text{cm}^2$ ]) was measured using the Living Image software (Perkin Elmer, Waltham, MA) and corrected by the TRE from the corresponding ROI in the background control animal. More specifically, for the *in vivo* analysis, brain and abdominal ROIs were drawn on the dorsal and ventral images, respectively, and for the *ex vivo* analysis, ROIs of each dissected organ were drawn in both dorsal and ventral positions (mean

values of both views were used for the analysis). All images were analysed blinded to the treatment group.

### 3.3.5. Magnetic Resonance Imaging (MRI)

Mice were anaesthetised with isoflurane via facemask (5% for induction, 0.5-1.5% for maintenance in 1 L/min O<sub>2</sub>) with respiratory frequency monitoring, and a recirculation water heating system integrated into the scanner bed was used to control the body temperature. T2-weighted fast spin-echo images were initially obtained in axial, sagittal and coronal planes to be used as reference images using the following parameters: effective echo time (TE<sub>eff</sub>) = 36 ms, TR = 2s, echo train length (ETL) = 8, FOV = 1.92×1.92 cm<sup>2</sup>, matrix = 128×128, and slice thickness = 1 mm. Then, coronal high-resolution MRI sections were determined over a 9.3 mm block starting at the olfactory bulb and towards the cerebellum. High-resolution T2WI (HR-T2WI) were acquired using a fast spin-echo sequence with ETL = 8, TE<sub>eff</sub> / TR = 60 ms / 4.2 s, FOV=1.6×1.6 cm<sup>2</sup>, matrix = 256×256, 17 contiguous slices with slice thickness = 0.5 mm and 0.05 mm gap between them. High-resolution T2\*WI (HR-T2\*WI) were acquired using a spoiled gradient-echo sequence with TE<sub>eff</sub> / TR = 10.5 ms / 350 ms, FA = 40°, FOV = 1.6×1.6 cm<sup>2</sup>, matrix = 320×320, 17 slices covering the same brain region as in HR-T2WI with slice thickness = 0.5 mm and 0.05 mm gap between them.

#### 3.3.5.1. MRI analysis

The superparamagnetic properties of the SPIONs embedded in the surface of the nanocarriers show good performance as transverse relaxation (T<sub>2</sub>) contrast agents, thus facilitating their tissue tracking as hypointense signal spots. To quantify the signal of NCs present in the brain after endovascular-ICA administration, ROIs were drawn dividing the cortical and subcortical areas of the ipsilateral and contralateral brain hemispheres on the T<sub>2</sub>\*WI. After a standardised pre-processing of the images, the number, area, and average size of the NC hypointense signals within each ROI

were analysed using the particle analysis tool from the ImageJ software, blinded to the treatment group.

### 3.3.6. Functional tests

Neurological deficits were evaluated in mice from *Safety study* and *Efficacy studies 1 and 2* by a researcher blinded to the treatments with a score based on a composite neurological scale<sup>195,196</sup> at 24 h, 48 h, 1 week and 2 weeks after MCAO (according to each experimental design). The neurological score ranges from 0 (healthy) to 39 and represents the sum of the general deficits (0-13): hair [0-2], ears [0-2], eyes [0-3], posture [0-3] spontaneous activity [0-3]; and focal deficits (0-26): body symmetry [0-2], gait [0-4], climbing on a surface held at 45° [0-3], circling behaviour [0-3], front limb symmetry [0-4], compulsory circling [0-3], whiskers response to a light touch [0-4] and gripping of the forepaws [0-3].

The forelimb force was also assessed in the animals from *Safety study* and *Efficacy studies 1 and 2* with the grip strength test as previously described.<sup>197</sup> The forelimb force was assessed as follows: habituation to the test was performed one day prior to the surgery to avoid neophobic behaviours and the grip strength was measured before the surgery and at 24 h, 48 h, 1 week and 2 weeks after MCAO (according to each experimental design). The grip strength score was recorded as the mean of 6 repeated measures.

### 3.3.7. Tissue sampling and processing

All animals were euthanised under deep anaesthesia by exsanguination followed by transcardial perfusion with cold saline, except mice from *Biodistribution studies 1, 2, and 3*, which were euthanised by cervical dislocation.

Brain, liver and spleen were collected from animals in *Biodistribution study 4*, fixed with 10% formalin, paraffin-embedded and sliced in 5 mm-thick sections with a microtome to confirm the presence of NC in the brain *ex vivo* (see sections 3.3.9 and 3.3.10).



For *Safety study* and *Efficacy study 1* the brains were collected and freshly sliced in 1 mm-thick coronal slices for infarct volume and haemorrhage evaluation (see section 3.3.11). The TTC-stained brains from *Efficacy study 1* were separated into the ipsilateral and contralateral hemispheres for homogenisation and brain vessels isolation, by following the protocol detailed in section 3.3.12 (**Figure 18**).

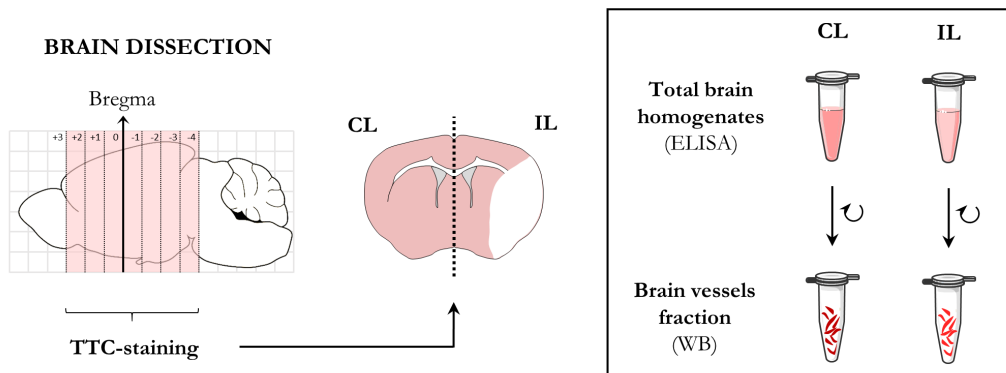


**Figure 18.** Dissection and processing of the brains collected in the short-term *Efficacy study 1*.

The brains from *Biodistribution study 5* were separated into the ipsilateral and contralateral hemispheres for homogenisation and brain vessels isolation, by following the protocol detailed in section 3.3.12.

For *Biodistribution study 6*, the brain was fixed in 4% paraformaldehyde overnight at 4°C before cryoprotection with 30% sucrose. The brain was then frozen and embedded in optimal cutting temperature (OCT), sliced in 12 µm-thick coronal sections with a cryostat and stored at -80°C until use.

For *Efficacy study 2*, the brain was dissected to collect a 1 mm-thick coronal slice starting at the bregma anatomical point as the core of the infarct tissue,<sup>198</sup> and the ipsilateral and contralateral hemispheres were separated, snap-frozen in liquid nitrogen and stored at -80°C until use. The remaining anterior and posterior brain fractions were fixed in 4% paraformaldehyde overnight at 4°C before cryoprotection with 30% sucrose. The brain fractions were frozen and embedded in OCT, sliced in

12  $\mu\text{m}$ -thick coronal sections with a cryostat and stored at  $-80^{\circ}\text{C}$  until use. The coronal slices were obtained serially starting from the respective posterior and anterior sides adjacent to the 1 mm-thick coronal slice previously collected for homogenates (Figure 19).

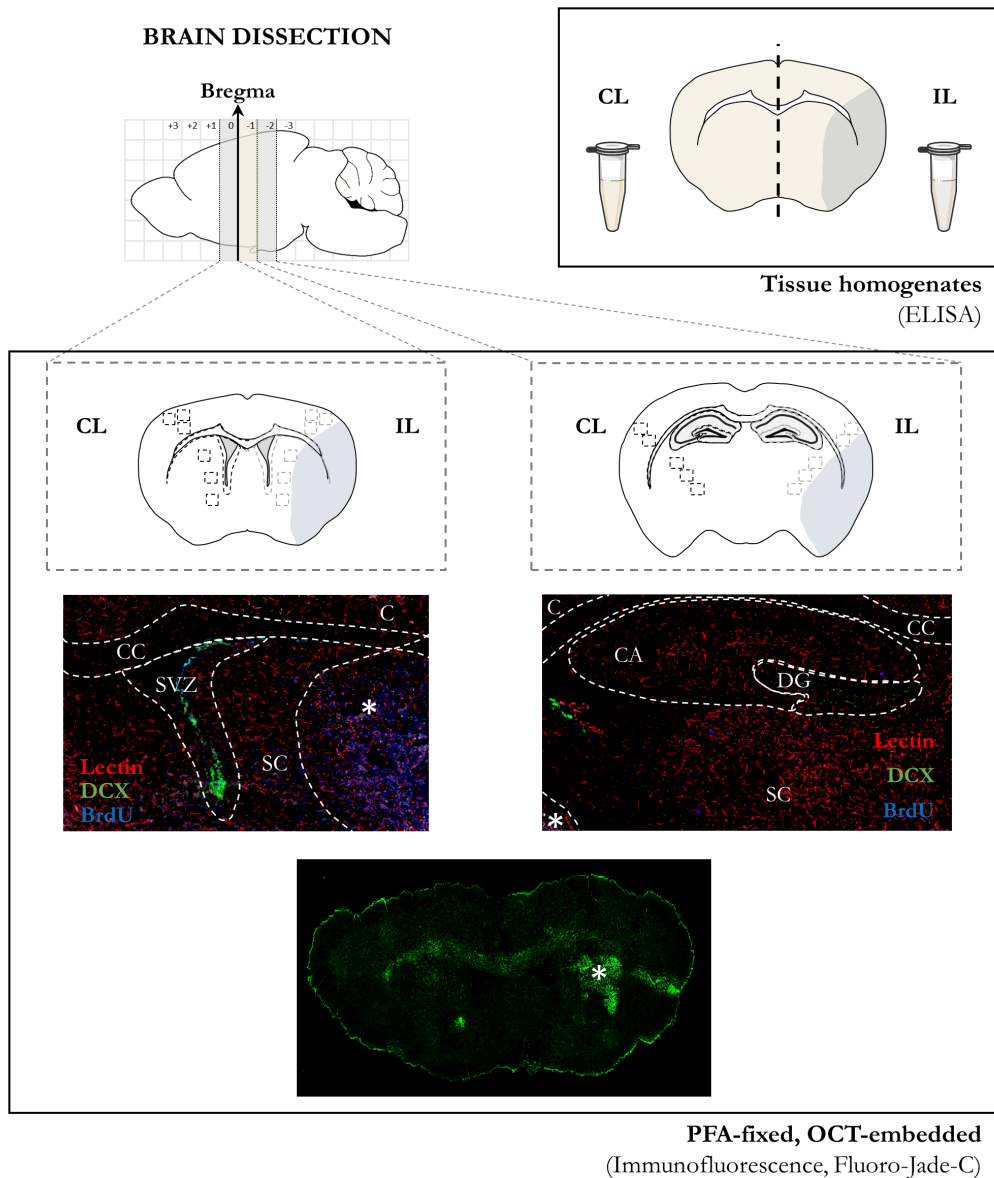


**Figure 19.** Dissection and processing of the brains from the long-term *Efficacy study 2*. Scheme (upper left) of the dissection of the ischaemic brain into a coronal slice

for homogenates (0 to -1 from bregma; upper right), and anterior and posterior brain fractions for tissue staining in the SVZ and hippocampal regions (below). PFA: paraformaldehyde, OCT: optimal cutting temperature, IL: ipsilateral, CL: contralateral, C: cortex, CC: corpus callosum, SC: subcortex. Asterisk showing the infarcted tissue.

### 3.3.8. Plasma biochemical analysis

Venous blood obtained from the right ventricle by cardiac puncture and collected in EDTA tubes was centrifuged (1,500 x g, 10 min at 4°C) to obtain plasma, which was stored at -80°C until analysis. Hepatic/pancreatic/renal toxicity was assessed by the plasmatic levels of alanine aminotransferase (ALT), aspartate aminotransferase (AST), creatine kinase (CK),  $\alpha$ -amylase, lipase, creatinine, urea, and  $\text{Na}^{2+}$  using an Olympus AU5800 clinical chemistry analyser. Haemolysed, icteric and lipaemic plasma samples were rejected from the analysis of the biochemical parameters described above.

### 3.3.9. Prussian blue staining

To indirectly confirm the presence of the NCs in the brain, we performed a specific staining for ferric iron as part of the SPIONs of the NCs. After deparaffinisation and rehydration, the sections were stained with a Prussian blue iron stain kit (Polysciences Inc, USA) following the manufacturer's protocol except for that potassium ferrocyanide:hydrochloric acid (HCl) mix solution was kept for a total of 40 min and nuclear Fast Red for 1 min. Images were acquired after dehydration and mounting with DPX medium (Ref. 06522, Sigma-Aldrich, St. Louis, USA) with a transmitted light microscope (Leica, Germany) and an automatic slide scanner (PANNORAMIC MIDI II, 3DHISTECH Ltd, Hungary).

### 3.3.10. Lectin vessel staining

To confirm the distribution of NCs in brain micro-vessel structures at 48 h after ischaemia and i.a. administration (as seen by Prussian blue staining in *Biodistribution study 4*), the vasculature was stained in consecutive brain slices from mice euthanised

at 48 h post-administration (*Biodistribution study 6*) with lectin-fluorescein isothiocyanate (FITC) as follows. After thawing and rehydration, the sections were incubated for 2 h with lectin-FITC from *Lycopersicon esculentum* (Ref. L0401, Sigma-Aldrich, Germany) diluted 1:200 in PBS-1% Tween20 (PBS-T). After dehydration and mounting with Fluoroshield mounting medium with DAPI (F6057, Sigma), images were acquired with a confocal laser scanning microscope (LSM980, Zeiss, Germany).

### 3.3.11. Infarct volume and intracerebral haemorrhage evaluation

Ischaemic C57 mice from the *Safety study* were euthanised at 48 h after administration post-reperfusion by cervical dislocation. Brains were removed, sliced in 1 mm thick coronal sections and stained with TTC (Sigma, St.Louis, MO, USA) in saline at room temperature (RT) for 15 min. Infarct volumes were quantified by a treatment-blinded researcher with the ImageJ software and corrected by oedema as previously described.<sup>199</sup> The number and extent of haemorrhagic events was determined by 3 independent treatment-blinded raters using a semi-quantitative method adapted from the ECASS classification as described elsewhere<sup>200</sup> by giving 0 to 4 scores as follows: 0 = absence of haemorrhage, 1–2 = increasing grades of haemorrhage infarction (HI1 and HI2), and 3–4 = homogeneous parenchymal haematomas of increasing grades (PH1 and PH2). The haemorrhage volume was also quantified with ImageJ following the same protocol as for the infarct volume.

### 3.3.12. Brain vessels isolation

The TTC-stained brain sections from *Efficacy study 1* were processed to obtain a total brain and a vascular-enriched fraction, as described in section 3.3.7 (**Figure 18**). The ipsilateral and contralateral hemispheres of the brain samples from *Efficacy study 1* were homogenised and processed separately to obtain the corresponding i) total brain homogenate fraction, and ii) a vascular-enriched fraction. The vascular-enriched fraction was isolated following a protocol previously described,<sup>201</sup> modified as follows.

Each brain hemisphere was homogenised in 2 mL of cold sucrose buffer (0.32 M sucrose (Sigma-Aldrich), 5 mM Hepes (Gibco)) using a Dounce homogeniser (55 times with A and 25 times with B pestle). The homogenate was transferred into a 15 mL tube together with 1 mL of buffer used to rinse the homogeniser. The final 3 mL homogenate was centrifuged (10 min, 1,000 x g, 4°C), after keeping 100 µL as the **total fraction**. After centrifugation, the pellet was used to obtain the vascular-enriched fraction, and the aforementioned centrifugation was repeated after resuspending the pellet in 3 mL of sucrose buffer. The new pellet was then resuspended in 1 mL of sucrose buffer and centrifuged (10 min, 400 x g, 4°C), repeating this step twice. The final pellet was lysed in 150 µL of RIPA lysis buffer (Sigma-Aldrich) containing protease inhibitors (1% phenylmethanesulfonyl fluoride-PMSF (Sigma-Aldrich), 0.5% aprotinin (Sigma-Aldrich), and 0.5% Phosphatase inhibitor cocktail-3 (Sigma-Aldrich)) for 15 min at 4°C and then centrifuged (15 min, 15,000 x g, 4°C) to obtain the final supernatant as the **vascular-enriched fraction**. The vascular-enriched fraction was used to evaluate BBB junctional proteins' expression (section 3.3.12), while the total brain fraction was used to assess neuro-inflammatory markers (section 3.3.13).

### 3.3.13. Western blot

The protein content from the brain vessels fraction, obtained as described in the previous section, was determined by the bicinchoninic acid (BCA) assay (Thermo Scientific™, IL, USA). A total amount of 20 µg of protein was mixed with 4x Laemmli Buffer (BioRad Cat#1610747) and 10% of 2-mercaptoethanol, heated at 95°C for 5 min. Then, the samples were subjected to electrophoresis (200 V, 45 min) in 10% (VE-Cadherin and zonula occludens 1 (ZO-1)) or 12% (Claudin-5 and Occludin) polyacrylamide electrophoresis gels and transferred (100 V, 1 h) into nitrocellulose membranes (Amersham™ Protein™ Premium 0.45 µM #10600003) using the BioRad Criterion™ Blotter (100 V, 1 h). Next, membranes were blocked for 1 h with 5% of skimmed milk in Tris-buffered saline containing 0.1% Tween20 (TBS-T) and 3% of normal goat serum (Sigma-Aldrich #G6767), and

incubated overnight at 4°C on a shaker with the following antibodies (1:1,000 in TBS-T): anti-Claudin-5 (Ab15106), anti-Occludin (Ab31721), anti-ZO-1 (Ab216880), or anti-VE-Cadherin (Ab33168). The membranes were then washed 3 times with TBS-T and incubated with a horseradish peroxidase-conjugated secondary antibody (goat anti-rabbit, Dako/Agilent Technologies) at 1:8,000 for 1 h at RT with gentle agitation. Finally, all membranes were washed 3 times with TBS-T and briefly incubated (5 min at RT) with the ECLTM Western Blotting detection reagent (Amersham, RPN2236) to visualise the chemiluminescence signal using the WB Imaging System Azure c600 (Azure Biosystems). A molecular weight marker (Precision Plus Protein™ All Blue standards, BioRad #1610373) was also run for reference values. Following the immunoblots of desirable targets, membranes were rinsed 3 times (10 min) and blocked for 30 min with 5% of skimmed milk in TBS-T. Afterwards, the membranes were stained with Coomassie Blue solution (Coomassie Blue R250 0.1% diluted in water/methanol/acetic acid (5:4:1)) for 1 min, and rigorously rinsed with a solution containing water/methanol/acetic acid (5:4:1) until removal of Coomassie Blue's excess. Finally, the membranes were dried and images were obtained using the WB Imaging System Azure c600 (Azure Biosystems).

The software TotalLab TL 100 1D gel Analysis was used for quantification of the relative immunoblots densities of the target proteins. Optical densities of the Coomassie Blue-stained membranes for total protein measurements were quantified using ImageJ. A standard mathematical correction was used based on the total protein to compensate for variability within samples (Bio-Rad Laboratories, Inc), as follows. A random reference lane was selected on the blot. Then a normalisation factor was determined for each sample by dividing the signal from the reference lane by the different sample lanes. This normalisation factor was then applied to the protein of interest in the tested samples by multiplying the optical density from the target protein by the corresponding normalisation factor.

### 3.3.14. Multiplexed enzyme-linked immunosorbent assays (ELISA)

A configurable multiplexed ELISA was used to investigate the inflammatory state in the brain samples (total homogenate fraction) collected 48 h after i.a. treatment with vehicle, NC-CM or f-CM (n=10/group) in ischaemic mice from the short-term *Efficacy study 1* (MILLIPLEX® Mouse High Sensitivity T Cell Magnetic Bead 11-plex Panel, MHSTCMAG-70K, MilliporeSigma). The following cytokines were multiplexed: granulocyte-macrophage colony-stimulating factor (GM-CSF), interferon-gamma (IFN $\gamma$ ), interleukin (IL)-1 $\alpha$  (IL-1 $\alpha$ ), IL-1 $\beta$ , IL-4, IL-6, IL-10, C-X-C motif chemokine ligand 1/keratinocyte-derived chemokine (CXCL1/KC), monocyte chemoattractant protein 1 (MCP-1), CXCL2/macrophage inflammatory protein 2 (MIP-2), and tumour necrosis factor  $\alpha$  (TNF $\alpha$ ).

For the brain homogenates (bregma coronal slice) from ischaemic mice at 2 weeks after receiving i.a. vehicle, NC-CM or f-CM (n=6-7/group, long-term *Efficacy study 2*), a configurable multiplexed ELISA was used to investigate angiogenesis-related proteins (MILLIPLEX® MAP Kit Mouse Angiogenesis/Growth Factor Magnetic Bead Panel, MAGPMAX-24K, MilliporeSigma). The following cytokines were multiplexed: Angiopoietin-2, G-CSF, EGF, IL-6, Endoglin, Endothelin-1, FGF-2, HGF, soluble CD31 / platelet endothelial cell adhesion molecule (sCD31/PECAM-1), MCP-1, SDF-1, and VEGF-A.

Both the total brain fraction for the neuro-inflammation multiplex (short-term *Efficacy study 1*) and the brain homogenates for the angiogenesis multiplex (long-term *Efficacy study 2*) were processed in lysis buffer (50 mM Tris-HCl, 150 mM NaCl, 5 mM CaCl<sub>2</sub>, 0.05% Brij35, 0.02% NaN<sub>3</sub>, 1% Triton-X-100) containing protease inhibitors (1% PMSF, 0.5% aprotinin (Sigma-Aldrich)), for 15 min at 4°C and then centrifuged (15 min, 15,000 x g, 4°C) to obtain the final supernatant.

All the results were analysed in duplicate with Luminex technology in a MAGPIX™ instrument, and samples with a coefficient of variation > 20% were excluded. In all cases, data were corrected by the amount of total protein determined by BCA assay.

### 3.3.15. Singleplex ELISA

A singleplex ELISA was used to determine the presence of Angiogenin (Human Angiogenin Quantikine ELISA Kit, DAN00, R&D systems), as a component of the administered EPCs-secretome, and the presence of urokinase-type plasminogen activator (uPA) (DUPA00, R&D SYSTEMS, MN, USA), as an alternative EPCs-CM component. The total brain homogenates and brain vessel fractions obtained from *Biodistribution study 6* were tested with the Angiogenin ELISA, while brain homogenates from naïve mice were tested with the uPA ELISA in order to discard mouse uPA cross-reactivity.

All samples were processed in lysis buffer, as described in section 3.3.14. All the results were analysed in duplicate and the optical densities were measured in a Synergy Mx microplate reader (BioTek Instruments Inc, USA). Samples falling under the range of the standard curve or with a coefficient of variation > 20% were excluded.

### 3.3.16. Immunofluorescence

To label dividing cells, mice from *Efficacy study 2* received daily single intraperitoneal injections of 5-Bromo-2'-deoxyuridine (BrdU, 50 mg/kg in saline, B9285, Sigma-Aldrich, USA) beginning at 24 h after MCAO and until euthanasia. Before euthanasia, mice were injected with Dylight 594-labelled tomato lectin (40 µg/mouse, DL-1177, Vector Laboratories, USA), which was allowed to circulate for 10 min to label functional blood vessels prior to exsanguination and intracardiac saline perfusion.

A minimum of 3 serial coronal sections were obtained between 0 and +1 from bregma, in the corresponding SVZ region, and a minimum of 3 serial coronal sections between -1 and -2 from bregma, in the corresponding hippocampal regions. Immunostaining with antibodies for proliferating cells (1:100 rat anti-BrdU; ab6326, Abcam, UK), and neuroblasts (1:200 rabbit anti-doublecortin, DCX; ab207175, Abcam, UK) was performed as follows.



The sections were thawed at RT for 30 min and transferred to PBS-T for hydration for 5 min. Then, cells were permeabilised with 0.3% PBS-Triton X-100 for 5 min. BrdU-stained sections were pre-treated with 2 M HCl-PBS for 1 h to open the deoxyribonucleic acid (DNA) structure and neutralised with 0.1 M borate buffer for 10 min. The sections were then blocked for 1 h in PBS-T blocking buffer containing 1% bovine serum albumin (BSA) and 5% goat serum. Primary antibodies were applied in blocking buffer overnight at 4°C and the slices were washed 3 times for 5 min at RT in PBS-T, followed by 1 h incubation at RT with the following secondary antibodies (1:500 in blocking buffer): Alexa Fluor 488 goat anti-rabbit IgG, and Alexa Fluor 405 goat anti-rat IgG.

The slices were finally washed 3 times for 5 min at RT in PBS-T, and mounted in Vectashield™ Antifade Mounting Medium (Vector Laboratories, USA). The whole coronal slices were imaged with the digital scanner Panoramic 250 FLASH (3D HISTECH). For quantification, the DCX+, BrdU+ or Lectin+ fluorescence areas were measured in the ROIs defined within the peri-infarct cortical and subcortical regions (**Figure 19**) using ImageJ and expressed as  $\mu\text{m}^2$ .

### 3.3.17. Fluoro-Jade C staining

Fluoro-Jade® C (FJC) staining was used to label degenerating neurons in mice from *Efficacy study 2*. A minimum of 3 serial coronal sections were obtained between 0 and +1 from bregma, in the corresponding SVZ region (**Figure 19**), and stained with the FJC ready-to-dilute staining kit (Biosensis), following the manufacturer's protocol modified as follows. Briefly, the sections were thawed at 60°C for 1 h and transferred to 80% ethanol containing 1% sodium hydroxide in distilled water for 5 min and then washed in distilled water for 2 min. For fluorescent background blocking and contrast optimisation, the sections were then treated with 5% potassium permanganate for 10 min and washed in distilled water for 2 min. The sections were stained in 5% FJC in distilled water for 10 min, washed in distilled water for 2 min, the nuclei were stained with Fluoroshield mounting medium with DAPI (F6057,

Sigma), and washed 3 times in distilled water for 1 min. The slices were finally dried at 60°C for 10 min, cleared in xylene and mounted with DPX medium (Ref. 06522, Sigma-Aldrich, St. Louis, USA). The whole coronal slices were imaged with the digital scanner Pannoramic 250 FLASH (3D HISTECH).

### 3.3.18. Pilot endovascular delivery study in pigs

A pilot study was conducted in order to assess the feasibility of endovascular NC delivery in pigs, as a large animal model with a gyrencephalic brain, resembling the human brain anatomy. For this purpose, the pigs were reused from a previous interventional training course. The animals were kept under general anaesthesia for the entire duration of the intervention and subsequent pilot experiment, and were euthanised without recovery. All the procedures were approved by the Ethics Committee for Animal Experimentation of the Vall d'Hebron Research Institute (VHI; registration number 92/17) and conducted in compliance with the Spanish legislation and in accordance with the directives of the European Union (2010/63/EU).

For the pilot study, hybrid female pigs (Large White x Landrace) were used (30-35 Kg; around 3 months old), purchased from the animal centre A. M. Animalia Bianya S.L. (Girona, Spain), entered in the register of breeding centres, suppliers and users of laboratory animals with the number G9900009 (GLP n° BPL808CAT). The animals were previously acclimated to our facilities and housed in conventional pens for 7-10 days, with *ad libitum* water and fed 2 times a day with conventional pig's diet. The animals were housed with other pigs, and the pen's temperature was maintained at  $21 \pm 2^\circ\text{C}$ . The relative humidity ranged from 40-60%, air renovation consisted of 10-15 air changes per hour, and the photoperiod was 12:12 h day/night. All animals were subjected to a clinical examination by the VHIR veterinary team, and underwent a fasting of 12 h prior to surgery, maintaining free access to water with diluted sucrose.

The endovascular delivery of NCs was performed as follows. A micro-catheter was introduced through the femoral vein, directed towards the CCA and placed at the ascending pharyngeal artery, proximal to the rete mirabile, in order to administer Cy7.5/Cy5-labelled NC towards the MCA vascular territory.

Two different doses of Cy7.5-labelled NCs were tested in a preliminary experiment (40 mg or 80 mg in 50 mL of saline; n=1/group), administered at a controlled infusion rate of 1 L/min. Ten mL of saline were finally infused in order to recover the nanomaterial from the catheter's dead volume. After infusion, the animals were euthanised by i.v. sodium thiopental (2 g) injection, and the brain was removed for *ex vivo* FMI.

Since the highest dose was tolerable, a second experiment was performed in pigs receiving 80 mg of Cy5-labelled NCs in 50 mL of saline (n=3) at 1 L/min, plus 10 mL of saline to recover the NCs. Venous blood samples from the jugular vein were collected before, during (at 10, 20 and 30 min), and at the end of the infusion (approximately 5 mL per time point). After infusion, the animals were euthanised by i.v. sodium thiopental (2 g) injection, and the brain was removed for *ex vivo* FMI. The brain of an additional pig without NCs administration was also used for background measurements.

TRE was quantified on ROIs manually drawn for the ipsilateral and contralateral brain hemispheres, corrected by their control animal. The blood samples were centrifuged (1,500 x g, 15 min, 4°C) to collect the serum, which was used to measure the circulating NCs fluorescence at different time points after endovascular nanocarriers delivery. Briefly, 100 µL of each serum sample were distributed in duplicates in 96-well plates, and the fluorescence was measured in a microplate fluorescence reader ( $\lambda_{ex}/\lambda_{em}$  650 nm/750 nm; Synergy Mx microplate reader, BioTek Instruments Inc, USA). All values were corrected by the basal serum fluorescence.

### 3.4. *Ex vivo* magnetic retention in a humanised model

In order to assess the feasibility and efficacy of NCs endovascular delivery followed by magnetic retention for possible human use, a preliminary *ex vivo* experiment was conducted using a three-dimensional (3D)-printed human-based vascular model and the human magnet prototype M3.

**These experiments were carried out in collaboration with the Stroke Laboratory (VHIR), with the help of Dr. Marc Ribó and Jiahui Li.**

#### 3.4.1. 3D printing

Briefly, neurovascular model manufacturing comprises the following steps: (i) medical image segmentation to generate the 3D geometry of the vascular anatomy, (ii) mesh modelling to prepare a printable anatomical model, (iii) 3D printing configuration, and (iv) post-printing processing. The 3D supra-aortic model used for the present study was constructed as follows.

DICOM data from i.v. contrast computed tomography scans from anonymous patients, provided by the Neuroradiology unit at the Hospital of Vall d'Hebron, were imported and loaded in the 3DSlicer software to obtain the preliminary 3D geometry of the model, through opacity threshold segmentation. Then, using the Autodesk Meshmixer software, the 3D geometry was simplified into anatomically relevant vessels for mechanical thrombectomy, that is to say, carotid arteries (CCAs, ECAs, ICAs), MCAs, anterior carotid arteries (ACAs), anterior communicating artery (ACoA), vertebral arteries (VAs), basilar artery (BA), posterior cerebral arteries (PCAs), and posterior communicating arteries (PCoAs). The proximal and distal segments were also adapted to create connection points of the model to the flow loop system, and 1 mm thickness was added to the vessel walls to provide consistency. Finally, mesh errors were corrected, and the virtual model was exported from Autodesk Meshmixer to PreForm to configure the printing material, resolution, optimal geometry orientation, and support structure for 3D printing. The model was printed with commercially available photopolymer clear resin (FormLabs, Boston,

MA, USA) at a resolution of 100  $\mu\text{m}$  with a Form 3 Printer (FormLabs, Boston, MA, USA). For post-printing processing, the support structures were removed from the model, which was then immersed in isopropyl alcohol and exposed to 305 nm UV light at 60°C for 20 min.

A temporal bone was also 3D-printed using the same methodology, using the scaffold material Durable (FormLabs, Boston, MA, with a final average thickness of 4.46 mm (3.5-9.86 mm).

### 3.4.2. Micro-catheter-guided infusion and monitoring

Briefly, the magnet was attached to a 3D-printed temporal bone, close the MCA territory, and an artificial bloodstream was created within the vascular model as a closed circuit connected to a peristaltic infusion pump. A constant flow of 580 mL/min was set based on the CBF distribution within the vascular tree represented in our vascular model (receiving approximately an 82% of the total CBF, which is approximately 710 mL/min).<sup>202</sup>

Cy5-labelled magnetic nanocarriers were infused through endovascular delivery with a micro-catheter guided towards the MCA. Specific magnetic retention in the targeted ipsilateral MCA of the nanocarriers was evaluated by FMI at 1 h after infusion.

### 3.5. Statistical analysis

Statistical analyses were performed using the GraphPad Prism 6 and SPSS softwares. The sample size of the *Safety study* was determined in a pilot study (n=4-5/group) by power analysis based on the infarct volume as primary outcome measure, using the software Ene 3.0 (GlaxoSmithKline SA), at 80% of statistical power and to a significance level of 5%. Randomisation of the experimental groups was generated using the standard = RAND() function in Microsoft Excel. All values are expressed as mean $\pm$ SD or median (InterQuartile Range, IQR) according to the normal or non-normal distribution of the represented variable, respectively. The normality of

continuous variables was assessed using the Shapiro-Wilk test ( $n < 30$ ) or Kolmogorov-Smirnov test ( $n \geq 30$ ). Normally distributed variables were analysed using t-test, one-way or two-way ANOVA (followed by Tukey's multiple comparisons post hoc test, or the Dunnett's multiple comparisons post hoc test for the *Efficacy studies* vs. Vehicle, and for the cell culture *in vitro* studies vs. cEBM). To analyse a dose-dependent effect in the cell culture *in vitro* studies (normally-distributed variables), a one-way ANOVA followed by a post hoc test for linear trend was performed. The Mann-Whitney U-test or Kruskal Wallis test (followed by Dunn's multiple comparisons post hoc test) were used for non-normally distributed variables. For the cell culture *in vitro* studies, the abovementioned analyses were performed considering the treatment conditions within a single experimental set-up as paired samples. Pearson's  $\chi^2$  test or Fisher exact test were used for categorical variables. Correlations were evaluated using Pearson's or Spearman's coefficient for normally or non-normally distributed variables, respectively. Body weight values monitored for the long-term *Efficacy study 2* were analysed by a generalized least squares model. Extreme values were excluded prior to data analyses using the outliers ROUT method ( $Q=1\%$ ). The significant level was set at  $P < 0.05$  at a 95% confidence level.



## RESULTS

---





#### 4.1. Angiogenic effects of EPCs-secretome on endothelial cells

A previous study, published by our group, demonstrated that EPCs-secretome obtained from ischaemic stroke patients EPCs in a high-scale production manner promoted angiogenic effects on mature ECs *in vitro* (**Annex II**).<sup>203</sup>

For the present work, we first aimed to confirm the pro-angiogenic effects of stroke patients EPCs-secretome, also obtained in a high-scale production manner, in both mouse/human and mature ECs/OECs.

Our results confirmed that stroke EPCs-secretome promotes both mouse and human mature brain ECs proliferation, and this effect is consistent amongst different secretome batches ( $P < 0.05$  vs. control basal media for all measures; **Figure 20A**).

An increase in both mouse and human OECs proliferation was also observed when treating with EPCs-secretome *in vitro* at 10  $\mu\text{g}/\text{mL}$  up to 50  $\mu\text{g}/\text{mL}$  in mouse OECs ( $P < 0.05$  vs. cEBM at the respective dose for all measures), and at 50  $\mu\text{g}/\text{mL}$  up to 250  $\mu\text{g}/\text{mL}$  in human OECs ( $P < 0.05$  vs. cEBM at the respective dose for all measures). Moreover, this effect was dose-dependent for both mouse and human OECs (post hoc for linear trend  $P < 0.0001$ ; slope/ $R^2 = 19.48/0.8612$ , and slope/ $R^2 = 8.056/0.6465$ , respectively). It should be highlighted that cEBM at the corresponding doses showed a dose-dependent decrease in mouse OECs viability (post hoc for linear trend  $P = 0.0318$ ; slope/ $R^2 = -1.895/0.1436$ ), although this effect was not statistically significant for human OECs (post hoc for linear trend  $P = 0.2710$ ; slope/ $R^2 = -0.6254/0.0226$ ). Even then, treatment with concentrated basal medium containing EPCs-secreted factors enhanced endothelial cell proliferation, as described above (**Figure 20B**).

It is noteworthy that the endothelial proliferative effects of human EPCs-derived secretome were higher in mouse-derived endothelial cells than human cells, since higher doses of secretome were required to significantly increase cell proliferation (**Figure 20B**).

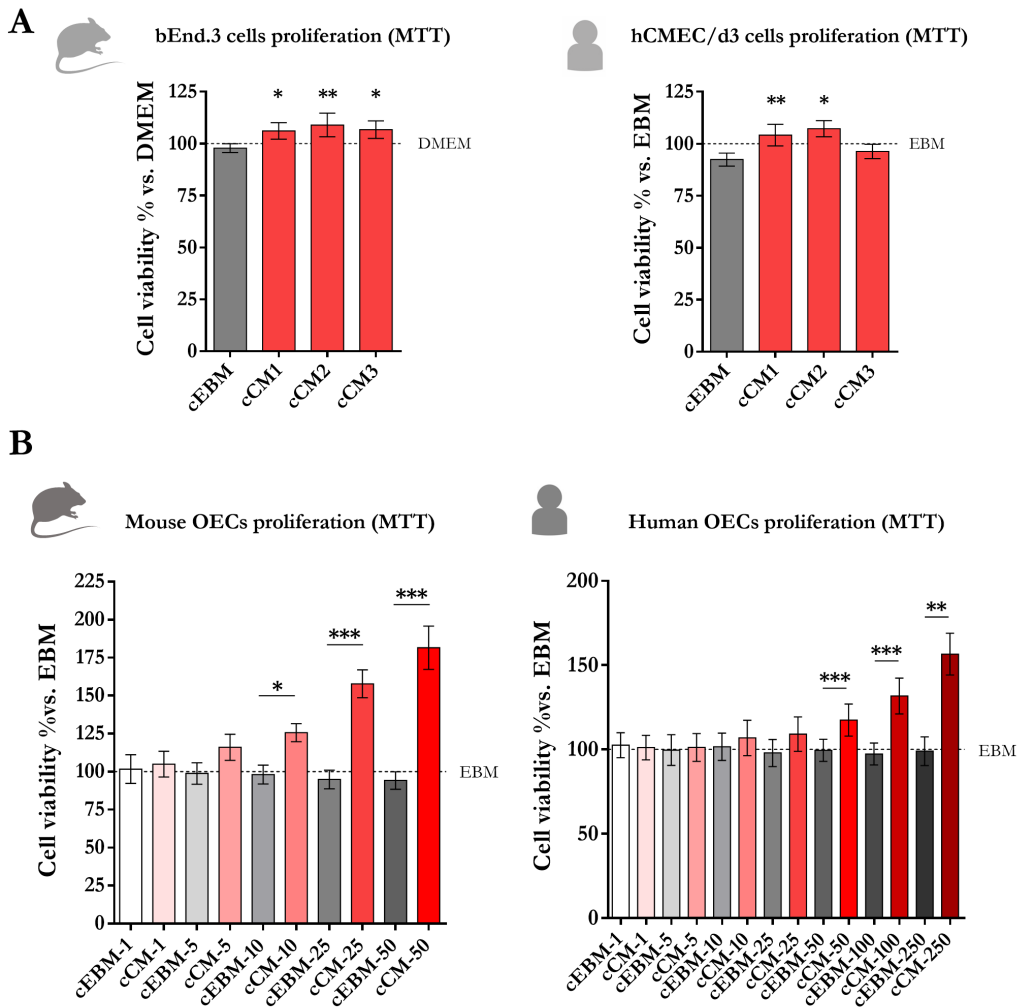


**Figure 20.** EPCs-secretome from stroke patients promotes mature ECs and OECs proliferation in both mouse- and human-derived cells *in vitro*. **A)** Graphs showing mouse ECs (bEnd.3 cells) and human ECs (hCMEC/d3 cells) proliferation, measured by the cell viability MTT assay at 24 h after treatment with different cCM batches (25  $\mu\text{g}/\text{mL}$ ;  $n=4$ ). **B)** Graphs showing mouse OECs and human OECs proliferation, measured by the cell viability MTT assay at 24 h after treatment with increasing doses (1  $\mu\text{g}/\text{mL}$  to 50  $\mu\text{g}/\text{mL}$  or 250  $\mu\text{g}/\text{mL}$ , respectively) of a single cCM batch ( $n=7-13$ ). All data are represented as mean $\pm$ SD. \* $P<0.05$ , \*\* $P<0.01$ , \*\*\* $P<0.001$ .

Next, we aimed to evaluate the angio-vasculogenic capacity of both mouse and human OECs *in vitro* after treatment with stroke patients-derived EPCs-secretome.

Our results showed that EPCs-secretome at a dose of 25  $\mu\text{g}/\text{mL}$  increased the tubulogenic capacity of mouse OECs *in vitro* in terms of tube length (perimeter of complete rings;  $P=0.0096$  vs. cEBM), and total number of loops (circular vessel-like structures;  $P=0.0235$  vs. cEBM); see **Figure 21**.

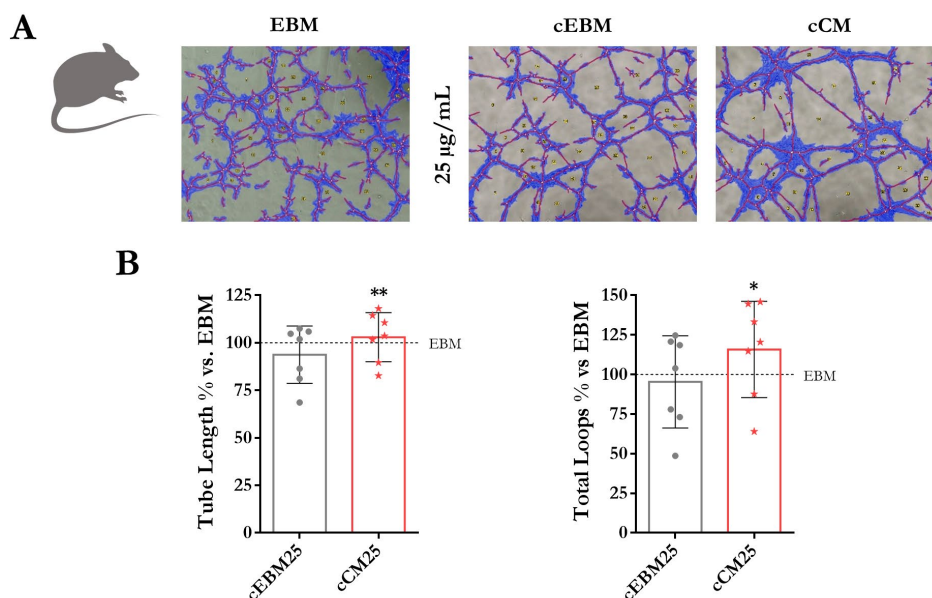


**Figure 21.** EPCs-secretome from stroke patients enhances the vasculo-angiogenic capacity of mouse OECs *in vitro*. **A)** Representative micrographs and automated analysis by Wimasis Image Analysis®, used for quantification. **B)** Graphs representing the tube length (left) and total loops (right);  $n=7$ . All data are represented as  $\text{mean} \pm \text{SD}$ . \* $P < 0.05$ , \*\* $P < 0.01$ .

The same effect was observed in human OECs, although to a lesser extent and, in the same line with the proliferation results described in the section above, a higher concentration of EPCs-secretome was needed in order to promote the tubulogenic capacity of human-derived cells. Specifically, treatment with EPCs-secretome at a dose of 50  $\mu\text{g}/\text{mL}$  increased the tube length, although not reaching statistical

significance ( $P=0.0956$  vs. cEBM). In contrast, the same dose did show a significant increase in the total loops compared to the control cEBM ( $P=0.0437$ ); **Figure 22**.

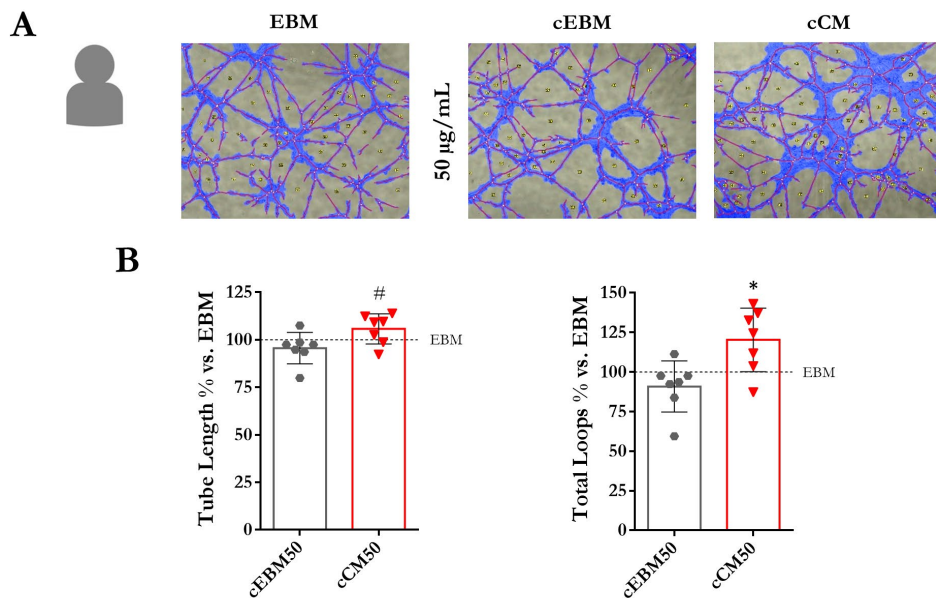


**Figure 22.** EPCs-secretome from stroke patients enhances the vasculo-angiogenic capacity of human OECs *in vitro*. **A)** Representative micrographs and automated analysis by Wimasis Image Analysis®, used for quantification. **B)** Graphs representing the tube length (left) and total loops (right);  $n=7$ . All data are represented as mean  $\pm$  SD. # $P<0.10$ , \* $P<0.05$ .

## 4.2. EPCs-secretome encapsulation

### 4.2.1. Angiogenic effects after EPCs-secretome encapsulation

Seizing the advantages of PLGA nanocapsules to encapsulate a large variety of molecules and undergo surface modification, we used magnetic PLGA nanocarriers, previously described by our group (**Annex II**)<sup>188</sup>, to encapsulate and deliver EPCs-secretome towards the ischaemic brain by external magnetic retention. This approach would potentially improve the specific targeting of the therapeutic EPCs-secretome and promote neurovascular repair in the context of cerebral ischaemia.

First, we addressed whether the encapsulation and release of EPCs-secretome was feasible and efficient, while maintaining the abovementioned biological functions.

As described above (sections 3.1.3 and 3.1.4), the secretome was lyophilised and reconstituted at the desired concentration (15 mg/mL) to optimise the therapeutic factors' encapsulation. In order to evaluate the pro-angiogenic potential of EPCs-secretome after the process of lyophilisation, encapsulation and release, NC-CM or their control NC-EBM were resuspended in EBM at a concentration of 2 mg/mL, and incubated at 37°C, on rotation, in the attempt to reproduce the physiological conditions of the nanomaterial in circulation after *in vivo* administration. After 48 h, we collected the released factors and assessed the angiogenic functions *in vitro* (**Figure 23A**).

Our results showed that EPCs-secretome preserved its biological function in promoting the proliferation of mouse OECs, as compared to the pre-lyophilised secretome. Specifically, both pre- and post-lyophilised secretome increased the proliferation of mouse OECs at 5 and 25 µg/mL ( $P < 0.05$  vs. cEBM at the respective concentration for all measures). Furthermore, no differences were observed between the cell proliferation after treating with EPCs-secretome before and after lyophilisation ( $P > 0.05$  for both treatment doses); **Figure 23B**.

Additionally, the secretome factors preserved their function after the encapsulation-release process, as demonstrated by an increase in the proliferation of mouse OECs after treatment with the 48 h-released factors ( $P = 0.0011$  vs. NC-EBM release); **Figure 23C**.

Finally, the released factors after 48 h also enhanced the *in vitro* tubulogenic capacity of mouse OECs, by increasing both the total loops number and total tube length ( $P = 0.0002$  and  $P = 0.0057$  vs. NC-EBM release, respectively); **Figure 23D**.

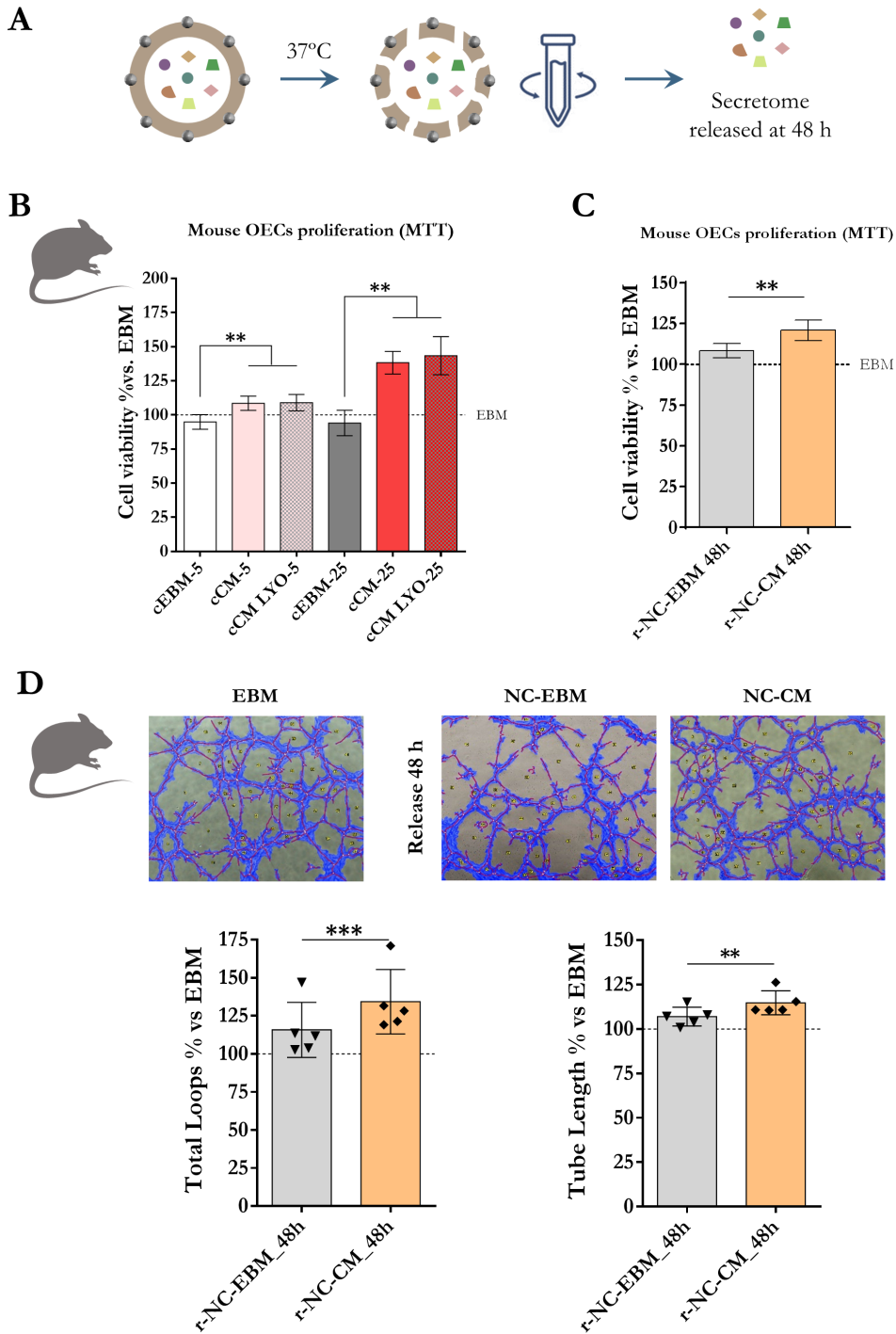


**Figure 23.** EPCs-secretome preserves its pro-angiogenic biological functions after processing for encapsulation in PLGA nanocarriers and subsequent release.

**A)** Scheme of the release process *in vitro* mimicking physiological conditions. Graphs representing the proliferation of mouse OECs after treating with **B)** pre- and post-lyophilised EPCs-secretome (n=6) and **C)** with the released factors after 48 h at the conditions depicted above (n=6). **D)** Representative micrographs and automated analysis by Wimasis Image Analysis®, and graphs representing the *in vitro* vasculo-angiogenic capacity of mouse OECs receiving the 48 h released factors from NC-CM, in terms of number of loops (left) and tube length (right); n=5. All data are represented as mean±SD. \*\*P<0.01, \*\*\*P<0.001. cCM: secretome pre-lyophilisation; cCM-LYO: secretome post-lyophilisation; r-NC-EBM/CM: released factors after 48 h from cEBM- or cCM-loaded nanocarriers, respectively.

We also sought to study whether NC-CM treatment could promote endothelial mature/progenitor cell proliferation *in vitro*. We tested increasing concentrations of NC-CM and none promoted the proliferation of neither mouse OECs nor human brain ECs (P>0.05 vs. cEBM at the respective concentration for all measures); **Figure 24**.

In addition, we observed a cytotoxic effect at increasing concentrations of both EBM- and CM-loaded NC, in both mouse OECs and human ECs, at the highest concentrations of 1,000 mg/mL and 2,000 mg/mL (P<0.05 vs. pure EBM for all measures), showing an average cell viability percentage vs. EBM below 55 % for both cell types treated with NC-EBM and NC-CM, at 1,000 mg/mL and 2,000 mg/mL; **Figure 24**. Therefore, we were technically unable to prove the therapeutic effect of NC-CM when treating with the whole nanoformulation in the tested cell lines.

The PLGA nanocarriers used for the present study were designed to target the ischaemic brain through magnetic retention. However, no additional moieties were incorporated onto the PLGA shell for a BBB specific transport mechanism. Yet, we aimed to evaluate whether endothelial cells, as the first barrier for brain delivery, were able to uptake these NCs *in vitro*. Our results show that, indeed, endothelial cells (both mature brain ECs and OECs) uptake the nanocarriers, presumably by



endocytosis, as the co-localisation of the NC fluorescent tag (Cy5) with internal membranes staining (DiOC) suggests (Figure 25).

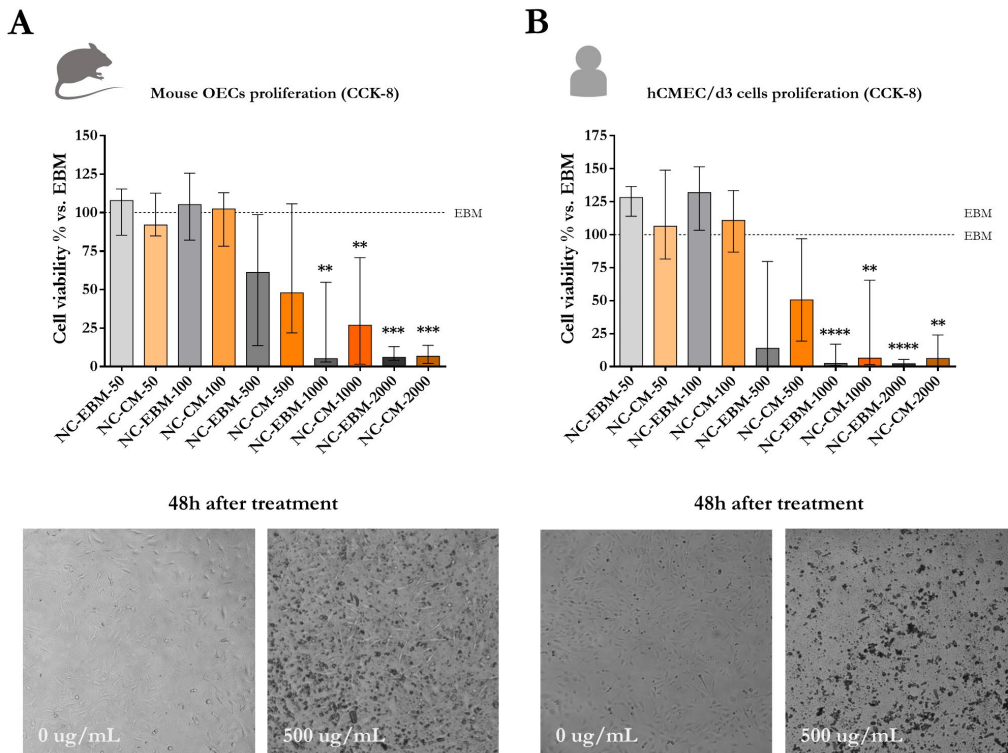


**Figure 24.** Effects of NC-CM on the proliferation of mouse OECs and human brain ECs. **A)** Graphs showing mouse OECs proliferation, measured by the cell viability CCK-8 assay at 48 h after treatment with increasing concentrations of NC-CM (50 to 2,000  $\mu\text{g}/\text{mL}$ ;  $n=4$ ). Below, representative micrographs showing mouse OECs in culture without (0  $\mu\text{g}/\text{mL}$ ) and treated with 500  $\mu\text{g}/\text{mL}$ , at 48 h after treatment. **B)** Graphs showing human brain ECs proliferation, measured by the cell viability CCK-8 assay at 48 h after treatment with increasing concentrations of NC-CM (50 to 2,000  $\mu\text{g}/\text{mL}$ ;  $n=4$ ). Below, representative micrographs showing hCMEC/d3 cells in culture without (0  $\mu\text{g}/\text{mL}$ ) and treated with 500  $\mu\text{g}/\text{mL}$ , at 48 h after treatment. All data are represented as median (IQR). \*\* $P<0.01$  vs. EBM, \*\*\* $P<0.001$  vs. EBM, \*\*\*\* $P<0.0001$  vs. EBM.

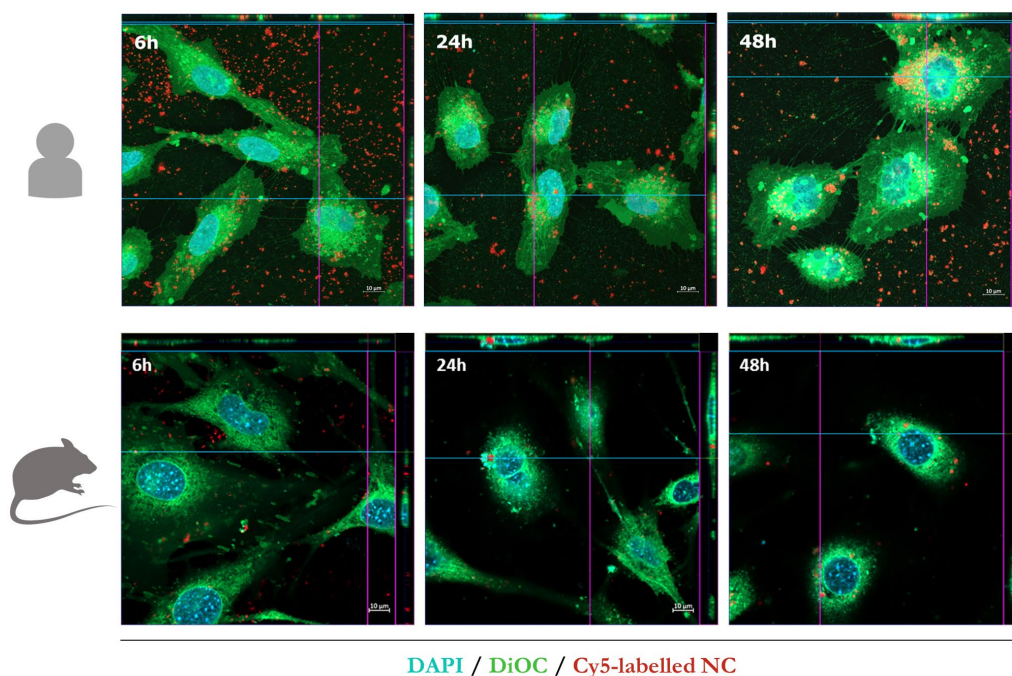


**Figure 25. Temporal NC-CM uptake by mature brain ECs and OECs.** Representative confocal micrographs showing the cellular uptake of Cy5-labelled NCs by hCMEC/d3 cells (above) and mouse OECs (below), at 6 h, 24 h and 48 h. Cell membranes were stained by the lipophilic dye DiOC (green), and nuclei stained with DAPI (blue). Scale bar: 10  $\mu\text{m}$ .

#### 4.2.2. Encapsulation efficiency

Previous studies have proven the versatility of PLGA nanocarriers for encapsulation or adsorption of different proteins.<sup>204,205</sup> However, in light of the large amount of factors in the EPCs-secretome, the composition of which has been previously described by our group (**Annex II**),<sup>203</sup> we aimed to determine the protein loading of NC-CM through quantification of total protein and specific representative EPCs-released proteins (**Table 8**).

Our results demonstrate the ability of PLGA nanocarriers to encapsulate different proteins, with a total protein loading of  $5.3 \pm 1.9 \mu\text{g}$  per mg of NCs.

**Table 8.** NC-CM encapsulation efficiency and drug loading.

	Drug loading (pg/mg NC)	EE%
<b>Multiplexed ELISA for specific proteins</b>		
<b>VEGF</b>	7.5±2.7	48.2±25.8
<b>PTX-3</b>	14.2±8.3	-
<b>GM-CSF</b>	4.5±1.8	29.4±20.9
<b>Angiogenin</b>	21.7±3.4	54.9±35.8
<b>Singleplex ELISA for specific proteins</b>		
<b>Angiogenin</b>	27.1±19.1	49.8±25.1
<b>CBQCA protein quantitation kit</b>		
<b>Total protein</b>	5,300±1870	41.1±13.3

All data are represented as mean±SD; n=4-8. EE% could not be calculated for PTX-3 due to pre-encapsulation CM protein measurement falling out of the range of the standard curve.

Taking into account both specific and total proteins, our EPCs-secretome encapsulation process into PLGA nanocarriers showed an average encapsulation efficiency of approximately 45%.

However, the encapsulation efficiency was different amongst proteins (ranging from 29.4±20.9% for GM-CSF to 54.9±35.8% for angiogenin), probably due to their different molecular weights and chemical-structural properties.

Importantly, the drug loading/encapsulation efficiency measured for angiogenin by two different techniques showed similar results, proving the reliability of the used methods (**Table 8**).

#### 4.2.3. Nanocarriers characterisation for *in vivo* studies

The magnetic PLGA nanocarriers used for the present study were further functionalised with fluorescent tags (Cy7.5 or Cy5) for *in vivo* imaging purposes.

The different Cy7.5- and Cy5-labelled NC batches used in this study presented a similar linear dose-dependent fluorescent signal (Total Radiant Efficiency, TRE) when imaged *ex vivo* although Cy5-labelled NCs displaying a higher signal-to-noise ratio, resulting in higher TRE values (**Figure 26**).

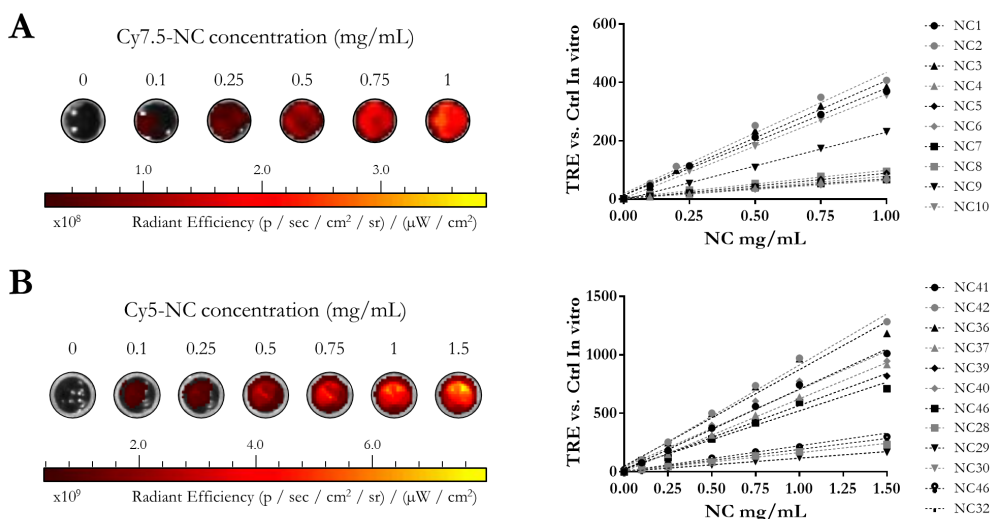


**Figure 26. Cy7.5/Cy5-labelled NC batches fluorescence *in vitro*.** **A)** Representative FMI images of increasing Cy7.5-NC concentrations in saline (0 mg/mL to 1 mg/mL). Graph representing the quantification of TRE on ROIs for each plate well at increasing NC concentrations, corrected by the TRE from the corresponding control well (saline). **B)** Representative FMI images of increasing Cy5-NC concentrations in saline (0 mg/mL to 1.5 mg/mL). Graph representing the quantification of TRE on ROIs drawn for each plate well at increasing NC concentrations, corrected by the TRE from the corresponding control well (saline).

### 4.3. Endovascular administration of magnetised nanocarriers to enhance brain delivery after stroke

#### 4.3.1. Administration route and magnetic retention

Our results showed a significant increase of the *in vivo* brain TRE at all the acquisition time points after i.a. administration compared to the i.v. route, both in the absence (F1) or presence (M1) of an external magnetic field ( $P=0.0062$ ,  $P=0.0062$  and  $P=0.0016$  for F1 at 30 min, 1 h and 3 h post-injection, respectively and  $P=0.0025$ ,  $P=0.0025$ ,  $P=0.0025$  for M1 at 30 min, 1 h and 3 h post-injection, respectively); see **Figure 27**.

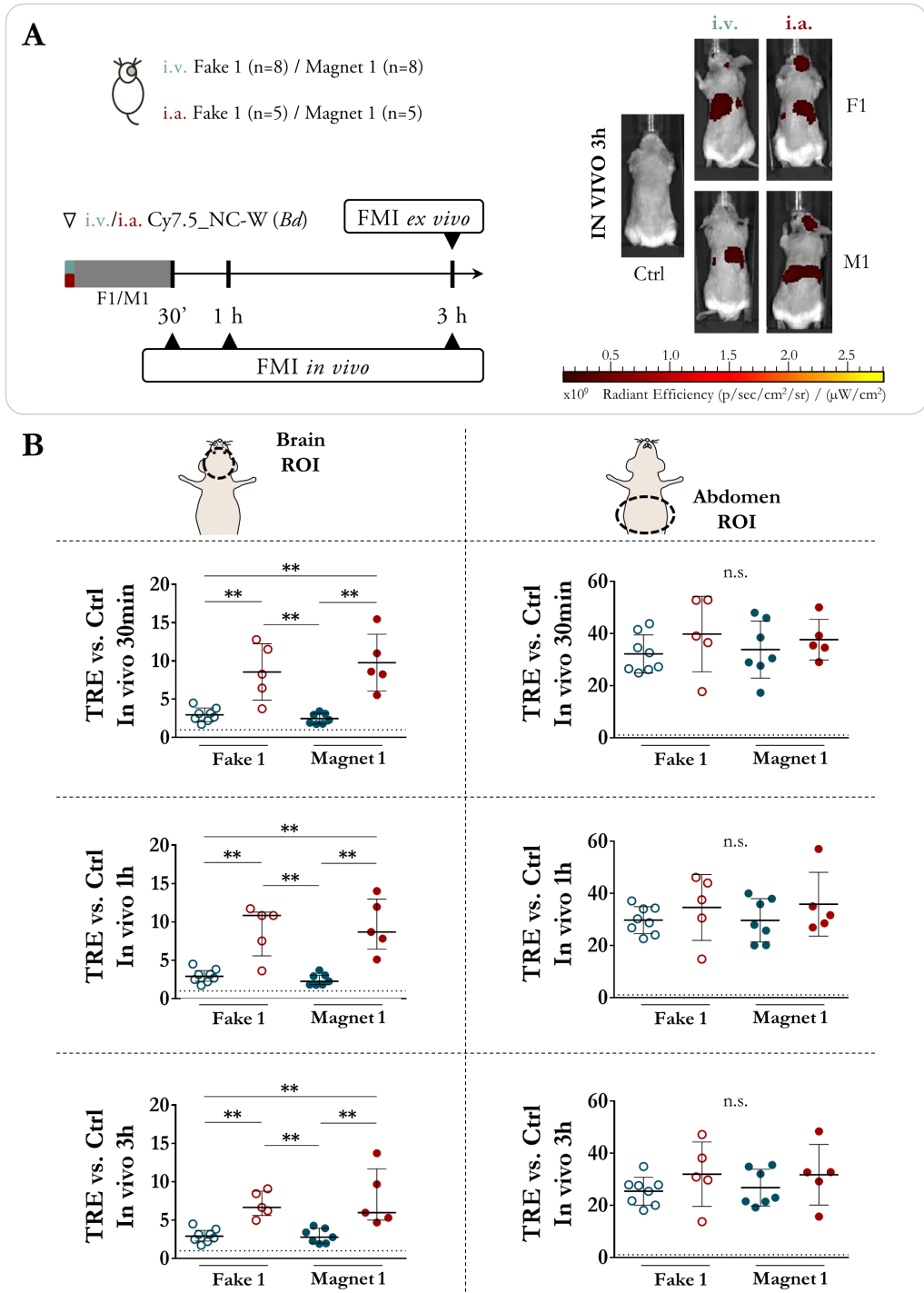


**Figure 27.** Biodistribution after NCs administration showing the advantage of the i.a. route for brain targeting in naïve mice. **A)** Scheme of the *Biodistribution study*

1 and representative *in vivo* FMI images at 3 h after i.v./i.a. NC injection. **B)** Graphs showing the TRE quantification on brain (left panel) and abdominal (right panel) ROIs from *in vivo* FMI acquisitions at 30 min, 1 h and 3 h after NCs administration. All data are shown as mean $\pm$ SD, except the graphs showing the TRE in the brain *in vivo*, which are shown as median (IQR). \*\*P<0.01, n.s.: non-significant.

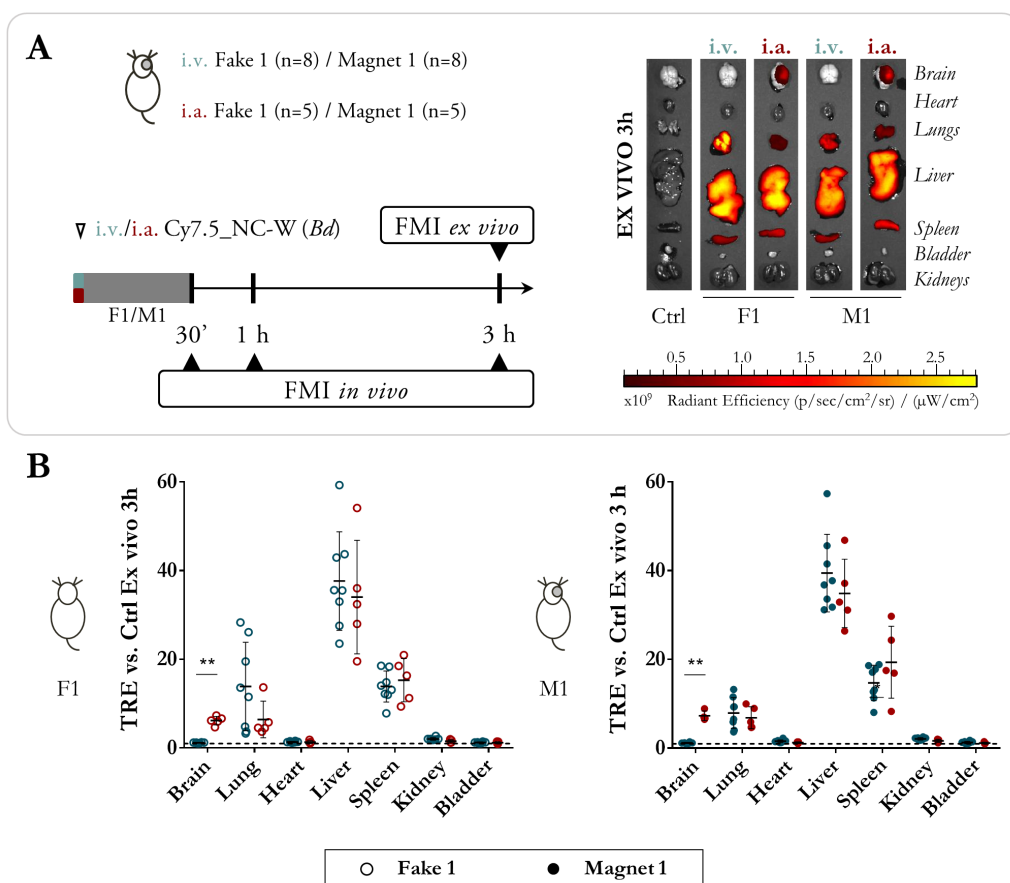


**Figure 28.** Biodistribution after NCs administration showing the advantage of the i.a. route for brain targeting in naïve mice. **A)** Scheme of the *Biodistribution study 1* and representative *ex vivo* FMI images at 3 h after i.v./i.a. NC injection. **B)** Graphs showing the TRE quantification on brain, lungs, heart, liver, spleen, kidneys, and bladder ROIs from the *ex vivo* FMI acquisition without magnetic retention (left; F1) or with magnetic retention (right; M1). All data are shown as mean $\pm$ SD. \*P<0.05, \*\*P<0.01.

**Figure 28** also shows the significant NC signal increase in the brain *ex vivo* at 3 h post-injection of animals receiving i.a. infusions vs. i.v. ( $P=0.0016$  for F1 and  $P=0.004$  for M1). Specifically, the brain fluorescent signal at 3 h after i.a. administration was increased  $2.53\pm 0.95$  times *in vivo* and  $5.65\pm 0.96$  *ex vivo*. Absolute fluorescence values were similar between administration routes in the abdominal region at all the *in vivo* acquisition time points (**Figure 27**) and *ex vivo* in all organs (except the brain) at 3 h post-injection (**Figure 28**), and did not change in the presence of a magnetic field ( $P>0.05$  for all measures).

However, when comparing the individual relative fluorescence in the abdominal region (as the TRE percentage on the abdominal ROIs versus the total TRE from all the ROIs drawn in *in vivo* FMI acquisitions) we found that it was significantly reduced in the i.a. administration vs. the i.v. route ( $P=0.0109$ ,  $P=0.0062$  and  $P=0.0031$  for F1 at 30min, 1 h and 3 h post-injection, respectively and  $P=0.0025$ ,  $P=0.0025$ ,  $P=0.0025$  for M1 at 30min, 1 h and 3 h post-injection, respectively; see **Figure 29**), and was also reduced in the liver *ex vivo* in the endovascular route with the magnet M1 ( $P=0.0012$ ); see **Figure 29**.

As shown in **Figure 27**, no differences were observed in the retention of the NCs in the whole brain when implanting the magnet M1 for 30 min ( $P>0.05$  for M1 vs. F1 for both administration routes). However, when dissecting the cortical and subcortical tissue we observed a significant increase ( $P=0.0382$ ; **Figure 30**) in the brain fluorescence in the ipsilateral cortex when the magnetic field was applied by M1, in areas under the influence of the magnetic field. Furthermore, a NC signal increase in the ipsilateral cortical and subcortical tissue was observed compared to the corresponding contralateral ( $P<0.05$  for all measures; see **Figure 30**).

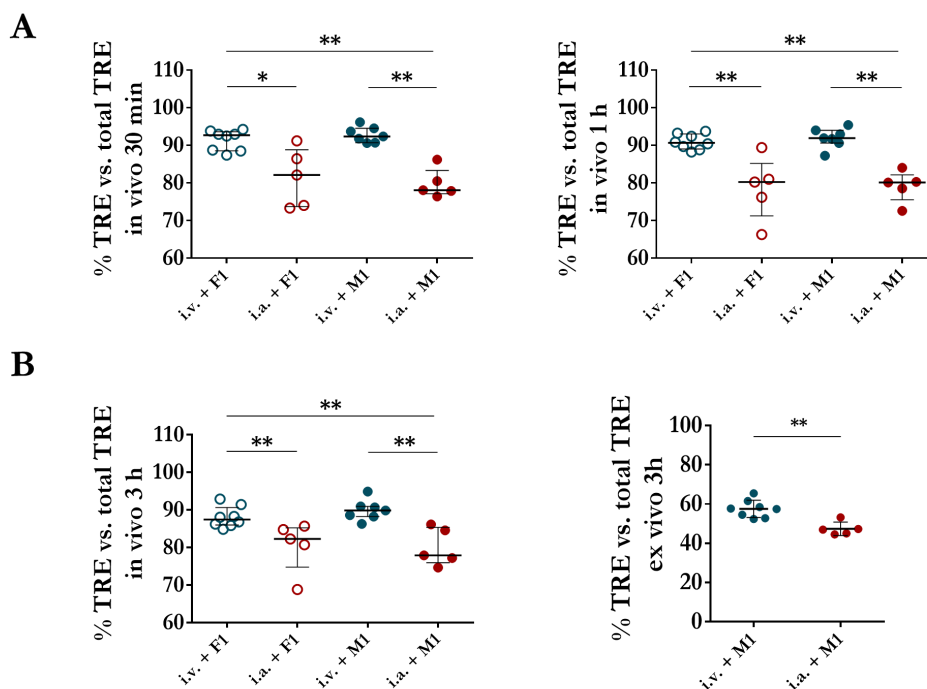


**Figure 29. Biodistribution after NCs administration showing the advantage of the i.a. route decreasing off-target accumulation. A)** Graphs showing the quantification of the TRE percentage on the abdominal ROIs versus the total TRE from all the ROIs drawn for each animal from *in vivo* FMI acquisitions at 30 min (left) and 1 h (right) after NCs infusion. **B)** Graphs showing the quantification of the TRE percentage on the abdominal ROIs versus the total TRE from all the ROIs *in vivo* (left), and on the liver ROI versus the total TRE from all the organ ROIs *ex vivo* (right), at 3 h after NC administration. All data are shown as median (IQR), except the TRE percentage on the liver *ex vivo*, showed as mean $\pm$ SD. \*P<0.05, \*\*P<0.01.



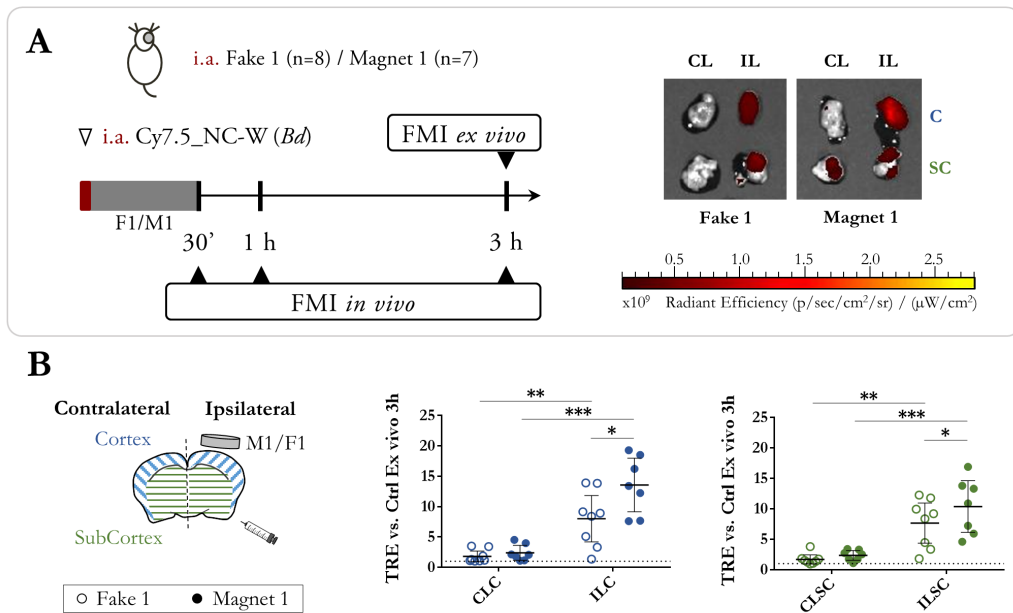


**Figure 30.** Brain nanocarriers distribution after MCAO and i.a. administration in naïve mice, showing the improved cortical NC brain targeting with the permanent magnet (M1). **A)** Scheme of the *Biodistribution study 2* and representative images *ex vivo* FMI of the ipsilateral (IL)/contralateral (CL) cortical (C) and subcortical (SC) brain regions at 3 h after i.a. NC injection. **C)** Graphs showing the corresponding quantification. Data shown as median (IQR). \*P<0.05, \*\*P<0.01, \*\*\*P<0.001.

#### 4.3.2. Safety of hyperacute endovascular administration of magnetised nanocarriers after cerebral ischaemia

Adverse events have been previously described after i.a. cell administration such as micro-occlusions or increased mortality rate.<sup>172,206,207</sup> In this regard, it should be highlighted that the average size of the nanomaterial used in the present study was  $273.21 \pm 34.7$  nm, within an acceptable range to avoid embolisation complications. Our protocol for the endovascular administration of NCs for brain targeting through the ICA in mice only transiently reduced the CBF at moderate levels for the first 10 min post-administration ( $34.8 \pm 29.2\%$  CBF reduction); see **Figure 31B**. Furthermore, no differences were observed in the mortality rate between ischaemic

mice receiving NCs or vehicle intraarterially (21.1% and 27.3%, respectively ( $P=0.727$ ); see **Figure 31C**). Importantly, we observed a trend ( $P=0.091$ ) between the total iron load dose and the mortality rate amongst ischaemic C57 mice receiving NCs intraarterially, which alerts us on potential harms of the use of certain nanomaterials.

The safety study also showed that the body weight loss after MCAO was similar amongst NCs and vehicle groups and within the expected values (**Figure 31D**). Our results also showed no significant differences in the functional outcome, infarct volume nor haemorrhagic transformations, as measured by the ECASS classification, number of haemorrhages and haemorrhage volume ( $P>0.05$  for all measures) (**Figure 31D, E, F**).

Potential systemic toxicity of the endovascular-ICA administration of NCs was studied at 48 h and 4 weeks after MCAO (**Table 9**) and no significant differences in the levels of ALT, lipase, creatinine, urea and  $\text{Na}^{2+}$  were observed amongst groups ( $P>0.05$  for all measures).

Only AST (an unspecific liver marker, also indicative of muscular injury) was increased at 48 h vs. the Naïve group ( $P=0.031$  and  $P=0.031$  for Vehicle and NC groups, respectively) and CK, a muscular injury-related enzyme, was increased at 48 h in the NC treatment vs. the Naïve group ( $P=0.027$ ). Importantly, the increased levels of AST and CK in the vehicle and NC groups returned to normal levels at 4 weeks ( $P>0.05$  for all comparisons), thus confirming the muscle injury-related increased levels of AST and CK acutely after the surgical intervention in the MCAO model.

Finally, regarding the pancreatic markers, the levels of  $\alpha$ -amylase were increased at 48 h after the ischaemia compared to the Naïve group ( $P=0.0025$  for the NC group), returning to normal levels at 4 weeks ( $P=0.0005$  vs. the NC group at 48 h post-ischaemia). On the other hand, plasma lipase levels were decreased at 48 h compared to the Naïve group, regardless of the treatment ( $P=0.011$  and  $P=0.0002$  for the

## Results

vehicle and NC groups, respectively). And importantly, the levels at 4 weeks were similar amongst groups and compared to the Naïve condition levels ( $P < 0.05$  for all measures), while the levels at 4 weeks were significantly increased in all groups compared to their respective levels at 48 h (MCAO controls  $P = 0.0024$  and NC-treated ischaemic mice  $P = 0.0016$ ), indicating an alteration related to the MCAO model, but not to the treatment.

**Table 9. Plasmatic toxicity markers from the *Safety study*.**

	Naïve (n=8)	MCAO		MCAO + Vehicle i.a.	MCAO + NC i.a.	
		48 h	4 wk	48 h	48 h	4 wk
<b>ALT</b> (UI/L)	37.7±16.7	38.8±16.2	43.6±24	46.9±29.5	46.3±14.1	25.5±12.4
<b>AST</b> (UI/L)	135.1±76.7	320±153.1	121.2±65.2	442.0±333.9 *	437.5±143.1 *	102.7±19.9
<b>CK</b> (UI/L)	406.9±154.2	494.5±152	289.2±175.7	818.0±256.7	973.1±447.8 *	292.4±65.3
<b>Creatinine</b> (mg/dL)	0.11±0.02	0.09±0.02	0.09±0.01	0.08±0.03	0.08±0.02	0.08±0.03
<b>Urea</b> (mg/dL)	51.5±9.3	41.5±0.7	29±2.7	39.3±6.5	40.3±11.9	34±8
<b>Na<sup>2+</sup></b> (mmol/L)	142.4±1.5	151.6±3.1	145.2±1.5	148.8±4.9	146.5±6.6	145±3.5
<b>α-amylase</b> (UI/L)	1,856±147.4	2,090±527	1,978.8±238.2	2,387±379.7	2,861.5±333.9 **	1,857.3±440.7 ***
<b>Lipase</b> (UI/L)	74.8±13.4	28±0	82±36.6 **	38.7±43.5 **	34.1±37 ***	63±13.6 **

Data represented as mean±SD. \* $P < 0.05$  vs. Naïve, \*\* $P < 0.01$  vs. Naïve, \*\*\* $P < 0.001$  vs. respective 48 h group

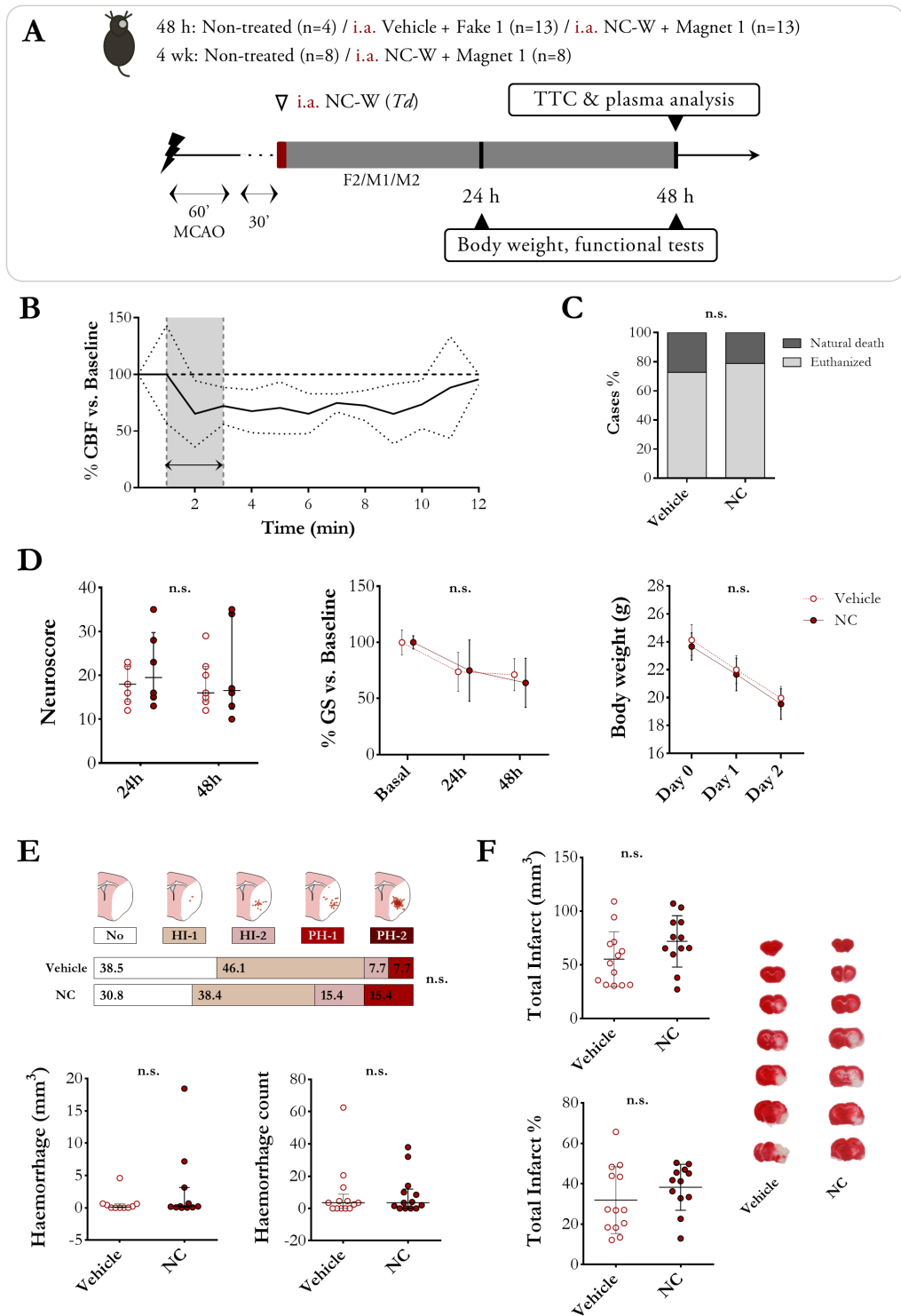


**Figure 31.** Safety of hyperacute i.a. NCs administration after MCAO and magnetic targeting. **A)** Scheme of the experimental design of the short-term *Safety*

*study* (C-F; n=13/group). **B)** CBF monitoring during and after i.a. administration of NCs (*Td*; n=6). **C)** Mortality rate amongst treatment groups. **D)** Graphs showing neuroscore and grip strength (GS) measurements, and body weight follow-up. **E)** Haemorrhages evaluation by visual classification according to ECASS criteria represented as the percentage of animals classified into each category (above), haemorrhage volume and haemorrhage counts (below). **F)** Graphs showing total infarct volume and percentage, and representative TTC-stained brains used for quantification. All data are represented as mean $\pm$ SD, except data represented in haemorrhage volume/count and neuroscore graphs, showing the median (IQR). n.s.: non-significant.

### 4.3.3. Magnetic field modelling to improve brain nanomaterial retention

We investigated the magnetic properties of the two FeNdB magnets designed as NC retention devices for the mouse brain, a permanent magnet (M1) and a focused magnet (M2). Experimental measurements of the spatial magnetic field distributions at different distance from the surface of the M1 and M2 showed that the magnetic force decreases as an inverse square law with the distance, displaying a higher magnetic force within the first 3 mm from the surface. However, M2 displays a 2.5-fold increase of the maximum values of the magnetic field and 5.5-fold increase of the magnetic force compared to M1, which is in agreement with the theoretical modelling of the magnetic field distribution of both magnet prototypes (**Figure 32A-B**). Finally, the magnetic retention capacity of both magnets was validated by means of a dust magnetic targeting test (**Figure 32C**), which was further confirmed for the focused magnet (M2) using a chicken egg model for MRI tracking of an injected magnetic fluid under the influence of the magnetic field (**Figure 32D**).

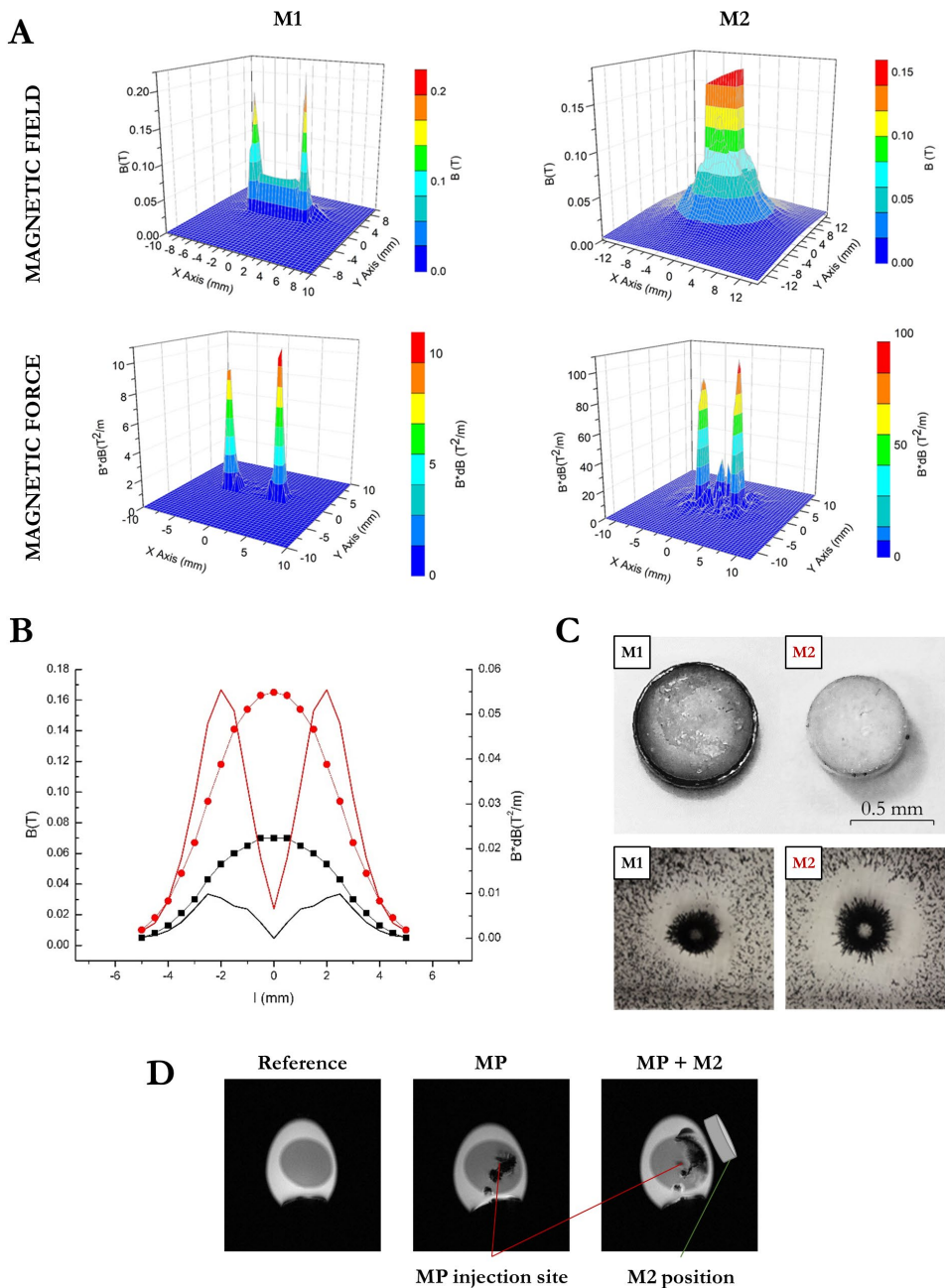


**Figure 32.** Characterisation of the magnet devices: magnetic field, magnetic force and magnetic targeting validation. **A)** Spatial distribution by computational modelling of the magnetic field and spatial distribution of the magnetic force for M1 (left) and M2 (right) at 3 mm above the magnet surface. **B)** Graph showing the magnetic field ( $B$ ; dotted lines) and magnetic force ( $B \cdot dB$ ; straight lines) of M1 (black) and M2

## Results

---

(red) at 3 mm above the magnet surface, measured by 3D Hall probe. **C)** Image (above) of M1 and M2 devices and illustrative image (below) of the dust effectivity test of magnetic targeting of ferrimagnetic magnetite microparticles (MP) for M1 and M2. **D)** T2\*WI for the tracking of a magnetic fluid under the influence of the focused magnet M2 at 45 min after injection in a chicken egg model, indicating the injection and magnet implantation sites.

Next, we aimed to prove the *in vivo* effectiveness of M1 and M2 devices on magnetic brain targeting after hyperacute endovascular NCs administration at the calculated *therapeutic dose* after cerebral ischaemia by FMI (**Figure 33A**). Our results show a significant  $2.42 \pm 0.78$ -fold increase of *in vivo* NC signal reaching the brain region at 3 h only by the M2 device compared with the F2 control ( $P=0.0209$ ). This advantage was maintained at 48 h post-injection *in vivo* ( $2.56 \pm 0.53$ -fold increase,  $P=0.0001$ ) and confirmed *ex vivo* ( $2.16 \pm 0.8$ -fold increase,  $P=0.0398$ ). On the other hand, the M1 device showed a  $1.72 \pm 0.51$ -fold increase in brain NC signal *in vivo* at 48 h post-injection compared to the F2 control, although not significant ( $P=0.055$ ). Importantly, M2 device showed  $1.49 \pm 0.31$  times more brain NC signal at 48 h than M1 *in vivo* ( $P=0.0182$ ). In parallel, FMI values were similar in the abdominal region *in vivo* at 3 h and 48 h post-injection and *ex vivo* in all organs ( $P>0.05$  for all measures, **Figure 33B**).

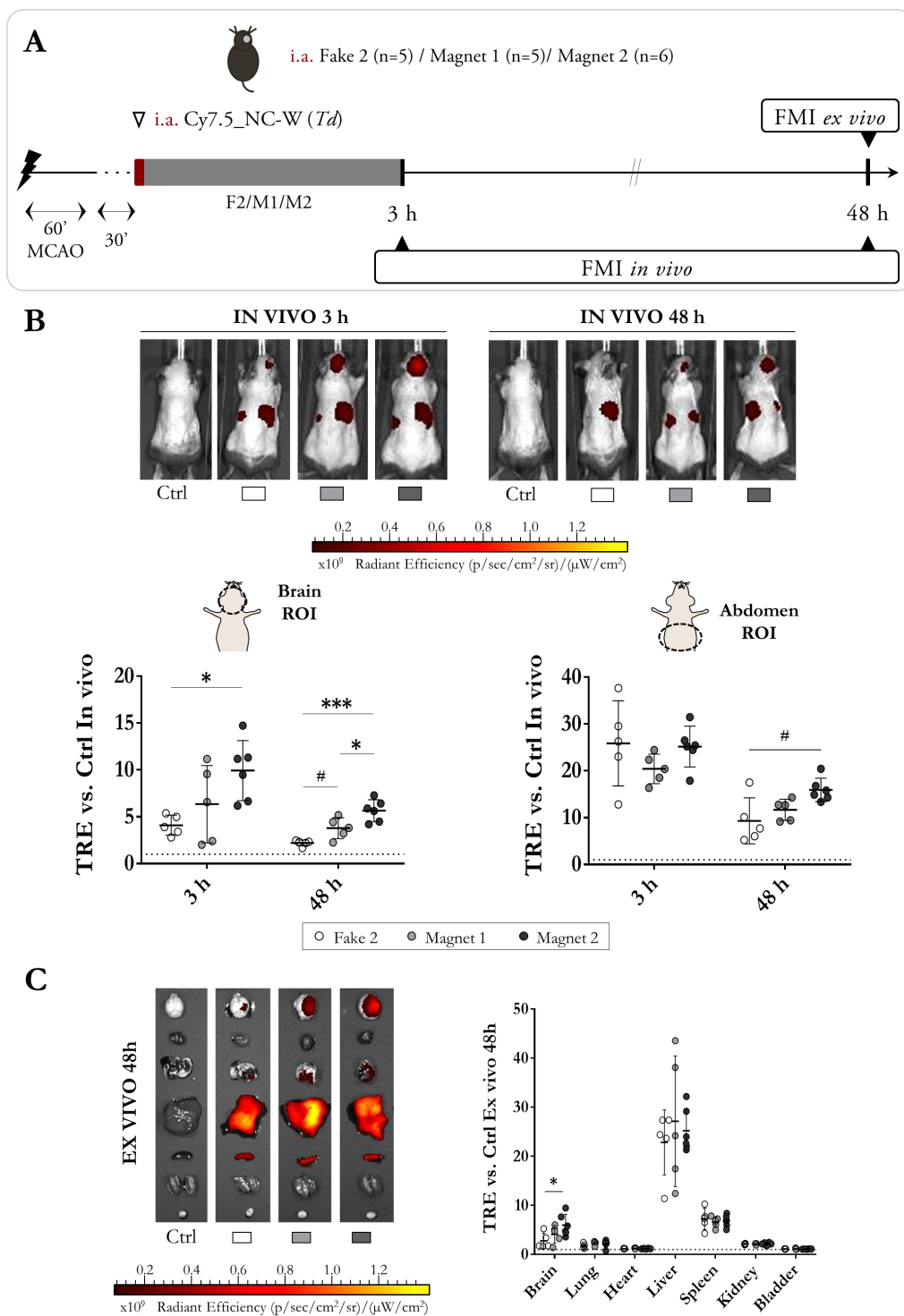


**Figure 33.** Biodistribution after MCAO and i.a. NCs administration showing the improved NC brain targeting with different magnetic devices and superior



**performance of the focused magnet (M2).** **A)** Scheme of the experimental *Biodistribution study 3*. **B)** Representative *in vivo* FMI images at 3 h and 48 h after i.a. NCs administration and graphs showing the corresponding quantification on brain and abdominal ROIs, corrected by their control animal. **C)** Representative *ex vivo* FMI images 3 h after i.a. NC administration and graph showing the quantification of TRE on ROIs from organs imaged by FMI *ex vivo* after the last *in vivo* acquisition. Data are shown as mean $\pm$ SD. #P<0.10, \*P<0.05, \*\*\*P<0.001.

Importantly, no associations between NC batch fluorescence and treatment group were observed, discarding batch-dependent biased results for the FMI data described above (**Figure 34**).

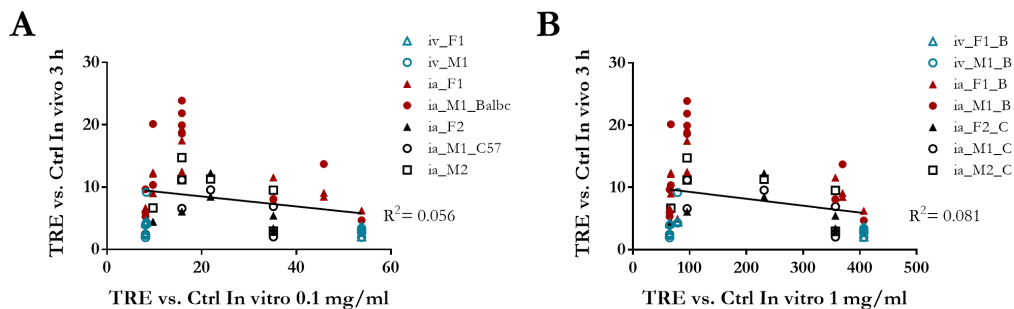


**Figure 34.** Cy7.5-labelled NC batches fluorescence *in vitro*: distribution of NC batches amongst *in vivo Biodistribution studies 1-3*. **A)** Correlation between TRE on brain ROIs quantified by FMI *in vivo* at 3 h after Cy7.5-NCs injection and the TRE quantified by FMI *in vitro* of the corresponding Cy7.5-NC batch at 0.1 mg/mL. **B)** Correlation between TRE on brain ROIs quantified by FMI *in vivo* at 3 h after Cy7.5-NC injection and the TRE quantified by FMI *in vitro* of the corresponding Cy7.5-NC batch at 1 mg/mL.

From a translational perspective, we aimed to confirm the results by MRI, a clinically-relevant technique, to better define the spatial brain distribution of the NCs after M2 implantation using the T2 relaxation properties of the SPIONs; see **Figure 35**. In accordance with the results observed by FMI, a significant increase in the particles

count was observed in the ipsilateral cortex when the M2 device was implanted vs. the F2 control ( $P=0.0125$ ), thus confirming the success in magnetic retention of the NCs in the brain cortex.

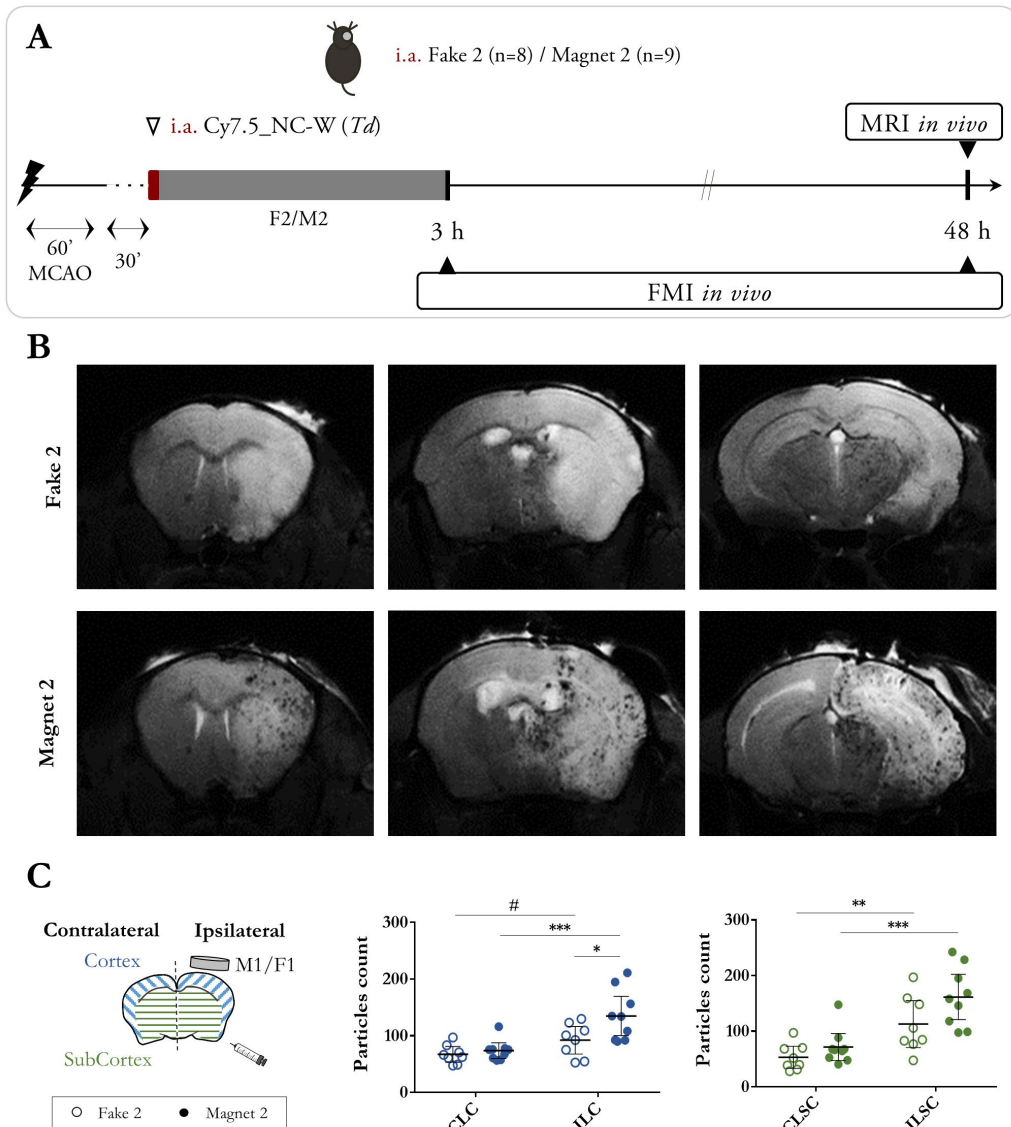


**Figure 35.** Spatial brain distribution of the NCs after i.a. administration and magnetic retention with the improved focused magnet (M2) in the MCAO model. **A)** Scheme of the *Biodistribution study 4*. **B)** Representative brain T2\*WI 48 h after i.a. NCs administration and graphs showing the corresponding particle analysis of the

## Results

hypointense signals attributed to SPIONs in ipsilateral (IL)/contralateral (CL) cortical (C) and subcortical (SC) regions. Data represented as median (IQR). # $P < 0.10$ , \* $P < 0.05$ , \*\* $P < 0.01$ , \*\*\* $P < 0.001$ .

Finally, a specific Prussian blue staining was conducted to confirm the MRI findings, to identify the location of ferric iron of the nanomaterial in tissues. Spleen slices were used as ferric iron-stain controls<sup>208</sup> and liver slices were also stained to confirm the presence of NCs in tissues, as they typically accumulate in the liver. Representative images of liver and spleen from animals receiving NCs intraarterially in the presence of M2 magnetic retention are shown in **Figure 36**.

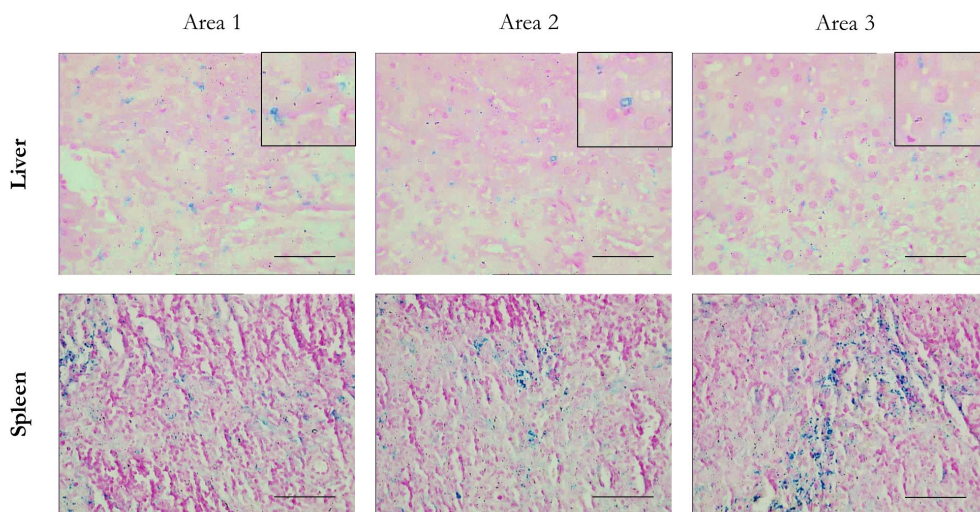


**Figure 36. Verification of NCs staining by Prussian blue.** Liver and spleen slices were stained as controls of NCs stain and endogenous ferric iron, respectively. Upper insets show magnified positive signals. Scale bar: 30  $\mu\text{m}$ .

Brain slices from mice receiving NCs intraarterially, in the presence of M2 magnetic retention, showed extensive positive staining in the ipsilateral brain hemisphere, predominantly in micro-vessel-like structures, while the presence of ferric iron in the contralateral hemisphere was negligible, matching with the FMI and MRI results (see **Figure 37**).

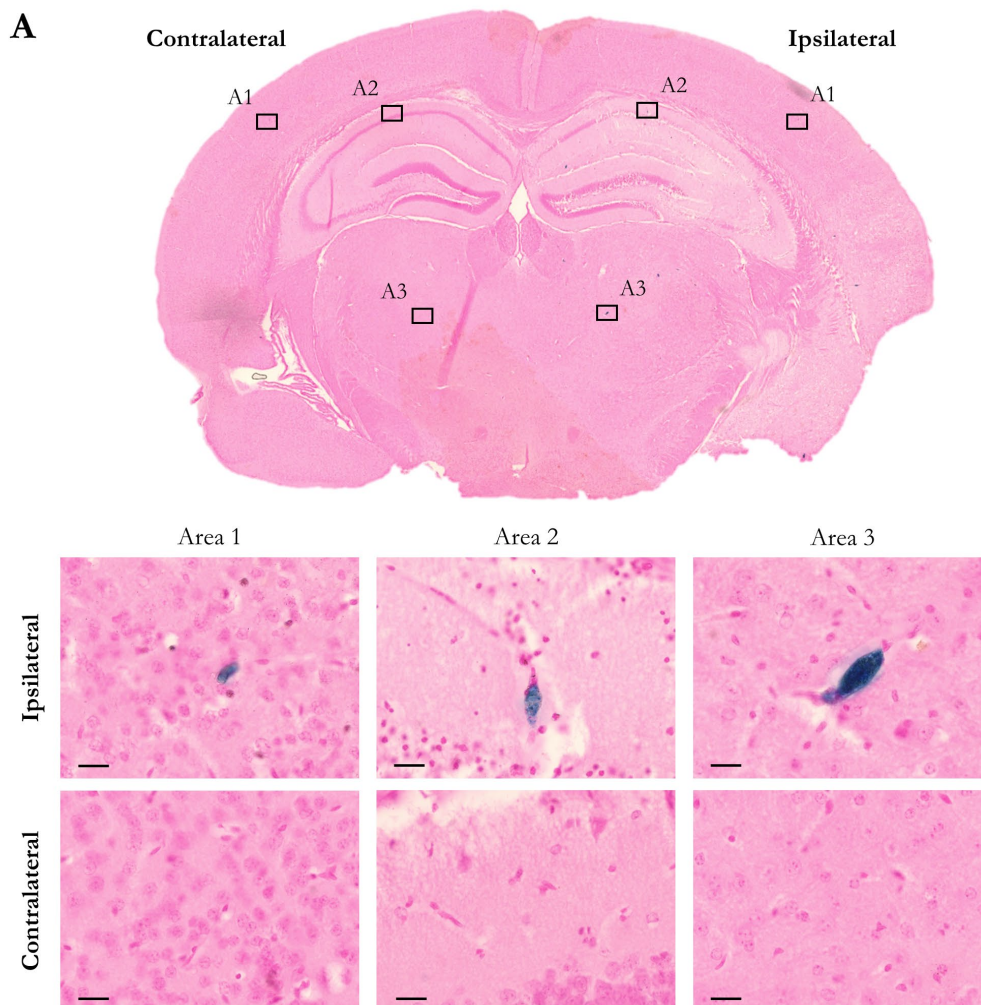


**Figure 37.** Verification of NCs brain distribution by Prussian blue ferric iron staining (contained in the SPIONs). Staining on brain shows a major and extensive signal in the ipsilateral hemisphere; note that most positive stain corresponds to microvessel-like structures in saline-perfused brains. Scale bar: 20  $\mu\text{m}$ .

### 4.4. Endovascular-nanotargeted EPCs-secretome treatment after cerebral ischaemia

#### 4.4.1. Short-term efficacy after hyperacute endovascular administration of free or nanotargeted EPCs-secretome in ischaemic mice

In light of the previous results proving a safe brain targeting improvement through hyperacute i.a. NCs administration and magnetic targeting (M2), we next aimed to evaluate whether the endovascular administration of nanotargeted EPCs-secretome was feasible, safe, and promoted neurovascular repair after cerebral ischaemia.

Considering the hyperacute treatment timing to take advantage of the i.a. route after mechanical reperfusion, a first group of ischaemic mice receiving vehicle, NC-CM with magnetic retention (M2) or f-CM (n=10-13/group), was followed for 48 h in order to evaluate the short-term therapeutic efficacy (*Efficacy study 1*). The results obtained are detailed in the following sections.

##### 4.4.1.1. Short-term functional outcome and brain damage

Our results showed no significant differences amongst groups in the functional outcome, body weight loss, nor mortality, during the first 48 h after MCAO ( $P > 0.05$  for all measures; **Figure 38**).

As described above, the results obtained in the *Safety study* did not show adverse events related to hyperacute i.a. NCs administration in the context of cerebral ischaemia. It should be highlighted that the average size of the NCs when encapsulating cCM or cEBM was slightly larger than the NC-W ( $312.1 \pm 32.0$  and  $295.5 \pm 61.4$  vs.  $266.2 \pm 28.8$ , respectively). However, we did not observe an increased infarct size nor haemorrhagic transformations in the NC-CM group compared to the vehicle group ( $P > 0.05$  for all measures; **Figures 39 and 40**). On the contrary, a slight increase in the cortical infarct percentage was observed in the f-CM group ( $P = 0.096$  vs. Vehicle; **Figure 39**). Yet, f-CM-treated mice did not show an increased risk of haemorrhagic transformation, as measured by the ECASS score, and haemorrhages

count and volume ( $P > 0.05$  vs. Vehicle for all measures). There was however a slight correlation between the cortical haemorrhages and infarct volumes in the f-CM group, yet not reaching statistical significance ( $r = 0.4262$ ,  $P = 0.1467$ , **Figure 40**).

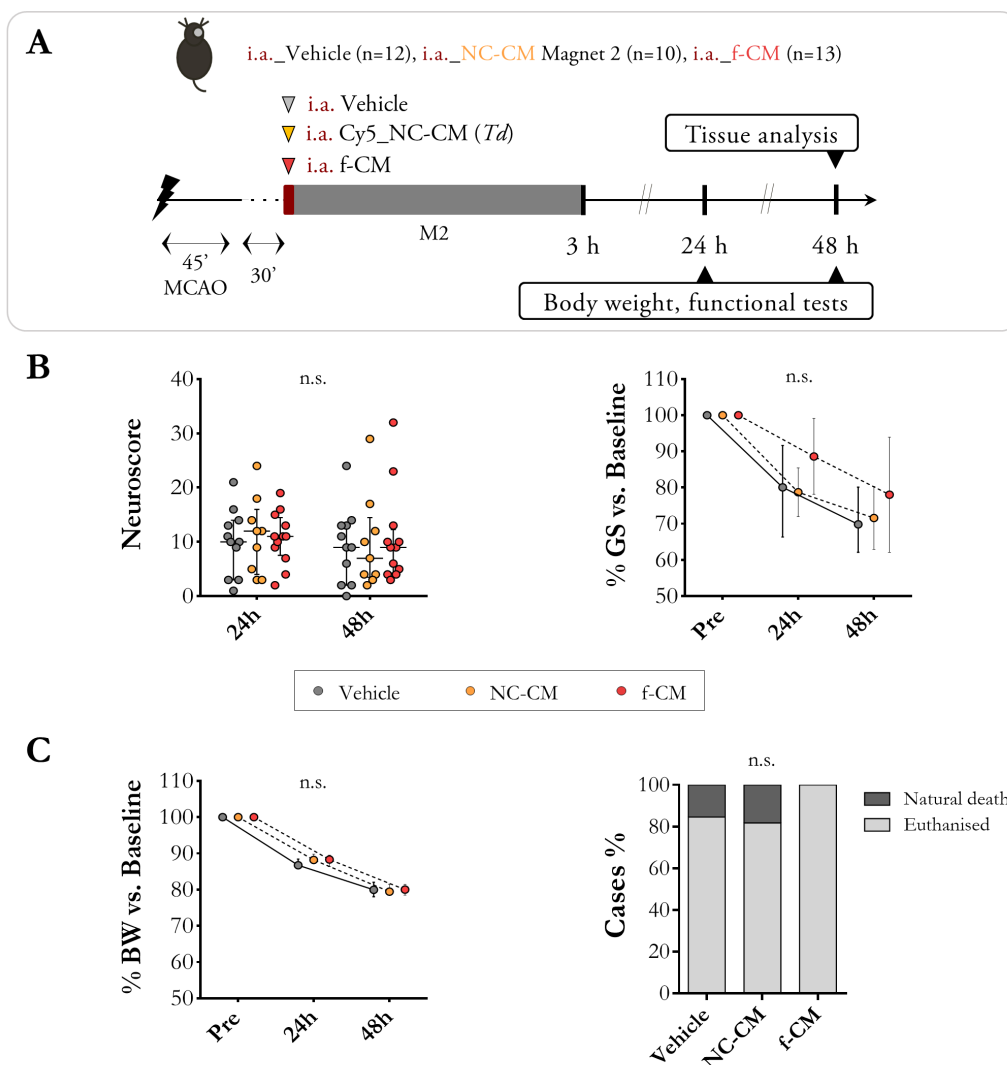


**Figure 38.** Functional outcome after hyperacute i.a. NC-CM or f-CM administration after MCAO and NCs magnetic targeting (M2). **A**) Scheme of the experimental design of the short-term *Efficacy study 1*. **B**) Graphs showing neuroscore and grip strength (GS) measurements, and body weight follow-up. **C**) Mortality rate after NC-CM or f-CM endovascular administration. All data are represented as median (IQR). n.s.: non-significant.

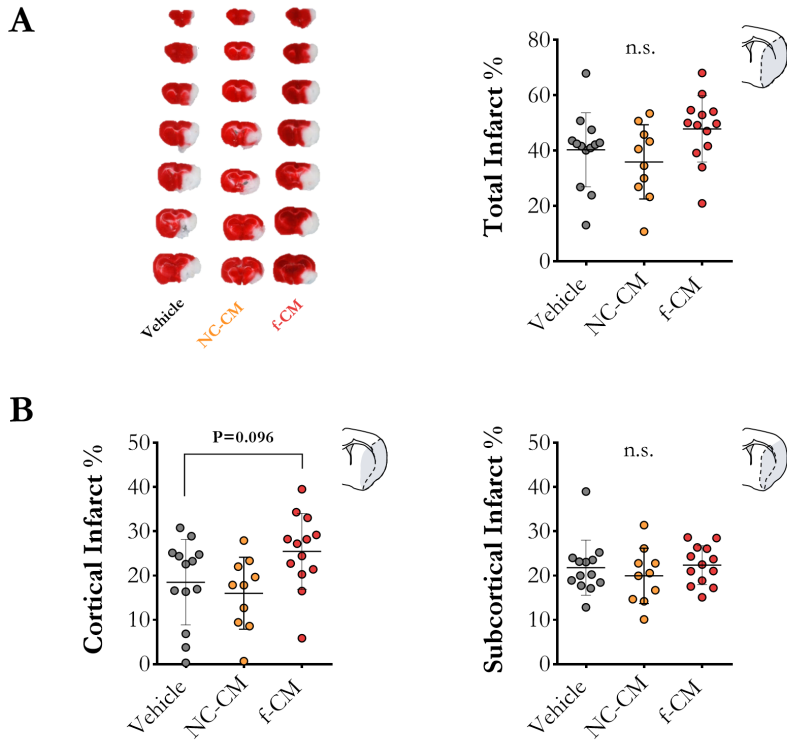


**Figure 39.** Infarct size after hyperacute i.a. NC-CM or f-CM administration after MCAO and NC magnetic targeting (M2) (*Efficacy study 1*). **A**) Representative TTC-stained brains used for quantification (left) and graph showing the total infarct percentage (right) **B**) Graphs showing the infarct percentage in the cortical and subcortical brain regions. All data are represented as mean±SD. n.s.: non-significant.

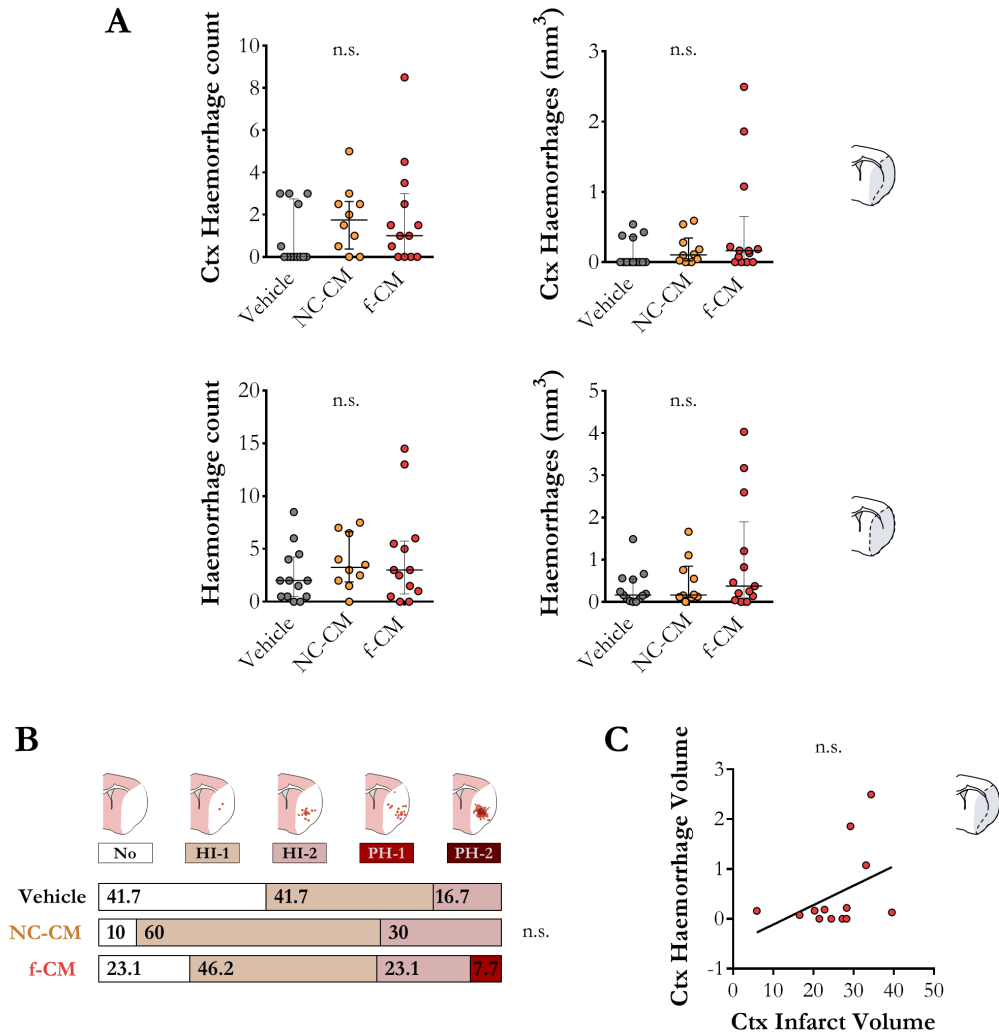


**Figure 40.** Haemorrhagic transformation after hyperacute i.a. NC-CM or f-CM administration after MCAO and NC magnetic targeting (M2) (*Efficacy study 1*). **A)** Graphs representing the cortical (Ctx; above) and total (below) haemorrhage count and volume. **B)** Haemorrhages evaluation by visual classification according to ECASS criteria represented as the percentage of animals classified into each category. **C)** Correlation between the cortical (Ctx) haemorrhage and infarct volumes. Data represented as median (IQR). n.s.: non-significant.



### 4.4.1.2. Effects of free or encapsulated EPCs-secretome on the BBB and the neuro-inflammatory response after cerebral ischaemia

The early administration of pro-angiogenic factors after cerebral ischaemia, such as VEGF, has been related to an increased BBB leakage, coupled with an enhanced risk of haemorrhagic transformation and increased infarct size.<sup>209</sup> Taking this into account and after observing an increased cortical infarct size in the group receiving free EPCs-secretome, we sought to evaluate the BBB through the expression of different junctional proteins in isolated brain vessels (**Figure 41**), and the neuro-inflammatory response through the expression of cytokines/chemokines in total brain homogenates (**Table 10/Figure 42**).

Our results suggest that the hyperacute i.a. treatment with f-CM might affect the junctional proteins' expression in the BBB (as seen by the reduced expression of some TJs proteins, while this effect is not induced when the secretome is administered encapsulated (NC-CM) (**Figure 41**).

Specifically, the expression of Claudin-5 was decreased in the contralateral brain vessels from mice receiving f-CM ( $P=0.0003$  vs. Vehicle), while no differences were observed in the NC-CM group ( $P>0.05$  vs. Vehicle) The same observations were found for ZO-1 which was significantly reduced in the contralateral brain vessels from f-CM-treated mice ( $P=0.0117$  vs. Vehicle), overall pointing to an off-target effect of the EPCs-secretome when given freely, but avoided when administered in the PLGA NCs.

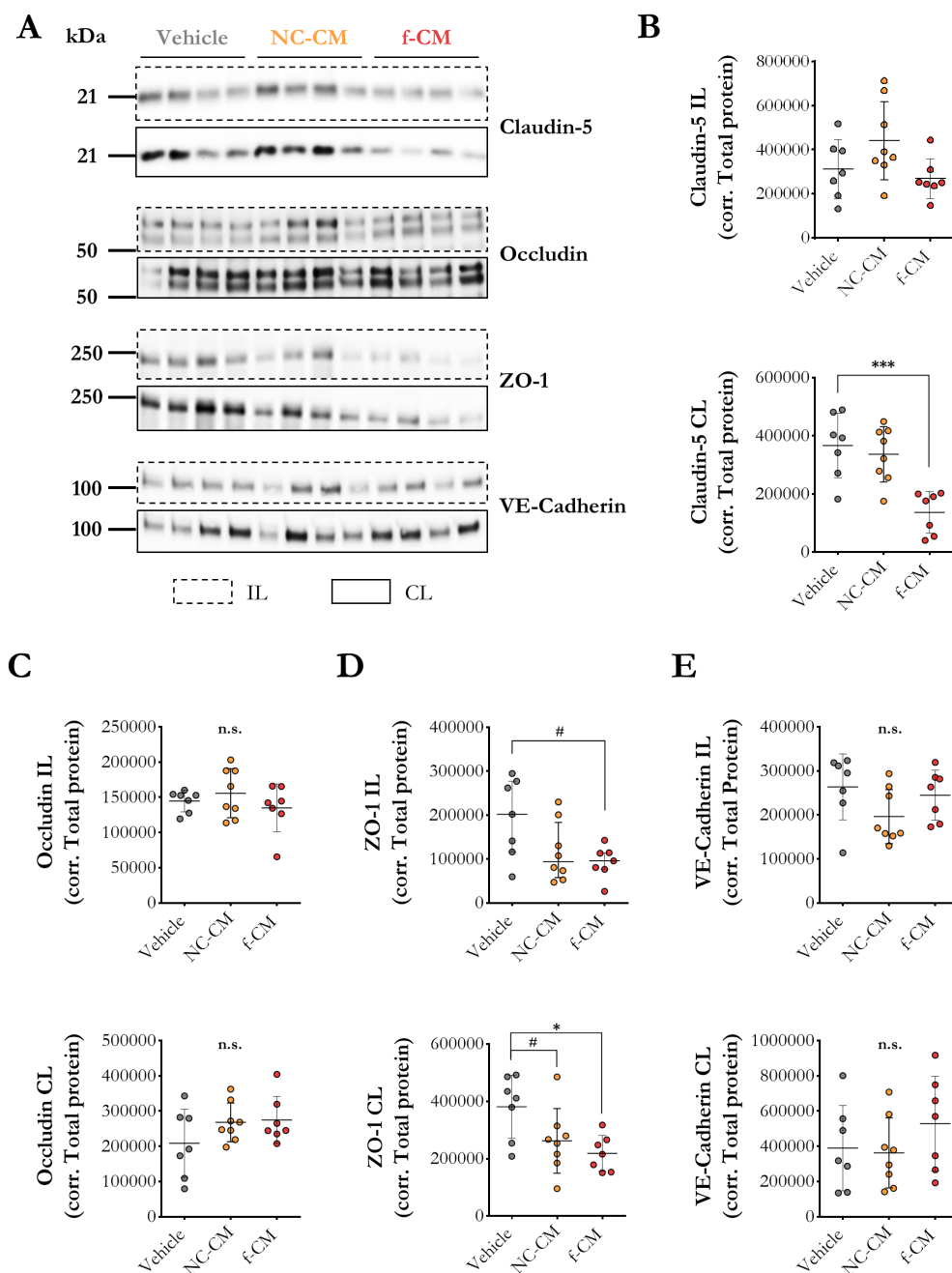


**Figure 41. Effect of hyperacute i.a. NC-CM or f-CM administration on BBB junctional proteins.** **A)** Representative images used for western blotting analysis of Claudin-5, Occludin, ZO-1 and VE-Cadherin. **B-E)** Graphs representing the expression of claudin-5, occludin, ZO-1 and VE-Cadherin corrected by Coomassie-stained total

## Results

---

protein, in the ipsilateral (IL; above) and contralateral (CL; below) brain blood vessels, respectively. All data are represented as mean±SD, except for ipsilateral ZO-1 values, which are represented as median (IQR). kDa: kilodaltons, n.s.: non-significant, #P<0.10, \*P<0.05, \*\*\*P<0.001.

Next, a multiplexed ELISA was performed to evaluate the inflammatory response in the brain at 48 h after cerebral ischaemia and hyperacute i.a. treatment with vehicle, NC-CM or f-CM. The results from all the multiplexed molecules are presented in **Table 10**, and those showing a significant difference amongst treatment groups are represented in **Figure 42**.

First, the levels of several pro-inflammatory cytokines (IL-6, KC, and MCP-1) were significantly increased in the ischaemic brain compared to the healthy hemisphere, regardless of the treatment (P<0.0001 vs. contralateral for all measures), confirming the acute inflammatory response in the ischaemic brain.

Furthermore, only the f-CM-treated mice presented increased levels of MIP-2 in the ipsilateral brain compared to the healthy brain (P=0.034), and a slight yet not significant increase in the ipsilateral levels of GM-CSF and TNF $\alpha$  compared to the contralateral (P=0.131 and P=0.126, respectively).

Importantly, the treatment with f-CM elevated the ipsilateral brain levels of GM-CSF and TNF $\alpha$  compared to the vehicle group (2.14-fold increase, P=0.0046, and 1.53-fold increase, P=0.0224, respectively).

In contrast, the brain levels from all of the chemokines/cytokines investigated were similar between NC-CM-treated mice and those receiving vehicle, both in ipsilateral and contralateral brain homogenates (P>0.05 for all measures vs. Vehicle).

**Table 10.** Brain levels of neuro-inflammatory molecules at 48 h after cerebral ischaemia and hyperacute i.a. treatment with free/nanotargeted EPCs-secretome.

Markers	Vehicle (pg/mg)	NC-CM (pg/mg)	f-CM (pg/mg)	ANOVA /K-W (P-value)	NC-CM vs. Vehicle (adj. P-v)	f-CM vs. Vehicle (adj. P-v)
<b>Ipsilateral brain</b>						
GM-CSF	25.9±12.7	26.0±16.0	55.4±22.6	<b>0.0036</b>	>0.999	<b>0.0046</b>
IFN $\gamma$	5.02±3.53	4.82±3.44	6.04±2.61	0.6663	0.9870	0.7023
IL-1 $\alpha$	379.8±229.8	290.6±199.9	449.7±295.8	0.3544	0.5722	>0.999
IL-1 $\beta$	8.60±3.93	6.06±3.06	8.42±3.65	0.3152	0.4151	>0.999
IL-4	0.71±0.26	0.54±0.32	0.88±0.36	<b>0.0361</b>	0.1976	0.7481
IL-6	438.8±352.7 ****	313.8±228.57 ****	619.1±400.9 ****	0.1506	>0.9999	0.3905
IL-10	33.7±18.0	26.2±18.6	48.6±25.7	<b>0.0373</b>	0.6690	0.2307
CXCL1/KC	163.1±141.4 ****	127.7±73.6 ****	170.3±88.6 ****	0.3882	>0.999	0.3946
MCP-1	131.8±67.3 ****	116.7±77.7 ****	170.1±19.9 ****	0.2570	>0.999	0.5062
CXCL2/MIP-2	34.0±13.0	27.4±10.6	46.7±18.3 *	<b>0.0178</b>	0.4847	0.1043
TNF $\alpha$	4.05±1.48	3.13±1.71	6.18±2.07	<b>0.0021</b>	0.4127	<b>0.0224</b>
<b>Contralateral brain</b>						
GM-CSF	31.9±18.2	36.5±20.3	42.8±29.0	0.4827	0.8663	0.4660
IFN $\gamma$	3.72±2.15	5.28±3.56	6.23±4.40	0.4162	0.5411	0.4571
IL-1 $\alpha$	265.5±126.7	251.0±137.9	337.8±241.2	0.9114	>0.999	>0.999
IL-1 $\beta$	6.62±2.74	6.57±3.15	6.4±2.0	0.973	0.9990	0.9666
IL-4	0.64±0.26	0.66±0.48	0.69±0.34	0.8323	>0.999	>0.999
IL-6	21.3±13.0	26.8±18.4	35.5±18.4	0.1087	0.6857	<b>0.0718</b>
IL-10	27.6±14.4	29.7±18.3	37.0±18.2	0.4304	>0.999	0.4168
CXCL1/KC	24.1±6.6	26.0±10.1	33.6±11.6	0.2325	>0.999	0.2846
MCP-1	39.6±28.7	33.4±15.9	40.9±18.7	0.6750	>0.999	>0.999
CXCL2/MIP-2	28.4±10.7	26.0±10.6	30.2±9.4	0.6647	0.8361	0.8987
TNF $\alpha$	3.48±1.50	3.47±1.44	4.8±1.8	0.1411	0.9999	0.1629

Data represented as mean±SD. \*P<0.05 vs. respective contralateral, \*\*\*\*P<0.0001 vs. respective contralateral. Adj. P-v: adjusted P-value.

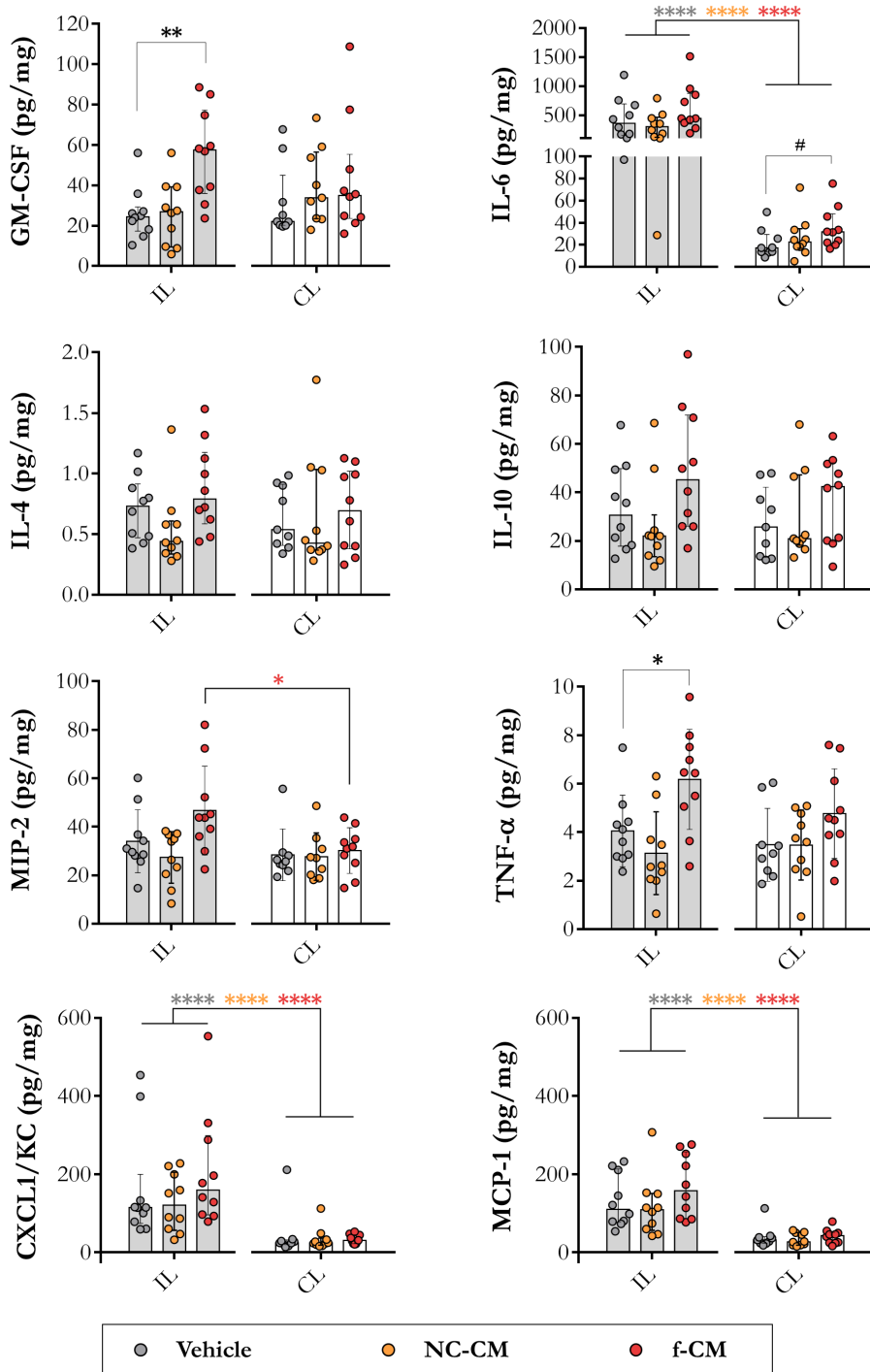


**Figure 42.** Effects of hyperacute i.a. NC-CM or f-CM administration on the brain inflammatory status at 48 h after cerebral ischaemia. Graphs representing neuro-

inflammatory molecules differently expressed amongst ipsilateral (IL)/contralateral (CL) brains or amongst treatment groups (n=10/group). All data are expressed as pg of protein per mg of total protein, and represented as median (IQR), except MIP-2 and TNF $\alpha$ , which are represented as mean $\pm$ SD. #P<0.10, \*P<0.05, \*\*P<0.01, \*\*\*P<0.0001 (the colours represent comparisons between brain hemispheres within each treatment group, respectively).

#### 4.4.2. Long-term efficacy after hyperacute endovascular administration of free or nanotargeted EPCs-secretome in ischaemic mice

It should be noted that we were unable to confirm the efficient arrival of nano-encapsulated EPCs-secretome proteins in the brain (*Biodistribution study 5*). The optical densities from the tested samples (brain homogenates and brain vascular fractions from ischaemic mice at 3 h after acute i.a. NC-CM administration), fell under the limit of detection of the technique (*data not shown*), probably due to the low amount of single specific proteins loaded in the *biodistribution dose* of 1.6 mg of NC-CM. Furthermore, the samples were not tested with the uPA ELISA given the cross-reactivity detected with the mouse-derived protein in the brain samples of non-treated mice (*data not shown*).

Despite this, we aimed to evaluate the long-term therapeutic efficacy in ischaemic mice at 2 weeks after receiving hyperacute i.a. vehicle, NC-CM with magnetic retention (M2) or f-CM (n=9-10/group; *Efficacy study 2*).

##### 4.4.2.1. Long-term NCs biodistribution

First, in order to study the nanomaterial biodistribution beyond the acute phase, two different groups of ischaemic mice receiving i.a. NC-CM with magnetic retention (M2) were followed for 48 h or 1 week, respectively, when NC-CM biodistribution was assessed by *in vivo* and *ex vivo* FMI (*Biodistribution study 6*; **Figure 43**).

The Cy5-NC signal was still detectable in the brain at 1 week after administration, but also in off-target organs, as seen both by *in vivo* and *ex vivo* FMI (**Figure 43**).

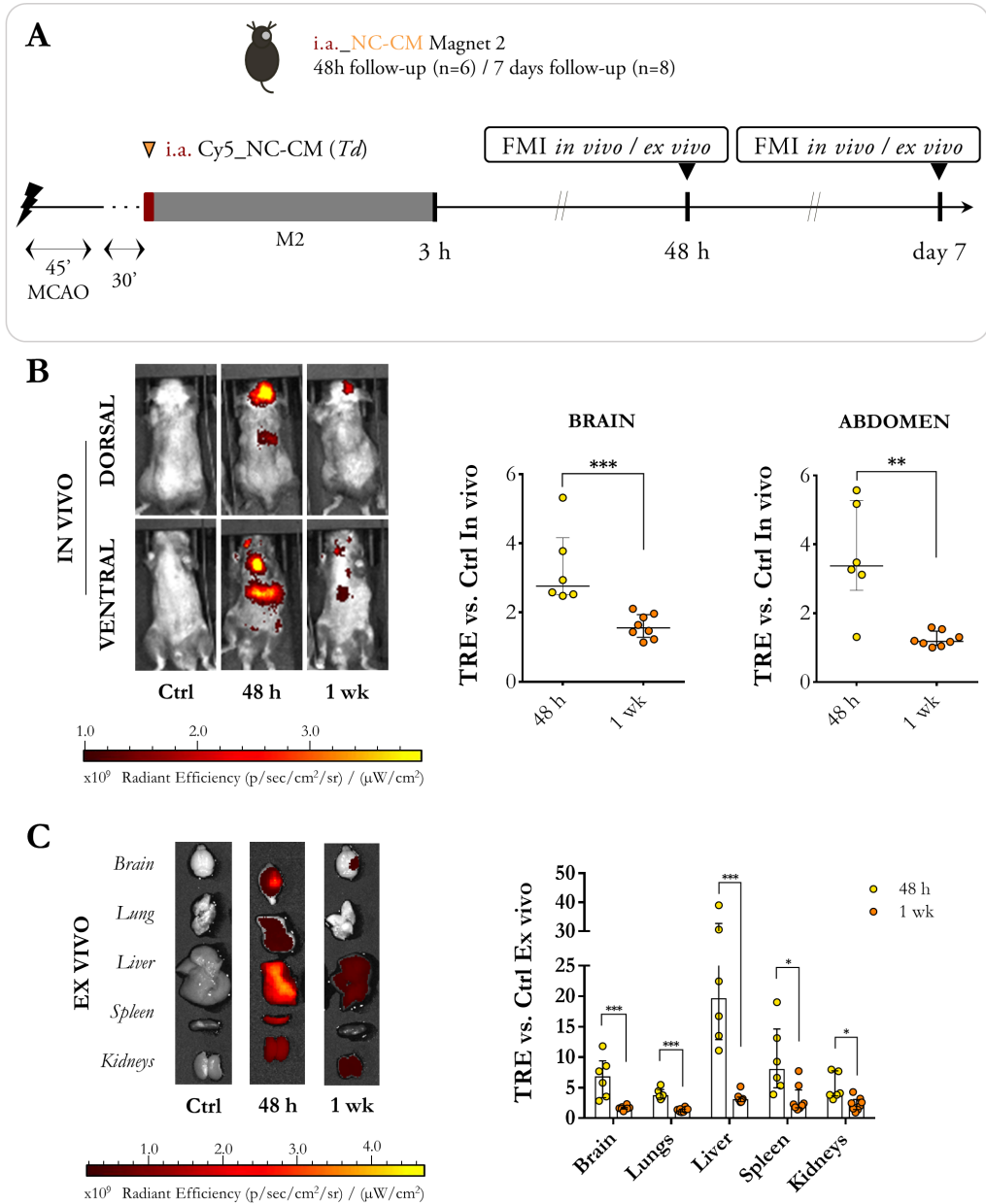


**Figure 43. Biodistribution after i.a. NC-CM administration and magnetic targeting (M2) in ischaemic mice showing the NCs clearance at 1 week after administration. A)** Scheme of the experimental design of *Biodistribution study 6*. **B)** Representative *in vivo* FMI images at 48 h and 1 week after i.a. NCs administration and graphs showing the corresponding TRE quantification on brain and abdominal ROIs corrected by their control animal. **C)** Representative *ex vivo* FMI images at 48 h and 1

week after i.a. NCs administration and graph showing the quantification of TRE on ROIs from all organs corrected by their control animal. Data are shown as median (IQR). \*\* $P < 0.01$ , \*\*\* $P < 0.001$ .

Nevertheless, a significant clearance of the NCs signal was observed when comparing the *in vivo* and *ex vivo* TRE values at 1 week vs. 48 h. Specifically, our results showed a significant 2.04-fold decrease of the *in vivo* NCs signal reaching the brain region, and a significant 2.92-fold decrease of the *in vivo* NCs signal reaching the abdominal region at 1 week vs. 48 h ( $P = 0.0007$  and  $P = 0.0027$ , respectively). *Ex vivo*, a significant decrease of the TRE was also observed in all of the organs investigated at 1 week vs. 48 h post-administration (Brain: 4.07-fold,  $P = 0.0007$ ; Lungs: 2.94-fold,  $P = 0.0007$ ; Liver: 6.85-fold,  $P = 0.0007$ ; Spleen: 3.09-fold,  $P = 0.0127$ ; Kidneys: 2.21-fold;  $P = 0.0127$ ). Furthermore, the Cy5-labelled NCs fluorescence co-localised with vessels (stained with FITC-conjugated lectin), as seen in *ex vivo* perfused brain slices at 48 h after i.a. NCs administration (**Figure 44**).

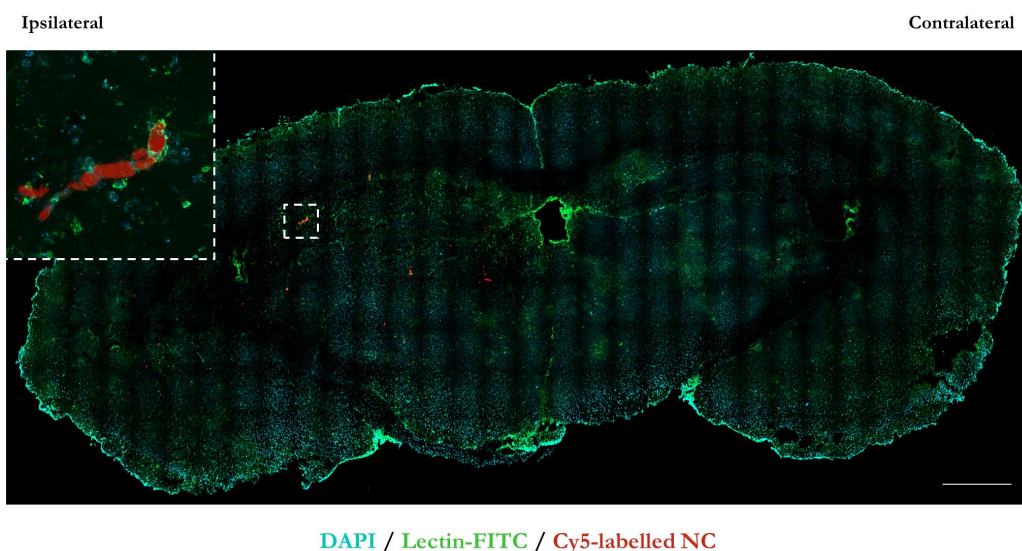


**Figure 44.** *Ex vivo* Cy5-NCs fluorescence showing ipsilateral accumulation in micro-vessels at 48 h after i.a. administration and magnetic retention (M2). Scale bar: 500  $\mu\text{m}$ . Upper insets show magnified blood vessel (lectin-FITC) with positive Cy5 signal.



### 4.4.2.2. Long-term safety and functional outcome

Potential systemic toxicity arising from the endovascular administration of NC-CM or f-CM was studied in the animals from *Efficacy studies 1 and 2*, at 48 h and 2 weeks after MCAO (**Table 11**).

The levels of ALT were slightly increased in the NC-CM group at 2 weeks compared to its respective levels at 48 h ( $P=0.0627$ ). Importantly, though, no differences were observed in the levels of ALT between treatment groups at any of the time points analysed ( $P>0.05$  for all measures). In the same line, the levels of AST were similar between treatment groups at all the time points ( $P>0.05$  for all measures). On the other hand, AST levels were decreased at 2 weeks vs. 48 h in all groups receiving vehicle, NC-CM or f-CM ( $P=0.004$ ,  $P=0.0057$ , and  $P=0.0016$ , respectively). Moreover, CK levels were increased in the f-CM group vs. the vehicle control group at 48 h ( $P=0.0498$ ), but no differences were observed at 2 weeks between treatment groups ( $P>0.05$ ). A significant decrease was observed in the CK levels at 2 weeks vs. 48 h in the f-CM group ( $P=0.0068$ ), and in the group receiving NC-CM, although not reaching statistical significance ( $P=0.0743$ ). No differences were observed instead between the levels of CK at the different time points in the vehicle group ( $P>0.05$ ).

The results observed in the AST and CK levels are in line with those reported in the *Safety study* (section 4.3.2, **Table 9**), indicating an acute muscular injury likely related to the surgical procedure, which is resolved at a later stage. However, it should be highlighted that, as described above, this acute muscular injury was exacerbated in the f-CM group.

Regarding the markers of renal function, no differences were observed in the plasma urea levels in the NC-CM vs. the vehicle group, at any of the time points analysed ( $P>0.05$  for all measures), and no differences were found in neither the vehicle nor the NC-CM group between their respective time points ( $P>0.05$  for all measures).

However, the urea levels were slightly increased in the group receiving f-CM compared to the vehicle group, at 48 h ( $P=0.0970$ ). These increased levels in the f-CM group were however normalised at 2 weeks, although not reaching statistical significance ( $P=0.068$ ), and the values at 2 weeks were similar amongst groups ( $P>0.05$  for all measures). Furthermore, no differences were observed between time points nor amongst treatment groups in the plasmatic  $\text{Na}^{2+}$  levels ( $P>0.05$  for all measures).

Finally, regarding the pancreatic markers, no significant differences were found in the levels of  $\alpha$ -amylase nor lipase amongst treatment groups at any of the time points analysed ( $P>0.05$  for all measures), although a significant decrease was detected in  $\alpha$ -amylase at 2 weeks in the NC-CM group vs. its respective 48 h levels ( $P=0.0349$ ). On the other side, lipase levels were increased at 2 weeks in all treatment groups compared to their respective levels at 48 h (Vehicle  $p=0.0028$ , NC-CM  $P=0.0029$ , f-CM  $P=0.0042$ ), indicating an alteration related to the surgical procedure, but not to the treatment. Furthermore, these results are in line with those reported in the *Safety study*.

**Table 11. Plasmatic toxicity markers from the *Efficacy studies 1 and 2*.**

	MCAO + Vehicle		MCAO + NC-CM		MCAO + f-CM	
	48 h	2 wk	48 h	2 wk	48 h	2 wk
<b>ALT</b> (UI/L)	27.7±9.8	43.0±29.5	30.8±17.5	46.6±26.1 #	29.4±15.6	43.0±30.3
<b>AST</b> (UI/L)	166.6±36.9	110.0±39.8 **	177.4±60.7	87.9±25.2 **	179.0±35.3	97.8±52.1 **
<b>CK</b> (UI/L)	283.9±90.2	275.7±116.5	345.6±127.1	232.6±87.5 #	423.2±182.7 *	214.4±84.2 **
<b>Urea</b> (mg/dL)	28.8±5.7	29.1±7.9	28.0±3.4	31.2±9.4	34.0±7.6 #	26.1±4.8 #
<b>Na<sup>2+</sup></b> (mmol/L)	139.5±2.4	141.2±3.1	138.1±2.9	142.7±4.1	139.8±3.2	141.7±4.3
<b><math>\alpha</math>-amylase</b> (UI/L)	1832.4±418	2110.6±948.6	2079.7±660.6	1542.6±256.8 *	2167.3±480.7	2009.5±861.7
<b>Lipase</b> (UI/L)	27.7±9.4	63.9±25.0 **	27.0±6.7	62.0±27.7 **	21.4±5.0	71.2±35.8 **

Data represented as mean±SD. # $P<0.10$  vs. Vehicle, # $P<0.10$  vs. respective 48 h group, \* $P<0.05$  vs. respective 48 h group, \*\* $P<0.01$  vs. respective 48 h group.

The body weight changes and mortality were similar during the 2 weeks following MCAO and hyperacute i.a. treatment with either vehicle, NC-CM or f-CM ( $P>0.05$ ; **Figure 45B**). Also, no major changes were observed in terms of functional outcome during 2 weeks of follow-up amongst treatment groups, yet some modest variations were found in the functional recovery patterns over time within treatment groups, which are described below (**Figure 45C**).

An overall significant difference was indeed observed in the neuroscore along time, regardless of the treatment ( $P<0.0001$ ). Specifically, a significant improvement in the neuroscore was observed at 1 week compared to 24 h in the f-CM group ( $P=0.0431$ ) and in the NC-CM, although not reaching statistical significance ( $P=0.1066$ ), but not in the group receiving vehicle ( $P=0.2703$ ). At 2 weeks, a significant improvement was observed in all vehicle, NC-CM and f-CM groups ( $P=0.0467$ ,  $P=0.0201$ , and  $P=0.0006$  vs. 24 h, respectively). However, no overall significant differences were observed in the neuroscore based on the treatment ( $P=0.1242$ ). Despite this, and although it did not reach statistical significance, the neuroscore was higher at 24 h and 48 h in the group receiving f-CM, but not significantly ( $P=0.1546$  and  $P=0.1276$  vs. Vehicle, respectively). The grip strength measurements also showed overall significant differences along time, regardless of the treatment ( $P<0.0001$ ). Specifically, the forelimb strength decreased at 48 h in the groups receiving vehicle or f-CM, but did not change in the NC-CM group ( $P=0.001$ ,  $P=0.0332$ , and  $P=0.3937$  vs. 24 h, respectively). This forelimb strength decrease was also observed at 1 and at 2 weeks in all vehicle, NC-CM and f-CM groups ( $P<0.0001$ ,  $P=0.0021$ , and  $P=0.0002$  at 1 week vs. 24 h, respectively;  $P<0.0001$ ,  $P<0.0001$ , and  $P=0.0002$  at 2 weeks vs. 24 h, respectively).

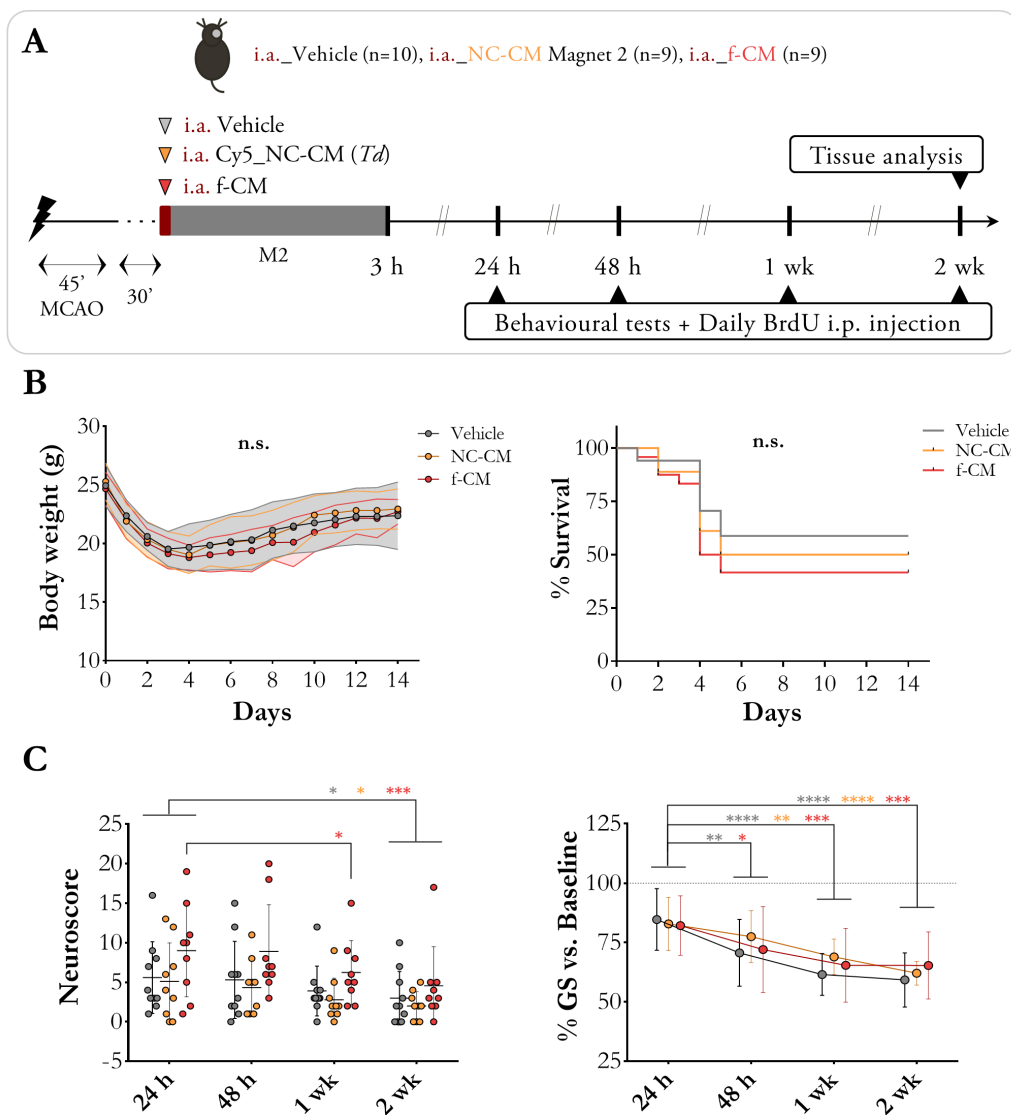


**Figure 45.** Functional outcome after hyperacute i.a. NC-CM or f-CM administration and NC magnetic targeting (M2) in ischaemic mice. **A)** Scheme of the experimental design of the long-term *Efficacy study 2*. **B)** Graphs showing body weight follow-up and survival rate. **C)** Graphs showing neuroscore and grip strength (GS) percentage vs. the corresponding pre-MCAO GS (dashed line). All data are expressed as mean $\pm$ SD. n.s.: non-significant, \* $P$ <0.05, \*\* $P$ <0.01, \*\*\* $P$ <0.001, \*\*\*\* $P$ <0.0001 (the colours represent comparisons within each treatment group, respectively).

#### 4.4.2.3. Effects of free or encapsulated EPCs-secretome on brain angiogenesis

Brain angiogenesis was evaluated through lectin functional vessels-staining in the anatomical SVZ and hippocampal areas, as representative anterior and posterior brain infarcted regions, respectively. Overall, brain angiogenesis was enhanced in ischaemic mice at 2 weeks after receiving either encapsulated (NC-CM) or free (f-CM) EPCs-secretome (**Figures 46-49**). Nonetheless, some relevant differences regarding the specific regions of enhanced vascular density were observed amongst both treatments, which are described below.

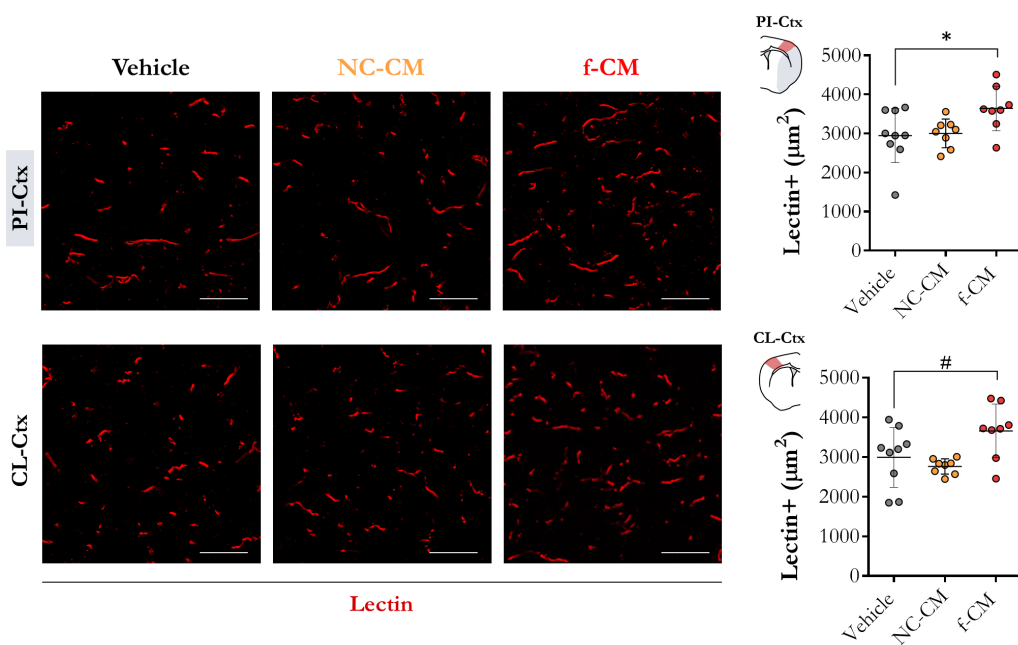


**Figure 46. Cortical peri-infarct angiogenesis in the anterior ischaemic brain.**

Representative cortical (Ctx) micrographs from lectin immunofluorescence used for quantification (scale bar: 50  $\mu\text{m}$ ), in the peri-infarct (PI) and contralateral (CL) anterior infarcted brain region from ischaemic mice at 2 weeks after receiving i.a. vehicle, NC-CM with magnetic targeting (M2), or f-CM (long-term *Efficacy study 2*; n=8-9/group). Graphs represent the lectin-positive area in the depicted ROIs for each region. All data are represented as mean $\pm$ SD. #P<0.10, \*P<0.05.

Our results show that **peri-infarct cortical vessel density** was significantly increased in **f-CM-treated** animals, both in the anterior and posterior infarcted brain ( $P=0.0352$ , and  $P=0.0052$  vs. Vehicle, **Figures 46 and 48**, respectively). Surprisingly, the vessel density of f-CM-treated animals was slightly increased also in the **contralateral cortical tissue**, both in the anterior and posterior regions of study ( $P=0.0594$  vs. Vehicle, and  $P=0.0253$  vs. Vehicle, **Figures 46 and 48**, respectively).

In contrast, no differences were seen in the vessel density in the peri-infarct nor the contralateral **subcortical** brain tissue, in neither NC-CM nor f-CM treated animals ( $P>0.05$  for all measures; **Figures 47 and 49**), except for the ipsilateral subcortex in the posterior brain region of f-CM-treated mice ( $P=0.0366$  vs. Vehicle; **Figure 49**).

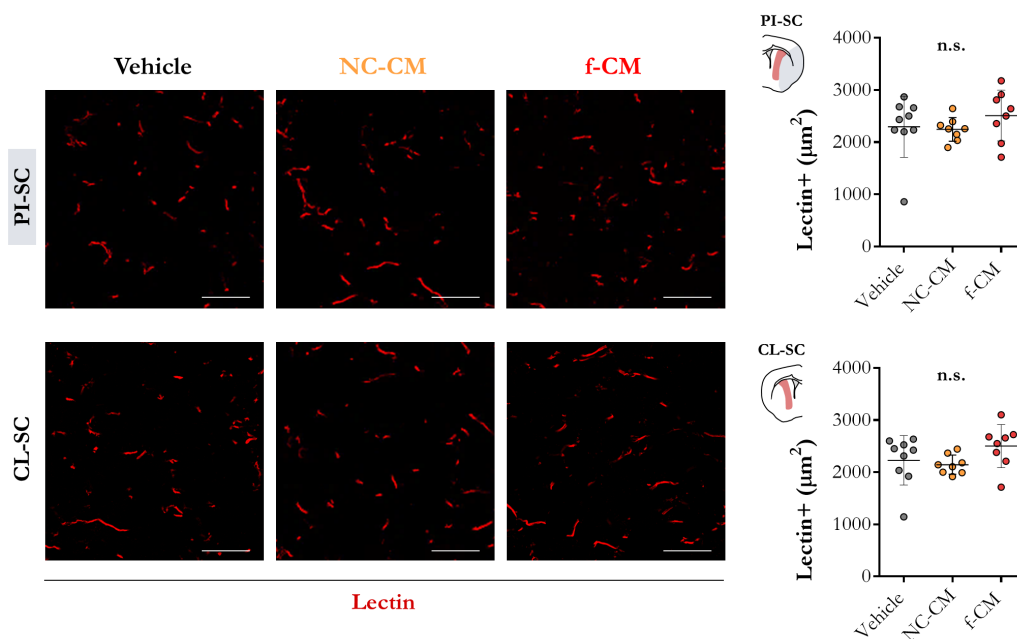


**Figure 47. Subcortical peri-infarct angiogenesis in the anterior ischaemic brain.**

Representative subcortical (SC) micrographs from lectin immunofluorescence used for quantification (scale bar: 50  $\mu\text{m}$ ), in the peri-infarct (PI) and contralateral (CL) anterior infarcted brain region from ischaemic mice at 2 weeks after receiving i.a. vehicle, NC-CM with magnetic targeting (M2), or f-CM (long-term *Efficacy study 2*;  $n=8-9/\text{group}$ ). Graphs represent the lectin-positive area in the depicted ROIs for each region. All data are represented as mean  $\pm$  SD. n.s. non-significant.

## Results

Finally, **peri-infarct cortical vessel density** was not increased in the anterior ischaemic brain of **NC-CM-treated animals** ( $P>0.05$  vs. Vehicle), however it did promote angiogenesis in the peri-infarct cortical posterior brain ( $P=0.0262$  vs. Vehicle) and, importantly, there was no off-target increase in vessel density, as seen in f-CM-treated mice (see **Figures 46-48**).

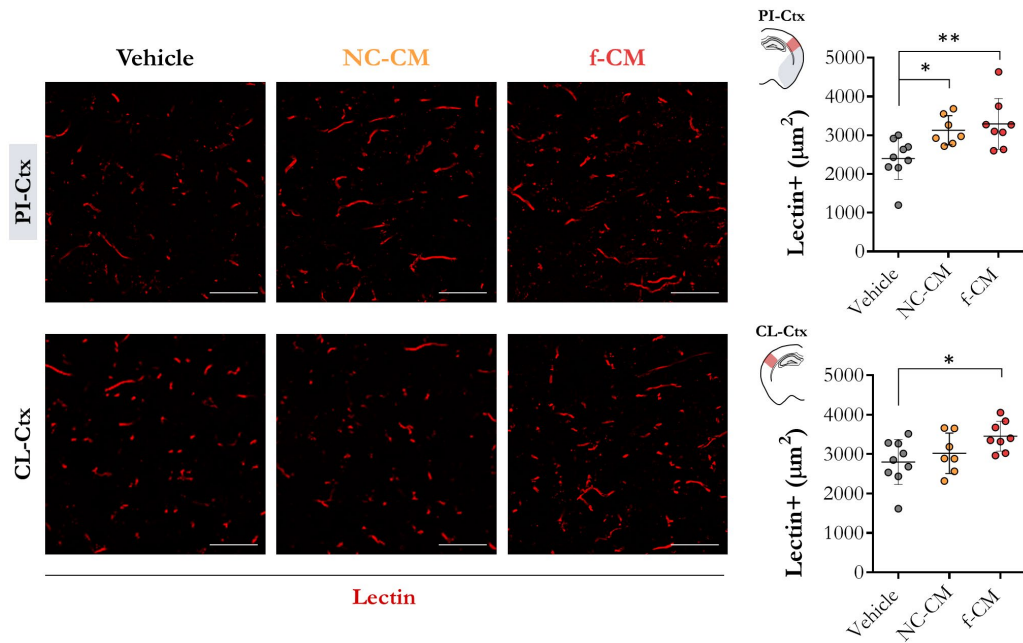


**Figure 48. Cortical peri-infarct angiogenesis in the posterior ischaemic brain.** Representative cortical (Ctx) micrographs from lectin immunofluorescence used for quantification (scale bar: 50  $\mu\text{m}$ ), in the peri-infarct (PI) and contralateral (CL) posterior infarcted brain region from ischaemic mice at 2 weeks after receiving i.a. vehicle, NC-CM with magnetic targeting (M2), or f-CM (long-term *Efficacy study 2*;  $n=7-9/\text{group}$ ). Graphs represent the lectin-positive area in the depicted ROIs for each region. All data are represented as mean  $\pm$  SD. # $P<0.10$ , \* $P<0.05$ , \*\* $P<0.01$ .

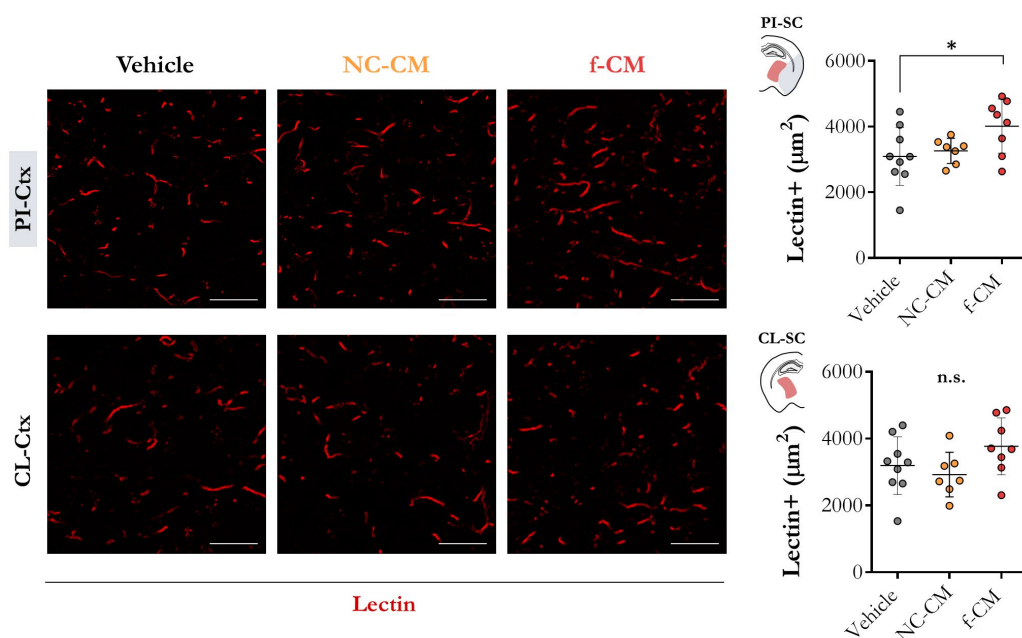


**Figure 49.** Subcortical peri-infarct angiogenesis in the posterior ischaemic brain.

Representative cortical (Ctx) micrographs from lectin immunofluorescence used for quantification (scale bar: 50  $\mu\text{m}$ ), in the peri-infarct (PI) and contralateral (CL) posterior infarcted brain region from ischaemic mice at 2 weeks after receiving i.a. vehicle, NC-CM with magnetic targeting (M2), or f-CM (long-term *Efficacy study 2*; n=7-9/group). Graphs represent the lectin-positive area in the depicted ROIs for each region. All data are represented as mean  $\pm$  SD. \*P<0.05, n.s.: non-significant.

In order to identify potential molecules involved in the underlying mechanisms of the EPCs-secretome pro-angiogenic effects described above, a mouse angiogenesis multiplexed ELISA was performed. For this purpose, brain homogenates from the ischaemic and corresponding contralateral tissue were obtained from representative samples of the same mice in which angiogenesis was studied (n=6-7/group, long-term *Efficacy study 2*). The results from all the multiplexed molecules are presented in **Table 12**.



**Table 12.** Brain levels of angiogenesis-related molecules at 2 weeks after cerebral ischaemia and hyperacute i.a. treatment with free/nanotargeted EPCs-secretome.

Markers	Vehicle (pg/mg)	NC-CM (pg/mg)	f-CM (pg/mg)	ANOVA /K-W (P-value)	NC-CM vs. Vehicle (adj. P-v)	f-CM vs. Vehicle (adj. P-v)
<b>Ipsilateral brain</b>						
Angiopoietin-2	85.3±23.0 *	68.0±24.1	88.5±33.0 *	0.3530	0.4246	0.9689
G-CSF	15.6±16.1 *	11.7±6.9 **	19.8±17.6 *	0.8675	>0.999	>0.999
EGF	13.7±2.5 *	12.7±2.9 **	12.9±2.6 *	0.2266	0.7529	0.8267
IL-6	6.54±3.0 *	5.88±2.06 **	5.90±2.55 *	0.9970	>0.999	>0.999
Endoglin	260.9±120.8 **	156.6±121.0 *	254.3±143.1 *	0.1721	0.1530	>0.999
Endothelin-1	2.26±0.67 *	1.81±0.71	2.0±0.64 *	0.5133	0.4122	0.8116
FGF-2	1524.3±406.3 *	1409.5±396.3 *	1923.1±866.8 #	0.2935	0.9146	0.4124
HGF	2305.3±597.1 *	2402.5±645.7 *	2433.1±774.6	0.9427	0.9523	0.9249
sCD31	109.3±36.5 **	96.8±42.3 *	112.5±27.4 **	0.7139	0.7631	0.9839
MCP-1	42.2±23.8 *	26.7±12.5 #	45.7±29.0 **	0.2861	0.3756	0.9464
SDF-1	247.8±69.2	225.1±71.3	180.2±65.0	0.2509	0.7796	0.1851
VEGF-A	1.08±0.28	0.89±0.22	0.91±0.18	0.3234	0.2818	0.3721
<b>Contralateral brain</b>						
Angiopoietin-2	57.9±11.0	54.2±14.7	53.2±3.5	0.7422	0.7792	0.6862
G-CSF	2.02±1.33	1.45±0.72	1.84±1.55	0.7006	0.8940	0.8833
EGF	8.56±1.76	7.49±1.39	8.41±1.55	0.4244	0.3856	0.9808
IL-6	3.33±0.66	3.18±0.74	2.87±0.75	0.5424	0.9050	0.4544
Endoglin	82.6±27.1	69.9±29.2	76.0±23.3	0.3664	0.3818	>0.999
Endothelin-1	1.41±0.28	1.34±0.45	1.28±0.21	0.8008	0.8989	0.7318
FGF-2	1028.2±162.4	982.0±153.5	1084.9±268.1	0.6561	0.8821	0.8404
HGF	1666.5±199.5	1667.1±345.1	1794.2±586.7	0.8191	>0.999	0.8103
sCD31	60.1±6.5	60.7±5.5	56.3±9.4	0.5233	0.9830	0.5771
MCP-1	14.2±6.0	15.9±8.1	8.80±2.32	<b>0.0545</b>	>0.999	0.1026
SDF-1	200.7±38.2	197.5±50.7	163.5±25.6	0.2326	0.9853	0.2204
VEGF-A	0.92±0.2	0.80±0.20	0.84±0.11	0.3669	0.3097	>0.999

Data represented as mean±SD. #P<0.10 vs. respective contralateral, \*P<0.05 vs. respective contralateral, \*\*P<0.01 vs. respective contralateral, \*\*\*P<0.0001 vs. respective contralateral. Adj. P-v: adjusted P-value.

Most of the angiogenesis-related molecules showed increased levels in the ipsilateral brain hemisphere at 2 weeks after cerebral ischaemia, compared to the contralateral brain, which is indicative of a spontaneously-active repair in the post-ischaemic brain. Specifically, all molecules shown in **Table 12** except SDF-1 and VEGF-A, were increased in the infarcted brain of vehicle-treated mice ( $P < 0.05$  vs. contralateral for all measures). However, the levels of angiopoietin-2, endothelin-1, and MCP-1 were not significantly different in the ipsilateral brain of NC-CM treated mice, as seen in vehicle- and f-CM-treated mice ( $P > 0.05$  for all measures vs. contralateral). On the other hand, the group receiving f-CM showed an increased ipsilateral expression of the same molecules as the vehicle-treated group ( $P < 0.05$  vs. contralateral for all measures), except for FGF-2, which did not reach a statistically significant difference ( $P = 0.078$  vs. contralateral).

Furthermore, it should be highlighted that a marked correlation was found between the overall ipsilateral brain levels of endothelin-1 and angiopoietin-2 ( $r = 0.8901$ ,  $P < 0.0001$ ), MCP-1 and angiopoietin-2 ( $r = 0.4992$ ,  $P = 0.0296$ ), and MCP-1 and endothelin-1 ( $r = 0.5986$ ,  $P = 0.0068$ ). The same association was found between the overall contralateral brain levels of endothelin-1 and angiopoietin-2 ( $r = 0.9190$ ,  $P < 0.0001$ ), MCP-1 and angiopoietin-2 ( $r = 0.7510$ ,  $P = 0.0002$ ), and MCP-1 and endothelin-1 ( $r = 0.6954$ ,  $P = 0.0009$ ).

Despite the increased vessel density observed predominantly in the peri-infarct cortical brain tissue of NC-CM and f-CM-treated mice, we failed to detect differences in the brain levels of angiogenesis-related proteins, at 2 weeks after cerebral ischaemia and treatment ( $P > 0.05$  vs. vehicle for all measures). Only a trend was observed in the contralateral levels of MCP-1, which were slightly decreased in the f-CM group ( $P = 0.1026$  vs. vehicle).

#### 4.4.2.4. Effects of free or encapsulated EPCs-secretome on neurogenesis and delayed neurodegeneration

We also sought to study whether free or encapsulated EPCs-secretome therapy had an effect on neurogenesis, assessed by neuroblasts immunofluorescence staining (DCX+ cells) and proliferative cells (BrdU+ cells) in the SVZ (**Figure 50**) and SGZ (**Figure 51**). However, we failed to detect significant differences between treatment groups ( $P > 0.05$  for all measures).

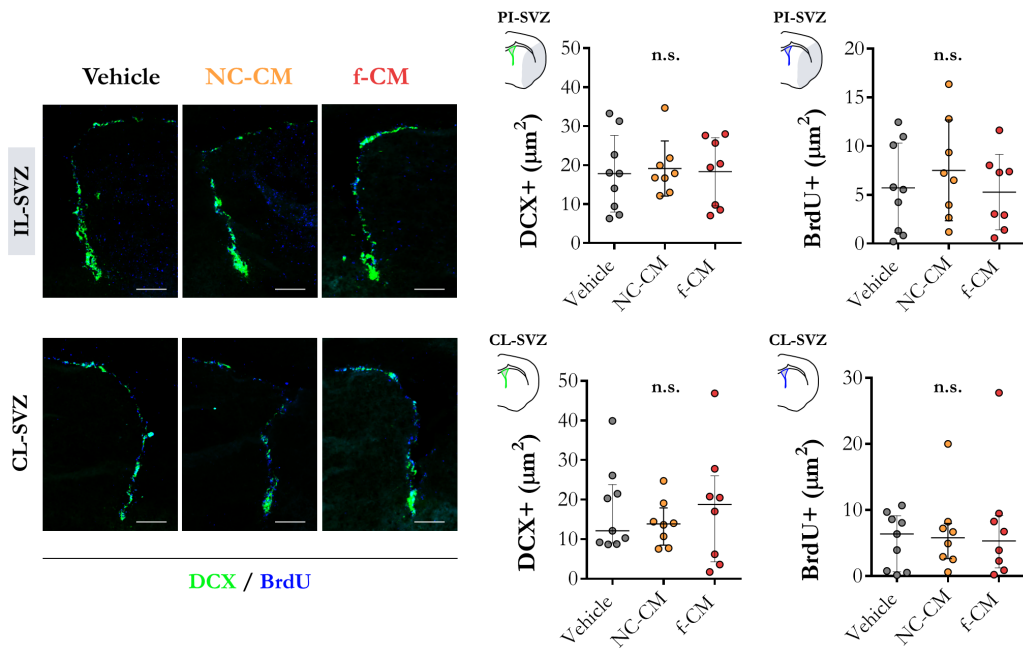


**Figure 50. SVZ neurogenesis at two weeks after cerebral ischaemia.** Composition of representative micrographs for DCX (green) and DAPI (blue) showing proliferative neuroblasts in the SVZ in each treatment group (long-term *Efficacy study 2*;  $n=7-9$ /group). Graphs represent the quantification of DCX-positive and BrdU-positive areas in both the ipsilateral (above) and contralateral (below) SVZ. All data are expressed as mean  $\pm$  SD, except DCX-positive area and BrdU-positive area in the contralateral SVZ, which are represented as median (IQR). n.s.: non-significant.

DCX+ neuroblasts were observed in both the SVZ and hippocampal SGZ of the DG of all ischaemic mice, and co-staining with BrdU+ cells indicated that most of these cells were also under proliferation (Figures 50 and 51). However, neither the amount of neuroblasts expressed as DCX-positive area in the SVZ or the DG, nor the proliferative cells expressed as BrdU-positive area in the SVZ, were different between groups ( $P>0.05$  for all measures; Figures 50 and 51). However, the proliferative cells, quantified as the BrdU-positive area in the ipsilateral DG were significantly increased in f-CM-treated mice ( $P=0.0253$  vs. Vehicle; Figure 51).

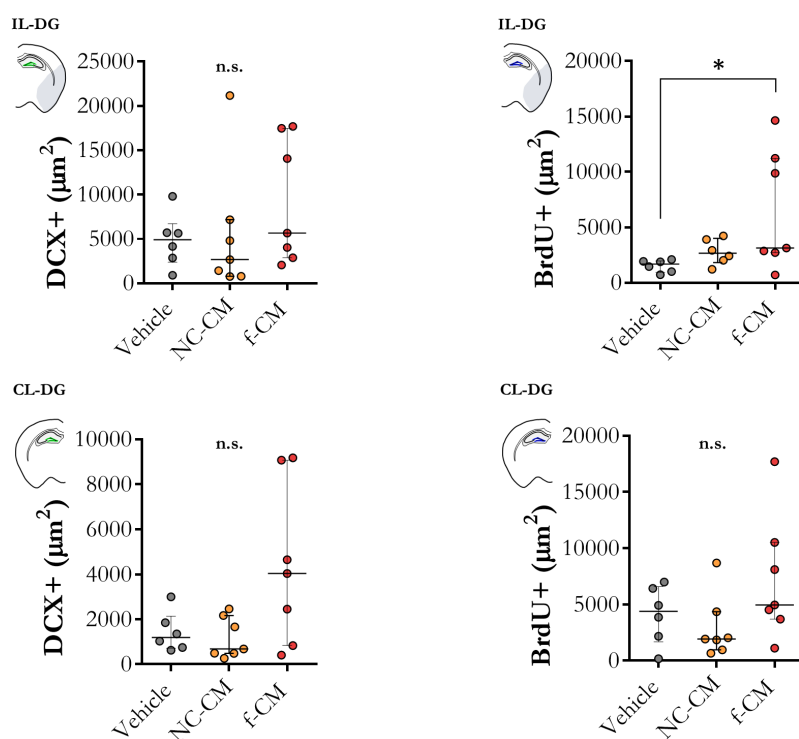


**Figure 51. Hippocampal DG neurogenesis at two weeks after cerebral ischaemia.**

Graphs represent the quantification of DCX-positive and BrdU-positive areas in both the ipsilateral (above) and contralateral (below) hippocampal DG. All data are expressed as median (IQR). n.s.: non-significant,  $*p<0.05$ .

## Results

Next, we evaluated neural degeneration in the SVZ anatomical brain region at 2 weeks after cerebral ischaemia and treatment, by means of Fluoro-Jade C staining.<sup>210</sup> Our results showed that hyperacute i.a. treatment with NC-CM reduced the cortical neurodegeneration at 2 weeks after the ischaemic event ( $P=0.0783$  vs. Vehicle), while no differences were observed in the f-CM group ( $P>0.05$  vs. Vehicle). Furthermore, the subcortical and total FJC-positive area was similar amongst groups ( $P>0.05$ ). It should be highlighted that the mechanisms for which FJC stains degenerating neurons remain unclear, and several authors suggest an unspecific labelling of resting or activated astrocytes and microglia.<sup>211</sup>

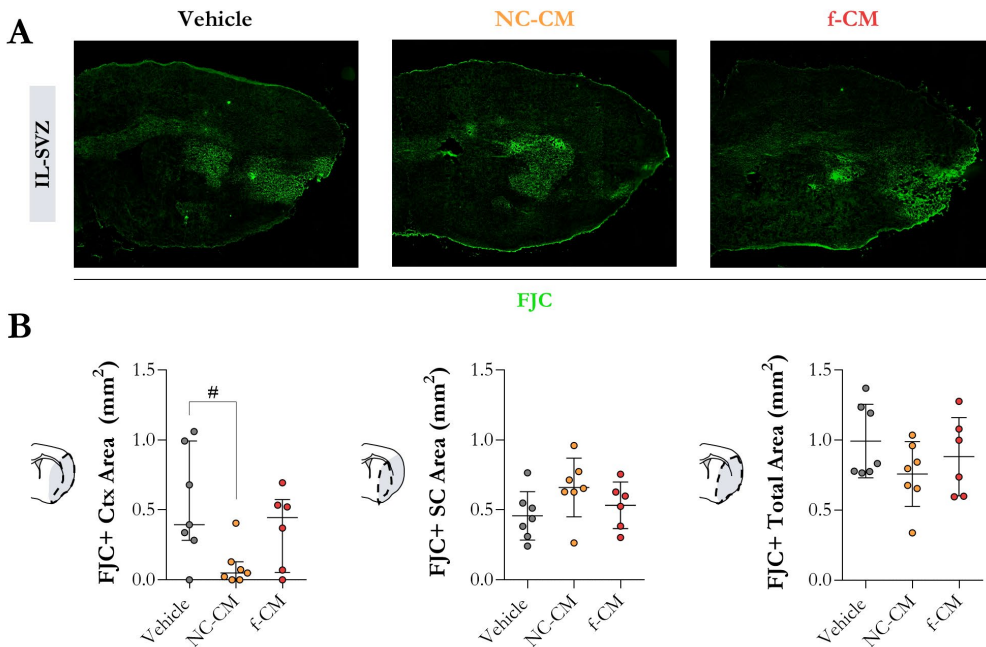


**Figure 52. Fluoro-Jade C staining showing neurodegeneration at two weeks after cerebral ischaemia. A)** Representative images showing neurodegenerating brain areas as FJC-positive regions in the ipsilateral brain (SVZ anatomical region), in all treatment groups (long-term *Efficacy study 2*;  $n=6-7$ /group). **B)** Graphs showing the quantification of cortical, subcortical or total FJC-positive area. All data are represented as mean $\pm$ SD, except the cortical FJC-positive area, which is represented as median (IQR). # $P<0.10$ .

## 4.5. Translational feasibility of endovascular delivery and magnetic retention for nanomaterial brain retention

### 4.5.1. Endovascular nanocarriers delivery in naïve pigs

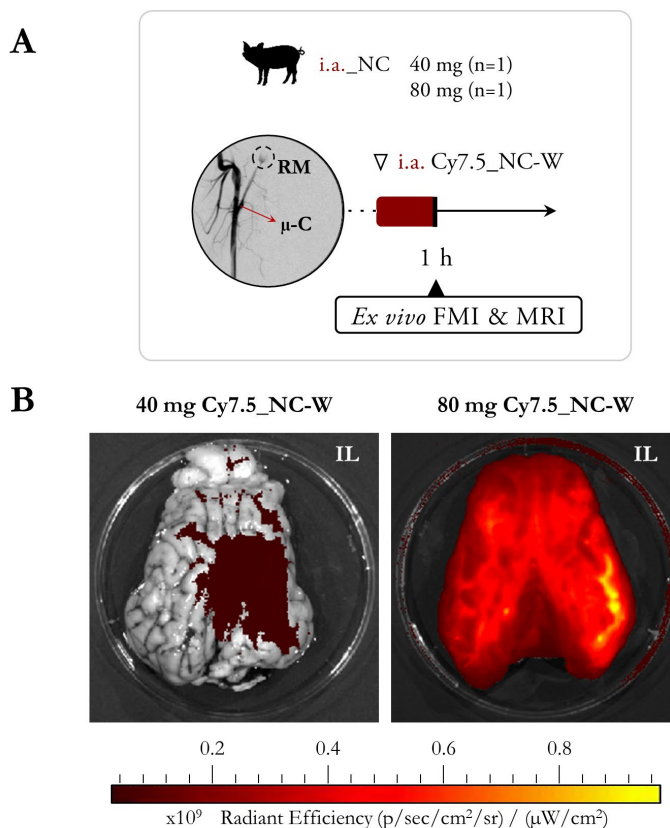


**Figure 53.** Pilot study to assess the translational feasibility of endovascular NCs delivery in healthy adult pigs receiving different doses of Cy7.5-labelled NCs (n=1/group). **A**) Scheme of the experimental design, with an angiography insert showing the micro-catheter ( $\mu$ -C) position for endovascular infusion, proximal to the rete mirabile (RM). **B**) Brain *ex vivo* FMI images at 1 h after i.a. NC administration. IL: ipsilateral.

As previously mentioned, the administration of nanomaterials has raised safety concerns related to infusion reactions leading to cardiopulmonary complications, associated with complement activation (CARPA).

For this reason, a preliminary experiment was performed in order to determine the optimal NCs dosage prior to the pre-clinical testing of the proposed nanoformulation in large animals (**Figure 53A**). Traditionally, the aforementioned reaction is prevented by controlling the administration at slow infusion rates. In this light, a first dose of 40 mg of Cy5-labelled NC-W and an infusion rate of 0.8 mg/min were determined based on the recommended infusion rate described in the literature (1 mg/min), while ensuring a reasonable duration of the intervention for translational purposes.<sup>212</sup>

No adverse reactions were observed during the intervention in terms of arterial pressure, respiratory nor heart rate alterations. Furthermore, the NCs fluorescence was detectable in brain by FMI *ex vivo* at 1 h after the start of the infusion, especially in the right ipsilateral brain hemisphere (**Figure 53B**).

Next, we tested a higher dose (80 mg) in order to enhance the NCs brain delivery while maintaining the intervention duration and flow rate, for which the nanomaterial infusion rate was increased to 1.6 mg/min. Again, no adverse reactions were observed during the intervention, and the NCs fluorescent signal was higher in the brain as seen by FMI *ex vivo* (**Figure 53B**).

Since the highest dose was well tolerated and led to a higher NC brain accumulation, a new group of animals receiving endovascular Cy5-labelled nanocarriers were monitored for systemic NCs availability and brain targeting by *ex vivo* FMI (**Figure 54A**). Our results showed that the endovascular administration of NCs was successful to target the brain, showing a preferential ipsilateral accumulation (**Figure 54B-C**). However, no significant differences were observed between the ipsilateral and contralateral TREs ( $P>0.05$ ); **Figure 54C**.

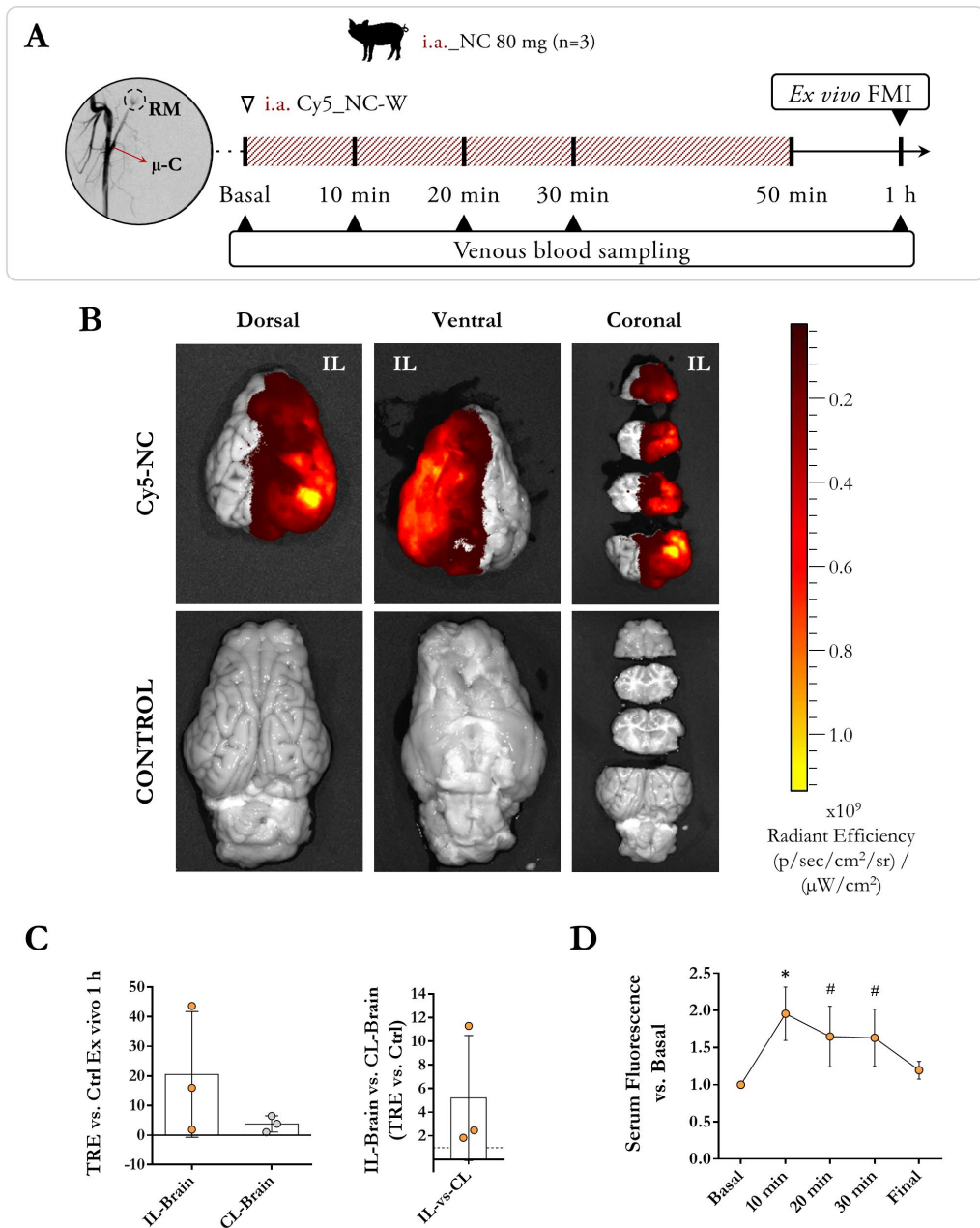


**Figure 54.** Pilot study to assess the translational feasibility of endovascular NC delivery in healthy adult pigs receiving the highest dose (80 mg) of Cy5-labelled NC (n=3). **A**) Scheme of the experimental design, with an angiography insert showing the micro-catheter ( $\mu$ -C) position for endovascular infusion, proximal to the rete mirabile (RM). **B**) *Ex vivo* FMI images of the brain in dorsal, ventral and coronal views,



at 1 h after i.a. NCs administration. **C)** Graphs showing the quantification of TRE on ROIs from the ipsilateral (IL) and contralateral (CL) brain (left), corrected by their control animal, and the ratio between IL and CL brain TRE (right). **D)** Graph showing the serum fluorescence during and after endovascular NC infusion, corrected by the basal fluorescence before NCs administration. All data are represented as mean $\pm$ SD. #P<0.10, \*P<0.05 (vs. Basal serum fluorescence).

We also measured the Cy5 fluorescence in serum obtained from blood samples collected before, during and after NCs infusion (**Figure 54D**). The fluorescence was detectable at all the time points during the infusion, but was almost negligible early after the end of administration. Specifically, the TRE was significantly higher in the serum collected at 10 min after the start of the infusion (P=0.0103 vs. basal TRE), and although the NCs fluorescence was also detected at 20 and 30 min, the difference in the TRE values was not statistically different from the basal TRE (P=0.0767 and P=0.0858, respectively). Finally, the serum fluorescence at the end of the infusion did not differ from the basal TRE (P=0.8455), indicating that the NCs are rapidly cleared from the system circulation after administration.

### 4.5.2. 3D vascular model

As a preliminary step for the translation of the proposed therapeutic approach to the clinical setting, we also tested the efficacy of a magnet adapted for human use (M3) to guide the nanocarriers towards a region of interest in a 3D-printed humanised vascular model. The magnet was attached to a 3D-printed temporal bone, close the MCA territory, and an artificial bloodstream was created at a constant flow rate of 580 mL/min, as described above. The endovascular delivery of the magnetised nanocarriers was performed with a micro-catheter guided towards the MCA (**Figure 55**).

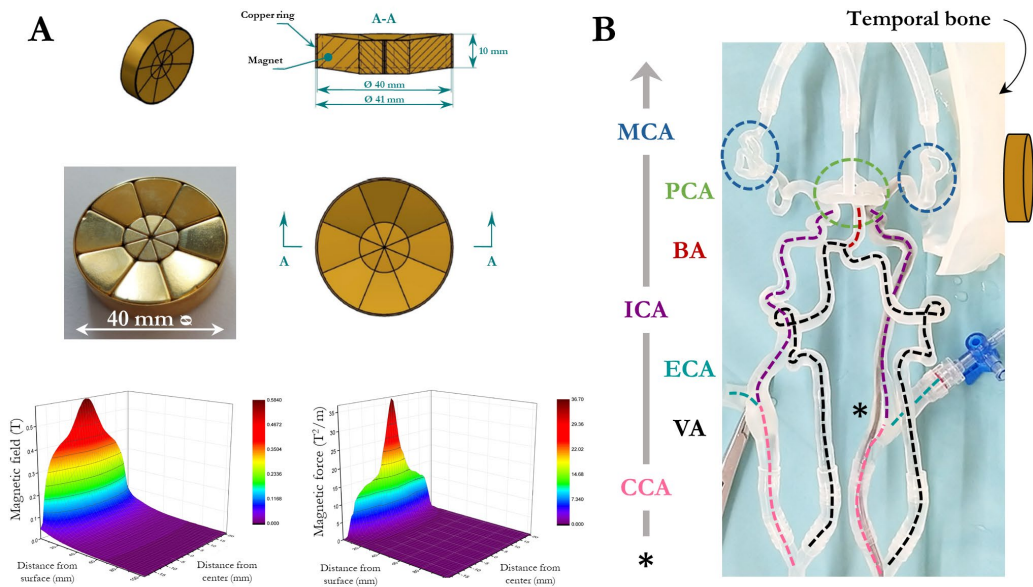


**Figure 55. Experimental set-up for endovascular NCs delivery and magnetic retention in a humanised vascular model. A)** Scheme of the design and image of the focused magnet (M3) adapted to the human anatomy (above), and graphs showing the magnetic field and magnetic force for M3, measured by Magscan, according to the distance from the surface and centre of the magnet (below). **B)** 3D-printed vascular model, temporal bone and M3 position for micro-catheter (asterisk) guided NCs infusion and magnetic retention towards the MCA. PCA: posterior cerebral artery, BA: basilar artery, ECA: external carotid artery, VA: vertebral artery, MCA middle cerebral artery, ICA: internal carotid artery, CCA: common carotid artery.

Specific magnetic retention was successfully achieved in the target ipsilateral MCA, as seen by FMI at 1 h after infusion (**Figure 56**), with a significantly higher TRE in the ipsilateral MCA territory compared to the contralateral MCA ( $P=0.0443$ ).

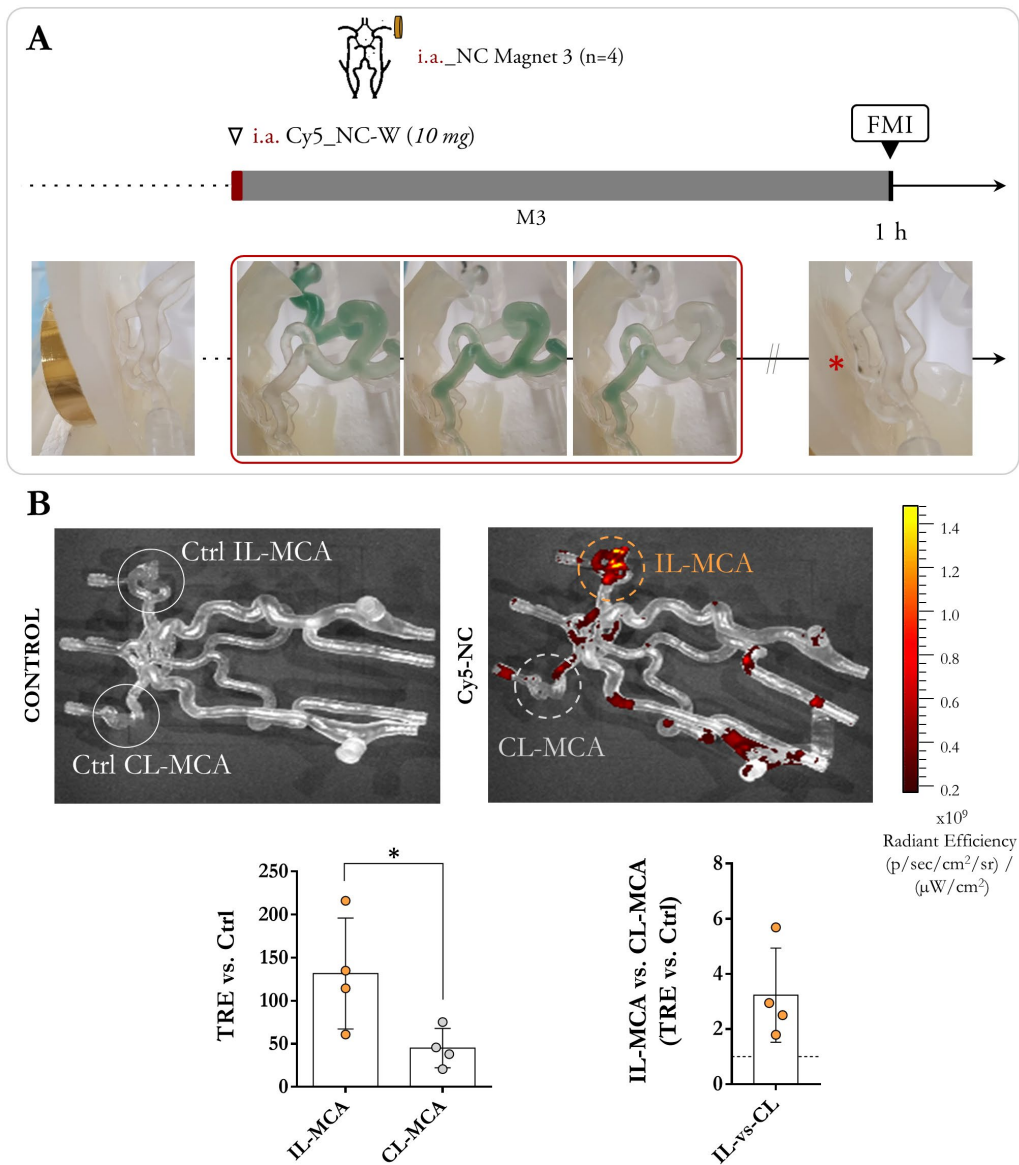


**Figure 56. Endovascular infusion of Cy5-labelled NCs and magnetic retention towards the MCA in a humanised 3D-vascular model. A)** Scheme of the experimental design (n=4) and inserts showing the MCA before, during and 1 h after infusion (asterisk showing the NCs deposition under the magnetic influence). **B)** Representative FMI images used for quantification (above), and graphs (below) showing the quantification of TRE on ROIs from the ipsilateral (IL) and contralateral (CL) MCA corrected by their control model (left), and the ratio between IL and CL MCA TRE (right). All data are represented as mean±SD. \*P<0.05.

## DISCUSSION

---



### 5.1. Enhancing brain delivery through endovascular administration and magnetic nanotargeting

The increasing use of mechanical thrombectomy for acute stroke management provides an opportunity to deliver therapeutics directly to the site of injury. In parallel, nanomedicine has become a booming field offering promising tools to enhance specific drug delivery. In this study, we tested the use of biocompatible nanomaterials to improve brain targeting after stroke, taking advantage of the endovascular route to reach the brain vasculature and the use of functionalised nanocarriers for imaging and magnetic targeting. Our data prove the safety and feasibility of hyperacute endovascular infusion of multimodal biocompatible PLGA nanocarriers to significantly improve brain targeting in a mouse model of cerebral ischaemia, paving the way for future nanomaterial-based treatments in the context of endovascular treatments.

A crucial aspect to consider while investigating a new therapeutic approach is the ideal administration route in terms of safety and efficient delivery while considering the particularities of a given pathological condition. As mentioned above, endovascular treatments present the advantage of a more selective targeting while minimising the side effects of systemic drug delivery in filtering organs.<sup>171,172</sup> In consistency with previous studies,<sup>188,213,214</sup> this work proves that intravenously administered NCs predominantly accumulate in the liver, lungs and spleen, while their retention in the brain is almost negligible. In contrast, the presented data confirm the significant advantage for stroke-affected brain targeting following the intraarterial-ICA administration route,<sup>215,216</sup> as seen both by MRI and FMI. The preferential ipsilateral and negligible contralateral hemisphere NCs accumulation observed in this thesis, as seen in both naïve and ischaemic mice, as well as in naïve pigs, has already been described by Lesniak and colleagues in a study showing a preferential ipsilateral accumulation of i.a. Bevacizumab both alone and following BBB opening with mannitol.<sup>149</sup> Further investigations are required for a deeper understanding of the underlying mechanisms for this specific ipsilateral uptake and

to fully elucidate the effects of this approach on the integrity of the BBB. Importantly though, we did not observe major haemorrhagic events after i.a. vehicle nor NCs administration following MCAO, evidencing the safety in the context of cerebral ischaemia. Furthermore, no major alterations were observed in terms of junctional proteins' expression, as markers of the BBB integrity, at 48 h after cerebral ischaemia after early i.a. NC-CM treatment, which is a crucial phase in detrimental TJs disassembly in the well-known biphasic BBB permeability after stroke.<sup>217</sup> Similarly, the SAVER-I Phase I trial has also demonstrated the feasibility and safety of the i.a. administration of free verapamil after standard thrombectomy, with no evidence of haemorrhagic transformations.<sup>174</sup> In the same vein, no intracerebral haemorrhages were observed in the brain of naïve pigs after intraarterial NCs administration.

Brain delivery of therapeutic agents in minimally invasive approaches has been a major challenge which could be faced with new nanomedicine tools. Due to the inherent nanocarriers accumulation in filtering organs, many strategies have been focused on adding affinity moieties to increase the specific accumulation in target organs but have been hindered by numerous challenges. A recent study has nicely reported a substantial increase of nanocarriers accumulation in the brain by using red blood cells as vascular carriers for NCs administration through the ICA, confirming the enormous advantage of this endovascular delivery route, which can be further improved with nanomedicine-based strategies.<sup>218</sup> In this light, seizing the advantages of polymeric nanoparticles to administer therapeutic agents with a sustained release, increased half-life *in vivo* and reduced systemic toxicity,<sup>219</sup> we have used a PLGA-based nanocarrier with biocompatible properties and tailor-made functionalisation moieties, previously described by our group (**Annex II**).<sup>188</sup> For the present study, the proposed nanocarriers have been functionalised with SPIONs and/or Cy7.5/Cy5 for a magnetically guided retention and *in vivo* tracking by MRI and FMI, respectively. This thesis proposes the use of biocompatible biomaterials with improved magnetic targeting, which are approved for medical use (PLGA and SPIONs), as a potential advantage for the clinical translation of nanomedical products. However, other non-

magnetised PLGA formulations or alternative biogenic/synthesised biomaterials could be used to achieve a successful brain delivery using the endovascular route after stroke.

To further improve the guided transport of the nanocarriers, these were functionalised with SPIONs to allow their retention by a magnetic field device to specific brain areas. The first results failed to show an advantage in magnetic targeting using permanent magnets (M1) and short implantation times (30 min) in whole hemispheres. Nonetheless, finest experiments further proved a successful brain targeting by our FeNdB devices in cortical areas, with particular success with the focused magnet (M2). This was achieved by focusing on the specific area of magnetic field influence (within 3 mm, corresponding to the cortical brain areas) with FMI. Specific cortical targeting was also demonstrated with a better spatial resolution in MRI using the improved focused magnet (M2), which showed a better performance related to a higher magnetic field and magnetic field gradient in deeper positions, as previously described.<sup>220,221</sup> This is the first time that a focused magnet designed for mouse brains is used to target the cortical delivery of nanocarriers after stroke in endovascular-ICA administrations. However, other authors have also used an external magnet to enhance the delivery of magnetised cells to specific organs, including the brain after i.v. stem cell administration and BBB opening in a rat model of traumatic brain injury, or to enhance the delivery of tPA through chitosan-coated magnetic nanoparticles in a mouse model of hindlimb ischaemia.<sup>180,222</sup>

Interestingly, even though a substantial amount of the NCs still remains in filtering organs such as the lungs, liver and spleen, this study also proves that the endovascular administration diminishes the accumulation of NCs in the liver, a known site of nanomaterials off-target accumulation. Importantly, this unavoidable off-site accumulation did not alter known biomarkers of liver/pancreas/renal damage at short- nor at long-term after i.a. infusion, and only alterations related to the surgical intervention were found transiently altered. Furthermore, the results presented here show a clearance of the NCs fluorescence, as part of the nanoformulation, in all of



the studied organs at 1 week after administration, altogether supporting the safety of the NCs treatment in terms of systemic toxicity.

As previously mentioned, the pre-clinical use of the i.a. administration route has raised safety concerns in previous investigations since thromboembolisms have been described as a common related complication, mainly associated with the infusion rate, dose or cell size.<sup>172,206,223</sup> To prevent this major complication, NCs with an average diameter below 300 nm were freshly prepared in a saline suspension, vortexed and sonicated before the endovascular infusion to avoid the NC aggregation. The CBF, which was monitored during a controlled infusion, was only transiently and moderately reduced, as similarly reported in previous studies using mesenchymal stem cells by i.a. administration,<sup>206,223</sup> but the intraarterial-ICA infusion of NCs was not associated to mortality, a worsening of the ischaemic damage nor a higher risk of haemorrhages, suggesting a low risk of thromboembolisms. Nonetheless, from a translational perspective, future pre-clinical studies should refine these endovascular delivery approaches and study the observed CBF changes with advanced imaging techniques. On the other hand, the maintenance of iron homeostasis in the context of cerebral ischaemia is of great importance, as iron catalyses the formation of free radicals and hence, can cause oxidative stress and worsen the ischaemic damage.<sup>224</sup> Importantly, the present work does not show an increase in the infarct volume nor haemorrhages following hyperacute endovascular NCs administration (containing SPIONs) after stroke compared to the vehicle infusion, suggesting the safety in the tested conditions. Nevertheless, the first *in vivo* studies (*Biodistribution studies 1-4* and *Safety study*) suggested a slight association between higher total iron load dose and increased mortality, only in ischaemic mice but not in naïve, indicating a potential iron load-related risk in the context of ischaemic cerebral damage. This alerted on the importance of strictly adjusting the iron dose when using magnetised nanocarriers as drug delivery systems for stroke. However, the subsequent *Efficacy studies 1 and 2* did not show adverse consequences in terms of infarct size, cerebral haemorrhages nor mortality, suggesting that the iron

load of the tested *therapeutic dose* is safe in the context of cerebral ischaemia. As mentioned above, iron deposition is known to exacerbate the ischaemic insult.<sup>224</sup> Yet, a recent study using a liposomal-encapsulated iron chelator demonstrated that the reduction of iron deposition in the ischaemic brain reverses intrinsic brain plasticity changes, thereby delaying the neurological function recovery after cerebral ischaemia. The same study showed that the exogenous administration of iron and consequent increase in iron brain deposition, also resulted in a worsening of the long-term functional outcome, suggesting a dual role that is presumably accountable to the need for a strict balance.<sup>225</sup>

It is worth noting that this thesis work has been able to detect by different *in vivo* and *ex vivo* imaging techniques the presence of the NCs in the brain up to 1 week after the endovascular infusion, suggesting that a substantial proportion of the administered nanocarriers remains available in the target organ for a long time period, easing the sought-after sustained release of the encapsulated therapeutic agents.

On the other hand, the histological findings suggest an endothelial uptake, as seen by a preferential accumulation of the NCs in micro-vessel structures through indirect *ex vivo* tracking of the SPIONs and Cy5, as components of the nanoformulation. These observations are in agreement with the endothelial uptake seen *in vitro* in both mature brain ECs and OECs, presumably through endocytic mechanisms. However, it is worth noting that the administration timing used in the present study coincides with the early stage of the aforementioned biphasic BBB permeability increase after stroke. Therefore, specific cellular or extracellular localisations within the brain parenchyma upon hyperacute endovascular administration and magnetic brain targeting are yet to be investigated. In this regard, this approach could be further combined with strategies aiming at the BBB crossing of therapeutic agents if needed, such as the selective BBB temporary opening with nanoagonists such as adenosine 2A receptor agonist-labelled dendrimers<sup>148</sup> or the functionalisation of nanoparticles with selective antibodies for a BBB receptor-mediated transcytosis.<sup>226</sup>

### 5.2. Neurovascular repair can be achieved through early nanoencapsulated EPCs-secretome intraarterial delivery after stroke reperfusion

As earlier pointed out, there is a clear need to develop therapeutic strategies beyond the acute phase of stroke. In this regard, EPCs have been in the spotlight of ischaemic tissue repair as a therapeutic strategy to enhance neovascularisation. Given their ability to release a large variety of pro-angiogenic molecules, several studies published by our group and others place the use of EPC-secretome as a promising cell-based but cell-free strategy to boost tissue repair.<sup>134,135,137,227</sup>

On the other side, therapeutic brain targeting remains a challenge that limits the development of neurovascular repair strategies. The present investigation provides evidence supporting the feasibility and advantages of the endovascular delivery of magnetised PLGA nanocarriers for brain targeting. These drug delivery systems have proven the versatility for the encapsulation or adsorption of a large variety of proteins, ranging from 8 to 66.5 kDa (e.g. VEGF, SDF, BDNF or albumin), showing successful encapsulation efficiencies, and posterior *in vitro* release with preserved functionality of the released factors.<sup>188,204,205</sup> On this basis, the present study aimed to administer EPCs-secretome taking advantage of the combination of magnetic nanotargeting and the endovascular route to enhance specific brain delivery and promote neurovascular repair after stroke.

The therapeutic secretome used in the present study was obtained from EPCs isolated from the peripheral blood of a stroke patient, and produced in a high-scale production manner. The same EPCs-secretome was tested in a study recently published by our group (**Annex II**), demonstrating that not only it promoted angiogenesis but also enhanced endothelial barrier tightness and protected the BBB from hypoxia-induced vascular leakage *in vitro*.<sup>203</sup>

In the present study, the pro-angiogenic effects of different EPCs-secretome batches were confirmed *in vitro* in both mouse and human mature ECs and OECs, in terms

of endothelial proliferation and tubulogenic capacity. Furthermore, this effect was dose-dependent and, interestingly, more prominent in mouse-derived cells *in vitro*, despite the human origin of the secretome, which could be due to the fact that mice have a higher mass-specific metabolic rate than humans.<sup>228</sup> Importantly, we were able to encapsulate the secretome into our nanoformulation, as confirmed by the detection of several known EPCs-released proteins. Moreover, the cargo molecules preserved their functionality after the lyophilisation-encapsulation-release process.

Other authors have shown that i.v. administration of EPCs one day after MCAO leads to an improved long-term functional recovery in a rat model of cerebral ischaemia, with reduced reactive astrogliosis and apoptosis, and increased angiogenesis, which were attributed to a paracrine effect.<sup>122</sup> In our hands, EPCs-secretome treatment one day after MCAO has shown long-term beneficial neurorepair effects in a mouse model of cerebral ischaemia, with improved functional recovery and peri-infarct neoangiogenesis.<sup>135</sup> However, this is the first time that EPCs-secretome is administered intraarterially and hyperacutely after reperfusion. For this reason, we tested the therapeutic potential of the free secretome therapy alongside the nanotargeted approach. To emulate the equivalent therapeutic dose of the NC-CM after encapsulation-administration-release, we determined the free secretome dose based on an estimation of the cCM encapsulation efficiency. It should be noted, however, that there seems to be a potential restriction on the molecular weight of the encapsulated factors, as seen by different encapsulation efficiencies for the studied proteins. Therefore, the composition of the released NC-CM factors could potentially differ from the formulation of the free secretome. This limitation should be further studied for specific neuroprotective or neurorestorative agents, always in balance with suitable nanoformulation sizes for a safe endovascular delivery, and proving its advantage against free drug deliveries.

Importantly, the results obtained in the short-term *Efficacy study 1* suggest that hyperacute i.a. administration of the free therapy could exacerbate the ischaemic brain injury through an increased neuro-inflammatory response and BBB damage,

although this was not reflected in a worsening of the functional outcome, whereas these deleterious effects are absent in the nanotargeted EPCs-secretome therapy.

As expected, we observed a neuro-inflammatory state in the brain samples analysed at 48 h after ischaemia, as seen by increased levels of IL-6, CXCL1/KC and MCP-1 in the ischaemic brain regardless of the treatment, in accordance with previous findings.<sup>229</sup> This ischaemic-induced inflammatory response was however amplified in ischaemic mice receiving free EPCs-secretome, showing increased levels of GM-CSF, TNF $\alpha$  and MIP-2 in the ischaemic brain.

GM-CSF is mainly produced by activated leukocytes, and exerts pro-inflammatory effects through recruitment and activation of myeloid cells, and promoting a pro-inflammatory macrophage phenotype.<sup>230</sup> However, it has also been shown that GM-CSF exerts a beneficial arteriogenic effect by mechanisms involved in the mobilisation of monocytes/macrophages.<sup>231,232</sup> TNF $\alpha$  is a key mediator in the pathophysiology of stroke, apparently contributing directly to neuronal injury. Several studies have found an association between higher TNF $\alpha$  levels and poor outcome or larger infarcts,<sup>25</sup> and although contradictory results have shown neuroprotective effects after cerebral ischaemia,<sup>233</sup> many studies have demonstrated that its blockage has neuroprotective effects in pre-clinical ischaemic stroke models.<sup>234,235</sup> MIP-2 is a chemoattractant and activating factor for neutrophils, and has been related to BBB permeability and brain oedema after intracerebral haemorrhage.<sup>236</sup> On the other hand, the levels of the anti-inflammatory IL-10 seemed to be slightly increased in the ischaemic brains of mice receiving free secretome, which could be indicative of a counterbalance mechanism. Indeed, TNF $\alpha$  can also induce IL-10 production, which itself inhibits the expression of TNF $\alpha$ , resulting in an auto-regulatory feedback loop.<sup>237</sup>

In this line, it is known that EPCs not only release pro-angiogenic factors but also thrombo-inflammatory mediators, adhesion molecules, and pro-inflammatory cytokines/chemokines, such as MCP-1 which regulates the migration and infiltration of monocytes/macrophages.<sup>238</sup> Although several of the secretome cytokines play a

pro-angiogenic role, the inflammation-driven effects of EPCs-secretome could explain the abovementioned results, which alerts us on potential treatment-related hazards in the context of ischaemic stroke.

However, the use of EPCs or EPCs-secretome therapy has yielded conflicting data in this regard. For instance, EPCs have been reported to improve long-term functional recovery in a rat model of cerebral ischaemia receiving EPCs 4 h after ischaemia, presumably through downregulation of the inflammation-associated stroke vasculome (inflammatory genes specifically upregulated in brain endothelial cells upon stroke).<sup>239</sup> Another study using EPCs-secretome in a rodent model of spinal cord injury reported anti-inflammatory effects through decreased M1 macrophage activation and cytokines release, together with increased angiogenesis and neuroprotection.<sup>136</sup>

In contrast, these results suggest that direct intraarterial brain administration of EPCs-secretome hyperacutely after cerebral ischaemia-reperfusion at the tested concentrations exerts a pro-inflammatory response that could outweigh the beneficial effects suggested by other authors, exacerbating the ischaemic injury. Such discrepancies highlight the importance of developing therapeutic strategies in a timely manner. Furthermore, it is worth noting that the specific contribution of the different cytokines/chemokines involved in the ischaemic cascade has been controversial, since complex interactions occur, including overlapping, synergistic and antagonistic effects.<sup>240</sup>

Furthermore, although this was not reflected in a worsening of the functional outcome nor an increased risk of haemorrhagic transformation, there seems to be a slight association between the increased cortical infarct size and cortical haemorrhages in the free secretome-treated group.

Additionally, our results showed that hyperacute i.a. administration of free EPCs-secretome after cerebral ischaemia could induce BBB damage in off-target areas, as seen by an altered expression of the junctional proteins claudin-5 and ZO-1. These

results are inconsistent with a previous study in which we observed that the same secretome promoted endothelial barrier tightness and protected the BBB from hypoxic injury *in vitro*,<sup>203</sup> which is further supported by another study demonstrating that OECs protect the BBB against ischaemic injury.<sup>241</sup> Nonetheless, it should be kept in mind that cell-culture systems are simple emulations of the complexity of *in vivo* systems, which lack of a peripheral immune system and glial or synaptic connections that might be essential for cytokine action, added to the difficulty of treatment timing and dose scalability from *in vitro* to *in vivo* studies.

Moreover, as earlier pointed out, the inflammatory burst might outweigh these mechanisms. Post-ischaemic neuro-inflammation is known to damage the BBB by disrupting the structural integrity of junctional proteins.<sup>242</sup> In this light, despite the difficulty of distinguishing between the cytokine response to injury and the early expression that might contribute to cell death,<sup>240</sup> our results suggest that hyperacute endovascular treatment with free EPCs-derived secretome worsens the ischaemic damage through an exacerbated inflammatory response. However, these observations warrant further research in order to elucidate the specific underlying mechanisms.

On the other side, the present study confirms the angiogenic potential of EPCs-secreted factors after cerebral ischaemia. Moreover, as expected from the *in vitro* studies, the therapeutic secretome was successfully administered through endovascular delivery and magnetic brain nanotargeting, preserving the angiogenic function of the released factors. To our knowledge, this is the first time that EPCs-secretome-loaded nanocarriers are used in combination with magnetic retention and endovascular delivery in a mouse model of cerebral ischaemia, although other authors have recently used polymeric nanoparticles to deliver EPCs-secretome in a mouse model of hindlimb ischaemia.<sup>243</sup> In line with the results of this thesis, those secretome-loaded polymeric nanoparticles showed an improved perfusion through increased angiogenesis in hindlimb ischaemic mice, compared to both free secretome- and non-treated mice, highlighting the advantage of nanotargeted EPCs-

secretome delivery. In the same line, Felice and colleagues also reported different encapsulation efficiencies for the studied proteins and, still, a beneficial effect was observed when using the encapsulated EPCs-secreted factors *in vivo*.<sup>243</sup>

In our hands, the NC-CM treatment did not outperform the angiogenic effect observed with the free secretome therapy. However, it is worth noting that, while the non-encapsulated treatment showed a ubiquitous angiogenic effect, NC-CM increased the vessel density only in the peri-infarct target region. These results position this approach as a potential nanotargeted strategy to deliver multiple neuroprotective or neurorestorative agents in a selective manner, minimising undesired off-site effects. Furthermore, the nanotargeted delivery of EPCs-secretome presented the advantage of promoting angiogenesis without the free EPCs-secretome exacerbated acute brain injury, while taking advantage of the intraarterial route, which could be implemented in the context of mechanical thrombectomy for acute stroke management.

In light of the angiogenic effect observed with both free and encapsulated EPCs-secretome, the brain expression of several angiogenesis-related proteins was analysed, but the results failed to show differentially expressed factors that could mechanistically explain the free/encapsulated treatments' angiogenesis-boosting effects. Most of the studied factors were significantly increased in the ischaemic brain, except VEGF and SDF-1 (which have been previously reported to increase during the first 7 and 3 days after ischaemia, respectively, returning to basal levels thereafter)<sup>244</sup>, suggesting an intrinsically active vascular remodelling at 2 weeks after cerebral ischaemia. Interestingly, the ischaemic mice receiving NC-CM did not show increased levels of angiopoietin-2, endothelin-1 nor MCP-1 in the ischaemic brain, as opposed to free secretome- and vehicle-treated mice.

Angiopoietin-2 is a growth factor belonging to the angiopoietin/Tie (tyrosine kinase with Ig and EGF homology domains) signalling pathway. It acts as an antagonist for angiopoietin-1, inhibiting the receptor Tie2-mediated signalling, and decreasing blood vessel maturation and stabilisation.<sup>245</sup> The expression of angiopoietin-2 is



triggered by hypoxia, reducing vascular pericyte coverage through the activation of pericyte migration and detachment from the basement membrane, therefore increasing BBB permeability.<sup>246</sup> It has shown a biphasic expression pattern after stroke, peaking during the first 3 days, which has been related to deleterious BBB permeability, and at 2 weeks, which has been associated to vascular stabilisation and maturation.<sup>244</sup> On the other hand, a study using mesenchymal stem cells-secretome through intranasal delivery showed an enhanced vascular remodelling, along with decreased angiotensin-2 and increased angiotensin-1 expression at 2 weeks after cerebral ischaemia.<sup>245</sup> Interestingly, a recent study reported an improved neurological recovery after treatment with an angiotensin-1 mimetic peptide in diabetic rats after stroke, through increased vascular and white matter remodelling, along with decreased levels of MCP-1 and endothelin-1.<sup>247</sup>

Moreover, the present study showed a marked correlation in the overall levels of angiotensin-2, MCP-1 and endothelin-1, suggesting a mechanistic association between the molecular pathways in which these factors are involved. In light of these findings, the association between these factors and their differential expression observed only in NC-CM-treated mice in our study deserves further research.

However, it should be acknowledged that the experimental design used here presents several limitations that should be taken into account. First, the molecular analysis was broadly performed in whole brain hemispheres, without dissecting the infarct and peri-infarct regions from the healthy tissue. And secondly, with the objective to study the molecular expression in the same mice in which vessel density was assessed, the angiogenesis-related factors expression was analysed 2 weeks after treatment, when the intrinsic remodelling processes are likely to mask molecular changes occurring earlier. Therefore, further research is needed in order to scrutinise the subjacent molecular mechanisms of the tested treatments.

Finally, hyperacute endovascular treatment with neither free nor encapsulated EPCs-secretome did not result in an increased neurogenic response at 2 weeks after cerebral ischaemia. Interestingly though, mice treated with NC-CM showed a decreased

cortical neurodegeneration, assessed through Fluoro-Jade C staining. Nonetheless, it should be kept in mind that the specificity of this staining has been called into question, as the exact mechanism by which FJC stains degenerating neurons has not been fully elucidated, and several findings have shown that FJC could also stain both resting/activated astrocytes and microglia.<sup>211</sup> Further research is therefore needed in order to draw conclusions from these findings.

As earlier pointed out, neurorepair strategies should ideally promote simultaneously neurogenesis, angiogenesis, myelinogenesis and neural plasticity. In this regard, in a hypothetical scenario, the therapeutic approach presented herein could be implemented in combination with other neuroprotective or neurorestorative therapeutic agents tackling multiple pathways to synergistically enhance tissue repair and functional recovery.

Overall, the different results obtained with the free or encapsulated treatment could be partially explained by a distinct effective timing of the therapeutic factors, being immediately available in the brain vasculature after free secretome i.a. administration, as opposed to a plausible controlled and sustained release when given encapsulated. However, as discussed above, the composition of the original EPCs-secretome is likely to differ from the released NC-CM factors, considering the differential encapsulation efficiencies, and, importantly, that the free secretome dose is based on an indirect calculation, and should not be strictly compared to the NC-CM dose. Finally, as the biodistribution studies suggest, the increased brain NCs accumulation when combining the endovascular delivery of magnetised nanocarriers and their magnetic retention with an improved focused magnet, is also accompanied by a decreased off-target accumulation of the therapeutic system. Taking this into account, it would be interesting to study whether there might be relevant differences in the peripheral effect of the EPCs-secretome therapy when given free or encapsulated, that could affect the therapeutic response.

### 5.3. Paving the way towards the clinical implementation of endovascular treatments, advanced therapies and nanotheranostics

From a translational perspective, studies in large animals with gyrencephalic brains and larger vessels/capillaries or in humanised prototypes should be used to demonstrate the feasibility of the proposed therapy.

The rodent brain is barely one-thousandth of the weight of the human brain. On the other hand, lissencephalic species (including rodents) show no neocortical folding and thus a much smaller neocortical area relative to the rest of the brain than gyrencephalic species, resulting in relevant differences in the brain circuitry and gray-white matter ratio.<sup>248,249</sup>

Therefore, the use of large gyrencephalic animal models has been recommended to bridge the gap from pre-clinical findings to the clinical setting. For ischaemic stroke, these models currently include, amongst others, dogs, swine, sheep, and non-human primates. Considering the ethical issues around the use of dogs or non-human primates, pigs are large animal models of particular interest, which display complex individual and social behaviours that can be analysed with multiple tests resembling the clinical scenario.<sup>250</sup> Importantly, pigs share some neurovascular characteristics with humans that make them suitable for the validation of endovascular devices prior to human use, which relies on the scope of the present investigation for the implementation of endovascular therapies.<sup>251</sup>

Nonetheless, modelling MCAO in large animals has been hindered by a relevant anatomical difference. In contrast to humans, several large animals, including pigs and sheep, present an extracranial network of small vessels at the base of the brain, proximal to the ICA, the rete mirabile, which represents an obstacle to access intracranial vessels such as the MCA. Therefore, most of the swine MCAO models are achieved through a craniotomy in order to access the MCA.<sup>249</sup> However, pigs have been widely used as models to test thrombectomy devices, due to the

anatomical and physiological similarities of their cardiovascular system with that of humans.<sup>252</sup>

On the other side, the administration of nanomaterials triggers the aforementioned CARPA reaction in both pigs and humans, while rodents show a much milder complement response to nanomaterials, highlighting the importance of large animals testing prior to the clinical implementation of nanomedicine-based treatments.<sup>166,253</sup> Additionally, intraarterial treatments have raised safety concerns related to the risk of thromboembolisms. In this regard, we hypothesize that this potential risk would be minimised in humans and large animals as compared to rodents, given the differences in the micro-vessels caliber. Furthermore, the potential differences in the biodistribution patterns described herein when translated to humans should be addressed, considering the abovementioned anatomical differences.

With this scenario, we aimed to conduct a pilot study in pigs to assess the feasibility of endovascular NCs delivery, as a preliminary translational approach. To do so, we included pigs that were reused from interventional training courses for the use of mechanical thrombectomy devices. As previously described, a micro-catheter was introduced through the femoral vein, and directed towards the ascending pharyngeal artery, proximal to the rete mirabile, in order to administer Cy7.5/Cy5-labelled NCs towards the MCA vascular territory.

The results presented herein showed that the endovascular administration of NCs was successful to target the brain, showing a preferential ipsilateral accumulation, as seen by *ex vivo* FMI. Furthermore, the fluorescence of the administered nanocarriers was detected in systemic circulation, observing a rapid clearance after the end of the infusion. Such findings could help modulating the experimental design for a hypothetical clinical implementation, taking into account, for instance, the appropriate timing for magnetic retention in order to enhance brain retention during this window of bioavailability. Importantly, the initial dose recommended to prevent the abovementioned CARPA reaction was doubled without deaths nor major complications. However, it should be noted that, although a complete monitoring of

the vital constants was carried out during the whole intervention, these could not be duly assessed, since prior surgical interventions could interfere with the clinical evolution during the procedure. Therefore, future studies should be exclusively designed for the present purpose, with controlled variables, in order to draw robust conclusions.

As an additional preliminary step for the translation of the proposed therapeutic approach, we also tested the efficacy of a magnet adapted for human use (M3) to guide the magnetic nanocarriers towards a region of interest in a 3D-printed humanised vascular model. The experimental set-up was designed to mimic the human biophysical conditions to the best of our possibilities. However, due to restrictions of the 3D-printing process, we were not able to represent the microvessel and capillary network, which would potentially modify the biodynamic properties affecting the nanocarriers distribution. Furthermore, *ex vivo* models lack, for instance, of circulating proteins or cells that may interfere with the administered nanocompound in physiological conditions. However, the focused magnet designed for human use showed an efficient magnetic retention capacity, overcoming relevant parameters such as the anatomical vascular morphology and the biodynamics of the bloodstream, suggesting a potential efficacy for the clinical use.

### 5.4. Limitations of the study and future perspectives

The present study proves the advantage and safety of intraarterially delivered magnetised nanocarriers for specific brain targeting, which could be used to selectively administer neuroprotective or neurorestorative therapeutic agents in the context of cerebral ischaemia.

Nonetheless, aside from the limitations highlighted above this study presents several weaknesses that should not be overlooked.

Despite demonstrating an enhanced brain delivery through the combination of the endovascular route with magnetic nanotargeting, the therapeutic benefit observed when used for EPCs-secretome therapy after cerebral ischaemia was modest. The

results obtained regarding the functional outcome suggested a mild hastening of the functional recovery in mice receiving NC-CM, but did not outperform the intrinsic long-term functional recovery in free secretome- and non-treated ischaemic mice. This could be due, amongst other factors, to the following reasons: (i) the neoangiogenic effect was insufficient to be translated into a significant functional improvement, and should occur along with other relevant neurorepair processes, (ii) the *therapeutic dose* tested was suboptimal, (iii) the high inter-individual variability and low samples sizes mitigated potential differences in the recovery, and (iv) the behavioural tests used are scarce and not sensitive enough.

The *therapeutic dose* was determined based on approved doses of iron (Endorem®) for human use. However, this dose was not scaled based on the mouse body weight. Plus, dose scaling should also consider other relevant factors such as body surface area or pharmacokinetics, especially considering the fact that mice have a different mass-specific metabolic rate than humans, as earlier pointed out. Therefore, the optimal NC-CM dosage in either single or multiple administrations should be further investigated to determine an appropriate risk-benefit. Importantly though, the potential iron load-derived toxicity or benefits, as well as the clearance mechanism and kinetics of this type of magnetic nanocarriers is yet to be fully elucidated. On the other hand, alternative nanocarriers holding a higher loading capacity could also improve the benefit of the proposed therapy.

On another note, the experimental design should ideally assess the evolution of the initial brain injury throughout the study, for instance with *in vivo* imaging techniques, such as MRI. A more exhaustive study, together with larger sample sizes, would potentially minimise the drawback of inter-individual variability, strengthening the reliability of the results.

The use of high-scale-produced EPCs-secretome is a potential advantage for the clinical translation of the proposed therapy, which could be readily used hyperacutely after stroke, taking advantage of the intraarterial route. Furthermore, the present study demonstrated the reproducibility of different secretome and NC-CM batches.

It should not be overlooked, however, that the secretome used for both the free and encapsulated treatment was obtained from EPCs isolated from a single donor. This adds to the aforementioned controversies regarding the adequate definition of EPCs subtypes. In this light, it is of great importance to precisely define these subtypes for a better understanding of their angiogenic potential, to maximise their therapeutic efficacy.

It would also be relevant to readdress the biodistribution and safety of the proposed nanocarriers for different encapsulated molecules or upon the addition/removal of imaging or affinity moieties. Moreover, our nanoformulation can be tailored in a modular approach to incorporate different imaging/functional moieties without significantly altering its morphochemical properties nor the loading capacity. In this regard, these nanocarriers could be adapted for specific purposes in the different steps towards a clinical application. Besides, other imaging tags could be investigated for different clinically relevant imaging techniques such as contrast agents for CT imaging, as an alternative to iron particles.

Finally, this thesis highlights the importance of using large animals to bridge the gap between pre-clinical research and the clinical setting. However, the proposed therapy should be tested in different pre-clinical stroke models such as the thromboembolic, in order to assess its feasibility and safety in combination with thrombolytic drugs, which would be clinically relevant, for instance, for cases in which tPA or TNK are administered prior to mechanical thrombectomy.

In the same vein, the proposed therapy should be tested in both sexes and in aged animals with relevant comorbidities, before jumping to the clinical scenario. An illustrative example that underscores the importance of including such diversity is a recent study in rodents showing that the intraarterial administration protocol requires adaptations for an optimal ipsilateral brain targeting due to sex differences.<sup>254</sup>

## CONCLUSIONS

---





The conclusions of this doctoral thesis are the following:

1. The factors secreted by EPCs isolated from ischaemic stroke patients promotes angio-vasculogenesis in both mouse and human endothelial cell models *in vitro*.
2. EPCs-secretome can be successfully encapsulated into PLGA nanocarriers, preserving the angiogenic functional activity upon release.
3. The endovascular delivery of magnetically-guided PLGA nanocarriers safely enhances focal brain targeting and reduces off-site accumulation in a mouse model of cerebral ischaemia.
4. Hyperacute endovascular delivery of EPCs-secretome might exacerbate the post-ischaemic neuro-inflammatory response and promote ubiquitous brain angiogenesis in a mouse model of cerebral ischaemia.
5. Hyperacute endovascular delivery of nanotargeted EPCs-secretome is feasible and safe, and promotes cortical peri-infarct brain angiogenesis in a mouse model of cerebral ischaemia.
6. From a translational perspective, enhancing brain nanotargeting through endovascular delivery is feasible in large animals with gyrencephalic brains, and magnetic nanotargeting could be successfully achieved with focused magnets adapted to the human anatomy.



## REFERENCES

---



1. Sacco, R. L. *et al.* An Updated Definition of Stroke for the 21st Century. *Stroke* **44**, 2064–89 (2013).
2. Yew, K. S. & Cheng, E. M. Diagnosis of acute stroke. *Am. Fam. Physician* **91**, 528–36 (2015).
3. Coupland, A. P., Thapar, A., Qureshi, M. I., Jenkins, H. & Davies, A. H. The definition of stroke. *J. R. Soc. Med.* **110**, 9–12 (2017).
4. Lindsay, M. P. *et al.* World Stroke Organization (WSO): Global Stroke Fact Sheet 2019. *Int. J. Stroke* **14**, 806–817 (2019).
5. Townsend, N., Nichols, M., Scarborough, P. & Rayner, M. Cardiovascular disease in Europe - Epidemiological update 2015. *Eur. Heart J.* **36**, 2673–4 (2015).
6. Boehme, A. K., Esenwa, C. & Elkind, M. S. V. Stroke Risk Factors, Genetics, and Prevention. *Circ. Res.* **120**, 472–495 (2017).
7. Chojdak-Lukasiewicz, J., Dziadkowiak, E. & Budrewicz, S. Monogenic causes of strokes. *Genes (Basel)*. **12**, 1855 (2021).
8. Adams, H. P. *et al.* Classification of subtype of acute ischemic stroke. Definitions for use in a multicenter clinical trial. TOAST. Trial of Org 10172 in Acute Stroke Treatment. *Stroke*. **24**, 35–41 (1993).
9. Knight-Greenfield, A., Nario, J. J. Q. & Gupta, A. Causes of Acute Stroke: A Patterned Approach. *Radiol. Clin. North Am.* **57**, 1093–1108 (2019).
10. Bamford, J., Sandercock, P., Dennis, M., Warlow, C. & Burn, J. Classification and natural history of clinically identifiable subtypes of cerebral infarction. *Lancet* **337**, 1521–1526 (1991).
11. World Health Organisation. ICD-11 for Mortality and Morbidity Statistics (ICD-11 MMS) 2018 version. <https://icd.who.int/Browse11/L-M/En> (2018).
12. D'Souza, S. Aneurysmal subarachnoid hemorrhage. *J. Neurosurg. Anesthesiol.*

- 27, 222–240 (2015).
13. Powers, W. J. *et al.* Guidelines for the early management of patients with acute ischemic stroke: 2019 update to the 2018 guidelines for the early management of acute ischemic stroke a guideline for healthcare professionals from the American Heart Association/American Stroke A. *Stroke* **50**, e344–e418 (2019).
  14. Vilela, P. Acute stroke differential diagnosis: Stroke mimics. *Eur. J. Radiol.* **96**, 133–144 (2017).
  15. Kleindorfer, D. O. *et al.* Designing a message for public education regarding stroke: Does FAST capture enough stroke? *Stroke* **38**, 2864–2868 (2007).
  16. Nor, A. M. *et al.* The Recognition of Stroke in the Emergency Room (ROSIER) scale: Development and validation of a stroke recognition instrument. *Lancet Neurol.* **4**, 727–734 (2005).
  17. Brott, T. *et al.* Measurements of acute cerebral infarction: A clinical examination scale. *Stroke* **20**, 864–870 (1989).
  18. Banks, J. L. & Marotta, C. A. Outcomes validity and reliability of the modified rankin scale: Implications for stroke clinical trials - A literature review and synthesis. *Stroke* **38**, 1091–1096 (2007).
  19. Dobkin, B. H. & Carmichael, S. T. The Specific Requirements of Neural Repair Trials for Stroke. *Neurorehabil. Neural Repair* **30**, 470–478 (2016).
  20. Mergenthaler, P., Dirnagl, U. & Meisel, A. Pathophysiology of stroke: Lessons from animal models. *Metab. Brain Dis.* **19**, 151–167 (2004).
  21. Jovin, T. G., Demchuk, A. M. & Gupta, R. Pathophysiology of acute ischemic stroke. *Contin. Lifelong Learn. Neurol.* **14**, 28–45 (2008).
  22. Lakhan, S. E., Kirchgessner, A. & Hofer, M. Inflammatory mechanisms in ischemic stroke: Therapeutic approaches. *J. Transl. Med.* **7**, 97 (2009).

23. Azad, T. D., Veeravagu, A. & Steinberg, G. K. Neurorestoration after stroke. *Neurosurg. Focus* **40**, E2 (2016).
24. Koh, S. H. & Park, H. H. Neurogenesis in Stroke Recovery. *Transl. Stroke Res.* **8**, 3–13 (2017).
25. Ramiro, L., Simats, A., García-Berrocso, T. & Montaner, J. Inflammatory molecules might become both biomarkers and therapeutic targets for stroke management. *Ther. Adv. Neurol. Disord.* **11**, 1756286418789340 (2018).
26. Morancho, A., Rosell, A., García-Bonilla, L. & Montaner, J. Metalloproteinase and stroke infarct size: Role for anti-inflammatory treatment? *Ann. N. Y. Acad. Sci.* **1207**, 123–133 (2010).
27. Iadecola, C. & Anrather, J. The immunology of stroke: From mechanisms to translation. *Nat. Med.* **17**, 796–808 (2011).
28. Faura, J., Bustamante, A., Miró-Mur, F. & Montaner, J. Stroke-induced immunosuppression: implications for the prevention and prediction of post-stroke infections. *J. Neuroinflammation* **18**, 127 (2021).
29. Simats, A., García-Berrocso, T. & Montaner, J. Neuroinflammatory biomarkers: From stroke diagnosis and prognosis to therapy. *Biochim. Biophys. Acta - Mol. Basis Dis.* **1862**, 411–424 (2016).
30. Kanazawa, M. *et al.* Angiogenesis in the ischemic core: A potential treatment target? *J. Cereb. Blood Flow Metab.* **39**, 753–769 (2019).
31. Rosell, A. & Lo, E. H. Multiphasic roles for matrix metalloproteinases after stroke. *Curr. Opin. Pharmacol.* **8**, 82–89 (2008).
32. Alia, C. *et al.* Cell-to-cell interactions mediating functional recovery after stroke. *Cells* **10**, 3050 (2021).
33. Cramer, S. C. Repairing the human brain after stroke: I. Mechanisms of spontaneous recovery. *Ann. Neurol.* **63**, 272–287 (2008).



34. Cassidy, J. M. & Cramer, S. C. Spontaneous and Therapeutic-Induced Mechanisms of Functional Recovery After Stroke. *Transl. Stroke Res.* **8**, 33–46 (2017).
35. Jones, T. A. Motor compensation and its effects on neural reorganization after stroke. *Nat. Rev. Neurosci.* **18**, 267–280 (2017).
36. Hunter, J. A treatise on the blood, inflammation and gunshot wounds. *Clin Orthop Relat Res.* **458**, 27–34 (1794).
37. Folkman, M. J. Tumor angiogenesis: therapeutic implications. *N. Engl. J. Med.* **285**, 1182–6 (1971).
38. Altman, J. Are new neurons formed in the brains of adult mammals? *Science (80- )*. **135**, 1127–1128 (1962).
39. Temple, S. Division and differentiation of isolated CNS blast cells in microculture. *Nature* **340**, 471–473 (1989).
40. Eriksson, P. S. *et al.* Neurogenesis in the adult human hippocampus. *Nat. Med.* **4**, 1313–1317 (1998).
41. Regenhardt, R. W., Takase, H., Lo, E. H. & Lin, D. J. Translating concepts of neural repair after stroke: Structural and functional targets for recovery. *Restor. Neurol. Neurosci.* **38**, 67–92 (2020).
42. Hermann, D. M. & Chopp, M. Promoting brain remodelling and plasticity for stroke recovery: Therapeutic promise and potential pitfalls of clinical translation. *Lancet Neurol.* **11**, 369–380 (2012).
43. Ming, G. li & Song, H. Adult Neurogenesis in the Mammalian Brain: Significant Answers and Significant Questions. *Neuron* **70**, 687–702 (2011).
44. Pino, A., Fumagalli, G., Bifari, F. & Decimo, I. New neurons in adult brain: distribution, molecular mechanisms and therapies. *Biochem. Pharmacol.* **141**, 4–22 (2017).

45. Imitola, J. *et al.* Directed migration of neural stem cells to sites of CNS injury by the stromal cell-derived factor 1 $\alpha$ /CXC chemokine receptor 4 pathway. *Proc. Natl. Acad. Sci. U. S. A.* **101**, 18117–18122 (2004).
46. Fontán-Lozano, Á. *et al.* To Become or Not to Become Tumorigenic: Subventricular Zone Versus Hippocampal Neural Stem Cells. *Front. Oncol.* **10**, 602217 (2020).
47. Lim, D. A. & Alvarez-Buylla, A. The adult ventricular–subventricular zone (V-SVZ) and olfactory bulb (OB) neurogenesis. *Cold Spring Harb. Perspect. Biol.* **8**, a018820 (2016).
48. Faiz, M. *et al.* Adult Neural Stem Cells from the Subventricular Zone Give Rise to Reactive Astrocytes in the Cortex after Stroke. *Cell Stem Cell* **17**, 624–634 (2015).
49. Ceanga, M., Dahab, M., Witte, O. W. & Keiner, S. Adult Neurogenesis and Stroke: A Tale of Two Neurogenic Niches. *Front. Neurosci.* **15**, 700297 (2021).
50. Cuartero, M. I. *et al.* Post-stroke Neurogenesis: Friend or Foe? *Front. Cell Dev. Biol.* **9**, 657846 (2021).
51. Zhang, R., Chopp, M. & Zhang, Z. G. Oligodendrogenesis after cerebral ischemia. *Front. Cell. Neurosci.* **7**, 201 (2013).
52. Kuhn, S., Gritti, L., Crooks, D. & Dombrowski, Y. Oligodendrocytes in Development, Myelin Generation and Beyond. *Cells* **8**, 1424 (2019).
53. Wilkins, A., Chandran, S. & Compston, A. A role for oligodendrocyte-derived IGF-1 in trophic support of cortical neurons. *Glia* **36**, 48–57 (2001).
54. Prinjha, R. *et al.* Inhibitor of neurite outgrowth in humans. *Nature* **403**, 383–384 (2000).
55. Carmeliet, P. & Jain, R. K. Molecular mechanisms and clinical applications of angiogenesis. *Nature* **473**, 298–307 (2011).

56. Arai, K., Jin, G., Navaratna, D. & Lo, E. H. Brain angiogenesis in developmental and pathological processes: Neurovascular injury and angiogenic recovery after stroke. *FEBS J.* **276**, 4644–4652 (2009).
57. Slevin, M., Kumar, P., Gaffney, J., Kumar, S. & Krupinski, J. Can angiogenesis be exploited to improve stroke outcome? Mechanisms and therapeutic potential. *Clin. Sci.* **111**, 171–183 (2006).
58. Talwar, T. & Srivastava, M. V. P. Role of vascular endothelial growth factor and other growth factors in post-stroke recovery. *Ann. Indian Acad. Neurol.* **17**, 1–6 (2014).
59. Hatakeyama, M., Ninomiya, I. & Kanazawa, M. Angiogenesis and neuronal remodeling after ischemic stroke. *Neural Regen. Res.* **15**, 16–19 (2020).
60. Rust, R. Insights into the dual role of angiogenesis following stroke. *J. Cereb. Blood Flow Metab.* **40**, 1167–1171 (2020).
61. Bell, A. H., Miller, S. L., Castillo-Melendez, M. & Malhotra, A. The Neurovascular Unit: Effects of Brain Insults During the Perinatal Period. *Front. Neurosci.* **13**, 1452 (2020).
62. Thored, P. *et al.* Long-term neuroblast migration along blood vessels in an area with transient angiogenesis and increased vascularization after stroke. *Stroke* **38**, 3032–3039 (2007).
63. Tsai, H. H. *et al.* Oligodendrocyte precursors migrate along vasculature in the developing nervous system. *Science (80-. ).* **351**, 379–384 (2016).
64. Ohab, J. J., Fleming, S., Blesch, A. & Carmichael, S. T. A Neurovascular Niche for Neurogenesis after Stroke. *J. Neurosci.* **26**, 13007–13016 (2006).
65. Joy, M. T. & Carmichael, S. T. Encouraging an excitable brain state: mechanisms of brain repair in stroke. *Nat. Rev. Neurosci.* **22**, 38–53 (2021).
66. Loubinoux, I., Brihmat, N., Castel-Lacanal, E. & Marque, P. Cerebral imaging of post-stroke plasticity and tissue repair. *Rev. Neurol. (Paris)*. **173**, 577–583

- (2017).
67. Cirillo, C. *et al.* Post-stroke remodeling processes in animal models and humans. *J. Cereb. Blood Flow Metab.* **40**, 3–22 (2020).
  68. Katsanos, A. H. *et al.* Intravenous Thrombolysis With Tenecteplase in Patients With Large Vessel Occlusions. *Stroke* **52**, 308–312 (2021).
  69. Maingard, J., Foo, M., Chandra, R. V. & Leslie-Mazwi, T. M. Endovascular Treatment of Acute Ischemic Stroke. *Curr. Treat. Options Cardiovasc. Med.* **21**, 225–558 (2019).
  70. Smith, W. S. *et al.* Safety and efficacy of mechanical embolectomy in acute ischemic stroke: Results of the MERCI trial. *Stroke* **36**, 1432–1438 (2005).
  71. Furlan A, Higashida R, Wechsler L, Gent M, Rowley H, Kase C, Pessin M, Ahuja A, Callahan F, Clark WM, Silver F, R. F. Intra-arterial prourokinase for acute ischemic stroke. The PROACT II study: a randomized controlled trial. Prolyse in Acute Cerebral Thromboembolism. *J. Am. Med. Assoc.* **282**, 2003–11 (1999).
  72. Ogawa, A. *et al.* Randomized trial of intraarterial infusion of urokinase within 6 hours of middle cerebral artery stroke: The Middle Cerebral Artery Embolism Local Fibrinolytic Intervention Trial (MELT) Japan. *Stroke* **38**, 2633–2639 (2007).
  73. Haussen, Di. C., Lima, A. & Nogueira, R. G. The Trevo XP 320 mm retriever (‘Baby Trevo’) for the treatment of distal intracranial occlusions. *J. Neurointerv. Surg.* **8**, 295–9 (2016).
  74. Schwaiger, B. J. *et al.* The pREset Stent Retriever for Endovascular Treatment of Stroke Caused by MCA Occlusion: Safety and Clinical Outcome. *Clin. Neuroradiol.* **26**, 47–55 (2016).
  75. Kaneko, N., Komuro, Y., Yokota, H. & Tateshima, S. Stent retrievers with segmented design improve the efficacy of thrombectomy in tortuous vessels.

- J. Neurointerv. Surg.* **11**, 119–122 (2019).
76. Fennell, V. S. *et al.* What to do about fibrin rich ‘tough clots’? Comparing the Solitaire stent retriever with a novel geometric clot extractor in an in vitro stroke model. *J. Neurointerv. Surg.* **10**, 907–910 (2018).
77. Gruber, P. *et al.* Embolus Retriever with Interlinked Cages versus other stent retrievers in acute ischemic stroke: An observational comparative study. *J. Neurointerv. Surg.* **10**, e31 (2018).
78. Nogueira, R. G. *et al.* Thrombectomy 6 to 24 hours after stroke with a mismatch between deficit and infarct. *N. Engl. J. Med.* **378**, 11–21 (2018).
79. Albers, G. W. *et al.* Thrombectomy for stroke at 6 to 16 hours with selection by perfusion imaging. *N. Engl. J. Med.* **378**, 708–718 (2018).
80. Desai, S. M., Rocha, M., Jovin, T. G. & Jadhav, A. P. High Variability in Neuronal Loss: Time Is Brain, Requantified. *Stroke* **50**, 34–37 (2019).
81. Zerna, C., Thomalla, G., Campbell, B. C. V., Rha, J. H. & Hill, M. D. Current practice and future directions in the diagnosis and acute treatment of ischaemic stroke. *Lancet* **392**, 1247–1256 (2018).
82. Winstein, C. J. *et al.* Guidelines for Adult Stroke Rehabilitation and Recovery: A Guideline for Healthcare Professionals From the American Heart Association/American Stroke Association. *Stroke* **47**, e98–e169 (2016).
83. Sommer, C. J. & Schäbitz, W. R. Principles and requirements for stroke recovery science. *J. Cereb. Blood Flow Metab.* **41**, 471–485 (2021).
84. Su, F. & Xu, W. Enhancing Brain Plasticity to Promote Stroke Recovery. *Front. Neurol.* **11**, 554089 (2020).
85. Alawieh, A., Zhao, J. & Feng, W. Factors affecting post-stroke motor recovery: Implications on neurotherapy after brain injury. *Behav. Brain Res.* **340**, 94–101 (2018).

86. Benjamin, E. J. *et al.* American Heart Association Council on Epidemiology and Prevention Statistics Committee and Stroke Statistics Subcommittee Heart Disease and Stroke Statistics-2018 Update: A Report From the American Heart Association. *Circulation* **137**, e67–e492 (2018).
87. Fluri, F., Schuhmann, M. K. & Kleinschnitz, C. Animal models of ischemic stroke and their application in clinical research. *Drug Des. Devel. Ther.* **9**, 3445–54 (2015).
88. Fisher, M. *et al.* Update of the stroke therapy academic industry roundtable preclinical recommendations. *Stroke* **40**, 2244–2250 (2009).
89. du Sert, N. P. *et al.* The arrive guidelines 2.0: Updated guidelines for reporting animal research. *PLoS Biol.* **17**, 3617–3624 (2020).
90. Stroke Therapy Academic Industry Roundtable (STAIR). Recommendations for standards regarding preclinical neuroprotective and restorative drug development. *Stroke* **30**, 2752–8 (1999).
91. Hermann, D. M., Popa-Wagner, A., Kleinschnitz, C. & Doeppner, T. R. Animal models of ischemic stroke and their impact on drug discovery. *Expert Opin. Drug Discov.* **14**, 315–326 (2019).
92. Dirnagl, U. & Walz, W. Rodent Models of Stroke. *Neuromethods* **21**, 86 (2016).
93. Kumar, A., Aakriti & Gupta, V. A review on animal models of stroke: An update. *Brain Res. Bull.* **122**, 35–44 (2016).
94. Sommer, C. J. Ischemic stroke: experimental models and reality. *Acta Neuropathol.* **133**, 245–261 (2017).
95. Henninger, N. & Mayasi, Y. Nucleic Acid Therapies for Ischemic Stroke. *Neurotherapeutics* **16**, 299–313 (2019).
96. Zhang, B., Kim, H., Wu, H., Gao, Y. & Jiang, X. Sonothrombolysis with magnetic microbubbles under a rotational magnetic field. *Ultrasonics* **98**, 62–71 (2019).

97. Li, Q., Liu, X., Chang, M. & Lu, Z. Thrombolysis enhancing by magnetic manipulation of Fe<sub>3</sub>O<sub>4</sub> nanoparticles. *Materials (Basel)*. **11**, 2313 (2018).
98. Chamorro, Á., Lo, E. H., Renú, A., Van Leyden, K. & Lyden, P. D. The future of neuroprotection in stroke. *J. Neurol. Neurosurg. Psychiatry* **92**, 129–135 (2021).
99. Kumar, A. & Kitago, T. Pharmacological Enhancement of Stroke Recovery. *Curr. Neurol. Neurosci. Rep.* **19**, 43 (2019).
100. Angels Font, M., Arboix, A. & Krupinski, J. Angiogenesis, Neurogenesis and Neuroplasticity in Ischemic Stroke. *Curr. Cardiol. Rev.* **6**, 238–244 (2010).
101. Koh, S. H. *et al.* Differential effects of isoxazole-9 on neural stem/progenitor cells, oligodendrocyte precursor cells, and endothelial progenitor cells. *PLoS One* **10**, e0138724 (2015).
102. Chrostek, M. R., Fellows, E. G., Crane, A. T., Grande, A. W. & Low, W. C. Efficacy of stem cell-based therapies for stroke. *Brain Res.* **1722**, 146362 (2019).
103. Suda, S. *et al.* Recent advances in cell-based therapies for ischemic stroke. *Int. J. Mol. Sci.* **21**, 1–24 (2020).
104. He, J. Q., Sussman, E. S. & Steinberg, G. K. Revisiting Stem Cell-Based Clinical Trials for Ischemic Stroke. *Front. Aging Neurosci.* **12**, 575990 (2020).
105. Li, Z. *et al.* Stem cell-based therapies for ischemic stroke: a systematic review and meta-analysis of clinical trials. *Stem Cell Res. Ther.* **11**, 252 (2020).
106. Kawabori, M., Shichinohe, H., Kuroda, S. & Houkin, K. Clinical trials of stem cell therapy for cerebral ischemic stroke. *Int. J. Mol. Sci.* **21**, 1–21 (2020).
107. Palma-Tortosa, S., Coll-San Martín, B., Kokaia, Z. & Tornero, D. Neuronal Replacement in Stem Cell Therapy for Stroke: Filling the Gap. *Front. Cell Dev. Biol.* **9**, 662636 (2021).
108. Savitz, S. I. Developing Cellular Therapies for Stroke. *Stroke* **46**, 2026–2031

- (2015).
109. Love, C. J., Selim, M., Spector, M. & Lo, E. H. Biomaterials for Stroke Therapy. *Stroke* **50**, 2278–2284 (2019).
  110. Asahara, T. *et al.* Isolation of putative progenitor endothelial cells for angiogenesis. *Science (80-. )*. **275**, 964–967 (1997).
  111. Fadini, G. P., Losordo, D. & Dimmeler, S. Critical reevaluation of endothelial progenitor cell phenotypes for therapeutic and diagnostic use. *Circ. Res.* **110**, 624–637 (2012).
  112. Basile, D. P. & Yoder, M. C. Circulating and Tissue Resident Endothelial Progenitor Cells. *J. Cell. Physiol.* **229**, 10–16 (2014).
  113. Chong, M. S. K., Ng, W. K. & Chan, J. K. Y. Concise Review: Endothelial Progenitor Cells in Regenerative Medicine: Applications and Challenges. *Stem Cells Transl. Med.* **5**, 530–538 (2016).
  114. Esquivia, G., Grayston, A. & Rosell, A. Revascularization and endothelial progenitor cells in stroke. *Am. J. Physiol. - Cell Physiol.* **315**, C664–C674 (2018).
  115. Bhatwadekar, A. D., Shaw, L. C. & Grant, M. B. Promise of endothelial progenitor cell for treatment of diabetic retinopathy. *Expert Rev. Endocrinol. Metab.* **5**, 29–37 (2010).
  116. Medina, R. J. *et al.* Endothelial progenitors: A consensus statement on nomenclature. *Stem Cells Transl. Med.* **6**, 1316–1320 (2017).
  117. Huizer, K., Mustafa, D. A. M., Spelt, J. C., Kros, J. M. & Sacchetti, A. Improving the characterization of endothelial progenitor cell subsets by an optimized FACS protocol. *PLoS One* **12**, e0184895 (2017).
  118. Fujisawa, T. *et al.* Endothelial Progenitor Cells Do Not Originate From the Bone Marrow. *Circulation* **140**, 1524–1526 (2019).
  119. Taguchi, A. *et al.* Administration of CD34+ cells after stroke enhances



- neurogenesis via angiogenesis in a mouse model. *J. Clin. Invest.* **114**, 330–338 (2004).
120. Ohta, T. *et al.* Administration of ex vivo-expanded bone marrow-derived endothelial progenitor cells attenuates focal cerebral ischemia-reperfusion injury in rats. *Neurosurgery* **59**, 679–686 (2006).
121. Shyu, W. C., Lin, S. Z., Chiang, M. F., Su, C. Y. & Li, H. Intracerebral peripheral blood stem cell (CD34+) implantation induces neuroplasticity by enhancing  $\beta$ 1 integrin-mediated angiogenesis in chronic stroke rats. *J. Neurosci.* **26**, 3444–3453 (2006).
122. Moubarik, C. *et al.* Transplanted Late Outgrowth Endothelial Progenitor Cells as Cell Therapy Product for Stroke. *Stem Cell Rev. Reports* **7**, 208–220 (2011).
123. Fan, Y. *et al.* Endothelial progenitor cell transplantation improves long-term outcome in mice. *Ann Neurol.* **67**, 488–497 (2011).
124. Pellegrini, L. *et al.* Therapeutic benefit of a combined strategy using erythropoietin and endothelial progenitor cells after transient focal cerebral ischemia in rats. *Neurol. Res.* **35**, 937–947 (2013).
125. Kong, Z., Hong, Y., Zhu, J., Cheng, X. & Liu, Y. Endothelial progenitor cells improve functional recovery in focal cerebral ischemia of rat by promoting angiogenesis via VEGF. *J. Clin. Neurosci.* **55**, 116–121 (2018).
126. Bayraktutan, U. Endothelial progenitor cells: Potential novel therapeutics for ischaemic stroke. *Pharmacol. Res.* **144**, 181–191 (2019).
127. Lodi, D., Iannitti, T. & Palmieri, B. Stem cells in clinical practice: applications and warnings. *J. Exp. Clin. Cancer Res.* **30**, 9 (2011).
128. Borlongan, C. V. Concise Review: Stem Cell Therapy for Stroke Patients: Are We There Yet? *Stem Cells Transl. Med.* **8**, 983–988 (2019).
129. Venkat, P., Chopp, M. & Chen, J. Cell-Based and Exosome Therapy in Diabetic Stroke. *Stem Cells Transl. Med.* **7**, 451–455 (2018).

130. Borlongan, C. V. *et al.* May the force be with you: Transfer of healthy mitochondria from stem cells to stroke cells. *Journal of Cerebral Blood Flow and Metabolism* vol. 39 367–370 (2019).
131. Doeppner, T. R. *et al.* Extracellular Vesicles Improve Post-Stroke Neuroregeneration and Prevent Postischemic Immunosuppression. *Stem Cells Transl. Med.* **4**, 1131–1143 (2015).
132. Vizoso, F. J., Eiro, N., Cid, S., Schneider, J. & Perez-Fernandez, R. Mesenchymal stem cell secretome: Toward cell-free therapeutic strategies in regenerative medicine. *Int. J. Mol. Sci.* **18**, 1852 (2017).
133. Alwjaj, M., Rais Reskiawan, A. K. & Bayraktutan, U. The secretome of endothelial progenitor cells: A potential therapeutic strategy for ischemic stroke. *Neural Regen. Res.* **16**, 1483–1489 (2021).
134. di Santo, S. *et al.* Novel cell-free strategy for therapeutic angiogenesis: In vitro generated conditioned medium can replace progenitor cell transplantation. *PLoS One* **4**, e5643 (2009).
135. Rosell, A. *et al.* Factors Secreted by Endothelial Progenitor Cells Enhance Neurorepair Responses after Cerebral Ischemia in Mice. *PLoS One* **8**, e73244 (2013).
136. Wang, T., Fang, X. & Yin, Z. S. Endothelial progenitor cell-conditioned medium promotes angiogenesis and is neuroprotective after spinal cord injury. *Neural Regen. Res.* **13**, 887–895 (2018).
137. Maki, T. *et al.* Endothelial Progenitor Cell Secretome and Oligovascular Repair in a Mouse Model of Prolonged Cerebral Hypoperfusion. *Stroke* **49**, 1003–1010 (2018).
138. Zhou, Y. *et al.* Exosomes from endothelial progenitor cells improve outcomes of the lipopolysaccharide-induced acute lung injury. *Crit. Care* **23**, 44 (2019).
139. Hinkel, R. *et al.* Thymosin beta4 is an essential paracrine factor of embryonic

- endothelial progenitor cell-mediated cardioprotection. *Circulation* **117**, 2232–40 (2008).
140. Dernbach, E. *et al.* Antioxidative stress-associated genes in circulating progenitor cells: Evidence for enhanced resistance against oxidative stress. *Blood* **104**, 3591–3597 (2004).
141. Habgood, M. & Ek, J. Delivering drugs into the brain: Barriers and possibilities. *Ther. Deliv.* **1**, 483–488 (2010).
142. Haumann, R., Videira, J. C., Kaspers, G. J. L., van Vuurden, D. G. & Hulleman, E. Overview of Current Drug Delivery Methods Across the Blood–Brain Barrier for the Treatment of Primary Brain Tumors. *CNS Drugs* **34**, 1121–1131 (2020).
143. Ahlawat, J. *et al.* Nanocarriers as Potential Drug Delivery Candidates for Overcoming the Blood-Brain Barrier: Challenges and Possibilities. *ACS Omega* **5**, 12583–12595 (2020).
144. Gosselet, F., Loiola, R. A., Roig, A., Rosell, A. & Culot, M. Central nervous system delivery of molecules across the blood-brain barrier. *Neurochem. Int.* **144**, 104952 (2021).
145. Idbaih, A. *et al.* Safety and feasibility of repeated and transient blood-brain barrier disruption by pulsed ultrasound in patients with recurrent glioblastoma. *Clin. Cancer Res.* **25**, 3793–3801 (2019).
146. Lipsman, N. *et al.* Blood–brain barrier opening in Alzheimer’s disease using MR-guided focused ultrasound. *Nat. Commun.* **9**, 2336 (2018).
147. Bidros, D. S., Liu, J. K. & Vogelbaum, M. A. Future of convection-enhanced delivery in the treatment of brain tumors. *Futur. Oncol.* **6**, 117–125 (2010).
148. Gao, X. *et al.* Nanoagonist-mediated endothelial tight junction opening: A strategy for safely increasing brain drug delivery in mice. *J. Cereb. Blood Flow Metab.* **37**, 1410–1424 (2017).

149. Lesniak, W. G. *et al.* A Distinct Advantage to Intraarterial Delivery of <sup>89</sup>Zr-Bevacizumab in PET Imaging of Mice With and Without Osmotic Opening of the Blood-Brain Barrier. *J. Nucl. Med.* **60**, 617–622 (2019).
150. Ji, R. *et al.* Cavitation-modulated inflammatory response following focused ultrasound blood-brain barrier opening. *J. Control. Release* **337**, 458–471 (2021).
151. Al-Ahmady, Z. S. *et al.* Selective Liposomal Transport through Blood Brain Barrier Disruption in Ischemic Stroke Reveals Two Distinct Therapeutic Opportunities. *ACS Nano* **13**, 12470–12486 (2019).
152. Trinh, D. *et al.* Microbubble drug conjugate and focused ultrasound blood brain barrier delivery of AAV-2 SIRT-3. *Drug Deliv.* **29**, 1176–1183 (2022).
153. Pegtel, D. M. & Gould, S. J. Exosomes. *Annu. Rev. Biochem.* **88**, 487–514 (2019).
154. Kalluri, R. & LeBleu, V. S. The biology, function, and biomedical applications of exosomes. *Science (80-. ).* **367**, eaau6977 (2020).
155. Tian, T. *et al.* Surface functionalized exosomes as targeted drug delivery vehicles for cerebral ischemia therapy. *Biomaterials* **150**, 137–149 (2018).
156. Webb, R. L. *et al.* Human Neural Stem Cell Extracellular Vesicles Improve Tissue and Functional Recovery in the Murine Thromboembolic Stroke Model. *Transl. Stroke Res.* **9**, 530–539 (2018).
157. Bleeker, E. A. J. *et al.* Considerations on the EU definition of a nanomaterial: Science to support policy making. *Regul. Toxicol. Pharmacol.* **65**, 119–125 (2013).
158. Ahlawat, J., Henriquez, G. & Narayan, M. Enhancing the delivery of chemotherapeutics: Role of biodegradable polymeric nanoparticles. *Molecules* **23**, 2157 (2018).
159. Fisher, D. G. & Price, R. J. Recent advances in the use of focused ultrasound for magnetic resonance image-guided therapeutic nanoparticle delivery to the central nervous system. *Front. Pharmacol.* **10**, 1348 (2019).

160. Mitchell, M. J. *et al.* Engineering precision nanoparticles for drug delivery. *Nat. Rev. Drug Discov.* **20**, 101–124 (2021).
161. Saraiva, C. *et al.* Nanoparticle-mediated brain drug delivery: Overcoming blood-brain barrier to treat neurodegenerative diseases. *J. Control. Release* **235**, 34–47 (2016).
162. Gustafson, H. H., Holt-Casper, D., Grainger, D. W. & Ghandehari, H. Nanoparticle uptake: The phagocyte problem. *Nano Today* **10**, 487–510 (2015).
163. Wolfram, J. *et al.* Safety of Nanoparticles in Medicine. *Curr. Drug Targets* **16**, 1671–1681 (2015).
164. Li, Y. *et al.* Complement opsonization of nanoparticles: Differences between humans and preclinical species. *J. Control. Release* **338**, 548–556 (2021).
165. Tavano, R. *et al.* C1q-Mediated Complement Activation and C3 Opsonization Trigger Recognition of Stealth Poly(2-methyl-2-oxazoline)-Coated Silica Nanoparticles by Human Phagocytes. *ACS Nano* **12**, 5834–5847 (2018).
166. Szebeni, J., Simberg, D., González-Fernández, Á., Barenholz, Y. & Dobrovolskaia, M. A. Roadmap and strategy for overcoming infusion reactions to nanomedicines. *Nat. Nanotechnol.* **13**, 1100–1108 (2018).
167. Dong, X. Current strategies for brain drug delivery. *Theranostics* **8**, 1481–1493 (2018).
168. Jahangiri, A. *et al.* Convection-enhanced delivery in glioblastoma: A review of preclinical and clinical studies. *J. Neurosurg.* **126**, 191–200 (2017).
169. Patel, M. M. & Patel, B. M. Crossing the Blood–Brain Barrier: Recent Advances in Drug Delivery to the Brain. *CNS Drugs* **31**, 109–133 (2017).
170. Ye, D. *et al.* Focused ultrasound combined with microbubble-mediated intranasal delivery of gold nanoclusters to the brain. *J. Control. Release* **286**, 145–153 (2018).

171. Griauzde, J., Ravindra, V. M., Chaudhary, N., Gemmete, J. J. & Pandey, A. S. Neuroprotection for ischemic stroke in the endovascular era: A brief report on the future of intra-arterial therapy. *J. Clin. Neurosci.* **69**, 289–291 (2019).
172. Guzman, R., Janowski, M. & Walczak, P. Intra-arterial delivery of cell therapies for stroke. *Stroke* **49**, 1075–1082 (2018).
173. Bhatia, V., Gupta, V., Khurana, D., Sharma, R. R. & Khandelwal, N. Randomized assessment of the safety and efficacy of intra-arterial infusion of autologous stem cells in subacute ischemic stroke. *Am. J. Neuroradiol.* **39**, 899–904 (2018).
174. Fraser, J. F. *et al.* Intra-arterial verapamil post-thrombectomy is feasible, safe, and neuroprotective in stroke. *J. Cereb. Blood Flow Metab.* **37**, 3531–3543 (2017).
175. Wu, C. *et al.* Safety, feasibility, and potential efficacy of intraarterial selective cooling infusion for stroke patients treated with mechanical thrombectomy. *J. Cereb. Blood Flow Metab.* **38**, 2251–2260 (2018).
176. Bonnard, T., Gauberti, M., Martinez De Lizarrondo, S., Campos, F. & Vivien, D. Recent Advances in Nanomedicine for Ischemic and Hemorrhagic Stroke. *Stroke* **50**, 1318–1324 (2019).
177. Han, L. & Jiang, C. Evolution of blood–brain barrier in brain diseases and related systemic nanoscale brain-targeting drug delivery strategies. *Acta Pharm. Sin. B* **11**, 2306–2325 (2021).
178. Bernardo-Castro, S. *et al.* Therapeutic nanoparticles for the different phases of ischemic stroke. *Life* **11**, 482 (2021).
179. Dong, X., Gao, J., Su, Y. & Wang, Z. Nanomedicine for ischemic stroke. *Int. J. Mol. Sci.* **21**, 1–22 (2020).
180. Chen, J. P., Yang, P. C., Ma, Y. H. & Wu, T. Characterization of chitosan magnetic nanoparticles for in situ delivery of tissue plasminogen activator. *Carbohydr. Polym.* **84**, 364–372 (2011).

181. Carena, E. *et al.* In vitro angiogenic performance and in vivo brain targeting of magnetized endothelial progenitor cells for neurorepair therapies. *Nanomedicine Nanotechnology, Biol. Med.* **10**, 225–234 (2014).
182. Voros, E. *et al.* TPA Immobilization on Iron Oxide Nanocubes and Localized Magnetic Hyperthermia Accelerate Blood Clot Lysis. *Adv. Funct. Mater.* **25**, 1709–1718 (2015).
183. Hu, J. *et al.* Tissue Plasminogen Activator-Porous Magnetic Microrods for Targeted Thrombolytic Therapy after Ischemic Stroke. *ACS Appl. Mater. Interfaces* **10**, 32988–32997 (2018).
184. Li, C., Sun, T. & Jiang, C. Recent advances in nanomedicines for the treatment of ischemic stroke. *Acta Pharm. Sin. B* **11**, 1767–1788 (2021).
185. Parvez, S. *et al.* Dodging blood brain barrier with ‘nano’ warriors: Novel strategy against ischemic stroke. *Theranostics* **12**, 689–719 (2022).
186. Ma, J. *et al.* Targeted Drug Delivery to Stroke via Chemotactic Recruitment of Nanoparticles Coated with Membrane of Engineered Neural Stem Cells. *Small* **15**, e1902011 (2019).
187. Navarro-Sobrinho, M. *et al.* Mobilization, endothelial differentiation and functional capacity of endothelial progenitor cells after ischemic stroke. *Microvasc. Res.* **80**, 317–323 (2010).
188. Zhang, Y. *et al.* PLGA protein nanocarriers with tailor-made fluorescence/MRI/PET imaging modalities. *Nanoscale* **12**, 4988–5002 (2020).
189. Weksler, B. *et al.* Blood-brain barrier- specific properties of a human adult brain endothelial cell line. **19**, 1872–1874 (2005).
190. Omid, Y. *et al.* Evaluation of the immortalised mouse brain capillary endothelial cell line, b.End3, as an in vitro blood-brain barrier model for drug uptake and transport studies. *Brain Res.* **990**, 95–112 (2003).
191. Morancho, A. *et al.* Cerebral ischaemia and matrix metalloproteinase-9

- modulate the angiogenic function of early and late outgrowth endothelial progenitor cells. *J. Cell. Mol. Med.* **17**, 1543–1553 (2013).
192. Rosell, A. *et al.* Interleukin-1 $\beta$  augments angiogenic responses of murine endothelial progenitor cells in vitro. *J. Cereb. Blood Flow Metab.* **29**, 933–943 (2009).
193. Clark, W. M., Lessov, N. S., Dixon, M. P. & Eckenstein, F. Monofilament intraluminal middle cerebral artery occlusion in the mouse. *Neurol. Res.* **19**, 641–8 (1997).
194. Hundt, W., Petsch, R., Helmberger, T. & Reiser, M. Signal changes in liver and spleen after Endorem administration in patients with and without liver cirrhosis. *Eur. Radiol.* **10**, 409–16 (2000).
195. Orsini, F. *et al.* Targeting mannose-binding lectin confers long-lasting protection with a surprisingly wide therapeutic window in cerebral ischemia. *Circulation* **126**, 1484–94 (2012).
196. De Simoni, M. G. *et al.* Neuroprotection by complement (C1) inhibitor in mouse transient brain ischemia. *J. Cereb. Blood Flow Metab.* **23**, 232–9 (2003).
197. Rosell, A. *et al.* Distal Occlusion of the Middle Cerebral Artery in Mice: Are We Ready to Assess Long-Term Functional Outcome? *Transl. Stroke Res.* **4**, 297–307 (2013).
198. Lee, S. *et al.* Middle cerebral artery occlusion methods in rat versus mouse models of transient focal cerebral ischemic stroke. *Neural Regen. Res.* **9**, 757–758 (2014).
199. Morancho, A. *et al.* A new method for focal transient cerebral ischaemia by distal compression of the middle cerebral artery. *Neuropathol. Appl. Neurobiol.* **38**, 617–27 (2012).
200. García-Yébenes, I. *et al.* A mouse model of hemorrhagic transformation by delayed tissue plasminogen activator administration after in situ



- thromboembolic stroke. *Stroke* **42**, 196–203 (2011).
201. Tontsch, U. & Bauer, H. C. Isolation, characterization, and long-term cultivation of porcine and murine cerebral capillary endothelial cells. *Microvasc. Res.* **37**, 148–161 (1989).
202. Zarrinkoob, L. *et al.* Blood flow distribution in cerebral arteries. *J. Cereb. Blood Flow Metab.* **35**, 648–654 (2015).
203. Loiola, R. A. *et al.* Secretome of endothelial progenitor cells from stroke patients promotes endothelial barrier tightness and protects against hypoxia-induced vascular leakage. *Stem Cell Res. Ther.* **12**, 552 (2021).
204. Carezza, E. *et al.* Encapsulation of VEGF165 into magnetic PLGA nanocapsules for potential local delivery and bioactivity in human brain endothelial cells. *J. Mater. Chem. B* **3**, 2538–2544 (2015).
205. Pakulska, M. M. *et al.* Encapsulation-free controlled release: Electrostatic adsorption eliminates the need for protein encapsulation in PLGA nanoparticles. *Sci. Adv.* **2**, e1600519 (2016).
206. Cui, L. L. *et al.* The cerebral embolism evoked by intra-arterial delivery of allogeneic bone marrow mesenchymal stem cells in rats is related to cell dose and infusion velocity. *Stem Cell Res. Ther.* **6**, 11 (2015).
207. Argibay, B. *et al.* Intraarterial route increases the risk of cerebral lesions after mesenchymal cell administration in animal model of ischemia. *Sci. Rep.* **7**, 40758 (2017).
208. Sukhbaatar, N. & Weichhart, T. Iron regulation: Macrophages in control. *Pharmaceuticals* **11**, 137 (2018).
209. Zhang, Z. G. *et al.* VEGF enhances angiogenesis and promotes blood-brain barrier leakage in the ischemic brain. *J. Clin. Invest.* **106**, 829–838 (2000).
210. Schmued, L. C., Albertson, C. & Slikker, W. Fluoro-Jade: A novel fluorochrome for the sensitive and reliable histochemical localization of

- neuronal degeneration. *Brain Res.* **751**, 37–46 (1997).
211. Ikenari, T., Kurata, H., Satoh, T., Hata, Y. & Mori, T. Evaluation of Fluoro-Jade C Staining: Specificity and Application to Damaged Immature Neuronal Cells in the Normal and Injured Mouse Brain. *Neuroscience* **425**, 146–156 (2020).
212. Goram, A. L. & Richmond, P. L. Pegylated liposomal doxorubicin: Tolerability and toxicity. *Pharmacotherapy* **21**, 751–763 (2001).
213. Cruz, L. J. *et al.* Effect of PLGA NP size on efficiency to target traumatic brain injury. *J. Control. Release* **223**, 31–41 (2016).
214. Wiley, D. T., Webster, P., Gale, A. & Davis, M. E. Transcytosis and brain uptake of transferrin-containing nanoparticles by tuning avidity to transferrin receptor. *Proc. Natl. Acad. Sci. U. S. A.* **110**, 8662–8667 (2013).
215. Pendharkar, A. V. *et al.* Biodistribution of neural stem cells after intravascular therapy for Hypoxic-ischemia. *Stroke* **41**, 2064–70 (2010).
216. Li, L. *et al.* Effects of administration route on migration and distribution of neural progenitor cells transplanted into rats with focal cerebral ischemia, an MRI study. *J. Cereb. Blood Flow Metab.* **30**, 653–62 (2010).
217. Knowland, D. *et al.* Stepwise Recruitment of Transcellular and Paracellular Pathways Underlies Blood-Brain Barrier Breakdown in Stroke. *Neuron* **82**, 603–617 (2014).
218. Brenner, J. S. *et al.* Red blood cell-hitchhiking boosts delivery of nanocarriers to chosen organs by orders of magnitude. *Nat. Commun.* **9**, 2684 (2018).
219. Ding, D. & Zhu, Q. Recent advances of PLGA micro/nanoparticles for the delivery of biomacromolecular therapeutics. *Mater. Sci. Eng. C* **92**, 1041–1060 (2018).
220. Kopcansky, P. *et al.* Numerical modeling of magnetic drug targeting. *Phys. Part. Nucl. Lett.* **8**, 502–505 (2011).

221. Kopčanský P, Bánó M, Repášan M, Potočová I, Timko M, Hrnčiar V, Demjan, S. Magnetic targeted drug delivery using focused magnet. *Magnetohydrodynamics* **40**, 369–378 (2004).
222. Shen, W. Bin *et al.* Magnetic enhancement of stem cell–targeted delivery into the brain following MR-guided focused ultrasound for opening the blood–brain barrier. *Cell Transplant.* **26**, 1235–1246 (2017).
223. Walczak, P. *et al.* Dual-modality monitoring of targeted intraarterial delivery of mesenchymal stem cells after transient ischemia. *Stroke* **39**, 1569–1574 (2008).
224. Minhas, G., Modgil, S. & Anand, A. Role of iron in ischemia-induced neurodegeneration: mechanisms and insights. *Metab. Brain Dis.* **29**, 583–591 (2014).
225. Guo, X. *et al.* Iron promotes neurological function recovery in mice with ischemic stroke through endogenous repair mechanisms. *Free Radic. Biol. Med.* **182**, 59–72 (2022).
226. Yemisci, M. *et al.* Systemically administered brain-targeted nanoparticles transport peptides across the blood-brain barrier and provide neuroprotection. *J. Cereb. Blood Flow Metab.* **35**, 469–475 (2015).
227. Haider, K. H., Aziz, S. & Al-Reshidi, M. A. Endothelial progenitor cells for cellular angiogenesis and repair: Lessons learned from experimental animal models. *Regen. Med.* **12**, 969–982 (2017).
228. Demetrius, L. Of mice and men. *EMBO Rep.* **6**, S39-44 (2005).
229. Benakis, C., Vaslin, A., Pasquali, C. & Hirt, L. Neuroprotection by inhibiting the c-Jun N-terminal kinase pathway after cerebral ischemia occurs independently of interleukin-6 and keratinocyte-derived chemokine (KC/CXCL1) secretion. *J. Neuroinflammation* **9**, 76 (2012).
230. Ushach, I. & Zlotnik, A. Biological role of granulocyte macrophage colony-

- stimulating factor (GM-CSF) and macrophage colony-stimulating factor (M-CSF) on cells of the myeloid lineage. *J. Leukoc. Biol.* **100**, 481–489 (2016).
231. Buschmann, I. R., Busch, H. J., Mies, G. & Hossmann, K. A. Therapeutic induction of arteriogenesis in hypoperfused rat brain via granulocyte-macrophage colony-stimulating factor. *Circulation* **108**, 610–615 (2003).
232. Schneeloch, E., Mies, G., Busch, H. J., Buschmann, I. R. & Hossmann, K. A. Granulocyte-macrophage colony-stimulating factor-induced arteriogenesis reduces energy failure in hemodynamic stroke. *Proc. Natl. Acad. Sci. U. S. A.* **101**, 12730–12735 (2004).
233. Lambertsen, K. L. *et al.* Microglia protect neurons against ischemia by synthesis of tumor necrosis factor. *J. Neurosci.* **29**, 1319–1330 (2009).
234. Arango-Dávila, C. A. *et al.* Soluble or soluble/membrane TNF- $\pm$  inhibitors protect the brain from focal ischemic injury in rats. *Int. J. Neurosci.* **125**, 936–940 (2015).
235. Hosomi, N., Naya, T. & Kohno, M. Tumor necrosis factor-alpha neutralization reduced cerebral edema following transient focal cerebral ischemia. *J. Cereb. Blood Flow Metab.* **25**, S8–S8 (2005).
236. Wu, H., Cong, Y., Wang, D., Zhao, R. & Qi, J. Correlation of macrophage inflammatory protein-2 expression and brain edema in rats after intracerebral hemorrhage. *Int. J. Clin. Exp. Pathol.* **2**, 83–90 (2009).
237. Zhai, Q. H., Futrell, N. & Chen, F. J. Gene expression of IL-10 in relationship to TNF- $\alpha$ , IL-1 $\beta$  and IL-2 in the rat brain following middle cerebral artery occlusion. *J. Neurol. Sci.* **152**, 119–124 (1997).
238. Zhang, Y. *et al.* Release of proinflammatory mediators and expression of proinflammatory adhesion molecules by endothelial progenitor cells. *Am. J. Physiol. - Hear. Circ. Physiol.* **296**, H1675-82 (2009).
239. Acosta, S. A., Lee, J. Y., Nguyen, H., Kaneko, Y. & Borlongan, C. V.

- Endothelial Progenitor Cells Modulate Inflammation-Associated Stroke Vasculome. *Stem Cell Rev. Reports* **15**, 256–275 (2019).
240. Allan, S. M. & Rothwell, N. J. Cytokines and acute neurodegeneration. *Nat. Rev. Neurosci.* **2**, 734–744 (2001).
241. Kadir, R. R. A., Alwjwaj, M. & Bayraktutan, U. Treatment with outgrowth endothelial cells protects cerebral barrier against ischemic injury. *Cytotherapy* **24**, 489–499 (2022).
242. Jayaraj, R. L., Azimullah, S., Beiram, R., Jalal, F. Y. & Rosenberg, G. A. Neuroinflammation: Friend and foe for ischemic stroke. *J. Neuroinflammation* **16**, 142 (2019).
243. Felice, F. *et al.* Endothelial progenitor cell secretome delivered by novel polymeric nanoparticles in ischemic hindlimb. *Int. J. Pharm.* **542**, 82–89 (2018).
244. Moisan, A. *et al.* Microvascular plasticity after experimental stroke: A molecular and MRI study. *Cerebrovasc. Dis.* **38**, 344–353 (2014).
245. Zhao, Q. *et al.* Intranasal administration of human umbilical cord mesenchymal stem cells-conditioned medium enhances vascular remodeling after stroke. *Brain Res.* **1624**, 489–496 (2015).
246. Akwii, R. G., Sajib, M. S., Zahra, F. T. & Mikelis, C. M. Role of Angiotensin-2 in Vascular Physiology and Pathophysiology. *Cells* **8**, 471 (2019).
247. Venkat, P. *et al.* Treatment with an Angiotensin-1 mimetic peptide promotes neurological recovery after stroke in diabetic rats. *CNS Neurosci. Ther.* **27**, 48–59 (2021).
248. Gordon, K. & Kral, A. Animal and human studies on developmental monaural hearing loss. *Hear. Res.* **380**, 60–74 (2019).
249. Arikan, F. *et al.* Malignant infarction of the middle cerebral artery in a porcine model. A pilot study. *PLoS One* **12**, e0172637 (2017).

- 
250. Melià-Sorolla, M. *et al.* Relevance of porcine stroke models to bridge the gap from pre-clinical findings to clinical implementation. *Int. J. Mol. Sci.* **21**, 1–30 (2020).
251. Ashwini, C. A., Shubha, R. & Jayanth, K. S. Comparative anatomy of the circle of Willis in man, cow, sheep, goat and pig. *Neuroanatomy* **7**, 54–65 (2008).
252. Schomberg, D. T. *et al.* Miniature Swine for Preclinical Modeling of Complexities of Human Disease for Translational Scientific Discovery and Accelerated Development of Therapies and Medical Devices. *Toxicol. Pathol.* **44**, 299–314 (2016).
253. Onwukwe, C. *et al.* Engineering Intravenously Administered Nanoparticles to Reduce Infusion Reaction and Stop Bleeding in a Large Animal Model of Trauma. *Bioconjug. Chem.* **29**, 2436–2447 (2018).
254. Messmer, S. J., Fraser, J. F., Pennypacker, K. R. & Roberts, J. M. Method of intra-arterial drug administration in a rat: Sex based optimization of infusion rate. *J. Neurosci. Methods* **357**, (2021).



## ANNEX I – Curriculum Vitae

---





## Academic background

---

- **PhD in Neurosciences** (*ongoing*). Universitat Autònoma de Barcelona (UAB), Bellaterra (Spain). Neurovascular research laboratory, Vall d'Hebron Research Institute (VHIR), Barcelona (Spain). Pre-doctoral contract for training in research into health (PFIS) - ISCIII - FI17/00073.
- **MSc in Translational Biomedical Research** (2016-2017). Universitat Autònoma de Barcelona (UAB), Spain. Neurovascular research laboratory, Vall d'Hebron Research Institute (VHIR), Barcelona (Spain). Fundació Banc Sabadell Scholarship.
- **BSc in Biomedical Sciences** (2012-2016). Universitat Autònoma de Barcelona (UAB), Spain. Molecular Neuropharmacology laboratory, Institut de Recerca Biomèdica Sant Pau – Institut de Neurociències (UAB), Bellaterra (Spain). Ítaca Salary Santander Scholarship for Talented Young People.

## Scientific visits

---

- **Medicine Nuclear Department, I.R.C.C.S. Ospedale San Raffaele.** Milan (Italy). 04/02/2019 – 24/05/2019. Mobility of research staff contracted within the framework of the Health Research and Development Strategy (M-AES) – ISCIII – MV18/00006.

## Scientific publications

---

- Grzelak J, Teles M, Roher N, **Grayston A**, Rosell A, Gich M, Roig A. Bioevaluation of magnetic mesoporous silica rods: cytotoxicity, cell uptake and biodistribution in zebrafish and rodents. *ACS Nano* (*under review*)
- Grzelak J, Gàzquez J, **Grayston A**, Herranz F, Rosell A, Roig A, Gich M. Magnetic mesoporous silica nanorods for theranostics: multimodal imaging and ceria loading. *ACS Applied Nanomaterials* 5, 2113-2125 (2022)

- Loiola RA, Garcia-Gabilondo M, **Grayston A**, Bugno P, Kowalska A, Duban-Deweer S, Rizzi E, Hachani J, Sano Y, Shimizu F, Kanda T, Mysiorek C, Mazurek MP, Rosell A, Gosselet F. Secretome of endothelial progenitor cells from stroke patients promotes endothelial barrier tightness and protects against hypoxia-induced vascular leakage. *Stem Cell Research & Therapy* 12, 552 (2021)
- **Grayston A**, Zhang Y, Garcia-Gabilondo Y, Arrúe M, Martin A, Kopcansky P, Timko M, Kovac J, Strbak O, Castellote L, Belloli S, Moresco RM, Picchio M, Roig A, Rosell A. Endovascular administration of magnetized nanocarriers targeting brain delivery after stroke. *Journal of Cerebral Blood Flow & Metabolism* 42, 237-252 (2021)
- Gabriel-Salazar M<sup>†</sup>, Lei T<sup>†</sup>, **Grayston A**, Costa C, Medina-Gutiérrez E, Comabella M, Montaner J, Rosell A. Angiogenin in the neurogenic subventricular zone after stroke. *Frontiers in neurology* 12, 662235 (2021) <sup>†</sup>Equal contribution.
- Seras-Franzoso J, Díaz-Riascos ZV, Corchero JL, González P, García-Aranda N, Mandaña M, Riera R, Boullosa A, Mancilla S, **Grayston A**, Moltó-Abad M, Garcia-Fruitós E, Mendoza R, Pintos-Morell G, Albertazzi L, Rosell A, Casas J, Villaverde A, Schwartz S Jr, Abasolo I. Extracellular Vesicles from Recombinant Cell Factories Improve the Activity and Efficacy of Enzymes Defective in Lysosomal Storage Disorders. *Journal of Extracellular Vesicles* 10, e12058 (2021)
- Zhang Y, Garcia-Gabilondo M, **Grayston A**, Feiner IVJ, Anton-Sales I, Loiola RA, Llop J, Ramos-Cabrer P, Barba I, Garcia-Dorado D, Gosselet F, Rosell A, Roig A. PLGA protein nanocarriers with tailor-made fluorescence/MRI/PET imaging modalities. *Nanoscale. The Royal Society of Chemistry* 12, 4988-5002 (2020)
- Oleshkevicha E, Morancho A, Saha A, Galenkamp KMO, **Grayston A**, Geninatti S, Alberti D, Protti N, Comella JX, Teixidor F, Rosell A, Viñas C. Combining Magnetic Nanoparticles and Icosahedral Boron Clusters in

Biocompatible Inorganic Nanohybrids for Cancer Therapy. *Nanomedicine: Nanotechnology, Biology, and Medicine* 20, 101986 (2019)

- Pradillo JM, **Grayston A**, Medina-Alonso V, Arrúe M, Lizasoain I, Rosell A. Effects of aging and comorbidities on endothelial progenitor cells. *Conditioning Medicine* 2, 18-29 (2019).
- Esquivá G, **Grayston A**, Rosell A. Revascularization and Endothelial Progenitor Cells in Stroke. *American journal of physiology. Cell physiology* 315, C664-C674 (2018)

### Involvement in research projects

---

- New neurovascular remodelling strategies for neurorepair after stroke: from nanomedicine to neurorehabilitation therapies (EoI for Collaborative efforts on Regenerative Medicine 2019) – Vall d’Hebron Research Institute (VHIR). 2019 - 2020. PI: Anna Rosell Novel
- New MAGnetic Biomaterials for Brain Repair and Imaging after Stroke (MAGBBRIS). AC17/00004 – Vall d’Hebron Research Institute (VHIR). 2018 - 2021. PIs: Anna Rosell Novel; Anna Roig; Fabien Gosselet; Maria Picchio; Filip Jelen; Peter Kopkanksy
- SMARRTS-II: Marcadores de Angiogénesis y Reparación durante Terapia Rehabilitadora tras el ictus: Estudio clínico multicéntrico y modelo animal de neurorehabilitación en ratón. PI16/00981 – Vall d’Hebron Research Institute (VHIR). 2017 - 2019. PI: Anna Rosell Novel
- New strategies in the treatment of diabetic neuropathy. PI14/00927 – Institut de Recerca de l’Hospital de la Santa Creu i Sant Pau. PI: Olga Pol Rigau

### Scientific communications in national and international meetings

---

- **Grayston A**, Garcia-Gabilondo M, Zhang Y, Stephany A, Mekseriwattana W, Timko M, Kovac J, Kopcansky P, Castellote L, Li J, Ribó M, Roig A, Rosell A. *Nanotargeted endovascular endothelial progenitor cells-secretome therapy for ischemic stroke. BRAIN & BRAIN PET 2022*. Glasgow (Scotland, United Kingdom).

29/05/2022 – 01/06/2022. **Candidate for Niels Lassen award** (Oral communication)

- **Grayston A**, Garcia-Gabilondo M, Zhang Y, Stephany A, Mekseriwattana W, Timko M, Kovac J, Kopcansky P, Castellote L, Li J, Ribó M, Loiola RA, Gosselet F, Belloli S, Moresco RM, Picchio M, Kowalska A, Mazurek M, Roig A, Rosell A. *Administración intraarterial de secretoma de células progenitoras endoteliales en nanocápsulas magnetizadas como “cell-free therapy” para el tratamiento del ictus*. **V Congreso Anual de la Red de Enfermedades Vasculares Cerebrales - INVICTUS+**. Santiago de Compostela (Spain). 18/11/2021 – 19/11/2021. (Oral communication)
- **Grayston A**, Garcia-Gabilondo M, Zhang Y, Stephany A, Timko M, Kovac J, Kopcansky P, Castellote L, Li J, Ribó M, Belloli S, Moresco RM, Picchio M, Kowalska A, Mazurek M, Roig A, Rosell A. *Endovascular administration of biocompatible magnetized nanocarriers for brain delivery after stroke*. **7th European Stroke Organisation Conference (ESOC)**. Online Meeting. 01/09/2021-03/09/2021. **Young investigator award** (Oral communication)
- **Grayston A**, Garcia-Gabilondo M, Zhang Y, Stephany A, Timko M, Kovac J, Loiola RA, Castellote L, Kowalska A, Belloli S, Li J, Ribó M, Moresco RM, Picchio M, Mazurek M, Kopcansky P, Gosselet F, Roig A, Rosell A. *New Magnetic Biomaterials for Brain Repair and Imaging after Stroke (MAGBBRIS)*. **EuroNanoMed3 - Review Seminar Joint Translational Call 2017**. Online Meeting. 20/04/2021. (**Poster**)
- **Grayston A**, Zhang Y, Garcia-Gabilondo M, Barba I, Garcia-Dorado D, Ramos-Cabrer P, Martín A, Roig A, Rosell A. *Intraarterial administration of Endothelial Progenitor Cell secretome in magnetized nanocapsules for a sustained release in a mouse model of transient cerebral ischemia*. **13th Vall d'Hebron Reserach Institute (VHIR) Scientific Session and 23rd Vall d'Hebron Annual Conference**. Barcelona (Spain). 12/12/2019 – 13/12/2019. **Pre-doctoral category award** (Poster and oral communication)

- **Grayston A**, Garcia-Gabilondo M, Zhang Y, Simats A, Arrué M, Belloli S, Canu T, Picchio M, Moresco RM, Barba I, Ramos-Cabrer P, Martín A, Roig A, Rosell A. *Administración intraarterial de secretoma de células progenitoras endoteliales en nanocápsulas magnetizadas y biocompatibles como “cell-free therapy” para promover la neuroreparación tras el ictus. III Congreso Anual de la Red de Enfermedades Vasculares Cerebrales - INVICTUS+.* Santiago de Compostela (Spain). 07/09/2018 – 08/09/2018. ([Oral communication](#))
- **Grayston A**, Garcia-Gabilondo M, Zhang Y, Simats A, Arrué M, Belloli S, Canu T, Picchio M, Moresco RM, Barba I, Ramos-Cabrer P, Martín A, Roig A, Rosell A. *Intraarterial administration of endothelial progenitor cell secretome in biocompatible magnetized nanocapsules as a targeted cell-free therapy for neurorepair after stroke. VII INC Scientific Conferences 2019.* Sant Feliu de Guíxols (Spain). 01/10/2019 – 03/10/2019. ([Oral communication](#))
- **Grayston A**, Zhang Y, Garcia-Gabilondo M, Barba I, Garcia-Dorado D, Ramos-Cabrer P, Martín A, Roig A, Rosell A. *Intraarterial administration of therapeutic endothelial progenitor cell secretome in biocompatible magnetized nanocapsules for sustained release in a mouse model of transient cerebral ischemia. 5th European Stroke Organisation Conference (ESOC).* Milan (Italy). 22/05/2019 – 24/05/2019. ([Poster](#))
- **Grayston A**, Zhang Y, Garcia-Gabilondo M, Barba I, Gabriel-Salazar M, Roig A, Rosell A. *Encapsulating Endothelial Progenitor Cell secretome in magnetized biocompatible nanocapsules for targeted cell-free therapy for neurorepair after stroke. 10th International Symposium on Neuroprotection and Neurorepair.* Dresden, Radebeul (Germany). 09/10/2018 – 11/10/2018. ([Oral communication](#))

### Additional training

---

- **Theoretical-practical course in Optical Imaging.** Alterations in metabolism, cellular stress and neurodegenerative processes. C.N.R. – Istituto di Bioimmagini e Fisiologia Molecolare (IBFM). April 2019

- **Training Course in Laboratory Animal Science for Scientists Responsible for the Design or Conduct of Animal Experiments.** Functions a,b,c,d according to Directive EU63/2010 for mouse, rat and fish (*Danio rerio*, zebrafish; *Carassius spp*, Goldfish; *Sparus Aurata*, Gilthead Seabream). UAB - FELASA F002/03. February 2018

### Teaching experience

---

**Master in Translational Biomedical Research (VHIR – UAB).** Module in Brain and Peripheral Nervous System. Practicum: In vivo models of Stroke. 2019-2022

## ANNEX II – Related Publications

---





## **Revascularization and endothelial progenitor cells in stroke**

---

DOI: 10.1152/ajpcell.00200.2018



## THEME | *Vascular and Cellular Pathophysiology of Stroke*

# Revascularization and endothelial progenitor cells in stroke

Gema Esquiva, Alba Grayston, and Anna Rosell

Neurovascular Research Laboratory and Neurology Department, Vall d'Hebron Research Institute, Universitat Autònoma de Barcelona, Barcelona, Spain

Submitted 22 May 2018; accepted in final form 9 August 2018

**Esquiva G, Grayston A, Rosell A.** Revascularization and endothelial progenitor cells in stroke. *Am J Physiol Cell Physiol* 315: C664–C674, 2018. First published August 22, 2018; doi:10.1152/ajpcell.00200.2018.—Stroke is one of the leading causes of death and disability worldwide. Tremendous improvements have been achieved in the acute care of stroke patients with the implementation of stroke units, thrombolytic drugs, and endovascular thrombectomies. However, stroke survivors with neurological deficits require long periods of neurorehabilitation, which is the only approved therapy for poststroke recovery. With this scenario, more treatments are urgently needed, and only the understanding of the mechanisms of brain recovery might contribute to identify new therapeutic agents. Fortunately, brain injury after stroke is counteracted by the birth and migration of several populations of progenitor cells towards the injured areas, where angiogenesis and vascular remodeling play a key role providing trophic support and guidance during neurorepair. Endothelial progenitor cells (EPCs) constitute a pool of circulating bone-marrow derived cells that mobilize after an ischemic injury with the potential to incorporate into the damaged endothelium, to form new vessels, or to secrete trophic factors stimulating vessel remodeling. The circulating levels of EPCs are altered after stroke, and several subpopulations have proved to boost brain neurorepair in preclinical models of cerebral ischemia. The goal of this review is to discuss the current state of the neuroreparative actions of EPCs, focusing on their paracrine signaling mechanisms through their secretome and released extracellular vesicles.

angiogenesis; endothelial progenitor cells; neurogenesis; secretome; stroke

## INTRODUCTION

### *Stroke Disease and Brain Injury*

Stroke is one of the leading causes of death and long-term disabilities worldwide. According to the World Health Organization (WHO), 15 million people suffer a stroke every year. Nearly 5 million of these people die and another 5 million are permanently disabled. Stroke occurs when a blood clot or thrombus blocks a brain artery (ischemic) or when an intracranial artery ruptures (hemorrhagic), leading to cell death in specific brain areas if blood flow is not rapidly restored. Therefore, stroke is considered a medical emergency that requires a rapid diagnosis and intervention to minimize brain injury because the sudden reduction of the physiological levels of oxygen and glucose is followed by cellular edema, inflammation, neurodegeneration, blood-brain barrier (BBB) injury, and the loss of neurological functions (45, 57). In the case of ischemic strokes, during reperfusion of the artery, additional damage can occur related to the arrival of new oxygen to the tissue. Such injury includes oxidative stress and BBB break-

down with subsequent intracerebral hemorrhages, and the initial ischemic lesion can expand in minutes to hours in parallel with the activation of spontaneous mechanisms of repair that will continue for weeks to months (55).

Fortunately, research in the stroke field over the last decades has provided enormous improvements for acute stroke. Together with stroke care in specialized stroke units, hyperacute thrombolytic treatments and the newest thrombectomy strategies are available, providing treatments for artery recanalization within the first 8 hours of symptom onset for ischemic stroke candidates (8, 28, 37, 89). However, despite all of medical efforts, stroke survivors with neurological deficits require long periods of neurorehabilitation, which is the only approved therapy for poststroke recovery, to achieve functional independence. Evidence-based stroke rehabilitation care includes several types of health interventions, such as early admission to specialized stroke rehabilitation units and intensive rehabilitation programs (46, 92), with the goal of helping stroke survivors become as independent as possible in the performance of living activities and achieving the best possible quality of life in the long term. Beyond the proven benefits of multidisciplinary rehabilitation programs, they do not guarantee complete recovery for all patients despite their wide therapeutic window and long-lasting rehabilitation programs.

Address for reprint requests and other correspondence: A. Rosell, Vall d'Hebron Research Institute, Passeig Vall d'Hebron 119-129, 08035 Barcelona, Spain (e-mail: anna.rosell@vhir.org).

Therefore, it is necessary to develop new stroke treatments that could be used to treat a large number of patients and provide treatments in the delayed phases of the disease to repair and rewire the injured tissue. This need is connected to the accepted concept that endogenous neurovascular plasticity and remodeling are also activated in the earliest phases of ischemic events and participate in functional recovery after stroke (55).

*Stroke Neurorepair*

The nature of stroke disease leads to a scenario in which severely damaged tissue is in very close proximity to functional peri-infarct tissue. The classical view of neuron rescue/repair has changed in the last decades in favor of a more global understanding of the brain as a whole and now includes other cell types (e.g., glia and inflammatory and progenitor cells), the extracellular matrix, and the communication between these components. Therefore, endogenous mechanisms of neurovascular repair include angio-vasculogenesis (the formation of new blood vessels), gliogenesis (the formation of new glia), neurogenesis (the formation of new neurons), remyelination (the construction of new myelin sheaths on demyelinated axons), and other mechanisms. Several of these endogenous mechanisms are activated in the minutes following the ischemic trigger in the peri-infarct areas (12, 54), and different populations of newborn progenitor cells have been identified in remodeling areas (12, 36, 69), such as neural progenitor cells (NPCs), endothelial progenitor cells (EPCs), and oligodendrocyte progenitor cells (OPCs). Moreover, trophic support has been described to occur in areas in which brain endothelial cells secrete soluble factors that maintain the CNS stem cell self-renewal and neurogenic potentials in vitro (84). The cross talk between the endothelium and oligodendrocytes/oligodendrocyte progenitors is nourished by trophic factors that are

released by endothelial cells, and this cross talk has been described in the normal and ischemic brain in which brain-derived neurotrophic factor (BDNF), TGF- $\beta$ , VEGF, or matrix metalloproteinases (MMPs) could be responsible for maintaining the oligovascular niche (65, 76).

All of these facts demonstrate the plastic nature of the brain and oppose the more classical view of a passively dying brain. In this context, the scope of the present review will focus on the role of EPCs as cellular mediators of vascular remodeling and repair in the poststroke brain during recovery (Fig. 1).

**ENDOTHELIAL PROGENITOR CELLS**

*Introduction to Endothelial Progenitor Cells*

The formation of new blood vessels was formerly thought to be limited to embryogenic vasculogenesis and to be followed by the sprouting of endothelial cells from preexisting vessels during angiogenesis (75). Nonetheless, Asahara and colleagues (3) discovered the presence of endothelial progenitor cells (EPCs) in adult peripheral blood, being first identified as CD34 antigen-positive (CD34<sup>+</sup>) mononuclear cells (MNCs) with endothelial characteristics. The proportion of these cells generally ranges between 0.1 and 2% of the total MNC in the bone marrow (BM), peripheral blood, and cord blood. EPCs are mobilized from the BM into the peripheral blood as an endogenous response to the pathophysiological demands of neovascularization and can be differentiated into functional endothelial cells in vitro and ex vivo. EPCs are known to play an important role in adult vasculogenesis and angiogenesis by participating not only in the formation of vessels but also in vessel repair and remodeling (52). For this reason, EPCs have become a focus of study in the field of neurorepair strategies, including in ischemia-related diseases (24, 52, 67).

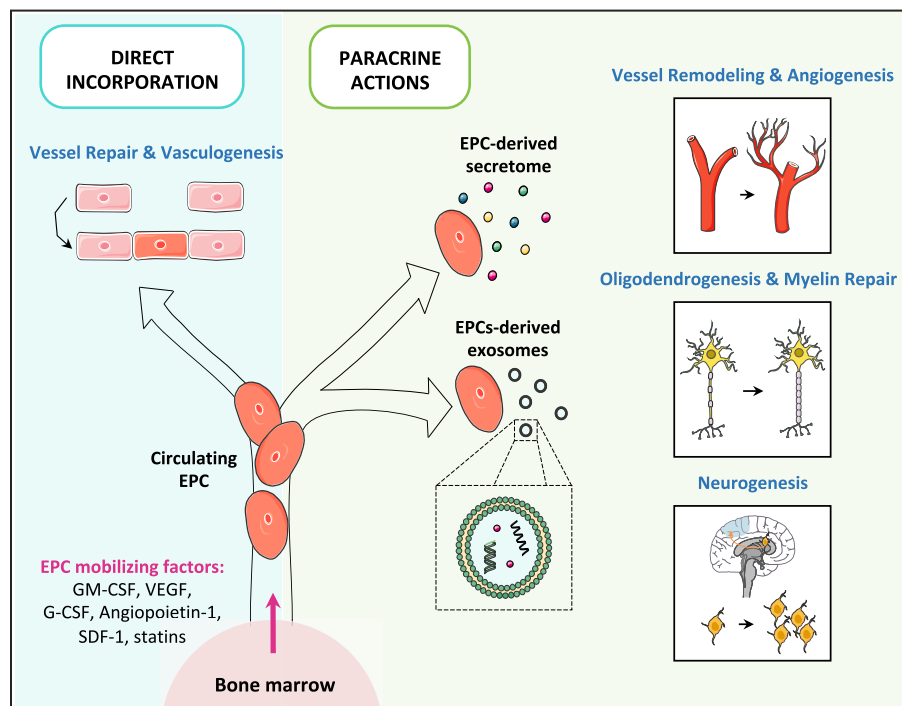


Fig. 1. Scheme of the main EPC functions related to neovascularization and contribution to mechanisms of neurorepair after stroke. Direct actions include the incorporation to damaged vessels or vessel remodeling by vasculogenesis whereas indirect contributions on vessel remodeling, remyelination, oligodendrogenesis, or neurogenesis are mediated by secreted molecules, including exosomes. EPC, endothelial progenitor cell; G-CSF, granulocyte-colony stimulating factor; GM-CSF, granulocyte macrophage-colony stimulating factor; SDF-1, stromal-derived factor-1. [Parts of this figure were supported by Servier Medical Art with permission under the Creative Commons Attribution 3.0 Unported License.]

### Classification

EPCs are defined as cells that express both stem cell markers and endothelial cell markers, although these cells continue to be controversial because no single marker has been identified for their unique identification (6, 19). However, the most widely accepted phenotypic definition is the coexpression of the cell-surface markers CD34 and VEGF receptor 2 (VEGFR-2; 51, 82). Because EPC subtypes have demonstrated different proliferative and angiogenic capabilities, it is of great importance to precisely define these subtypes to determine their specific natures and mechanisms of action. Such knowledge would enable a true and greater understanding of their angiogenic potential *in vitro* and *in vivo* and allow for the highest therapeutic revascularization efficacy in the setting of ischemic diseases.

Inconsistent results have been obtained among EPC studies regarding the definitions and classifications of the subpopulations that emerge from peripheral blood MNC-derived EPCs at different times in culture, exhibiting phenotypes that are between the hematopoietic and the endothelial lineages. However, there is a consensus about the classification of these cells into two major types that emerge from MNC cultures, which were initially named as “early EPC” or circulating angiogenic cells (CACs) and “late EPC” or outgrowth endothelial cells (OECs). These types of cells have different origins and provide different contributions to angiogenesis (19, 61). The early EPC appear after 3–10 days of peripheral blood MNC culture, and the late EPCs appear after 2–3 weeks approximately. While the early EPCs present with a spindle shape within heterogeneous populations of cells, the late OECs or endothelial colony-forming cells (ECFCs) form cobblestone and palisading colonies and exhibit clonogenic capacity (27, 34). Minami et al. (63) redefined this classification by further classifying OECs into the following three subpopulations: “moderate”-outgrowth EPCs (MOCs), which emerge in culture at days 10–16; “late”-outgrowth EPCs (LOCs), which emerge at days 17–23; and “very late”-outgrowth EPCs (VOCs), which emerge at days 24–30. The recruitment of OECs is known to contribute to both angiogenesis and arteriogenesis in a paracrine manner and is directly involved in neovascularization and the incorporation of new blood vessels. Thus, OECs exhibit proliferative and tubulogenic potentials (27, 34, 80, 83), whereas early populations are thought to contribute to angiogenesis mainly through paracrine signals (19). Among the late EPCs, LOCs have been found to exhibit the highest levels of expression of angiogenic genes and are the only cells that significantly promote blood flow recovery and increase capillary collateral formation in a mouse model of hindlimb ischemia. LOCs mediate this process by incorporating into newly formed vessels and promoting the release of proangiogenic factors (63). More recently, Huizer et al. (33) improved the characterization of OECs using a FACs sorting protocol in which they defined homogeneously highly expressed and stable markers (i.e., CD146, CD144, CD105, CD31) on the one hand, and heterogeneous and unstable markers on the other (i.e., CD34, c-kit, CD133). The lack of consistency among studies in the identification and classification of EPC subsets has been attributed to the low frequencies of these cells in the bloodstream, the different methods used for their isolation, and differences in the immunophenotyping protocols that have been performed thus far. However, based

on the perspective of the last 20 years of research in the field, it has also been proposed that this lack of consistency may indicate that endothelial progenitors exhibit a dynamic phenotype in space and time (19).

### Endothelial Progenitor Cell Mobilization

Regarding the kinetics of EPCs, several factors have been found to promote EPC mobilization from the BM into the peripheral circulation from which they eventually incorporate into sites of neovascularization. These mobilizing factors include, among others, the following: granulocyte macrophage-colony stimulating factor (GM-CSF); vascular endothelial growth factor (VEGF) (3, 91); granulocyte-colony stimulating factor (G-CSF) (24); angiopoietin-1 (29); stromal-derived factor-1 (SDF-1), which interacts with the CXCR receptor 4 (CXCR4) that is present in EPCs (74); and HMG-CoA reductase inhibitors (statins) (17, 53, 98). We would like to highlight the SDF-1/CXCR4 axis because it has been reported to play a key role in EPC mobilization in response to hypoxia or injury. The basal levels of SDF-1 in the circulation and BM are low, but after an ischemic event, hypoxia-inducible factor-1 (HIF-1) is upregulated, and it can activate both SDF-1 and VEGF. EPCs are then mobilized to the ischemic region because they follow SDF-1 gradients (Fig. 2). This axis is important for the homing or recruitment of circulating EPCs to the ischemic site where their angiogenic and repairing functions occur in the context of tissue remodeling (13, 15, 103).

Interestingly, HMG-CoA reductase inhibitors (statins), which were drugs originally used as inhibitors of cholesterol biosynthesis showing other pleiotropic effects, were found to stimulate EPCs in different ways. On one hand, statin therapy

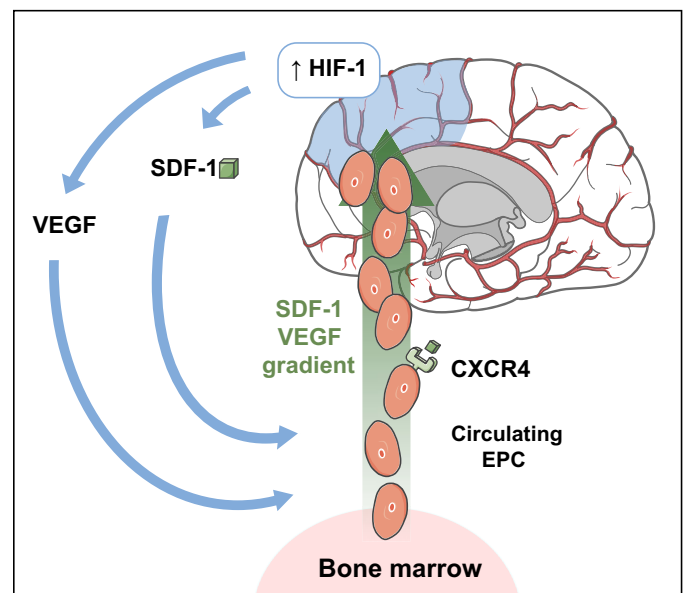


Fig. 2. Scheme of the SDF-1/CXCR4 axis. Cellular and molecular mechanism by which HIF-1 activates SDF-1 and VEGF to mobilize EPCs to the ischemic region for tissue remodeling in response to hypoxia or injury. [Parts of this figure were supported by Servier Medical Art with permission under the Creative Commons Attribution 3.0 Unported License.] CXCR4, CXC chemokine receptor 4; HIF-1, hypoxia-inducible factor 1; SDF-1, stromal-derived factor-1.

has been shown to stimulate the growth of new blood vessels in ischemic limbs of normocholesterolemic rabbits (44), and further investigations showed that this proangiogenic effect was due to an increase in the mobilization of EPCs by mediating the phosphatidylinositol 3-kinase (PI3K)/Akt pathway (62). Similar results have been described in a mouse model of hindlimb ischemia related to the SDF-1 $\alpha$ /CXCR4 axis and nitric oxide regulation (14). Other examples of the effect of statins on EPC mobilization have been described in both rodent (98) and human studies (45) under statin therapy showing increased EPC levels, and more recently in the context of ischemic stroke (26).

#### *Endothelial Progenitor Cells and Poststroke Neurorepair*

EPCs are involved in the direct repair of damaged blood vessel and angiogenesis in ischemic tissues, but they are also indirectly involved through paracrine signaling (Fig. 1). These cells have become a focus of study in the field of neurorepair strategies in ischemia-related diseases and have gained increasing importance in cerebral ischemia treatments because they are known to play critical roles in both the physiopathology and tissue repair associated with ischemic stroke. There are several mechanisms by which EPCs participate in endothelial repair. Ischemia mobilizes bone marrow-derived EPCs that interact with endothelial cells, extravasate, and reach the ischemic site, where they can directly incorporate into the vascular wall (32, 111). Moreover, EPCs are known to release protective cytokines and growth factors that can induce the self-repair of injured endothelial cells (ECs) or promote the extension of normal ECs into the injured sites and thereby assume a repair function (50, 51). In this regard, it is believed that the regenerating effect of EPCs may be attributable not only to the addition of new cells to new vessels but also to the secretion of factors that influence pathways of paracrine communication (59, 81, 82). These factors can induce the aforementioned mechanisms of the repair of damaged blood vessels, participate in the formation of new blood vessels from preexisting vessels, and promote the de novo formation of blood vessels in ischemic sites (50, 51).

Additionally, these growth factors can explain the relationship between angiogenesis and neurogenesis that guides the migration of neuroblasts and increases their survival in the so-called neurovascular niche (69). Neurogenesis in the adult brain occurs in two areas, i.e., the hippocampal subgranular zone (SGZ) and subventricular zone (SVZ) (68, 69); these areas renew cells in the dentate gyrus and olfactory bulb, respectively. Neural stem cells (NSCs) reside in specific niches, such as the SVZ, and display partial differentiation and enhanced proliferation with specific fates, for example, neuroblasts or oligodendrocyte progenitor cells (OPCs) (69). After cerebral ischemia, these areas that are rich in neural progenitor niches have been demonstrated to exhibit cells that can proliferate, migrate, and graft into most perilesional brain areas where they can differentiate into new neurons or glial cells and renew the cell population (68). For this process to happen there must be signals that guide the migrating neuroblasts to areas in which cell renewal can occur, and EPCs could be the source of these signals (81).

#### *Therapeutic Potential of the Use of Endothelial Progenitor Cells*

Several preclinical studies have reported beneficial effects of the transplantation of EPCs after cerebral ischemia (Table 1). The first studies utilized a mouse model of transient middle cerebral artery occlusion (MCAO) to demonstrate that the administration of human early EPCs was associated with a reduction in infarct volume, reduced cortical atrophy, increased angiogenesis, and improved neurobehavioral outcomes (20, 70, 81). Furthermore, the administration of outgrowth populations of human EPCs improved the neurological function in a rat model of ischemia-reperfusion (66).

Despite all of the preclinical evidence suggesting the benefits of EPC treatments for stroke by enhancing neurorepair mechanisms, there is a lack of clinical trials testing the safety and/or efficacy of EPC therapy treatments. To our knowledge only one Phase I clinical trial has tested and proved the safety and feasibility of administering intra-arterially autologous, bone marrow-derived CD34<sup>+</sup> cells (which includes the EPC population) in five stroke patients (5). Several reasons could influence the current scenario such as: 1) the relatively recent identification of EPCs in adult humans (3); 2) the existence of other accessible stem/progenitor cells used for regenerative purposes in stroke, including commercial genetically modified stem cells or whole bone-marrow aspirates/peripheral blood-derived mononuclear cells (101); 3) the use of other stem cells such as mesenchymal stem cells early after their identification in a large number of clinical trials showing safety (88); 4) the fact that EPCs were first thought to exclusively influence vascular repair when other repair/remodeling mechanisms have been described later to also benefit from the cross talk with EPCs (58); 5) the anatomical/structural barrier to reach the brain tissue which limits the delivery of any cell product with minimally invasive procedures and good delivery efficiencies (101) might have discouraged the design of cell-based stroke clinical trials; and 6) the lack of consensus for standardized isolation and cell culture methods to expand the low numbers of circulating EPCs in healthy subjects (9).

In this context, further efforts have been applied from the preclinical side to offer improved efficiencies of treatments based on the use of EPCs. For example, EPCs transfected with lentiviral vectors encoding the human adiponectin gene elicit improvements in behavioral function, infarct extension, microvessel density, and cell apoptosis rates (109). Another study has recently demonstrated that the application of CXCL12-engineered EPCs with a lentivirus (used to deliver the cxcl12 gene into human umbilical cord blood EPCs) in a preclinical model of stroke at 1 week after ischemia resulted in increased blood vessel density but also promoted myelin sheath integrity and the proliferation and migration of OPCs (49).

However, it is important to highlight that despite the lack of clinical trials using EPCs in ischemic diseases, several observational studies have been carried out to assess the levels of circulating EPCs in patients with ischemic diseases such as stroke or myocardial infarction (15, 79), thus suggesting their use as a biomarker of endothelial function, integrity, or repair response.

In stroke patients different studies have shown an increase in circulating EPCs in the acute and subacute phases of the

Table 1. Publications testing the therapeutic actions of EPCs in preclinical models of cerebral ischemia

Reference	Animal Model	EPC Source/Dose/Route	Outcome
Chen J et al., 2001 (13b)	Adult male rats. Transient MCAO 2 h occlusion.	HUBSCs containing MSCs and EPCs ( $3 \times 10^6$ cells at 24 h postischemia or 7 days, via tail vein.	HUBSCs at 24 h: $\uparrow$ neurobehavioral outcome. HUBSCs at day 7: $\uparrow$ neurobehavioral outcome.
Zhang et al., 2002 (111)	Male mice (N-TgN, TIE2LacZ). Embolic MCAO. Male mice. Permanent MCAO.	BM transplantation ( $2 \times 10^6$ BM cells) 4 wk before MCAO, via tail vein. $5 \times 10^5$ CD34 <sup>+</sup> cells at 48 h postischemia, via tail vein.	Incorporation of Tie-2-LacZ-positive cells into sites of neovascularization at the border of the infarct. $\uparrow$ Neovascularization and neurogenesis, $\uparrow$ NPC migration towards ischemic area, and $\downarrow$ cortical atrophy.
Shyu et al., 2006 (85a)	Male rats. Transient MCAO 90 min occlusion.	$5 \times 10^5$ autologous CD34 <sup>+</sup> peripheral blood (obtained after G-CSF injection), stereotaxically injected 7 days following ischemia.	$\uparrow$ Neurobehavioral outcome, $\uparrow$ neuronal activity, $\uparrow$ endogenous mobilization and engraftment of stem cells, $\uparrow$ reactive cerebral blood flow, $\uparrow$ neurotrophic factors, angiogenesis and neurogenesis.
Ohta et al., 2006 (70)	Male rats. Transient MCAO, 90 min occlusion.	$2.5 \times 10^5$ EPCs immediately after ischemia, via internal carotid artery.	$\downarrow$ Infarct volume and neurological functional deficits, $\uparrow$ regional cerebral cortical blood flow and $\downarrow$ infiltration of myeloperoxidase immunoreactive cells.
Fan et al., 2010 (20)	Adult nude mice. Transient MCAO, 60 min occlusion.	$10^6$ EPCs at 1 h postischemia, via left jugular vein.	$\downarrow$ Infarct volume, $\downarrow$ cortical atrophy, $\uparrow$ neurobehavioral outcome and $\uparrow$ angiogenesis.
Moubarik et al., 2011 (66)	Adult male rats. Transient MCAO, 60 min occlusion.	$4 \times 10^6$ ECFCs at 24 h postischemia, via femoral vein.	$\uparrow$ Neurobehavioral outcome, $\uparrow$ angiogenesis, $\uparrow$ neurogenesis and $\downarrow$ cerebral apoptosis
Pellegrini et al., 2013 (74a)	Adult male rats. Transient MCAO, 60 min occlusion.	$4 \times 10^6$ ECFCs at 24 h postischemia, via femoral vein.	ECFCs: $\uparrow$ neurobehavioral outcome, $\downarrow$ cerebral apoptosis, $\uparrow$ angiogenesis and neurogenesis. ECFCs+EPO: $\uparrow$ $\uparrow$ neurobehavioral outcome, $\downarrow$ $\downarrow$ cerebral apoptosis, $\uparrow$ $\uparrow$ angiogenesis and neurogenesis.
Hecht et al., 2014 (29a)	Adult male rats, permanent MCAO.	$10^6$ Embryonic EPCs immediately after chronic cerebral hypoperfusion and at day 7 and 14, tail vein.	$\uparrow$ Cerebrovascular reserve capacity, $\uparrow$ collateral vessel growth and capillary density.
Chen C. et al., 2014 (13a)	Adult male mice. Transient MCAO, 90 min occlusion.	$10^6$ hPB-EPCs from stroke patients, after 90 min of tMCAO, jugular vein.	$\downarrow$ Brain atrophy and $\uparrow$ angiogenesis.
Bai et al., 2015 (4)	Adult male mice, MCAO via photochemical reaction.	$10^6$ EPCs at 24 h of ischemia, via ipsilateral internal carotid artery.	$\downarrow$ Infarct volume and neurological deficits, $\uparrow$ angiogenesis and $\uparrow$ neurogenesis and neuronal survival, $\uparrow$ axonal growth. Activation of eNOS and expression of BDNF.
Xin et al., 2016 (102a)	Adult male mice. Permanent MCAO. Groups: Ad libitum diet vs. Prolonged fasting (PF) diet.	$10^6$ EPCs (obtained from each group) immediately after ischemia, via tail vein.	Control-EPCs vs. control group/PF-EPCs vs. control group/ PF-EPCs vs. control-EPC: $\downarrow$ infarct volume, $\downarrow$ cortical atrophy, $\uparrow$ neurobehavioral outcome and $\uparrow$ angiogenesis.
Rosell et al., 2013 (81)	Adult male mice. Permanent MCAO.	$10^4$ to $2 \times 10^5$ EPCs vs. EPC secretome, tail vein.	$\uparrow$ Neurobehavioral outcome and microvessel density in both groups compared with vehicle.
Zhang et al., 2017 (9)	Adult male rats. Transient MCAO, 2 h occlusion.	$2 \times 10^6$ EPC/LV-APN-EPCs after 2 h of reperfusion, via tail vein.	Control-EPCs vs. control group/LV-APN-EPCs vs. control group/LV-APN-EPCs vs. control-EPCs: $\downarrow$ infarct volume, $\uparrow$ neurobehavioral outcome and microvessel density and $\downarrow$ cerebral apoptosis.

BDNF, brain-derived neurotrophic factor; BM, bone marrow; ECFCs, endothelial colony-forming cells; eNOS, endothelial nitric oxide synthase; EPCs, endothelial progenitor cells; EPO, erythropoietin; G-CSF, granulocyte-colony stimulating factor; HUBSCs, human umbilical cord blood cells; LV-APN, left ventricle adiponectin; MCAO, middle cerebral artery occlusion; MSCs, mesenchymal stem cells; NPCs, neural progenitor cells.

disease including a peak in EPCs after 7 days of ischemic stroke (55, 60, 90) that is associated with better outcomes (55, 108), a positive correlation with infarct volume (15), suggesting that the mobilization of EPC from the bone marrow into peripheral circulation occurs as a stress response to an ischemic event, or a decrease in the EPCs counts at 3 months of the event (56). A recent study has also related for the first time EPC levels with poststroke reha-

bilitation therapy showing that the expected long-term decrease in circulating EPC does not occur in patients under intensive rehabilitation therapy (23). However, other investigations have reported lower baseline circulating EPC levels in acute ischemic stroke patients in comparison with the control group (15, 95), perhaps related to the presence of cardiovascular risk factors such as blood pressure and or hypercholesterolemia (15).



### *Endothelial Progenitor Cells as Boosters of Cell Communication*

Cell communication is an essential process in living organisms. Intercellular communication was long thought to be mediated exclusively through direct cell-to-cell interactions and the secretion of soluble intercellular molecules (e.g., growth factors, cytokines, neurotransmitters, lipids, hormones, etc.) that transmit the signal by binding to specific receptors on the target cell and/or via uptake into that cell. Recently, extracellular vesicles (EVs), which were initially considered to be intracellular debris, have been proposed as a new frontier of cell-to-cell communication (48). The presence of these vesicles is commonly related to a large number of diseases and pathologic conditions, and it is believed that they exert an important role in pathologies because the dysregulation of intercellular communication leads the progress of the disease (10). As described in the previous section, although EPCs have demonstrated therapeutic effects when transplanted into several animal models of ischemic disease, it has been reported that very few cells incorporate into the newly formed vessels in the ischemic regions, which suggests that there must be a paracrine mechanism that accounts for their beneficial effects (66). In this regard, it is known that EPCs communicate and interact with neurons, cerebral endothelial cells, astrocytes, and the surrounding extracellular matrix in the so-called neurovascular unit, and all of these interactions contribute to neurovascular remodeling after stroke (47, 54) (Fig. 1).

### *Endothelial Progenitor Cell-Derived Secretome*

The repair capacities of EPCs are not exclusively due to their homing and engraftment because circulating EPCs also contribute to reendothelization and tissue regeneration following ischemic events by releasing paracrine proangiogenic factors, such as stromal-derived factor-1 (SDF-1), insulin-like growth factor-1, hepatocyte growth factor (HGF), G-CSF, VEGF, endothelial nitric oxide synthase, inducible nitric oxide synthase, IL-8, and IL-9 among many others (59). These factors can promote endothelial cell proliferation and reduce cell apoptosis, but are also involved in the regulation of endogenous progenitor cell recruitment, vascular growth, and remodeling (34, 35, 77, 80, 82, 96). The paracrine factors released by EPCs not only promote the angiogenic activities of vascular cells but also preserve this capacity and protect differentiated endothelial cells from apoptosis under conditions of oxidative stress (106). Other studies supporting the therapeutic effect of EPC-secreted factors have reported that cultured cortical neurons that are exposed to oxygen-glucose deprivation exhibit less axon degeneration when they are treated with EPC-conditioned media (72). The release of these factors appears to be increased by hypoxia; for example, Di Santo and colleagues (82) found that angiogenin, HGF, IL-8, platelet-derived growth factor homodimer BB (PDGF-BB), SDF-1, and VEGF-A are increased in EPC-conditioned media in hypoxic conditions, which supports the protective role of EPCs in the context of cerebral ischemia.

As explained above, several studies have suggested that early EPCs are capable of secreting large amounts of proteins, although this secretion is not the only role of this EPC population. Abe et al. (1) reported the contribution of EPC-conditioned medium (CM), in which EPCs secrete VEGF, on three-

dimensional (3D) microvessel formation using an in vitro model. These authors demonstrated that EPC induced 3D network invasion into gels by creating a local VEGF gradient. In another study, Hur and colleagues (34) found higher levels of VEGF in the supernatant of early EPCs compared with late EPCs. VEGF produces nitric oxide (NO) in endothelial cells through the kinase insert domain receptor (KDR), and it is known that the upregulation of KDR on endothelial cells causes an increase in VEGF-mediated tube formation on Matrigel matrices. These authors also describe a greater expression of KDR by late EPCs, which might explain the higher tubulogenic potential of this population. Based on these findings, it has been proposed that early EPCs contribute to neovascularization mainly by secreting proangiogenic factors that promote endothelial cell recruitment and induce endothelial cell proliferation and survival. In contrast, late EPCs contribute to neovascularization also through their high proliferation rate that provides a source of endothelial cells (34, 66, 86).

Interestingly, EPC-derived CM has aroused interest as an alternative to cell therapy in the last years. Many studies have reported therapeutic effects in animal models of different ischemic diseases following a cell-free but cell-based therapeutic approach. The first study demonstrated that EPC-CM transplantation stimulated neovascularization and vascular maturation and thereby improved hindlimb perfusion and muscle function (82). More recently, intravenously administered EPC-CM appeared to enhance vascular remodeling in a cortical model of stroke and led to better functional outcomes (81). Moreover, for the first time, Maki et al. (59) observed recovery from white matter injury after EPC-CM administration in a prolonged hypoperfusion model that was mediated by increased vessel density, increased numbers of proliferating oligodendrocyte-lineage cells, and enhanced myelination in the corpus callosum accompanied by an improved cognitive function.

Several growth factors that are present in EPC-derived CM appear to be involved not only in angiogenesis but also in neurogenic processes and have been linked to stroke-induced neurogenesis by different authors (31, 38, 66). Some of the EPC-secreted factors reported in these investigations include the following: growth-regulated oncogene-a (GRO-a), interleukin 8 (IL-8), tissue inhibitors of metalloproteinases (TIMP-1 and TIMP-2), metalloproteinases 2 and 9 (MMP-2 and MMP-9), epidermal growth factor (EGF), monocyte chemoattractant protein-1 (MCP-1), PDGF-BB, angiopoietin 2 (Ang-2), erythropoietin (EPO), VEGF, G-CSF, fibroblast growth factor-2 (FGF-2), brain-derived neurotrophic factor (BDNF), insulin-like growth factor (IGF-1), and stem cell factor (SCF), among many others.

This neurovascular niche supports adult neurogenesis from neural progenitor cells by signaling mechanisms that include contact-mediated and vascular-derived soluble factors (47, 69) (Fig. 1). Direct contact between NPCs and vascular endothelial cells in neurogenic sites maintains NPC quiescence through contact-dependent signaling (71), while soluble endothelial factors have been demonstrated to promote the proliferation of NPCs and to stimulate brain remodeling processes (30). These findings are in accordance with a study in which cocultured human EPCs and NPCs obtained from induced pluripotent stem cells synergistically protected ECs from hypoxia/reoxygenation-induced apoptosis and dysfunction, and these benefits

resulted from paracrine activation of the PI3K/Akt signaling pathway mediated by VEGF and BDNF (99). G-CSF, which is among the factors present in the EPC-derived secretome, also plays a role in neurogenesis through VEGF. When G-CSF binds to its receptor, cytoplasmic tyrosine kinases are recruited, and these kinases activate STAT proteins. Activated STAT translocates to the nucleus, where it regulates gene expression and thereby promotes cell proliferation and mobilization. STAT3 has been reported to directly upregulate VEGF expression, and its kinase receptors VEGFR-1 (Flt-1) and VEGFR-2 (Flk-1 and KDR) are also expressed in nonvascular cells, such as neurons and NPCs (38). In a study performed by Zhu et al. (112) that utilized a mouse model of permanent focal ischemia, IGF-1 was demonstrated to enhance vascular density in the peri-infarct region and to increase neurogenesis at 7 days poststroke. However, whether IGF-1 directly promoted neurogenesis or this effect resulted from increased vascular density was not determined. Others have found that Ang-2 promotes an increase in the number of proliferating NSCs in culture (2). Ang-2 activates a pathway downstream of the Notch receptor that is known to induce the expansion of NSC populations, and NSCs in the subventricular zone (SVZ) and throughout the brain express the angiopoietin receptor Tie-2; furthermore, these cells appear to be in close proximity to blood vessels (2).

Other examples of the neurotrophic actions of factors secreted by EPCs relate to NPC migration from the SVZ neurogenic niche to the injured region of the brain that is guided by several receptor-ligand signaling pathways and molecular factors such as SDF-1/CXCR4 and MMP (41, 69, 100). These studies demonstrated how, after ischemic stroke, SDF-1 is released from endothelial cells, and its receptor CXCR4 is expressed in NSC and migrating neuroblasts.

#### *Endothelial Progenitor Cell-Derived Exosomes*

The secretion of extracellular vesicles (EVs) is a phenomena that is evolutionarily conserved from simple to complex multicellular organisms. EVs are considered comunicasomes, i.e., nanosized extracellular organelles that are limited by lipid bilayers, have an average diameter of 30–500 nm, and play diverse pathophysiological roles in intercellular communication (7, 78, 97). EVs are normally found in all environments and in all body fluids, including the blood, saliva, breast milk, urine, and cerebrospinal fluid, as well as in stool. EVs have physiological functions, such as coagulation, regulation of immune responses, communication in the brain, and functions during pregnancy. EVs also have deleterious functions, e.g., they can suppress immune responses in a manner that leads to pathological conditions such as premetastatic niche formation and tumor angiogenesis (94).

Among other methods, EVs can be isolated by the centrifugation of either biofluids or cell-cultured supernatants (102, 104). There is no consensus in the nomenclature of the different EVs because of their heterogeneity, but some authors have named EVs according to the cell type from which they originate, for example, oncosomes (tumor-derived microvesicles), prostasomes (secreted by the prostate gland epithelial cells into the seminal fluid), and many others. However, we can classify EVs into three subtypes based on their biogenesis: exosomes, ectosomes, (shedding microvesicles), and apoptotic bodies. EVs are known to be secreted by a cell into the extracellular

space. Exosomes are released by exocytosis, ectosomes are secreted by outward budding of the plasma membrane, and apoptotic bodies are released by dying cells during the later stages of apoptosis (39). EVs contain and deliver cargo that reflects their cellular origins and can include DNA, mRNA, microRNA (miRNA), proteins, and lipids (42). Moreover, the different intracellular origins of EVs are probably related to their different functions (73). However, the subtypes of EVs are not well characterized. Despite separate biogenesis pathways, definitive markers of EV subtypes are nonexistent (40, 42, 64).

Exosomes are small membrane vesicles (30–150 nm) that are produced via the endosomal pathway and are secreted from intracellular stores called multivesicular bodies (MVBs) and subsequently incorporated into the intracellular spaces of target/host cells through three different pathways: fusion with the plasma membrane, pinocytosis or phagocytosis, and binding to specific receptors. Interestingly, exosomes induce significant cell proliferation and migration in recipient cells (40). For example, in the specific case of ECs, van Balkom and colleagues (97a) reported that these cells require miR-214 to secrete exosomes that suppress senescence and stimulate angiogenesis.

#### *Exosomes and Stroke*

After stroke, exosomes secreted by cerebral endothelial cells and NPCs regulate intercellular communication between components of the neurovascular unit and thus contribute to the coupling of neurogenesis and angiogenesis during brain repair. These exosomes exhibit a bidirectional exchange of genetic and molecular information between stem cells and injured cells and reprogram the latter cells to repair damaged tissues (10). In this manner, increased levels of exosomes of mainly endothelial origin have been observed in cardiovascular pathology (87). These vesicles have been well documented to play an important role in angiogenesis, and it has been demonstrated that miRNAs are crucial in vascular endothelial cell angiogenesis as well as in stroke pathogenesis (107). Furthermore, it has been reported that cargo proteins are altered in the exosomes of plasma endothelial cells after stroke (25).

In vitro and in vivo experiments have demonstrated that exosomes from EPCs transfer miRNAs, such as miR-126 and miR-296, which activate the PI3K/Akt signaling pathway and lead to angiogenesis (11, 16). Moreover, the upregulation of miR-27b (43) and miR-181d (93) enhance angiogenesis, whereas the upregulation of miR-328 enhances cell migration (105) and promotes good clinical outcomes after ischemic stroke. In contrast, the downregulation of miRNA-15a in a mouse model of focal cerebral ischemia also promotes stroke-induced angiogenesis in the cerebral vessels of the peri-infarct region by increasing FGF-2 and VEGF levels (107).

Beyond exosome vascular stimulation, NSCs also exchange molecular signals with blood vessels, neighboring cells, cerebrospinal fluid, and astrocytes through exosomes to mediate synaptic and axonal plasticity (18), and these signals could be involved in brain remodeling following ischemia. Furthermore, these signals may also communicate with the immune system after stroke (110). Regarding glial cells, it has been reported that cultured oligodendrocytes secrete exosomes that contribute to the neuronal-mediated coordination of myelination (22), and exosomes from oligodendrocytes can also improve neuron

viability under cell stress conditions and reduce ischemic neuronal death through the transfer of superoxide dismutase, catalase, and other antioxidant enzymes (21). Moreover, microglia exosomes can regulate oligodendrogenesis and neurogenesis under physiological and pathological conditions (85), including ischemic stroke.

**CONCLUSIONS**

EPCs have been documented to be confident candidates for preclinical regenerative medicine approaches for ischemic stroke, contributing to the recovery of neurological functions and activating neurorepair mechanisms after EPC transplantation. EPCs contribute to tissue repair by both direct incorporation into remodeling vessels or by indirect secretion of proteins or molecule-containing vesicles supporting cell communication, serving as blood biomarkers of injury, cardiovascular risk, or poststroke recovery. However, despite the well-known neuroreparative potential of these cells in the context of an ischemic event, this therapeutic approach has not reached the clinical setting yet and to date, only two clinical trials using EPCs are being registered (<https://www.clinicaltrials.gov>). Several limitations for this scenario have been discussed in this review including the extensive use of other stem cells for tissue regeneration such as mesenchymal stem cells, the complex administration and delivery of cell products in the brain, and the lack of a standardized protocol for the isolation, culture, and expansion of EPCs. It is in this light that cell-free (but cell-based) therapies are now also considered as an alternative to standard cell therapies, taking advantage of the capacity of EPCs to release soluble growth and communicating molecules (106). Special interest should also be focused on future treatments increasing EPC mobilization from the bone marrow to peripheral circulation to increase the pool of EPCs that would eventually reach the ischemic site to promote neurorepair; available drugs such as HMG-CoA reductase inhibitors have already shown this ability, but additional investigations on new pharmacotherapies to increase the pool or function of EPC will also be part of these future cell-based (but cell-free) strategies. These approaches would avoid the disadvantages related to the direct administration of cells in more classical approaches, but could trigger a wider neurorestorative response by activating different mature and precursors cell types at once. For this reason, in the coming years it would also be important to investigate the exosomes derived from EPCs as future therapeutic agents or therapeutic targets to regulate as communicating agents during stroke repair.

**ACKNOWLEDGMENTS**

A. Grayston holds a predoctoral fellowship from Instituto de Salud Carlos III (PI17/00073), A. Rosell is supported by the Miguel Servet program (CPII15/00003), and G. Esquiva holds a postdoctoral fellowship from the Catalan Research and Innovation Department (PERIS SLT002/16/00352).

**GRANTS**

This work was supported by Instituto de Salud Carlos III, Spain Grants PI16/00981, AC17/00004, and RETICS INVICTUS RD16/0019/0021, cofinanced by the European Regional Development Fund. AC17/00004 is part of the MAGBBRIS project, funded under the Euronanomed III 8th joint call on innovative nanomedicine.

**DISCLOSURES**

No conflicts of interest, financial or otherwise, are declared by the authors.

**AUTHOR CONTRIBUTIONS**

G.E., A.G., and A.R. prepared figures; G.E., A.G., and A.R. drafted manuscript; G.E., A.G., and A.R. edited and revised manuscript; G.E., A.G., and A.R. approved final version of manuscript.

**REFERENCES**

1. Abe Y, Ozaki Y, Kasuya J, Yamamoto K, Ando J, Sudo R, Ikeda M, Tanishita K. Endothelial progenitor cells promote directional three-dimensional endothelial network formation by secreting vascular endothelial growth factor. *PLoS One* 8: e82085, 2013. doi:10.1371/journal.pone.0082085.
2. Androutsellis-Theotokis A, Rueger MA, Park DM, Boyd JD, Padmanabhan R, Campanati L, Stewart CV, LeFranc Y, Plenz D, Walbridge S, Lonser RR, McKay RD. Angiogenic factors stimulate growth of adult neural stem cells. *PLoS One* 5: e9414, 2010. doi:10.1371/journal.pone.0009414.
3. Asahara T, Murohara T, Sullivan A, Silver M, van der Zee R, Li T, Witzenbichler B, Schatteman G, Isner JM. Isolation of putative progenitor endothelial cells for angiogenesis. *Science* 275: 964–966, 1997. doi:10.1126/science.275.5302.964.
4. Bai YY, Peng XG, Wang LS, Li ZH, Wang YC, Lu CQ, Ding J, Li PC, Zhao Z, Ju SH. Bone marrow endothelial progenitor cell transplantation after ischemic stroke: an investigation into its possible mechanism. *CNS Neurol Ther* 21: 877–886, 2015. doi:10.1111/cns.12447.
5. Banerjee S, Bentley P, Hamady M, Marley S, Davis J, Shlebak A, Nicholls J, Williamson DA, Jensen SL, Gordon M, Habib N, Chataway J. Intra-arterial immunoselected CD34<sup>+</sup> stem cells for acute ischemic stroke. *Stem Cells Transl Med* 3: 1322–1330, 2014. doi:10.5966/sctm.2013-0178.
6. Basile DP, Yoder MC. Circulating and tissue resident endothelial progenitor cells. *J Cell Physiol* 229: 10–16, 2014. doi:10.1002/jcp.24423.
7. Belting M, Witttrup A. Nanotubes, exosomes, and nucleic acid-binding peptides provide novel mechanisms of intercellular communication in eukaryotic cells: implications in health and disease. *J Cell Biol* 183: 1187–1191, 2008. doi:10.1083/jcb.200810038.
8. Berkheer OA, Fransen PSS, Beumer D, van den Berg LA, Lingsma HF, Yoo AJ, Schonewille WJ, Vos JA, Nederkoorn PJ, Wermer MJH, van Walderveen MAA, Staals J, Hofmeijer J, van Oostayen JA, Lycklama à Nijeholt GJ, Boiten J, Brouwer PA, Emmer BJ, de Bruijn SF, van Dijk LC, Kappelle LJ, Lo RH, van Dijk EJ, de Vries J, de Kort PL, van Rooij WJ, van den Berg JS, van Hasselt BA, Aerden LA, Dallinga RJ, Visser MC, Bot JC, Vroomen PC, Eshghi O, Schreuder TH, Heijboer RJ, Keizer K, Tielbeek AV, den Hertog HM, Gerrits DG, van den Berg-Vos RM, Karas GB, Steyerberg EW, Flach HZ, Marquering HA, Sprengers ME, Jenniskens SF, Beenen LF, van den Berg R, Koudstaal PJ, van Zwam WH, Roos YB, van der Lugt A, van Oostenbrugge RJ, Majoie CB, Dippel DW; MR CLEAN Investigators. A randomized trial of intraarterial treatment for acute ischemic stroke. *N Engl J Med* 372: 11–20, 2015. doi:10.1056/NEJMoa1411587.
9. Bueno-Betí C, Novella S, Lázaro-Franco M, Pérez-Cremades D, Heras M, Sanchís J, Hermenegildo C. An affordable method to obtain cultured endothelial cells from peripheral blood. *J Cell Mol Med* 17: 1475–1483, 2013. doi:10.1111/jcmm.12133.
10. Camussi G, Deregius MC, Bruno S, Cantaluppi V, Biancone L. Exosomes/microvesicles as a mechanism of cell-to-cell communication. *Kidney Int* 78: 838–848, 2010. doi:10.1038/ki.2010.278.
11. Cantaluppi V, Biancone L, Figliolini F, Beltramo S, Medica D, Deregius MC, Galimi F, Romagnoli R, Salizzoni M, Tetta C, Segoloni GP, Camussi G. Microvesicles derived from endothelial progenitor cells enhance neoangiogenesis of human pancreatic islets. *Cell Transplant* 21: 1305–1320, 2012. doi:10.3727/096368911X627534.
12. Carmichael ST. Themes and strategies for studying the biology of stroke recovery in the poststroke epoch. *Stroke* 39: 1380–1388, 2008. doi:10.1161/STROKEAHA.107.499962.
13. Ceradini DJ, Kulkarni AR, Callaghan MJ, Tepper OM, Bastidas N, Kleinman ME, Capla JM, Galiano RD, Levine JP, Gurtner GC. Progenitor cell trafficking is regulated by hypoxic gradients through HIF-1 induction of SDF-1. *Nat Med* 10: 858–864, 2004. doi:10.1038/nm1075.
- 13a. Chen C, Lin X, Wang J, Tang G, Mu Z, Chen X, Xu J, Wang Y, Zhang Z, Yang GY. Effect of HMGB1 on the paracrine action of EPC promotes post-ischemic neovascularization in mice. *Stem Cells* 32: 2679–2689, 2014. doi:10.1002/stem.1754.

- 13b. Chen J, Sanberg PR, Li Y, Wang L, Lu M, Willing AE, Sanchez-Ramos J, Chopp M. Intravenous administration of human umbilical cord blood reduces behavioral deficits after stroke in rats. *Stroke* 32: 2682–2688, 2001. doi:10.1161/hs1101.098367.
14. Chiang KH, Cheng WL, Shih CM, Lin YW, Tsao NW, Kao YT, Lin CT, Wu SC, Huang CY, Lin FY. Statins, HMG-CoA reductase inhibitors, improve neovascularization by increasing the expression density of CXCR4 in endothelial progenitor cells. *PLoS One* 10: e0136405, 2015. doi:10.1371/journal.pone.0136405.
15. Deng Y, Wang J, He G, Qu F, Zheng M. Mobilization of endothelial progenitor cell in patients with acute ischemic stroke. *Neurol Sci* 39: 437–443, 2018. doi:10.1007/s10072-017-3143-y.
16. Deregibus MC, Cantaluppi V, Calogero R, Lo Iacono M, Tetta C, Biancone L, Bruno S, Bussolati B, Camussi G. Endothelial progenitor cell derived microvesicles activate an angiogenic program in endothelial cells by a horizontal transfer of mRNA. *Blood* 110: 2440–2448, 2007. doi:10.1182/blood-2007-03-078709.
17. Dimmeler S, Aicher A, Vasa M, Mildner-Rihm C, Adler K, Tiemann M, Rütten H, Fichtlscherer S, Martin H, Zeiher AM. HMG-CoA reductase inhibitors (statins) increase endothelial progenitor cells via the PI 3-kinase/Akt pathway. *J Clin Invest* 108: 391–397, 2001. doi:10.1172/JCI200113152.
18. Edelstein L, Smythies J. The role of epigenetic-related codes in neuro-computation: dynamic hardware in the brain. *Philos Trans R Soc Lond B Biol Sci* 369: 20130519, 2014. doi:10.1098/rstb.2013.0519.
19. Fadini GP, Losordo D, Dimmeler S. Critical reevaluation of endothelial progenitor cell phenotypes for therapeutic and diagnostic use. *Circ Res* 110: 624–637, 2012. doi:10.1161/CIRCRESAHA.111.243386.
20. Fan Y, Shen F, Frenzel T, Zhu W, Ye J, Liu J, Chen Y, Su H, Young WL, Yang GY. Endothelial progenitor cell transplantation improves long-term stroke outcome in mice. *Ann Neurol* 67: 488–497, 2010. doi:10.1002/ana.21919.
21. Fröhlich D, Kuo WP, Frühbeis C, Sun JJ, Zehendner CM, Luhmann HJ, Pinto S, Toedling J, Trotter J, Krämer-Albers EM. Multifaceted effects of oligodendroglial exosomes on neurons: impact on neuronal firing rate, signal transduction and gene regulation. *Philos Trans R Soc Lond B Biol Sci* 369: 20130510–20130510, 2014. doi:10.1098/rstb.2013.0510.
22. Frühbeis C, Fröhlich D, Kuo WP, Krämer-Albers EM. Extracellular vesicles as mediators of neuron-glia communication. *Front Cell Neurosci* 7: 182, 2013. doi:10.3389/fncel.2013.00182.
23. Gabriel-Salazar M, Moranchó A, Rodríguez S, Buxó X, García-Rodríguez N, Colell G, Fernandez A, Giralt D, Bustamante A, Montaner J, Rosell A. Importance of angiogenin and endothelial progenitor cells after rehabilitation both in ischemic stroke patients and in a mouse model of cerebral ischemia. *Front Neurol* 9: 508, 2018. doi:10.3389/fneur.2018.00508.
24. Gehling UM, Ergün S, Schumacher U, Wagener C, Pantel K, Otte M, Schuch G, Schaffhausen P, Mende T, Kilic N, Kluge K, Schäfer B, Hossfeld DK, Fiedler W. In vitro differentiation of endothelial cells from AC133-positive progenitor cells. *Blood* 95: 3106–3112, 2000.
25. Goetzl EJ, Schwartz JB, Mustapic M, Lobach IV, Daneman R, Abner EL, Jicha GA. Altered cargo proteins of human plasma endothelial cell-derived exosomes in atherosclerotic cerebrovascular disease. *FASEB J* 31: 3689–3694, 2017. doi:10.1096/fj.201700149.
26. Golab-Janowska M, Paczkowska E, Machalinski B, Meller A, Kotlega D, Safranow K, Wankowicz P, Nowacki P. Statins therapy is associated with increased populations of early endothelial progenitor (CD133+/VEGFR2+) and endothelial (CD34-/CD133-/VEGFR2+) cells in patients with acute ischemic stroke. *Curr Neurovasc Res* 15: 120–128, 2018. doi:10.2174/1567202615666180611120546.
27. Gulati R, Jevremovic D, Peterson TE, Chatterjee S, Shah V, Vile RG, Simari RD. Diverse origin and function of cells with endothelial phenotype obtained from adult human blood. *Circ Res* 93: 1023–1025, 2003. doi:10.1161/01.RES.0000105569.77539.21.
28. Hacke W, Kaste M, Bluhmki E, Brozman M, Dávalos A, Guidetti D, Larrue V, Lees KR, Medeghri Z, Machnig T, Schneider D, von Kummer R, Wahlgren N, Toni D; ECASS Investigators. Thrombolysis with alteplase 3 to 4.5 hours after acute ischemic stroke. *N Engl J Med* 359: 1317–1329, 2008. doi:10.1056/NEJMoa0804656.
29. Hattori K, Dias S, Heissig B, Hackett NR, Lyden D, Tateno M, Hicklin DJ, Zhu Z, Witte L, Crystal RG, Moore MAS, Rafii S. Vascular endothelial growth factor and angiopoietin-1 stimulate postnatal hematopoiesis by recruitment of vasculogenic and hematopoietic stem cells. *J Exp Med* 193: 1005–1014, 2001. doi:10.1084/jem.193.9.1005.
- 29a. Hecht N, Schneider UC, Czabanka M, Vinci M, Hatzopoulos AK, Vajkoczy P, Woitzik J. Endothelial progenitor cells augment collateralization and hemodynamic rescue in a model of chronic cerebral ischemia. *J Cereb Blood Flow Metab* 34: 1297–1305, 2014. doi:10.1038/jcbfm.2014.78.
30. Hermann DM, Chopp M. Promoting brain remodelling and plasticity for stroke recovery: therapeutic promise and potential pitfalls of clinical translation. *Lancet Neurol* 11: 369–380, 2012. doi:10.1016/S1474-4422(12)70039-X.
31. Hermann DM, Peruzzotti-Jametti L, Schlechter J, Bernstock JD, Doeppner TR, Pluchino S. Neural precursor cells in the ischemic brain—integration, cellular crosstalk, and consequences for stroke recovery. *Front Cell Neurosci* 8: 291, 2014. doi:10.3389/fncel.2014.00291.
32. Hristov M, Weber C. Endothelial progenitor cells: characterization, pathophysiology, and possible clinical relevance. *J Cell Mol Med* 8: 498–508, 2004. doi:10.1111/j.1582-4934.2004.tb00474.x.
33. Huizer K, Mustafa DAM, Spelt JC, Kros JM, Sacchetti A. Improving the characterization of endothelial progenitor cell subsets by an optimized FACS protocol. *PLoS One* 12: e0184895, 2017. doi:10.1371/journal.pone.0184895.
34. Hur J, Yoon CH, Kim HS, Choi JH, Kang HJ, Hwang KK, Oh BH, Lee MM, Park YB. Characterization of two types of endothelial progenitor cells and their different contributions to neovascularogenesis. *Arterioscler Thromb Vasc Biol* 24: 288–293, 2004. doi:10.1161/01.ATV.0000114236.77009.06.
35. Ii M, Nishimura H, Iwakura A, Wecker A, Eaton E, Asahara T, Losordo DW. Endothelial progenitor cells are rapidly recruited to myocardium and mediate protective effect of ischemic preconditioning via “imported” nitric oxide synthase activity. *Circulation* 111: 1114–1120, 2005. doi:10.1161/01.CIR.0000157144.24888.7E.
36. Jin K, Wang X, Xie L, Mao XO, Zhu W, Wang Y, Shen J, Mao Y, Banwait S, Greenberg DA. Evidence for stroke-induced neurogenesis in the human brain. *Proc Natl Acad Sci USA* 103: 13198–13202, 2006. doi:10.1073/pnas.0603512103.
37. Jovin TG, Chamorro A, Cobo E, de Miquel MA, Molina CA, Rovira A, San Román L, Serena J, Abilleira S, Ribó M, Millán M, Urra X, Cardona P, López-Cancio E, Tomasello A, Castaño C, Blasco J, Aja L, Dorado L, Quesada H, Rubiera M, Hernandez-Pérez M, Goyal M, Demchuk AM, von Kummer R, Gallofré M, Dávalos A; REVASCAT Trial Investigators. Thrombectomy within 8 hours after symptom onset in ischemic stroke. *N Engl J Med* 372: 2296–2306, 2015. doi:10.1056/NEJMoa1503780.
38. Jung KH, Chu K, Lee ST, Kim SJ, Sinn DI, Kim SU, Kim M, Roh JK. Granulocyte colony-stimulating factor stimulates neurogenesis via vascular endothelial growth factor with STAT activation. *Brain Res* 1073-1074: 190–201, 2006. doi:10.1016/j.brainres.2005.12.037.
39. Kalra H, Drummen GPC, Mathivanan S. Focus on extracellular vesicles: introducing the next small big thing. *Int J Mol Sci* 17: 170, 2016. doi:10.3390/ijms17020170.
40. Keerthikumar S, Gangoda L, Liem M, Fonseka P, Atukorala I, Ozcitti C, Mechler A, Adda CG, Ang CS, Mathivanan S. Proteomic analysis reveals exosomes are more oncogenic than ectosomes. *Oncotarget* 6: 15375–15396, 2015. doi:10.18632/oncotarget.3801.
41. Kokovay E, Goderie S, Wang Y, Lotz S, Lin G, Sun Y, Roysam B, Shen Q, Temple S. Adult SVZ lineage cells home to and leave the vascular niche via differential responses to SDF1/CXCR4 signaling. *Cell Stem Cell* 7: 163–173, 2010. doi:10.1016/j.stem.2010.05.019.
42. Kowal J, Arras G, Colombo M, Jouve M, Morath JP, Prindal-Bengtson B, Dingli F, Loew D, Tkach M, Théry C. Proteomic comparison defines novel markers to characterize heterogeneous populations of extracellular vesicle subtypes. *Proc Natl Acad Sci USA* 113: E968–E977, 2016. doi:10.1073/pnas.1521230113.
43. Kuehbacher A, Urbich C, Zeiher AM, Dimmeler S. Role of Dicer and Drosha for endothelial microRNA expression and angiogenesis. *Circ Res* 101: 59–68, 2007. doi:10.1161/CIRCRESAHA.107.153916.
44. Kureishi Y, Luo Z, Shiojima I, Bialik A, Fulton D, Lefer DJ, Sessa WC, Walsh K. The HMG-CoA reductase inhibitor simvastatin activates the protein kinase Akt and promotes angiogenesis in normocholesterolemic animals. *Nat Med* 6: 1004–1010, 2000. [Erratum in *Nat Med* 7: 129, 2001.] doi:10.1038/79510.
45. Lakhani SE, Kirchgessner A, Hofer M. Inflammatory mechanisms in ischemic stroke: therapeutic approaches. *J Transl Med* 7: 97, 2009. doi:10.1186/1479-5876-7-97.

46. Langhorne P, Bernhardt J, Kwakkel G. Stroke rehabilitation. *Lancet* 377: 1693–1702, 2011. doi:10.1016/S0140-6736(11)60325-5.
47. Lau M, Li J, Cline HT. In vivo analysis of the neurovascular niche in the developing *Xenopus* brain. *eNeuro* 4: ENEURO.0030-17.2017, 2017. doi:10.1523/ENEURO.0030-17.2017.
48. Lee TH, D’Asti E, Magnus N, Al-Nedawi K, Meehan B, Rak J. Microvesicles as mediators of intercellular communication in cancer—the emerging science of cellular ‘debris’. *Semin Immunopathol* 33: 455–467, 2011. doi:10.1007/s00281-011-0250-3.
49. Li Y, Chang S, Li W, Tang G, Ma Y, Liu Y, Yuan F, Zhang Z, Yang GY, Wang Y. cxcl12-engineered endothelial progenitor cells enhance neurogenesis and angiogenesis after ischemic brain injury in mice. *Stem Cell Res Ther* 9: 139, 2018. doi:10.1186/s13287-018-0865-6.
50. Li YF, Ren LN, Guo G, Cannella LA, Chernaya V, Samuel S, Liu SX, Wang H, Yang XF. Endothelial progenitor cells in ischemic stroke: an exploration from hypothesis to therapy. *J Hematol Oncol* 8: 33, 2015. doi:10.1186/s13045-015-0130-8.
51. Liao S, Luo C, Cao B, Hu H, Wang S, Yue H, Chen L, Zhou Z. Endothelial progenitor cells for ischemic stroke: update on basic research and application. *Stem Cells Int* 2017: 2193432, 2017. doi:10.1155/2017/2193432.
52. Liman TG, Endres M. New vessels after stroke: postischemic neovascularization and regeneration. *Cerebrovasc Dis* 33: 492–499, 2012. doi:10.1159/000337155.
53. Llevadot J, Murasawa S, Kureishi Y, Uchida S, Masuda H, Kawamoto A, Walsh K, Isner JM, Asahara T. HMG-CoA reductase inhibitor mobilizes bone marrow-derived endothelial progenitor cells. *J Clin Invest* 108: 399–405, 2001. doi:10.1172/JCI200113131.
54. Lo EH, Dalkara T, Moskowitz MA. Mechanisms, challenges and opportunities in stroke. *Nat Rev Neurosci* 4: 399–415, 2003. doi:10.1038/nrn1106.
55. Lo EH. A new penumbra: transitioning from injury into repair after stroke. *Nat Med* 14: 497–500, 2008. doi:10.1038/nm1735.
56. Lodi D, Iannitti T, Palmieri B. Stem cells in clinical practice: applications and warnings. *J Exp Clin Cancer Res* 30: 9, 2011. doi:10.1186/1756-9966-30-9.
57. Lopez-Nebolina F, Toledo AH, Toledo-Pereyra LH. Molecular biology of apoptosis in ischemia and reperfusion. *J Invest Surg* 18: 335–350, 2005. doi:10.1080/08941930500328862.
58. Ma F, Morancho A, Montaner J, Rosell A. Endothelial progenitor cells and revascularization following stroke. *Brain Res* 1623: 150–159, 2015. doi:10.1016/j.brainres.2015.02.010.
59. Maki T, Morancho A, Martínez-San Segundo P, Hayakawa K, Takase H, Liang AC, Gabriel-Salazar M, Medina-Gutiérrez E, Washida K, Montaner J, Lok J, Lo EH, Arai K, Rosell A. Endothelial progenitor cell secretome and oligovascular repair in a mouse model of prolonged cerebral hypoperfusion. *Stroke* 49: 1003–1010, 2018. doi:10.1161/STROKEAHA.117.019346.
60. Martí-Fàbregas J, Delgado-Mederos R, Crespo J, Peña E, Marín R, Jiménez-Xarrié E, Fernández-Arcos A, Pérez-Pérez J, Martínez-Domeño A, Camps-Renom P, Prats-Sánchez L, Casoni F, Badimon L. Circulating endothelial progenitor cells and the risk of vascular events after ischemic stroke. *PLoS One* 10: e0124895, 2015. doi:10.1371/journal.pone.0124895.
61. Medina RJ, Barber CL, Sabatier F, Dignat-George F, Melero-Martín JM, Khosrotehrani K, Ohneda O, Randi AM, Chan JKY, Yamaguchi T, Van Hinsbergh VWM, Yoder MC, Stitt AW. Endothelial progenitors: a consensus statement on nomenclature. *Stem Cells Transl Med* 6: 1316–1320, 2017. doi:10.1002/sctm.16-0360.
62. Miller-Kasprzak E, Jagodziński PP. Endothelial progenitor cells as a new agent contributing to vascular repair. *Arch Immunol Ther Exp (Warsz)* 55: 247–259, 2007. doi:10.1007/s00005-007-0027-5.
63. Minami Y, Nakajima T, Ikutomi M, Morita T, Komuro I, Sata M, Sahara M. Angiogenic potential of early and late outgrowth endothelial progenitor cells is dependent on the time of emergence. *Int J Cardiol* 186: 305–314, 2015. doi:10.1016/j.ijcard.2015.03.166.
64. Minciacchi VR, You S, Spinelli C, Morley S, Zandian M, Aspúria PJ, Cavallini L, Ciardiello C, Reis Sobreiro M, Morello M, Kharmate G, Jang SC, Kim DK, Hosseini-Behesti E, Tomlinson Gums E, Gleave M, Gho YS, Mathivanan S, Yang W, Freeman MR, Di Vizio D. Large oncosomes contain distinct protein cargo and represent a separate functional class of tumor-derived extracellular vesicles. *Oncotarget* 6: 11327–11341, 2015. doi:10.18632/oncotarget.3598.
65. Miyamoto N, Pham LD, Seo JH, Kim KW, Lo EH, Arai K. Crosstalk between cerebral endothelium and oligodendrocyte. *Cell Mol Life Sci* 71: 1055–1066, 2014. doi:10.1007/s00018-013-1488-9.
66. Moubarik C, Guillet B, Youssef B, Codaccioni JL, Piercecchi MD, Sabatier F, Lionel P, Dou L, Foucault-Bertaud A, Velly L, Dignat-George F, Pisano P. Transplanted late outgrowth endothelial progenitor cells as cell therapy product for stroke. *Stem Cell Rev* 7: 208–220, 2011. doi:10.1007/s12015-010-9157-y.
67. Navarro-Sobrinho M, Rosell A, Hernandez-Guillamon M, Penalba A, Ribó M, Alvarez-Sabín J, Montaner J. Mobilization, endothelial differentiation and functional capacity of endothelial progenitor cells after ischemic stroke. *Microvasc Res* 80: 317–323, 2010. doi:10.1016/j.mvr.2010.05.008.
68. Ohab JJ, Carmichael ST. Poststroke neurogenesis: emerging principles of migration and localization of immature neurons. *Neuroscientist* 14: 369–380, 2008. doi:10.1177/1073858407309545.
69. Ohab JJ, Fleming S, Blesch A, Carmichael ST. A neurovascular niche for neurogenesis after stroke. *J Neurosci* 26: 13007–13016, 2006. doi:10.1523/JNEUROSCI.4323-06.2006.
70. Ohta T, Kikuta K, Imamura H, Takagi Y, Nishimura M, Arakawa Y, Hashimoto N, Nozaki K. Administration of ex vivo-expanded bone marrow-derived endothelial progenitor cells attenuates focal cerebral ischemia-reperfusion injury in rats. *Neurosurgery* 59: 679–686, 2006. doi:10.1227/01.NEU.0000229058.08706.88.
71. Ottone C, Krusche B, Whitby A, Clements M, Quadrato G, Pitulescu ME, Adams RH, Parrinello S. Direct cell-cell contact with the vascular niche maintains quiescent neural stem cells. *Nat Cell Biol* 16: 1045–1056, 2014. doi:10.1038/ncb3045.
72. Park HJ, Friston K. Structural and functional brain networks: from connections to cognition. *Science* 342: 1238411, 2013. doi:10.1126/science.1238411.
73. Pegtel DM, Peferoen L, Amor S. Extracellular vesicles as modulators of cell-to-cell communication in the healthy and diseased brain. *Philos Trans R Soc Lond B Biol Sci* 369: 20130516–20130516, 2014. doi:10.1098/rstb.2013.0516.
74. Peichev M, Naiyer AJ, Pereira D, Zhu Z, Lane WJ, Williams M, Oz MC, Hicklin DJ, Witte L, Moore MA, Rafii S. Expression of VEGFR-2 and AC133 by circulating human CD34<sup>+</sup> cells identifies a population of functional endothelial precursors [Online]. *Blood* 95: 952–958, 2000. https://www.ncbi.nlm.nih.gov/pubmed/10648408.
- 74a. Pellegrini L, Bennis Y, Guillet B, Velly L, Garrigue P, Sabatier F, Dignat-George F, Bruder N, Pisano P. Therapeutic benefit of a combined strategy using erythropoietin and endothelial progenitor cells after transient focal cerebral ischemia in rats. *Neurol Res* 35: 937–947, 2013. doi:10.1179/1743132813Y.0000000235.
75. Pepper MS. Manipulating angiogenesis. From basic science to the bedside. *Arterioscler Thromb Vasc Biol* 17: 605–619, 1997. doi:10.1161/01.ATV.17.4.605.
76. Pham LD, Hayakawa K, Seo JH, Nguyen MN, Som AT, Lee BJ, Guo S, Kim KW, Lo EH, Arai K. Crosstalk between oligodendrocytes and cerebral endothelium contributes to vascular remodeling after white matter injury. *Glia* 60: 875–881, 2012. doi:10.1002/glia.22320.
77. Pula G, Mayr U, Evans C, Prokopi M, Vara DS, Yin X, Astrouklakis Z, Xiao Q, Hill J, Xu Q, Mayr M. Proteomics identifies thymidine phosphorylase as a key regulator of the angiogenic potential of colony-forming units and endothelial progenitor cell cultures. *Circ Res* 104: 32–40, 2009. doi:10.1161/CIRCRESAHA.108.182261.
78. Ratajczak J, Wysoczynski M, Hayek F, Janowska-Wieczorek A, Ratajczak MZ. Membrane-derived microvesicles: important and underappreciated mediators of cell-to-cell communication. *Leukemia* 20: 1487–1495, 2006. doi:10.1038/sj.leu.2404296.
79. Regueiro A, Cuadrado-Godia E, Bueno-Betí C, Diaz-Ricart M, Oliveras A, Novella S, Gené GG, Jung C, Subirana I, Ortiz-Pérez JT, Roqué M, Freixa X, Núñez J, Escolar G, Marrugat J, Hermenegildo C, Valverde MA, Roquer J, Sanchis J, Heras M. Mobilization of endothelial progenitor cells in acute cardiovascular events in the PRO-CELL study: time-course after acute myocardial infarction and stroke. *J Mol Cell Cardiol* 80: 146–155, 2015. doi:10.1016/j.yjmcc.2015.01.005.
80. Rehman J, Li J, Orschell CM, March KL. Peripheral blood “endothelial progenitor cells” are derived from monocyte/macrophages and secrete angiogenic growth factors. *Circulation* 107: 1164–1169, 2003. doi:10.1161/01.CIR.0000058702.69484.A0.
81. Rosell A, Morancho A, Navarro-Sobrinho M, Martínez-Saez E, Hernández-Guillamon M, Lope-Piedrafita S, Barceló V, Borrás F, Penalba A,

- García-Bonilla L, Montaner J. Factors secreted by endothelial progenitor cells enhance neurorepair responses after cerebral ischemia in mice. *PLoS One* 8: e73244, 2013. doi:10.1371/journal.pone.0073244.
82. Di Santo S, Yang Z, Wyler von Ballmoos M, Voelzmann J, Diehm N, Baumgartner I, Kalka C. Novel cell-free strategy for therapeutic angiogenesis: in vitro generated conditioned medium can replace progenitor cell transplantation. *PLoS One* 4: e5643, 2009. doi:10.1371/journal.pone.0005643.
  83. Schmidt-Lucke C, Fichtlscherer S, Aicher A, Tschöpe C, Schultheiss H-P, Zeiher AM, Dimmeler S. Quantification of circulating endothelial progenitor cells using the modified ISHAGE protocol. *PLoS One* 5: e13790, 2010. doi:10.1371/journal.pone.0013790.
  84. Shen Q, Goderie SK, Jin L, Karanth N, Sun Y, Abramova N, Vincent P, Pumiglia K, Temple S. Endothelial cells stimulate self-renewal and expand neurogenesis of neural stem cells. *Science* 304: 1338–1340, 2004. doi:10.1126/science.1095505.
  85. Shigemoto-Mogami Y, Hoshikawa K, Goldman JE, Sekino Y, Sato K. Microglia enhance neurogenesis and oligodendrogenesis in the early postnatal subventricular zone. *J Neurosci* 34: 2231–2243, 2014. doi:10.1523/JNEUROSCI.1619-13.2014.
  - 85a. Shyu WC, Lin SZ, Chiang MF, Su CY, Li H. Intracerebral peripheral blood stem cell (CD34<sup>+</sup>) implantation induces neuroplasticity by enhancing beta1 integrin-mediated angiogenesis in chronic stroke rats. *J Neurosci* 26: 3444–3453, 2006. doi:10.1523/JNEUROSCI.5165-05.2006.
  86. Sieveking DP, Buckle A, Celermajer DS, Ng MK. Strikingly different angiogenic properties of endothelial progenitor cell subpopulations: insights from a novel human angiogenesis assay. *J Am Coll Cardiol* 51: 660–668, 2008. doi:10.1016/j.jacc.2007.09.059.
  87. Simak J, Gelderman MP. Cell membrane microparticles in blood and blood products: potentially pathogenic agents and diagnostic markers. *Transfus Med Rev* 20: 1–26, 2006. doi:10.1016/j.tmr.2005.08.001.
  88. Squillaro T, Peluso G, Galderisi U. Clinical trials with mesenchymal stem cells: an update. *Cell Transplant* 25: 829–848, 2016. doi:10.3727/096368915X689622.
  89. Stroke Unit Trialists' Collaboration. Organised inpatient (stroke unit) care for stroke. In: *Cochrane Database of Systematic Reviews*, edited by Langhorne P. Chichester, UK: John Wiley & Sons, Ltd, 2007, p. CD000197.
  90. Taguchi A, Soma T, Tanaka H, Kanda T, Nishimura H, Yoshikawa H, Tsukamoto Y, Iso H, Fujimori Y, Stern DM, Naritomi H, Matsuyama T. Administration of CD34<sup>+</sup> cells after stroke enhances neurogenesis via angiogenesis in a mouse model. *J Clin Invest* 114: 330–338, 2004. doi:10.1172/JCI200420622.
  91. Takahashi T, Kalka C, Masuda H, Chen D, Silver M, Kearney M, Magner M, Isner JM, Asahara T. Ischemia- and cytokine-induced mobilization of bone marrow-derived endothelial progenitor cells for neovascularization. *Nat Med* 5: 434–438, 1999. doi:10.1038/7434.
  92. Teasell R, Rice D, Richardson M, Campbell N, Madady M, Hussein N, Murie-Fernandez M, Page S. The next revolution in stroke care. *Expert Rev Neurother* 14: 1307–1314, 2014. doi:10.1586/14737175.2014.968130.
  93. Templin C, Volkmann J, Emmert MY, Mocharla P, Müller M, Kraenkel N, Ghadri JR, Meyer M, Styp-Rekowska B, Briand S, Klingenberg R, Jaguszewski M, Matter CM, Djonov V, Mach F, Windecker S, Hoerstrup SP, Thum T, Lüscher TF, Landmesser U. Increased proangiogenic activity of mobilized CD34<sup>+</sup> progenitor cells of patients with acute ST-segment-elevation myocardial infarction: role of differential microRNA-378 expression. *Arterioscler Thromb Vasc Biol* 37: 341–349, 2017. doi:10.1161/ATVBAHA.116.308695.
  94. Théry C, Ostrowski M, Segura E. Membrane vesicles as conveyors of immune responses. *Nat Rev Immunol* 9: 581–593, 2009. doi:10.1038/nri2567.
  95. Tsai NW, Hung SH, Huang CR, Chang HW, Chang WN, Lee LH, Wang HC, Lin YJ, Lin WC, Cheng BC, Chiang YF, Su YJ, Tsai TR, Lu CH. The association between circulating endothelial progenitor cells and outcome in different subtypes of acute ischemic stroke. *Clin Chim Acta* 427: 6–10, 2014. doi:10.1016/j.cca.2013.09.029.
  96. Urbich C, Aicher A, Heeschen C, Dernbach E, Hofmann WK, Zeiher AM, Dimmeler S. Soluble factors released by endothelial progenitor cells promote migration of endothelial cells and cardiac resident progenitor cells. *J Mol Cell Cardiol* 39: 733–742, 2005. doi:10.1016/j.yjmcc.2005.07.003.
  97. Valadi H, Ekström K, Bossios A, Sjöstrand M, Lee JJ, Lötvall JO. Exosome-mediated transfer of mRNAs and microRNAs is a novel mechanism of genetic exchange between cells. *Nat Cell Biol* 9: 654–659, 2007. doi:10.1038/ncb1596.
  - 97a. van Balkom BW, de Jong OG, Smits M, Brummelman J, den Ouden K, de Bree PM, van Eijndhoven MAJ, Pegtel DM, Stoorvogel W, Würdinger T, Verhaar MC. Endothelial cells require miR-214 to secrete exosomes that suppress senescence and induce angiogenesis in human and mouse endothelial cells. *Blood* 121: 3997–4006, 2013. doi:10.1182/blood-2013-02-478925.
  98. Walter DH, Rittig K, Bahlmann FH, Kirchmair R, Silver M, Murayama T, Nishimura H, Losordo DW, Asahara T, Isner JM. Statin therapy accelerates reendothelialization: a novel effect involving mobilization and incorporation of bone marrow-derived endothelial progenitor cells. *Circulation* 105: 3017–3024, 2002. doi:10.1161/01.CIR.0000018166.84319.55.
  99. Wang J, Chen Y, Yang Y, Xiao X, Chen S, Zhang C, Jacobs B, Zhao B, Bihl J, Chen Y. Endothelial progenitor cells and neural progenitor cells synergistically protect cerebral endothelial cells from hypoxia/reoxygenation-induced injury via activating the PI3K/Akt pathway. *Mol Brain* 9: 12, 2016. doi:10.1186/s13041-016-0193-7.
  100. Wang L, Zhang ZG, Zhang RL, Gregg SR, Hozeska-Solgot A, LeTourneau Y, Wang Y, Chopp M. Matrix metalloproteinase 2 (MMP2) and MMP9 secreted by erythropoietin-activated endothelial cells promote neural progenitor cell migration. *J Neurosci* 26: 5996–6003, 2006. doi:10.1523/JNEUROSCI.5380-05.2006.
  101. Wechsler LR, Bates D, Stroemer P, Andrews-Zwilling YS, Aizman I. Cell therapy for chronic stroke. *Stroke* 49: 1066–1074, 2018. doi:10.1161/STROKEAHA.117.018290.
  102. Witwer KW, Buzás EI, Bemis LT, Bora A, Lässer C, Lötvall J, Nolte-’t Hoen EN, Piper MG, Sivaraman S, Skog J, Théry C, Wauben MH, Hochberg F. Standardization of sample collection, isolation and analysis methods in extracellular vesicle research. *J Extracell Vesicles* 2: 20360, 2013. doi:10.3402/jev.v2i0.20360.
  - 102a. Xin B, Liu CL, Yang H, Peng C, Dong XH, Zhang C, Chen AF, Xie HH. Prolonged Fasting Improves Endothelial Progenitor Cell-Mediated Ischemic Angiogenesis in Mice. *Cell Physiol Biochem* 40: 693–706, 2016. doi:10.1159/000452581.
  103. Yamaguchi J, Kusano KF, Masuo O, Kawamoto A, Silver M, Murasawa S, Bosch-Marce M, Masuda H, Losordo DW, Isner JM, Asahara T. Stromal cell-derived factor-1 effects on ex vivo expanded endothelial progenitor cell recruitment for ischemic neovascularization. *Circulation* 107: 1322–1328, 2003. doi:10.1161/01.CIR.0000055313.77510.22.
  104. Yamashita T, Takahashi Y, Nishikawa M, Takakura Y. Effect of exosome isolation methods on physicochemical properties of exosomes and clearance of exosomes from the blood circulation. *Eur J Pharm Biopharm* 98: 1–8, 2016. doi:10.1016/j.ejpb.2015.10.017.
  105. Yang SF, Lee WJ, Tan P, Tang CH, Hsiao M, Hsieh FK, Chien MH. Upregulation of miR-328 and inhibition of CREB-DNA-binding activity are critical for resveratrol-mediated suppression of matrix metalloproteinase-2 and subsequent metastatic ability in human osteosarcomas. *Oncotarget* 6: 2736–2753, 2015. doi:10.18632/oncotarget.3088.
  106. Yang Z, Di Santo S, Kalka C. Current developments in the use of stem cell for therapeutic neovascularisation: is the future therapy “cell-free”? *Swiss Med Wkly* 140: w13130, 2010. doi:10.4414/smw.2010.13130.
  107. Yin KJ, Hamblin M, Chen YE. Angiogenesis-regulating microRNAs and ischemic stroke. *Curr Vasc Pharmacol* 13: 352–365, 2015. doi:10.2174/1570161113119990016.
  108. Yip HK, Chang LT, Chang WN, Lu CH, Liou CW, Lan MY, Liu JS, Youssef AA, Chang HW. Level and value of circulating endothelial progenitor cells in patients after acute ischemic stroke. *Stroke* 39: 69–74, 2008. doi:10.1161/STROKEAHA.107.489401.
  109. Zhang R, Xie X, Yu Q, Feng H, Wang M, Li Y, Liu Y. Constitutive expression of adiponectin in endothelial progenitor cells protects a rat model of cerebral ischemia. *Neural Plast* 2017: 6809745, 2017. doi:10.1155/2017/6809745.
  110. Zhang ZG, Chopp M. Exosomes in stroke pathogenesis and therapy. *J Clin Invest* 126: 1190–1197, 2016. doi:10.1172/JCI81133.
  111. Zhang ZG, Zhang L, Jiang Q, Chopp M. Bone marrow-derived endothelial progenitor cells participate in cerebral neovascularization after focal cerebral ischemia in the adult mouse. *Circ Res* 90: 284–288, 2002. doi:10.1161/hh0302.104460.
  112. Zhu W, Fan Y, Hao Q, Shen F, Hashimoto T, Yang GY, Gami M, Bartus RT, Young WL, Chen Y. Postischemic IGF-1 gene transfer promotes neurovascular regeneration after experimental stroke. *J Cereb Blood Flow Metab* 29: 1528–1537, 2009. doi:10.1038/jcbfm.2009.75.



## Effects of aging and comorbidities on endothelial progenitor cells

---

[www.conditionmed.org](http://www.conditionmed.org)





## REVIEW ARTICLE | OPEN ACCESS

# Effects of aging and comorbidities on endothelial progenitor cells

Jesús M. Pradillo<sup>1</sup>, Alba Grayston<sup>2</sup>, Violeta Medina-Alonso<sup>1</sup>, Mercedes Arrúe<sup>2</sup>, Ignacio Lizasoain<sup>1</sup>, Anna Rosell<sup>2</sup>

Endothelial Progenitor Cells (EPCs) are postulated to participate in the function of the vessel endothelium and are emerging as key cellular elements of vessel and tissue repair. These bone marrow-derived cells play a central role in maintaining blood vessel health and function under physiological conditions. Several investigations have identified these cells as mediators of repair; however, their number and function vary among subjects according to age, sex, and comorbid circumstances, which may negatively condition the characteristics and functions of EPCs. Lifestyle habits in developed countries increase the prevalence of comorbid conditions, including cardiovascular diseases and disorders in which the health of the vascular system is compromised. In this review, we describe how age, diabetes, hypertension, and obesity (significant comorbid conditions) may influence the opportunities for vascular remodeling by modifying the bio-distribution and functions of EPCs. We provide evidence for the need to improve cardiovascular protection beyond endothelial function and the vascular wall structure by preserving the endogenous mechanisms of vascular repair based on the actions of the endothelial progenitor pools.

**Keywords:** endothelial progenitor cells, stroke, cardiovascular disease, aging, comorbidity, vascular repair

### 1. Introduction

Cardiovascular diseases (CVDs) comprise a group of disorders of the heart and blood vessels, including coronary heart disease, cerebrovascular disease, and peripheral arterial disease, among others. These diseases cause 17.9 million deaths every year and account for 31% of all global deaths, according to the World Health Organization (WHO). CVDs primarily manifest as heart attacks and strokes, which are associated with several lifestyle habits, including tobacco use, an unhealthy diet, physical inactivity, and alcohol abuse. Such lifestyle choices increase the prevalence of raised blood pressure, elevated blood glucose, high cholesterol, and obesity, which are risk factors that negatively affect cardiovascular health primarily by damaging and narrowing or obstructing the blood vessels (Beaglehole, 2001). Apart from these direct effects on the vascular walls, the presence of one or multiple comorbid conditions can influence other organs, cellular metabolism and function, tissue repair mechanisms, or the number and function of stem/progenitor cells. Therefore, the preservation of endothelial function and blood vessel health is essential for the prevention of the progression of CVDs, both in aged and young individuals.

A dysfunctional or damaged endothelium, with limited regenerative capacity, leads to platelet aggregation, unbalanced

hemostasis, immune cell infiltration, increased oxidative stress, reduced vasomotor capabilities, and cellular turnover of the blood vessels (Ross, 2018; Widmer and Leman, 2014). A dysfunctional or damaged endothelium is also associated with arterial atherosclerosis, blood clot formation, reduced vessel repair, and impaired angiogenesis or tissue remodeling. In this context, endothelial progenitor cells (EPCs), also known as circulating angiogenic cells, which derive from bone marrow (BM), play a central role in maintaining blood vessel health and function (Esquivia et al., 2018) in the following ways: EPCs provide a source for physiological endothelial cell replacement; EPCs provide a source for endothelial repair via incorporation into the damaged vasculature as mature endothelial cells; EPCs promote angiogenesis by stimulating other endothelial cells to proliferate; and EPCs promote whole tissue remodeling in the recovery phases of stroke or cardiac injury. However, the number and function of EPCs may be negatively conditioned by the presence of the abovementioned risk factors. In this review, we highlight the importance of EPCs as key cellular elements of endothelial function and vessel and tissue repair. The influence of aging and comorbid conditions, which are associated with CVD, on EPC function, will also be discussed.

<sup>1</sup>Departamento de Farmacología y Toxicología, Facultad de Medicina, Universidad Complutense de Madrid (UCM), Instituto de Investigación Hospital 12 de Octubre (i+12), Madrid, Spain. <sup>2</sup>Neurovascular Research Laboratory and Neurology Department, Vall d'Hebron Research Institute, Universitat Autònoma de Barcelona, Barcelona, Spain.

## 2. Endothelial Progenitor Cells

### 2.1. Background: EPC populations and functions

The formation of new blood vessels was once thought to result from embryonic vasculogenesis followed by an outbreak of endothelial cells from existing vessels (Pepper, 1997). However, this dogma was questioned with the discovery of BM-derived EPCs in adult peripheral blood, which were first identified as CD34 antigen-positive (CD34<sup>+</sup>) mononuclear cells (MNC) with endothelial characteristics (Asahara et al., 1997). The proportion of these cells generally ranges between 0.1 and 2% of the total MNCs in the BM, peripheral blood, and cord blood. EPCs are mobilized from the BM into the peripheral blood as an endogenous response to the physiopathological demands of neovascularization and can be differentiated into functional endothelial cells *in vitro* and *ex vivo*. Currently, these cells play an important role in adult vasculogenesis and angiogenesis by participating not only in the formation of vessels but also in vessel repair and remodeling (Liman and Endres, 2012). However, the identification of EPCs remains controversial, as no single marker has been identified for this type of cell. Currently, these cells are defined as cells expressing both stem cell and endothelial markers, and flow cytometry is the most commonly

applied approach to count EPCs. Most accepted definitions describe EPCs as proliferating cells that express the cell-surface markers of stem cells (CD34 or CD133) and endothelial cells (vascular endothelial growth factor (VEGF) receptor-2) (Liman and Endres, 2012), although other progenitor or endothelial markers have also been used (Fadini et al., 2012). Despite the lack of a simple and rapid marker for identifying EPCs, there is consensus regarding the classification of these cells into two major types that emerge from MNC cultures, which were initially named “early EPCs” or circulating angiogenic cells (CAC) and “late EPCs” or outgrowth endothelial cells (OEC). These types of cells have distinct origins and contribute differently to angiogenesis (Fadini et al., 2012; Medina et al., 2017). The early EPCs appear rapidly in culture under specific conditions for endothelial cell growth, and the late EPCs appear after 2 to 3 weeks and expand in culture. While the early-EPCs exhibit a spindle shape within heterogeneous populations of cells, the late-OECs or endothelial colony-forming cells (ECFCs) exhibit cobblestone colonies with a characteristic clonogenic capacity (Hur et al., 2004; Gulati et al., 2003). Regardless of these controversies, it has been demonstrated that EPCs are capable of differentiating *ex vivo* into endothelial-like cells and therefore represent a new model for endothelial

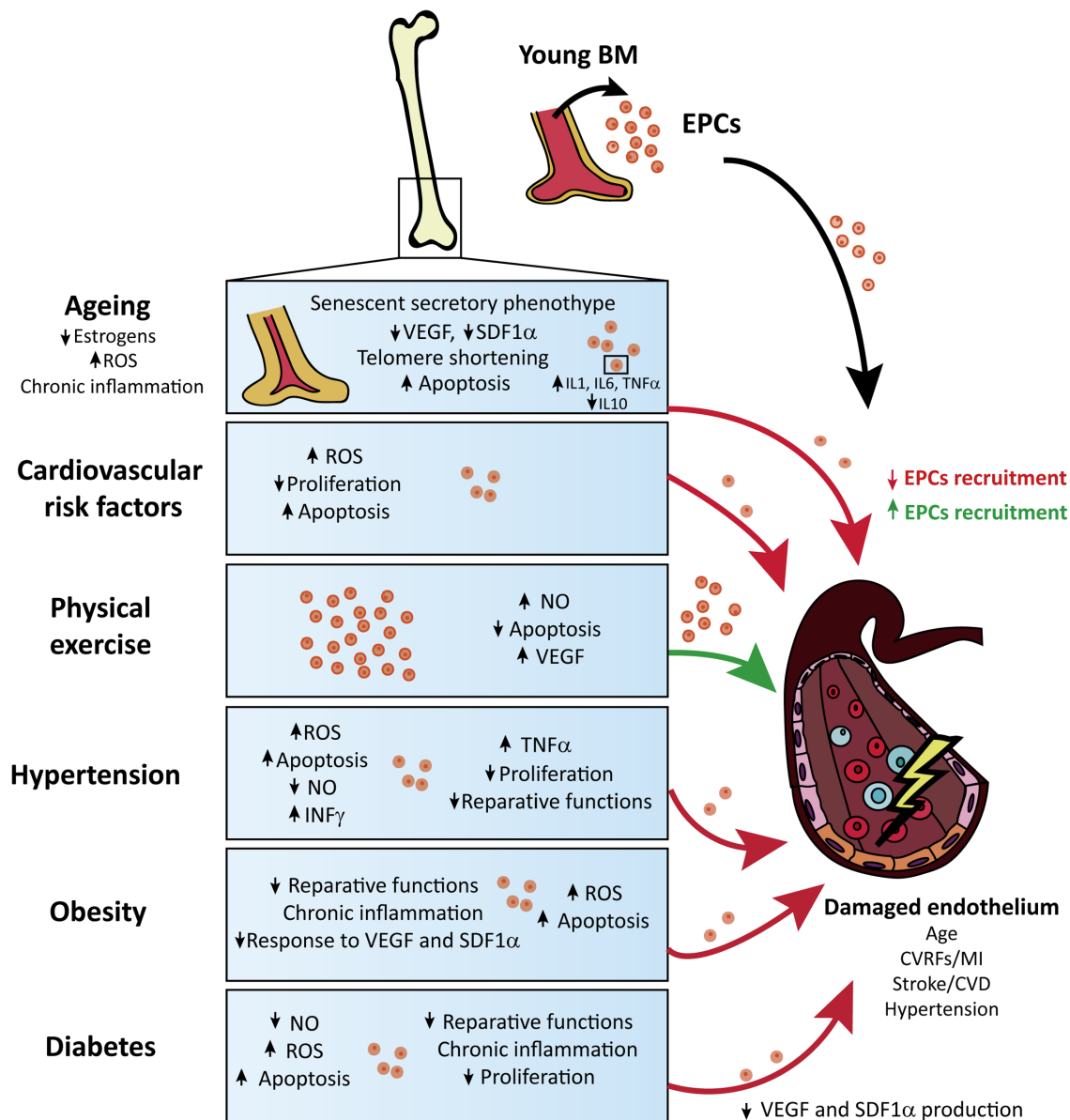


Figure 1. Schematic representation of the reported effects of comorbid conditions on EPC function and endothelial health in the context of cardiovascular disease.

Table 1. Most cited articles regarding the effects of aging on the biology of EPCs.

	Title	Journal	Main Results	Type of study	Cit.	Ref.
A g i n g	Age-dependent depression in circulating endothelial progenitor cells in patients undergoing coronary artery bypass grafting	Journal of the American College of Cardiology	Preoperative values of EPCs in 43 to 80 years old patients with stable coronary artery disease undergoing CABG were lowered with increasing age, similar to the lowering of plasma VEGF levels. Despite a significant increase in EPCs and release of cytochemokines during CABG, age was a major limiting factor for mobilization of EPCs.	Clinical research	303	Scheubel et al 2003
	Age-dependent impairment of endothelial progenitor cells is corrected by growth hormone mediated increase of insulin-like growth factor-1	Circulation Research	The age-related decline in EPC number and function can be restored by growth hormone mediated increase of IGF-1 levels.	Clinical research and Experimental research	213	Thum et al 2007
	Age decreases endothelial progenitor cell recruitment through decreases in hypoxia-inducible factor 1alpha stabilization during ischemia	Circulation	Aging impairs EPC trafficking to sites of ischemia through a failure of aged tissues to normally stabilize the HIF1 $\alpha$ induced by hypoxia in ischemic tissues.	Clinical research and Experimental research	145	Chang et al 2007
	Aging, exercise, and endothelial progenitor cell clonogenic and migratory capacity in men	Journal of Applied Physiology	Aging adversely affects EPC function in terms of migration and CFU number, but a 3-months aerobic exercise intervention improved EPC clonogenic and migratory capacity in middle-aged and older healthy men.	Clinical research and Experimental research	112	Hoetzer et al 2007
	Estrogen reduces endothelial progenitor cell senescence through augmentation of telomerase activity	Journal of Hypertension	Estrogen prevented the onset of EPC senescence, probably through the stimulation of telomerase, and potentiated their proliferative activity and network formation in vitro.	Experimental research	104	Imanishi et al 2005

**Foot note:** In order to summarize the most relevant publications associating EPC levels and function with aging, a search on Scopus database was undertaken. Keywords included “endothelial progenitor cells”, “EPC”, and “aging”. Only original articles were selected. Results were sorted according to the number of citations. The 5 most cited and relevant papers in the field of this comorbidity are listed, sorted from the most cited to the less according to Scopus database. Abbreviations: Cit (Citations), Ref (Reference), Endothelial Progenitor Cells (EPCs), Coronary Artery Bypass Grafting (CABG), Vascular Endothelial Growth Factor (VEGF), Insulin-like Growth Factor-1 (IGF-1), Hypoxia-Inducible Factor 1alpha (HIF1 $\alpha$ ), Colony Forming Units (CFU).

regeneration, vessel repair, and angio-vasculogenesis.

In addition to the therapeutic interest in endothelial progenitors for vascular regeneration due to their homing and engraftment into new or damaged blood vessels, it is also known that EPCs secrete a large number of growth factors, which contribute to vessel and tissue regeneration through stromal cell-derived factor 1 (SDF-1), VEGF, granulocyte-colony stimulating factor, endothelial nitric oxide synthase (eNOS), inducible NOS (iNOS), interleukin (IL)-8, and several matrix metalloproteinases (MMPs), among many others (Ma et al., 2015). These factors can promote endothelial cell proliferation and migration, reduce cell apoptosis, regulate the recruitment of endogenous progenitor cells, and promote vascular growth and remodeling (Urbich et al., 2005; Di Santo et al., 2009; Rosell et al., 2013). Moreover, the release of these factors appears to be increased by hypoxia; for example, Di Santo and colleagues showed that angiogenin, hepatocyte growth factor, IL-8, platelet-derived growth factor-BB, SDF-1, and VEGF-A are increased in EPC-conditioned media under hypoxic conditions (Di Santo et al., 2009), which supports the protective role of EPCs in the context of cerebral ischemia.

## 2.2. EPCs in tissue repair and their role in stroke neurorepair

Stroke is a CVD with a clear need for new therapies beyond the acute phase of the disease, during which reperfusion therapies have already demonstrated a clear impact on improving stroke management and neuroprotection (Hacke et al., 2005; Urra et al., 2015; Nogueira et al., 2017). The nature of this devastating disease leads to severely damaged tissue/cells in very close proximity to healthy peri-infarct tissue. The classical view of neuronal rescue/repair has changed in the last decades into a more global understanding of the brain as a whole. This view has expanded to include other cell types (glial cells, inflammatory cells, stem/progenitor cells), the extracellular matrix, and the communication between these components. Therefore, the endogenous mechanisms of neurovascular repair include angio-vasculogenesis (formation of new blood vessels),

gliogenesis (formation of new glial cells), neurogenesis (formation of new neurons), remyelination (new myelin sheaths on demyelinated axons), among others. Several of these endogenous mechanisms are activated in the minutes following the ischemic trigger in peri-infarct areas (Lo, 2005; Carmichael, 2008). Several populations of newborn progenitor cells have been identified in remodeling areas (Ohab et al., 2006; Jin et al., 2006), such as neural progenitor cells (NPCs), EPCs, or oligodendrocyte progenitor cells (OPCs). These findings demonstrate the plastic nature of the brain, in contrast to the more classical views of brains passively dying.

The following two elements must be highlighted in the natural neurorepair process: the neurovascular coupling and the neurovascular niche (Shen et al., 2004; Ohab et al., 2006). The former refers to the neurogenesis phenomenon which is closely linked to post-stroke angiogenesis, and the latter refers to the factors released by the tissue cells, which create an appropriate niche for neurorepair. The importance of this coupling was demonstrated when ischemic mice that received systemic endostatin to inhibit angiogenesis abolished the normal patterns of neuroblast migration through the peri-infarct areas from the subventricular zone (Ohab et al., 2006). The authors of that study elegantly demonstrated that the vascular production of SDF-1 and angiopoietin 1 (Ang1) promote neuroblast migration to peri-infarct cortex (newly generated neurons expressing C-X-C chemokine receptor type (CXCR4) or Tie-2, which are the receptors for SDF-1 and Ang1, respectively). Meanwhile, other authors have identified proliferating neuroblasts in peri-infarct areas of the human brain in close proximity to blood vessels (Jin et al., 2006). Moreover, it has been described that the trophic support of endothelial cells to the neural stem cell niche also occurs in non-pathological conditions, wherein brain endothelial cells secrete soluble factors that maintain CNS stem cell self-renewal and neurogenic potential *in vitro* (Shen et al., 2004). The crosstalk between the endothelium and oligodendrocyte/oligodendrocyte progenitors, which involves nourishing trophic factors that are released by endothelial

Table 2. Most cited articles regarding the effects of hypertension on the biology of EPCs.

	Title	Journal	Main Results	Type of study	Cit.	Ref.
H y p e r t e n s i o n	Number and migratory activity of circulating endothelial progenitor cells inversely correlate with risk factors for coronary artery disease	Circulation research	Number of isolated EPCs was reduced in CAD patients compared to healthy volunteers. These EPCs presented impaired migratory response. Number of (Atherosclerotic) risk factors correlated with the reduction of EPCs and inversely with the migratory response capacity. This decrease in EPC number and function may contribute to impaired vascularization in CAD patients.	Clinical research	1906	Vasa et al. 2001
	Endothelial progenitor cell senescence is accelerated in both experimental hypertensive rats and patients with essential hypertension	Journal of hypertension	EPCs from hypertensive patients and both spontaneously hypertensive and DOCA-SH rats showed accelerated senescence and lower telomerase activity. EPC senescence may affect vascularization processes in hypertensive patients.	Experimental research and Clinical research	191	Imanishi et al 2005
	Impaired endothelial repair capacity of early endothelial progenitor cells in prehypertension: Relation to endothelial dysfunction	Hypertension	The re-endothelialized area of the EPCs from prehypertensive/hypertensive patients was lower than healthy subjects. Senescence of EPCs in prehypertension/hypertension was increased whereas NO production was reduced. Reduced endothelial repair capacity of EPCs was related to accelerated senescence and impaired endothelial function.	Clinical research	133	Giannotti et al 2010
	Effects of an ARB on endothelial progenitor cell function and cardiovascular oxidation in hypertension	American Journal of Hypertension	Candesartan, an ARB used as an antihypertensive drug: increased the number of EPCs, reduced their oxidative stress response and the expression of NADPH oxidase subunits in cardiovascular organs of spontaneously hypertensive rats, improving EPC dysfunction.	Experimental research	83	Yu et al 2008
	Losartan improves the impaired function of endothelial progenitor cells in hypertension via an antioxidant effect	Hypertension Research	Number, colony formation and migration of EPCs was reduced in SHR-sp compared to controls. After administration of Losartan (ARB), an increase in the number of circulating EPCs and in their colony formation capacity was observed together with an inhibition of oxidation in SHR-sp. Antihypertensives can be useful to repair vascular injuries related to hypertension.	Experimental research	80	Yao et al 2007

**Foot note:** In order to summarize the most relevant publications associating EPC levels and function with hypertension, a search on Scopus database was undertaken. Keywords included “endothelial progenitor cells”, “EPC”, and “hypertension”. Only original articles were selected. Results were sorted according to the number of citations. The 5 most cited and relevant papers in the field of this comorbidity are listed, sorted from the most cited to the less according to Scopus database. Abbreviations: Cit (Citations), Ref (Reference), Endothelial Progenitor Cells (EPCs), Coronary Artery Disease (CAD), deoxycorticosterone acetate-salt hypertensive (DOCA-SH), Nitric Oxide (NO), Angiotensin II Receptor Blocker (ARB), Nicotinamid-Adenin-Dinucleotide-Phosphate Nicotinamide adenine dinucleotide phosphate (NADPH), Spontaneously Hypertensive Stroke Prone Rat (SHR-sp).

cells, has also been described in the normal and ischemic brain, wherein brain derived neurotrophic factor, transforming growth factor-beta, VEGF or MMPs may be responsible for maintaining the oligovascular niche (Miyamoto et al., 2014; Pham et al., 2012).

In this context, increasing evidence demonstrates that EPCs are present after ischemic stroke. The first studies of EPC mobilization in response to tissue ischemia (Takahashi et al., 1999) showed that this process was potentially related to the maintenance of endothelial integrity and the need for vascular remodeling. Other studies have demonstrated the incorporation of EPCs into neovessels (Asahara et al., 1997), and Taguchi and colleagues first reported that CD34<sup>+</sup>/CD133<sup>+</sup> cells, as an EPC-enriched population, were a marker of cerebrovascular function (Taguchi et al., 2004). Further research in the field demonstrate that, following injury, unidentified signals induce EPC mobilization in the blood and produce a variety of growth factors as well as cytokines, which recruit EPCs to the injury site for neovascularization and tissue repair (Reinisch et al., 2009; Navarro-Sobrino et al., 2010; Massot et al., 2013). One of the most relevant signaling systems that participates in the endogenous recruitment of EPCs to the injured tissue is the CXCR4/SDF-1 axis, which is activated in animal models of middle cerebral artery occlusion (MCAO) in rodents (Mao et al., 2014). In humans, studies show that after stroke, there is an increase in circulating EPCs in the acute phases, which is related to better outcomes (Navarro-Sobrino et al., 2010; Pías-Peleiteiro et al., 2016), and is followed by a decrease in the EPC counts at 3 months (Martí-Fábregas et al., 2013). Moreover, a recent study suggests that the initial stroke-driven increase in EPCs could be maintained in response to post-stroke rehabilitation therapy during the months after the ischemic

insult (Gabriel-Salazar et al., 2018).

### 2.3. Cell-therapy opportunities involving EPCs

Transplantation of EPCs has emerged as a promising approach to enhance tissue repair. Initial studies demonstrate that EPC therapy enhance angio-vasculogenic responses in ischemic conditions. However, later studies demonstrate that these cells are capable of communicating with other cell types to participate in other repair mechanisms beyond vessel remodeling, including neurogenesis, in the context of stroke (Ma et al., 2015). EPCs can be mobilized in response to a hypoxic event, can home in to sites of neovascularization, and can differentiate into endothelial cells. They can also secrete growth factors and exosome bodies in cell-to-cell communication mechanisms (Urbich et al., 2005; Esquiva et al., 2018).

Although many pre-clinical studies support the benefits of EPC treatments for stroke by enhancing vascular remodeling and neurorepair in the context of stroke, there is still a lack of trials investigating the safety and/or efficacy of EPC therapy. However, even without trials several therapeutic approaches are possible, including autologous transplantation after blood extraction or BM aspiration, posterior cell isolation and/or expansion, heterologous cell administration of EPCs obtained from healthy donors, and even the administration of EPC-secreted factors in a cell-free strategy. However, clinical data that evaluate the best strategy are still missing. Moreover, with the new endovascular treatments to remove cerebral blood clots in stroke patients, new therapeutic approaches can now be considered to physically deliver the therapeutic product (e.g. EPCs or EPCs-secreted factors) directly to the affected brain territory. However to date, one Phase I clinical trial has confirmed the safety and feasibility of administering intra-

arterially autologous BM-derived CD34<sup>+</sup> cells (which includes the EPC population) in a small number of stroke patients (Banerjee et al., 2014). Most recently, a new randomized controlled Phase IIa trial has been initiated to investigate the reduction in infarct volume in stroke patients who receive intrarterial CD34<sup>+</sup> cells in the acute phase (Sargento-Freitas et al., 2018).

Finally, growing evidence suggest that the regenerative potential of the cell therapies that are being currently investigated are, in part, orchestrated by the proteins secreted by the cells (the secretome), which reflect the functional competence of a given cell. The secretome is also responsible for the crosstalk between cells and with the extracellular matrix via trophic factors, cytokines, or other bioactive molecules. In this regard, cell-free strategies have been proposed for regenerative medicine, and several authors have already proposed to treat cerebral ischemia (Rosell et al., 2013), wound healing in the context of diabetes (Kim et al., 2010), hindlimb ischemia (Di Santo et al., 2009) and, more recently, white matter damage induced by chronic hypoperfusion (Maki et al., 2018). The use of these cell-based but cell-free EPC strategies warrants further testing in the stroke clinical setting.

### 3. Comorbid conditions and EPCs

Aging is an inevitable process characterized by the progressive degeneration of tissue and organ systems, the deterioration of body functions, and the declining ability to respond to stress. Aging can also trigger the emergence of other risk factors and, consequently, increase the risk of age-related diseases. These comorbidities include hypertension, diabetes, obesity, atherosclerosis, CVD, and stroke, and their development accelerates and aggravates the process of aging, leading to disability and premature death (Tian and Li, 2014; Bao et al.,

2014).

The Endothelium is one of the structures that is strongly affected by aging and by the comorbidities described above. Endothelial cells respond to physical/chemical stimulation by releasing appropriate substances to maintain vasomotor balance and vascular hemostasis. However, in pathological circumstances, the damaged endothelium needs to be repaired by the action of EPCs to recover its normal functions. Due to the important role of EPCs in vascular repair, specifically in CVD and stroke, the effect of various comorbidities on these stem cells will be reviewed in the following sections (see tables 1 to 5 and Figure 1). It is important to highlight that the different preclinical works described in the following sections have studied how each individual risk factor separately affects the properties of EPCs. However, following the Stroke Treatment Academic Industry Roundtable, or STAIR recommendations for stroke and CVD (Fisher et al., 2009; Kahle et al., 2012), the influence of several of the aforementioned risk factors on EPCs should be analyzed in the same animal model to increase the translation from bench to bed side and increase the potential reparative effects of these stem cells in comorbid patients.

#### 3.1. Aging

Aging is a complex and multifactorial process that is determined to a large extent by genetics and influenced by a wide range of environmental factors. One of the effects of aging is the structural and functional decline of the cardiovascular system, which is primarily attributable to the accumulation of senescent cells within the vascular wall. In young people, after endothelial damage, BM-derived EPCs proliferate, enter the circulation and migrate to the site of injury, improving endothelial function. In elderly patients, however, there are two main types of age-related processes that impair vascular repair. The first process is

Table 3. Most cited articles regarding the effects of Obesity on the biology of EPCs.

	Title	Journal	Main Results	Type of study	Cit.	Ref.
O b e s i t y	Decreased number of circulating progenitor cells in obesity: Beneficial effects of weight reduction	European heart journal	Obesity is associated with decreased numbers of CPCs and increased IMT: Inverse correlation between BMI and waist circumference and CPCs was observed. IMT increased together with BMI and correlated inversely with the number of EPCs. After diet, there was an increase in EPCs that correlated with the decrease in BMI and with the increase in CPC. Diet and weight loss may contribute to regression of IMT.	Clinical research and Experimental research	82	Müller-Ehmsen et al 2008
	Adiponectin promotes endothelial progenitor cell number and function	FEBS letters	Adiponectin is downregulated in obese subjects; EPC levels did not increase in adiponectin deficient mice in response to hindlimb ischemia. But adenovirus mediated delivery of adiponectin increased EPC levels in both WT and KO mice. Incubation of human blood mononuclear cells with adiponectin led to an increase in the number of EPCs. Adiponectin also induced EPC differentiation into network structures and served as chemoattractant in EPC migration assays. The deficiency of adiponectin may contribute to decreased levels of EPC in obese patients.	Experimental research	74	Shibata et al 2008
	Endothelial progenitor cell levels in obese men with the metabolic syndrome and the effect of simvastatin monotherapy vs. simvastatin/ezetimibe combination therapy	European heart journal	Circulating EPC levels were reduced in obese men compared to non-obese healthy controls. Monotreatment of statins vs combination with a cholesterol absorption inhibitor both increased EPC circulating levels compared to control subjects. Treatment could contribute to endothelial regeneration and protect against cardiovascular disease.	Clinical research	64	Westerweel et al. 2008
	Influence of BMI on level of circulating progenitor cells	Obesity	Obesity is associated with fivefold increased frequency of CPCs but the number of mature endothelial cells is unaffected by the condition. Obesity could promote mobilization of progenitor cells.	Clinical research and Experimental research	60	Bellows et al 2011
	Leptin receptor and functional effects of leptin in human endothelial progenitor cells	Atherosclerosis	High concentrations of leptin inhibited human EPC migration but did not have any effect on EPC proliferation. Thus, leptin may affect EPC function both in physiological and hyperleptinemic conditions.	Experimental research	59	Wolk et al 2005

**Foot note:** In order to summarize the most relevant publications associating EPC levels and function with obesity, a search on Scopus database was undertaken. Keywords included “endothelial progenitor cells”, “EPC”, and “obesity”. Only original articles were selected. Results were sorted according to the number of citations. The 5 most cited and relevant papers in the field of this comorbidity are listed, sorted from the most cited to the less according to Scopus database. Abbreviations: Cit (Citations), Ref (Reference), Circulating Progenitor Cells (CPC), Intima Media Thickness (IMT), Body Mass Index (BMI), Endothelial Progenitor Cells (EPCs), Wild Type (WT), Knockout (KO).

Table 4. Most cited articles regarding the effects diabetes on the biology of EPCs.

	Title	Journal	Main Results	Type of study	Cit.	Ref.
D i a b e t e s	Human endothelial progenitor cells from type II diabetics exhibit impaired proliferation, adhesion, and incorporation into vascular structures	Circulation	Type II diabetes may alter EPC biology: Proliferative capacity of diabetic EPCs was decreased compared to control subjects. Though EPCs had a normal adhesion to fibronectin, collagen and quiescent endothelial cells. They were also less likely to form tubules.	Experimental research	1153	Tepper et al 2002
	Endothelial Progenitor Cell Dysfunction: A Novel Concept in the Pathogenesis of Vascular Complications of Type 1 Diabetes	Diabetes	The number of EPCs obtained from type 1 diabetic patients was lower than EPCs of control subjects, as well as their angiogenesis capacity. This dysfunction could contribute to the vascular complications in type 1 diabetes.	Experimental Research	672	Loomans et al 2004
	Circulating endothelial progenitor cells are reduced in peripheral vascular complications of type 2 diabetes mellitus	Journal of the American College of Cardiology	The number of CPCs and EPCs from diabetic patients was reduced compared to healthy subjects. This reduction may be involved in the pathogenesis of peripheral vascular complications such as peripheral vascular disease.	Experimental Research	515	Fadini et al 2005
	Diabetic impairments in NO-mediated endothelial progenitor cell mobilization and homing are reversed by hyperoxia and SDF-1 $\alpha$	Journal of Clinical investigation	Diabetic mice showed impaired phosphorylation of BM eNOS which decreases the number of circulating EPCs. In a situation of hyperoxia the amounts of BM NO and circulating EPCs increased. Hyperoxia reverses the diabetic defect in EPC mobilization	Experimental Research	438	Gallagher et al 2007
	Number and function of endothelial progenitor cells as a marker of severity for diabetic vasculopathy	Arteriosclerosis, Thrombosis and Vascular Biology	EPC number is related to the severity to PAD complications in diabetic patients. Also, EPC function is altered in Diabetic patients with peripheral arterial disease. In this study patients with PAD showed a reduction in circulating EPCs versus non-PAD patients. Also, the clonogenic and adhesion capacity of these cells was lower in the diabetic PAD patients.	Clinical research and Experimental research	316	Fadini et al 2006

**Foot note:** In order to summarize the most relevant publications associating EPC levels and function with diabetes, a search on Scopus database was undertaken. Keywords included "endothelial progenitor cells", "EPC", "diabetes". Only original articles were selected. Results were sorted according to the number of citations. The 5 most cited and relevant papers in the field of this comorbidity are listed, sorted from the most cited to the less according to Scopus database. Abbreviations: Cit (Citations), Ref (Reference), Endothelial Progenitor Cell (EPC), Circulating Progenitor Cells (CPC), Bone Marrow (BM), endothelial Nitric Oxide Synthase (eNOS), Nitric Oxide (NO), Peripheral Arterial Disease (PAD).

the alteration of the microenvironment and structure of the BM, which is the main niche of EPCs, and the second process is a direct effect of aging on EPCs (Rurali et al., 2016).

Regarding the effects of aging on BM structure, the most important factor is the progressive reduction of hematopoietic tissue mass (also called red or active BM, which contains the EPC populations) paralleled by an increase in adipose tissue mass (also called inactive or yellow BM because of its typical color due to fatty replacement) (Ricci et al., 1990). In fact, it has been demonstrated that BM cellularity is strictly dependent upon a patient's age, and a 30% reduction in active BM mass in the iliac crest has been demonstrated at 70 years of age (Gilleece, 1993). However, BM stem cells are also strongly dependent upon extra-niche factors, such as hormonal levels (estrogens), reactive oxygen species (ROS) overproduction, or chronic inflammation. In women, menopause is one of the physiological mechanisms of senescence that is characterized by the reduction of estrogens. It has been shown that a reduction of estrogens in menopausal women leads to an increase in pro-inflammatory cytokines, such as IL-6, favoring the accumulation of adipose tissue in the BM (Pfeilschifter et al., 2002). Interestingly, type 2 diabetes may also cause BM niche dysfunction through the generation of advanced glycation end-products, which accumulate in the extracellular matrix and can suppress proliferation, induce apoptosis, and increase ROS production (Leslie et al., 2012).

Another age-related effect on BM cellularity is the reduction in tissue renewal and the switch to a senescent secretory phenotype resulting from the accumulation of senescent cells. The secretory content of EPCs is very important, for instance, after stroke or in vascular dementia. In both pathologies, but primarily in stroke, not only is there an increase in proliferation/migration and the incorporation of EPCs into the blood vessels at the site of injury, but it has also been shown that EPCs release protective cytokines and growth factors that can induce the self-repair of injured endothelial cells (Esquivia et al., 2018; Maki et al., 2018). Senescent cells, however, secrete biologically active

molecules that can disrupt the normal tissue microenvironment and affect the behavior of neighboring cells. For example, aging results in an increase in pro-inflammatory cytokines (IL-1, IL6 and tumor necrosis factor- $\alpha$  (TNF- $\alpha$ ), a decrease in anti-inflammatory cytokines, such as IL-10, and a decrease in hematopoietic growth factors. These changes finally converge into the disappearance of the red BM (Abdelmagid et al., 2015).

The second age-related process that impairs vascular repair is the direct effect of aging on EPCs due to mechanisms such as telomere shortening, an exaggerated production of inflammatory cytokines/ROS, increased apoptosis, and a reduction of EPC-stimulating factors. Telomeres are the regions at the ends of the chromosomes, and their main function is to protect the chromosome from degradation during DNA replication. With each cycle of cell division, the telomeres progressively shorten until they reach a critical length, below which senescence is achieved (Kushner et al., 2009). Interestingly, EPCs, like others stem cells, can elongate their telomeres by expressing the telomerase reverse transcriptase enzyme (TERT), but aging induces a decreased activity of this enzyme by increasing oxidative stress and decreasing the bioavailability of NO (Herrera et al., 2010). Another age-related factor that causes EPC senescence is low grade but chronic inflammation, which leads to an increase in cytokines such as TNF- $\alpha$ . This cytokine, in particular, can induce premature EPC senescence and apoptosis by acting on silent information regulator type-1 (SIRT1). In fact, SIRT1 inhibition reduces telomere length and increases the activity of the pro-apoptotic factor p53 (Du et al., 2014). Moreover, TNF- $\alpha$  reduces EPC proliferation by increasing the phosphorylation of p38 and, consequently, the activation of CREB and cyclin D1 (Seeger et al., 2005).

Aging is also associated with a pro-apoptotic EPC phenotype that is characterized by the decreased expression of key anti-apoptotic proteins and an enhanced susceptibility to pro-apoptotic factors. For example, it has been demonstrated that EPCs obtained from healthy aged men exhibit increased levels

of active caspase-3, which is an important enzyme involved in apoptosis, when compared with EPCs from younger patients (Kushner et al., 2011).

Finally, as indicated throughout this review, after any kind of injury, such as CVD or stroke, there is an increase in the release of factors that promote both the proliferation and migration of EPCs to the site of injury. These factors include VEGF and SDF-1, which are produced throughout the stabilization of intracellular hypoxia-inducible factor 1-alpha (HIF-1 $\alpha$ ) in response to hypoxic conditions. In fact, one of the age-related effects resulting in decreased EPC recruitment is the increase in the degradation of HIF-1 $\alpha$ , which indirectly reduces the levels of VEGF and SDF-1 (Chang et al., 2007). A summary of selected publications on aging and EPCs function can be found in Table 1.

**3.2. Cardiovascular risk factors**

CVD is one of the leading causes of death in many parts of the world. CVD is also a recognized age-dependent condition whose incidence is increased due to a longer life expectancy and by the combination of several factors, known as cardiovascular risk factors (CVRFs), including tobacco use, physical inactivity, hypertension, elevated low-density lipoprotein cholesterol, atherosclerosis, and a cluster of interrelated metabolic risk factors. All these factors have been shown to produce endothelial damage, which could be resolved by the action of EPCs; however, unfortunately, CVRFs also produce EPC dysfunction. One of the consequences of smoking is a higher level of oxidative stress and, as previously mentioned, an increase in the production of ROS inhibits proliferation and mobilization of EPCs, and promotes the apoptosis of EPCs. In fact, it has been demonstrated that there is a 50% reduction in the number of EPCs in smokers compared to controls (Michaud et al., 2006).

Regarding another CVRF, physical inactivity, it has

been shown that physical exercise results in increased NO production, which has been shown to be related to increased EPC mobilization. In a study evaluating the effect of physical exercise on EPCs from patients with stable coronary artery disease, a higher number of circulating EPCs and reduced apoptosis on day 28 of physical exercise was reported, compared with the first day. It was also demonstrated that physical exercise increased the number of EPCs in the BM and peripheral blood due to the upregulation of NO and VEGF (Laufs et al., 2004).

Hypercholesterolemia is a major risk factor for atherosclerosis, and both conditions appear to be significantly correlated with endothelial damage. It has been shown that patients with hypercholesterolemia with high levels of oxidized low-density lipoprotein (oxLDL) exhibit a reduction in the number of EPCs, as these oxLDL are uptaken by EPCs, which generates oxidative stress and can therefore lead to apoptosis of these stem cells (Tie et al., 2010).

**3.3. Hypertension**

Although hypertension is a CVRF, it is considered separately in this review because it is one of the most prevalent diseases worldwide and is a major risk factor for CVD and stroke. Hypertension, like the other CVRFs, causes damage to the vascular endothelium and requires the protective actions of EPCs. Unfortunately, there are many clinical studies demonstrating that hypertension is the most important independent predictor of EPC functional decline in patients with coronary artery diseases (Vasa et al., 2001; see Table 2). Hypertension has also been associated with alterations in the circulating levels of EPCs, the impairment of their angiogenic properties, and alterations in their gene expression and cellular life span. In an attempt to summarize the effect of hypertension on EPCs from all of these clinical studies, first, the EPC functional decline appears to occur earlier than the reduction

Table 5. Most cited articles regarding the effects of other comorbidities on the biology of EPCs.

	Title	Journal	Main Results	Type of study	Cit.	Ref.
O t h e r  c o m o r b i d i t i e s	Circulating endothelial progenitor cells, vascular function, and cardiovascular risk	New England Journal of Medicine	EPCs from subjects at high risk for cardiovascular events had higher rates of in vitro senescence than cells from subjects at low risk. Levels of EPCs may be a surrogate biologic marker for vascular function and cumulative cardiovascular risk.	Clinical research and Experimental research	2779	Hill et al 2003
	Selective Functional Exhaustion of Hematopoietic Progenitor Cells in the Bone Marrow of Patients With Postinfarction Heart Failure	Journal of the American College of Cardiology	Ischemic cardiomyopathy is associated with selective impairment of progenitor cell function in the bone marrow and in the peripheral blood, which may contribute to an unfavorable left ventricular remodeling process	Clinical research and Experimental research	189	Kissel et al 2007
	p38 mitogen-activated protein kinase downregulates endothelial progenitor cells	Circulation	Incubation with glucose or TNF- $\alpha$ reduces the number of EPCs in vitro through the activation of p38 MAPK, while its inhibition by SB203580 (specific inhibitor of p38) prevents these negative effects.	Clinical research and Experimental research	182	Seeger et al. 2005
	Oxidized low-density lipoprotein induces endothelial progenitor cell senescence, leading to cellular dysfunction	Clinical and Experimental Pharmacology and Physiology	ox-LDL, a potential pro-atherosclerotic lipoprotein, accelerated the onset of EPC senescence, which may be related to telomerase inactivation, and lead to the impairment of their proliferative capacity and network formation in vitro.	Experimental research	169	Imanishi et al 2004
	Circulating CD34-positive cells provide an index of cerebrovascular function	Circulation	There is a strong inverse correlation between numbers of circulating EPCs and cerebral infarction, providing a potential marker of cerebrovascular function.	Clinical research	158	Taguchi et al 2004

**Foot note:** In order to summarize the most relevant publications associating EPC levels and function with other comorbidities different to those shown in tables 1 to 4, a search on Scopus database was undertaken. Keywords included “endothelial progenitor cells”, “EPC”, “comorbidity”, and “comorbidities”. Only original articles were selected. Results were sorted according to the number of citations. The 5 most cited and relevant papers are listed, sorted from the most cited to the less according to Scopus database. Abbreviations: Cit (Citations), Ref (Reference), Endothelial Progenitor Cell (EPC), Tumor Necrosis Factor alpha (TNF- $\alpha$ ), p38 Mitogen-Activated Protein Kinase (p38 MAPK), oxidized Low-Density Lipoprotein (ox-LDL).



in EPC quantity in patients with hypertension. Second, the reduction in both EPC count and EPC function can be restored with antihypertensive treatment. Third, different types of EPCs may be differentially affected in patients with hypertension, i.e., late EPCs undergo more significant declines in their proliferative activity compared with other types of EPCs. Finally, the quantitative and functional decline of EPCs become more pronounced with advanced stages of hypertension, which can be manifested as intractable high blood pressure, increased incidence of adverse vascular events, and severe organ damage (Luo et al., 2016).

There are several possible molecular explanations for these effects of hypertension on EPCs, which are common to the other CVRFs. For example, hypertension is associated with an accumulation of ROS, which causes an increase in apoptosis and senescence of EPCs. ROS also reduce NO availability, causing a reduction in EPC mobilization. Hypertension leads to a chronic increase in inflammatory molecules, such as TNF- $\alpha$  and interferon gamma (INF- $\gamma$ , leading to a decrease in EPC proliferation, migration, and reparative functions (Luo et al., 2016).

### 3.4. Obesity and diabetes

Obesity is a widespread, increasingly prevalent disease with a crucial role in the development of endothelial dysfunction. Obesity is also associated with several comorbidities, including chronic inflammation, lipid metabolic disorder, accelerated atherosclerosis, increased risk for thrombosis, hypertension, hyperinsulinemia, insulin resistance, and type 2 diabetes mellitus, all of which can trigger CVD and stroke.

Endothelial dysfunction caused by obesity also requires the actions of EPCs to replace and regenerate the body vasculature (see highlighted publications summarized in Table 3). However, as with the other comorbidities, obesity affects the reparative functions of EPCs. In fact, in an experimental model of murine obesity, a reduced number of circulating EPCs with impaired functions were observed (Tsai et al. 2012). These experimental data have also been confirmed clinically; for example, a reduced number of circulating EPCs were shown in obese men with metabolic syndrome (MS) compared with lean men without MS (Westerweel et al., 2008). In another clinical study performed on obese subjects without diabetes or CVD, patients not only exhibited a decreased number of circulating EPCs but also an impaired functionality of these stem cells, compared to control subjects (Jialal et al., 2010). However, if this comorbidity is treated, as was shown in an interesting clinical study performed by Heida and colleagues in 2010, the poor pro-angiogenic properties of EPCs isolated from obese patients can be recovered after 6 months of weight loss therapy (Heida et al., 2010).

There are many molecular mechanisms through which obesity impairs EPC functions. One of the main consequences of obesity is the induction of chronic inflammation, a process that is also involved in the production of oxidative stress in many tissues, including the endothelium and the BM. As explained above, both mechanisms are implicated in EPC apoptosis and senescence, for example, by altering the expression of various cyclins, which are important regulators of the cellular cycle (Tobler et al., 2010). EPCs from obese patients have been shown to exhibit a decreased response to growth factors, such as VEGF and SDF-1, and a reduced paracrine potency, as they release reduced amounts of pro-angiogenic molecules such as IL-8 and monocyte chemoattractant protein-1 (MCP-1). Such alterations are, in part, prevented by inhibiting the MAP-kinase pathway (Heida et al., 2010).

As mentioned repeatedly throughout this review, the reparative actions of EPCs are very important in pathologies such as CVD and stroke. A clinical study performed on patients

with CVD with and without MS demonstrated that, although there was an increased number of EPCs in CVD patients with MS when compared with patients without MS, interestingly, increased oxidative DNA damage, decreased telomerase activity, and decreased telomere length, a marker of increased senescence in EPCs, were observed in CVD patients with MS in comparison with the CVD patients without MS (Satoh et al., 2008). In the stroke field, it has been demonstrated that an increase in circulating EPCs after acute ischemic stroke is associated with good functional outcomes and reduced infarcts, even if patients have large-artery atherosclerosis and small-vessel disease (Marti-Fabregas et al., 2013; Sobrino et al., 2007). In this context, data from our research on aged and obese rats subjected to cerebral ischemia suggest a reduction in the circulating levels of EPCs, poorer pro-angiogenic properties *in vitro*, a reduction in the plasma levels of SDF-1, a worse post-stroke angiogenesis, and a worse functional recovery compared to aged lean animals (Pradillo et al., unpublished).

Diabetes, which is another CVRF, is a disease with increasing incidence in all societies. In most cases, diabetes develops as a consequence of obesity or MS. Diabetes is a complex metabolic disorder that is characterized by impaired glucose metabolism with hyperglycemia and alterations in the induction of endothelial damage with micro- or macro-vascular consequences, such as retinopathy, nephropathy, and accelerated atherosclerosis. A decrease in NO production by eNOS plays a critical role in the development and progression of endothelial damage and atherosclerosis in diabetes. Clinical studies have reported that EPCs are markedly reduced in patients with either type 1 or type 2 diabetes, and EPCs from diabetic patients also exhibit a reduced capacity to induce angiogenesis *in vitro* (Tepper et al., 2002). Likewise, impaired post-ischemic EPC mobilization in diabetic animals has been previously demonstrated (Fadini et al., 2006; Huang et al., 2010).

Several primary mechanisms have been proposed to explain the reduced number and dysfunction of EPCs that are associated with impaired glucose metabolism and diabetes. These mechanisms are inflammation, oxidative stress, reduced release of chemo-attracting factors, and reduction of NO. EPCs are first affected by diabetes in regard to their proliferation/mobilization from the BM. Both experimental and human studies have demonstrated eNOS dysfunction and reduced SDF-1 $\alpha$  levels in the BM, both of which result in decreased EPC proliferation/mobilization from their niche (Fadini et al., 2013; Gallagher et al., 2007). The second level of by which diabetes affects EPC is by impairing EPC trafficking to the injured/ischemic area and their survival. In this setting, it has been shown that diabetes alters the cytokine gradient, reduces the VEGF and SDF-1 $\alpha$  levels, decreases NO production, and increases the ROS levels and glycation end products, which are mechanisms involved in the diabetes-related EPC migration and survival effects. Finally, another level of influence by this disease is the process of EPC homing to the site of injury. For example, in this step, the local release of factors such as VEGF or SDF-1 $\alpha$  is very important. In patients with diabetes, the high-glucose environment reduces the secretion levels of these factors from endothelial cells through mechanisms such as an increased degradation of the HIF-1 $\alpha$  factor, which is the main transcription factor involved in the synthesis of the homing factors (Yiu and Tse, 2014). Table 4 highlights the findings of relevant publications demonstrating the negative effects of diabetes on EPCs.

### 4. Conclusions and Future Perspectives.

As discussed, EPCs are progenitor cells found in adult subjects under physiological conditions, which respond to injury signals and hypoxic conditions by primarily contributing to vessel repair, angiogenesis, and vasculogenesis. Current literature highlights the importance of EPCs in maintaining a healthy

vascular system, but has also shown strong evidence relating comorbid conditions such as hypertension, obesity and diabetes (strongly associated with CVDs), and aging, with EPCs decline and malfunction. These impaired abilities include reduced mobilization from the BM, smaller pools of circulating cells, decreased proliferation, altered endothelial functions, or declined paracrine potency. The good news is that some of these aberrant malfunctions of EPCs can be improved when the pathological conditions are reversed (e.g. with healthy diet, reduced glucose levels, or drug treatments such as statins), demonstrating that these cells might become future therapeutic targets to improve vascular health to prevent the manifestation of CVDs. Finally, beyond the importance of those negative conditioning aspects in the context of CVDs, we should not forget the impact that they could also display in neurological diseases where the vascular crosstalk with other brain cells and the extracellular matrix is known to participate in disease progression or recovery.

### Acknowledgments

A. G. holds a predoctoral fellowship (FI17/00073) and A.R. is supported by the Miguel Servet program (CPII15/00003), both from Instituto de Salud Carlos III. This research has been funded with research grants from Fundació La Marató de TV3 (agreement 201731), SGR 2017/1427 from the Generalitat de Catalunya (AGAUR), S2017/BMD-3688 and M+Vision Fellowship from Comunidad de Madrid, and the PI16/00981 and PI17/01601, AC17/00004 and the INVICTUS RD16/0019/0021 and RD16/0019/0009 grants from the Instituto de Salud Carlos III, Spain, co-financed by the European Regional Development Fund. AC17/00004 is also part of the Euronanomed III funded Project MAGBBRIS.

### References

- Abdelmagid SM, Barbe MF, Safadi FF (2015) Role of inflammation in the aging bones. *Life Sci* 123:25-34.
- Asahara T, Murohara T, Sullivan A, Silver M, van der Zee R, Li T, Witzenbichler B, Schatteman G, Isner JM (1997) Isolation of Putative Progenitor Endothelial Cells for Angiogenesis. *Science* 275: 964–966.
- Bao Q, Pan J, Qi H, Qian H, Jiang F, Shao Z, Xu F, Tao Z, Ma Q, Nelson P, Hu X (2014) Aging and age-related diseases—from endocrine therapy to target therapy. *Mol Cell Endocrinol* 394:115-118.
- Beaglehole R (2001) Global cardiovascular disease prevention: time to get serious. *358*: 661-663.
- Bellows CF, Zhang Y, Simmons PJ, Khalsa AS, Kolonin MG (2011) Influence of BMI on level of circulating progenitor cells. *Obesity (Silver Spring)* 19:1722-1726.
- Banerjee S, Bentley P, Hamady M, Marley S, Davis J, Shlebak A, Nicholls J, Williamson DA, Jensen SL, Gordon M, Habib N, Chataway J (2014) Intra-Arterial Immunoselected CD34<sup>+</sup> Stem Cells for Acute Ischemic Stroke. *Stem Cells Transl Med* 3: 1322–1330.
- Carmichael ST (2008) Themes and strategies for studying the biology of stroke recovery in the poststroke epoch (*Stroke*) 39:1380-1388.
- Chang EI, Loh SA, Ceradini DJ, Lin SE, Bastidas N, Aarabi S, Chan DA, Freedman ML, Giaccia AJ, Gurtner GC (2007) Age decreases endothelial progenitor cell recruitment through decreases in hypoxia-inducible factor 1alpha stabilization during ischemia. *Circulation* 116:2818-2829.
- Di Santo S, Yang Z, Wyler von Ballmoos M, Voelzmann J, Diehm N, Baumgartner I, Kalka C (2009) Novel Cell-Free Strategy for Therapeutic Angiogenesis: *In Vitro* Generated Conditioned Medium Can Replace Progenitor Cell Transplantation. *PLoS One* 4: e5643.
- Du G, Song Y, Zhang T, Ma L, Bian N, Chen X, Feng J, Chang Q, Li Z (2014) Simvastatin attenuates TNFalpha-induced apoptosis in endothelial progenitor cells via the upregulation of SIRT1. *Int J Mol Med* 34:177-182.
- Esquiva G, Grayston A, Rosell A (2018) Revascularization and Endothelial Progenitor Cells in Stroke. *Am J Physiol Cell Physiol* 2018 Aug 22. doi: 10.1152/ajpcell.00200.2018. [Epub ahead of print].
- Fadini GP, Miorin M, Facco M, Bonamico S, Baesso I, Grego F, Menegolo M, de Kreutzenberg SV, Tiengo A, Agostini C, Avogaro A (2005) Circulating endothelial progenitor cells are reduced in peripheral vascular complications of type 2 diabetes mellitus. *J Am Coll Cardiol* 45:1449-1457.
- Fadini GP, Sartore S, Schiavon M, Albiero M, Baesso I, Cabrelle A, Agostini C, Avogaro A (2006) Diabetes impairs progenitor cell mobilisation after hindlimb ischaemia-reperfusion injury in rats. *Diabetologia* 49:3075-3084.
- Fadini GP, Sartore S, Albiero M, Baesso I, Murphy E, Menegolo M, Grego F, Vigili de Kreutzenberg S, Tiengo A, Agostini C, Avogaro A (2006) Number and function of endothelial progenitor cells as a marker of severity for diabetic vasculopathy. *Arterioscler Thromb Vasc Biol* 26:2140-2146.
- Fadini GP, Losordo D, Dimmerler S (2012) Critical re-evaluation of endothelial progenitor cell phenotypes for therapeutic and diagnostic use. *Circ Res* 110: 624–637.
- Fadini GP, Albiero M, Vigili de Kreutzenberg S, Boscaro E, Cappellari R, Marescotti M, Poncina N, Agostini C, Avogaro A (2013) Diabetes impairs stem cell and proangiogenic cell mobilization in humans. *Diabetes Care* 36:943-949.
- Fisher M, Feuerstein G, Howells DW, Hurn PD, Kent TA, Savitz SI, Lo EH; STAIR Group (2009) Update of the stroke therapy academic industry roundtable preclinical recommendations. *Stroke* 40:2244-50.
- Gabriel-Salazar M, Morancho A, Rodriguez S, Buxó X, García-Rodríguez N, García-Rodríguez N, Colell G, Fernandez A, Giralt D, Bustamante A, Montaner J, Rosell A (2018) Importance of Angiogenin and Endothelial Progenitor Cells After Rehabilitation Both in Ischemic Stroke Patients and in a Mouse Model of Cerebral Ischemia. *Front Neurol* 9:508.
- Gallagher KA, Liu ZJ, Xiao M, Chen H, Goldstein LJ, Buerk DG, Nedeau A, Thom SR, Velazquez OC (2007) Diabetic impairments in NO-mediated endothelial progenitor cell mobilization and homing are reversed by hyperoxia and SDF-1 alpha. *J Clin Invest* 117:1249-1259.
- Giannotti G, Doerries C, Mocharla PS, Mueller MF, Bahlmann FH, Horváth T, Jiang H, Sorrentino SA, Steenken N, Manes C, Marzilli M, Rudolph KL, Lüscher TF, Drexler H, Landmesser U (2010) Impaired endothelial repair capacity of early endothelial progenitor cells in prehypertension: relation to endothelial dysfunction. *Hypertension* 55:1389-1397.
- Gilleece MH, Dexter TM (1993) The biological aging of bone marrow. *Rev Clin Gerontol* 3:317–325.
- Gulati R, Jevremovic D, Peterson TE, Chatterjee S, Shah V, Vile RG, Simari RD (2003) Diverse Origin and Function of Cells with Endothelial Phenotype Obtained from Adult Human Blood. *Circ Res* 93: 1023–1025.
- Hacke W, Kaste M, Bluhmki E, Brozman M, Dávalos A, Guidetti D, Larrue V, Lees KR, Medeghri Z, Machnig T, Schneider D, von Kummer R, Wahlgren N, Toni D; ECASS Investigators (2005) Thrombolysis with Alteplase 3 to 4.5 Hours after Acute Ischemic Stroke. *Clin Trials* 359:1317–1329.
- Heida NM, Muller JP, Cheng IF, Leifheit-Nestler M, Faustin V, Riggert J, Hasenfuss G, Konstantinides S, Schäfer K

- (2010) Effects of obesity and weight loss on the functional properties of early outgrowth endothelial progenitor cells. *J Am Coll Cardiol* 55:357-367.
- Herrera MD, Mingorance C, Rodriguez-Rodriguez R, Alvarez de Sotomayor M (2010) Endothelial dysfunction and aging: an update. *Ageing Res Rev* 9:142-152.
- Hill JM, Zalos G, Halcox JP, Schenke WH, Waclawiw MA, Quyyumi AA, Finkel T (2003) Circulating endothelial progenitor cells, vascular function, and cardiovascular risk. *N Engl J Med* 348:593-600.
- Hoetzer GL, Van Guilder GP, Irmiger HM, Keith RS, Stauffer BL, DeSouza CA (1985) Aging, exercise, and endothelial progenitor cell clonogenic and migratory capacity in men. *J Appl Physiol* 102:847-852.
- Huang PH, Tsai HY, Wang CH, Chen YH, Chen JS, Lin FY, Lin CP, Wu TC, Sata M, Chen JW, Lin SJ (2010) Moderate intake of red wine improves ischemia-induced neovascularization in diabetic mice-roles of endothelial progenitor cells and nitric oxide. *Atherosclerosis* 212:426-435.
- Hur J, Yoon CH, Kim HS, Choi JH, Kang HJ, Hwang KK, Oh BH, Lee MM, Park YB (2004) Characterization of Two Types of Endothelial Progenitor Cells and Their Different Contributions to Neovascularization. *Arterioscler Thromb Vasc Biol* 24: 288–293.
- Imanishi T, Hano T, Sawamura T, Nishio I (2004) Oxidized low-density lipoprotein induces endothelial progenitor cell senescence, leading to cellular dysfunction. *Clin Exp Pharmacol Physiol* 31:407-413.
- Imanishi T, Moriwaki C, Hano T, Nishio I (2005) Endothelial progenitor cell senescence is accelerated in both experimental hypertensive rats and patients with essential hypertension. *J Hypertens* 23:1831-1837.
- Imanishi T, Hano T, Nishio I (2005) Estrogen reduces endothelial progenitor cell senescence through augmentation of telomerase activity. *J Hypertens* 23:1699-1706.
- Jialal I, Devaraj S, Singh U, Huet BA (2010) Decreased number and impaired functionality of endothelial progenitor cells in subjects with metabolic syndrome: implications for increased cardiovascular risk. *Atherosclerosis* 211:297-302.
- Jin K, Wang X, Xie L, Mao XO, Zhu W, Wang Y, Shen J, Mao Y, Banwait S, Greenberg DA (2006) Evidence for stroke-induced neurogenesis in the human brain. *Proc Natl Acad Sci U S A* 103:13198-13202.
- Kahle MP, Bix GJ. Successfully Climbing the "STAIRs": Surmounting Failed Translation of Experimental Ischemic Stroke Treatments (2012) *Stroke Res Treat* 2012:374098.
- Kim JY, Song SH, Kim KL, Ko JJ, Im JE, Yie SW, Ahn YK, Kim DK, Suh W (2010) Human cord blood-derived endothelial progenitor cells and their conditioned media exhibit therapeutic equivalence for diabetic wound healing. *Cell Transplant* 19:1635-1644.
- Kissel CK, Lehmann R, Assmus B, Aicher A, Honold J, Fischer-Rasokat U, Heeschen C, Spyridopoulos I, Dimmeler S, Zeiher AM (2007) Selective functional exhaustion of hematopoietic progenitor cells in the bone marrow of patients with postinfarction heart failure. *J Am Coll Cardiol* 49:2341-2349.
- Kushner EJ, MacEneaney OJ, Weil BR, Greiner JJ, Stauffer BL, DeSouza CA (2011) Aging is associated with a proapoptotic endothelial progenitor cell phenotype. *J Vasc Res* 48:408-414.
- Kushner EJ, Van Guilder GP, Maceneaney OJ, Cech JN, Stauffer BL, DeSouza CA (2009) Aging and endothelial progenitor cell telomere length in healthy men. *Clin Chem Lab Med* 47:47-50.
- Laufs U, Werner N, Link A, Endres M, Wassmann S, Jürgens K, Miche E, Böhm M, Nickenig G (2004) Physical training increases endothelial progenitor cells, inhibits neointima formation, and enhances angiogenesis. *Circulation* 109:220-226.
- Leslie WD, Rubin MR, Schwartz AV, Kanis JA (2012) Type 2 diabetes and bone. *J Bone Miner Res* 27:2231-2237.
- Liman TG, Endres M (2012) New vessels after stroke: Postischemic neovascularization and regeneration. *Cerebrovasc Dis* 33: 492–499.
- Lo EH (2008) A new penumbra: transitioning from injury into repair after stroke. *Nat Med* 14:497-500.
- Loomans CJ, de Koning EJ, Staal FJ, Rookmaaker MB, Verseyden C, de Boer HC, Verhaar MC, Braam B, Rabelink TJ, van Zonneveld AJ (2004) Endothelial progenitor cell dysfunction: a novel concept in the pathogenesis of vascular complications of type 1 diabetes. *Diabetes* 53:195-159.
- Luo S, Xia W, Chen C, Robinson EA, Tao J (2016) Endothelial progenitor cells and hypertension: current concepts and future implications. *Clin Sci (Lond)* 130:2029-2042.
- Ma F, Morancho A, Montaner J, Rosell A (2015) Endothelial progenitor cells and revascularization following stroke. *Brain Res* 1623: 150–159.
- Maki T, Morancho A, Martinez-San Segundo P, Hayakawa K, Takase H, Liang AC, Gabriel-Salazar M, Medina-Gutiérrez E, Washida K, Montaner J, Lok J, Lo EH, Arai K, Rosell A (2018) Endothelial Progenitor Cell Secretome and Oligovascular Repair in a Mouse Model of Prolonged Cerebral Hypoperfusion. *Stroke* 49:1003-1010.
- Mao L, Huang M, Chen SC, Li YN, Xia YP, He QW, Wang MD, Huang Y, Zheng L, Hu B (2014) Endogenous endothelial progenitor cells participate in neovascularization via CXCR4/ SDF-1 axis and improve outcome after stroke. *CNS Neurosci Ther* 20: 460–468.
- Marti-Fabregas J, Crespo J, Delgado-Mederos R, Martinez-Ramirez S, Peña E, Marín R, Diniá L, Jiménez-Xarrié E, Fernández-Arcos A, Pérez-Pérez J, Querol L, Suárez-Calvet M, Badimon L (2013) Endothelial progenitor cells in acute ischemic stroke. *Brain Behav* 3:649-655.
- Massot A, Navarro-Sobrino M, Penalba A, Arenillas JF, Giralt D, Ribó M, Molina CA, Alvarez-Sabín J, Montaner J, Rosell A (2013) Decreased levels of angiogenic growth factors in intracranial atherosclerotic disease despite severity-related increase in endothelial progenitor cell counts. *Cerebrovasc Dis* 35: 81–88.
- Medina RJ, Barber CL, Sabatier F, Dignat-George F, Melero-Martin JM, Khosrotehrani K, Ohneda O, Randi AM, Chan JKY, Yamaguchi T, Van Hinsbergh VWM, Yoder MC, Stitt AW (2017) Endothelial Progenitors: A Consensus Statement on Nomenclature. *Stem Cells Transl Med* 6: 1316–1320.
- Michaud SE, Dussault S, Haddad P, Groleau J, Rivard A (2006) Circulating endothelial progenitor cells from healthy smokers exhibit impaired functional activities. *Atherosclerosis* 187:423-432.
- Miyamoto N, Pham LD, Seo JH, Kim KW, Lo EH, Arai K (2014) Crosstalk between cerebral endothelium and oligodendrocyte. *Cell Mol Life Sci* 71:1055-1066.
- Müller-Ehmsen J, Braun D, Schneider T, Pfister R, Worm N, Wielckens K, Scheid C, Frommolt P, Flesch M (2008) Decreased number of circulating progenitor cells in obesity: beneficial effects of weight reduction. *Eur Heart J* 29:1560-1568.
- Navarro-Sobrino M, Rosell A, Hernandez-Guillamon M, Penalba A, Ribó M, Alvarez-Sabín J, Montaner J (2010) Mobilization, endothelial differentiation and functional capacity of endothelial progenitor cells after ischemic

- stroke. *Microvasc Res* 80:317–323.
- Nogueira RG, et al. (2017) Thrombectomy 6 to 24 Hours after Stroke with a Mismatch between Deficit and Infarct. *N Engl J Med* 378:11–3721.
- Ohab JJ, Fleming S, Blesch A, Carmichael ST (2006) A neurovascular niche for neurogenesis after stroke. *J Neurosci* 26:13007–13016.
- Pepper MS (1997) Manipulating angiogenesis: From basic science to the bedside. *Arterioscler Thromb Vasc Biol* 17:605–19.
- Pfeilschifter J, Koditz R, Pfohl M, Schatz H (2002) Changes in proinflammatory cytokine activity after menopause. *Endocr Rev* 23:90–119.
- Pham LD, Hayakawa K, Seo JH, Nguyen MN, Som AT, Lee BJ, Guo S, Kim KW, Lo EH, Arai K (2012) Crosstalk between oligodendrocytes and cerebral endothelium contributes to vascular remodeling after white matter injury. *Glia* 60:875–81.
- Pías-Peleiteiro J, Pérez-Mato M, López-Arias E, Rodríguez-Yáñez M, Blanco M, Campos F, Castillo J, Sobrino T (2016) Increased endothelial progenitor cell levels are associated with good outcome in intracerebral hemorrhage. *Sci Rep* 6:28724.
- Reinisch A, Hofmann NA, Obenaus AC, Kashofer K, Rohde E, Schallmoser K, Flicker K, Lanzer G, Linkesch W, Speicher MR, Strunk D (2009) Humanized large-scale expanded endothelial colony-forming cells function *in vitro* and *in vivo*. *Blood* 113:6716–6725.
- Ricci C, Cova M, Kang YS, Yang A, Rahmouni A, Scott WW Jr, Zerhouni EA (1990) Normal age-related patterns of cellular and fatty bone marrow distribution in the axial skeleton: MR imaging study. *Radiology* 177:83–88.
- Rosell A, Morancho A, Navarro-Sobrino M, Martínez-Saez E, Hernández-Guillamon M, Lope-Piedrafita S, Barceló V, Borrás F, Penalba A, García-Bonilla L, Montaner J (2013) Factors Secreted by Endothelial Progenitor Cells Enhance Neurorepair Responses after Cerebral Ischemia in Mice. *PLoS One* 8: e73244.
- Ross MD (2018) Endothelial Regenerative Capacity and Aging: Influence of Diet, Exercise and Obesity. *Curr Cardiol Rev* 14:233–244.
- Rurali E, Bassetti B, Perrucci GL, Zanobini M, Malafronte C, Achilli F, Gambini E (2016) BM ageing: Implication for cell therapy with EPCs. *Mech Ageing Dev* 159:4–13.
- Sargento-Freitas J, Pereira A, Gomes A, Amorim P, Matos T, Cardoso CMP, Silva F, Santo GC, Nunes C, Galego O, Carda J, Branco J, Lourenço V, Cunha L, Ferreira L (2018) STROKE34 Study Protocol: A Randomized Controlled Phase IIa Trial of Intra-Arterial CD34<sup>+</sup> Cells in Acute Ischemic Stroke. *Front Neurol* 9:302.
- Satoh M, Ishikawa Y, Takahashi Y, Itoh T, Minami Y, Nakamura M (2008) Association between oxidative DNA damage and telomere shortening in circulating endothelial progenitor cells obtained from metabolic syndrome patients with coronary artery disease. *Atherosclerosis* 198:347–353.
- Scheubel RJ, Zorn H, Silber RE, Kuss O, Morawietz H, Holtz J, Simm A (2003) Age-dependent depression in circulating endothelial progenitor cells in patients undergoing coronary artery bypass grafting. *J Am Coll Cardiol* 42:2073–2080.
- Seeger FH, Haendeler J, Walter DH, Rochwalsky U, Reinhold J, Urbich C, Rössig L, Corbaz A, Chvatchko Y, Zeiher AM, Dimmeler S (2005) p38 mitogen-activated protein kinase downregulates endothelial progenitor cells. *Circulation* 111:1184–1191.
- Shen Q, Goderie SK, Jin L, Karanth N, Sun Y, Abramova N, Vincent P, Pumiglia K, Temple S (2004) Endothelial cells stimulate self-renewal and expand neurogenesis of neural stem cells. *Science* 304:1338–1340.
- Shibata R, Skurk C, Ouchi N, Galasso G, Kondo K, Ohashi T, Shimano M, Kihara S, Murohara T, Walsh K (2008) Adiponectin promotes endothelial progenitor cell number and function. *FEBS Lett* 582:1607–1612.
- Sobrino T, Hurtado O, Moro MA, Rodríguez-Yanez M, Castellanos M, Brea D, Moldes O, Blanco M, Arenillas JF, Leira R, Dávalos A, Lizasoain I, Castillo J (2007) The increase of circulating endothelial progenitor cells after acute ischemic stroke is associated with good outcome. *Stroke* 38:2759–2764.
- Taguchi A, Mastsuyama T, Moriwaki H, Hayashi T, Hayashida K, Nagatsuka K, Todo K, Mori K, Stern DM, Soma T, Naritomi H (2004) Circulating CD34-positive cells provide an index of cerebrovascular function. *Circulation* 109:2972–2975.
- Takahashi T, Kalka C, Masuda H, Chen D, Silver M, Kearney M, Magner M, Isner JM, Asahara T (1999) Ischemia and cytokine-induced mobilization of bone marrow-derived endothelial progenitor cells for neovascularization. *Nat Med* 5:434–438.
- Tepper OM, Galiano RD, Capla JM, Kalka C, Gagne PJ, Jacobowitz GR, Levine JP, Gurtner GC (2002) Human endothelial progenitor cells from type II diabetics exhibit impaired proliferation, adhesion, and incorporation into vascular structures. *Circulation* 106:2781–2786.
- Thum T, Hoeber S, Froese S, Klink I, Stichtenoth DO, Galuppo P, Jakob M, Tsikas D, Anker SD, Poole-Wilson PA, Borlak J, Ertl G, Bauersachs J (2007) Age-dependent impairment of endothelial progenitor cells is corrected by growth-hormone-mediated increase of insulin-like growth-factor-1. *Circ Res* 100:434–443.
- Tian XL, Li Y (2014) Endothelial cell senescence and age-related vascular diseases. *J Genet Genomics* 41:485–495.
- Tie G, Yan J, Yang Y, Park BD, Messina JA, Raffai RL, Nowicki PT, Messina LM (2010) Oxidized low-density lipoprotein induces apoptosis in endothelial progenitor cells by inactivating the phosphoinositide 3-kinase/Akt pathway. *J Vasc Res* 47:519–530.
- Tobler K, Freudenthaler A, Baumgartner-Parzer SM, Wolzt M, Ludvik B, Nansalmaa E, Nowotny PJ, Seidinger D, Steiner S, Luger A, Artwohl M (2010) Reduction of both number and proliferative activity of human endothelial progenitor cells in obesity. *Int J Obes (Lond)* 34:687–700.
- Tsai TH, Chai HT, Sun CK, Yen CH, Leu S, Chen YL, Chung SY, Ko SF, Chang HW, Wu CJ, Yip HK (2012) Obesity suppresses circulating level and function of endothelial progenitor cells and heart function. *J Transl Med* 10:137.
- Urbich C, Aicher A, Heeschen C, Dernbach E, Hofmann WK, Zeiher AM, Dimmeler S (2005) Soluble factors released by endothelial progenitor cells promote migration of endothelial cells and cardiac resident progenitor cells. *J Mol Cell Cardiol* 39:733–742.
- Urra X, Abilleira S, Dorado L, Ribó M, Cardona P, Millán M, Chamorro A, Molina C, Cobo E, Dávalos A, Jovin TG, Gallofré M; Catalan Stroke Code and Reperfusion Consortium (2015) Mechanical thrombectomy in and outside the REVASCAT trial: Insights from a concurrent population-based stroke registry. *Stroke* 46:3437–3442.
- Vasa M, Fichtlscherer S, Aicher A, Adler K, Urbich C, Martin H, Zeiher AM, Dimmeler S (2001) Number and migratory activity of circulating endothelial progenitor cells inversely correlate with risk factors for coronary artery disease. *Circ Res* 89:E1–7.
- Westerweel PE, Visseren FL, Hajer GR, Olijhoek JK, Hofer IE, de Bree P, Rafii S, Doevendans PA, Verhaar MC (2008) Endothelial progenitor cell levels in obese men

- with the metabolic syndrome and the effect of simvastatin monotherapy vs. simvastatin/ezetimibe combination therapy. *Eur Heart J* 29:2808-2817.
- Widmer RJ, Lerman A (2014) Endothelial dysfunction and cardiovascular disease. *Glob Cardiol Sci Pract.* 2014:291-308.
- Wolk R, Deb A, Caplice NM, Somers VK (2005) Leptin receptor and functional effects of leptin in human endothelial progenitor cells. *Atherosclerosis* 183:131-139.
- Yao EH, Fukuda N, Matsumoto T, Kobayashi N, Katakawa M, Yamamoto C, Tsunemi A, Suzuki R, Ueno T, Matsumoto K (2007) Losartan improves the impaired function of endothelial progenitor cells in hypertension via an antioxidant effect. *Hypertens Res* 30:1119-1128.
- Yiu KH, Tse HF (2014) Specific role of impaired glucose metabolism and diabetes mellitus in endothelial progenitor cell characteristics and function. *Arterioscler Thromb Vasc Biol* 34:1136-1143.
- Yu Y, Fukuda N, Yao EH, Matsumoto T, Kobayashi N, Suzuki R, Tahira Y, Ueno T, Matsumoto K (2008) Effects of an ARB on endothelial progenitor cell function and cardiovascular oxidation in hypertension. *Am J Hypertens* 21:72-77.

**PLGA protein nanocarriers with tailor-made fluorescence /  
MRI / PET imaging modalities**

---

DOI: 10.1039/c9nr10620k





Cite this: DOI: 10.1039/c9nr10620k

## PLGA protein nanocarriers with tailor-made fluorescence/MRI/PET imaging modalities†

Yajie Zhang,<sup>a</sup> Miguel García-Gabilondo,<sup>b</sup> Alba Grayston,<sup>b</sup> Irene V. J. Feiner,<sup>c</sup> Irene Anton-Sales,<sup>d</sup> Rodrigo A. Loiola,<sup>d</sup> Jordi Llop,<sup>c,e</sup> Pedro Ramos-Cabrer,<sup>f,g</sup> Ignasi Barba,<sup>h</sup> David Garcia-Dorado,<sup>‡</sup> Fabien Gosselet,<sup>d</sup> Anna Rosell\*<sup>b</sup> and Anna Roig<sup>id</sup>\*<sup>a</sup>

Designing theranostic nanocarriers with high protein payload and multimodality tracking without cross interferences between the different imaging probes and the delicate protein cargo is challenging. Here, chemical modifications of poly(lactic-co-glycolic acid) (PLGA) to produce nanocapsules (NCs) that incorporate several imaging moieties are reported. The biocompatible and biodegradable PLGA-NCs can be endowed with a magnetic resonance imaging (MRI) reporter, two fluorescence imaging probes (blue/NIR) and a positron emission tomography (PET) reporter. The modular integration of these imaging moieties into the shell of the NCs is successfully achieved without affecting the morphochemical properties of the nanocarrier or the protein loading capacity. *In vivo* biodistribution of the NCs is monitored by MRI, PET and NIRF and the results from different techniques are analyzed comparatively. The viabilities of two different human endothelial cells *in vitro* show no toxicity for NC concentration up to 100  $\mu\text{g mL}^{-1}$ . The morbidity of mice for 2 weeks after systemic administration and the hepatic/pancreatic enzymes at the plasma level indicate their *in vivo* biosafety. In summary, the new theranostic PLGA nanoplatform presented here shows versatile *in vitro/in vivo* multimodal imaging capabilities, excellent biosafety and over 1 wt% protein loading.

Received 16th December 2019,  
Accepted 20th January 2020

DOI: 10.1039/c9nr10620k

rs.c.li/nanoscale

## Introduction

Drug delivery nanocarriers can be extremely advantageous to administer insoluble, sensitive or multi-component drugs by protecting the encapsulated therapeutic molecules from clearance, inactivation or degradation, as well as by reducing poten-

tial toxicity, increasing blood circulation time or tissue specificity.<sup>1–5</sup> Poly(lactic-co-glycolic acid) (PLGA) has demonstrated optimal properties for the encapsulation of a large variety of therapeutic agents and it is extensively employed in nanomedicine.<sup>6,7</sup> Moreover, PLGA-based nanocarriers have been used as drug delivery systems to administer proteins,<sup>8,9</sup> DNA<sup>10</sup> and anticancer drugs among others.<sup>1,11,12</sup> Nonetheless, despite their compositional similarities, any novel PLGA-based drug delivery system will require a thorough evaluation to address potential toxicity issues and study the pharmacokinetics and the pharmacodynamics of each specific carrier. Such preclinical *in vitro* and *in vivo* studies, comprising multiple biological characterization phases, could be expedited by endowing the carrier with complementary imaging capacities. For instance, *in vitro* cellular uptake can be easily imaged with fluorescence<sup>13,14</sup> while radioimaging<sup>15,16</sup> or near infrared (NIR) imaging<sup>1,17</sup> are well suited for *in vivo* biodistribution studies. However, the simultaneous incorporation of all these imaging probes into a single nanocarrier unnecessarily increases the complexity of the system, potentially limiting translation to the clinics. Moreover, any additional component of the theranostic carrier will have an enormous impact on the manufacturing process, production cost and in complying with the medical regulations. In this sense, a drug delivery nanocarrier easily

<sup>a</sup>Institut de Ciència de Materials de Barcelona (ICMAB-CSIC), 08193 BellaterraCatalonia, Spain. E-mail: anna.roig@csic.es

<sup>b</sup>Neurovascular Research Laboratory, Vall d'Hebron Institut de Recerca, Universitat Autònoma de Barcelona, 08035 BarcelonaCatalonia, Spain. E-mail: anna.rosell@vhir.org

<sup>c</sup>Radiochemistry and Nuclear Imaging Group, CIC biomaGUNE, Basque Research and Technology Alliance (BRTA), 20014 San Sebastian, Guipúzcoa, Spain

<sup>d</sup>University of Artois, Blood-Brain Barrier Laboratory (BBB Lab), UR2465, F-62300 Lens, France

<sup>e</sup>CIBERES, Centro de Investigación Biomédica en Red, 28029 Madrid, Spain

<sup>f</sup>Magnetic Resonance Imaging Laboratory, CIC biomaGUNE, Basque Research and Technology Alliance (BRTA), 20014 San Sebastian, Guipúzcoa, Spain

<sup>g</sup>Ikerbasque, Basque Foundation for Science, 48013 Bilbao, Spain

<sup>h</sup>Cardiovascular Diseases Research Group, Vall d'Hebron University Hospital and Research Institute, Universitat Autònoma de Barcelona, 08035 Barcelona, Spain

†Electronic supplementary information (ESI) available. See DOI: 10.1039/c9nr10620k

‡In memory of our colleague Dr Garcia-Dorado who passed away on August 16th 2019.





adaptable to incorporate one or several imaging moieties in a modular approach can be a smart strategy to guide the carrier preclinical development while guaranteeing that a simpler formula is used for the final product. However, this strategy is suitable only when the inclusion or removal of the imaging probes do not affect the size, shape and main compositional traits of the final carrier.

Furthermore, conventional approaches to physically blend imaging probes within the carrier can lead to incomplete conclusions or misinterpretations on the carrier's biodistribution.<sup>18,19</sup> For example, loading two different molecules as probes into the same carrier led to opposite conclusions regarding the kinetics of brain-specific delivery.<sup>19</sup> A growing body of evidence suggests that new methods will be required to monitor nanocarriers' biodistribution avoiding interference of the imaging moieties with the encapsulated drug or leaching of the imaging probes.<sup>19,20</sup>

Here, we report on PLGA nanocapsules (NCs) as a multimodal theranostic platform for *in vivo* drug delivery. We describe the chemical synthetic routes to covalently label the PLGA with biocompatible small molecule fluorophores or radioligands. It involves the fabrication of PLGA NCs integrating several moieties for their *in vitro* and *in vivo* imaging. Specifically, superparamagnetic iron oxide nanoparticles (SPIONs) enabled magnetic resonance imaging (MRI), fluorescence imaging at different emitting wavelengths (blue and NIR) and <sup>89</sup>Zr-labeling enabled positron emission tomography (PET) imaging. We show that the morphology and size of PLGA NCs are not altered by either the incorporation or the removal of one of the several imaging probes. In all cases, the imaging moieties are chemically attached to the PLGA shell matrix as opposed to being entrapped in the core of the nanocapsule.<sup>13–15,17</sup> This approach is advantageous to avoid interferences of the imaging moieties with the cargo in the core.<sup>21</sup> This is especially important for delicate payloads such as proteins, enzymes or microRNAs. For this, we have used bovine serum albumin (BSA) as a model protein to evaluate the protein loading capability.

## Experimental section

All reagents were purchased from Sigma Aldrich unless otherwise specified. The Ethics Committee of Animal Experimentation of the Vall d'Hebron Research Institute approved all experimental animal procedures (protocol number 70.18), which were performed in accordance with the Spanish legislation and the Directives of the European Union. Experiments performed at CIC biomaGUNE were approved by the Ethical Committee of the Institution and by the corresponding authorities (Departamento de Promoción Económica, Turismo y Medio Rural, Diputación Foral de Guipúzcoa; project codes PRO-AE-SS-059 and PRO-AE-SS-067).

### Modification and functionalization of the commercial PLGA

**Synthesis of -NH<sub>2</sub> terminated PLGA (PLGA-NH<sub>2</sub>).** In order to introduce a terminal amine group into PLGA, the carboxylic

acid terminal group of PLGA (lactic:glycolic ratio 50:50, RG502H, *M<sub>w</sub>* 12 000) was activated and reacted with ethylenediamine. The carboxylic groups were firstly activated with *N,N'*-dicyclohexylcarbodiimide (DCC) and *N*-hydroxysuccinimide (NHS). 0.025 mmol of PLGA was dissolved in 8 ml of dichloromethane (DCM), and then 0.1 mmol of DCC in 1 mL of DCM and 0.1 mmol of NHS in 0.5 mL of acetone were added into the polymer solution under magnetic stirring. PLGA-NHS activation was achieved after 4 h at room temperature (RT). The coupling reaction was accomplished by adding an excess amount of ethylenediamine (0.15 mmol) in 1 mL of DCM to the solution and further stirring for 2 h. The majority of the insoluble by-product, dicyclohexylurea, was removed by centrifuging the solution after reaction at 9391 rcf for 15 min at 4 °C and discarding the pellet. The supernatant was filtered (0.2 μm PTFE syringe filter) to remove any trace of the insoluble by-product. PLGA-NH<sub>2</sub> was precipitated by slowly pouring the supernatant into an excess amount of ethanol (10-fold), where the un-reacted NHS/DCC/ethylenediamine was separated from PLGA-NH<sub>2</sub> due to their solubility in ethanol. Precipitated PLGA-NH<sub>2</sub> was redissolved in DCM and reprecipitated in ethanol twice for purification. The purified PLGA-NH<sub>2</sub> was dried under vacuum.

**Synthesis of fluorophore terminated PLGA using fluorescamine (PLGA-fluoram).** Fluorescamine (fluoram) is a non-fluorescent compound that reacts with primary amines (R-NH<sub>2</sub>) fast and near completely forming the fluorophore of fluoram derivative which emits strong fluorescence at λ<sub>em</sub> = 465 nm (λ<sub>ex</sub> = 390 nm).<sup>22</sup> 0.025 mmol of the as-synthesized PLGA-NH<sub>2</sub> and 0.075 mmol of fluoram were mixed and dissolved in 4 mL of acetone and the reaction took place in a dark room after 2 h at RT under magnetic stirring. Then the solution was slowly dropped into an excess amount of ethanol (10-fold) to precipitate the product PLGA-fluoram. The PLGA-fluoram was collected by centrifugation, redissolved in acetone and reprecipitated in ethanol twice for purification. The purified PLGA-fluoram was dried under vacuum.

**Synthesis of fluorophore terminated PLGA using Cy7.5 (PLGA-Cy7.5).** NIR fluorophore cyanine7.5 (λ<sub>em</sub> = 808 nm, λ<sub>ex</sub> = 788 nm) was introduced at the end of PLGA-NH<sub>2</sub> by forming an amide bond between the PLGA terminal amine group and amine reactive Cy7.5 NHS ester (Lumiprobe GmbH, Hannover, Germany). 0.025 mmol of the as-synthesized PLGA-NH<sub>2</sub> and 0.05 mmol of Cy7.5 NHS ester were mixed and dissolved in 4 mL of acetone and 0.05 mmol of Et<sub>3</sub>N were added as the catalyst. The reaction took place in the dark after 6 h at RT under magnetic stirring. Then the solution was slowly poured into an excess amount of ethanol (10-fold) to precipitate PLGA-Cy7.5. The product was collected by centrifugation, redissolved in acetone and precipitated in ethanol twice for purification. The purified PLGA-Cy7.5 was dried under vacuum.

**Synthesis of DFO terminated PLGA (PLGA-DFO).** <sup>89</sup>Zr chelator deferoxamine (DFO) was introduced at the terminal amine of PLGA-NH<sub>2</sub> by forming a thiocarbamide bond between the PLGA terminal amine group and amine reactive p-NCS-Bz-DFO



(CheMatech, Dijon, France). 0.025 mmol of the as-synthesized PLGA-NH<sub>2</sub> and 0.05 mmol of p-NCS-Bz-DFO ester were mixed and dissolved in 4 mL of DMSO and 0.05 mmol of Et<sub>3</sub>N were added as the catalyst. The reaction was accomplished after 12 h at RT under magnetic stirring. Then the DMSO solution was mixed with 2-fold DCM and slowly dropped into 10-fold diethyl ether to precipitate PLGA-DFO and unreacted p-NCS-Bz-DFO, which were collected by centrifugation at 9391 rcf for 10 min. The PLGA-DFO/p-NCS-Bz-DFO mixture pellet was dissolved in 1.5 mL of DCM and centrifuged at 13 171 rcf for 60 min to remove the insoluble p-NCS-Bz-DFO. The supernatant was further filtered (0.2 μm PTFE syringe filter) to remove the traces of p-NCS-Bz-DFO. Finally PLGA-DFO was precipitated by slowly dropping the supernatant into 10-fold diethyl ether, collected by centrifugation and dried under vacuum.

### Synthesis of SPIONs coated with oleic acid (OA-SPIONs)

SPIONs were synthesized through a microwave assisted thermal decomposition in a microwave oven (Discover SP, CEM Corporation) at a frequency of 2.45 GHz and 300 W of power and then coated with oleic acid (OA).<sup>23</sup> Briefly, the process to obtain homogeneous OA-SPIONs with an average diameter of 9 nm was as follows. In a microwave reaction glass tube 3.5 mmol of iron precursor Fe(acac)<sub>3</sub> was dissolved in 4.5 mL of benzyl alcohol. The tube was closed and microwave irradiation occurred with the power set at 300 W. The solution was kept at 60 °C for 5 min to fully dissolve the precursor and subsequently heated to 210 °C and kept at this temperature for 30 min and then cooled down to room temperature. After the reaction, a black colored dispersion formed which suggested the formation of a magnetic material. Then 3.17 mmol of oleic acid in 4 mL of toluene was added to the product dispersion and sonicated for 1 h. Then 5-fold of acetone was added followed by centrifugation to sediment the product pellet. The pellet was redispersed in 4 mL of toluene and transferred into a glass vial, a magnet was attached on the wall and after 5 s the suspension containing SPIONs with smaller size and lower magnetization was discarded. Then the pellet was redispersed in 6 mL of DCM followed by centrifugation at 1075 rcf for 5 min to sediment the unstable big particles. The OA-SPIONs of 9 nm stable in DCM were precipitated by adding 5-fold acetone and centrifugation. The final black product was dried under vacuum and redispersed in DCM at the concentration required for use.

### Fabrication of PLGA-based NCs and encapsulation of BSA

BSA encapsulated PLGA-based NCs were prepared by the double emulsion solvent evaporation method. Briefly, 50 μL of the inner aqueous phase (W<sub>1</sub>) containing BSA (30 mg mL<sup>-1</sup>) was emulsified in 500 μL of DCM organic phase (O) composed of 50 mg of different proportions of PLGA/functional PLGA and a certain amount of OA-SPIONs by sonication at 200 W for 28 s (VC505, Sonics & Materials, Inc., USA) to form the first emulsion (W<sub>1</sub>/O). Then 2 mL of external aqueous phase (W<sub>2</sub>) with PVA (20 mg mL<sup>-1</sup>) was added and the second emulsion

(W<sub>1</sub>/O/W<sub>2</sub>) was formed by sonication for an additional 28 s. The temperature during the whole emulsion process was kept at 4 °C by using an ice bath. The resulting double emulsion was poured into 50 mL of MilliQ water and mechanically stirred at RT for 2 h to allow complete evaporation of the organic solvent and formation of NCs. Finally, the NC pellet was obtained by centrifugation at 9391 rcf for 15 min and washed three times with 50 mL of MilliQ water and then lyophilized in 6 mL of trehalose (2 mg mL<sup>-1</sup>) aqueous solution. The as-obtained powder was stored at 4 °C with desiccant silica gel.

### Physicochemical characterization of the polymers, SPIONs and PLGA-NC

**ATR-FTIR, UV/Vis, TG, DLS.** Attenuated total reflectance-Fourier transform infrared (ATR-FTIR) characterization of the polymers was performed on a Bruker Vertex 70 FTIR spectrometer with a Pike Miracle Single-Bounce diamond crystal plate accessory at room temperature. FTIR spectra were recorded over a wavelength range of 4000–500 cm<sup>-1</sup> with a resolution of 4 cm<sup>-1</sup>. The ultraviolet-visible infrared (UV/Vis) spectra of the fluorescent polymers were recorded on a Varian Cary-5000 UV/Vis spectrophotometer using a quartz cuvette with an optical path of 1 cm. Thermogravimetric (TG) analysis of oleic acid coated SPIONs was carried out on a SETSYS Evolution TGA (Setaram) from room temperature to 800 °C at a heating rate of 10 °C min<sup>-1</sup> and under a dynamic dry air flow. Dynamic light scattering (DLS) (Malvern Zetasizer) measurements of the hydrodynamic diameter and size distribution of NCs by intensity were performed by redispersing 0.5 mg of lyophilized powder into 1 mL of MilliQ water.

**Electron microscopies.** A field emitting scanning electron microscope (SEM, FEI Quanta 200 FEG) and a transmission electron microscope (TEM, JEOL JEM-1210) were used to study the morphologies of SPIONs and NCs. For the SEM sample preparation of NCs, 0.5 mg of lyophilized powder was redispersed in 1 mL of MilliQ water and centrifuged at 4000 rpm for 10 min. Then the supernatant was discarded to remove the trehalose and 1 mL of fresh water was added, and the pellet of NCs was redispersed in water with ultrasound. Finally, 6 μL of the slightly turbid suspension was deposited onto a small slice of silicon wafer stuck on top of a carbon layer and dried at room temperature overnight. The sample was sputtered with Au-Pd (Emitech K550 Sputter Coater, 20 mA for 2 min). TEM samples were prepared by placing and drying one drop of the corresponding NC or SPION dispersion on a copper grid at room temperature.

**SQUID.** Superconductive quantum interference device (SQUID, Quantum Design MPMS5XL) was used to measure the magnetization of NCs and SPIONs and calculate the experimental SPION loading (wt%<sub>SPIONs</sub>) and EE%<sub>SPIONs</sub> of NCs. A gelatin capsule filled with about 7 mg of samples topped with some cotton wool was inserted into the SQUID magnetometer sample holder and the hysteresis loop was measured from -50 kOe to 50 kOe at 5 K. The remnant magnetization of the magnetic NCs ( $M_{R, NCs}$ , emu g<sup>-1</sup>) and of SPIONs ( $M_{R, SPIONs}$ , emu



$\text{g}^{-1}$ ) at 5 K was used to calculate  $\text{wt}\%_{\text{SPIONs}}$  and  $\text{EE}\%_{\text{SPIONs}}$  as follows:

$$\text{wt}\%_{\text{SPIONs}} = \frac{M_{\text{R, NCs}}}{M_{\text{R, SPIONs}}} \times 100\%$$

$$\text{EE}\%_{\text{SPIONs}} = \frac{\text{Experimental SPION loading}}{\text{Nominal SPION loading}} \times 100\%$$

**Fluorescence properties.** Fluorescence spectra of the polymer PLGA-fluram were acquired on a PerkinElmer LS45 spectrofluorometer. Both the excitation and emission-slit widths were set at 10 nm. The quantum yield of the polymer was measured by the Williams' method<sup>24</sup> shown in Fig. S3a.† The molar extinction coefficient ( $\epsilon$ ,  $\text{mol}^{-1} \text{L cm}^{-1}$ ) of PLGA-fluram was calculated according to the Beer-Lambert law,  $A = \epsilon CL$ . Here  $C$  and  $L$  are the concentration ( $\text{mol L}^{-1}$ ) and length (cm) of the dye solution in a UV/Vis cuvette respectively. Brightness and photostability are two important intrinsic photophysical properties of fluorescent materials. The brightness intensity of PLGA-fluram can be calculated by the extinction coefficient multiplied by the quantum yield. Photostability was measured by continuously illuminating polymer solution with excitation light at 390 nm and measuring the resulting emission at 483 nm for 3 h. The photostability of rhodamine B as a reference was tested with its maximum excitation at 540 nm and maximum emission at 625 nm for the same 3 h in aqueous solution. Fluorescence signals of different concentrations of PLGA-fluram NC in saline were quantified in a 96-well plate by a microplate reader. The NCs were excited at the maximal excitation wavelength and the fluorescence signal was collected at the maximal emission wavelength.

### *In vitro* and *in vivo* MRI of the NC-SPIONs

*In vitro* agarose phantoms of NCs were prepared by filling a series of glass microtubes with solutions of 0.63% agarose in water (Conda, Madrid), into which different amounts of NCs were admixed. The corresponding iron doses ( $\text{mmol L}^{-1}$ ) were calculated according to the  $\text{wt}\%$  of SPIONs in each sample.  $T_2$  weighted images (T2WI) of the phantoms were acquired at 7 T in a 70/30 Bruker USR Biospec system (Bruker GmbH, Ettlingen) as follows: multi-slice multi-echo (MSME) sequence with echo time (TE) = 8 ms, repetition time (TR) = 2600 ms, average  $N = 2$ , matrix size =  $160 \times 160$ , field of view (FOV) =  $24 \times 24$  mm, 14 slices of 1 mm thickness, and spectrometer bandwidth (BW) of 474 Hz per pixel. Quantitative  $T_2$  values were obtained from hand-drawn regions of interest (ROIs) by using curve fitting in the Image Sequence Analysis (ISA) Tool (ParaVision v.5.1).

Balb/c female mice (16–17 weeks of age,  $n = 2$ ) were anesthetized with isoflurane (IsoFlo; Abbott Laboratories). T2WI were acquired pre- and 15–20 min post-administration of NCs (1.6 mg in 150  $\mu\text{L}$  of saline through tail vein) using the following imaging parameters: MSME pulse sequence, 20 echo times with  $\Delta\text{TE} = 8$  ms, TR = 2.6 s,  $N = 2$  averages, a matrix of  $256 \times 256$  points covering a FOV of  $25.6 \times 25.6 \text{ mm}^2$ , giving a

resolution of 100  $\mu\text{m}$  in plane, 14 continuous slices of 1 mm thickness, and BW = 75 kHz. The images were acquired with a respiratory gating by using a SAI Model 1030 monitoring & gating system (Small Animals Instruments, Stony Brook, NY, USA). Fat suppression was achieved by a saturation pulse of 1050 Hz.  $T_2$  maps were constructed off-line using Image-J 1.50b (National Institutes of Health), and data were fitted to a three parameter exponential decay equation ( $S = A + S_0 \exp(-\text{TE}/T_2)$ , where  $S$  represents signal intensity,  $A$ ,  $S_0$  and  $T_2$  are the fitting parameters), achieved by the “exponential decay with offset” equation of the fitting routine of ImageJ. Signal intensities in T2WI and  $T_2$  maps were quantified manually in selected ROIs using ImageJ. Afterwards mice were euthanized and organs were preserved for histological analyses.

### *In vitro* and *in vivo* NIRF imaging of NC-PLGA-Cy7.5

A series of concentrations of NCs in 100  $\mu\text{L}$  of saline ( $n = 3$ ) were prepared in a 96-well plate and imaged using a Xenogen IVIS® spectrum ( $\lambda_{\text{ex}}/\lambda_{\text{em}}$  710/820 nm). BALB/cAnNRJ male mice (Janvier; 7–8 weeks of age,  $n = 2$ ) were deeply anesthetized with isoflurane and were injected *via* the tail vein with NCs at a dose of 1.6 mg in 200  $\mu\text{L}$  of saline. The NIRF images were acquired on a Xenogen IVIS® spectrum imaging system at 0.5 h, 1 h and 3 h post injection. At the end of the 3 h scan, the mice were euthanized to image the signal intensity of the principal organs *ex vivo* together with blood and urine.

### *In vivo* PET imaging of $^{89}\text{Zr}$ labelled NC-PLGA-DFO

NC-PLGA-DFO were labelled with  $^{89}\text{Zr}$  as follows: [ $^{89}\text{Zr}$ ]ZrC<sub>2</sub>O<sub>4</sub> was produced in house following a standard protocol. The as-obtained 1500  $\mu\text{L}$  of 1 M oxalic acid containing  $^{89}\text{Zr}$  (8.2 mCi, 303.4 MBq) were neutralized with 2 M sodium carbonate (pH = 7.2) and the volume was adjusted to 3.5 mL with 0.5 M HEPES buffer. Six aliquots (1.6 mg each) of the lyophilized particles were dispersed in 50  $\mu\text{L}$  MQ-water, and 450  $\mu\text{L}$  of the freshly prepared  $^{89}\text{Zr}$ -solution was added to each and mixed well by sonication. After incubating overnight at room temperature the particles were purified by centrifugation and washed two times with MQ-water followed by one wash with saline to remove all non-bound  $^{89}\text{Zr}$ . The pellet of the last wash was dispersed in 120  $\mu\text{L}$  of saline with an average calculated radiochemical yield of 70.1% (decay-corrected). As the achieved samples were too high in activity, a one to one dilution with non-labelled particles was performed. The final injections (150  $\mu\text{L}$ ) were performed intravenously *via* the tail vein of healthy female mice (CrI:CD1(ICR)) with an average injected activity of 161  $\mu\text{Ci}$  (6.0 MBq).

Imaging studies were conducted using positron emission tomography (PET) in combination with computerized tomography (CT), using the  $\beta$ - and X-cube microsystem of Molecubes. Static whole body images (1 bed) were acquired in a 511 keV  $\pm$  30% energetic window at 1 h, 4 h, 23 h and 47 h post injection (acquisition time 5 min for 1 h and 4 h, 20 min for 23 h and 47 h). PET images were analyzed using PMOD image analysis software (PMOD Technologies Ltd, Zurich, Switzerland).



### Prussian blue stain

Liver samples from the mice subjected to PET were embedded in an optimal cutting temperature (OCT) compound and kept at  $-80\text{ }^{\circ}\text{C}$  until sliced in  $8\text{ }\mu\text{m}$  sections with a cryostat. After rehydration, the sections were stained with a Prussian blue iron stain kit (Polysciences Inc, USA) following the manufacturer's protocol except that potassium ferrocyanide: hydrochloric acid solution was kept for a total of 40 minutes and nuclear Fast Red for 1 minute. Images were acquired after dehydration with a transmitted light microscope (Leica, Germany).

### *In vitro* and *in vivo* toxicity evaluation of the NCs

**Cell viability evaluation.** The toxicity of the NCs on human brain endothelial cells (hCMEC/D3) and  $\text{CD34}^+$  endothelial cells<sup>25,26</sup> was assessed by performing a viability assay with 3-(4,5-dimethylthiazol-2-yl)-2,5-diphenyl tetrazolium bromide (MTT). For the hCMEC/D3 cells,  $2 \times 10^4$  viable cells were distributed on a 24-well plate in  $400\text{ }\mu\text{L}$  Endothelial Growth Media (EGM2 from Lonza with 2% fetal bovine serum and half the amount of the growth factors included in the kit) whereas  $5 \times 10^3$  viable  $\text{CD34}^+$  endothelial cells were seeded on a 96-well plate in complete media. Both cell types were incubated for 24 h at  $37\text{ }^{\circ}\text{C}$  and 5% of  $\text{CO}_2$ . After this period, culture supernatants were substituted with basal cell culture media (serum-free medium) containing increasing doses of NCs at concentrations of  $25\text{ }\mu\text{g mL}^{-1}$ ,  $50\text{ }\mu\text{g mL}^{-1}$ , and  $100\text{ }\mu\text{g mL}^{-1}$  ( $N = 3$ , triplicate). The MTT assay was performed after 48 h of incubation, and the absorbance of the resulting formazan crystals diluted in DMSO was determined at  $540\text{ nm}$ . Cell viability was referred to as the percentage of viability compared with the control conditions (without NC).

***In vivo* safety.** Body weights of mice were monitored periodically at 0 d, 1 d, 5 d, 8 d, 11 d and 13 d after i.v. injection of NCs in  $150\text{ }\mu\text{L}$  of saline at a dose of  $0.84\text{ mg Fe per kg}$  ( $n = 5$ ), where the vehicle group received  $150\text{ }\mu\text{L}$  of saline ( $n = 5$ ) and the naïve group without treatment served as control ( $n = 3$ ). At the end of 13 days blood samples were collected and liver/pancreas toxicity based on specific enzyme levels in plasma was analysed in all groups: alanine aminotransferase (ALT), alkaline phosphatase (ALK), aspartate aminotransferase (AST) and

$\alpha$ -amylase using an Olympus AU5800 clinical chemistry analyser.

### BSA loading content

The albumin content was determined directly using the CBQCA protein assay kit (Invitrogen™ ref. C6667), which determines the protein concentration based on the production of fluorescent products measurable at  $\lambda_{\text{ex}}/\lambda_{\text{em}} = 450\text{ nm}/550\text{ nm}$  *via* non-covalent interaction between CBQCA and primary aliphatic amines of proteins. This highly sensitive fluorescence-based method showed compatibility with DMSO, SPIONS, detergents and other substances which interfere with many commonly used protein determination methods. Lyophilized NCs encapsulating albumin as well as empty NCs as control were fully dissolved in DMSO at  $100\text{ mg mL}^{-1}$ . The protein contents in the NC lysates were measured and calculated based on the difference in fluorescence with control and a calibration curve drawn with standard albumin solutions, and the protein contents in the BSA solutions used for encapsulation were also measured. All determinations were performed in duplicate for each NC batch. The experimental BSA loading content was expressed as  $\mu\text{g}$  of BSA per  $\text{mg}$  of NCs ( $\mu\text{g mg}^{-1}$ ). The encapsulation efficiency (EE%) was calculated as follows:

$$\text{EE\% BSA} = \frac{\text{Experimental BSA loading}}{\text{Nominal BSA loading}} \times 100\%$$

## Results and discussion

PLGA NCs reported here incorporate several biocompatible multimodal imaging modalities (Fig. 1): fluram and cyanine 7.5 (Cy7.5) as fluorescent probes in the blue and the near-infrared (NIR) wavelengths,  $^{89}\text{Zr}$  chelated with DFO as a radio imaging probe and SPIONS as a MRI contrast agent. The fluorescent probes and the DFO chelator were anchored to an aminated PLGA, PLGA-NH<sub>2</sub>, resulting from the modification of the commercial carboxylic acid-terminated PLGA. BSA encapsulated PLGA NCs could then be prepared by a double emulsion solvent evaporation method where selected imaging moieties were incorporated into the PLGA shell by adding the desired

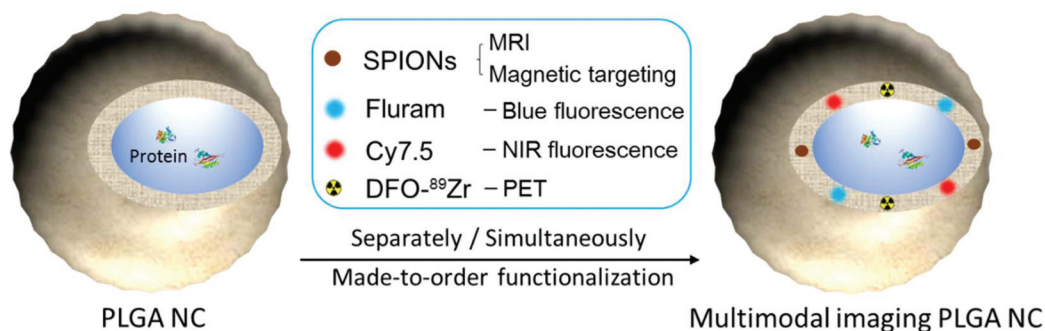


Fig. 1 Schematic illustration of a PLGA NC as a tailor-made multimodal theranostic platform.



proportions of a given functional PLGA and oleic acid coated SPIONs to the organic phase while the BSA was added to the aqueous phase.

### Chemical modification of the PLGA with functional moieties

Fig. 2 shows the schematic representation for terminal modifications and functionalization of the PLGA. Firstly, the carboxylic acid end group of PLGA was activated with DCC and NHS to conjugate ethylenediamine and form PLGA-NH<sub>2</sub>, bearing a free primary amine group in the PLGA end (Fig. 2a). An excess amount of ethylenediamine (6:1 ethylenediamine:PLGA mole ratio) was used to suppress the coupling reaction of PLGA-PLGA that could occur due to the homo-functional crosslinker ethylenediamine. Subsequently, the three functional moieties with amine-reactive groups (fluram, Cy7.5, DFO) could be respectively integrated at the end of the PLGA molecule through coupling reactions (Fig. 2b). Further details are reported in the Experimental section.

ATR-FTIR spectra of the commercial PLGA-COOH and the PLGA-NH<sub>2</sub> product confirmed their similar chemical structure and successful modification (Fig. S1 in the ESI<sup>†</sup>). The reaction efficiency of PLGA-COOH to PLGA-NH<sub>2</sub> was quantified by measuring the conjugated amount of fluram to the -NH<sub>2</sub> groups. The UV absorbance of the PLGA-NH<sub>2</sub> product ( $M_w$

12 000 g mol<sup>-1</sup>) in chloroform at 390 nm due to the conjugation of fluram was compared with a standard calibration curve constructed from different concentrations of ethylenediamine prepared under the same conditions (Fig. S2<sup>†</sup>). A reaction efficiency of 86% of PLGA-COOH to PLGA-NH<sub>2</sub> was estimated, which means that the molar fraction of pure PLGA-NH<sub>2</sub> in the product was 0.86.

Fluram is a non-fluorescent compound that reacts quickly and almost quantitatively with primary amines (R-NH<sub>2</sub>) to form a fluorescent derivative, which emits strong fluorescence at around 480 nm when excited at 390 nm.<sup>22</sup> The conjugation of this compound to the -NH<sub>2</sub> end of PLGA for fluorescence application is very advantageous considering that neither free fluram itself nor its hydrolysis product show fluorescence. As shown in Fig. 3a, the characteristic absorption peak of the fluorophore at 390 nm occurred in the UV-Vis spectrum of the conjugation product PLGA-fluram but this was not observed either in PLGA-NH<sub>2</sub> or in fluram. The disappearance of the 309 nm absorption band of fluram in the PLGA-fluram product indicates that the purification process removes the vast majority of free fluram. The fluorescence of the obtained PLGA-fluram was evaluated and the excitation and emission spectra are depicted in Fig. 3b. Importantly, the fluorescence intensity of PLGA-fluram decreased only slightly (<5%) after continuous UV excitation at the maximum excitation wave-

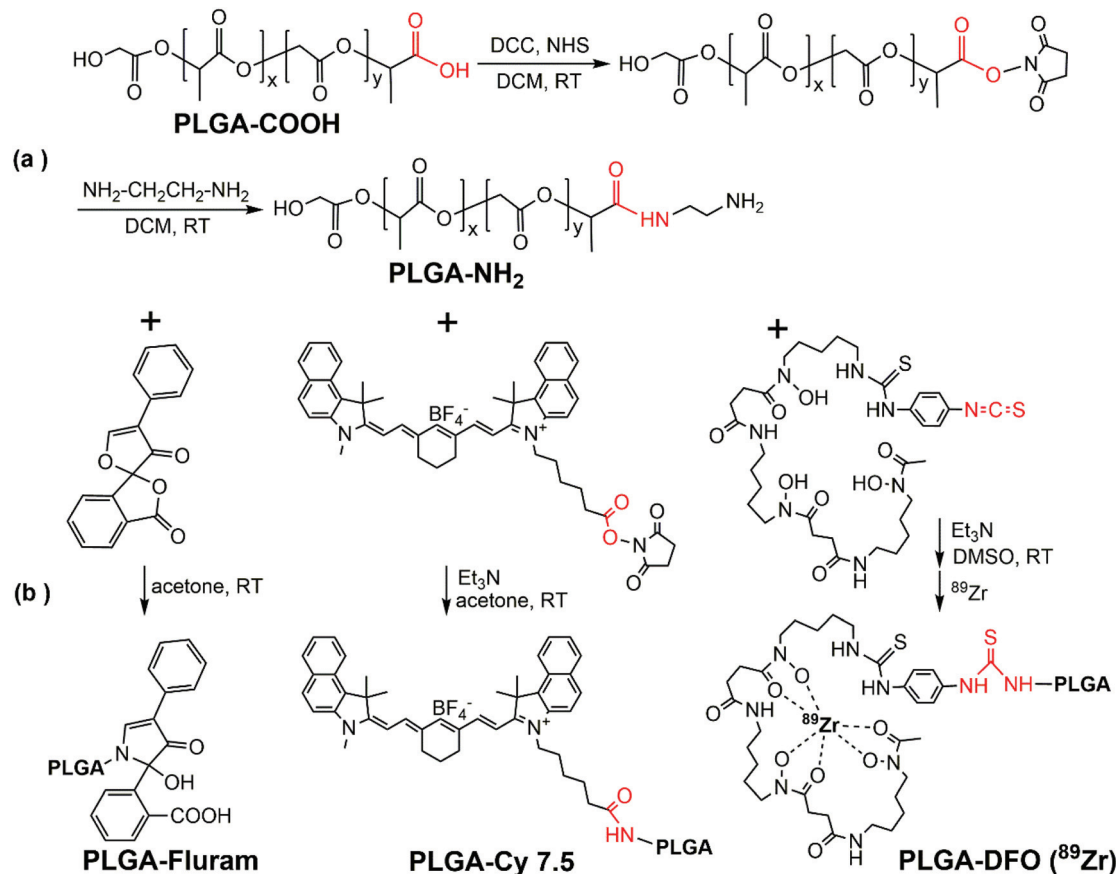
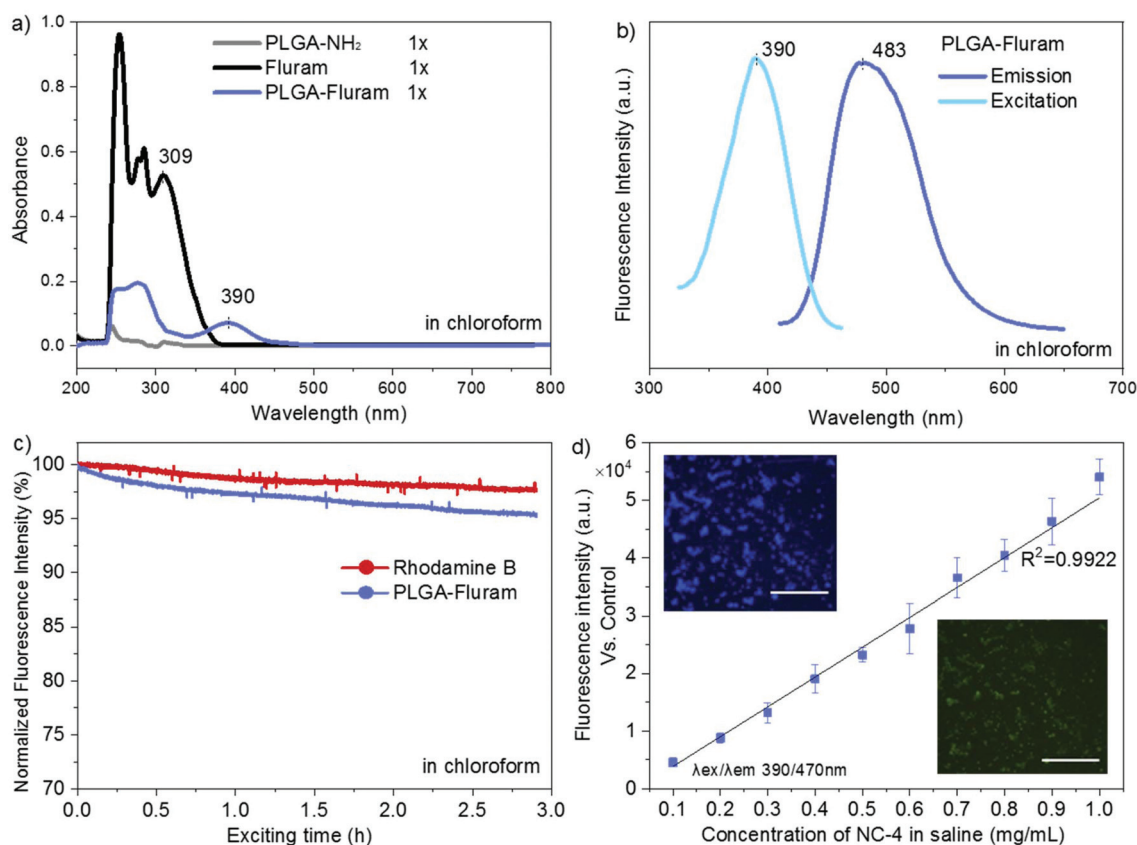


Fig. 2 PLGA chemical modifications. Synthetic schemes of terminal modifications and functionalization of the PLGA.





**Fig. 3** PLGA-fluram system spectroscopic and fluorescence characterization. (a) UV-Vis absorption spectra of PLGA and PLGA/fluram samples; (b) excitation and emission spectra of PLGA-fluram; (c) photostability evaluation of PLGA-fluram and control dye rhodamine B, fluorescence intensity expressed as the percentage vs. time 0; (d) fluorescence intensity of different concentrations of NC-PLGA-fluram (NC-4) vs. NC-control (NC-3) measured by using a microplate reader ( $n = 3$ , values represent mean  $\pm$  SEM); insert: lyophilized NC-4 observed under a fluorescence microscope with DAPI/GFP filters, scale bar 60  $\mu\text{m}$ .

length for 3 h, thus exhibiting a photostability just slightly lower (2%) than rhodamine-B, a widely used commercial fluorescent dye (Fig. 3c). The photostability of PLGA-fluram using a confocal microscope configuration is also included in Fig. S3b.† The fluorescence intensity of NCs fabricated by PLGA-fluram decreased by only 13% after 10 min of continuous illumination at 10% of laser power (401 nW). Considering that the laser power applied to observe stained cells is generally less than 10%, our fluorescent NCs would exhibit good photostability under *in vitro* conditions. Note that the calculated quantum yield of PLGA-fluram (18%) (Fig. S3a†) is much higher than the values reported for fluorescent proteins such as green fluorescent protein (GFP) (7.3%) and its blue variants (7.9%),<sup>27</sup> and similar to other polymeric fluorescent materials such as poly(amido amine)s.<sup>28,29</sup> Finally, the calculated fluorescent brightness of PLGA-fluram (25056) is also much higher than that of other reported biodegradable photo-luminescent poly(lactide-co-glycolide) (BPLP-co-PLGA) (6550–19230)<sup>30</sup> and other frequently used small organic dyes such as Alexa Fluor 430 (8800) or DAPI (15660). The fluorescence intensities of the fabricated NCs show linear dependency on the NC concentration, and NCs can be clearly imaged with a fluorescence

microscope (Fig. 3d). Although in this work we have focused on *in vivo* imaging modalities, the remarkable fluorescence properties shown here endow the PLGA-fluram system with very interesting features for *in vitro* fluorescence tracking studies.

Next, the NIR fluorophore Cy7.5 was introduced into the terminal amine of PLGA-NH<sub>2</sub> via an amide bond between the PLGA terminal amine group and amine-reactive Cy7.5 NHS ester. The absorption band of Cy7.5 appeared in the UV-Vis spectrum of the PLGA-Cy7.5 product, which confirmed the successful conjugation of Cy7.5 (Fig. S4a†). The amount of conjugated Cy7.5 in the PLGA-Cy7.5 product was quantified by comparing the fluorescence intensity of the PLGA-Cy7.5 product with free Cy7.5 (Fig. S4b†) in DMSO. Pure PLGA-Cy7.5 with a molar fraction of 0.65 was estimated in the product and a conjugation efficiency of 76% of the Cy7.5 NHS ester to PLGA-NH<sub>2</sub> was calculated considering that the fraction of pure PLGA-NH<sub>2</sub> is 0.86.

For radiolabelling functionalization the <sup>89</sup>Zr chelator DFO was introduced at the end of PLGA-NH<sub>2</sub> by forming a thiocarbamide bond between the PLGA terminal amine group and the amine reactive -NCS group in the DFO derivative



p-NCS-Bz-DFO. Compared to the IR spectrum of PLGA-NH<sub>2</sub>, some new bands corresponding to the DFO conjugate appear in the spectrum of PLGA-DFO, indicating the successful conjugation of DFO (Fig. S1†). The amount of conjugated DFO in the PLGA-DFO product was quantified by measuring the amount of unreacted PLGA-NH<sub>2</sub> through the fluram method described above (Fig. S2c†). Pure PLGA-DFO with a molar fraction of 0.75 was estimated in the product, and a conjugation efficiency of 88% of p-NCS-Bz-DFO to PLGA-NH<sub>2</sub> was calculated considering that the fraction of pure PLGA-NH<sub>2</sub> is 0.86.

### Fabrication of PLGA NCs with selected combinations of imaging moieties

PLGA NCs with encapsulated BSA were prepared by a double emulsion solvent evaporation method.<sup>31</sup> Imaging moieties were incorporated into the PLGA shell by adding to the organic phase various proportions of functionalized PLGA as well as the oleic acid (OA) coated SPIONs (Table 1). Compositional changes of the organic phase did not affect the encapsulation process, and all types of NCs prepared showed mean hydrodynamic sizes within a diameter range of 250–300 nm and a polydispersity index (PdI) <0.2. As seen in Table 1 from NC-1 to NC-3, neither increasing the SPION size nor increasing two-fold its loading affected the mean size of the NCs compared to plain PLGA NCs (NC-0). Note that for the same loading of SPIONs, the magnetization of NC-2 is much higher than that of NC-1 given the larger size of SPIONs for NC-2. Therefore optimal formulation regarding SPIONs (6 wt%, with 9 nm nanoparticles) yields an average saturation magnetization value of 4.06 emu g<sup>-1</sup> NCs which is more than four-fold larger than our previously reported value (0.90 emu g<sup>-1</sup>).<sup>31</sup> As will be shown later, the increase of the magnetic moment of NCs resulting from using larger size SPIONs and increasing their load will positively impact on the MRI signal intensity.<sup>32</sup>

Furthermore, the size of NCs as well as the encapsulation efficiency (EE%) of SPIONs were not affected when various proportions of PLGA-fluram (NC-4), PLGA-DFO (NC-5) or PLGA-Cy7.5 (NC-6) were incorporated into the PLGA matrix, even when incorporating various moieties simultaneously (NC-7). Importantly, we had found that the PLGA-based NCs can be fabricated using either up to 100 wt% of any modified PLGA (PLGA-DFO, PLGA-Cy7.5 or PLGA-fluram) or with any mixed proportion of them without affecting the morphology of NCs and EE% of SPIONs. This can be explained by the forming process of the NCs: the different functional moieties at the end of the comparatively extra-long PLGA molecules do not affect the film-forming of PLGA and the entrapment of SPIONs in the polymeric matrix. Finally, PEGylation of the PLGA NCs was achieved by adding a given amount of the commercial amphiphilic block copolymer PLGA-PEG (PEG *M<sub>n</sub>* 5000 and PLGA *M<sub>n</sub>* 7000) to the organic phase. The morphology and size of NCs (NC-8) are maintained up to a maximal fraction of 7 wt% amphiphilic PLGA-PEG (3 wt% PEG, Table 1) and are not affected when co-incorporating other hydrophobic modified PLGA (*i.e.*, PLGA-Fluram/PLGA-DFO/PLGA-Cy7.5) (data not shown).

Fig. 4 shows a representative scanning electron microscopy (SEM) image of the NCs (NC-3) presenting homogeneous spherical morphologies. The inset is a dynamic light scattering (DLS) size distribution histogram of lyophilized NCs redispersed in water. In this case, the mean hydrodynamic diameter of the NCs is 276 nm with a polydispersity index (PdI) of 0.18 reflecting good redispersibility of the NCs in water after the lyophilization process. As mentioned, all types of NCs listed in Table 1 had similar morphologies and sizes (Fig. S7†), which were considered to be suitable for intravenous administration.<sup>33</sup> The upper inset in Fig. 4 shows a representative broken NC, exposing the hollow core, ideal for the loading of protein drugs. The transmission electron microscopy (TEM)

**Table 1** Summary of the formulations of PLGA-based NCs. Different proportions of modified PLGA and SPIONs were mixed in the organic phase during the double emulsion process

Sample type	PLGA information (wt%)					SPIONs					Size (DLS)	
	PLGA	PLGA-Fluram	PLGA-DFO	PLGA-Cy7.5	PLGA-PEG	Size <sup>a</sup> (nm)	Loading <sup>b</sup> (wt%)	EE% <sup>b</sup>	<i>M<sub>R</sub></i> (emu g <sup>-1</sup> )	<i>M<sub>S</sub></i> (emu g <sup>-1</sup> )	d.nm	PdI
NC-0	100	—	—	—	—	—	—	—	—	—	255	0.10
NC-1	100	—	—	—	—	6	2.9	92%	0.4	1.0	279	0.17
NC-2	100	—	—	—	—	9	3.0	90%	0.8	1.9	264	0.19
NC-3	100	—	—	—	—	9	6.1	95%	1.6	3.9	276	0.18
NC-4	50	50	—	—	—	9	6.2	95%	1.6	4.7	260	0.15
NC-5	40	—	60	—	—	9	6.3	97%	1.6	4.3	271	0.19
NC-6	40	—	—	60	—	9	5.9	91%	1.5	3.6	245	0.11
NC-7	—	50	50	—	—	9	5.9	91%	1.5	3.7	268	0.18
NC-8	93	—	—	—	7	9	6.0	92%	1.6	3.8	265	0.13
OA-SPIONs <sup>c</sup>						6			14.0	50.8		
						9			26.1	75.1		

<sup>a</sup> The size of SPIONs was determined by statistics from TEM images (Fig. S5†). <sup>b</sup> SPION loading and entrapment efficiency (EE%) were determined by SQUID measurements at 5 K. <sup>c</sup> The fraction of SPIONs in OA-SPIONs was determined by thermogravimetric analysis (TGA) and the magnetization is expressed as emu g<sup>-1</sup> SPIONs (Fig. S6†).



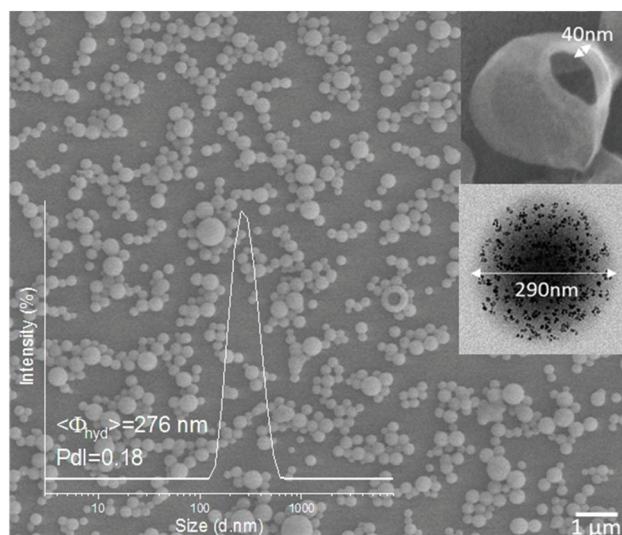


**Fig. 4** Morphological data of a representative PLGA NC system (NC-3). SEM image of lyophilized PLGA based NCs with the upper inset showing the hollow core of the NC; lower inset TEM image shows a spherical NC with SPIONs visible as black spots, uniformly distributed in the polymer matrix; DLS curve of NC water suspension after lyophilization with a mean diameter of 276 nm and 0.18 polydispersity.

image in the lower inset revealed the embedding and finely homogeneous distribution of the SPIONs within the polymeric matrix.

#### NC magnetic properties, accumulation and biodistribution by MRI

The magnetic hysteresis loop at room temperature of lyophilized NC-3 is displayed in Fig. 5a showing the superparamagnetic character of the NCs (lack of coercivity). The superparamagnetic behavior of the NCs after SPION encapsulation is important since in the absence of an external magnetic field, it ensures lack of interactions among NCs thus minimizing the risk of embolization for i.v. administration. The magnetic retention of NCs is illustrated with the use of an external magnet. As seen in Fig. 5b, the colloidal water suspension of 2 mg mL<sup>-1</sup> of NC-3 forms a round pellet next to the magnet after 7 h. The solution becomes completely clear indicating that a great majority of the NCs are retained by the magnet. Previous experiments using magnetic PLGA nanoparticles<sup>34</sup> or microparticles loaded with only 1 wt% iron oxide<sup>35</sup> already demonstrated magnetic retention in rodent brain or knees, indicating that our protein loaded magnetic NCs with a higher magnetic load (6 wt%,  $M_S = 4 \text{ emu g}^{-1}$ ) may still have better characteristics to address magnetic targeting.

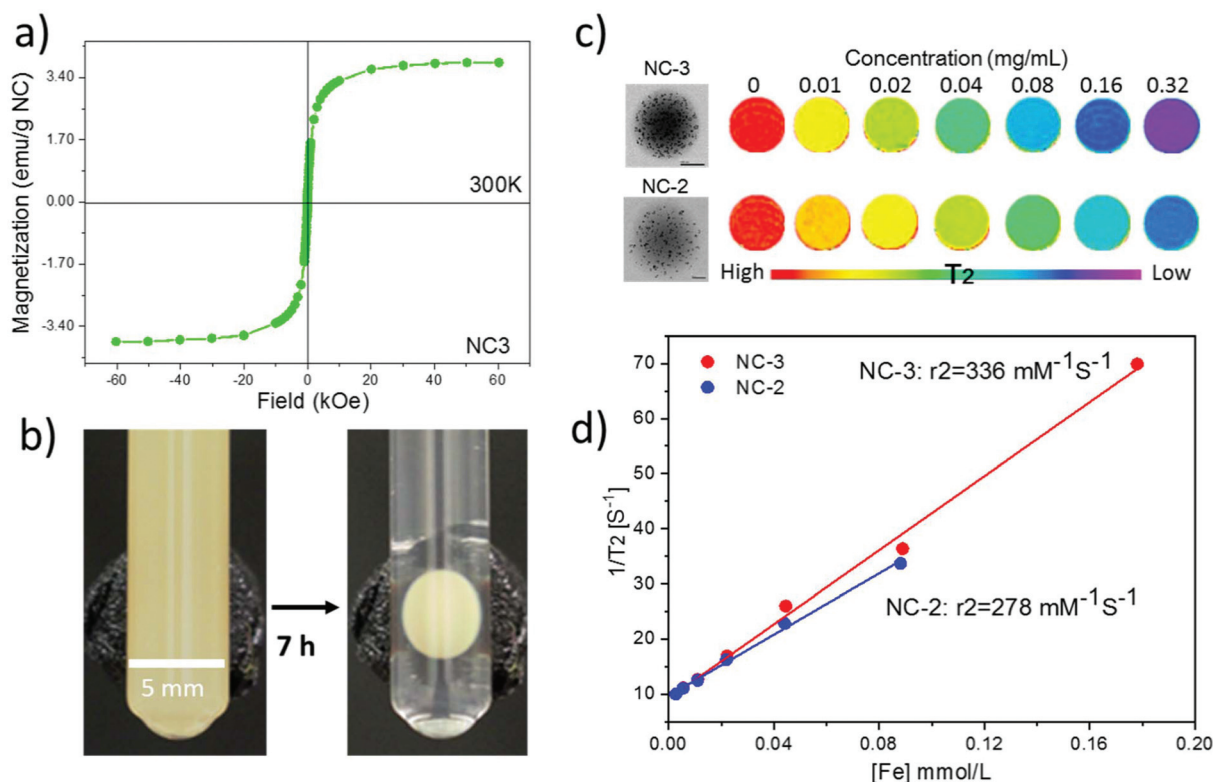


**Fig. 5** Magnetic characterization, retention and MRI phantoms of PLGA-SPIONs NCs. (a) Hysteresis loop of the lyophilized batch NC-3 at 300 K, showing superparamagnetism at room temperature; (b) glass tube with water suspension of NC-3 at a concentration of 2 mg mL<sup>-1</sup>. A permanent magnet (diameter 8 mm, surface field ~0.4 T) was placed on the wall. After 7 h, the NCs adsorbed to the tube wall on the magnet side; (c) T<sub>2</sub>-weighted phantoms obtained by mixing lyophilized NCs with agarose at increasing NC concentrations, on the left are TEM images of NCs; (d) evaluation of  $r_2$  relaxivities for NC-3 and NC-2 (3 wt% and 6 wt%; 9 nm diameter).





Phantom studies were conducted to confirm the MRI performance of the NCs. Phantoms from two batches (NC-2 and NC-3) with different SPION loadings (3 wt% and 6 wt%; 9 nm diameter) at a series of concentrations were prepared (Fig. 5c). Spin-spin relaxation time ( $T_2$ ) weighted color-coded MRI images clearly exhibit signal decay in a concentration dependent manner. Importantly, at the same concentration NC-3 with 6 wt% SPIONs showed a higher  $T_2$  signal decay rate than NC-2 with 3 wt% SPIONs indicating that NC-3 will be easier to track *in vivo* by MRI. Furthermore, the transverse relaxivity ( $r_2$ ) value at 7 Tesla of NC-3 ( $336 \text{ mM}^{-1} \text{ s}^{-1}$ ) was higher, as expected, than that of NC-2 ( $278 \text{ mM}^{-1} \text{ s}^{-1}$ ) as seen in Fig. 5d, indicating that the denser packing of SPIONs in a single NC of NC-3 endows the NCs with a larger magnetic moment and increases its efficiency as a spin-spin relaxation agent.<sup>36</sup> Compared with other clinically used SPION systems such as Feridex ( $98 \text{ mM}^{-1} \text{ s}^{-1}$ ) and Resovist ( $151 \text{ mM}^{-1} \text{ s}^{-1}$ ),<sup>37</sup> the much higher  $r_2$  value in our final NC formula (6 wt% SPIONs of 9 nm in diameter) is expected to be useful for *in vivo* MRI tracking of the NCs.

As the representative abdominal images show in Fig. 6b, a much clearer increase of the contrast of the liver was observed in both T2WI and T2 maps after NC administration, illustrating the fast accumulation of NCs in the liver. Quantitative ROI analysis in Fig. 6c shows a 55% drop of signal intensity (SI) on T2W images and a 26% drop of  $T_2$  relaxation time in the liver, while a negligible signal drop was observed in the kidney, which further demonstrate the large accumulation of NCs in this organ. To further confirm the presence of NCs in the tissue, Prussian blue staining on liver sections confirmed the presence of ferric iron (Fig. 6d) after the *in vivo* MRI.

#### Biodistribution of the NCs monitored by PET

With a  $\sim 3$  day half-life,  $^{89}\text{Zr}$ -based PET imaging holds great potential as a useful tool for long-term monitoring of the dynamic biodistribution, biodegradation and clearance pathway of nanoparticles *in vivo*.<sup>38</sup> Our results showed that  $^{89}\text{Zr}$ -labelling has a yield of about 70% for NC-PLGA-DFO (NC-5) after overnight incubation at room temperature at a concentration of  $3 \text{ mg mL}^{-1}$ . A DFO challenge study has been

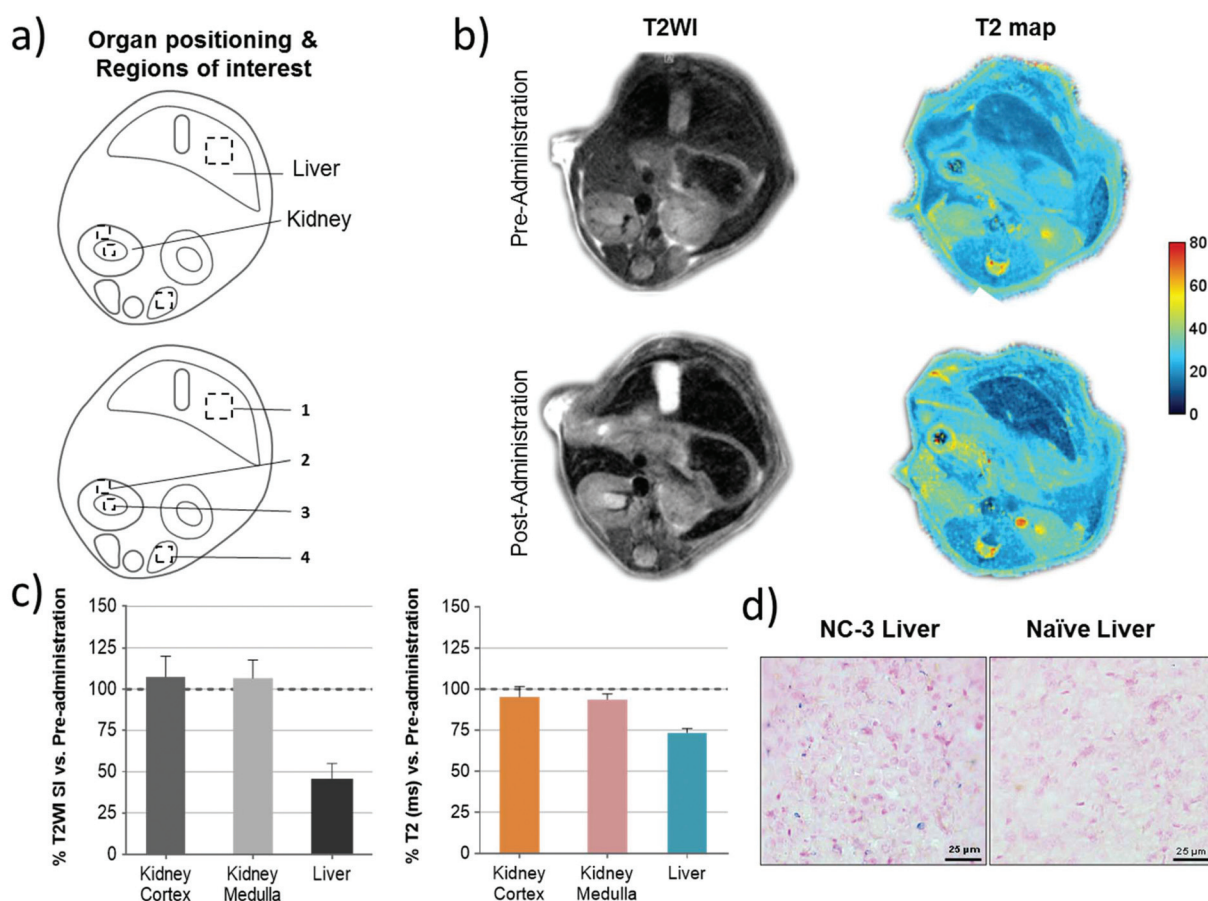


**Fig. 6** *In vivo* mouse MRI of the PLGA-SPIONs NCs and liver Prussian blue iron-stain. (a) Representation of the abdominal region with organ positioning and ROI quantification in the kidney and liver (1: liver, 2: kidney cortex, 3: kidney medulla, 4: paravertebral muscle used for normalization). (b) Representative images of T2W and T2 maps before and after NC-3 administration. (c) Signal intensity (SI) and relaxation time (ms) were calculated for each ROI corresponding to the analyzed anatomical structures which were then corrected by muscle ROI SI. Final data are represented as post-administration SI or  $T_2$  relaxation as the percentage of the pre-administration values (mean  $\pm$  SEM;  $n = 2$ ). (d) Representative images of Prussian blue stain for ferric iron in liver sections of naïve and treated animals administered with NC-3 in the MRI study (blue spots).



reported to demonstrate the radiostability of  $^{89}\text{Zr}$ -labelled nanoparticles.<sup>39</sup> In our study, the as-obtained NC-PLGA-DFO- $^{89}\text{Zr}$  was suspended in 1 mM DFO aqueous solution and incubated at 37 °C for 23 h. Then the NCs were separated by centrifugation and 100% were still labelled, with no presence of  $^{89}\text{Zr}$ -DFO in the supernatant, demonstrating a strong binding affinity of  $^{89}\text{Zr}$  to the NC-PLGA-DFO.

$^{89}\text{Zr}$  labelled NC-PLGA-SPIONs-DFO- $^{89}\text{Zr}$  (NC-5) were then injected *via* the tail vein with the same iron dosage as for the MRI study (1.68 mg Fe per  $\text{kg}^{-1}$ ) to anesthetized mice. Static whole body PET-CT images were acquired at 1 h, 4 h, 23 h and 47 h p.i. Dominant liver, spleen and lung uptake was observed (Fig. 7a) and confirmed by the quantitative ROI analysis (Fig. 7b) within two days, which can be related to phagocytic cell uptake by the mononuclear phagocyte system,<sup>1</sup> as expected for i.v. injected PLGA nanoparticles of this size.<sup>17</sup> Interestingly, noticeable bladder accumulation ( $\sim 22\% \text{ID cm}^{-3}$ ) was observed at 1 h p.i., with a sharp decrease at 4 h p.i. ( $\sim 6\% \text{ID cm}^{-3}$ ) likely due to uncontrolled animals' urination between scans. The early stage activity in the bladder could also be confirmed by continuous PET-CT acquisition (Fig. S8†), which showed a

linear increase of activity within 3 h p.i. It is hard to assign the activity in the urine to the detachment of free  $^{89}\text{Zr}$  from the NCs, since detached free  $^{89}\text{Zr}$  is a well-known osteophilic cation with a fast and retained uptake in bones,<sup>38,40</sup> which is not detectable in our case. In the study of Chen *et al.*,<sup>38</sup> for both free  $^{89}\text{Zr}$ -oxalate or  $^{89}\text{Zr}$  labelled  $\text{SiO}_2$  nanoparticles, fast and sustained uptake of free/detached  $^{89}\text{Zr}$  in bones and joints was observed from the first few hours up to three weeks, while the accumulation in the bladder was negligible. We thus hypothesized that the erosion of the soft polymeric NCs had happened at an early stage in the complex blood circulation environment. The detached  $^{89}\text{Zr}$ -molecular fragments from the NCs, either by degradation of ester bonds in PLGA molecular chains or thiocarbamide bonds between PLGA and DFO or by mechanical force, with a size smaller than 15 nm (ref. 41) underwent renal clearance and were observed in the bladder. Additional experiments showed erosion of NCs clearly observed after *in vitro* incubation in mouse plasma at 37 °C for 24 h (Fig. 7c). Small holes appeared on the NCs while under the same conditions NCs incubated in saline did not show the same eroded surface (Fig. 7d). Considering the *in vivo* blood

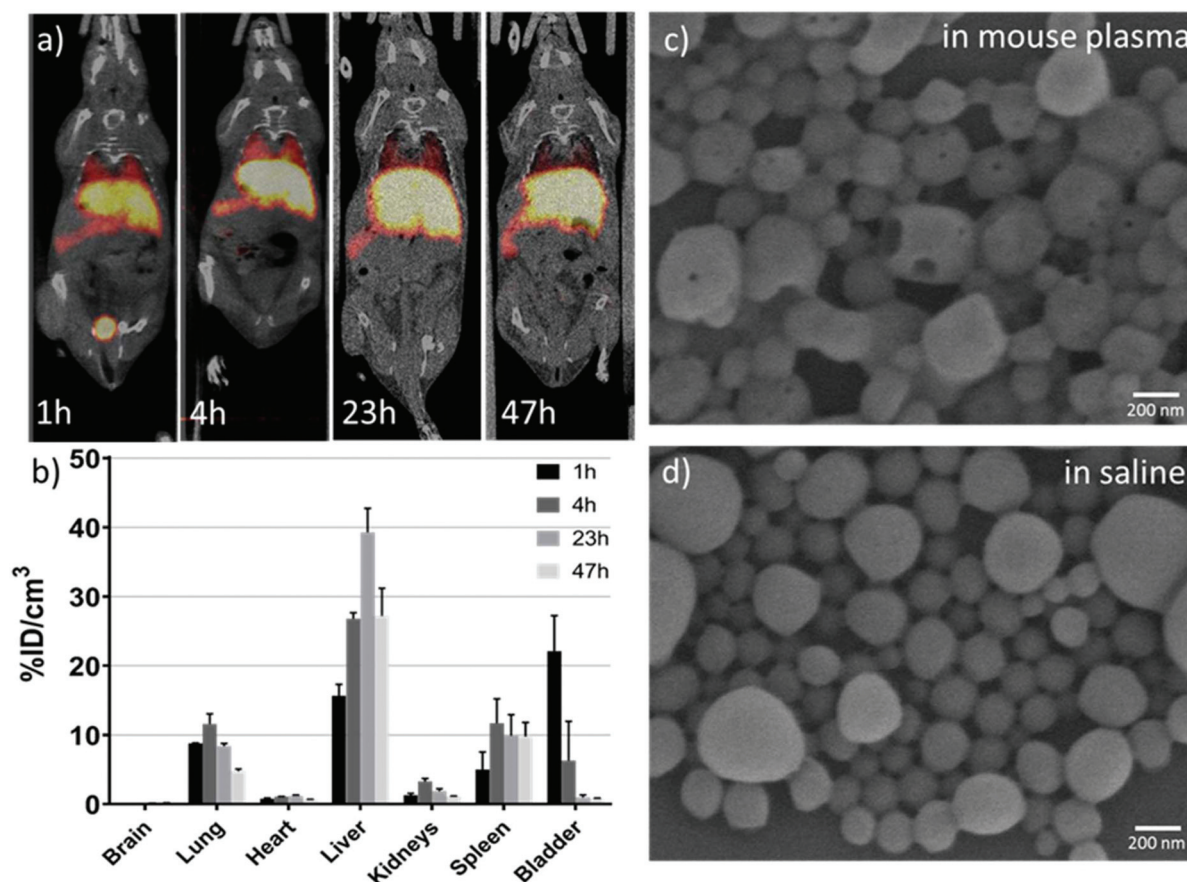


**Fig. 7** PET biodistribution study of PLGA-SPIONs-DFO- $^{89}\text{Zr}$  NCs. (a) Representative PET-CT coronal images of mice obtained at different time points after intravenous (i.v.) administration of NC-PLGA-SPIONs-DFO- $^{89}\text{Zr}$  (NC-5). PET images (maximum intensity projections) have been co-registered with CT images (slices) of the same animals for localization of the radioactivity signal; (b) accumulation of radioactivity, expressed as a percentage of injected dose per  $\text{cm}^3$  of tissue ( $\% \text{ID cm}^{-3}$ ) at 1 h, 4 h, 23 h and 47 h p.i. (mean  $\pm$  SEM of  $n = 2$ ); (c) and (d) SEM images of the NCs after incubation for 24 h at 37 °C in mouse plasma or saline.



circulation setting, the erosion of PLGA NCs would be much faster as reported by Swider.<sup>42</sup> Not surprisingly, at late time points the concentration of radioactivity in the bladder decreases likely due to the fast accumulation of the NCs in the liver/spleen.

### NC biodistribution monitored by near infrared fluorescence (NIRF) imaging

To investigate the feasibility of the formulation of NC-PLGA-Cy7.5 (NC-6) for *in vivo* NIRF imaging, *in vitro* fluorescence performance was firstly checked. The *in vitro* fluorescence intensity of NC-6 was linearly dependent on the concentrations of NCs, showing strong fluorescence and no quenching up to a high level of 1 mg mL<sup>-1</sup> (Fig. 8a). Real-time whole-body imaging revealed a dominant abdominal distribution of the NCs with a total radiant efficiency (TRE) of ~42.40 vs. control at 2 h p.i. At the end of the observation, main organs including brain, heart, lungs, liver, spleen, kidneys, and bladder were collected. Fig. 8c shows a representative *ex vivo* fluorescence picture of those organs and Fig. 8d shows the quantified result of the biodistribution of the NCs.

Dominant liver, spleen and lung accumulation was observed which was consistent with the data acquired with PET. Note that we also did see the bladder signal during the real-time imaging, which further demonstrated that the erosion of NCs really occurred at the early stage p.i., considering that the NIRF imaging is less sensitive than PET. The unobservable *ex vivo* bladder signal may result from the uncontrolled urination and urine sample collection.

From the above discussion, similar biodistribution of the NCs with different imaging probes for MRI/PET/NIRF was evidenced. That was expected since the only difference among the NCs for these three imaging modalities is the existence or not of small molecule <sup>89</sup>Zr-DFO or Cy7.5 at the end of the PLGA molecular chain. As we have demonstrated, the imaging probes in the matrix of the PLGA shell do not affect the size of the NCs, which is a key attribute influencing the biodistribution and pharmacokinetics of the nanocarriers.<sup>17,41,43</sup> Thus, the incorporation or removal of these small molecules in the shell does not affect the NCs' *in vivo* biodistribution and tailor-made capsules can be fabricated with the appropriate imaging probe needed for each specific *in vivo* and *in vitro*

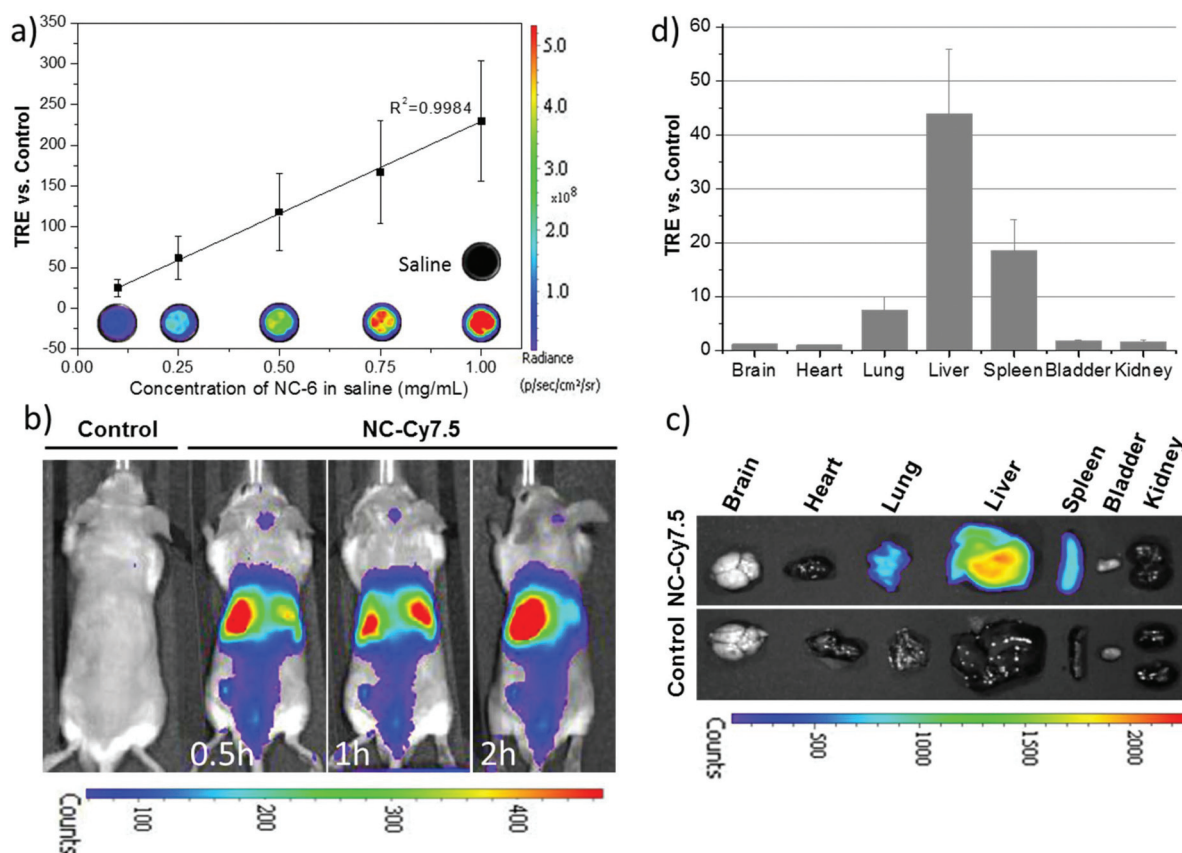


**Fig. 8** Fluorescence molecular imaging of PLGA-SPIONs-Cy7.5 NCs. A Xenogen IVIS® imaging system ( $\lambda_{ex}/\lambda_{em}$  710/820 nm) was used to monitor the NIRF signal of NC-6, and the fluorescence intensity was quantified as total radiant efficiency (TRE) vs. the corresponding control. (a) Quantitative *in vitro* NIRF intensity of different concentrations of NCs vs. control saline ( $n = 3$ , mean  $\pm$  SEM) and representative images of NCs in the well; (b) representative whole body *in vivo* images obtained at different time points after i.v. injection; (c) representative *ex vivo* images of excised organs at the end of the *in vivo* experiment; (d) *ex vivo* quantification of biodistribution of NCs determined by the averaged organ TRE vs. the control mouse ( $n = 2$ , mean  $\pm$  SEM).



study. Moreover, simultaneous multimodal imaging is an option through custom-tuning the functional moieties in the capsules. Despite that bare (non-PEGylated) NCs were used here, the PLGA NCs can also be easily pegylated as shown for the NC-8 system (3 wt% PEG Mn 5000) and modify the blood circulation time of NCs. Moreover, the magnetic functionality could be exploited for magnetic targeting in a selected organ or tissue.

### *In vitro* and *in vivo* safety studies of NCs

*In vitro* and *in vivo* safety studies of NC-3 (PLGA-SPIONs NCs) were conducted considering that this is the simplest therapeutic formulation for magnetically targeted delivery. We tested the effect of NC-3 on the proliferation/viability of human endothelial cells since endothelial cells lining the blood vessels are the first NC target following their intravenous administration. Thus, human brain endothelial cells (hCMEC/D3), a cell line derived from brain microcirculation, and primary cultures of human CD34<sup>+</sup>-derived endothelial cells were exposed to NC-3 and its cytotoxicity was evaluated by performing a MTT assay. As shown in Fig. 9a, the cells did not exhibit a decrease in viability after being exposed for 48 h to

the NCs from 25 to 100  $\mu\text{g mL}^{-1}$ , and the differences in cell viability between groups were not significant (ANOVA >0.05), thus our results suggest that the NCs are biocompatible for the studied range of concentrations and time. Thereafter, the systemic effect of NCs *via* i.v. administration was evaluated. Fig. 9b shows that after injection of NCs, all animals maintained the body weight within normal values for two weeks (no differences between groups at the end of the experimental period), with no significant morbidity and no potential adverse effects. At the same time, blood sample tests to monitor potential liver and pancreatic toxicity showed that none of the biomarker enzymes were significantly different between groups and similar to those measured in non-treated mice (Fig. 9c; ANOVA >0.05), suggesting a normal activity of these organs. All the above results reinforce the biosafety of this formulation of nanocarriers for future clinical translational practice.

### Protein loading

The protein loading content was determined as  $11.3 \pm 1.0 \mu\text{g}$  BSA per mg NCs (1.13 wt%) with an encapsulation efficiency of  $46.0 \pm 1.4\%$ , the average of six different batches measured. The

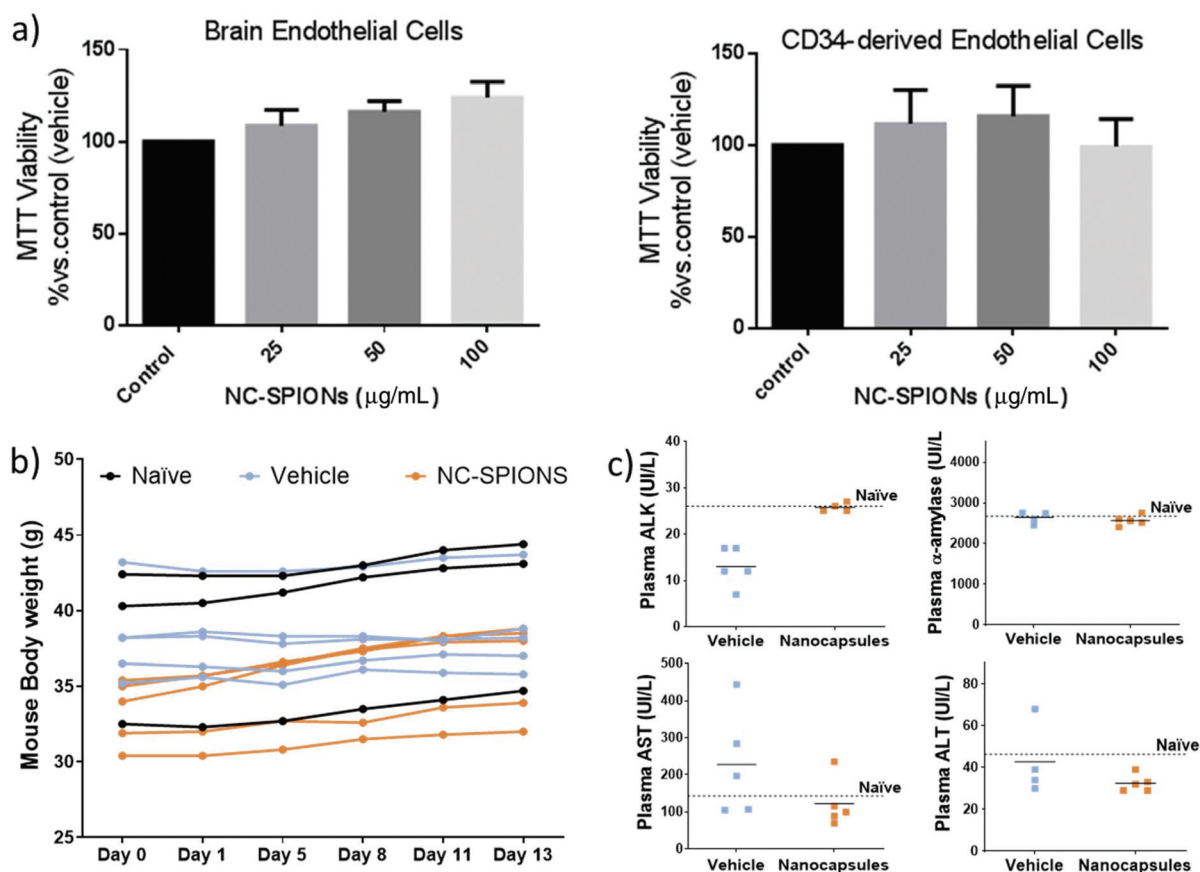


**Fig. 9** *In vitro* and *in vivo* safety of PLGA-SPION NCs (NC-3). (a) Cell viability after exposing to an increasing dose of NCs for 48 h, expressed as a percentage of untreated cells (control media), determined by MTT assay ( $n = 3$ , mean  $\pm$  SEM); (b) the curve of body weight of the observed mice throughout the experiment, the naïve group was not treated serving as control ( $n = 3$ ), the vehicle group received 150  $\mu\text{L}$  of saline ( $n = 5$ ) and the NC group received 0.84 mg NCs in 150  $\mu\text{L}$  of saline ( $n = 5$ ); (c) liver and pancreatic toxicity after 13 days of NC injection based on specific enzyme levels in plasma: alanine aminotransferase (ALT), alkaline phosphatase (ALK), aspartate aminotransferase (AST) and  $\alpha$ -amylase.



protein loading of 1.13 wt% is much higher than the reported value (0.03 wt%) of vessel endothelial growth factor loaded PLGA NCs<sup>31</sup> and the EE% is comparable to the PLGA NCs loaded with neurotrophin-3 (47 ± 2%) or brain-derived neurotrophic factor (47 ± 7%).<sup>8</sup>

## Conclusions

By covalently bonding PLGA with small molecules of fluorophores and radioligands as well as by incorporating iron oxide nanoparticles we propose here chemical synthetic approaches to transform PLGA NCs into a sensitive, multimodal theranostic platform for drug delivery. We have shown that the size of PLGA NCs remained unaltered after incorporation or removal of one or several imaging moieties. We have proposed a modular approach for capsules with multimodal capacities to be used at several development phases and investigated by different imaging modalities including MRI, fluorescence at different emitting wavelengths (blue and NIR) or <sup>89</sup>Zr-labeling enabled positron emission tomography (PET) imaging. In all cases, the imaging moieties are chemically attached to the PLGA and with minimal interaction with the encapsulated drug thus avoiding leaching and interferences with the therapeutic agent.

The theranostic PLGA NCs show no toxicity *in vitro* or *in vivo*. In this regard, the NCs did not affect the viability of two different human endothelial cells (brain endothelial cells and CD34<sup>+</sup> derived endothelial cells) for concentration up to 100 µg mL<sup>-1</sup>. *In vivo* biosafety was shown based on the lack of morbidity of mice for 2 weeks after the systemic NC administration and the fact that none of the biomarker enzymes monitored were significantly different between groups and similar to those measured in non-treated mice.

Finally, we have shown that the NCs can contain over 1 wt% of protein in their core achieved at the fabrication level. Interestingly, PLGA NCs decorated with iron oxide nanoparticles can be exploited for magnetic retention or magnetic guiding and biodistribution could be modified by using PEG-PLGA NCs.

## Author contributions

Y. Zhang contributed to the experimental design, data acquisition and analysis, and manuscript writing. M. García contributed to protein loading and *in vitro* safety study. A. Grayston contributed to the *in vivo* safety and IVIS study. I. Feiner and J. Llop contributed to the radiolabelling and PET study. R. Loiola and F. Gosselet participated in the *in vitro* safety study. P. Cabrer, I. Barba and D. Dorado contributed to the MRI study. I. Anton participated in the NC preparation. A. Rosell and A. Roig contributed to the design of experiments, coordination of the study, and manuscript writing. All authors revised the manuscript.

## Conflicts of interest

The authors declare no conflicts of interest.

## Acknowledgements

The Acciones Complementarias program from the Instituto de Salud Carlos III, Spain, co-financed by the European Regional Development Fund (AC17/00004 grant) as part of the MAGBBRIS project (Euronanomed III 8th joint call), and the RETICS INVICTUS RD16/0019/0021 are acknowledged. The Miguel Servet program (CPII15/00003) and PFIS program (FI17/00073) from Fondo de Investigaciones Sanitarias-Instituto de Salud Carlos III and ERDF supported A. Rosell and A. G. research contracts. This work was also partially supported by the Spanish Ministry of Science, Innovation and Universities through the grants PCIN-2017-090, RTI2018-096273-B-I00, CTQ2017-87637-R, SAF2017-87670-R, SEV-2015-0496 and MDM-2017-0720 and by the Generalitat de Catalunya grants (2017SGR765 & 2017SGR1427). Yajie Zhang is supported by the China Scholarship Council (CSC). FG and RAL are supported by the French national agency (ANR) through the grant ANR-17-ENM3-0005-01. The authors thank Dr Vanessa Gómez-Vallejo, Dr Unai Cossío, Dr Xabier Rios and Zuriñe Baz for support in labelling and PET *in vivo* experimentation. We acknowledge support of the publication fee by the CSIC Open Access Publication Support Initiative through its Unit of Information Resources for Research (URICI).

## References

- R. Klippstein, J. T. W. Wang, R. I. El-Gogary, J. Bai, F. Mustafa, N. Rubio, S. Bansal, W. T. Al-Jamal and K. T. Al-Jamal, *Small*, 2015, **11**, 4704–4722.
- T. Sudha, D. J. Bharali, M. Yalcin, N. H. Darwish, M. Debrel Coskun, K. A. Keating, H. Y. Lin, P. J. Davis and S. A. Mousa, *Int. J. Nanomed.*, 2017, **12**, 1305–1315.
- R. Yang, J. Xu, L. Xu, X. Sun, Q. Chen, Y. Zhao, R. Peng and Z. Liu, *ACS Nano*, 2018, **12**, 5121–5129.
- N. Bertrand, J. Wu, X. Xu, N. Kamaly and O. C. Farokhzad, *Adv. Drug Delivery Rev.*, 2014, **66**, 2–25.
- Z. Ouyang, T. Tan, C. Liu, J. Duan, W. Wang, X. Guo, Q. Zhang, Z. Li, Q. Huang and P. Dou, *Biomaterials*, 2019, **205**, 50–63.
- F. Danhier, E. Ansorena, J. M. Silva, R. Coco, A. Le Breton and V. Preat, *J. Controlled Release*, 2012, **161**, 505–522.
- D. Bobo, K. J. Robinson, J. Islam, K. J. Thurecht and S. R. Corrie, *Pharm. Res.*, 2016, **33**, 2373–2387.
- M. M. Pakulska, I. E. Donaghue, J. M. Obermeyer, A. Tuladhar, C. K. McLaughlin, T. N. Shendruk and M. S. Shoichet, *Sci. Adv.*, 2016, **2**, e1600519.
- X. Qin, C. Yu, J. Wei, L. Li, C. Zhang, Q. Wu, J. Liu, S. Q. Yao and W. Huang, *Adv. Mater.*, 2019, **31**, 1902791.



- 10 A. Harguindey, D. W. Domaille, B. D. Fairbanks, J. Wagner, C. N. Bowman and J. N. Cha, *Adv. Mater.*, 2017, **29**, 1700743.
- 11 C. J. Bowerman, J. D. Byrne, K. S. Chu, A. N. Schorzman, A. W. Keeler, C. A. Sherwood, J. L. Perry, J. C. Luft, D. B. Darr, A. M. Deal, M. E. Napier, W. C. Zamboni, N. E. Sharpless, C. M. Perou and J. M. DeSimone, *Nano Lett.*, 2017, **17**, 242–248.
- 12 B. Colzani, L. Pandolfi, A. Hoti, P. A. Iovene, A. Natalello, S. Avvakumova, M. Colombo and D. Prospero, *Int. J. Nanomed.*, 2018, **13**, 957–973.
- 13 W. Tao, X. Zeng, J. Wu, X. Zhu, X. Yu, X. Zhang, J. Zhang, G. Liu and L. Mei, *Theranostics*, 2016, **6**, 470–484.
- 14 P. Kumar, T. V. Treuren, A. P. Ranjan, P. Chaudhary and J. K. Vishwanatha, *Nanotechnology*, 2019, **30**, 265101.
- 15 A. C. Souza, A. L. Nascimento, N. M. de Vasconcelos, M. S. Jeronimo, I. M. Siqueira, L. R-Santos, D. O. Cintra, L. L. Fuscaldi, O. R. Pires Junior, R. Titze-de-Almeida, M. F. Borin, S. N. Bao, O. P. Martins, V. N. Cardoso, S. O. Fernandes, M. R. Mortari, A. C. Tedesco, A. C. Amaral, M. S. Felipe and A. L. Bocca, *Eur. J. Med. Chem.*, 2015, **95**, 267–276.
- 16 J. Llop, P. Jiang, M. Marradi, V. Gomez-Vallejo, M. Echeverria, S. Yu, M. Puigivila, Z. Baz, B. Szczupak and C. Perez-Campana, *J. Mater. Chem. B*, 2015, **3**, 6293–6300.
- 17 L. J. Cruz, M. A. Stammes, I. Que, E. R. van Beek, V. T. Knol-Blankevoort, T. J. A. Snoeks, A. Chan, E. L. Kaijzel and C. Lowik, *J. Controlled Release*, 2016, **223**, 31–41.
- 18 M. M. Abdel-Mottaleb, A. Beduneau, Y. Pellequer and A. Lamprecht, *Int. J. Pharm.*, 2015, **494**, 471–478.
- 19 R. L. Cook, K. T. Householder, E. P. Chung, A. V. Prakapenka, D. M. DiPerna and R. W. Sirianni, *J. Controlled Release*, 2015, **220**, 89–97.
- 20 S. Florinas, M. Liu, R. Fleming, L. Van Vlerken-Ysla, J. Ayriss, R. Gilbreth, N. Dimasi, C. Gao, H. Wu and Z.-Q. Xu, *Biomacromolecules*, 2016, **17**, 1818–1833.
- 21 K. Qian, J. Wu, E. Zhang, Y. Zhang and A. Fu, *Int. J. Nanomed.*, 2015, **10**, 4149.
- 22 S. Udenfriend, S. Stein, P. Bohlen, W. Dairman, W. Leimgruber and M. Weigele, *Science*, 1972, **178**, 871–872.
- 23 E. Carenza, V. Barcelo, A. Morancho, J. Montaner, A. Rosell and A. Roig, *Acta Biomater.*, 2014, **10**, 3775–3785.
- 24 J. Yang, Y. Zhang, S. Gautam, L. Liu, J. Dey, W. Chen, R. P. Mason, C. A. Serrano, K. A. Schug and L. Tang, *Proc. Natl. Acad. Sci. U. S. A.*, 2009, **106**, 10086–10091.
- 25 R. Cecchelli, S. Aday, E. Sevin, C. Almeida, M. Culot, L. Dehouck, C. Coisne, B. Engelhardt, M. P. Dehouck and L. Ferreira, *PLoS One*, 2014, **9**, e99733.
- 26 F. Shimizu, Y. Sano, M. a. Abe, T. Maeda, S. Ohtsuki, T. Terasaki and T. Kanda, *J. Cell. Physiol.*, 2011, **226**, 255–266.
- 27 K. Muring, V. Krasnenko and S. Miller, *J. Lumin.*, 2007, **122**, 291–293.
- 28 D. Wang, T. Imae and M. Miki, *J. Colloid Interface Sci.*, 2007, **312**, 8–13.
- 29 W. Yang and C. Y. Pan, *Macromol. Rapid Commun.*, 2009, **30**, 2096–2101.
- 30 J. Hu, J. Guo, Z. Xie, D. Shan, E. Gerhard, G. Qian and J. Yang, *Acta Biomater.*, 2016, **29**, 307–319.
- 31 E. Carenza, O. Jordan, P. Martinez-San Segundo, R. Jiřík, Z. Starčuk Jr., G. Borchard, A. Rosell and A. Roig, *J. Mater. Chem. B*, 2015, **3**, 2538–2544.
- 32 Y.-w. Jun, Y.-M. Huh, J.-s. Choi, J.-H. Lee, H.-T. Song, S. Kim, S. Kim, S. Yoon, K.-S. Kim and J.-S. Shin, *J. Am. Chem. Soc.*, 2005, **127**, 5732–5733.
- 33 R. Gref, M. Lück, P. Quellec, M. Marchand, E. Dellacherie, S. Harnisch, T. Blunk and R. Müller, *Colloids Surf., B*, 2000, **18**, 301–313.
- 34 Y. Cui, M. Zhang, F. Zeng, H. Jin, Q. Xu and Y. Huang, *ACS Appl. Mater. Interfaces*, 2016, **8**, 32159–32169.
- 35 N. Butoescu, C. A. Seemayer, G. Palmer, P. A. Guerne, C. Gabay, E. Doelker and O. Jordan, *Arthritis Res. Ther.*, 2009, **11**, R72.
- 36 E. Taboada, R. Solanas, E. Rodríguez, R. Weissleder and A. Roig, *Adv. Funct. Mater.*, 2009, **19**, 2319–2324.
- 37 Y. X. Wang, *Quant. Imaging Med. Surg.*, 2011, **1**, 35–40.
- 38 F. Chen, S. Goel, H. F. Valdovinos, H. Luo, R. Hernandez, T. E. Barnhart and W. Cai, *ACS Nano*, 2015, **9**, 7950–7959.
- 39 E. Boros, A. M. Bowen, L. Josephson, N. Vasdev and J. P. Holland, *Chem. Sci.*, 2015, **6**, 225–236.
- 40 D. S. Abou, T. Ku and P. M. Smith-Jones, *Nucl. Med. Biol.*, 2011, **38**, 675–681.
- 41 M. Cataldi, C. Vigliotti, T. Mosca, M. Cammarota and D. Capone, *Int. J. Mol. Sci.*, 2017, **18**, 1249.
- 42 E. Swider, S. Maharjan, K. Houkes, N. K. van Riessen, C. G. Figdor, M. Srinivas and O. Tagit, *ACS Appl. Bio Mater.*, 2019, **2**(3), 1131–1140.
- 43 J. M. Caster, S. K. Yu, A. N. Patel, N. J. Newman, Z. J. Lee, S. B. Warner, K. T. Wagner, K. C. Roche, X. Tian, Y. Min and A. Z. Wang, *Nanomedicine*, 2017, **13**, 1673–1683.





**Endovascular administration of magnetised nanocarriers  
targeting brain delivery after stroke**

---

DOI: 10.1177/0271678X211028816





# Endovascular administration of magnetized nanocarriers targeting brain delivery after stroke

Journal of Cerebral Blood Flow & Metabolism  
2022, Vol. 42(2) 237–252  
© The Author(s) 2021  
Article reuse guidelines:  
sagepub.com/journals-permissions  
DOI: 10.1177/0271678X211028816  
journals.sagepub.com/home/jcbfm



Alba Grayston<sup>1</sup> , Yajie Zhang<sup>2</sup> , Miguel Garcia-Gabilondo<sup>1</sup>, Mercedes Arrúe<sup>1</sup>, Abraham Martin<sup>3,4</sup>, Peter Kopcansky<sup>5</sup>, Milan Timko<sup>5</sup>, Jozef Kovac<sup>5</sup>, Oliver Strbak<sup>6</sup>, Laura Castellote<sup>7</sup>, Sara Belloli<sup>8,9</sup>, Rosa M Moresco<sup>8,10</sup>, Maria Picchio<sup>8,11</sup>, Anna Roig<sup>2</sup> and Anna Rosell<sup>1</sup> 

## Abstract

The increasing use of mechanical thrombectomy in stroke management has opened the window to local intraarterial brain delivery of therapeutic agents. In this context, the use of nanomedicine could further improve the delivery of new treatments for specific brain targeting, tracking and guidance. In this study we take advantage of this new endovascular approach to deliver biocompatible poly(D-L-lactic-co-glycolic acid) (PLGA) nanocapsules functionalized with superparamagnetic iron oxide nanoparticles and Cy7.5 for magnetic targeting, magnetic resonance and fluorescent molecular imaging. A complete biodistribution study in naïve (n = 59) and ischemic (n = 51) mice receiving intravenous or intraarterial nanocapsules, with two different magnet devices and imaged from 30 min to 48 h, showed an extraordinary advantage of the intraarterial route for brain delivery with a specific improvement in cortical targeting when using a magnetic device in both control and ischemic conditions. Safety was evaluated in ischemic mice (n = 69) showing no signs of systemic toxicity nor increasing mortality, infarct lesions or hemorrhages. In conclusion, the challenging brain delivery of therapeutic nanomaterials could be efficiently and safely overcome with a controlled endovascular administration and magnetic targeting, which could be considered in the context of endovascular interventions for the delivery of multiple treatments for stroke.

## Keywords

Stroke, endovascular treatment, PLGA, nanocarrier, magnetic targeting

Received 27 January 2021; Revised 8 June 2021; Accepted 8 June 2021

<sup>1</sup>Neurovascular Research Laboratory, Vall d'Hebron Institut de Recerca, Universitat Autònoma de Barcelona (VHIR-UAB), Barcelona, Spain

<sup>2</sup>Nanoparticles and Nanocomposites Group, Institut de Ciència de Materials de Barcelona (ICMAB-CSIC), Bellaterra, Spain

<sup>3</sup>Achucarro Basque Center for Neuroscience, Laboratory of Neuroimaging and Biomarkers of Inflammation, Leioa, Spain

<sup>4</sup>Ikerbasque Basque Foundation for Science, Bilbao, Spain

<sup>5</sup>Department of Magnetism, Institute of Experimental Physics, SAS, Kosice, Slovakia

<sup>6</sup>Biomedical Center Martin, Jessenius Faculty of Medicine in Martin, Comenius University in Bratislava, Martin, Slovakia

<sup>7</sup>Department of Clinical Biochemistry, Clinical Laboratories, Vall d'Hebron University Hospital, Barcelona, Spain

<sup>8</sup>Nuclear Medicine Department, IRCCS San Raffaele Scientific Institute, Milan, Italy

<sup>9</sup>Institute of Molecular Bioimaging and Physiology (IBFM), CNR, Segrate, Italy

<sup>10</sup>Department of Medicine and Surgery, University of Milano – Bicocca, Monza (MB), Italy

<sup>11</sup>School of Medicine, Vita-Salute San Raffaele University, Milan, Italy

## Corresponding authors:

Anna Rosell, Neurovascular Research Laboratory Vall d'Hebron Research Institute (VHIR), Passeig Vall d'Hebron 119-129; 08035, Barcelona, Catalonia, Spain.  
Email: anna.rosell@vhir.org

Anna Roig, Institut de Ciència de Materials de Barcelona (ICMAB-CSIC), Campus UAB, 08193 Bellaterra, Catalonia, Spain.  
Email: roig@icmab.es

## Introduction

Given the narrow time-window and insufficient performance of thrombolytic therapies in large vessel occlusion strokes, endovascular therapy (EVT) has been in the spotlight of stroke management over the past years.<sup>1</sup> EVT is now increasingly used throughout developed countries, with substantially improved devices showing successful recanalization rates within the first 6 h after symptoms onset.<sup>2–6</sup> Furthermore, the current American Stroke Association/American Heart Association guidelines have extended this time window up to 24 h in patients that meet specific eligibility criteria as demonstrated in the DAWN or DEFUSE clinical trials.<sup>7–9</sup> However, despite these enormous advances in stroke management, the stroke community is still investigating on new treatments to improve functional recovery beyond the acute phase, when rehabilitation therapies are the only approved treatments.<sup>10</sup> In this context, the extensive use of EVT in the daily clinical practice has also opened the opportunity for direct deliveries to the brain vasculature, through which neuroprotective or neurorestorative treatments could be directly administered in the ischemic hemisphere thus helping to overcome a significant drawback of systemic drug delivery.<sup>11,12</sup> In this regard this administration route has already been used in stroke clinical trials to administer autologous stem cells,<sup>13</sup> drugs such as verapamil<sup>14</sup> or to induce cerebral hypothermia by administering cold isotonic saline.<sup>15</sup>

In this scenario nanomedicine-based strategies are optimal candidates to synergistically exploit the advantages of endovascular approaches by tracking the therapeutic agent with imaging tags, reducing drug doses with a sustained release or improving brain targeting with functionalized biomaterials. In this light, we aimed at studying for the first time the advantages of the post-stroke endovascular delivery of biocompatible nanomaterials combined with specific magnetic brain targeting providing a complete safety, feasibility and biodistribution study. For this we have chosen poly (D-L-lactic-co-glycolic acid) (PLGA) as an FDA-approved biocompatible polymer that is currently used in over 10 therapeutic nanoformulations, with the potential to encapsulate a large variety of therapeutic agents and integrate different imaging moieties.<sup>16,17</sup> For the present study, the PLGA nanocapsules (NC) were functionalized with superparamagnetic iron oxide nanoparticles (SPION) and Cy7.5 for the improved magnetic targeting and brain imaging.

Our data provides evidence of the potential use and advantages of the endovascular delivery of nanomaterials after cerebral ischemia, which could be considered in the context of EVT to deliver multiple therapeutic agents.

## Materials and methods

### Animals

All procedures were approved by the Ethics Committee for Animal Experimentation of the Vall d'Hebron Research Institute and Universitat Autònoma de Barcelona (protocol numbers 70/18 and CEEA-4784) and conducted in compliance with the Spanish legislation and in accordance with the Directives of the European Union. A total of 129 C57BL/6JRj (C57) and 88 Balbc AnNRj (Balbc) adult male mice ( $23.7 \pm 1.5$  g and  $23.8 \pm 1.2$  g, respectively, 7 to 9 weeks), purchased from Janvier laboratories (Saint Berthevin, France), were used in this study. Mice were housed in groups and kept in a climate-controlled environment on a 12 h light/dark cycle. Food and water were available *ad libitum*. At the end of the study, a total of 59 mice were excluded: 21 due to failure/complications of the experimental procedures, 34 due to mortality after the interventions and 4 according to the exclusion criteria of the experimental model. A total of 38 mice were used for background control during fluorescent molecular imaging (FMI) acquisitions. All *in vivo* experiments are reported according to the ARRIVE 2.0 guidelines.<sup>18</sup> Complete schemes of the experimental designs are presented in Figures 1 to 4 and 6.

### Middle cerebral artery occlusion (MCAo)

C57BL/6 mice were subjected to 60 min MCAo by introducing an intraluminal filament through the right internal carotid artery (ICA), as described elsewhere.<sup>19</sup> All animals were anesthetized with isoflurane via facemask (5% for induction, 1.5% for maintenance in air, 79% N<sub>2</sub>:21% O<sub>2</sub>). Body temperature was maintained at 37°C using a self-regulated heating pad connected to a rectal probe. Mice eyes were protected from corneal damage during surgery using an ophthalmic lubricating ointment (Lipolac<sup>TM</sup>; Angelini Farmaceutica, Barcelona, Spain), and analgesia (subcutaneous buprenorphine 0.1 mg/kg; Divasa Farma-Vic S.A., Barcelona, Spain) was given before starting the surgical procedure and daily during the first 5 days after the surgery to minimize their pain and discomfort. Additionally, 0.5 mL of saline was daily administered subcutaneously for post-surgical recovery during the first 5 days. Nutritionally fortified water gel (DietGel Recovery<sup>®</sup>, ClearH2O<sup>®</sup>, Portland, ME, USA) was given to mice from *Safety study 2* one week prior to surgery for habituation and was available *ad libitum* after surgery.

After surgical exposure of the right Common Carotid Artery (CCA) bifurcation into the External Carotid Artery (ECA) and the ICA, a silicone-coated nylon monofilament (Doccol Corporation, Sharon,

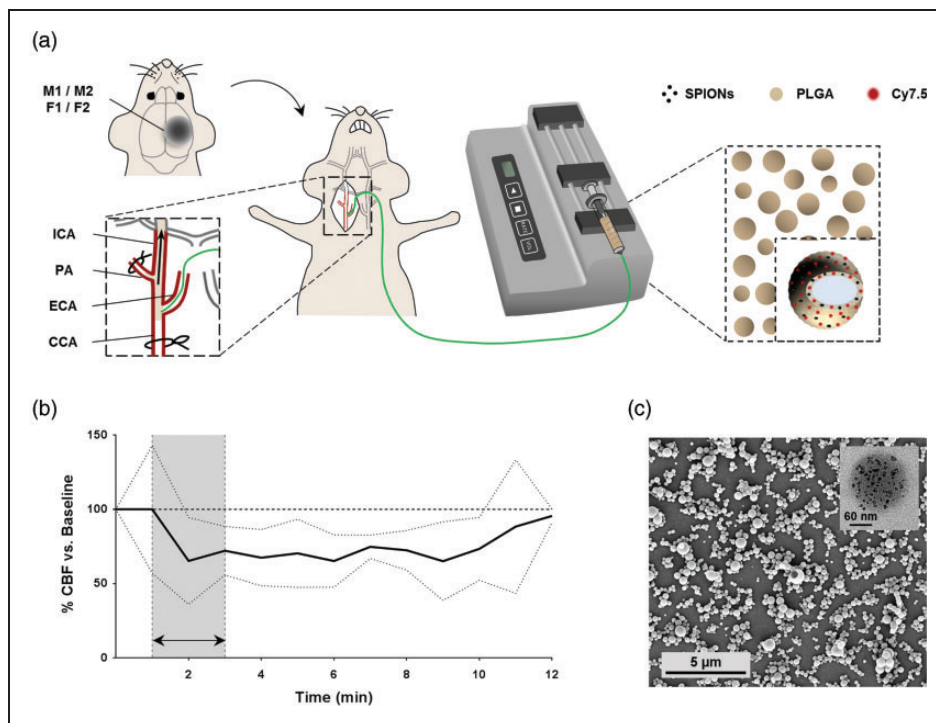


**Figure 1.** Endovascular-ICA administration of functionalized NC. (a) Scheme of the subcutaneous magnet implantation and the surgical procedure for intraarterial NC administration. (b) CBF during and after intraarterial administration of 0.8 mg of NC in 150  $\mu$ L of saline ( $n = 6$ ). Data shown as mean  $\pm$  SD. (c) Representative SEM image of NC. Inset showing a single NC TEM image, with SPION visible as black spots uniformly distributed in the PLGA. PA: pterygopalatine artery.

MA, USA, reference number: 602256PK10Re) was introduced through the ECA and directed towards the ICA to occlude the MCA. Occlusion was monitored by laser Doppler flowmetry using a flexible fibreoptic probe (Moor Instruments, Devon, UK) placed on the surface of the distal MCA branch, and confirmed by the decrease of the registered cerebral blood flow (CBF)  $>80\%$  (100% being considered as the pre-ischemia CBF value). After occlusion, animals woke up and were re-anesthetized for reperfusion 60 min later as described above by removing the monofilament. Only animals recovering  $>80\%$  of CBF after filament removal were finally included.

### Nanocarriers synthesis

PLGA-NC were synthesized by a double emulsion solvent evaporation method and functionalized with SPION and Cy7.5 (Figure 1(a) and (c)), as described previously.<sup>20</sup> Briefly, SPION were embedded in the PLGA shell by adding oleic acid-coated SPION with an average diameter of 9 nm in the PLGA organic phase during the first emulsification, and modified PLGA-Cy7.5 was also added in the organic phase in addition to the commercial PLGA. The obtained NCs suspension in trehalose aqueous solution was

lyophilized and stored at 4 °C with desiccant silica gel until each experimental use when they were resuspended in saline. The NC were freshly dispersed at the desired concentration before use, vortexed for 1 min and sonicated in an ultrasound bath for 3 min at 83.3 W/L and 48 kHz. Details of the different NC batches used in this study are listed in the Supplementary Table S1.

**Administration routes.** Systemic intravenous administration through the tail vein and intraarterial administration through the ICA of the NC dispersed in saline (either 1.6 or 0.8 mg/animal, corresponding to the *biodistribution* and *therapeutic doses*, respectively) were conducted; see Figure 1(a). The *therapeutic dose* corresponds to the approved doses of iron Feridex<sup>®</sup> (Endorem<sup>®</sup>).<sup>21</sup> The surgical procedure for the intraarterial administration was protocolized in the intraluminal MCAo model by cannulating the ECA 30 min after reperfusion under anesthesia as described above, with a polyimide microcatheter (0.2–0.22 mm OD, 0.14–0.15 mm ID; MicroLumen, Oldsmar, FL) directed towards the ICA and connected to an infusion pump (PHD 2000 Advance Syringe Pump, Harvard Apparatus, Holliston, Massachusetts, US) at an infusion rate of 75  $\mu$ L/min, total volume 150  $\mu$ L. Sham animals underwent the same surgical procedure as for the

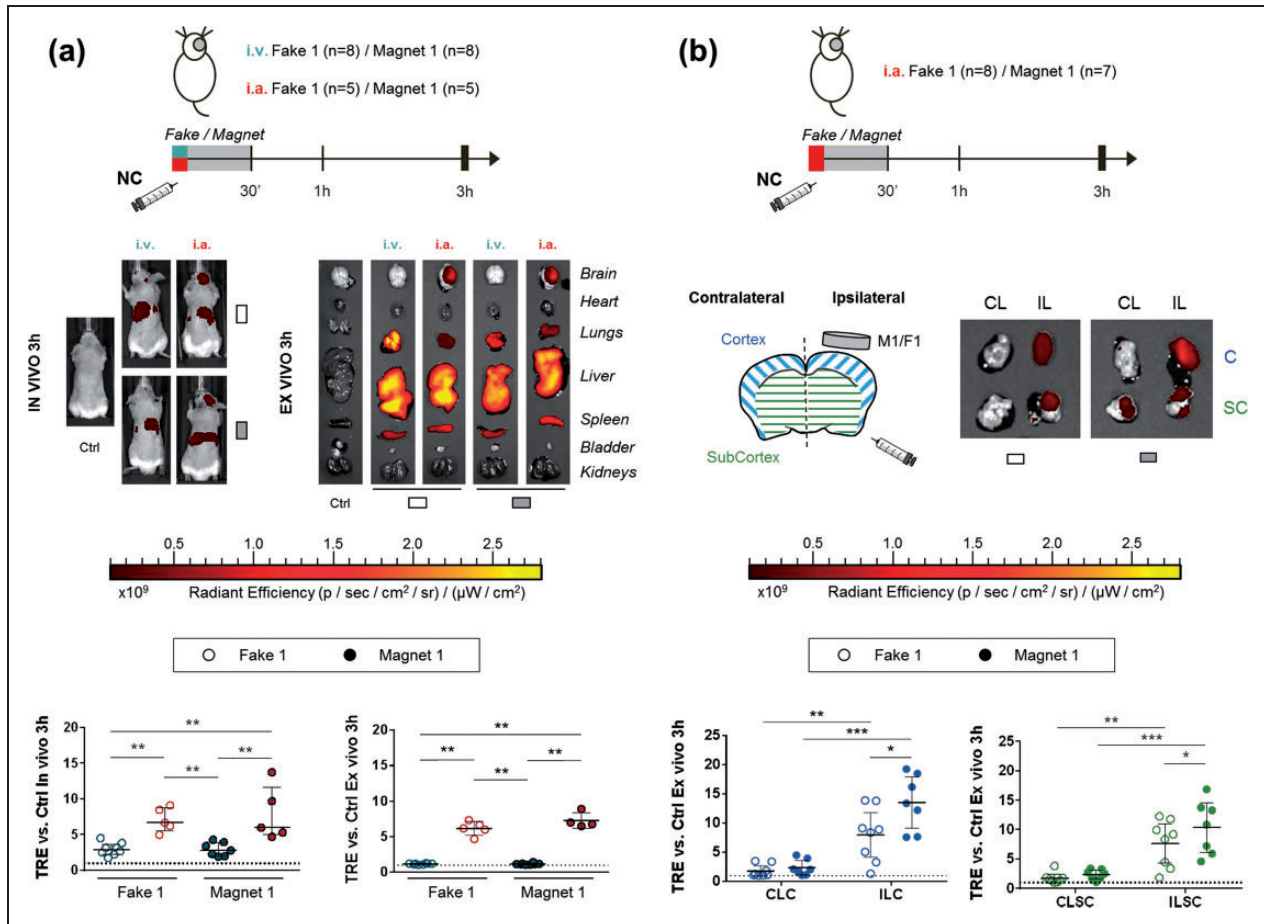


**Figure 2.** Biodistribution after NC administration showing the advantage of intraarterial-ICA route and magnetic targeting in naïve mice. (a) Scheme of the *Biodistribution study 1*, representative *in vivo* and *ex vivo* FMI images at 3 h after intravenous/intraarterial NC injection and graphs showing the corresponding quantification on brain regions of interest (ROIs). Data shown as median (IQR). (b) Scheme of the *Biodistribution study 2*, representative images *ex vivo* FMI of the ipsilateral/contralateral cortical and subcortical brain regions at 3 h after intraarterial NC injection and graphs showing the corresponding quantification. Data shown as median (IQR). \* $P < 0.05$ , \*\* $P < 0.01$ , \*\*\* $P < 0.001$ .

i.v.: intravenous; i.a.: intraarterial; Ctrl: control; ILC: ipsilateral cortex; ILSC: ipsilateral subcortex; CLC: contralateral cortex; CLSC: contralateral subcortex.

intraluminal MCAo model except that the microcatheter was introduced through the ECA without previously occluding the MCA. Note that the pterygopalatine artery was permanently sutured in all cases to avoid perfusion towards off-target areas. The cortical CBF was registered before, during and after intraarterial administration of the NC as described above and according to the experimental design in each group. On the other hand, for intravenous administrations a volume of 150  $\mu$ L NC suspension was administered using a 25 G needle through the lateral tail vein after vessel dilatation using a heat lamp.

### Magnet devices

To study the advantages of an external magnetic field for specific brain targeting of the magnetized NC, two

different iron-neodymium-boron (FeNdB) magnets were constructed considering the mouse brain anatomy: permanent Magnet 1 (M1) and focused Magnet 2 (M2), together with non-magnetic pieces serving as controls, minimally differing on the final size: Fake 1 (F1) and Fake 2 (F2).

M1 consists of a circular FeNdB permanent magnet of 5x2 mm covered by a soft iron yoke and a biocompatible polymer support frame (final size of the device was 8x3 mm). M2 consists of a focused FeNdB magnet with a 2x1mm matrix of submagnets covered with nickel and a thin biocompatible polyurethane/epoxy film, with a final cylindrical shape of 6x3 mm. F1 and F2 were manufactured as M1 and M2, respectively, except for a brass core instead of FeNdB. The spatial distribution of the magnetic field and magnetic force of M1 and M2 was characterized with the

standard QUICKFIELD software. The modelling was calculated in the plane 3 mm over the surface of the magnet devices (Figure 5).

The magnetic field induction and magnetic field gradient of the magnet devices M1 and M2 were measured by 3 D Hall probe. The magnetic force was calculated according to the distance from the center of the magnet at 3 mm in height from the magnet surface.

The magnet/fake device was implanted on the right (ipsilateral) hemisphere prior to the NC administration (under anesthesia, as described in the supplementary materials) attached to the skull with superglue. The skin was closed over the device using Histoacryl® (Figure 1(a)) and the piece was removed before the first *in vivo* image acquisition.

### Biodistribution by FMI

FMI was performed to characterize the fluorescence of the Cy7.5\_NC *in vitro* (for details, please see the supplementary materials) and to track the NC biodistribution *in vivo* and *ex vivo* in single organs using a Xenogen IVIS® spectrum. Prior to *in vivo* administrations, the fluorescence of Cy7.5\_NC batches was characterized by FMI. Briefly, a series of concentrations of Cy7.5-labeled NC in 100 µL of saline were prepared for each batch in a 96-well plate and imaged using a Xenogen IVIS® spectrum ( $\lambda_{ex}/\lambda_{em}$  710/820 nm, respectively); see Figure S1.

The general protocol for the *in vivo* biodistribution studies started with mice being anesthetized with isoflurane via facemask (5% for induction, 1.5% for maintenance in 95% O<sub>2</sub>) and images being acquired at different time points post-injection according to each experimental design ( $\lambda_{ex}/\lambda_{em}$  710/820 nm, respectively) in dorsal and ventral views of the whole body. Between image acquisitions mice recovered from anesthesia in temperature-controlled recovery cages. All animals were euthanized by cervical dislocation under anesthesia after the last *in vivo* acquisition and brain, heart, lungs, liver, spleen, kidney and bladder were dissected for the *ex vivo* imaging ( $\lambda_{ex}/\lambda_{em}$  745/820 nm, respectively) in dorsal and ventral views. For details of the FMI analysis, please see the supplementary materials.

**Biodistribution study 1:** To first study biodistribution of the NC following systemic or endovascular routes and the influence of the first magnet device for brain targeting, randomly assigned naïve Balbc mice were injected either intravenously (n = 16) or intraarterially (n = 10) with the 1.6 mg *biodistribution dose* of Cy7.5\_NC following the aforementioned protocols. Each intravenous/intraarterial group was further randomly divided into the M1 and the control F1 groups. The fake/magnet devices were implanted for 30 min after the NC administration and FMI *in vivo* images

were acquired at 30 min, 1 h and 3 h post-injection (Figures 1(a) and 2(a)). After the last acquisition, mice organs were obtained for *ex vivo* imaging as described above. **Biodistribution study 2:** to further investigate the influence of the magnetic field on the NC brain retention, naïve Balbc mice receiving the 1.6 mg *biodistribution dose* of Cy7.5\_NC intraarterially were randomly assigned into the M1 (n = 7) and the control F1 (n = 8) groups, implanted and administered as described above. A single image acquisition was conducted at 3 h post-injection when the brain was removed and divided into cortical and subcortical regions for the *ex vivo* acquisition (Figures 1(a) and 2(b)).

**Biodistribution study 3:** next, we studied the biodistribution of the NC after acute intraarterial administration in the MCAo model, with magnetic guidance by two magnet devices with different magnetic fields. A total of 16 C57 mice receiving the 0.8 mg *therapeutic dose* of Cy7.5\_NC intraarterially were randomly divided into the two magnet groups (M1 and M2) and a control fake F2 group. The magnet/fake devices were removed after 3 h before the first FMI acquisition time-point which was repeated at 48 h post-injection. After the last image acquisition organs were obtained for *ex vivo* imaging (Figures 1(a) and 5(a)).

### Biodistribution by magnetic resonance imaging (MRI)

**Biodistribution study 4:** MRI was performed to further characterize the retention and spatial distribution of the NC in the brain after acute intraarterial administration in the MCAo model with magnetic guidance by the M2 device, which showed a better performance in the FMI *Biodistribution study 3* (Figures 1(a) and 5(b)). A total of 17 C57 mice receiving the 0.8 mg *therapeutic dose* of Cy7.5\_NC through the ICA were randomly divided into the M2 and the control F2 groups, implanted and administered as in *Biodistribution study 3*. A single *in vivo* MRI was carried out at 48 h post-injection using a BioSpec 70/30 USR scanner with a 7 T horizontal magnet (Bruker BioSpin, Ettlingen, Germany) equipped with a 72 mm inner diameter linear volume coil as a transmitter and a mouse brain surface coil as a receiver. High-resolution T2-weighted and high-resolution T2\*-weighted images were acquired to visualize the ischemic lesion and the hypointensities representing the SPION-labelled NC, respectively. For details of the acquisition protocols and MRI analysis, please see the supplementary materials.

### Safety study in the MCAo model

**Safety study 1:** to assess the safety of acute endovascular NC administration after cerebral ischemia, a total

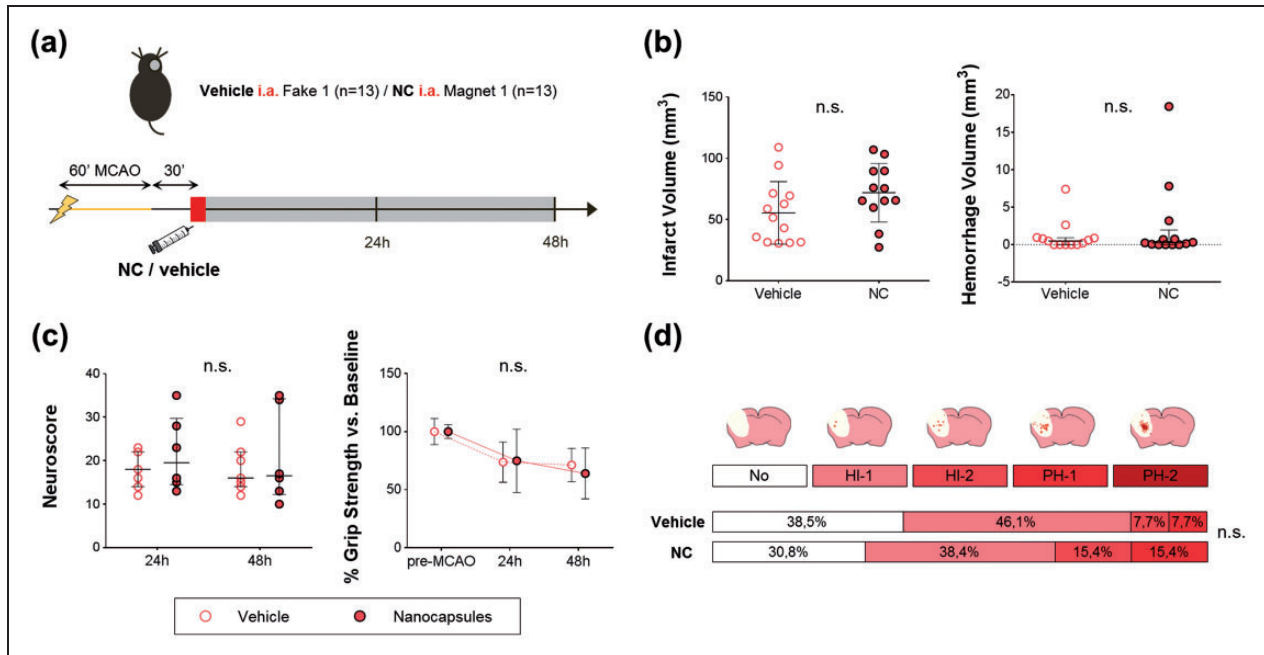


**Figure 3.** Safety of acute intraarterial-ICA NC administration after MCAO and magnetic targeting. (a) Scheme of the experimental design of *Safety study 1*. (b) Graphs showing infarct and hemorrhage volumes. (c) Graphs showing neuroscore and grip strength measurements. (d) Hemorrhages evaluation by visual classification according to ECASS criteria in TTC-stained brains represented as the percentage of animals classified in each category. Data represented in Infarct volume and Grip strength show the mean $\pm$ SD, and data represented in Hemorrhage volume and Neuroscore graphs show the median (IQR). n.s.: non-significant.

of 26 C57 ischemic mice were randomly assigned into 2 groups: the vehicle group receiving 150  $\mu$ L of saline (n=13) with a fake magnet (F1), and the treatment group receiving the 0.8 mg *therapeutic dose* of NC in 150  $\mu$ L of saline (n=13) with a magnet (M1), following the aforementioned protocols of pre-clinical stroke and endovascular administration through the ICA (Figures 1(a), 3(a) and 4(a)). Both groups were followed for 48 h, when blood was collected from the right ventricle in EDTA tubes for biochemical analysis and animals were euthanized under deep anesthesia by cervical dislocation to dissect the brain for 2,3,5-triphenyltetrazolium chloride (TTC) staining and intracerebral hemorrhage evaluation.

*Safety study 2:* C57 ischemic mice (n=8) receiving the 0.8 mg *therapeutic dose* of NC through the ICA were followed for 4 weeks when under deep anesthesia blood was collected from the right ventricle in EDTA tubes for biochemical analysis. Plasma control samples were also included from naïve C57 mice (n=8) and ischemic C57 mice without treatment followed at 48 h (n=4) and at 4 weeks (n=8). (Figures 1(a) and 4(a)).

#### Prussian blue and vessel staining with lectin-FITC

To confirm the presence of the NC in the brain, we performed specific staining for ferric iron as part of

the SPION of the NC. Animals from *Biodistribution study 4* were euthanized under deep anesthesia by exsanguination followed by transcardial perfusion with cold saline and the brain, liver and spleen were fixed with 10% formalin, paraffin-embedded and sliced in 5  $\mu$ m-thick sections with a microtome. After deparaffinization and rehydration, the sections were stained with a Prussian blue iron stain kit (Polysciences Inc, USA) following the manufacturer's protocol except for that potassium ferrocyanide: hydrochloric acid mix solution was kept for a total of 40 min and nuclear Fast Red for 1 min. Images were acquired after dehydration and mounting with DPX medium (Ref. 06522, Sigma-Aldrich, St. Louis, USA) with a transmitted light microscope (Leica, Germany) and an automatic slide scanner (PANNORAMIC MIDI II, 3DHISTECH Ltd, Hungary).

To confirm the distribution of NC (Cy7.5-labeled) in brain microvessel structures as seen by Prussian blue staining, vasculature was stained in consecutive brain slices with lectin-FITC as follows: after deparaffinization and rehydration, the sections were incubated overnight with lectin-FITC from *Lycopersicon esculentum* (Ref. L0401, Sigma-Aldrich, Germany) diluted 1:200 in PBS-1% Tween20. After dehydration and mounting with antifade mounting medium (Vectashield, CA,

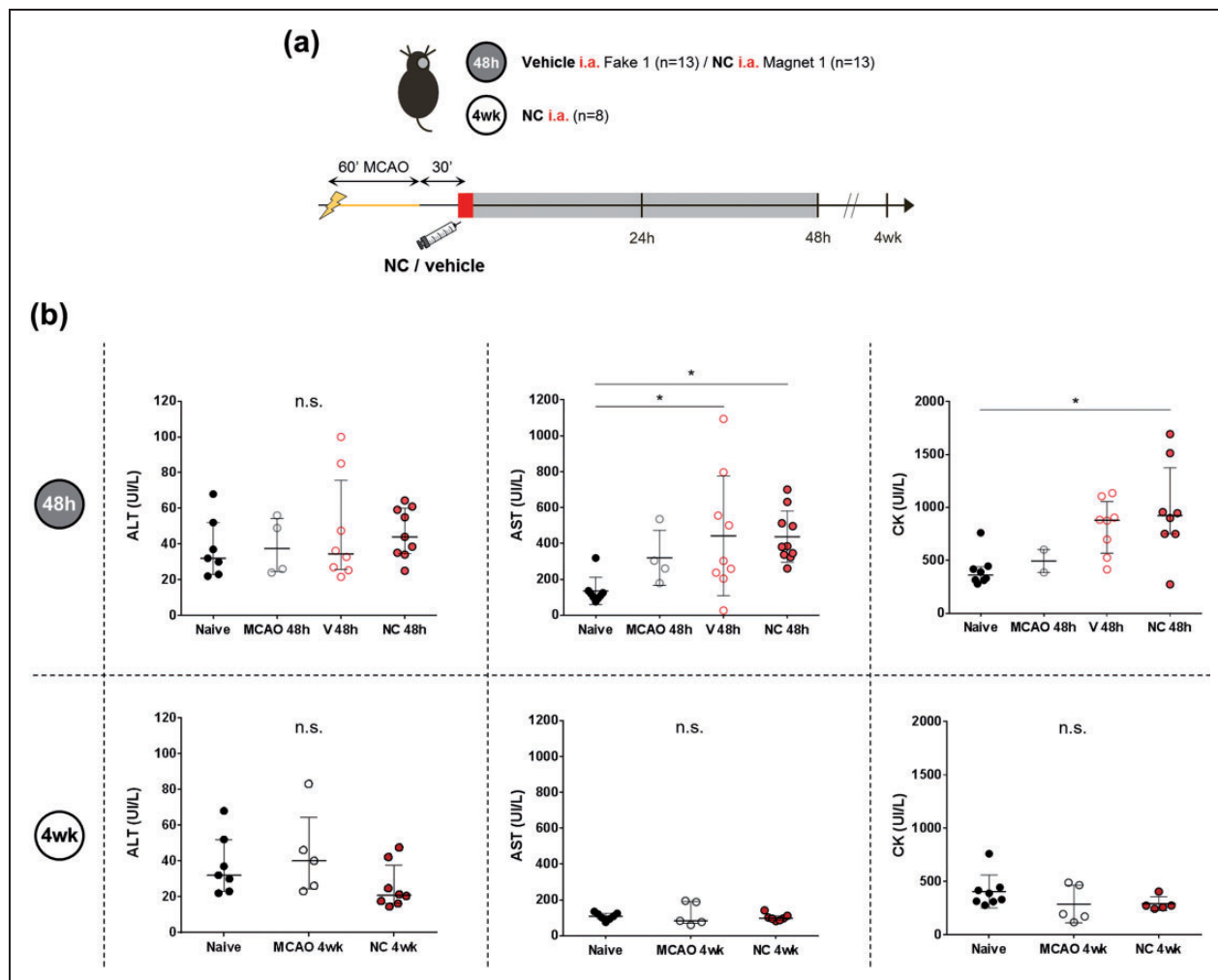


**Figure 4.** Systemic toxicity study at 48 h and 4 weeks after MCAo and intraarterial-ICA NC administration. (a) Scheme of the experimental design of *Safety studies 1* and *2*. (b) Plasma levels of AST, ALT and CK represented in graphs show the median (IQR), except for the graphs showing AST levels at 48 h and CK levels at 4 weeks, where the data is showing mean ± SD. \* $P < 0.05$ , n.s.: non-significant. Abbreviations: V: vehicle; NC: nanocapsule.

USA), images were acquired with a confocal laser scanning microscope (LSM880, Zeiss, Germany).

### Infarct volume and intracerebral hemorrhage evaluation

Ischemic C57 mice from *Safety study 1* were euthanized at 48 h after administration post-reperfusion by cervical dislocation. Brains were removed, sliced in 1 mm thick coronal sections and stained with TTC (Sigma, St. Louis, MO, USA) in saline at room temperature for 15 min. Infarct volumes were quantified by a treatment-blinded researcher with the Image J software and corrected by edema as previously described.<sup>22</sup> The number and extent of hemorrhagic events was determined by 3 independent treatment-blinded raters using a semi-quantitative method adapted from the ECASS

classification as described elsewhere<sup>23,24</sup> by giving 0 to 4 scores as follows: 0 = absence of hemorrhage, 1–2 = increasing grades of hemorrhage infarction (HI1 and HI2), and 3–4 = homogeneous parenchymal hematomas of increasing grades (PH1 and PH2); see Figure 3(d). The hemorrhage volume was also quantified with Image J following the same protocol as for the infarct volume.

### Functional tests

Neurological deficits were evaluated in mice from *Safety study 1* by a researcher blinded to the treatments with a 0 to 39 score based on a composite neurological scale<sup>25,26</sup> at 24 h and 48 h after MCAo. The forelimb force was also assessed in the animals from *Safety study*



1 with the grip strength test as previously described.<sup>27</sup> For details, please see the supplementary materials.

### Biochemical analysis

Venous blood obtained from the right ventricle by cardiac puncture in EDTA tubes was centrifuged (1500 g, 10 min at 4°C) to obtain plasma which was stored at -80°C until analysis. Liver/pancreas/renal toxicity based on specific enzyme levels in plasma was assessed in the animals from *Safety studies 1* and *2*; for details see the supplementary materials.

### Statistical analysis

Statistical analyses were performed using the GraphPad Prism 6 and SPSS softwares. The sample size of the *Safety study 1* was determined in a pilot study ( $n=4-5/\text{group}$ ) by power analysis based on the infarct volume as primary outcome measure, using the software Ene 3.0 (GlaxoSmithKline SA), at 80% of statistical power and to a significance level of 5%. Randomization of the experimental groups was generated using the standard = RAND() function in Microsoft Excel. All values are expressed as mean  $\pm$  SD or median (InterQuartile Range, IQR) according to the normal or non-normal distribution of the represented variable, respectively. The normality of continuous variables was assessed using the Shapiro-Wilk test ( $n < 30$ ) or Kolmogorov-Smirnov test ( $n \geq 30$ ). Normally distributed variables were analyzed using t-test or ANOVA (followed by Tukey's multiple comparisons post hoc test). The Mann-Whitney U-test or Kruskal Wallis test (followed by Dunn's multiple comparisons post hoc test) were used for non-normally distributed variables. Pearson's  $\chi^2$  test or Fisher exact test were used for categorical variables. A total of 14 extreme values were excluded prior to data analyses using the outliers ROUT method ( $Q=1\%$ ), corresponding to the biochemical parameters analysis ( $n=11$ ), the NC biodistribution in naïve mice ( $n=2$ ) and the safety NC administration in ischemic mice ( $n=1$ ). The significant level was set at  $P < 0.05$ .

## Results

### *Intraarterial administration of nanomaterials shows a robust advantage for brain targeting*

Our protocol for the endovascular administration of NC for brain targeting through the ICA in mice only transiently reduced the CBF at moderate levels for the first 10 min post-administration ( $34.8 \pm 29.2\%$  CBF reduction); see Figure 1.

The different Cy7.5\_NC batches used in this study presented a similar dose-dependent fluorescent signal when imaged *ex vivo* (Supplementary Figures S1(a) and S1(b)) and no associations between NC batch-fluorescence and treatment group were observed, discarding batch-dependent biased results for the FMI data (Supplementary Figures S1(c) and S1(d)).

Our results show a significant increase of the *in vivo* brain NC fluorescent signal (Total Radiant Efficiency, TRE) at all the acquisition time points after intraarterial administration compared to the intravenous route, both in the absence (F1) or presence (M1) of an external magnetic field ( $P=0.0062$ ,  $P=0.0062$  and  $P=0.0016$  for F1 at 30 min, 1 h and 3 h post-injection, respectively and  $P=0.0025$ ,  $P=0.0025$ ,  $P=0.0025$  for M1 at 30 min, 1 h and 3 h post-injection, respectively); see Figure 2(a) and Supplementary Figure S2(a) and S2(b). Figure 2(a) also shows the significant NC signal increase in the brain *ex vivo* at 3 h post-injection of animals receiving intraarterial infusions vs. intravenous ( $P=0.0016$  for F1 and  $P=0.004$  for M1). Specifically, the brain fluorescent signal at 3 h after intraarterial administration was increased  $2.53 \pm 0.95$  times *in vivo* and  $5.65 \pm 0.96$  *ex vivo*. Absolute fluorescence values were similar between administration routes in the abdominal region at all the *in vivo* acquisition time points and *ex vivo* in all organs (except the brain) at 3 h post-injection, and did not change in the presence of a magnetic field ( $P > 0.05$  for all measures, Supplementary Figure S2). However, when comparing the individual relative fluorescence in the abdominal region we found that it was significantly reduced in the intraarterial administration vs. the intravenous route ( $P=0.0109$ ,  $P=0.0062$  and  $P=0.0031$  for F1 at 30 min, 1 h and 3 h post-injection, respectively and  $P=0.0025$ ,  $P=0.0025$ ,  $P=0.0025$  for M1 at 30 min, 1 h and 3 h post-injection, respectively), and was also reduced in the liver *ex vivo* in the endovascular route with the magnet M1 ( $P=0.0012$ ); see Supplementary Figure S3.

### *Improved cortical NC targeting*

As shown in Figure 2(a), no differences were observed in the retention of the NC in the whole brain when implanting the magnet M1 for 30 min ( $P > 0.05$  for M1 vs. F1 for both administration routes). However, when dissecting the cortical and subcortical tissue we observed a significant increase ( $P=0.0382$ ; Figure 2(b)) in the brain fluorescence in the ipsilateral cortex when the magnetic field was applied by M1, in areas under the influence of the magnetic. Furthermore, a NC signal increase in the ipsilateral cortical and subcortical tissue was observed compared to the corresponding contralateral ( $P < 0.05$  for all measures; see Figure 2(b)).

### Acute endovascular administration of magnetized nanocarriers after cerebral ischemia is feasible and safe

The safety study showed that the body weight loss and the mortality rate after MCAo were similar among NC and vehicle groups and within the expected values (Supplementary Figures S4(a) and S4(b)). Our results also showed no significant differences in functional outcome, infarct volume nor hemorrhagic transformations ( $P > 0.05$  for all measures) (Figure 3).

Potential systemic toxicity of the endovascular-ICA administration of NC was studied at 48 h and 4 weeks after MCAo and no significant differences in the levels of alanine aminotransferase (ALT), lipase, creatinine, urea and sodium were observed among groups ( $P > 0.05$  for all measures). Only aspartate aminotransferase (AST) was increased at 48 h vs. the Naïve group ( $P = 0.031$  and  $P = 0.031$  for Vehicle and NC groups, respectively) and creatine kinase (CK), a muscular injury-related enzyme, was increased at 48 h in the NC treatment vs. the Naïve group ( $P = 0.027$ ). Importantly, the increased levels of AST and CK in the vehicle and NC groups returned to normal levels at 4 weeks ( $P > 0.05$  for all comparisons), thus confirming the muscle injury-related increased levels of AST and CK acutely after the surgical intervention in the MCAo model. Finally, the levels of  $\alpha$ -amylase were increased at 48 h after the ischemia compared to the Naïve group ( $P = 0.0025$  for the NC group), returning to normal levels at 4 weeks ( $P = 0.0005$  vs. the NC group at 48 h post-ischemia). See Figure 4 and Supplementary Figure S4(c).

### Modelling magnetic field properties increases brain nanomaterial retention after ischemia

We investigated the magnetic properties of the two FeNdB magnets designed as NC retention devices for the mouse brain, a permanent magnet (M1) and a focused magnet (M2) (Figures 5 and S5). Experimental measurements of the spatial magnetic field distributions at different distance from the surface of the M1 and M2 showed that the magnetic force decreases as an inverse square law with the distance, displaying a higher magnetic force within the first 3 mm from the surface. However, M2 displays a 2.5-fold increase of the maximum values of the magnetic field and 5.5-fold increase of the magnetic force compared to M1, which is in agreement with the theoretical modelling of the magnetic field distribution of both magnet prototypes (Figure 5).

Next, we aimed to prove the *in vivo* effectiveness of M1 and M2 devices on magnetic brain targeting after acute endovascular NC administration at the

calculated *therapeutic dose* after cerebral ischemia by FMI (Figure 6(a)). Our results show a significant  $2.42 \pm 0.78$ -fold increase of *in vivo* NC signal reaching the brain region at 3 h only by the M2 device compared with the F2 control ( $P = 0.0209$ ). This advantage was maintained at 48 h post-injection *in vivo* ( $2.56 \pm 0.53$ -fold increase,  $P = 0.0001$ ) and confirmed *ex vivo* ( $2.16 \pm 0.8$ -fold increase,  $P = 0.0398$ ). On the other hand, the M1 device showed a  $1.72 \pm 0.51$ -fold increase in brain NC signal *in vivo* at 48 h post-injection compared to the F2 control, although not significant ( $P = 0.055$ ). Importantly, M2 device showed  $1.49 \pm 0.31$  times more brain NC signal at 48 h than M1 *in vivo* ( $P = 0.0182$ ). In parallel, FMI values were similar in the abdominal region *in vivo* at 3 h and 48 h post-injection and *ex vivo* in all organs ( $P > 0.05$  for all measures, Supplementary Figure S6(b)).

From a translational perspective, we aimed to confirm the results by MRI, a clinically-relevant technique, to better define the spatial brain distribution of the NC after M2 implantation using the T2 relaxation properties of the SPION; see Figure 6(b). In accordance with the results observed by FMI, a significant increase in the particles count was observed in the ipsilateral cortex when the M2 device was implanted vs. the F2 control ( $P = 0.0125$ ; see Figure 6(b)), thus confirming the success in magnetic retention of the NC in the brain cortex.

Finally, a specific Prussian blue staining was conducted to confirm the MRI findings, to identify the location of the nanomaterial in tissues. Representative images of brain, liver and spleen from animals receiving NC intraarterially in the presence of M2 are shown in Figure 7 and Supplementary Figure S7. Spleen slices were used as Prussian blue controls<sup>28</sup> and liver slices were also stained to confirm the presence of the NC in tissues as NC typically accumulate in the liver (Supplementary Figure S7). Brain slices showed extensive positive staining in the ipsilateral brain hemisphere, predominantly in microvessel-like structures, while the presence of ferric iron in the contralateral hemisphere was negligible, matching with the FMI and MRI results (see Figure 7). Additionally, the predominant distribution of NC in ipsilateral brain microvessels was confirmed by co-localization of the Cy7.5 fluorescence with lectin-FITC stained microvessels (Figure 7).

### Administration-related cautions

Adverse events have been previously described after intraarterial cell administration such as micro-occlusions or increased mortality rate.<sup>12,29,30</sup> In this regard, it should be highlighted that the average size of the nanomaterial used in the present study was  $273.21 \pm 34.7$  nm, within an acceptable range to avoid

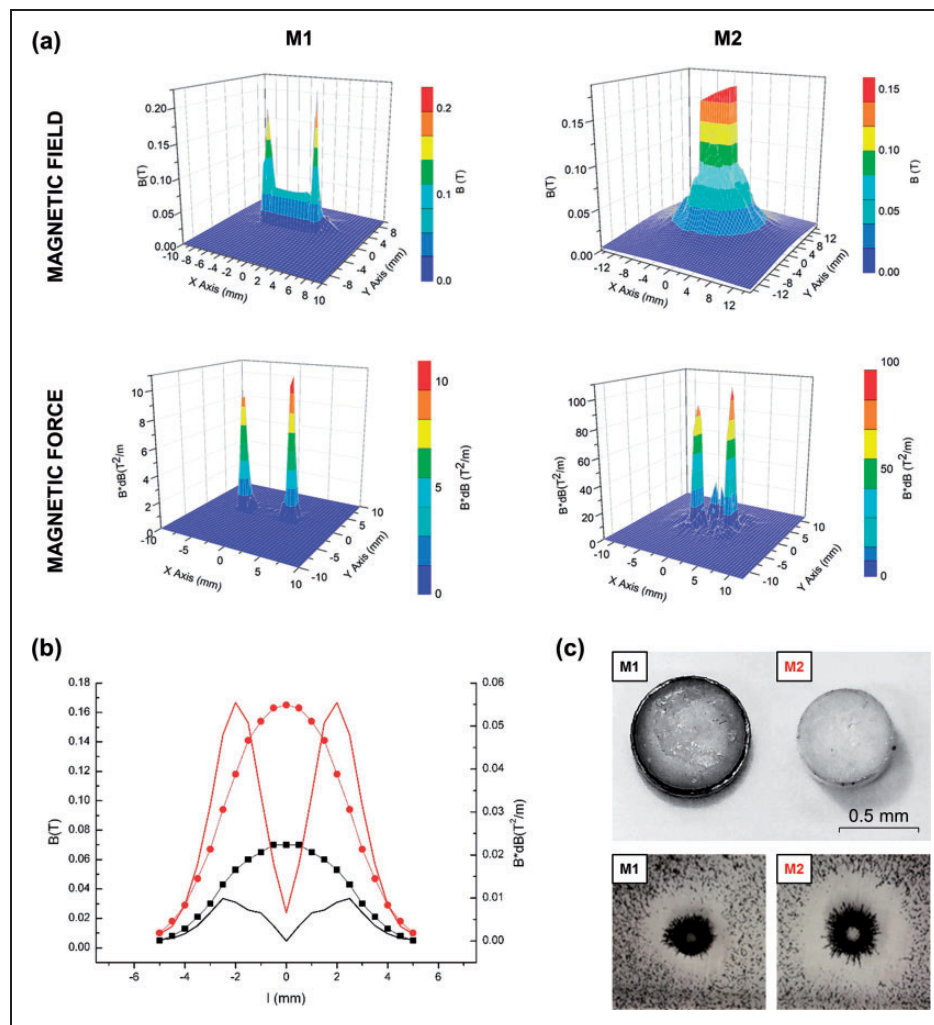


**Figure 5.** Characterization of the magnetic field and magnetic force of the magnet devices. (a) Spatial distribution by computational modelling of the magnetic field and spatial distribution of the magnetic force for M1 (left) and M2 (right) at 3 mm above the magnet surface. (b) Graph showing the magnetic field ( $B$ ; dotted lines) and magnetic force ( $B^2/dB$ ; straight lines) of M1 (black) and M2 (red) at 3 mm above the magnet surface, measured by 3D Hall probe. (c) Image (above) of M1 and M2 devices and illustrative image (below) of the dust effectivity test of magnetic targeting of ferrimagnetic magnetite microparticles for M1 and M2.

embolization complications. Indeed, no differences were observed in the mortality rate between ischemic mice receiving NC or vehicle intraarterially (*Safety study 1*: 21.1% and 27.3%, respectively ( $P=0.727$ ); see Supplementary Figure S4(b)). Importantly, we observed a trend ( $P=0.091$ ) between the total iron load dose and the mortality rate among ischemic C57 mice receiving NC intraarterially, which alerts us on potential harms of the use of certain nanomaterials.

## Discussion

In this study, we tested the use of biocompatible nanomaterials to improve brain targeting after stroke taking advantage of the endovascular route to reach the brain vasculature and the use of functionalized nanocarriers

for imaging and magnetic targeting. Our data prove the safety and feasibility of acute brain endovascular infusion of multimodal biocompatible PLGA-NC in a mouse model of cerebral ischemia to significantly improve brain delivery, paving the way for future nanomaterial-based treatments in the context of EVT.

A crucial aspect to consider while investigating a new therapeutic approach is the ideal administration route in terms of safety and efficient delivery while considering the particularities of a given pathological condition. As mentioned above, endovascular treatments have the advantage of a more selective targeting while minimizing the side effects of systemic drug delivery in filtering organs.<sup>11,12</sup> In consistency with previous studies,<sup>20,31,32</sup> we have observed that intravenously administered NC predominantly accumulate in the

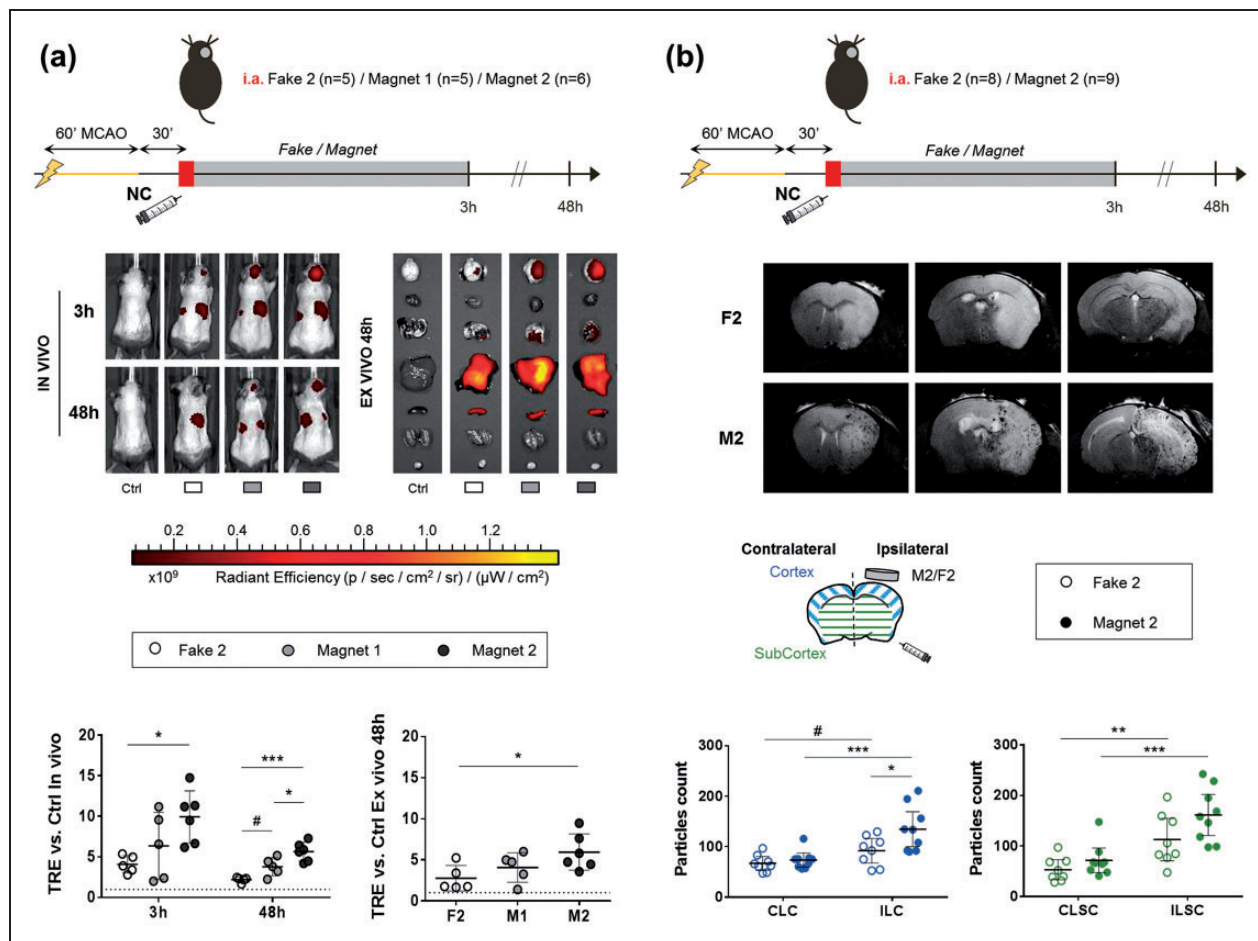


**Figure 6.** Biodistribution after MCAo and intraarterial-ICA NC administration showing the improved NC brain targeting with different magnetic devices and superior performance of the focused magnet design (M2). (a) Scheme of the experimental *Biodistribution study 3*, representative *in vivo* FMI images and *ex vivo* after intraarterial-ICA NC administration and graphs showing the corresponding quantification on brain ROIs. (b) Scheme of the *Biodistribution study 4*, representative brain T2\*WI 48 h after intraarterial-ICA NC administration and graphs showing the corresponding particle analysis of the hypointense signals attributed to SPION in ipsilateral/contralateral cortical and subcortical regions. All data are shown as mean  $\pm$  SD, except the graph showing the particles count in the subcortical regions, where data is represented as median (IQR). #P < 0.01, \*P < 0.05, \*\*P < 0.01, \*\*\*P < 0.001.

liver, lungs and spleen, while their retention in the brain is almost negligible. In contrast, our data confirm the significant advantage for stroke-affected brain tissue targeting following the intraarterial-ICA administration route,<sup>33,34</sup> as seen both by MRI and FMI when delivering small nanocarriers (below 300 nm in our study). The preferential ipsilateral and negligible contralateral hemisphere NC accumulation, seen both in healthy and ischemic mice in our study, has been already described by Lesniak and colleagues observing a preferential ipsilateral accumulation of Bevacizumab after intraarterial administration of the free antibody, which was further enhanced following the blood-brain barrier (BBB) opening with mannitol and preserving the preference for the ipsilateral hemisphere of the injection.<sup>35</sup> Further investigations are required for a deeper understanding of the underlying mechanisms

for this specific ipsilateral uptake and to fully elucidate the effects of this approach on the integrity of the BBB. However, we did not observe major hemorrhagic events after intraarterial vehicle nor NC administration following MCAo, evidencing the safety in the context of cerebral ischemia. Similarly, the SAVER-I Phase I trial has also demonstrated the feasibility and safety of the intraarterial administration of free verapamil after standard thrombectomy with no evidence of hemorrhagic transformations.<sup>14</sup>

Brain delivery of therapeutic agents in minimally invasive approaches has been a major challenge which could be faced with new nanomedicine tools. Due to the inherent nanocarriers accumulation in filtering organs, many strategies have been focused on adding affinity moieties to increase the specific accumulation in target organs but have been hindered by

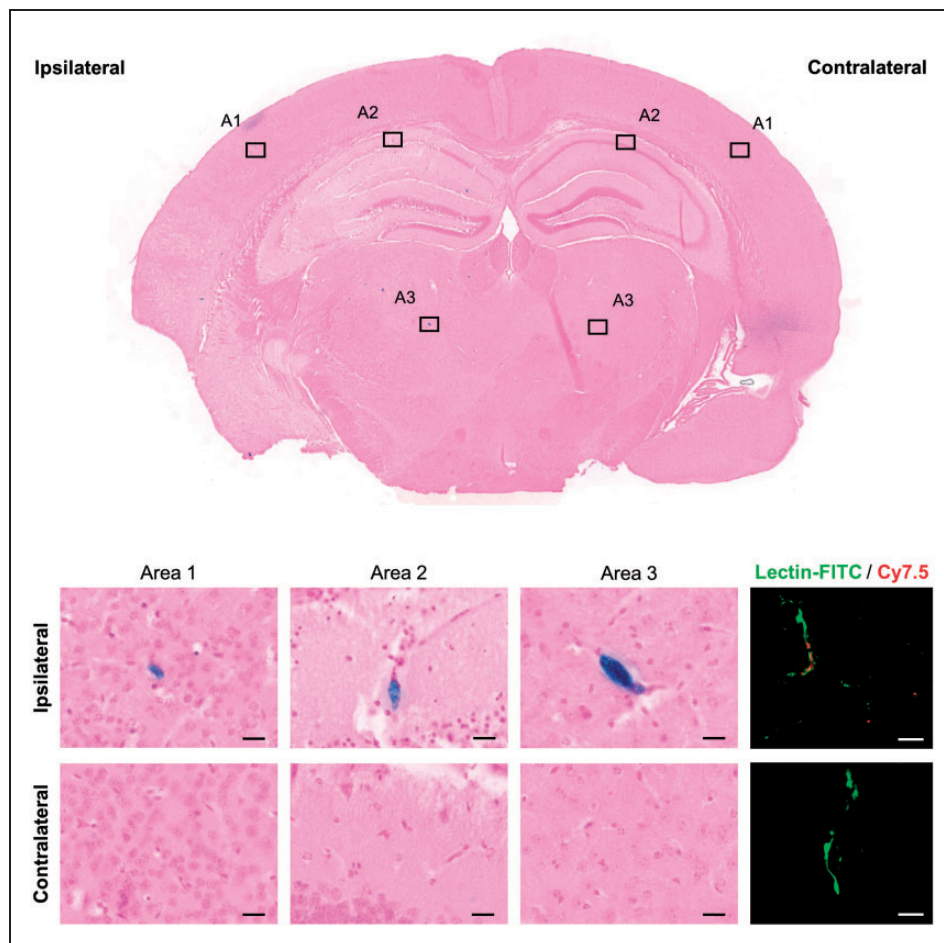


**Figure 7.** Verification of NC brain distribution by Prussian blue ferric iron staining (SPION) and fluorescence (Cy7.5). Staining on brain shows a major and extensive signal in the ipsilateral hemisphere; note that most positive stain corresponds to microvessel-like structures in saline-perfused brains. Scale bar: 20  $\mu\text{m}$ .

numerous challenges. A recent study has nicely reported a substantial increase of nanocarriers accumulation in the brain by using red blood cells as a vascular carrier for NC and administration through the ICA, confirming the enormous advantage of this endovascular delivery route in downstream organs, which can be further improved with nanomedicine-based strategies for brain targeting.<sup>36</sup> In this light, seizing the advantages of polymeric nanoparticles to administer therapeutic agents with a sustained release, increased half-life *in vivo* and reduced systemic toxic effects,<sup>37</sup> we have used a PLGA-based nanocarrier with biocompatible properties which has been functionalized with SPION and Cy7.5 for a magnetically guided retention and *in vivo* tracking by MRI and FMI as previously described by our group.<sup>20</sup> In our opinion, the use in the present study of biocompatible approved biomaterials for the medical use as PLGA and SPION with improved magnetic targeting is a potential advantage for the clinical translation of

nanomedical products, however other non-magnetized PLGA formulations or alternative biogenic/synthesized biomaterials could be used to achieve the successful brain delivery using the endovascular route after stroke.

To further improve the guided transport of the used nanocarriers, NC were functionalized with SPION to allow their retention by a magnetic field device to specific brain areas which was proved by our FeNdB devices in cortical areas under magnetic influence, with particular success with the focused magnet design (M2) showing better performance related to higher magnetic field and magnetic field gradient in deeper positions, as previously described.<sup>38,39</sup> This is the first time that a focused magnet designed for mouse brains is used to target the cortical delivery of nanocarriers after stroke in endovascular-ICA administrations, although other authors have also used an external magnet to enhance the delivery of magnetized cells to specific organs, including the brain after intravenous

stem cell administration and BBB opening in a rat model of traumatic brain injury.<sup>40</sup>

Our results first failed in showing an advantage in magnetic targeting using permanent magnets (M1) and short implantation times (30 min) in whole hemispheres. Nonetheless, finest experiments further proved the increased NC retention in the cortex after the advantageous intraarterial-ICA administration, by focusing on the specific area of magnetic field influence (several mm, corresponding to the cortical brain areas) with FMI and better spatial resolution in MRI using the improved focused magnet (M2). It is worth noting that we have also been able to detect by different *in vivo* and *ex vivo* imaging techniques the presence of the NC in the brain up to 48 h after the endovascular infusion, suggesting that a substantial proportion of the administered NC remains available in the target organ for a long time period, easing the sought-after sustained release of encapsulated therapeutic agents. Interestingly, even though a substantial amount of the NC still remains in filtering organs such as the lungs, liver and spleen, our study also proves that the endovascular administration diminished the accumulation of NC in the liver, a known off-target accumulation of nanomaterials in filtering organs. Importantly, this unavoidable accumulation of the NC observed in our study did not alter known biomarkers of liver/pancreas/renal damage at short- nor at long-term after intraarterial infusion compared to healthy mice, and only alterations related to the surgical intervention were found transiently altered, supporting the safety of the NC treatment in terms of systemic toxicity.

As previously mentioned, the pre-clinical use of the intraarterial administration route has raised safety concerns in previous investigations since thromboembolisms have been described as a common related complication, mainly associated with the infusion rate, dose or cell size.<sup>12,29,41</sup> To prevent this major complication, NC with an average diameter below 300 nm were freshly prepared in a saline suspension, vortexed and sonicated before the endovascular infusion to avoid the NC aggregation. The CBF, which was monitored during a controlled infusion, was only transiently and moderately reduced, as similarly reported in previous studies using mesenchymal stem cells by intraarterial administration,<sup>29,41</sup> but the intraarterial-ICA infusion of NC was not associated to mortality, a worsening of the ischemic damage nor a higher risk of hemorrhages, suggesting a low risk of thromboembolisms. Nonetheless, from a translational perspective, future pre-clinical studies should refine these endovascular delivery approaches and study the observed cerebral blood flow changes with advanced imaging techniques. On the other hand, the maintenance of iron homeostasis in the context of cerebral ischemia is of great

importance, as iron catalyzes the formation of free radicals and hence, can cause oxidative stress and worsen the ischemic damage.<sup>42</sup> Importantly, we did not observe an increase in the infarct volume nor hemorrhages following the acute endovascular-ICA NC administration (containing SPION) after stroke compared to the vehicle infusion, suggesting the safety in the tested conditions. Nevertheless, we observed a trend in higher total iron load dose and increased mortality only in ischemic mice but not in naïve, indicating a potential iron load-related risk in the context of acute ischemic cerebral damage. Hence, the iron load should be strictly adjusted when using magnetized nanocarriers as drug delivery systems in the context of cerebral ischemia. Although we have shown some data regarding long term safety at 2 weeks, additional studies with long-term monitoring of the administered NC in terms of safety and biodistribution are needed. Furthermore, our histological findings suggest an endothelial uptake of the nanocarriers, but other cellular or extracellular localizations within the brain parenchyma upon endovascular administration and magnetic brain targeting is yet to be investigated. In this light, this approach could be further combined with promising strategies aiming at the BBB crossing of therapeutic agents, such as the selective BBB temporary opening with nanoagonists such as adenosine 2A receptor agonist-labelled PAMAM dendrimers<sup>43</sup> or the functionalization of nanoparticles with selective antibodies for a BBB receptor-mediated transcytosis.<sup>44</sup> Finally, the present investigation provides evidence supporting the potential use and advantages of the endovascular delivery of PLGA nanocarriers which have already proven the versatility for the encapsulation or adsorption of a large variety of proteins, ranging from 8 to 66.5 kDa (e.g. VEGF, SDF, BDNF or albumin), showing successful encapsulation efficiencies, and posterior *in vitro* release with preserved functionality of the released factors.<sup>45–47</sup> This supports the encapsulation of therapeutic molecules for tissue repair, for example. However any potential restriction on the molecular weight of the cargo proteins should be further studied for specific neuroprotective or neurorestorative agents, always in balance with suitable nanoformulation sizes for a safe endovascular delivery and proving its advantage in front of free drug deliveries.

The present study proves the advantage and safety of intraarterially delivered magnetized nanocarriers for specific brain targeting in the context of cerebral ischemia. Nonetheless, there are several limitations that should be considered for future studies. The biodistribution and safety of the proposed nanocarriers should be readdressed for different encapsulated molecules or the addition/removal of imaging or affinity moieties. Furthermore, the iron load-derived toxicity, as well as

the clearance mechanism and kinetics of this type of magnetic nanocarrier is yet to be fully elucidated. Finally, from a translational perspective, studies in large animals with gyrencephalic brains and larger vessels/capillaries or in humanized prototypes should be used to demonstrate the feasibility of the proposed therapy.

### Data availability

Data related to this manuscript will be available upon reasonable request to the corresponding author.

### Funding

The author(s) disclosed receipt of the following financial support for the research, authorship, and/or publication of this article: This work has been supported under the Euronanomed MAGGBRIS collaborative project by grants from the Spanish Ministry of Science and Innovation (PCIN-2017-090 grant), the Instituto de Salud Carlos III (AC17/00004 with FEDER funds), the Slovak Research and Development Agency under the Contract No.APVV-19-0324 and the Italian Ministry of Health (Ricerca Corrente year 2017 funds); by the Expression of Interest (EoI) for Collaborative Projects on Regenerative Medicine 2019P-CMR[C]; programs 2017-SGR-1427 and 2017-SGR-765 from the Generalitat de Catalunya; RETICS-INVICTUS PLUS from ISCIII (RD16/0019/0021 with FEDER funds); the ‘Severo Ochoa’ Program for Centers of Excellence in R&D (CEX2019-000917-S) and the RYC-2017-22412 and PID2019-107989RB-I00. A.G has been supported by fellowships from ISCIII (FI17/00073 and MV18/00006), A.R by a visiting-scientist fellowship from ISCIII (BA17/00052) and Y. Z has been supported by the China Scholarship Council (CSC).

### Acknowledgements

We are grateful for the technical assistance received from the Pre-clinical imaging Platform at Vall d’Hebron Institut de Recerca, the Servei RMN at Universitat Autònoma de Barcelona, and the Unitat de Microscopia Òptica Avançada, Facultat de Medicina at the Universitat de Barcelona.

### Declaration of conflicting interests


The author(s) declared no potential conflicts of interest with respect to the research, authorship, and/or publication of this article.

### Authors’ contributions

A Rosell and A. Roig contributed to the study conception; AG, A Rosell., A Roig, PK, RMM and MP contributed to the study design; AG, MG and MA, AM, MT, JK, OS, SB and YZ conducted the experimental studies; AG, MT, LC and JK analyzed the data, AG and A Rosell wrote the paper and all authors contributed to the draft revisions.

### ORCID iDs

Alba Grayston  <https://orcid.org/0000-0002-1466-0099>

Yajie Zhang  <https://orcid.org/0000-0003-1566-1007>

Anna Rosell  <https://orcid.org/0000-0003-1082-3599>

### Supplementary material

Supplemental material for this article is available online.

### References

1. Maingard J, Foo M, Chandra RV, et al. Endovascular treatment of acute ischemic stroke. *Curr Treat Options Cardiovasc Med* 2019; 21: 225–558.
2. Haussen DC, Lima A and Nogueira RG. The trevo XP 320 mm retriever (‘Baby trevo’) for the treatment of distal intracranial occlusions. *J Neurointerv Surg* 2016; 8: 295–299.
3. Schwaiger BJ, Kober F, Gersing AS, et al. The pREset stent retriever for endovascular treatment of stroke caused by MCA occlusion: safety and clinical outcome. *Clin Neuroradiol* 2016; 26: 47–55.
4. Kaneko N, Komuro Y, Yokota H, et al. Stent retrievers with segmented design improve the efficacy of thrombectomy in tortuous vessels. *J NeuroIntervent Surg* 2019; 11: 119–122.
5. Fennell VS, Setlur Nagesh SV, Meess KM, et al. What to do about fibrin rich ‘tough clots’? Comparing the solitaire stent retriever with a novel geometric clot extractor in an in vitro stroke model. *J NeuroIntervent Surg* 2018; 10: 907–910.
6. Gruber P, Zeller S, Garcia-Esperon C, et al. Embolus retriever with interlinked cages versus other stent retrievers in acute ischemic stroke: an observational comparative study. *J NeuroIntervent Surg* 2018; 10: e31–e31.
7. Powers WJ, Rabinstein AA, Ackerson T, et al. Guidelines for the early management of patients with acute ischemic stroke: 2019 update to the 2018 guidelines for the early management of acute ischemic stroke a guideline for healthcare professionals from the American Heart Association/American Stroke A. *Stroke* 2019; 50: e344–e418.
8. Nogueira RG, Jadhav AP, Haussen DC, et al. Thrombectomy 6 to 24 hours after stroke with a mismatch between deficit and infarct. *N Engl J Med* 2018; 378: 11–21.
9. Albers GW, Marks MP, Kemp S, et al. Thrombectomy for stroke at 6 to 16 hours with selection by perfusion imaging. *N Engl J Med* 2018; 378: 708–718.
10. Gittler M and Davis AM. Guidelines for adult stroke rehabilitation and recovery. *Jama* 2018; 319: 820–821.
11. Griauzde J, Ravindra VM, Chaudhary N, et al. Neuroprotection for ischemic stroke in the endovascular era: a brief report on the future of intra-arterial therapy. *J Clin Neurosci* 2019; 69: 289–291.
12. Guzman R, Janowski M and Walczak P. Intra-arterial delivery of cell therapies for stroke. *Stroke* 2018; 49: 1075–1082.

13. Bhatia V, Gupta V, Khurana D, et al. Randomized assessment of the safety and efficacy of intra-arterial infusion of autologous stem cells in subacute ischemic stroke. *AJNR Am J Neuroradiol* 2018; 39: 899–904.
14. Fraser JF, Maniskas M, Trout A, et al. Intra-arterial verapamil post-thrombectomy is feasible, safe, and neuroprotective in stroke. *J Cereb Blood Flow Metab* 2017; 37: 3531–3543.
15. Wu C, Zhao W, An H, et al. Safety, feasibility, and potential efficacy of intraarterial selective cooling infusion for stroke patients treated with mechanical thrombectomy. *J Cereb Blood Flow Metab* 2018; 38: 2251–2260.
16. Danhier F, Ansorena E, Silva JM, et al. PLGA-based nanoparticles: an overview of biomedical applications. *J Control Release* 2012; 161: 505–522.
17. Wang Y and Qu W. CS. FDA's regulatory science program for generic PLA/PLGA-based drug products. *Am Pharm Rev* 2017; 19: 5–9.
18. Du Sert NP, Hurst V, Ahluwalia A, et al. The ARRIVE guidelines 2.0: updated guidelines for reporting animal research. *J Cereb Blood Flow Metab* 2020; 40: 1769–1777.
19. Clark WM, Lessov NS, Dixon MP, et al. Monofilament intraluminal Middle cerebral artery occlusion in the mouse. *Neurol Res* 1997; 19: 641–648.
20. Zhang Y, García-Gabilondo M, Grayston A, et al. PLGA protein nanocarriers with tailor-made fluorescence/MRI/PET imaging modalities. *Nanoscale* 2020; 12: 4988–5002.
21. Hundt W, Petsch R, Helmberger T, et al. Signal changes in liver and spleen after endorem administration in patients with and without liver cirrhosis. *Eur Radiol* 2000; 10: 409–416.
22. Morancho A, García-Bonilla L, Barceló V, et al. A new method for focal transient cerebral ischaemia by distal compression of the Middle cerebral artery. *Neuropathol Appl Neurobiol* 2012; 38: 617–627.
23. García-Yébenes I, Sobrado M, Zarruk JG, et al. A mouse model of hemorrhagic transformation by delayed tissue plasminogen activator administration after in situ thromboembolic stroke. *Stroke* 2011; 42: 196–203.
24. Campos M, García-Bonilla L, Hernández-Guillamon M, et al. Combining statins with tissue plasminogen activator treatment after experimental and human stroke: a safety study on hemorrhagic transformation. *CNS Neurosci Ther* 2013; 19: 863–870.
25. Orsini F, Villa P, Parrella S, et al. Targeting mannose-binding lectin confers long-lasting protection with a surprisingly wide therapeutic window in cerebral ischemia. *Circulation* 2012; 126: 1484–1494.
26. De Simoni MG, Storini C, Barba M, et al. Neuroprotection by complement (C1) inhibitor in mouse transient brain ischemia. *J Cereb Blood Flow Metab* 2003; 23: 232–239.
27. Rosell A, Agin V, Rahman M, et al. Distal occlusion of the Middle cerebral artery in mice: are We ready to assess Long-Term functional outcome? *Transl Stroke Res* 2013; 4: 297–307.
28. Sukhbaatar N and Weichhart T. Iron regulation: Macrophages in control. *Pharmaceuticals* 2018; 11: 137.
29. Cui LL, Kerkelä E, Bakreen A, et al. The cerebral embolism evoked by intra-arterial delivery of allogeneic bone marrow mesenchymal stem cells in rats is related to cell dose and infusion velocity. *Stem Cell Res Ther* 2015; 6: 11.
30. Argibay B, Trekker J, Himmelreich U, et al. Intraarterial route increases the risk of cerebral lesions after mesenchymal cell administration in animal model of ischemia. *Sci Rep* 2017; 7: 40758.
31. Cruz LJ, Stammes MA, Que I, et al. Effect of PLGA NP size on efficiency to target traumatic brain injury. *J Control Release* 2016; 223: 31–41.
32. Wiley DT, Webster P, Gale A, et al. Transcytosis and brain uptake of transferrin-containing nanoparticles by tuning avidity to transferrin receptor. *Proc Natl Acad Sci USA* 2013; 110: 8662–8667.
33. Pendharkar AV, Chua JY, Andres RH, et al. Biodistribution of neural stem cells after intravascular therapy for hypoxic-ischemia. *Stroke* 2010; 41: 2064–2070.
34. Li L, Jiang Q, Ding G, et al. Effects of administration route on migration and distribution of neural progenitor cells transplanted into rats with focal cerebral ischemia, an MRI study. *J Cereb Blood Flow Metab* 2010; 30: 653–662.
35. Lesniak WG, Chu C, Jablonska A, et al. PET imaging of intra-arterial 89 Zr bevacizumab in mice with and without osmotic opening of the blood-brain barrier: distinct advantage of intra-arterial delivery. *J Nucl Med* 2019; 60: 617–622.
36. Brenner JS, Pan DC, Myerson JW, et al. Red blood cell-hitchhiking boosts delivery of nanocarriers to chosen organs by orders of magnitude. *Nat Commun* 2018; 9: 2684.
37. Ding D and Zhu Q. Recent advances of PLGA micro/nanoparticles for the delivery of biomacromolecular therapeutics. *Mater Sci Eng C Mater Biol Appl* 2018; 92: 1041–1060.
38. Kopcansky P, Timko M, Hnatic M, et al. Numerical modeling of magnetic drug targeting. *Phys Part Nuclei Lett* 2011; 8: 502–505.
39. Kop-anský P, Bánó M, Repašan M, et al. Magnetic targeted drug delivery using focused magnet. *Magneto hydrodynamics* 2004; 40: 369–378.
40. Bin SW, Anastasiadis P, Nguyen B, et al. Magnetic enhancement of stem cell-targeted delivery into the brain following MR-guided focused ultrasound for opening the blood-brain barrier. *Cell Transplant* 2017; 26: 1235–1246.
41. Walczak P, Zhang J, Gilad AA, et al. Dual-modality monitoring of targeted intraarterial delivery of mesenchymal stem cells after transient ischemia. *Stroke* 2008; 39: 1569–1574.
42. Minhas G, Modgil S and Anand A. Role of iron in ischemia-induced neurodegeneration: mechanisms and insights. *Metab Brain Dis* 2014; 29: 583–591.
43. Gao X, Wang YC, Liu Y, et al. Nanoagonist-mediated endothelial tight junction opening: a strategy for safely increasing brain drug delivery in mice. *J Cereb Blood Flow Metab* 2017; 37: 1410–1424.



44. Yemisci M, Caban S, Gursoy-Ozdemir Y, et al. Systemically administered brain-targeted nanoparticles transport peptides across the blood–brain barrier and provide neuroprotection. *J Cereb Blood Flow Metab* 2015; 35: 469–475.
45. Zhang Y, García-Gabilondo M, Rosell A, et al. MRI/photoluminescence dual-modal imaging magnetic PLGA nanocapsules for theranostics. *Pharmaceutics* 2020; 12: 16.
46. Carezza E, Jordan O, Martínez-San Segundo P, et al. Encapsulation of VEGF165 into magnetic PLGA nanocapsules for potential local delivery and bioactivity in human brain endothelial cells. *J Mater Chem B* 2015; 3: 2538–2544.
47. Pakulska MM, Donaghue IE, Obermeyer JM, et al. Encapsulation-free controlled release: electrostatic adsorption eliminates the need for protein encapsulation in PLGA nanoparticles. *Sci Adv* 2016; 2: e1600519.

**Secretome of endothelial progenitor cells from stroke patients  
promotes endothelial barrier tightness and protects against  
hypoxia-induced vascular leakage**

---

DOI: 10.1186/s13287-021-02608-y




RESEARCH

Open Access



# Secretome of endothelial progenitor cells from stroke patients promotes endothelial barrier tightness and protects against hypoxia-induced vascular leakage

Rodrigo Azevedo Loiola<sup>1</sup>, Miguel García-Gabilondo<sup>2</sup>, Alba Grayston<sup>2</sup>, Paulina Bugno<sup>3</sup>, Agnieszka Kowalska<sup>3</sup>, Sophie Duban-Deweert<sup>1</sup>, Eleonora Rizzi<sup>1</sup>, Johan Hachani<sup>1</sup>, Yasuteru Sano<sup>4</sup>, Fumitaka Shimizu<sup>4</sup>, Takashi Kanda<sup>4</sup>, Caroline Mysiorek<sup>1</sup>, Maciej Piotr Mazurek<sup>3</sup>, Anna Rosell<sup>2</sup> and Fabien Gosselet<sup>1,5\*</sup> 

## Abstract

**Background:** Cell-based therapeutic strategies have been proposed as an alternative for brain repair after stroke, but their clinical application has been hampered by potential adverse effects in the long term. The present study was designed to test the effect of the secretome of endothelial progenitor cells (EPCs) from stroke patients (scCM) on *in vitro* human models of angiogenesis and vascular barrier.

**Methods:** Two different scCM batches were analysed by mass spectrometry and a proteome profiler. Human primary CD34<sup>+</sup>-derived endothelial cells (CD34<sup>+</sup>-ECs) were used for designing angiogenesis studies (proliferation, migration, and tubulogenesis) or *in vitro* models of EC monolayer (confluent monolayer ECs—CMECs) and blood–brain barrier (BBB; brain-like ECs—BLECs). Cells were treated with scCM (5 µg/mL) or protein-free endothelial basal medium (scEBM—control). CMECs or BLECs were exposed (6 h) to oxygen–glucose deprivation (OGD) conditions (1% oxygen and glucose-free medium) or normoxia (control—5% oxygen, 1 g/L of glucose) and treated with scCM or scEBM during reoxygenation (24 h).

**Results:** The analysis of different scCM batches showed a good reproducibility in terms of protein yield and composition. scCM increased CD34<sup>+</sup>-EC proliferation, tubulogenesis, and migration compared to the control (scEBM). The proteomic analysis of scCM revealed the presence of growth factors and molecules modulating cell metabolism and inflammatory pathways. Further, scCM decreased the permeability of CMECs and upregulated the expression of the junctional proteins such as occludin, VE-cadherin, and ZO-1. Such effects were possibly mediated through the activation of the interferon pathway and a moderate downregulation of Wnt signalling. Furthermore, OGD increased the permeability of both CMECs and BLECs, while scCM prevented the OGD-induced vascular leakage in both models. These effects were possibly mediated through the upregulation of junctional proteins and the regulation of MAPK/VEGFR2 activity.

**Conclusion:** Our results suggest that scCM promotes angiogenesis and the maturation of newly formed vessels while restoring the BBB function in ischemic conditions. In conclusion, our results highlight the possibility of using

\*Correspondence: [fabien.gosselet@univ-artois.fr](mailto:fabien.gosselet@univ-artois.fr)

<sup>5</sup> Laboratory of the Blood-Brain Barrier, Sciences Faculty Jean Perrin, Artois University, Lens, France

Full list of author information is available at the end of the article



© The Author(s) 2021. **Open Access** This article is licensed under a Creative Commons Attribution 4.0 International License, which permits use, sharing, adaptation, distribution and reproduction in any medium or format, as long as you give appropriate credit to the original author(s) and the source, provide a link to the Creative Commons licence, and indicate if changes were made. The images or other third party material in this article are included in the article's Creative Commons licence, unless indicated otherwise in a credit line to the material. If material is not included in the article's Creative Commons licence and your intended use is not permitted by statutory regulation or exceeds the permitted use, you will need to obtain permission directly from the copyright holder. To view a copy of this licence, visit <http://creativecommons.org/licenses/by/4.0/>. The Creative Commons Public Domain Dedication waiver (<http://creativecommons.org/publicdomain/zero/1.0/>) applies to the data made available in this article, unless otherwise stated in a credit line to the data.

EPC-secretome as a therapeutic alternative to promote brain angiogenesis and protect from ischemia-induced vascular leakage.

**Keywords:** Endothelial progenitor cells, Secretome, Blood–brain barrier, Stroke, Angiogenesis, Cell therapy, Cardiovascular disease, Regenerative medicine

## Background

Ischemic stroke is among the leading causes of mortality and disability worldwide [1]. In the past decades, recanalization therapy has dramatically reduced the mortality and functional disabilities [1]. However, there are no successful therapies targeting brain repair or vascular remodelling after stroke. Cerebral ischemia results in irreversible damage not only at the neuronal level but also in the brain microvasculature, namely the blood–brain barrier (BBB) [2]. Endothelial cells (ECs) forming a monolayer in brain microvessels are a major component of the BBB, which acts as a physical barrier due to the presence of tight junctions (TJs) between adjacent ECs and the absence of fenestration and pinocytotic activity of these cells [3, 4]. Besides, the delivery of essential nutrients to the brain parenchyma is strictly regulated by specific enzymes, receptors, and efflux pumps expressed at the luminal face of the BBB ECs [4]. BBB impairment and vascular disruption are early events following an ischemic stroke, exacerbating the brain injury and contributing to cognitive impairment [2, 5]. In this context, developing new therapies that combine the protection of the BBB integrity and the promotion of angiogenesis could be a potential strategy to improve the functional outcome after stroke. This hypothesis is supported by a body of evidence, suggesting that therapies promoting angiogenesis can stimulate neurogenesis and improve brain repair after stroke [6].

Over the last years, cell therapy with endothelial progenitor cells (EPCs) has been proposed as an alternative approach to promote angiogenesis and brain repair after stroke. EPCs constitute a pool of circulating bone marrow-derived cells that are mobilized towards the damaged tissues after an ischemic injury, where they promote angiogenesis through their incorporation into the vascular wall and the secretion of growth factors [7]. Although several pre-clinical studies have demonstrated that EPCs potentiate neurogenesis and angiogenesis in mouse models of stroke [8–10], the clinical translation of cell-based therapies still raises safety concerns due to their potential adverse side effects [11]. For this reason, clinical trials investigating the potential benefits of cell therapies for ischemic stroke are scarce [12]. In particular, one randomized phase I/IIa clinical trial (NCT01468064) testing the intravenous injection of autologous EPCs for acute stroke [13] did not show serious adverse effects or

allergic reactions related to the treatment. In this context, previous studies have reported that the administration of EPC-conditioned medium (EPC-secretome) promotes a beneficial response in pre-clinical models of cerebral ischemia and hypoperfusion [14, 15]. Despite these promising results, mainly obtained with animal cells and models, very few studies have been designed to characterize the effects of EPC-secretome on human cells, in particular in angiogenesis and barrier properties of ECs. The present study was therefore designed to evaluate the effect of EPC-secretome from stroke patients on in vitro models of angiogenesis and ischemia using primary human ECs. Our findings suggest that EPCs from stroke patients produce modulatory molecules which promote angiogenesis and vessel maturation while preventing the hypoxia-induced vascular leakage in oxygen–glucose deprivation (OGD) conditions in vitro. Altogether these data support the use of EPC-secretome to improve microvascular repair in the human brain after stroke.

## Methods

### Reagents

EC medium (ECM) and EC growth supplement (ECGS) were purchased from Sciencell (USA); foetal bovine serum (FBS) from Gibco (France); Dulbecco's modified Eagle medium (DMEM), vascular endothelial growth factor receptor 2 (VEGFR2) kinase inhibitor VII, AKT inhibitor VIII, UO126 monoethanolate, AZ6102, and fibroblast growth factor (FGF) receptor tyrosine kinase inhibitor were purchased from Sigma-Aldrich (France).

### EPC-secretome production

#### *EPC-isolation and culture*

The EPCs' isolation from stroke patients and healthy donors was performed as previously described [16]. Frozen EPCs were previously obtained from peripheral blood of both stroke patients (SP: 1—man, 66 years; 2—man, 77 years; 3—woman, 61 years) and healthy donors (HD: 1-woman, 43 years; woman, 39 years; man, 59 years). All donors (stroke or healthy) did not present any known malignant, infectious, or neurological disease (other than the stroke), which were exclusion criteria for the EPC collection. Briefly, blood was collected in EDTA tubes by venous puncture, and Ficoll gradient (1.078 g/L) was used to isolate human mononuclear cells. Isolated cells were seeded on human fibronectin (hFN)-coated

12-well plates at a density of  $10^7$  cells/well, cultured with EGM-2 in a 5% CO<sub>2</sub> incubator at 37 °C. After 3 days in culture, non-adherent cells were discarded and the medium was changed every other day. Colonies of outgrowth ECs appeared between 10 and 20 days after seeding and were further expanded. Immunophenotyping of EPCs was confirmed by von Willebrand factor (vWF—Dako), Ulex Europaeus Agglutinin—1 (UEA-1—Sigma-Aldrich), CD34 (Santa Cruz) and VEGFR2 (Santa Cruz). For EPCs seeding, all flasks were previously pre-coated (37 °C, 45 min) with hFN (1:100) diluted in H<sub>2</sub>O.

#### Low-scale production (LSP) of EPC-secretome

The LSP was performed to obtain small quantities of EPC-secretome from both stroke patients and healthy donors as usually performed in academic laboratories for studying EPCs. Briefly, EPCs ( $3 \times 10^6$  cells) from HD and SP were resuspended in 12 mL of complete EGM-2 and seeded in T75 flasks (75 cm<sup>2</sup>). After 72 h, cells were rinsed (PBS-CMF) and incubated (1 h) with DMEM. Then, DMEM was discarded and cells were cultivated with 12 mL of endothelial basal medium (EBM—Lonza) without the addition of any supplements. After 24 h, the conditioned medium (HD-CM or SP-CM) was collected.

#### High-scale production (HSP) of EPC-secretome

The HSP was performed in 10-layer culture flasks to provide higher content of proteins in the conditioned medium, which is desirable to consider future studies and treatments in patients. Briefly, EPCs ( $1 \times 10^7$  cells) from SP-1 donor were resuspended in 25 mL of EGM-2 and seeded in a T175 flask (175 cm<sup>2</sup>). After 96 h, EPCs were trypsinized and split in three T300 flasks (300 cm<sup>2</sup>). For

**Table 2** List of antibodies used in the study

Target	Reference	Provider
COX-2	AF4198	R&D Systems
Phospho-VEGFR2	AF1766	R&D Systems
Phospho-AKT	MAB887	R&D Systems
pan-VEGFR2	sc6251	SantaCruz
Non-phospho(active)-β catenin	19,807	CellSignalling
Phospho-ERK1/2	9106	CellSignalling
pan-ERK1/2	9102	CellSignalling
pan-AKT	4691	CellSignalling
pan-β catenin	Ab6302	Abcam
BCRP	Ab3380	Abcam
ICAM-1	Ab53013	Abcam
VCAM-1	Ab98954	Abcam
Tricellulin	Ab253067	Abcam
ABCA1	Ab18180	Abcam
β-actin	A5541	Sigma Aldrich
P-gp	C219	Genetex
VE-cadherin	Ab33168	Abcam
ZO-1	Ab216880	Abcam
Claudin 5	Ab15106	Abcam
Occludin	Ab31721	Abcam

every T300 flask,  $2 \times 10^7$  cells were seeded in 70 mL of complete EGM-2 medium. After 72 h, EPCs were trypsinized, resuspended ( $2.48 \times 10^8$  cells) in 1 L of EGM-2, and seeded in a CF10 flask (Nunc™ EasyFill™ Cell Factory™ Systems, culture area 6320 cm<sup>2</sup>). After 96 h (100% confluence), the EGM-2 medium was discarded and cells were rinsed with PBS-CMF. Next, cells were incubated

**Table 1** List of primers used in the study and their corresponding sequence

Target	Gene	Primer sequence
Cyclin D1	<b>CCND1</b>	Forward: GAAGATCGTCGCCACCTGGA Reverse: CAGGCGCTCTTTTTCACGG
APC Downregulated 1	<b>APCDD1</b>	Forward: ACTGATGCCACCCAGAGGATG Reverse: AGATGATCCGACAGGCGATGC
Axin 2	<b>Axin 2</b>	Forward: CCTGGGGGCGAGGAGTATTA Reverse: TTGGGCAAGGTACTGCCTCT
Vascular endothelial growth factor A	<b>VEGFA</b>	Forward: AGAAGGAGGAGGGCAGAATC Reverse: ACACAGGATGGCTTGAAGATG
Cyclophilin A	<b>PPIA</b>	Forward: CTGAGGACTGGAGAGAAAGGAT Reverse: GAAGTCACCACCTGACACATA
Glucose transporter 1 (GLUT1)	<b>SLC2A1</b>	Forward: CTTCTCCAAGTGGACCTCAAAT Reverse: AGGAGCACAGTGAAGATGATGA
Hypoxia-induced factor 1α (HIF1α)	<b>HIF1A</b>	Forward: GGATCAGACACCTAGTCTCT Reverse: ATCCATTGGGATATAGGGAG

in DMEM medium, which was discarded after 1 h and replaced with 1L of EBM without supplements. After 24 h, CM was collected and filtered/concentrated.

#### Filtration and concentration of EPC-secretome

EPC-secretome obtained by LSP (HD-CM and SP-CM) or HSP (CM), and fresh protein-free EBM (control) were filtered through a 0.22- $\mu\text{m}$  vacuum filter to remove cells and debris. Centricon Plus-70 filters (3 kDa Ultracel-PL membrane—Millipore) were filled with EPC-secretome or EBM and centrifuged (3500 $\times$ g) at 4 °C for 60 min. The super-concentrated EPC-secretomes (scHD-CM, scSP-CM, scCM) or EBM (scEBM) was recovered by centrifuging in collection mode at 1000 g for 1 min. Finally, the protein content was determined by Bradford assay and frozen at  $-80$  °C in low-protein binding tubes.

#### Treatments

All experiments were performed in the absence of serum or other commercial growth factors. The EPC-secretome (5  $\mu\text{g}/\text{mL}$  of either scSP-CM, scHD-CM, or scCM) or scEBM (control) was diluted in serum-free ECM containing bovine serum albumin (BSA) 0.1%. For the experiments using inhibitors, CD34<sup>+</sup>-ECs were pre-treated 30 min before adding scEBM or scCM using the following concentrations: UO126 (MAPK inhibitor—1  $\mu\text{mol}/\text{L}$ ); VEGFR2 kinase inhibitor VII (10  $\mu\text{mol}/\text{L}$ ); AKT inhibitor VIII (1  $\mu\text{mol}/\text{L}$ ); AZ6102 (Wnt inhibitor—1  $\mu\text{mol}/\text{L}$ ); FGFR tyrosine kinase inhibitor (1  $\mu\text{mol}/\text{L}$ ). For experiments using TNF $\alpha$  cells were pre-treated (24 h) with scCM or scEBM, and then, TNF $\alpha$  (10 ng/mL—Sigma-Aldrich) was added. After 24 h, a permeability assay and sample collection were performed.

#### Cells

CD34<sup>+</sup> cells were isolated from human umbilical cord blood and differentiated into ECs (CD34<sup>+</sup>-ECs), as previously described [17]. CD34<sup>+</sup>-ECs were seeded in 100-mm 1% gelatin-coated dishes with ECM-containing ECGS and 5% FBS (named ECM5). After two days, cells were trypsinized and seeded for the experiments of angiogenesis (cell proliferation, tubulogenesis, and migration) or the preparation of CMECs and BLECs, as further described.

For the co-culture approach (in vitro BBB model), human–brain pericytes (HBPs) were grown in DMEM containing 4.5 g/L D-glucose, 10% FBS, 1% L-glutamine, and 1% penicillin–streptomycin, as previously described [18, 19].

#### Cell proliferation

CD34<sup>+</sup>-ECs were seeded ( $5 \times 10^3$  cells/well) in 1% gelatin-coated 96-well plates. After 24 h, CD34<sup>+</sup>-ECs were serum-starved in ECM with 0.1% BSA for 6 h. Then, cells were treated (24 h) with EPC-secretome (scHD-CM, scSP-CM, or scCM) or scEBM. Cell viability was evaluated by a resazurin assay, as previously reported [20]. ATP levels were measured with a luminescent kit (CellTiter Glo™, Promega, France) following the manufacturer's instructions (Additional File 1: Figure S1). To assess the effect of the treatment on cell proliferation/growth, CD34<sup>+</sup>-ECs were seeded at a low density, and the experiments were performed during the exponential growth phase, when no cell death was observed. Cell proliferation thus represents the cell viability (relative number of living cells) of EPC-secretome-treated CD34<sup>+</sup>-ECs compared to scEBM-treated cells. Cell proliferation data were represented as the relative percentage versus the scEBM (control) group.

#### Wound healing assay

CD34<sup>+</sup>-ECs ( $2 \times 10^5$  cells/well) were seeded in 1% gelatin-coated 24-well plates. After 24 h, CD34<sup>+</sup>-ECs were serum-starved in ECM with 0.1% BSA for 6 h. Then, a wound was created by scratching the cell monolayer with a 200- $\mu\text{L}$  tip. Cells were rinsed with DMEM to remove cell debris and treated with EPC-secretome (scHD-CM, scSP-CM, or scCM) or scEBM. Images of the wound were taken immediately after the scratch (time 0) and 16 h after the treatments using a phase-contrast microscope (Nikon). The wound healing of EPC-secretome-treated cells was calculated by measuring the difference between the initial (time 0) and final (time 16 h) wound area using the ImageJ software. The migration of EPC-secretome-treated CD34<sup>+</sup>-ECs was calculated as the relative percentage compared to the scEBM-treated cells.

(See figure on next page.)

**Fig. 1** EPC-secretome from stroke patients promotes in vitro angiogenesis. EPC-secretome obtained from stroke patients (scSP-CM) and healthy donors (scHD-CM) under low-scale production conditions have similar effects on CD34<sup>+</sup>-ECs proliferation (**a**), migration (**b**), and tubulogenesis (**c**). Further, EPC-secretome obtained from stroke patients produced at high-scale conditions (scCM) increased CD34<sup>+</sup>-ECs proliferation (**d**), migration (**e**), and tubulogenesis (**f**). Besides, two scCM batches were compared and showed similar effects (scCM-1, batch 1; scCM-2, batch 2). The effects of scCM were similar to those observed with VEGF-A (50 ng/mL). Data represent median (interquartile range) ( $n = 3-8$ ), \* $P < 0.05$  vs scEBM. Scale bar: 200  $\mu\text{m}$

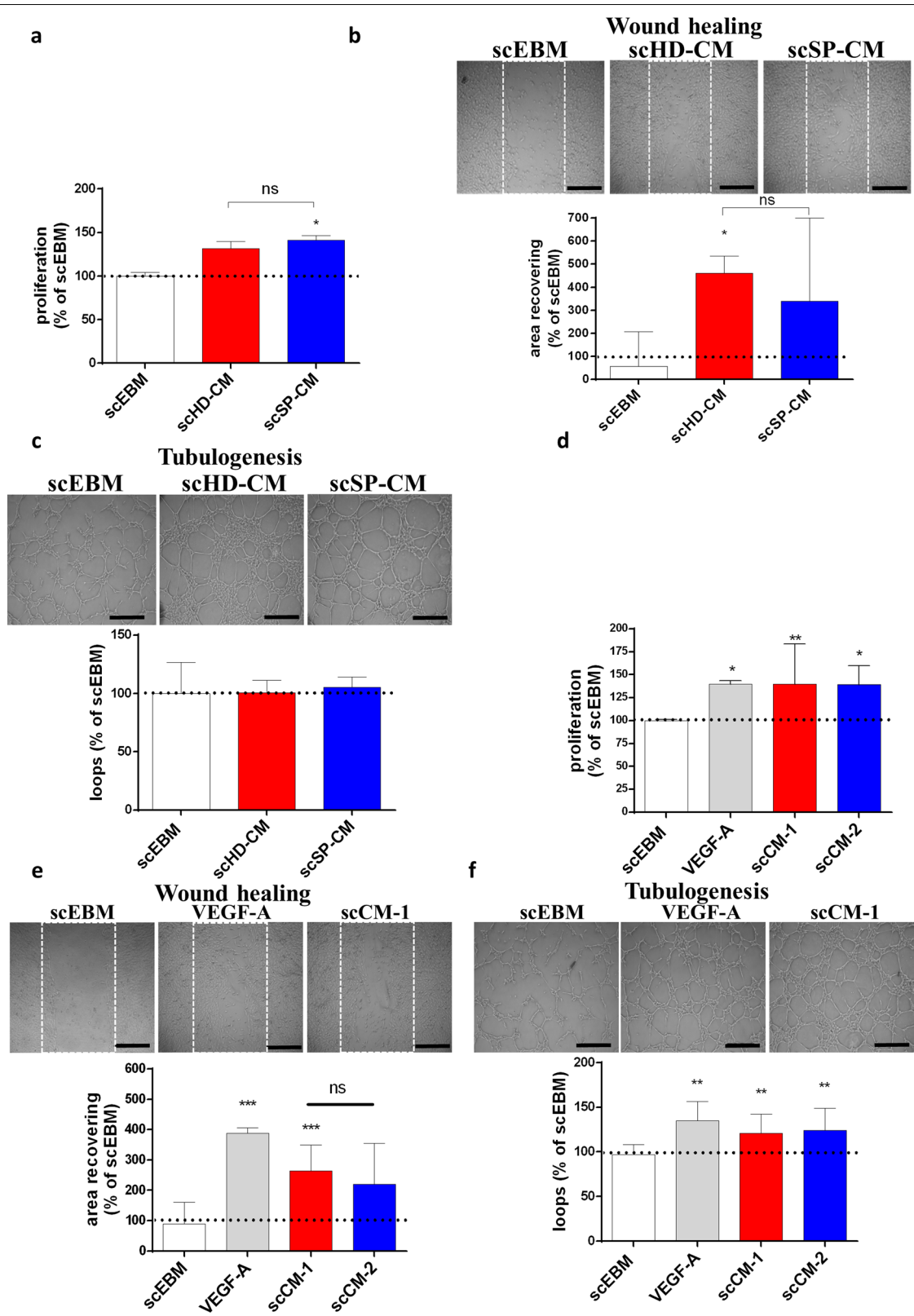


**Fig. 1** (See legend on previous page.)



### Capillary-like tubulogenesis assay

Angiogenesis  $\mu$ -slides (IBIDI, Germany) were coated with Matrigel™ (BD Biosciences—10  $\mu$ L/well) and incubated at 37 °C for 1 h, as previously described [21]. After serum-starvation (ECM + 0.1% BSA) for 16 h, CD34<sup>+</sup>-ECs were detached and seeded ( $12 \times 10^3$  cells/well) on the surface of polymerized Matrigel™ and treated with EPC-secretome (scSP-CM, scHD-CM, scCM) or scEBM. After 6-h incubation, pictures were taken using a phase-contrast microscope (Nikon) with a  $5 \times$  magnification objective. The number of tubular structures was determined using the Wimasis® Image Analysis software, and the tubulogenesis of EPC-secretome-treated CD34<sup>+</sup>-ECs was calculated as the relative percentage versus the scEBM-treated cells.

### Confluent monolayers of endothelial cells (CMECs)

Briefly, CD34<sup>+</sup>-ECs ( $8 \times 10^4$  cells/insert) were seeded in Matrigel™-coated Transwell inserts (Costar Transwell inserts, pore size 0.4  $\mu$ m). Filters were placed in 12-well plates containing ECM5, and after 4 days, cells were treated with scCM or scEBM. Then, 48 h later, permeability studies and sample collection were performed.

### In vitro BBB model with brain-like endothelial cells (BLECs)

The BBB model was reproduced as previously published [22]. Briefly, CD34<sup>+</sup>-ECs ( $8 \times 10^4$  cells/insert) were seeded into Matrigel™-coated filters (Costar Transwell inserts, pore size 0.4  $\mu$ m). Then, inserts were placed in collagen-coated 12-well plates containing HBPs ( $5 \times 10^4$  cells/well). After 5 days of co-culture, CD34<sup>+</sup>-ECs acquire the major BBB properties observed in vivo [23] and reproduce a suitable model to investigate BBB permeability and physiology [22, 24]. They are therefore named as brain-like ECs (BLECs). Once differentiated, BLECs were treated with scCM or scEBM and, 48 h later, permeability studies and sample collection were performed.

### Permeability assay

Permeability assays were performed as previously described [25]. HEPES-buffered Ringer's solution was added to empty wells in a 12-well plate (Costar). Filter inserts containing CMECs or BLECs were subsequently placed in the 12-well plate and filled with Ringer-Hepes

buffer (RH) containing the fluorescent integrity marker sodium fluorescein (Naf; 10  $\mu$ M; Life Technologies), which poorly crosses the BBB. Alternatively, some experiments were performed with radiolabeled sucrose-C<sup>14</sup>, another paracellular marker that also poorly crosses the BBB (Additional file 2: Figure S2a). After 1 h, filter inserts were withdrawn from the receiver compartment. Aliquots from the donor solution were taken at the beginning and the end of the experiments, and the fluorescence was quantified. The permeability coefficient was calculated as previously described [26]. Briefly, both insert permeability (PSf, for insert only coated with Matrigel™) and permeability of inserts containing either CMECs or BLECs (PSt, for insert with Matrigel™ and cells) were considered, according to the following formula:  $1/PSe = 1/PSt - 1/PSf$ . The permeability value for the CMECs' or BLECs' monolayer was then divided by the surface area of the insert (1.12 cm<sup>2</sup>) to obtain the permeability coefficient (Pe) of each molecule (cm/min).

### Immunofluorescence

Cells were fixed with cold methanol and rinsed twice with cold PBS-CMF. Unspecific binding was blocked (30 min, RT) using a Sea Block buffer solution (Thermo Fisher Scientific). Then, cells were incubated (60 min, RT) with the primary antibodies against claudin 5 (Invitrogen, 34-1600), ZO-1 (Invitrogen, 61-7300), VE-cadherin (Abcam, Ab33168), or occludin (Invitrogen, 71-500) in PBS-CMF containing 2% (v/v) normal goat serum (PBS-NGS). After rinsing, cells were incubated (30 min, RT) with a secondary polyclonal antibody (Life Technologies, A-11034). For F actin staining, cells were fixed with 4% paraformaldehyde (PFA) and permeabilized using Triton 0.1% in PBS-CMF (10 min, RT). Then, cells were incubated (30 min, RT) with phalloidin (Bodipy—588/568—Thermo Fisher, B3475) diluted in PBS-NGS. After rinsing, cells were mounted using ProLong Gold antifade mountant (Thermo Fisher) containing DAPI (nuclear staining). Images were acquired using a Leica microscope (DMRD; Leica Microsystems) and processed using the ImageJ software.

### qPCR

The mRNA from cells was extracted using the NucleoSpin® RNA/protein kit (Macherey–Nagel, Germany).

(See figure on next page.)

**Fig. 2** Identification of proteins in scCM. Detection of pro-angiogenesis factors in two batches of scCM was performed by Angiogenesis Proteome Profiler (a). Two different batches of scCM were analysed by MS. Over 1200 proteins were identified and the two batches of scCM shared 1041 proteins (b). The set of proteins shared between two batches of scCM (1041) were converted in gene identifiers and then submitted to an enrichment analysis using the GeneOntology/Panther software. The proteins were classified according to protein class (c), molecular (d), or biological function (e). Among the Panther pathways that were over-represented in the enrichment analysis of scCM samples, several were related to cell metabolism (f)

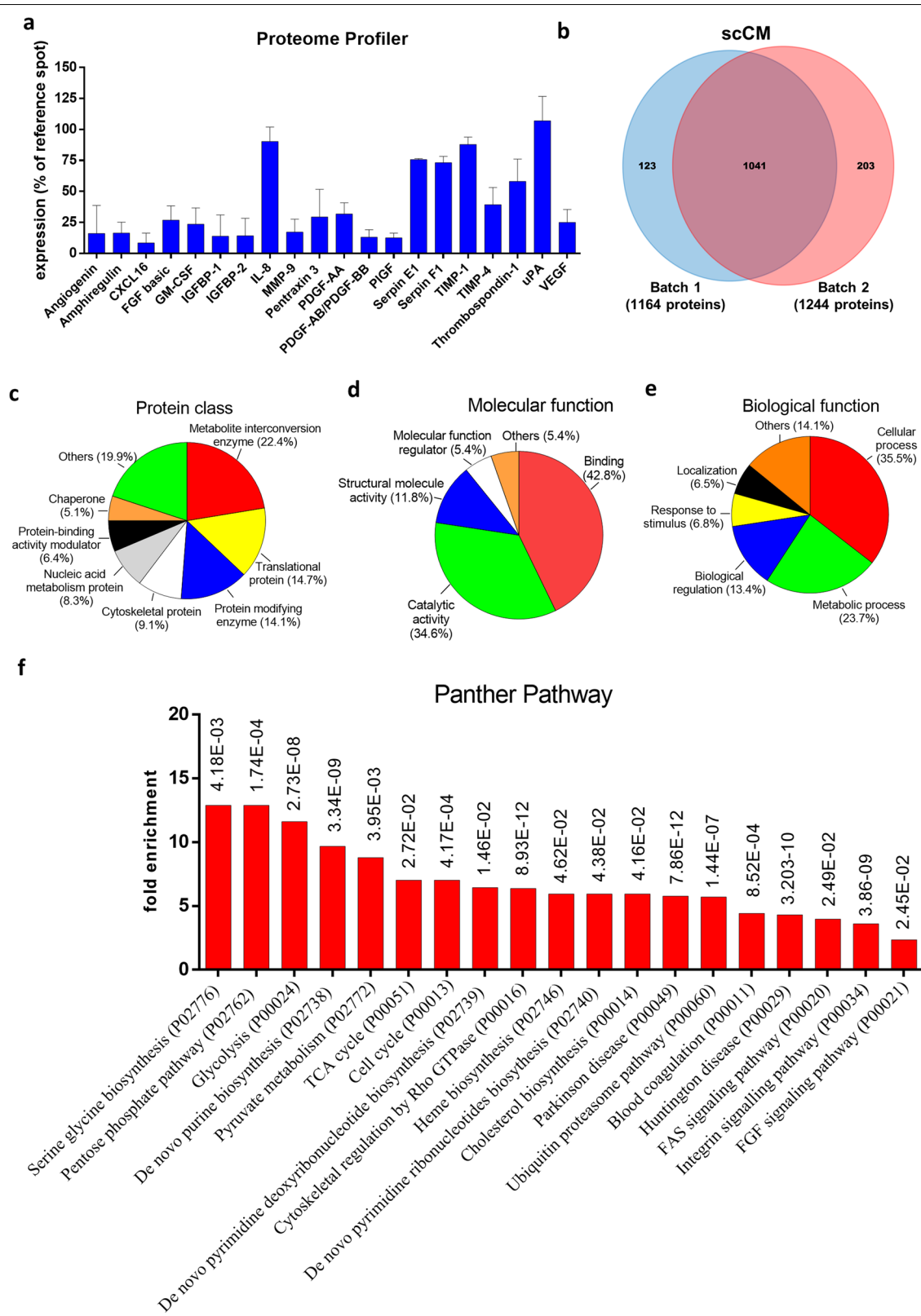


**Fig. 2** (See legend on previous page.)

cDNA was obtained from 250 ng of mRNA using IScript™ Reverse Transcription Supermix (BioRad, USA), following the manufacturer's instructions. qPCRs (10 µL) were prepared using SsoFast™ EvaGreen® Supermix (BioRad), primers (100 nM), deionized water, and cDNA. qPCR amplification was carried out for 40 cycles with an annealing temperature of 60 °C in a CFX96 thermocycler (BioRad). Ct data were obtained using the Bio-Rad CFX Manager software. Gene expression levels of the targets (Table 1) were calculated using the  $2^{-\Delta\Delta C_t}$  method, relative to the housekeeping gene *PPIA* (Cyclophilin A).

### Western blotting (WB)

Cells were collected with RIPA lysis buffer containing protease and phosphatase inhibitors (Sigma-Aldrich). Cell lysates (10–20 µg) were prepared, placed on sodium dodecyl sulphate–polyacrylamide gel electrophoresis (SDS-PAGE) and then transferred to nitrocellulose membranes (GE Healthcare, Germany). Non-specific binding was blocked using tris-buffered saline containing 0.1% Tween 20 (TBS-T) with 5% of skimmed milk (1 h, RT). Membranes were incubated (4 °C, overnight) with primary antibodies (Table 2), washed extensively and then incubated (1 h, RT) with a horseradish peroxidase-conjugated secondary antibody (Dako/Agilent Technologies). After rinsing, membranes were developed with a chemiluminescence reagent (GE Healthcare), and images were acquired using the WB Imaging System Azure c600 (Azure Biosystems). The software TotalLab TL 100 1D gel Analysis was used for quantification of the relative immunoblots densities. Conditions and concentrations of each antibody shown in Table 2 were previously optimized, as demonstrated in Additional file 3: Figure S3. Western blot images shown in this study were cropped, but original results obtained for each experiment performed are provided in Additional file 4: Figure S4, Additional file 5: Figure S5, Additional file 6: Figure S6, Additional file 7: Figure S7, Additional file 8: Figure S8, Additional file 9: Figure S9, Additional file 10: Figure S10, Additional file 11: Figure S11, Additional file 12: Figure S12, Additional file 13: Figure S13. More pictures and data can be provided upon request.

### In vitro oxygen–glucose deprivation (OGD) assay

The in vitro OGD model was designed to simulate the in vivo stroke conditions, with a shortage of oxygen (1% O<sub>2</sub>) and nutrients (glucose-free medium), which were achieved by using a hypoxic chamber (Whitley H35 Hypoxystation). In parallel, experiments performed under normoxic conditions (5% CO<sub>2</sub>/95% air and 1 g/L glucose) were used as controls. All media and solutions used for the OGD conditions were previously equilibrated in the hypoxic chamber. Then, inserts were submitted to OGD or normoxic conditions for 6 h and permeability assays or sample collection were performed. In another set of inserts, cells exposed to OGD or normoxic conditions were treated with scCM or scEBM and submitted to a reoxygenation phase (24 h), which consists in returning the cells to physiological conditions, thereby mimicking the in vivo reperfusion phase. After reoxygenation, permeability assay and sample collection were performed.

### scCM protein profile

The protein content was analysed in two independent batches of scCM using the Proteome Profiler Human Angiogenesis Array kit (R&D Systems, USA), which can detect the expression of 55 angiogenesis-related proteins. Briefly, scCM (150 µg of total protein) was mixed with the biotinylated detection antibodies provided in the kit and incubated (4 °C, overnight) in a nitrocellulose membrane containing the capture antibodies. After incubation, the membranes were washed and the Streptavidin-HRP and chemiluminescent detection reagents were applied. The spot signal was detected with the Luminescent Imaging System Azure c600 (Azure Biosystem), and quantification of the relative densities of the bands was performed using the TotalLab TL 100 1D gel Analysis software. scEBM was used as a negative control. Results are expressed as the percentage of the signal relative to the reference spot (loading control).

### Proteomic analysis of scCM

#### Preparation of the samples

Proteins were extracted from two independent batches of scCM (~100 µg each) in a 1.5 M Tris–HCl buffer (pH 8.5) containing 7 M guanidine hydrochloride (GuHCl),

(See figure on next page.)

**Fig. 3** scCM promotes in vitro angiogenesis mediated by MAPK and VEGFR2 activation. scCM induces a rapid and consistent increase in ERK1/2 phosphorylation, whereas it does not affect AKT or VEGFR2 activation (a). ERK1/2 activation remains until 4 h after treatment, while VEGFR2 phosphorylation is upregulated after 24 h of treatment (b). Pre-incubation with UO126 (MEK/ERK inhibitor—1 µmol/L), VEGFR2 kinase inhibitor VII (10 µmol/L) and FGFR tyrosine kinase inhibitor (1 µmol/L) reduced the scCM-induced proliferation (c) while VEGFR2 and FGFR inhibition reduced the scCM-induced migration (d). Western blot detection of ERK1/2 and VEGFR2 phosphorylation on cells treated with either vehicle (DMSO), MEK/ERK1/2, or VEGFR2, or FGFR inhibitors (e). Proteins classified as involved in angiogenesis [8], VEGF-A [4], and FGF [15] were grouped, then converted in gene identifiers and an interaction network was prepared using Cytoscape software (version 3.8.2, released 2020.10.24). Such pathways share in common the protein MAPK1 (ERK2) (f). Data represent median (interquartile range) (n = 3–7), \*P < 0.05 vs scEBM; \$P < 0.05 vs scCM vehicle

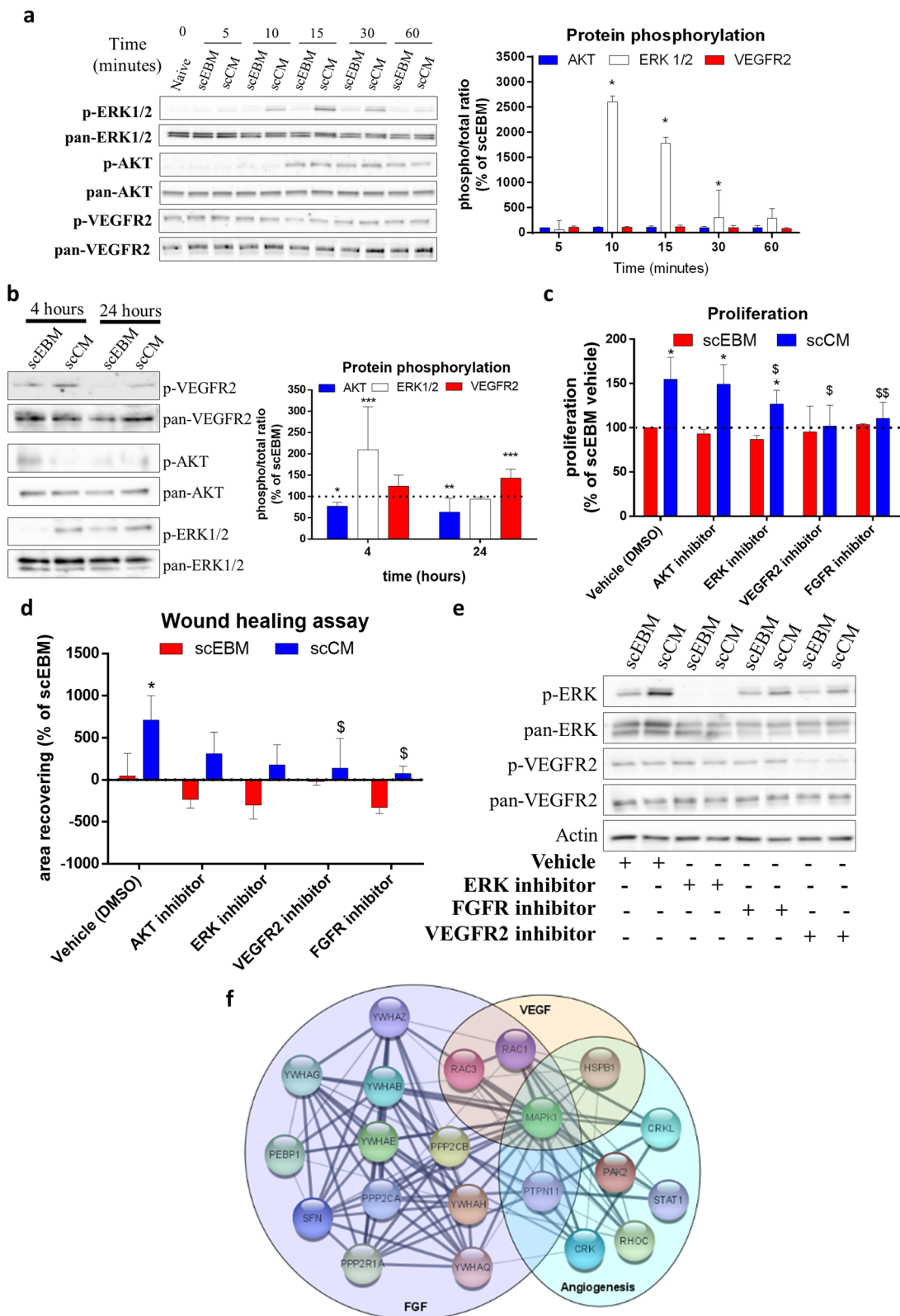


**Fig. 3** (See legend on previous page.)

20 mM ethylenediaminetetraacetate (EDTA), and 0.5 M dithiothreitol (DTT), and incubated for 1 h at 60 °C. The sulfhydryl groups of the proteins were carbamidomethylated with iodoacetamide used in a 2.5-fold excess (w/w) to DTT in the dark (20 min, RT). The suspension was centrifuged at 11,000 g for 15 min at 4 °C, and the supernatant was collected. Protein concentration was measured using the Quick start Bradford dye reagent (Biorad, Hercules, USA) with BSA as a standard protein. For each sample, 100 µg of protein was precipitated in 80% acetone overnight at –20 °C. After 15 min of centrifugation at 11,000 g, the pellet was enzymatically digested overnight using a sequencing grade modified trypsin (Promega, Madison, USA) with an enzyme/substrate ratio of 1/50 at 37 °C in 25 mM ammonium bicarbonate (NH<sub>4</sub>HCO<sub>3</sub>). The reaction was stopped by adding formic acid to a final concentration of 0.1% (v/v). Peptides were extracted using the HyperSep SpinTip Microscale C18 (Thermo Fisher Scientific, USA), and the peptides' concentration was measured using the Quantitative Colorimetric Peptide Assay (Thermo Fisher Scientific, USA).

#### Data-dependent acquisition by mass spectrometry (DDA-MS)

DDA consists in a proteomic approach in which digested peptides are ionized and analysed by MS. Peptide signals that raised in a full-scan mass spectrum with predefined MS parameters were selected for fragmentation, and then, their tandem product (MS/MS) mass spectra were matched to spectra in a protein database. Briefly, two micrograms of peptides from each sample was analysed using an Eksigent nano-LC 2D HPLC system connected to a quadrupole time-of-flight Triple TOF 5600+ mass spectrometer (Sciex, Redwood City, USA). After injection, peptide mixtures were transferred into a nano-HPLC column (ChromXP C18, 3 µm 120 Å, nanoLC column, 3C18-CL, 75 µm×15cm, Sciex, USA) at a flow rate of 300 nL/min using the following gradients for solvent B: 2 to 8% solvent B in A (from 0 to 5 min), 8 to 35% B (5 to 90 min), 35 to 40% B (90 to 100 min), 40 to 90% B (100 to 102 min), 90% B (102 to 107 min), 90 to 2% B (107 to 109 min) and finally 2% solvent B in A (109 to 140 min), with a total runtime of 140 min including a mobile phase equilibration. The following solvents were added in the mobile phase A: 2% acetonitrile/98% of 0.1% formic acid (v/v) in water; and in the mobile phase B: 98% acetonitrile/2% of 0.1% formic acid (v/v) in water. The eluted

peptides were directly injected for MS data acquisition in a hybrid quadrupole-TOF 5600+ System fitted with a Nano-spray III source. Ionization was obtained with an ion spray voltage of 2.2 kV, curtain gas set at 25 psi, and ion source gas at 3 psi, using positive-ion mode. DDA-MS survey scans were acquired at 250 ms from 400 to 1500 *m/z* and MS/MS scan from 100 to 2000 *m/z* (100 ms accumulation time, 50 mDa mass tolerance, rolling collision energy).

Peptide and protein identifications were performed using the Protein Pilot software (version 5.0.2, Sciex) with a Swiss-Prot/TrEMBL concatenated target-reverse decoy database (downloaded in November 2018), specifying iodoacetamide and methionine oxidation as variable modifications. The false discovery rate (FDR) was used to generate a spectral library and was set to 1% for both peptides and proteins.

#### TempO-Seq analysis

Targeted transcriptome quantification assay (TempO-Seq, BioSpyder) was performed in CMECs (*n* = 3 per group) treated with scCM (5 µg/mL) or scEBM (control). Cells were rinsed with sterile PBS-CMF, lysed using a TempO-Seq lysis buffer, and stored at –80 °C before shipment to BioClavis (Glasgow, UK), where the TempO-Seq assay was performed. The TempO-Seq analysis was performed as previously described [27]. Briefly, the toxicity pathway analysis was performed using a list of genes annotated to different stress response pathways (3565 probe-set representing 3257 genes). The FASTQ file from each sample was aligned against the TempO-Seq transcriptome using the Bowtie aligner, generating a table of counts per gene and sample, which was further analysed using the R software. The differential expression analysis was performed by comparing the scCM-treated samples with their suitable control (scEBM). Genes were considered significantly differentially expressed when the Benjamini Hochberg adjusted *P* value was < 0.05.

#### Statistical analysis

All statistics were analysed using GraphPad Prism® software version 6.0. The normality of continuous variables was assessed using the Shapiro–Wilk test (*n* < 30) or Kolmogorov–Smirnov test (*n* ≥ 30). For variables that were not normally distributed, Mann–Whitney or

(See figure on next page.)

**Fig. 4** scCM promotes endothelial barrier tightness. scCM reduced the permeability of CMECs, while it did not affect BLECs (a). scCM upregulated the expression of junctional proteins on CMECs (b). Heat map representing 23 genes upregulated by scCM on CMECs, most of them associated with the IFN pathway (c). scCM reduced the content of active β-catenin and claudin 3 (d) and downregulated mRNA expression of Wnt pathway targets APCDD1, Axin2, and CCND1 on CMECs (e). Co-incubation with Wnt inhibitor (AZ6102, 1 µmol/L) decreased barrier permeability of cells treated with scEBM (f). Data represent median (interquartile range) [b, d, and e] or mean ± SD [a and f] (*n* = 4–8). \**P* < 0.05 vs scEBM CMECs

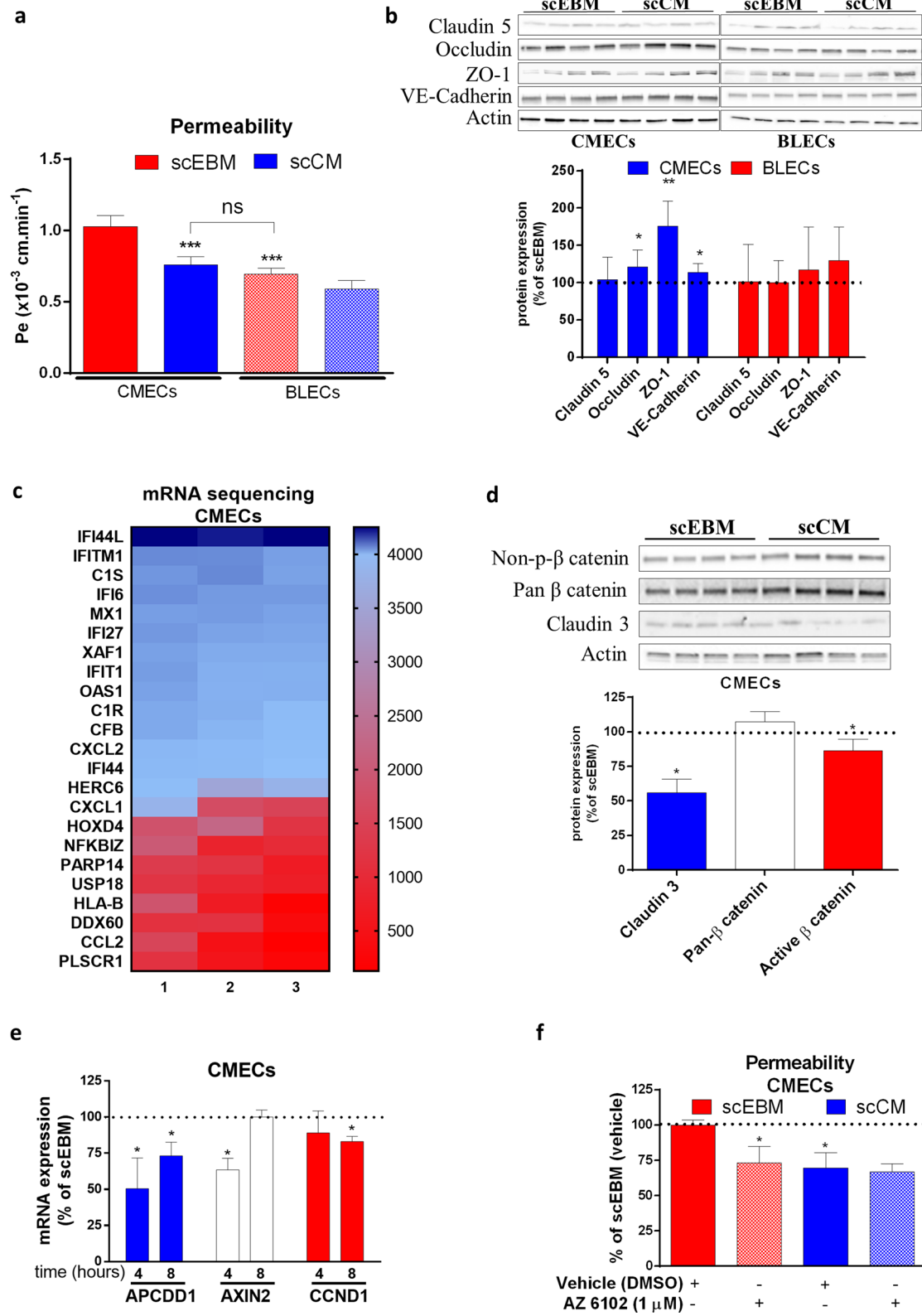


**Fig. 4** (See legend on previous page.)



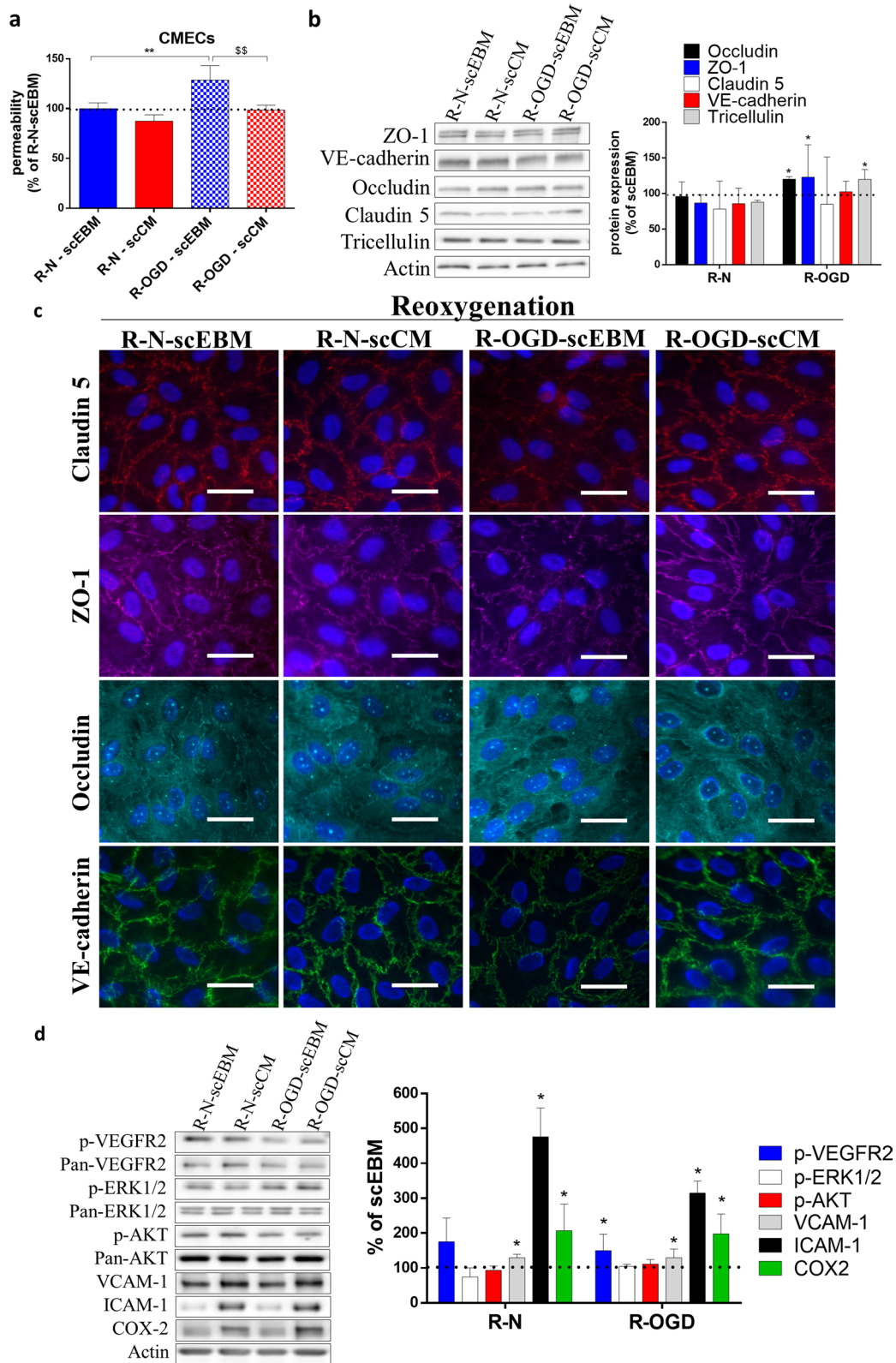


**Fig. 5** (See legend on previous page.)



(Fig. 2c), molecular function (Fig. 2d), and biological process (Fig. 2e). Besides, a Gene Ontology (GO) enrichment analysis revealed an overrepresentation (fold enrichment) of pathways involved in cell metabolism, such as serine glycine biosynthesis, pentose phosphate pathway, glycolysis, pyruvate metabolism, and TCA cycle (Fig. 2f and Additional file 14: Table S1).

#### scCM-induced angiogenesis is mediated through MAPK kinase and receptor tyrosine kinase (RTK) activation

To further investigate the underlying mechanisms of the observed scCM-induced effects, we evaluated the activation of MAPK, VEGFR2, and PI3K/AKT signalling pathways, key modulators of angiogenesis. scCM induced a strong and consistent ERK1/2 phosphorylation (scCM, 10 min: 2599% [1102–2723]), whereas it did not affect either AKT or VEGFR2 phosphorylation (Fig. 3a). Further, we observed that ERK1/2 activation lasts for at least 4 h, getting normalized after 24 h of treatment (Fig. 3b). Interestingly, AKT activation is reduced at 4 and 24 h after scCM treatment, while VEGFR2 phosphorylation is increased after 24 h of treatment (Fig. 3b). Inhibition of ERK pathway (using UO126), VEGFR2 (using VEGFR kinase inhibitor VII), and FGF receptor (using FGFR tyrosine kinase inhibitor) attenuated the scCM-induced increase on CD34<sup>+</sup>-EC proliferation (Fig. 3c). Additionally, VEGFR2 and FGFR inhibition reduced the scCM-induced migration (Fig. 3d). The efficiency of ERK1/2 and VEGFR2 inhibition was confirmed by WB (Fig. 3e). STRING analysis database (version 11.0, released 2019.01.19) was used to classify the scCM proteins as involved with “angiogenesis” (8 proteins), “VEGF-A pathway” (4 proteins), and “FGF pathway” (15 proteins). Among them, most were adapter proteins (14–3-3 superfamily and CRK), GTPases (RHOC, RAC1, and RAC3), or serine/threonine-protein phosphatases (PPP2R1A, PP2CA, and PPP2CB). By creating an interaction map among these proteins, we observed that MAPK1 (ERK2) was central in the network hub (Fig. 3f).

#### scCM promotes vascular tightness

To understand the effect of scCM on vascular permeability, CMECs were used as a model of newly formed vessels, which presents an elevated permeability in comparison with fully matured BBB microvessels. In parallel,

BLECs were used as an in vitro BBB model, characterized by the presence of TJ and an extremely low permeability. Indeed, the crossing of sucrose C<sup>14</sup>, a classical paracellular marker for permeability studies, showed a 2.45-fold increase through CMECs when compared to BLECs (Additional file 2: Figure S2a). Similar results were observed using the fluorescent marker Naf, although the difference between CMECs and BLECs was more discrete (+50%) (Fig. 4a). However, given the concerns associated with the manipulation and disposal of radioactive tracers, further experiments were performed with Naf. At such conditions, VEGF-A (50 ng/mL) promoted a consistent increase in the permeability of both CMECs (2.7-fold increase) and BLECs (2.3-fold increase) (Additional file 2: Figure S2b). scCM treatment decreased CMECs permeability (scEBM:  $1.03 \pm 0.08 \times 10^{-3}$  cm/min vs scCM:  $0.76 \pm 0.06 \times 10^{-3}$  cm/min), while it did not affect BLECs. WB analysis showed that scCM increases the expression of VE-Cadherin (113.5% [107.3–125.8]), ZO-1 (176% [104.6–209.3]), and occludin (121.1% [115.2–143.9]) in CMECs (Fig. 4b), whereas it had no effect on BLECs. IF analysis suggested that scCM favours the localization of TJ at the cell junctions and decreases its accumulation in the cytoplasm of CMECs (Additional file 2: Figure S2c). Besides, we observed that scCM-treated cells presented an accumulation of F-actin fibres at the cell junctions (Additional file 15: Figure S14a-b). Furthermore, scCM upregulated P-glycoprotein (Pg-p) in BLECs, one of the major efflux pumps of the ABC family restricting xenobiotics entrance into the CNS, while it had no effect in Breast Cancer Resistant Protein (BCRP) and ABC subfamily A member 1 (ABCA1) in neither CMECs nor BLECs (Additional file 15: Figure S14c).

#### scCM upregulates the expression of genes involved in the interferon pathway

We further investigated the underlying mechanisms of scCM effects in CMECs by performing an mRNA sequencing by TempO-seq. scCM upregulated the expression of 23 genes (Fig. 4c). By analysing the upregulated genes using the Panther software, we observed an overrepresentation of genes involved in interferon (IFN) pathways (Table 3 and Additional file 16: Table S2) according to the Reactome database. Given that previous studies have suggested that IFN response can inhibit the Wnt pathway

(See figure on next page.)

**Fig. 6** OGD-induced in vitro BBB leakage is prevented by scCM. Treatment with scCM during reoxygenation (24 h) abolished the OGD-induced increase in permeability on BLECs (a). WB analysis revealed that scCM increased claudin 5 expression (b) and favoured its localization at the cell junctions (c). scCM decreased VEGFR2 and ERK1/2 activation during reoxygenation (d). Moreover, scCM increased ICAM-1 expression in normoxic conditions but had no effect on BLECs exposed to OGD (d). Data represent median (interquartile range) [b and d] or mean  $\pm$  SD [a] ( $n = 3-5$ ).

\* $P < 0.05$  vs scEBM; \$ $P < 0.5$  vs R-OGD scEBM. Scale bar: 10  $\mu$ m

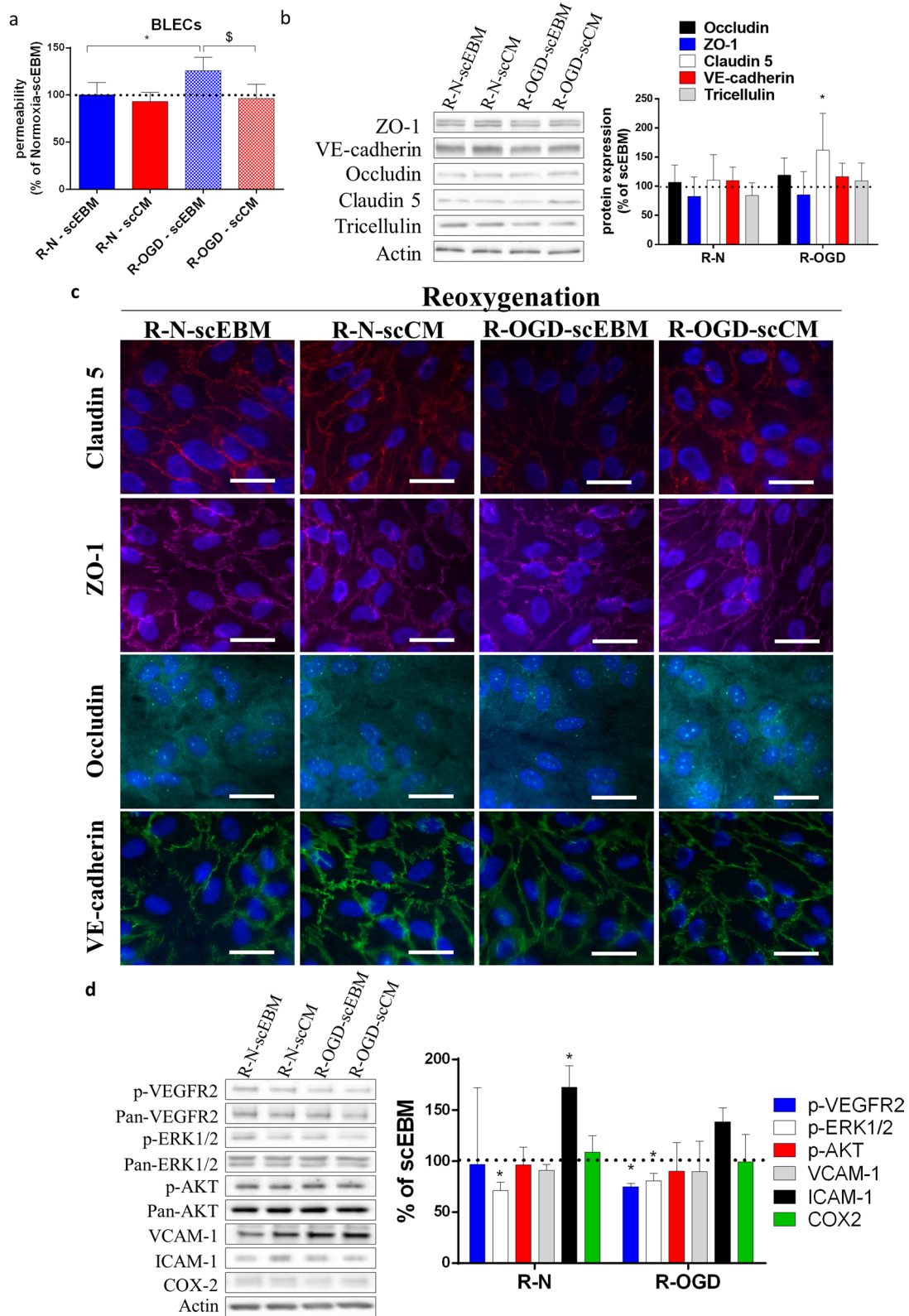


**Fig. 6** (See legend on previous page.)

activation [31], we investigated the effect of scCM on Wnt signalling. The levels of non-phosphorylated  $\beta$ -catenin, which translocates into the nucleus and transduces the Wnt pathway signalling, were reduced in scCM-treated cells (91.5% [80.8–92.6]) (Fig. 4d) together with a down-regulation of claudin 3 (53.7% [48.1–66.2]), a target which is positively correlated with Wnt activation (Fig. 4d). Further, we observed a reduction in the mRNA expression of Wnt pathway targets (APCDD1, Axin 2, CCND1) (Fig. 4e). Besides, Wnt pathway inhibitor (AZ6102, 1  $\mu$ mol/L) did not affect scCM-treated cells, while it caused a consistent decrease (scEBM vehicle:  $100 \pm 3.7\%$  vs scEBM AZ6102:  $73.2 \pm 11.8\%$ ) in the permeability of scEBM-treated cells (Fig. 4f).

#### scCM protects against OGD-induced barrier disruption

Next, CMECs and BLECs were exposed to OGD mimicking the conditions observed after stroke. OGD did not affect CMECs (Additional file 17: Figure S15a), while it induced a marked increase in the permeability of BLECs (normoxia: 0.66 [0.63–0.69] vs OGD:  $1.18 [0.92–1.25] \times 10^{-3}$  cm/min) (Additional file 17: Figure S15b). Besides, OGD upregulated the expression of hypoxia-target genes (HIF1A, VEGF-A, and GLUT1) in both CMECs and BLECs (Additional file 17: Figure S15c). While we could not detect any marked effect of OGD on TJ expression (Additional file 17: Figure S15d), IF suggested that OGD changed the distribution of junctional proteins (Additional file 17: Figure S15e–f).

To evaluate the protective effect of scCM under ischemic conditions, cells were treated after OGD or normoxia with scEBM or scCM during re-oxygenation (R-normoxia or R-OGD). CMECs exposed to OGD conditions presented a higher permeability (scEBM R-OGD:  $128.7 \pm 14.3\%$ ) in comparison with the control (scEBM R-Normoxia:  $100 \pm 5.8\%$ ) after reoxygenation, and scCM treatment reverted the OGD-induced barrier leakiness (scCM R-OGD:  $98.5 \pm 4.9\%$ ) (Fig. 5a). WB analysis revealed that scCM upregulated occludin (120.3% [107.5–123.8]), ZO-1 (123.2% [107.7–168.5]),

and tricellulin (120.1% [109.8–133.7]) expression (Fig. 5b). Besides, IF analysis suggested that scCM treatment preserved the TJ distribution at the cell boundaries (Fig. 5c). Interestingly, the VEGFR2 phosphorylation was increased in scCM-treated CMECs, with no changes detected in ERK1/2 nor AKT activation (Fig. 5d). Besides, scCM induced the expression of VCAM-1, ICAM-1, and COX2 in CMECs during reoxygenation (Fig. 5d).

In BLECs, OGD exposure increased the permeability after reoxygenation (scEBM R-normoxia:  $100 \pm 5.9\%$  vs scEBM R-OGD:  $125.8 \pm 14.3\%$ ) and scCM prevented the OGD-induced leakiness (scCM R-OGD:  $96.1 \pm 15.4\%$ ) (Fig. 6a). Such effect is possibly associated with the upregulation of claudin 5 (154.2% [106.9–224.7]) (Fig. 6b) and the restoration of TJ localization/assembly (Fig. 6c). Oppositely to the effects in CMECs, scCM inhibited both VEGFR2 and ERK1/2 activation, while it had no effect in the expression of VCAM-1, ICAM-1, and COX2 under OGD conditions (Fig. 6d).

#### scCM prevents TNF $\alpha$ -induced BBB leakage

The exacerbation of TNF $\alpha$  production by perivascular cells plays a key role in neuroinflammation and vascular leakage after stroke [32]. Since scCM had a protective effect in the vascular barrier under hypoxic conditions, we investigated whether it was also able to prevent the TNF $\alpha$ -induced barrier breakdown. In CMECs, TNF $\alpha$  did not significantly affect the permeability (Additional file 18: Figure S16a). On the other hand, TNF $\alpha$  induced a drastic elevation of BLECs permeability (scEBM control: 101.4% [93.3–106] vs scEBM TNF $\alpha$  473% [375.2–1049.1]) and scCM partially prevented the BBB leakage (245.8% [202.9–688.3]) (Additional file 18: Figure S16b). In parallel, TNF $\alpha$  treatment downregulated occludin expression (scEBM control:  $100 \pm 32.5\%$  vs scEBM TNF $\alpha$ :  $39.2 \pm 9.5\%$ ) and pre-treatment with scCM partially inhibited (scCM TNF $\alpha$ :

(See figure on next page.)

**Fig. 7** Network map of potential proteins/pathways involved in scCM-induced effects. **(a)** Schematic overview of angiogenesis process and in vitro assays proposed for evaluating EPC-secretome effects. Human CD34<sup>+</sup>-derived cord-blood hematopoietic endothelial cells (CD34<sup>+</sup>-ECs) were used to study angiogenesis (proliferation, cell migration, and tubulogenesis). To investigate mechanisms involved in vascular maturation, CD34<sup>+</sup>-EC were seeded on the surface of Matrigel<sup>™</sup>-coated Transwell inserts and cultivated in monocultures (CMECs). Finally, to study the effect of EPC-secretome on brain capillaries, we used an in vitro BBB model which consisted in seeding CD34<sup>+</sup>-ECs on Matrigel<sup>™</sup>-coated Transwell inserts and co-cultivating them with human brain pericytes, which enabled CD34<sup>+</sup>-ECs to acquire a brain-like endothelial cell phenotype (BLECs). **(b)** Proteins present in scCM were converted in gene identifiers and were then grouped according to their biological function/pathway (metabolic pathways, growth factors, inflammatory response, basal membrane (BM) regulation, cytoskeletal regulation, and integrin pathway). An interaction network was prepared using the Cytoscape software (version 3.8.2, released 2020.10.24). The regulation of MAPK activity might play an essential role in the scCM-induced angiogenesis in human primary ECs. In parallel, scCM promotes vascular maturation of newly formed vessels and protects the BBB integrity under ischemic and inflammatory conditions

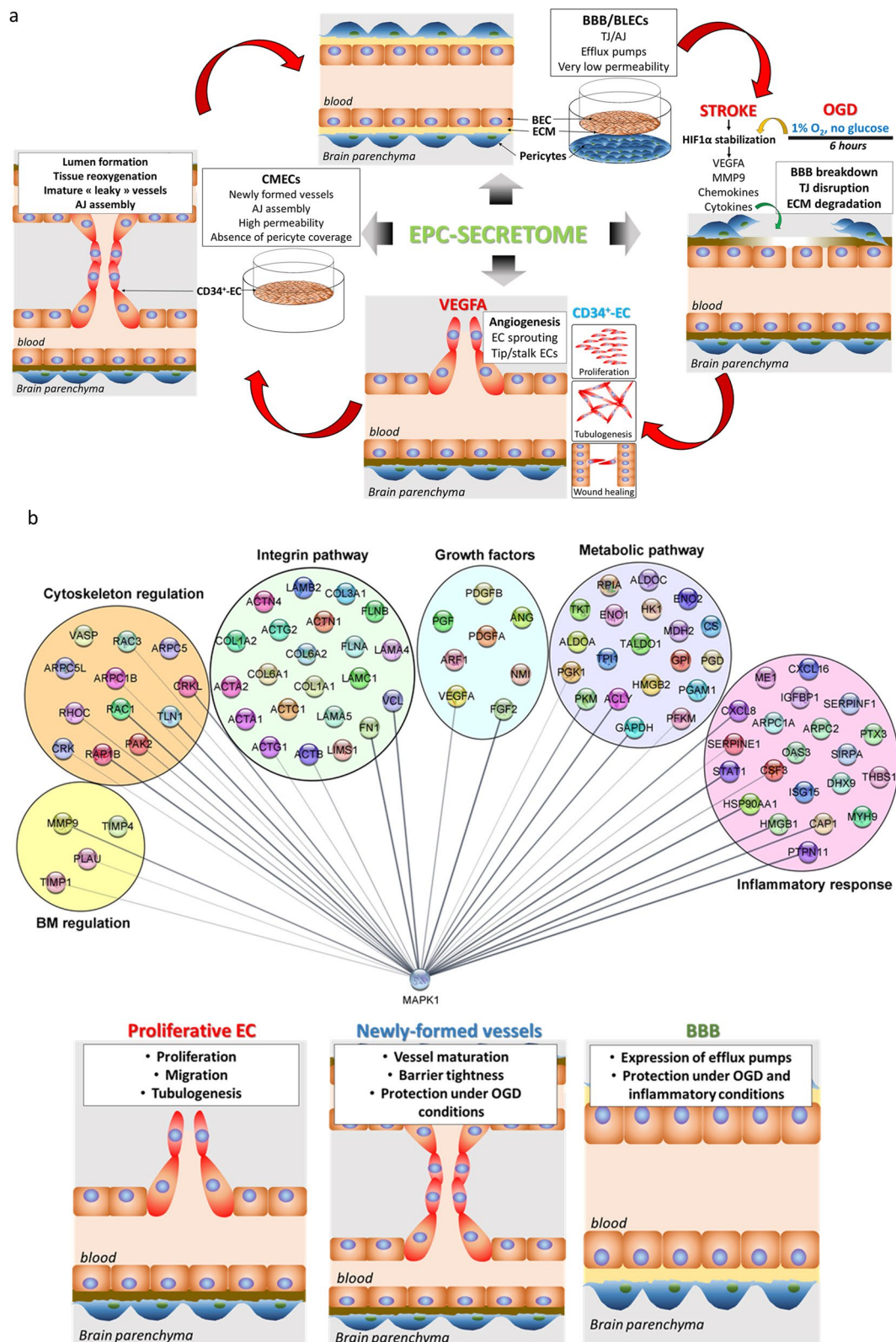


**Fig. 7** (See legend on previous page.)

64.8 ± 25.7%) this effect in BLECs (Additional file 18: Figure S16c).

## Discussion

Ischemic stroke is a major cause of death and disability worldwide, and the current therapeutic interventions targeting brain repair are still scarce. Over the last years, cell therapy with EPCs has been pinpointed as a promising approach for the enhancement of both vascular remodeling and neurogenesis after stroke [8, 9, 33]. However, concerns associated with cell-based therapies have limited their application for clinical purposes. In this context, cell-free therapies have been considered as an interesting alternative and some studies have reported beneficial effects of EPC-secretome in pre-clinical models of stroke and hypoperfusion [14, 15]. The present study reports a reproducible method for high-scale production of EPC-secretome (scCM) for therapeutic purposes. Further, we investigated the effect of scCM in primary human ECs, with a particular focus on angiogenesis and the regulation of vascular permeability (Fig. 7a). Overall, our results suggested that scCM exhibits an important angiogenic activity while lacking the negative effects of VEGF-A on vascular barrier properties. To the best of our knowledge, this is the first study evaluating the effect of EPC-secretome produced under high-scale conditions in a human *in vitro* BBB model. The results from this study expand the current knowledge about the mechanisms underlying the EPC-mediated effects on vascular cells and highlight proteins/pathways, which can be targeted for the simultaneous promotion of angiogenesis and vascular protection in the brain (Fig. 7b).

Initially, we have compared the angiogenic activity of the secretome produced by EPCs derived from SP and HD obtained by LSP. Although accumulating evidence has suggested that cardiovascular risk factors are associated with dysfunction and a reduced number of EPCs [34–37], the influence of cerebrovascular diseases on circulating EPCs is still debated. For instance, studies have shown that stroke was associated with a reduced number of circulating EPCs [38] and impairment of EPC function [39, 40]. On the other hand, some studies have also reported an increase in the number of circulating EPCs in stroke patients [16, 41]. Additionally, pre-clinical studies have shown that focal cerebral ischemia promotes EPCs mobilization and enhances the tubulogenesis of EPCs *in vitro* [10]. Besides, hypoxic pre-conditioning of EPCs has been proposed as a strategy to enhance their angiogenic properties [42]. In a nutshell, such studies have suggested that ischemia might improve the angiogenic abilities of EPCs and enhance therapeutic outcomes. Our *in vitro* studies (proliferation, migration, and tubulogenesis) have not found any difference in the angiogenic properties of EPC-secretome from stroke and healthy donors. Therefore, the use of autologous EPCs

from stroke patients might be the alternative for secretome production, as this approach would shorten ethical approvals. From our point of view, this study is a first step towards developing cell-based but cell-free formulations obtained under optimized GMP conditions for future clinical applications.

The EPC-secretome obtained under HSP conditions (scCM) showed a higher protein concentration (168-fold increase) in comparison with LSP. Additionally, the composition of LSP and HSP might be slightly different, since we observed a consistent effect of high-scale produced EPC-secretome on tubulogenesis, while the secretome produced under LSP had no effect. It is important to highlight that the standardization of HSP of EPC-secretome consisted in several challenging steps, such as controlling cell density at seeding, change of medium, and concentration of large volumes of conditioned medium. Therefore, further studies are necessary to understand the difference on composition of the secretome produced under low- and high-scale conditions; however, we consider it is an important step towards developing cell-based therapies for stroke treatment.

Proteome profiler analysis revealed an equitable presence of key angiogenesis-related proteins in two scCM batches, indicating low batch-to-batch variation under HSP conditions. Further, DDA-MS analysis of scCM revealed an overrepresentation of proteins associated with the modulation of cell metabolism, which is in agreement with previous studies reporting that the beneficial effects of cell therapy are due, at least in part, to metabolism regulation of injured cells [43–45]. Indeed, the delivery of key proteins involved in the regulation of glycolysis, pyruvate, and pentose phosphate pathways by EPC-secretome might boost cell metabolism or rescue metabolic activity in ischemic-injured cells. Additionally, the enrichment of proteins participating in cell cycle and cytoskeleton regulation might contribute to the scCM-induced promotion of CD34<sup>+</sup>-ECs proliferation, migration, and tubulogenesis, which were similar to the effects induced by VEGF-A, a key regulator of angiogenesis. The scCM-induced angiogenesis was partially mediated through MAPK activation, whereas PI3K/AKT pathway might not play a major role on this process. Our results are partially different from a previous study reporting that AKT is the main pathway underlying EPC-secretome-induced angiogenesis in rat immortalized brain ECs, while ERK activation plays a minor role in this process [46]. The RTK activation by growth factors might be the key event leading to downstream MAPK activation since the inhibition of both VEGFR2 and FGFR completely abolished scCM-induced angiogenesis. The presence of growth factors and adapter molecules on scCM possibly contribute to RTK/MAPK activation. Additionally, the presence of integrin ligands in scCM might contribute to VEGFR2/ERK

activation, given that integrins can increase the efficiency of RTK activation [47] and the coupling between upstream and downstream events in the RTK-Ras-MAPK cascade [48]. Besides, the crosstalk between VEGFR and integrin receptors is necessary to induce the VEGFR2-mediated angiogenesis [49]. In summary, our results suggest that the coordinated action of growth factors, adapter molecules, and integrin ligands plays a pivotal role in scCM-induced angiogenesis (Fig. 7b).

Vascular leakage following acute stroke is a major hazard that can compromise brain function as well as the therapeutic outcomes of treatments targeting brain repair. Considering that the local production of VEGF-A is critical for vascular disruption following stroke [50], we investigated the effect of scCM on permeability using an in vitro model of newly formed vessels (CMECs) and an already established BBB model in vitro (BLECs). As expected, VEGF-A evoked barrier leakage, while scCM promoted a consistent decrease in CMECs permeability together with an upregulation of junctional proteins. Interestingly, scCM upregulated P-gp expression in BLECs, suggesting that it might potentiate the transport of xenobiotics out of the brain through the BBB. Further, mRNA sequencing analysis of CMECs revealed that scCM upregulated the expression of several IFN-related genes. This finding is in accord with the presence of several proteins related to inflammatory pathways detected in scCM by MS analysis. Among them, STAT1 can translocate to the nucleus and activate the transcription of IFN-stimulated genes [51], while NMI, ISG15, and HMGB1 are IFN-induced proteins [52–54] (Fig. 7b). A body of evidence has highlighted a potential beneficial effect of the IFN pathway on the regulation of vessel maturation and inflammatory response. In this regard, IFN can stabilize barrier properties of in vitro BBB models [55] and act as a modulator of cytokine networks, reducing the cytokine-induced neutrophil infiltration and attenuating BBB disruption [56, 57]. Besides, IFN- $\beta$  might counteract the TJ disruption induced by the inflammatory response on brain ECs [56]. Such findings are in agreement with the protective effect of scCM against TNF $\alpha$ -induced disruption in BLECs. In parallel, our results suggest that scCM-induced barrier tightness is mediated through a moderate downregulation of Wnt activation, as highlighted by a decrease in active  $\beta$ -catenin content. Interestingly, some studies have reported evidence showing a common modulation of the Wnt and IFN pathways in the regulation of inflammatory responses. For instance, members of the miR-34 family, which are well-known repressors of Wnt/ $\beta$ -catenin signalling, potentiate the induction of IFN-responsive genes and their signalling pathways [58]. Another study has shown that PEGylated-IFN

inhibited  $\beta$ -catenin translocation to the nucleus and Wnt signalling in hepatoma cell lines [59]. Overall, our results suggest that the orchestrated modulation of the Wnt pathway and IFN signalling could be an underlying mechanism involved in scCM-induced barrier tightness under physiological conditions.

Next, we tested the potential beneficial effect of scCM on cells exposed to hypoxic conditions. In this regard, treatment with scCM completely abolished the OGD-induced leakage on CMECs and BLECs. This effect was possibly mediated through the regulation of junctional proteins expression and localization, leading to vascular protection against hypoxic-induced injury. The activity of integrin ligands and modulators of the extra-cellular matrix might be involved in scCM-mediated protection in OGD conditions since the degradation of the basal membrane involving the BBB is directly associated with ischemia-induced vascular disruption [60]. A potential activation of the IFN pathway by scCM also might contribute to the scCM-mediated vascular protection under ischemic conditions. Besides, the presence of small levels of growth factors in EPC-secretome might have a protective effect on injured cells, given that growth factors can promote anti-apoptotic effects [61]. Indeed, scCM increased VEGFR2 activation on CMECs exposed to OGD conditions. In parallel, scCM upregulated the expression of adhesion molecules (VCAM-1 and ICAM-1) and COX2, known molecular targets of VEGF pathway activation [62, 63]. Besides, the enrichment of proteins involved in inflammatory responses might contribute to the scCM-induced upregulation of adhesion molecules (Fig. 7b). VCAM-1 is important to promote close intercellular adhesion between ECs and pericytes, and it is required for blood vessel formation [64]. Besides, COX-2 plays a pivotal role in the VEGF-induced angiogenesis [65]. The scCM-induced adhesion molecule upregulation might favour the homing of leukocytes and circulating EPCs on injured vessels, which can further potentiate angiogenesis. On the other hand, the scCM-induced downregulation of VEGFR2 and ERK1/2 activation in BLECs exposed to OGD conditions might have a beneficial effect, considering that hypoxia-driven VEGF-A production is the main mechanism inducing BBB leakage [50] and that MAPK activation plays a key role in vascular injury induced by ischemia [66, 67]. Altogether, these results suggest that scCM can prevent the hypoxia-induced vascular leakiness, protecting the brain from edema-related deleterious effects.

Altogether, our results suggest that the scCM-elicited effects in proliferative and quiescent ECs were mediated through an orchestrated action of growth factors, integrin ligands, inflammatory mediators, enzymes regulating cell metabolism, and proteins regulating cytoskeleton

and basement membrane composition (Fig. 7b). The regulation of the MAPK pathway seems to be a key component of scCM-driven effects since a variety of proteins identified are directly linked to ERK1/2 activation and the scCM-treatment leads to the activation and/or inhibition of MAPK. However, other molecules present in the EPCs secretome, such as lipids and microRNAs, should be also considered but not addressed in this study. Certainly, further studies are necessary to better understand the mechanisms of EPC-secretome actions and identify the key molecules triggering its beneficial effects. It is noteworthy that we have used for this study cryopreserved EPCs obtained from freshly isolated PBMCs. Despite the fact that the effect of cryopreservation on EPCs' physiology is still controversial [68–70], such strategy allows the creation of a bank of EPCs from different donors or sources (e.g. bone marrow, blood, umbilical cord) for screening the cells with better angiogenic activity. We consider that a potential effect of cryopreservation needs to be taken into account for future studies in order to optimize EPC-secretome use as a therapeutic alternative for promoting brain angiogenesis and neurorepair. However, our study provides valuable information to understand the underlying mechanisms of EPC-mediated effects to develop cell-based therapies for stroke.

## Conclusions

Herein, we describe a reproducible method for a high-scale production of EPC-secretome and report pre-clinical evidence supporting its potential benefits for regenerative medicine. In particular, our results using human primary ECs suggest that scCM boosts angiogenesis-related processes while preserving the vascular barrier function in healthy vessels. In addition, scCM might promote vessel maturation and restore/preserve the BBB function in ischemic or inflammatory conditions. In conclusion, our results pave the way for future clinical trials employing EPC-secretome in order to promote brain repair after stroke.

## Abbreviations

AJ: Adherens junctions; AKT: Protein kinase B; ATP: Adenosine triphosphate; BBB: Blood–brain barrier; BLEC: Brain-like endothelial cells; BSA: Bovine serum albumin; CD34<sup>+</sup>-EC: CD34<sup>+</sup>-derived cord-blood hematopoietic endothelial cells; CM: Conditioned medium; CMEC: Confluent monolayer of endothelial cells; CNS: Central nervous system; COX-2: Cyclooxygenase 2; DTT: Dithiothreitol; ECGS: Endothelial cell growth supplement; EPC: Endothelial progenitor cells; ECM: Endothelial cell medium; EGM: Endothelial growth medium; ERK1/2: Extracellular signal-regulated kinase 1/2; HBP: Human brain pericytes; HD: Healthy donor; hFN: Human fibronectin; HSP: High-scale production; HIF1 $\alpha$ : Hypoxia-induced factor 1 $\alpha$ ; ICAM-1: Intercellular adhesion molecule 1; IFN: Interferon; LSP: Low-scale production; MAPK: Mitogen-activated protein kinase; Min: Minutes; MMP9: Metalloproteinase 9; MS: Mass spectrometry; Naf: Sodium fluorescein; NGS: Normal goat serum; OGD: Oxygen–glucose deprivation; PBS-CMF: Phosphate-buffered saline calcium magnesium-free; PDGF: Platelet-derived growth factor; Pe: Permeability coefficient; qRT-PCR:

Real-time quantitative reverse transcription polymerase chain reaction; RH: Ringer-Hepes buffer; RT: Room temperature; RTK: Receptor tyrosine kinase; scCM: Super-concentrated conditioned medium; SP: Stroke patient; TIMP1/4: Tissue inhibitor of metalloproteinase 1 and 4; TJ: Tight junction; VCAM-1: Vascular cell adhesion molecule 1; VEGF-A: Vascular endothelial cell growth factor A; VEGFR2: VEGF receptor 2; uPA: Urokinase-type plasminogen activator; WB: Western blot.

## Supplementary Information

The online version contains supplementary material available at <https://doi.org/10.1186/s13287-021-02608-y>.

**Additional file 1: Figure S1.** scCM increases CD34<sup>+</sup>-ECs proliferation. scHD-CM, scSP-CM, and scCM (batch 1 and 2) increase ATP production by CD34<sup>+</sup>-ECs. Data represent median (interquartile range) ( $n = 3-7$ ), \* $P < 0.05$  vs scEBM.

**Additional file 2: Figure S2** Effect of scCM treatment in the endothelial barrier properties. The permeability for radiolabelled-sucrose is enhanced in CMECs compared with BLECs (a). VEGF-A (50 ng/mL) induced vascular leakage in both CMECs and BLECs (b). Representative images of immunofluorescence performed in CMECs (c) and BLECs (d) for detection of claudin 5, ZO-1, occludin, and VE-cadherin. Data represent median (interquartile range) ( $n = 3-5$ ). Scale bar: 10  $\mu$ m.

**Additional file 3: Figure S3.** Representative images of pilot experiments performed to test the antibodies used in the study. Black arrows show the corresponding bands for every antibody according to the molecular weight predicted by the manufacturer. (a) phospho-AKT and pan-AKT; (b) phospho-VEGFR2 and pan-VEGFR2; (c) phospho-ERK1/2 and pan-ERK1/2; (d) non-phospho- $\beta$ -catenin and pan- $\beta$ -catenin; (e) ABCA1; (f) BCRP; (g) P-gp; (h) COX-2; (i) VCAM-1; (j) ICAM-1; (k) claudin 5; (l) VE-cadherin; (m) occludin; (n) ZO-1; (o) tricellulin; (p) claudin 3. For images A–D, membranes were firstly probed with phospho-antibodies and then reprobated with pan-antibodies.

**Additional file 4: Figure S4.** Images used for western blotting analysis of ERK1/2, AKT, and VEGFR2 phosphorylation in proliferative CD34<sup>+</sup>-EC in response to acute administration (0–60 min) of scCM (5  $\mu$ g/mL) (Fig. 3a). bFGF (basic FGF) represented in (a) was not considered for analysis.

**Additional file 5: Figure S5.** Images used for western blotting analysis of ERK1/2, AKT, and VEGFR2 phosphorylation in proliferative CD34<sup>+</sup>-EC in response to administration (4 or 24 h) of scCM (5  $\mu$ g/mL) (Figure 3b).

**Additional file 6: Figure S6.** Images used for western blotting analysis of ZO-1, VE-cadherin, occludin, claudin 5, claudin 3, non-phospho-catenin, and pan-catenin in CMECs in response to administration (48 h) of scCM (5  $\mu$ g/mL) (Fig. 4b and e). scCM-1: batch 1; scCM-2: batch 2. Analysis of scCM-2 were not presented in the manuscript.

**Additional file 7: Figure S7.** Images used for western blotting analysis of ZO-1, VE-cadherin, occludin, and claudin 5 in BLECs in response to administration (48 h) of scCM (5  $\mu$ g/mL) (Fig. 4b). scCM-1: batch 1; scCM-2: batch 2. Analysis of scCM-2 were not presented in the manuscript.

**Additional file 8: Figure S8.** Images used for western blotting analysis claudin 5, tricellulin, VEGFR2, VCAM-1, COX-2, occludin, VE-Cadherin, ZO-1, and ERK1/2 in CMECs exposed to normoxic (N) or OGD conditions and reoxygenation (R-N-scEBM; R-N-scCM; R-OGD-scEBM; R-OGD-scCM) (Fig. 5 and Additional file 17: Figure S15).

**Additional file 9: Figure S9.** Images used for western blotting analysis of claudin 5, ZO-1, VE-cadherin, VEGFR2, VCAM, AKT, ERK1/2, and occludin in CMECs exposed to normoxic (N) or OGD conditions and reoxygenation (R-N-scEBM; R-N-scCM; R-OGD-scEBM; R-OGD-scCM) (Fig. 5 and Additional file 17: Figure S15).

**Additional file 10: Figure S10.** Images used for western blotting analysis of VEGFR2, claudin 5, ZO-1, VE-cadherin, occludin, ICAM-1, AKT, ERK1/2, tricellulin, VCAM-1, and COX2 in BLECs exposed to normoxic (N) or OGD conditions and reoxygenation (R-N-scEBM; R-N-scCM; R-OGD-scEBM; R-OGD-scCM) (Fig. 6 and Additional file 17: Figure S15).

**Additional file 11: Figure S11.** Images used for western blotting analysis of VEGFR2, occludin, VE-cadherin, ZO-1, claudin 5, ERK1/2, AKT, and ICAM-1 in BLECs exposed to normoxic (N) or OGD conditions and reoxygenation (R-N-scEBM; R-N-scCM; R-OGD-scEBM; R-OGD-scCM) (Fig. 6 and Additional file 17: Figure S15).

**Additional file 12: Figure S12.** Images used for western blotting analysis of ABCA1, BCRP, and P-gp in CMECs (a–c) and BLECs (d–e) in response to administration (48 h) of scCM (5 µg/mL) (Additional file 15: Figure S14d). scCM-1: batch 1; scCM-2: batch 2. Analysis of scCM-2 were not presented in the manuscript.

**Additional file 13: Figure S13.** Images used for western blotting analysis of claudin 5, ZO-1, occludin, and VE-cadherin in BLECs treated with vehicle or TNFα (10 ng/mL) (Additional file 18: Figure S5c).

**Additional file 14: Table S1.**

**Additional file 15: Figure S14.** Effect of scCM treatment in the endothelial barrier properties. Co-staining with phalloidin and ZO-1 suggests that scCM promotes the accumulation of actin fibres at the cell borders (yellow arrowheads) and decreases its distribution across the cytoplasm of CMECs (a) and BLECs (b). scCM upregulates P-gp expression on BLECs, whereas it did not affect ABCA1 and BCRP expression (c). Data represent median (interquartile range) ( $n = 4–8$ ). \* $P < 0.05$  vs scEBM. Scale bar: 10 µm.

**Additional file 16: Table S2.**

**Additional file 17: Figure S15.** Effect of oxygen–glucose deprivation (OGD) on *in vitro* vascular permeability. OGD (6 h) had no effect on permeability of CMECs (a), while it induced vascular leakage in BLECs (b). OGD upregulated the mRNA expression of target genes, such as HIF1A, VEGF-A, and Glut-1 (c). Western blot analysis did not show a marked effect of OGD on the expression of junctional proteins (d); however, IF analysis suggested that OGD induces their accumulation in the cytoplasm (e). Data represent median (interquartile range) ( $n = 3–4$ ). \* $P < 0.05$  vs scEBM. Scale bar: 10 µm.

**Additional file 18: Figure S16.** Effect of TNFα on *in vitro* vascular permeability. CMECs and BLECs were pre-treated (24 h) with scEBM or scCM (5 µg/mL) and then TNFα (10 ng/mL) was administered to the cells. Whereas TNFα had no significant effect on permeability of CMECs (a), scCM partially prevented TNFα-induced leakage in BLECs (b). WB analysis showed that scCM partially restored the TNFα-induced downregulation of occludin in BLECs (c). Data represent median (interquartile range) [a and b] or mean  $\pm$  SD [c] ( $n = 4–8$ ). \* $P < 0.05$  vs scEBM control.

## Acknowledgements

Authors would like to acknowledge Dr. Julien Saint-Pol for helpful discussions and advices on experimental set-ups, Lucie Dehouck and Emanuel Sevin for supporting cell culture routine, Maxime Culote and Sara Wellens for collaborating with mRNA-sequencing experiments, and Gustavo Henrique de Oliveira Rocha for the help with the western blots.

## Authors' contributions

This study was designed by FG and AR. RAL designed and performed the experiments, data analysis and interpretation of proteomic and mRNA-sequencing data. AR, MGG, and AG isolated EPCs from patients and realized the low-scale production of secretome. PB, AK, and MPM performed and optimized the high-scale production of EPC-secretomes. YS, FS, and TK isolated, purified and characterized the human brain pericytes necessary to reproduce the human BBB *in vitro*. Proteomic analysis of the samples and the corresponding data interpretations were performed by SDD and JH. ER and CM developed and optimized the OGD protocol in both human barrier models. Manuscript was written by FG and RAL and then edited by all the authors. All authors read and approved the final manuscript.

## Funding

This work has been supported under the Euronanomed 8th Joint Call-MAG-GBRIS collaborative project by grants from the Spanish Ministry of Science and Innovation (PCIN-2017-090) the French national agency (ANR-ANR-17-ENM3-0005-01), the AC17/00004 grant from Instituto Carlos III (ISCIII) with FEDR funds, and the National Centre for Research and Development (NCBR

15/EuronanoMed/2018). A part of this study has been also funded in the frame of the NANOSTEM project, a Marie Skłodowska-Curie Innovative Training Network (ITN) by receiving grant from the European Union's Horizon 2020 research and innovation programme under grant agreement No. 764958 and the Expression of Interest (Eol) for Collaborative Projects on Regenerative Medicine 2019 P-CMR[C], and the programs 2017-SGR-1427 and 2017-SGR-765 from the Generalitat de Catalunya. Alba Grayston is supported by the fellowship F117/00073 from ISCIII with FEDR funds. Miguel Garcia-Gabilondo is supported by the PERIS grant SLT017/20/000197 from Generalitat de Catalunya. The mass spectrometer of the Spectrométrie de Masse de l'Artois (SMART) facilities used in this study was funded by the European Regional Development Fund (ERDF), the Hauts-de-France regional council, and the Université d'Artois (France).

## Availability of data and materials

The datasets used and/or analysed during this study are available from the corresponding authors upon reasonable request.

## Declarations

### Ethics approval and consent to participate.

Informed consent was obtained from all subjects with the approval of the Clinical Ethics Committee of the Hospital Vall d'Hebron (PR-AG-177-2011/2021). Collection of human umbilical cord blood was done with the signature of a consent form by infant's parents, in compliance with the French legislation. The protocol was approved by the French Ministry of Higher Education and Research (CODECOH Number DC2011-1321). All experiments were carried out in accordance with the approved protocol.

### Consent for publication

Not applicable.

### Competing interests

PB, AK, and MM are employees of Pure Biologics S.A. Authors report no competing interests.

### Author details

<sup>1</sup>UR 2465, Blood-Brain Barrier Laboratory (LBHE), Univ. Artois, 62300 Lens, France. <sup>2</sup>Neurovascular Research Laboratory, Vall d'Hebron Institut de Recerca, Universitat Autònoma de Barcelona, 08035 Barcelona, Catalonia, Spain. <sup>3</sup>Pure Biologics S.A., Duńska 11, 54-427 Wrocław, Poland. <sup>4</sup>Department of Neurology and Clinical Neuroscience, Graduate School of Medicine, Yamaguchi University, Ube, Japan. <sup>5</sup>Laboratory of the Blood-Brain Barrier, Sciences Faculty Jean Perrin, Artois University, Lens, France.

Received: 28 June 2021 Accepted: 25 September 2021

Published online: 26 October 2021

## References

- Prabhakaran S, Ruff I, Bernstein RA. Acute stroke intervention: a systematic review. *JAMA*. 2015;313(14):1451–62.
- Abdullahi W, Tripathi D, Ronaldson PT. Blood–brain barrier dysfunction in ischemic stroke: targeting tight junctions and transporters for vascular protection. *Am J Physiol Cell Physiol*. 2018;315(3):C343–56.
- Abbott NJ, Ronnback L, Hansson E. Astrocyte–endothelial interactions at the blood–brain barrier. *Nat Rev Neurosci*. 2006;7(1):41–53.
- Gosset F, Loiola RA, Roig A, Rosell A, Culot M. Central nervous system delivery of molecules across the blood–brain barrier. *Neurochem Int*. 2021;144:104952.
- Arai K, Jin G, Navaratna D, Lo EH. Brain angiogenesis in developmental and pathological processes: neurovascular injury and angiogenic recovery after stroke. *FEBS J*. 2009;276(17):4644–52.
- Ergul A, Alhusban A, Fagan SC. Angiogenesis: a harmonized target for recovery after stroke. *Stroke*. 2012;43(8):2270–4.
- Esquiva G, Grayston A, Rosell A. Revascularization and endothelial progenitor cells in stroke. *Am J Physiol Cell Physiol*. 2018;315(5):C664–74.
- Taguchi A, Soma T, Tanaka H, Kanda T, Nishimura H, Yoshikawa H, et al. Administration of CD34+ cells after stroke enhances neurogenesis via angiogenesis in a mouse model. *J Clin Investig*. 2004;114(3):330–8.



9. Bai Y-Y, Wang L, Chang D, Zhao Z, Lu C-Q, Wang G, et al. Synergistic effects of transplanted endothelial progenitor cells and RWJ 67657 in diabetic ischemic stroke models. *Stroke*. 2015;46(7):1938–46.
10. Morancho A, Hernandez-Guillamon M, Boada C, Barcelo V, Giral D, Ortega L, et al. Cerebral ischaemia and matrix metalloproteinase-9 modulate the angiogenic function of early and late outgrowth endothelial progenitor cells. *J Cell Mol Med*. 2013;17(12):1543–53.
11. Boltze J, Arnold A, Walczak P, Jolkkonen J, Cui L, Wagner DC. The dark side of the force—constraints and complications of cell therapies for stroke. *Front Neurol*. 2015;6:155.
12. Boncoraglio GB, Ranieri M, Bersano A, Parati EA, Del Giovane C. Stem cell transplantation for ischemic stroke. *Cochrane Database Syst Rev*. 2019;5:CD007231.
13. Fang J, Guo Y, Tan S, Li Z, Xie H, Chen P, et al. Autologous endothelial progenitor cells transplantation for acute ischemic stroke: a 4-year follow-up study. *Stem Cells Transl Med*. 2019;8(1):14–21.
14. Rosell A, Morancho A, Navarro-Sobrinho M, Martínez-Saez E, Hernández-Guillamon M, Lope-Piedrafitá S, et al. Factors secreted by endothelial progenitor cells enhance neurorepair responses after cerebral ischemia in mice. *PLoS ONE*. 2013;8(9):e73244.
15. Maki T, Morancho A, Martínez-San Segundo P, Hayakawa K, Takase H, Liang AC, et al. Endothelial progenitor cell secretome and oligovascular repair in a mouse model of prolonged cerebral hypoperfusion. *Stroke*. 2018;49(4):1003–10.
16. Navarro-Sobrinho M, Rosell A, Hernandez-Guillamon M, Penalba A, Ribo M, Alvarez-Sabin J, et al. Mobilization, endothelial differentiation and functional capacity of endothelial progenitor cells after ischemic stroke. *Microvasc Res*. 2010;80(3):317–23.
17. Pedroso DC, Tellechea A, Moura L, Fidalgo-Carvalho I, Duarte J, Carvalho E, et al. Improved survival, vascular differentiation and wound healing potential of stem cells co-cultured with endothelial cells. *PLoS ONE*. 2011;6(1):e16114.
18. Shimizu F, Sano Y, Abe M, Maeda T, Ohtsuki S, Terasaki T, et al. Peripheral nerve pericytes modify the blood–nerve barrier function and tight junctional molecules through the secretion of various soluble factors. *J Cell Physiol*. 2011;226(1):255–66.
19. Deligne C, Hachani J, Duban-Deweer S, Meignan S, Leblond P, Carcaboso AM, et al. Development of a human in vitro blood–brain tumor barrier model of diffuse intrinsic pontine glioma to better understand the chemoresistance. *Fluids Barriers CNS*. 2020;17:1–15.
20. Jennings P, Koppelstaetter C, Aydin S, Abberger T, Wolf AM, Mayer G, et al. Cyclosporine A induces senescence in renal tubular epithelial cells. *Am J Physiol-Renal Physiol*. 2007;293(3):F831–8.
21. Ma F, Martínez-San Segundo P, Barcelo V, Morancho A, Gabriel-Salazar M, Giral D, et al. Matrix metalloproteinase-13 participates in neuroprotection and neurorepair after cerebral ischemia in mice. *Neurobiol Dis*. 2016;91:236–46.
22. Cecchelli R, Aday S, Sevin E, Almeida C, Culot M, Dehouck L, et al. A stable and reproducible human blood–brain barrier model derived from hematopoietic stem cells. *PLoS ONE*. 2014;9(6):e99733.
23. Heymans M, Figueiredo R, Dehouck L, Francisco D, Sano Y, Shimizu F, Kanda T, Bruggmann R, Engelhardt B, Winter P, Gosselet F. Contribution of brain pericytes in blood–brain barrier formation and maintenance: a transcriptomic study of cocultured human endothelial cells derived from hematopoietic stem cells. *Fluids Barriers CNS*. 2020;17(1):48.
24. Luo H, Gauthier M, Tan X, Landry C, Poupon J, Dehouck M-P, et al. Sodium transporters are involved in lithium influx in brain endothelial cells. *Mol Pharm*. 2018;15(7):2528–38.
25. Cecchelli R, Dehouck B, Descamps L, Fenart L, Buée-Scherrer V, Duhem C, Lundquist S, Rentfel M, Torpier G, Dehouck MP. In vitro model for evaluating drug transport across the blood–brain barrier. *Adv Drug Deliv Rev*. 1999;36(2–3):165–78.
26. Siflinger-Birnboim A, del Vecchio PJ, Cooper JA, Blumenstock FA, Shepard JM, Malik AB. Molecular sieving characteristics of the cultured endothelial monolayer. *J Cell Physiol*. 1987;132(1):111–7.
27. Wellens S, Dehouck L, Chandrasekaran V, Singh P, Loiola RA, Sevin E, et al. Evaluation of a human iPSC-derived BBB model for repeated dose toxicity testing with cyclosporine A as model compound. *Toxicol in Vitro*. 2021;73:105112.
28. Lin C-P, Lin F-Y, Huang P-H, Chen Y-L, Chen W-C, Chen H-Y, et al. Endothelial progenitor cell dysfunction in cardiovascular diseases: role of reactive oxygen species and inflammation. *BioMed Res Int*. 2013;2013:845037.
29. Belkacemi L, Zhang SX. Anti-tumor effects of pigment epithelium-derived factor (PEDF): implication for cancer therapy. A mini-review. *J Exp Clin Cancer Res*. 2016;35:4.
30. Lawler PR, Lawler J. Molecular basis for the regulation of angiogenesis by thrombospondin-1 and -2. *Cold Spring Harbor Perspect Med*. 2012;2(5):a006627.
31. Li W, Huang X, Tong H, Wang Y, Zhang T, Wang W, et al. Comparison of the regulation of  $\beta$ -catenin signaling by type I, type II and type III interferons in hepatocellular carcinoma cells. *PLoS ONE*. 2012;7(10):e47040.
32. Doll DN, Barr TL, Simpkins JW. Cytokines: their role in stroke and potential use as biomarkers and therapeutic targets. *Aging Dis*. 2014;5(5):294–306.
33. Morancho A, Ma F, Barcelo V, Giral D, Montaner J, Rosell A. Impaired vascular remodeling after endothelial progenitor cell transplantation in MMP9-deficient mice suffering cortical cerebral ischemia. *J Cereb Blood Flow Metab: Off J Int Soc Cereb Blood Flow Metab*. 2015;35(10):1547–51.
34. Vasa M, Fichtlscherer S, Aicher A, Adler K, Urbich C, Martin H, et al. Number and migratory activity of circulating endothelial progenitor cells inversely correlate with risk factors for coronary artery disease. *Circ Res*. 2001;89(1):E1–7.
35. Pirro M, Schillaci G, Menecali C, Bagaglia F, Paltriccia R, Vaudo G, et al. Reduced number of circulating endothelial progenitors and HoxA9 expression in CD34+ cells of hypertensive patients. *J Hypertens*. 2007;25(10):2093–9.
36. Ho JC, Lai WH, Li MF, Au KW, Yip MC, Wong NL, et al. Reversal of endothelial progenitor cell dysfunction in patients with type 2 diabetes using a conditioned medium of human embryonic stem cell-derived endothelial cells. *Diabetes Metab Res Rev*. 2012;28(5):462–73.
37. Tepper OM, Galiano RD, Capla JM, Kalka C, Gagne PJ, Jacobowitz GR, et al. Human endothelial progenitor cells from type II diabetics exhibit impaired proliferation, adhesion, and incorporation into vascular structures. *Circulation*. 2002;106(22):2781–6.
38. Ghani U, Shuaib A, Salam A, Nasir A, Shuaib U, Jeerakathil T, et al. Endothelial progenitor cells during cerebrovascular disease. *Stroke*. 2005;36(1):151–3.
39. Kukumberg M, Zaw AM, Wong DHC, Toh CM, Chan BPL, Seet RCS, et al. Characterization and functional assessment of endothelial progenitor cells in ischemic stroke patients. *Stem Cell Rev Rep*. 2021;17(3):952–67.
40. Chu K, Jung KH, Lee ST, Park HK, Sinn DL, Kim JM, et al. Circulating endothelial progenitor cells as a new marker of endothelial dysfunction or repair in acute stroke. *Stroke*. 2008;39(5):1441–7.
41. Regueiro A, Cuadrado-Godia E, Bueno-Beti C, Diaz-Ricart M, Oliveras A, Novella S, et al. Mobilization of endothelial progenitor cells in acute cardiovascular events in the PROCELL study: time-course after acute myocardial infarction and stroke. *J Mol Cell Cardiol*. 2015;80:146–55.
42. Akita T, Murohara T, Ikeda H, Sasaki K, Shimada T, Egami K, et al. Hypoxic preconditioning augments efficacy of human endothelial progenitor cells for therapeutic neovascularization. *Lab Invest J Tech Methods Pathol*. 2003;83(1):65–73.
43. Hayakawa K, Chan SJ, Mandeville ET, Park JH, Bruzzese M, Montaner J, et al. Protective effects of endothelial progenitor cell-derived extracellular mitochondria in brain endothelium. *Stem cells*. 2018;36(9):1404–10.
44. Islam MN, Das SR, Emin MT, Wei M, Sun L, Westphalen K, et al. Mitochondrial transfer from bone-marrow-derived stromal cells to pulmonary alveoli protects against acute lung injury. *Nat Med*. 2012;18(5):759–65.
45. Kaza AK, Wamala I, Friehs I, Kuebler JD, Rathod RH, Berra I, et al. Myocardial rescue with autologous mitochondrial transplantation in a porcine model of ischemia/reperfusion. *J Thorac Cardiovasc Surg*. 2017;153(4):934–43.
46. Di Santo S, Seiler S, Fuchs AL, Staudigl J, Widmer HR. The secretome of endothelial progenitor cells promotes brain endothelial cell activity through PI3-kinase and MAP-kinase. *PLoS ONE*. 2014;9(4):e95731.
47. Soldi R, Mitola S, Strasly M, Defilippi P, Tarone G, Bussolino F. Role of  $\alpha$ v $\beta$ 3 integrin in the activation of vascular endothelial growth factor receptor-2. *EMBO J*. 1999;18(4):882–92.

48. Lin TH, Chen Q, Howe A, Juliano RL. Cell anchorage permits efficient signal transduction between Ras and its downstream kinases. *J Biol Chem*. 1997;272(14):8849–52.
49. West XZ, Meller N, Malinin NL, Deshmukh L, Meller J, Mahabeleshwar GH, et al. Integrin  $\beta$  3 crosstalk with VEGFR accommodating tyrosine phosphorylation as a regulatory switch. *PLoS ONE*. 2012;7(2):e31071.
50. Ma Y, Zechariah A, Qu Y, Hermann DM. Effects of vascular endothelial growth factor in ischemic stroke. *J Neurosci Res*. 2012;90(10):1873–82.
51. Khodarev NN, Roizman B, Weichselbaum RR. Molecular pathways: interferon/stat1 pathway: role in the tumor resistance to genotoxic stress and aggressive growth. *Clin Cancer Res: Off J Am Assoc Cancer Res*. 2012;18(11):3015–21.
52. Xu X, Chai K, Chen Y, Lin Y, Zhang S, Li X, et al. Interferon activates promoter of Nmi gene via interferon regulator factor-1. *Mol Cell Biochem*. 2018;441(1–2):165–71.
53. Zhao C, Collins MN, Hsiang TY, Krug RM. Interferon-induced ISG15 pathway: an ongoing virus-host battle. *Trends Microbiol*. 2013;21(4):181–6.
54. Rendon-Mitchell B, Ochani M, Li J, Han J, Wang H, Yang H, et al. IFN- $\gamma$  induces high mobility group box 1 protein release partly through a TNF-dependent mechanism. *J Immunol*. 2003;170(7):3890–7.
55. Kraus J, Voigt K, Schuller A, Scholz M, Kim K, Schilling M, et al. Interferon- $\beta$  stabilizes barrier characteristics of the blood–brain barrier in four different species in vitro. *Mult Scler J*. 2008;14(6):843–52.
56. Kuruganti PA, Hinojosa JR, Eaton MJ, Ehmann UK, Sobel RA. Interferon- $\beta$  counteracts inflammatory mediator-induced effects on brain endothelial cell tight junction molecules—implications for multiple sclerosis. *J Neuropathol Exp Neurol*. 2002;61(8):710–24.
57. Veldhuis WB, Derksen JW, Floris S, Van Der Meide PH, De Vries HE, Schepers J, et al. Interferon-beta blocks infiltration of inflammatory cells and reduces infarct volume after ischemic stroke in the rat. *J Cereb Blood Flow Metab*. 2003;23(9):1029–39.
58. Smith JL, Jeng S, McWeeney SK, Hirsch AJ. A microRNA screen identifies the Wnt signaling pathway as a regulator of the interferon response during flavivirus infection. *J Virol*. 2017;91(8):e02388–e2416.
59. Thompson MD, Dar MJ, Monga SP. Pegylated interferon alpha targets Wnt signaling by inducing nuclear export of  $\beta$ -catenin. *J Hepatol*. 2011;54(3):506–12.
60. Kwon I, Kim EH, del Zoppo GJ, Heo JH. Ultrastructural and temporal changes of the microvascular basement membrane and astrocyte interface following focal cerebral ischemia. *J Neurosci Res*. 2009;87(3):668–76.
61. Lanfranconi S, Locatelli F, Corti S, Candelise L, Comi GP, Baron PL, et al. Growth factors in ischemic stroke. *J Cell Mol Med*. 2011;15(8):1645–87.
62. Kim I, Moon S, Hoon Kim S, Jin Kim H, Soon Koh Y, Young KG. Vascular endothelial growth factor expression of ICAM-1, VCAM-1 and E-selectin through NF $\kappa$ B activation in endothelial cells. *J Biol Chem*. 2001;276:7614–20.
63. Akarasereenont P, Techatraisak K, Thaworn A, Chotewuttakorn S. The expression of COX-2 in VEGF-treated endothelial cells is mediated through protein tyrosine kinase. *Mediat Inflamm*. 2002;11(1):17–22.
64. Garmy-Susini B, Jin H, Zhu Y, Sung R-J, Hwang R, Varner J. Integrin  $\alpha$  4  $\beta$  1–VCAM-1–mediated adhesion between endothelial and mural cells is required for blood vessel maturation. *J Clin Investig*. 2005;115(6):1542–51.
65. Wu G, Luo J, Rana JS, Laham R, Sellke FW, Li J. Involvement of COX-2 in VEGF-induced angiogenesis via P38 and JNK pathways in vascular endothelial cells. *Cardiovasc Res*. 2006;69(2):512–9.
66. Narasimhan P, Liu J, Song YS, Massengale JL, Chan PH. VEGF Stimulates the ERK 1/2 signaling pathway and apoptosis in cerebral endothelial cells after ischemic conditions. *Stroke*. 2009;40(4):1467–73.
67. Maddahi A, Edvinsson L. Cerebral ischemia induces microvascular pro-inflammatory cytokine expression via the MEK/ERK pathway. *J Neuroinflamm*. 2010;7(1):1–13.
68. Lin RZ, Dreyzin A, Aamodt K, Dudley AC, Melero-Martin JM. Functional endothelial progenitor cells from cryopreserved umbilical cord blood. *Cell Transplant*. 2011;20(4):515–22.
69. Bogoslovsky T, Wang D, Maric D, Scattergood-Keeper L, Spatz M, Auh S, et al. Cryopreservation and enumeration of human endothelial progenitor and endothelial cells for clinical trials. *J Blood Disord Transfus*. 2013;4(5):158.
70. Béland S, Désy O, Bouchard-Boivin F, Gama A, De Serres SA. Endothelial colony forming cells generated from cryopreserved peripheral blood mononuclear cells. *Hum Immunol*. 2021;82(4):309–14.

## Publisher's Note

Springer Nature remains neutral with regard to jurisdictional claims in published maps and institutional affiliations.

Ready to submit your research? Choose BMC and benefit from:

- fast, convenient online submission
- thorough peer review by experienced researchers in your field
- rapid publication on acceptance
- support for research data, including large and complex data types
- gold Open Access which fosters wider collaboration and increased citations
- maximum visibility for your research: over 100M website views per year

At BMC, research is always in progress.

Learn more [biomedcentral.com/submissions](https://biomedcentral.com/submissions)

